ABSTRACT

Early Paleocene Fossil Floras, Paleoclimate, and Magnetostratigraphy
from the San Juan Basin, New Mexico, USA

Andrew G. Flynn, Ph.D.

Mentor: Daniel J. Peppe, Ph.D.

The San Juan Basin, located in northwestern New Mexico, preserves an excellent early Paleocene floral and faunal records in North America making it an ideal location to study the tempo and processes of terrestrial ecosystem recovery following the Cretaceous-Paleogene mass extinction. However, the lack of precise age constraints for fossil localities and poor sampling of the early Paleocene floral record has hampered previous work. To address this issue, I constructed a high-resolution age model for the early Paleocene Ojo Alamo Sandstone and lower Nacimiento Formation in the San Juan Basin using magnetostratigraphy, biostratigraphy, and detrital sanidine ages. This age model demonstrated that the earliest Paleocene Ojo Alamo Sandstone deposition was time transgressive, the Nacimiento Formation records a shift from low to high accommodation and an increase in basin subsidence, the Puercan-Torrejonian North America Land Mammal Age faunal transition occurred between 65.03 – 64.66 Ma, and this faunal transition may have been diachronous across North America.

Fossil leaves were collected from the Ojo Alamo Sandstone and lower Nacimiento Formation to evaluate changes in early Paleocene floral composition and paleoclimate. The fossil floras from San Juan Basin were diverse, laterally heterogeneous, and dominated by angiosperms. Leaf physiognomic paleoclimate estimates indicate warm temperatures and high precipitation through the entire record consistent with a modern tropical seasonal forest biome. The San Juan Basin flora had higher species richness and warmer paleoclimate estimates compared to contemporaneous northern North American localities indicating an early Paleocene latitudinal diversity and paleoclimate gradient.

Early Paleocene floral diversity dynamics were modeled from western North American collections during the first ~1.5 Myr of the Paleocene. Model results indicate simultaneous and volatile changes in floral diversity across western North America, especially during the first ~800 Kyr of the Paleocene, suggesting a global driver in early Paleocene floral diversity. Intervals of decreasing diversity during the early Paleocene correspond with a negative bulk organic $\delta^{13}C$ excursion and correlate with the onset of major Deccan Traps eruptive phases suggesting Deccan Traps volcanism impacted early Paleocene floral communities. These results highlight prolonged recovery and increased sensitivity to environmental perturbations in terrestrial ecosystems following the Cretaceous-Paleogene mass extinction.

Early Paleocene Fossil Floras, Paleoclimate, and Magnetostratigraphy
from the San Juan Basin, New Mexico, USA

by

Andrew G. Flynn, B.S.

A Dissertation

Approved by the Department of Geosciences

Steven Driese, Ph.D., Chairperson

Submitted to the Graduate Faculty of
Baylor University in Partial Fulfillment of the
Requirements for the Degree
of
Doctor of Philosophy

Approved by the Dissertation Committee

Daniel J. Peppe, Ph.D., Chairperson

Stacy C. Atchley, Ph.D.

Steve I. Dworkin, Ph.D.

William C. Hockaday, Ph.D.

Joseph D. White, Ph.D.

Accepted by the Graduate School
May 2020

J. Larry Lyon, Ph.D., Dean

Page bearing signatures is kept on file in the Graduate School.

TABLE OF CONTENTS

LIST OF FIGURES

LIST OF TABLES

ACKNOWLEDGMENTS

First, the work presented here would not have been possible without the patience and guidance of my advisor Dr. Dan Peppe. His invaluable support, direction, and encouragement has enabled my success and seen me through this process. This work was supported by numerous collaborators whose invaluable contributions elevated its quality: Thomas Williamson, Matt Heizler, Caitlin Leslie, Adam Davis, Ross Secord, Steve Brusatte, and C. William Fenley IV. This work would not have been possible without field and laboratory assistance from Baylor University undergraduate students Brittany Abbuhl, Jie Geng, Parker Wright, Hunter Anderson, Jeremiah Robinson, and Michaela Donahoo and graduate students Joseph Milligan, Aly Baumgartner, and Jennifer Wagner and I thank them for not leaving me in the desert when I told them one more hour of digging. I would also like to thank Ellen Currano for introducing me to paleobotany an undergraduate student at Miami University, Rich Barclay, Lisa Boucher, Regan Dunn, and Steve Manchester for their assistance in identifying fossil leaves from New Mexico, Lee Hsiang Liow for her assistance with Capture-Mark-Recapture methods, and Stacy Atchley, Steve Dworkin, William Hockaday, and Joseph White for providing feedback on this work. I greatly appreciate the generous support from the Geosciences Department and all the assistance from Paulette Penney, Janelle Atchley, and Jamie Ruth over the past seven years. I extend my gratitude to my fellow graduate students past and present, especially Emily Beverly, Ian Byram, Todd Longbottom, and Yohan Letourmy, for pushing me to be a better scientist and, more importantly, all the fun we had along the way. Lastly, I would like to my family and friends who have encouraged and inspired me on this journey and most importantly my parents, Magan and Will, for their unconditional support of a son who never quite got over dinosaurs.

This research was made possible by funding from the National Science Foundation, American Chemical Society Petroleum Research Fund, US Bureau of Land Management, Geologic Society of America, Dallas Paleontological Society, and Baylor University Department of Geosciences James Dixon Fund.

CHAPTER ONE

Introduction

This dissertation is comprised of three manuscripts corresponding to three separate chapters. These studies include contributions from collaborators who aided in the completion of each chapter. I collected and analyzed all data and samples, produced all figures and tables, and wrote the corresponding manuscript with the exceptions outlined below.

This dissertation focuses on the early Paleocene fossil floras and geochronology of terrestrial deposits from San Juan Basin, New Mexico which are important for understanding terrestrial ecosystem response to the Cretaceous-Paleogene mass extinction. While the San Juan Basin has arguably the most complete early Paleocene fossil mammalian record in North America, precise age constraints for many faunal localities were poor to nonexistent and the Paleocene floral record of the San Juan Basin has been understudied inhibiting our understanding of the tempo and processes of early Paleocene terrestrial ecosystem recovery. The first study develops a high-resolution age model for the Ojo Alamo Sandstone and lower Nacimiento Formation to constrain the age of fossil plant and mammal localities throughout the San Juan Basin. The second study looks at a unique and diverse fossil flora from the Ojo Alamo Sandstone which was deposited < 350 Kyr after the Cretaceous-Paleogene boundary. The final study models floral diversity dynamics using Capture-Mark-Recapture methods to estimate rates of floral diversity change during the first ~1.5 Myr of the Paleocene. The records of floral diversity change were then compared to coeval paleoclimate and stable C isotopic records to identify potential drivers of early Paleocene floral community diversity across western North America.

In Chapter Two, titled "Early Paleocene Magnetostratigraphy and Revised Biostratigraphy of the Ojo Alamo Sandstone and Lower Nacimiento Formation, San Juan Basin, New Mexico, USA", we use magnetostratigraphy, detrital sanidine ages, and biostratigraphy to generate a high-resolution age model for the Ojo Alamo Sandstone and lower Nacimiento Formation in the San Juan Basin. This work revises the ages of earliest Paleocene mammal localities, demonstrates that the earliest Paleocene Ojo Alamo Sandstone was time transgressive from northwest to the southeast across the basin, and documents a shift from low to high accommodation and an increase in basin subsidence in the lower Nacimiento Formation. D. Peppe and T. Williamson helped design the study. A. Davis, C. Leslie, D. Peppe, and T. Williamson helped collect paleomagnetic samples, measure sections, and assisted with fieldwork for the study. C. W. Fenley IV and D Peppe. assisted in analyzing and interpreting paleomagnetic and rock magnetism data. M. Heizler performed analyses and calculated detrital sanidine ages. S. Brusatte, R. Secord, and T. Williamson identified and measured mammal localities.

In Chapter Three, titled "Early Paleocene Tropical Forest from the San Juan Basin, New Mexico, USA", we analyzed the diversity and estimated paleoclimate using fossil leaves collected from the Ojo Alamo Sandstone which were deposited within < 350 Kyr after the Cretaceous-Paleogene Boundary. The Ojo Alamo Sandstone fossil flora was diverse (53 morphotypes), laterally heterogeneous, highly uneven, and dominated by angiosperms. Paleoclimate estimates based on the size and shape of leaves (leaf physiognomy) indicate warm temperatures (24.3 – 27.4 °C mean annual temperature) and relatively high precipitation (1554 - 1928 mm/yr mean annual precipitation), which is consistent with a modern tropical seasonal forest biome. When compared to contemporaneous floras from northern North America, the San Juan Basin flora had significantly higher species richness and warmer paleoclimate estimates indicating the presence of a relatively steep latitudinal species richness and paleoclimate gradient during the early Paleocene. D. Peppe assisted with fossil collection, measuring sections, and fossil identification.

In Chapter Four, titled "Terrestrial Ecosystem Instability Following the Cretaceous-Paleogene Boundary", we use Capture-Mark-Recapture methods to model floral diversity dynamics from the San Juan Basin, New Mexico, Denver Basin, Colorado, and Williston Basin, Montana and North Dakota during the first ~1.5 Myr of the Paleocene (66.0 – 64.5 Ma). Model results indicated simultaneous and volatile changes in floral diversity across western North America, especially during the first ~800 Kyr of the Paleocene, with approximately 70-80% plant species extinction at the Cretaceous-Paleogene boundary, two other intervals of comparable proportional species loss during the early Paleocene, and three intervals of rapid floral diversification, suggesting a regional and/or global driver in early Paleocene floral diversity. Intervals of decreasing diversity during the early Paleocene correspond with a -1.5 to 2.5 $\delta^{13}C$ bulk organic excursion and correlate with the onset of major Deccan Traps eruptive phases indicating the important contribution of Deccan Traps volcanism on early Paleocene floral community instability. S. Brusatte, D. Peppe, R. Secord, and T. Williamson helped design the study. B. Abbuhl, J. Geng, and D. Peppe collected fossils in the San Juan

Basin and assisted in fieldwork. B. Abbuhl and J. Geng prepared and measured fossil leaves from the San Juan Basin for paleoclimate analyses. R. Secord measured sections and performed bulk organic stable C isotope analyses.

CHAPTER TWO

Early Paleocene Magnetostratigraphy and Revised Biostratigraphy of the Ojo Alamo Sandstone and Lower Nacimiento Formation, San Juan Basin, New Mexico, USA

This chapter published as: Flynn, A.G., Davis, A.J., Williamson, T.E., Heizler, M., Fenley, C.W. IV, Leslie, C.E., Secord, R., Brusatte, S.L., and Peppe, D.J., *in press*, Early Paleocene Magnetostratigraphy and Revised Biostratigraphy of the Ojo Alamo Sandstone and Lower Nacimiento Formation, San Juan Basin, New Mexico, USA: *Geologic Society of America Bulletin*.

Abstract

The lower Paleocene Ojo Alamo Sandstone and Nacimiento Formation from the San Juan Basin (SJB) in northwestern New Mexico preserve arguably the best early Paleocene mammalian record in North America and is the type location for the Puercan (Pu) and Torrejonian (To) North American Land Mammal ages (NALMA). However, the lack of precise depositional age constraints for the Ojo Alamo Sandstone and lower Nacimiento Formation has hindered our understanding of the timing and pacing of mammalian community change in the SJB following the Cretaceous-Paleogene mass extinction. Here we produced a high-resolution age model for the Ojo Alamo Sandstone and lower Nacimiento Formation combining magnetostratigraphy and $^{40}Ar/^{39}Ar$ geochronology spanning the first ~3.5 m.y. of the Paleocene. Mean sediment accumulation rates during C29n were relatively low (<50 m/m.y.) and equalized from basin center to basin margin indicating an accommodation minimum; sediment accumulation rates approximately double (> 90 m/m.y.) during C28r and are highest in the basin center and lowest on basin margin, which indicates high accommodation and an increase in basin subsidence near the C29n/C28r boundary (ca. 64.96 Ma). Puercan fossil

localities were restricted to C29n, Torrejonian 1 localities to C28n, and lower Torrejonian 2 localities to C27r. Our revised age model for the SJB suggests that the first appearance of To1 mammals may have been diachronous across North America, with the Torrejonian 1 mammals first appearing in the north (Montana and North Dakota) during C29n, then in middle latitudes (Utah) in C28r, and lastly in southern North America (New Mexico) in C28n.

Introduction

The Ojo Alamo Sandstone and the Nacimiento Formation from the San Juan Basin (SJB) in northwestern New Mexico and southwestern Colorado (Fig. 2.1) preserve a nearly continuous succession of lower Paleocene terrestrial deposits (e.g., Baltz et al., 1966; O'Sullivan et al., 1972; Williamson, 1996; Williamson et al., 2008; Cather et al., 2019). The SJB also preserves one of the most complete records of early Paleocene mammalian evolution following the Cretaceous-Paleogene (K-Pg) mass extinction and has been extensively studied for over a century (e.g., Granger, 1917; Matthew, 1937; Simpson, 1959; Williamson and Lucas, 1992; Williamson, 1996; Williamson et al., 2016). The early Paleocene Puercan and Torrejonian North American Land Mammal ages (NALMAs) were defined using SJB fossil mammalian faunas (Wood et al., 1941). These land mammal ages were subsequently divided into biochrons, based largely on the SJB record, and are used for early Paleocene correlation across North America (Lindsay, 2003; Lofgren et al., 2004).

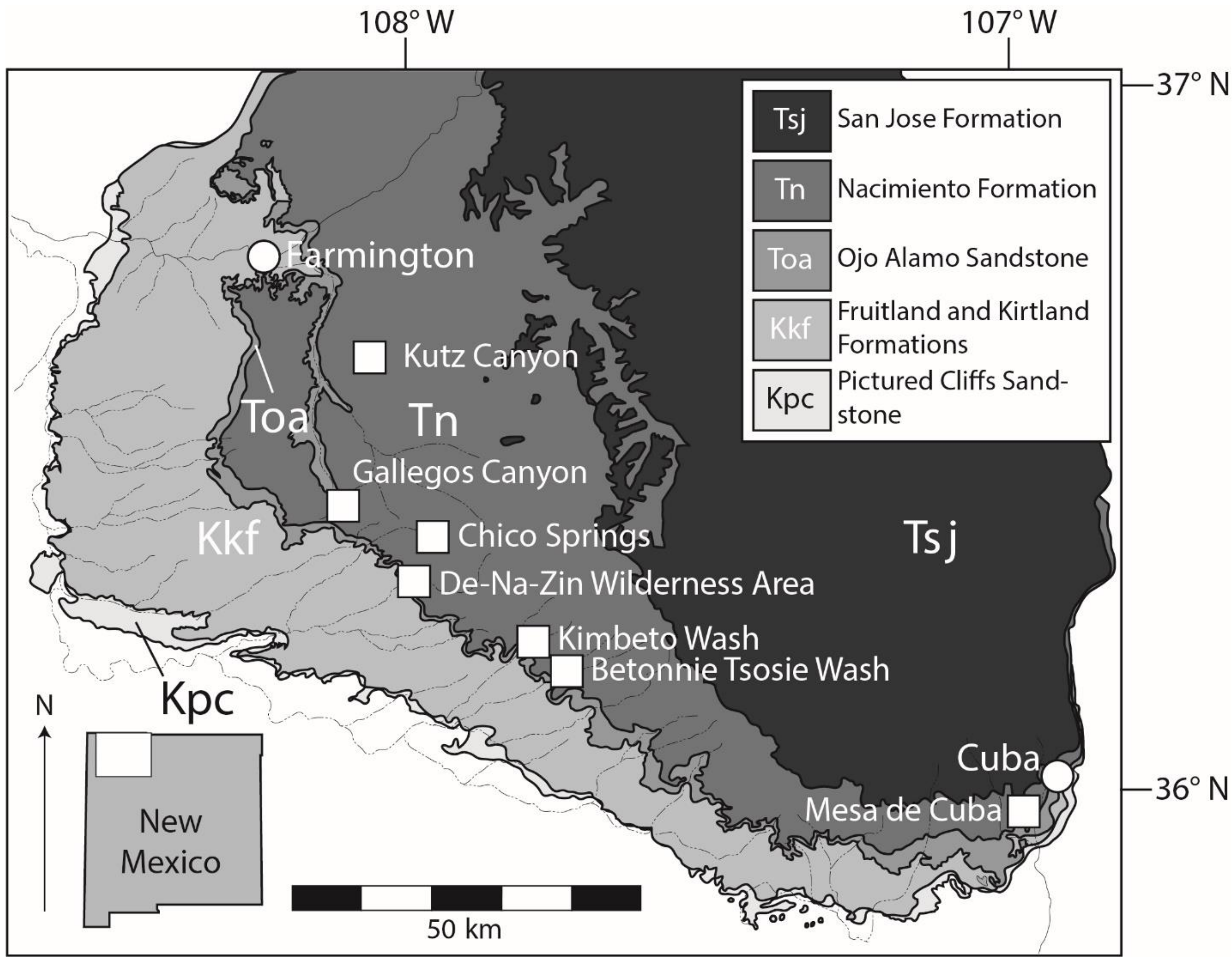

Figure 2.1. Geologic map of the San Juan Basin, New Mexico, showing Upper Cretaceous through lower Eocene strata. White squares show the locations of the seven measured sections used in this study: (1) Kutz Canyon, (2) Gallegos Canyon, (3) Chico Springs, (4) De-Na-Zin Wilderness Area, (5) Kimbeto Wash, (6) Betonnie Tsosie Wash, and (7) Mesa de Cuba (modified from Williamson et al., 2008).

Two intervals of potentially rapid mammalian turnover, between Puercan 2 (Pu2) and Puercan 3 (Pu3) and between Torrejonian 2 (To2) and Torrejonian 3 (To3) faunas, were documented by Williamson (1996). Additionally, the boundary between Pu3 and Torrejonian 1 (To1) records the near total replacement of mammalian communities with new species and potentially represents another time period of high mammalian turnover, but this pattern is somewhat unclear due to low sampling intensity in To1 (Williamson, 1996). Although Leslie et al. (2018b) were able to develop a high-resolution age model for the To2-To3 transition, no high-resolution age models exist for the Pu2-Pu3 and Pu3-To1 transitions in the SJB, which limits our understanding of the timing and rate of faunal change through this crucial time interval.

Previous work has used magnetostratigraphy to develop an age model for the Ojo Alamo Sandstone and lower Nacimiento Formation with the goal of identifying the K-Pg boundary and evaluating the chronology of mammalian evolution within the SJB (e.g., Butler et al., 1977; Butler and Taylor, 1978; Lindsay et al., 1978, 1981; Taylor and Butler, 1980; Butler and Lindsay, 1985; Fassett, 2009). However, sample spacing was relatively large and mammal localities were not always precisely correlated to magnetostratigraphic sections, which has meant that there is not a high-resolution age model for Ojo Alamo Sandstone or lower Nacimiento Formation. Additionally, the age and duration of type section of the Nacimiento Formation at Mesa de Cuba (Cope, 1875) has never been determined.

In this study, we developed a high-resolution magnetostratigraphic age model for the Ojo Alamo Sandstone and lower Nacimiento Formation spanning the Puercan and early Torrejonian (To1-To2) interval from seven measured sections encompassing the first ~3.5 m.y. of the Paleocene. These sections, from northwest to southeast, are (1) Kutz Canyon, (2) Gallegos Canyon, (3) Chico Springs, (4) De-Na-Zin, (5) Kimbeto Wash, (6) Betonnie Tsosie Wash, and (7) Mesa de Cuba (Fig. 2.1). Local polarity zones from each section, constrained by $^{40}Ar/^{39}Ar$ ash and detrital sanidine ages, were correlated to the global geomagnetic polarity time scale (GPTS) (Ogg, 2012). Sediment accumulation rates were calculated for each section and/or magnetic chrons within the sections and used to develop an age model for the Ojo Alamo Sandstone and the base of the Nacimiento Formation. This age model was then correlated with the magnetostratigraphic sections of Leslie and others (2018b) to develop a basin-wide geochronological framework for the entire lower Paleocene in the SJB to assess basin evolution during the early Paleocene. The age model was then used to constrain the age of Puercan and early Torrejonian (To1 – To2) fossil localities across the SJB. These revised ages for the Puercan and Torrejonian mammal sites have important implications for understanding the tempo of mammalian turnover after the end-Cretaceous mass extinction and the timing of key events in early mammal evolution.

Previous Studies

Geologic Background

The SJB is a Laramide foreland basin in northwest New Mexico and southwest Colorado that preserves a nearly continuous succession of Upper Cretaceous (Campanian) to lower Eocene terrestrial deposits (Baltz et al., 1966; Chapin and Cather, 1983). Cather (2004) argued for three distinct subsidence phases in the SJB: (1) an early phase during the late Campanian – early Maastrichtian, (2) a middle phase during the late

Maastrichtian – early Paleocene, and (3) a late phase during the Eocene. The middle phase of subsidence was hypothesized to allow for deposition of lower Paleocene sediments in the basin (Cather, 2004).

The SJB preserves two lower Paleocene formations: (1) the Ojo Alamo Sandstone and (2) the Nacimiento Formation (Baltz et al., 1966; O'Sullivan et al., 1972). The Ojo Alamo Sandstone unconformably overlies the Maastrichtian Naashoibito Member of the Kirtland Formation (e.g., Baltz et al., 1966; Powell, 1973; Chapin and Cather, 1983; Lehman, 1985; Cather, 2004; Sullivan et al., 2005; Williamson and Weil, 2008a; Williamson et al., 2008; Flynn and Peppe, 2019) and is composed of gold to yellow colored, cross-bedded, medium- to coarse-grained sandstone with interbedded sandstone and siltstone deposits and localized carbonaceous shale beds and local accumulations of large, nearly complete trees suggesting high depositional energies. These deposits have been interpreted to represent an alluvial plain in a seasonally dry, subtropical climate with one or more sediment sources in the southern Rocky Mountains (Baltz et al., 1966; O'Sullivan et al., 1972; Powell, 1973; Tidwell et al., 1981; Chapin and Cather, 1983; Sikkink, 1987; Cather, 2004; Flynn and Peppe, 2019). Differences in stratigraphic terminology related to the Ojo Alamo Sandstone and underlying Naashoibito Member have created confusion about the relationship between these two units (for example, see discussions in Williamson and Weil, 2008a, 2008b). Previous authors recognized the Naashoibito Member and Ojo Alamo Sandstone as unique stratigraphic units representing different formations (e.g., Baltz et al., 1966; Williamson, 1996; Williamson and Weil, 2008a; Williamson et al., 2008) or as different members of the same formation (Powell, 1973; Sullivan et al., 2005; Fassett, 2009; Cather et al., 2019). Herein we recognize the

Ojo Alamo Sandstone as a separate stratigraphic formation (*sensu* Baltz et al., 1966). For clarity in stratigraphic nomenclature used herein, the Ojo Alamo Sandstone as referenced in this paper is equivalent to the Kimbeto Member of the Ojo Alamo Formation proposed by Powell (1973) and Sullivan et al. (2005).

The lack of detailed geochronology for the Ojo Alamo Sandstone has led to uncertainty about the age and duration of the Ojo Alamo Sandstone and Naashoibito Member with some authors arguing that both units are Paleocene (Fassett, 2009b), that the Naashoibito Member is early Maastrichtian and the Ojo Alamo Sandstone is early Paleocene (Sullivan and Lucas, 2003; Sullivan et al., 2005), or that the Naashoibito is late Maastrichtian and the Ojo Alamo Sandstone is earliest Paleocene (Williamson and Weil, 2008a; Williamson et al., 2008; Peppe et al., 2013; Flynn et al., 2019). The lack of an age model for the Ojo Alamo Sandstone and confusion about stratigraphic terminology has also led some researchers to argue for the occurrence of early Paleocene dinosaurs from the San Juan Basin (e.g., Fassett et al., 2002, 2011; Fassett, 2009). However, these interpretations were made based on an incorrect interpretation of previously published geochronology and the purported presence of Paleocene pollen in the Naashoibito Member, which has not been replicated, casting doubts upon their validity (e.g., Lucas et al., 2009). Further, detailed work on the mammalian faunas, the floras, and recent geochronologic analyses also refute this interpretation. The mammalian faunas of the Naashoibito Member correlate to the Lancian Land Mammal Age, which suggests a late Maastrichtian age (Williamson and Weil, 2008a). Paleobotanical analyses on the megaflora and pollen indicates that the Ojo Alamo Sandstone is earliest Paleocene in age and is correlated with palynostratigraphic zones P1 or P2 (Anderson, 1959; Nichols, 2003; Williamson et al., 2008; Flynn and Peppe, 2019). Recent detrital sanidine and paleomagnetic work has constrained the Naashoibito Member to the latest Maastrichtian, which indicates that the K/Pg boundary is represented by the unconformity between the Naashoibito Member and the Ojo Alamo Sandstone (Peppe et al., 2013; Flynn et al., 2019). These data, coupled with previous sedimentological analyses, demonstrate that the Naashoibito Member is late Maastrichtian in age and the Ojo Alamo Sandstone is early Paleocene in age with an erosive unconformity, that cuts out the Cretaceous-Paleogene boundary, separating the two units.

The Nacimiento Formation conformably overlies the Ojo Alamo Sandstone and unconformably underlies the Eocene San Jose Formation. The Nacimiento Formation is subdivided into six members: (1) The Kutz , (2) Tsosie, (3) Angel Peak, (4) Arroyo Chijuillita, (5) Ojo Encino, and (6) Escavada Members (Williamson and Lucas, 1992; Williamson, 1996; Cather et al., 2019). This study focuses on the Kutz, Tsosie, Arroyo Chijuillita and Ojo Encino Members. The Arroyo Chijuillita and Ojo Encino Members are confined to the southern portion of the basin. The Arroyo Chijuillita Member is composed of drab mudstones and small lenticular sandstone beds (Davis et al., 2016). The Ojo Encino Member contains variegated red and drab mudstones, large sheet and channel sandstone units, and three persistent intervals consisting of numerous “black mudstone” paleosol horizons referred to as the “lower,” “middle,” and “upper black” (Leslie et al., 2018b). Both members have been interpreted to represent meandering fluvial systems deposited in a subtropical climate, and depositional energy increases from the Arroyo Chijuillita to Ojo Encino Member (Tidwell et al., 1981; Williamson, 1996; Davis et al., 2016; Flynn and Peppe, 2019). The Kutz Member is equivalent to the “main body" of Williamson (1996) and is primarily exposed in Kutz Canyon. It is a thick succession of cross-bedded channel sandstones, splay sandstones, and floodplain mudstones. The lower Kutz Member tends to be drab in color and becomes more variegated with reddish mudstones in the upper portion (Cather et al., 2019). The Tsosie Member is exposed in the southwestern part of the basin and is characterized by thick, cross-bedded channel sandstone complexes separated by mostly drab floodplain mudstones. The channel sandstones were interpreted as deposits from a river with a maximum depth of at least 5 m (Cather et al., 2019). Regional dip for the Ojo Alamo Sandstone and Nacimiento Formation varies between 1-5° (Baltz, 1967). Locally, the beds are flat lying.

Mammalian Biostratigraphy

Puercan Mammalian Biostratigraphy. The first mammalian biostratigraphy for the lower Nacimiento Formation was proposed by Sinclair and Granger (1914), who identified two zones - the lower *Ectoconus* zone and the upper *Taeniolabis* zone – in exposures from De-Na-Zin, Kimbeto, and Betonnie Tsosie washes. They distinguished the two zones by the presence of the large-bodied multituberculate *Taeniolabis* in the upper horizon but noted that *Ectoconus* was known from both horizons (Sinclair and Granger, 1914). Wood et al. (1941) later placed both the *Ecotconus* and *Taeniolabis* zones from Sinclair and Granger (1914) in the Puercan NALMA and designated the Nacimiento Formation fauna as representative of the Puercan. The significance of the *Ectoconus* and *Taeniolabis* zones as defined by Sinclair and Granger (1914) was debated due to both zones being present superpositionally only in De-Na-Zin and because the difference between the two zones may reflect differences in facies and/or collection intensity (Lindsay et al., 1981; Archibald et al., 1987; Williamson, 1996).

Archibald et al. (1987) redefined the early Paleocene NALMAs, subdividing the Puercan into three biochronologic zones: *Protungulatum – Ectoconus* zone (Pu1), *Ectoconus – Taeniolabis taoensis* zone (Pu2), and *Taeniolabis taoensis – Periptychus carnidens* zone (Pu3), and equating the younger two zones (Pu2 and Pu3) to the *Ectoconus* and *Taeniolabis* zones defined by Sinclair and Granger (1914) (only Pu2 and Pu3 are preserved in SJB). Williamson (1996) later revised the SJB biostratigraphy based on taxon ranges not included in Archibald et al. (1987) and approximately equated their Pu2 interval to the *Hemithlaeus kowalevskianus-Taeniolabis taoensis* zone (H-T Zone, referred to here as Pc1) and the Pu3 interval to the *Taeniolabis taoensis-Periptychus carinidens* zone (T-P Zone, referred to here as Pc2). We here refer to these last two biostratigraphic zones as Pc1 and Pc2, respectively, to distinguish them from the biochronological Puercan Pu2 and Pu3 subzones. The revision of early Paleocene NALMAs by Lofgren et al. (2004) used the same biozones defined by Archibald et al. (1987). Multiple authors (e.g., Archibald et al., 1987; Williamson and Lucas, 1992; Williamson, 1996) have noted that the fossil horizons in the SJB that yield both Pu2 and Pu3 mammalian faunas occur in C29n, which has made precise age control difficult and has inhibited temporal correlation both within the basin and across North America for each NALMA interval.

Williamson (1996) observed a potential decrease in species and generic diversity between the Pu2 and Pu3 mammalian faunas. Several mammalian taxa that are abundant in Pu2 faunas, mostly periptychid "condylarths," are absent from the succeeding Pu3 faunal interval (Williamson, 1996). Williamson (1996) also noted a relatively high rate of origination in the Pu3 interval but attributed this observation to immigration of taxa from northern North America. However, previous relatively low precision temporal constraints on this turnover have obscured the timing and rate of mammalian faunal changes.

Torrejonian Mammalian Biostratigraphy. Sinclair and Granger (1914) recognized two biostratigraphic faunal zones – a lower *Deltatherium* and an upper *Pantolambda* zone – stratigraphically above the Puercan faunas from Torreon Wash. Osborn (1929) treated the *Deltatherium* and *Pantolambda* zones as temporally distinct "life zones." Wood et al. (1941) placed the *Deltatherium* and *Pantolambda* zones within the Torrejonian NALMA, which was separated from the Puercan NALMA by the Dragonian NALMA. Tomida (1981) proposed a further subdivision of the Torrejonian NALMA with the retention of the previous *Deltatherium* and *Pantolambda* zones and the addition of an older *Periptychus-Loxolophus* zone. Additionally, because the "Dragonian" NALMA was shown to overlap with their *Periptychus-Loxolophus* zone (Tomida and Butler, 1980; Tomida, 1981; Archibald et al., 1987), Archibald et al. (1987) considered the "Dragonian" to be part of the Torrejonian NALMA.

Archibald et al. (1987) proposed three Torrejonian interval zones in their revision of the early Paleocene NALMAs: the *Periptychus carinidens-Tetraclaenodon* interval zone (To1), *Tetraclaenodon-Pantolambda* interval zone (To2), and *Pantolambda-Plesiadapis praecursor* interval zone (To3). The To1 zone was equivalent to the *Periptychus-Loxolophus* zone and the "Dragonian" interval (Wood et al., 1941; Tomida, 1981), and the To2 and To3 interval zones were approximately equivalent to the previous

Deltatherium and *Pantolambda* zones (Osborn, 1929; Tomida, 1981). Williamson (1996) subdivided the Torrejonian into six local biostratigraphic zones in the SJB based on new fossil discoveries — (1) *Periptychus carinidens-Protoselene opisthacus* Zone (P-P Zone; referred to here as Tj1), (2) *Protoselene opisthacus-Ellipsodon grangeri* Zone (P-E Zone; referred to here as Tj2), (3) *Ellipsodon grangeri-Arctocyon ferox* Zone (E-A Zone; referred to here as Tj3), (4) *Arctocyon ferox-Pantolamda cavirictum* Zone (A-P Zone; referred to here as Tj4), (5) *Pantolamda cavirictum-Mixodectes pugens* Zone (P-M Zone; referred to here as Tj5), and (6) *Mixodectes pugens* Zone (M Zone; referred to here as Tj6). This new zonation showed some temporal overlap in the mammalian taxa used to define the Torrejonian interval zones by Archibald et al. (1987).

In their update of early Paleocene NALMAs, Lofgren et al. (2004) redefined the To1 biochronologic interval zone as the *Periptychus carinidens-Protoselene opisthacus* zone (approximately equivalent to the P-P [Tj1] zone from Williamson, 1996), the To2 interval zone as the *Protoselene opisthacus-Mixodectes pugens* Zone (approximately equivalent to the P-E [Tj2], E-A [Tj3], A-P [Tj4], and P-M [Tj5] zones from Williamson, 1996), and To3 interval zone as the *Mixodectes pugens-Plesiadapis praecursor* Zone (approximately equivalent to the M [Tj6] Zone from Williamson, 1996).

In the SJB, the Tj1 zone (approximately temporally equivalent to To1) is poorly fossiliferous (Williamson, 1996), with fossil mammal collections existing from Kutz Canyon, De-Na-Zin, Kimbeto Wash, Betonnie Tsosie Wash, and Mesa de Cuba. Biozones Tj2 – Tj5 (approximately temporally equivalent to To2) are significantly more fossiliferous. and collections have been made primarily from Kutz Canyon, Gallegos Canyon, Kimbeto Wash, Escavada Wash, and Torreon Wash (Williamson, 1996; Leslie et al., 2018b). The Tj6 zone (approximately temporally equivalent to To3) is also relatively well collected, with samples primarily from Escavada, Alemita Arroyo, Torreon Wash, and San Isidro Arroyo (Williamson, 1996; Leslie et al., 2018b). Previous magnetostratigraphy in the SJB has constrained Tj1 fossil localities to within C28n, Tj2-Tj5 fossil localities to within C27r, and Tj6 fossil localities to within C27n (Lindsay et al., 1978; Butler and Lindsay, 1985; Williamson and Lucas, 1992; Leslie et al., 2018b).

Magnetostratigraphy and Rock Magnetism

There is a long history of magnetostratigraphy and rock magnetism research focused on the Ojo Alamo and Nacimiento Formations in the SJB. The original magnetostratigraphic studies of the Ojo Alamo Sandstone and Nacimiento Formation conducted analyses on measured sections in De-Na-Zin, Kimbeto Wash, Betonnie Tsosie Wash (also referred to as Tsosie Wash), and Kutz Canyon (Butler et al., 1977; Lindsay et al., 1978, 1981). In these studies, the K-Pg boundary was interpreted to be in C29n, the Ojo Alamo Sandstone was correlated with C28r, Puercan mammalian localities (*Ectoconus* and *Taeniolabis* Zones) were correlated with C28n, and the Torrejonian aged strata were correlated with C27n to C26n (Butler et al., 1977; Lindsay et al., 1978, 1981; Taylor and Butler, 1980). However, subsequent paleomagnetic and rock magnetic analyses of the San Juan Basin deposits by Butler and Lindsay (1985) documented zones of magnetic overprinting in the Lower Cretaceous and lower Paleocene samples that had been previously unrecognized, which demonstrated that the original magnetostratigraphic work (Butler et al., 1977; Lindsay et al., 1978, 1981; Taylor and

Butler, 1980) incorrectly correlated the local polarity stratigraphy to the GPTS. Using the reinterpretation of the local polarity stratigraphy based on the recognition of overprinted zones, Butler and Lindsay (1985) revised thee magnetostratigraphic interpretations for the SJB, placing the K-Pg boundary and deposition of the Ojo Alamo Sandstone in C29r, the Puercan zone mammalian localities in C29n, and the Torrejonian mammalian localities from Kutz Canyon in C28n-26n. Unfortunately, despite this correction, some researchers (e.g., Fasset, 2009) have continued to use the original, erroneous magnetostratigraphic interpretations to argue for the occurrence of Paleocene dinosaurs in the San Juan Basin based on the premise that the Naashoibito Member is Paleocene in age, which has caused some confusion in the literature over the age of the Ojo Alamo Sandstone and the basal Nacimiento Formation. However, all other researchers have used the GPTS interpretations of Butler and Lindsay (1985), which is in agreement with biostratigraphy and independent age interpretations (e.g., Williamson, 1996; Williamson and Weil, 2008a; Williamson et al., 2008; Cather et al., 2019; Flynn and Peppe, 2019).

Although Butler and Lindsay's (1985) new analyses and reinterpretation of previous work (Butler et al., 1977; Lindsay et al., 1978, 1981; Taylor and Butler, 1980) developed a magnetostratigraphic framework for the Ojo Alamo Sandstone and the Nacimiento Formation, the sample spacing in all of the studies was relatively coarse, making it difficult to precisely determine the stratigraphic position of chron boundaries or to calculate accurate sediment accumulation rates. Further, in many cases, the position of the chron boundaries relative to key mammal fossil sites was not precisely constrained and had to be determined later (e.g., Williamson, 1996). Thus, it has not been possible to estimate the age of the fossil localities in the SJB more precisely than a qualitative position within a chron. Additionally, although Mesa de Cuba is the type section for the Nacimiento Formation (Cope, 1875), no previous magnetic polarity stratigraphy has been constructed there.

Butler and Lindsay (1985) analyzed the rock magnetics of SJB samples from nine stratigraphic levels from the Upper Cretaceous through middle Paleocene and found that titanohematite of intermediate composition was the dominant magnetic mineral in the Nacimiento Formation. They suggested that the most likely source for this was the Cretaceous volcanic rocks of the San Juan Mountains to the north that were eroded during the Paleocene. The anisotropy of remanence analyses of Nacimiento Formation samples from Kutz Canyon measured by Kodama (1997) supported primary detrital magnetization for the Nacimiento Formation. Leslie et al. (2018b) found the upper Nacimiento Formation had a mixed magnetic mineralogy with titanohematite and maghemite as the characteristic remanent magnetization carriers. Goethite was also present in all upper Nacimiento lithologies and dominated low-temperature magnetic measurements but was not found to contribute to the characteristic remanence measurements (Leslie et al., 2018b).

Methods

Lithostratigraphy

Seven lithologic and magnetostratigraphic sections were measured across ~110 km northwest to southeast transect: (1) a 129 m section from Kutz Canyon, (2) a 68 m section at Gallegos Canyon, (3) a 58 m section at Chico Springs, (4) a 126 m section from De-Na-Zin, (5) an 82 m section from Kimbeto Wash, (6) a 115 m section from Betonnie Tsosie Wash, and (7) a 156 m section from Mesa de Cuba (Figs. 2.1-2.4). At Gallegos Canyon, De-Na-Zin, Betonnie Tsosie Wash, and Mesa de Cuba, the bases of the sections were measured from the lithologic contact between the Ojo Alamo Sandstone and Nacimiento Formation (Figs. 2.2 and 2.3). In the De-Na-Zin section the entire Ojo Alamo Sandstone was measured (i.e., both the upper and lower contacts of the formation), while in the Gallegos Canyon, Betonnie Tsosie Wash, and Mesa de Cuba sections only the uppermost part of the Ojo Alamo Sandstone was measured. The section at Kimbeto Wash began above the Ojo Alamo Sandstone-Nacimiento Formation contact at ~8 m below vertebrate horizon 2 (Table 2.1, Fig. 2.3) (Williamson, 1996). The Kutz Canyon section began ~4 m below vertebrate horizon 11 in the Nacimiento Formation (Williamson, 1996) to ensure overlap with correlative biozones. The top of the Kutz Canyon section was measured to the vertebrate locality "Bab's Basin", which is at the base of the Kutz Canyon measured section of Leslie et al. (2018b). The Chico Springs lithostratigraphic and magnetostratigraphic section began approximately 8 m below fossil horizon 13 in the Nacimiento Formation (Table 2.1, Fig. 2.4). Williamson (1996) produced relatively detailed measured sections through Kutz Canyon, De-Na-Zin, Kimbeto Wash, and Betonnie Tsosie Wash. Where possible, those sections were correlated to the measured sections presented here.

Each measured section was trenched to remove weathered material and to allow recording of lithologic contacts. The stratigraphic sections were measured at ~0.5 – 1.0 m resolution, and the lithology and sedimentary structures of each sampling horizon were documented. Additionally, the nature of lithologic contacts was documented. For relatively thick (> 3 m) heterolithic units, only the major rock types were recorded. For sandstones, the grain size(s) and relationship to surrounding strata were recorded. Potential unconformities were recognized by erosive contact and abrupt increases in grain size between adjacent strata.

The stratigraphic position of most vertebrate fossil intervals (Table 2.1, Table B.1) within each measured section was documented in the field. For those whose stratigraphic position was not measured directly in this study, their stratigraphic position relative to major lithologic contacts from Williamson (1996) was used and correlated with our measured sections (Figs. 2.2-2.4). Table 2.1 documents the 14 vertebrate fossil-bearing intervals, the generalized area, the NALMA interval zone (Lofgren et al., 2004),San Juan Basin biostratigraphic zone (Williamson, 1996), and the age of the vertebrate horizon calculated in this study using sediment accumulation rates. For vertebrate horizons 15-23, their generalized area, the associated biochronologic interval zone (Lofgren et al., 2004), San Juan Basin biozone (Williamson, 1996), and the calculated age of the vertebrate horizon are from Leslie et al. (2018b). The stratigraphic position and locality number(s) within each vertebrate horizon is included in Table B.1.

Magnetostratigraphy and Magnetic Mineralogy

Four paleomagnetic samples were collected from a single stratigraphic horizon from mudstones, shales, paleosols, and fine-grained sandstones at ~1.5 to 3 m intervals (0.20 m minimum, 20.75 m maximum) in each measured section. Lithologies coarser than fine-grained sandstones were avoided if possible, and site spacing was dictated primarily by both lithology and rock exposure. To generate paleomagnetic samples, a flat

Table 2.1 – San Juan Basin Mammal Fossil Localities

Vertebrate Fossil Horizon*	Location	NALMA†	San Juan Basin biozone§	Estimated age (Ma)
1	De-Na-Zin	Pu2	H-T/Pc1	65.68 - 65.63 (+0.01/-0.01)
2	Betonnie Tsosie	Pu2	H-T/Pc1	65.57 - 65.47 (+0.02/-0.04)
3	Kimbeto	Pu2	H-T/Pc1	65.49 - 65.34 (+0.03/-0.03)
4	De-Na-Zin	Pu3	T-P/Pc2	65.27 - 65.22 (+0.06/-0.06)
5	Gallegos Canyon	Pu3	T-P/Pc2	65.20 – 65.03 (+0.03/-0.01)
6	Mesa de Cuba	To1?	P-P/Tj1?	64.80 - 64.74 (+0.04/-0.02)
7	Kimbeto	To1	P-P/Tj1	64.66 - 64.58 (+0.02/-0.01)
8	Mesa de Cuba	To1	P-P/Tj1	64.52 - 64.50 (+0.03/-0.02)
9	Betonnie Tsosie	To1	P-P/Tj1	64.49 – 64.44 (+0.05/-0.01)
10	De-Na-Zin	To1	P-P/Tj1	64.46 – 64.40 (+0.05/-0.03)
11	Kutz Canyon	To1	P-P/Tj1	63.79 - 63.76 (+0.05/-0.08)
12	Kutz Canyon	To2	P-E/Tj2	63.48 - 63.44 (+0.01/-0.01)
13	Chico Springs	To2	P-E/Tj2	63.44 – 63.42 (+0.01/-0.01)
14	Kutz Canyon	To2	E-A/Tj3	62.97 - 62.91 (+0.10/-0.08)
15	Escavada Wash	To2	P-M/Tj5	62.80 – 62.71 (+0.08/-0.09)
16	Kutz Canyon	To2	A-P/Tj4	62.76 – 62.68 (+0.00/-0.04)
17	Torreon West	To2	A-P/Tj4	62.66 – 62.63 (+0.03/-0.03)
18	Torreon East	To2	A-P/Tj4	62.66 – 62.63 (+0.04/-0.03)
19	Kutz Canyon	To2	P-M/Tj5	62.63 (+0.01/-0.00)
20	Torreon West	To2	P-M/Tj5	62.59 (+0.03/-0.02)
21	Escavada Wash	To3	M/Tj6	62.35 – 62.29 (+0.06/-0.10)
22	Torreon East	To3	M/Tj6	62.47 – 62.28 (+0.05/-0.02)
23	Torreon West	To3	M/Tj6	62.46 - 62.27 (+0.04/-0.02)

*Horizons 1-14 from this study; horizons 15-23 from Leslie et al. (2018b)
†NALMA zones from Lofgren et al. (2004)
§SJB biozones from Williamson (1996)

face was created *in situ* on unweathered rock surfaces using a hand rasp, and the orientation of the created surface was measured using a Brunton Pocket Transit Compass. Beds on outcrop scale were flat lying, and dip was set to 0° for all strike and dip measurements. The samples were then cut into approximately 2-4 cm^3 cubes using a rock saw at Baylor University with each sample producing one cube.

Samples were collected from Gallegos Canyon, De-Na-Zin, Kimbeto Wash, and Betonnie Tsosie Wash across the entire Puercan interval; additionally, samples were collected from De-Na-Zin, Kimbeto Wash, and Betonnie Tsosie Wash from Tj1 strata (Figs. 2.2 and 2.3) (Williamson, 1996). Kutz Canyon samples spanned upper Tj1 toTj3 strata, and Chico Springs samples spanned lower Tj2 strata (Fig. 2.4) (Williamson, 1996; Williamson and Lucas, 1997). While the Mesa de Cuba section is poorly fossiliferous, and the position of the fossil localities relative to the biostratigraphic and biochronologic intervals is unclear, samples were collected from strata presumed to represent late Pc2 to Tj3 zones (Fig. 2.4) (Williamson, 1996).

Specimens were measured at Baylor University using a 2G Enterprises (Mountain View, California) cryogenic DC-SQuID magnetometer located in a two-layer magneto-static shielded room with a background field typically less than 300 nT. Thermal demagnetization steps were performed in 25-50 °C increments to a maximum unblocking temperature or until magnetization became erratic and unreliable, typically ranging between 250 °C and 580 °C. To minimize oxidation reactions, thermal demagnetization was conducted in a nitrogen atmosphere using an ASC Scientific (Carlsbad, California) controlled atmosphere thermal demagnetizer.

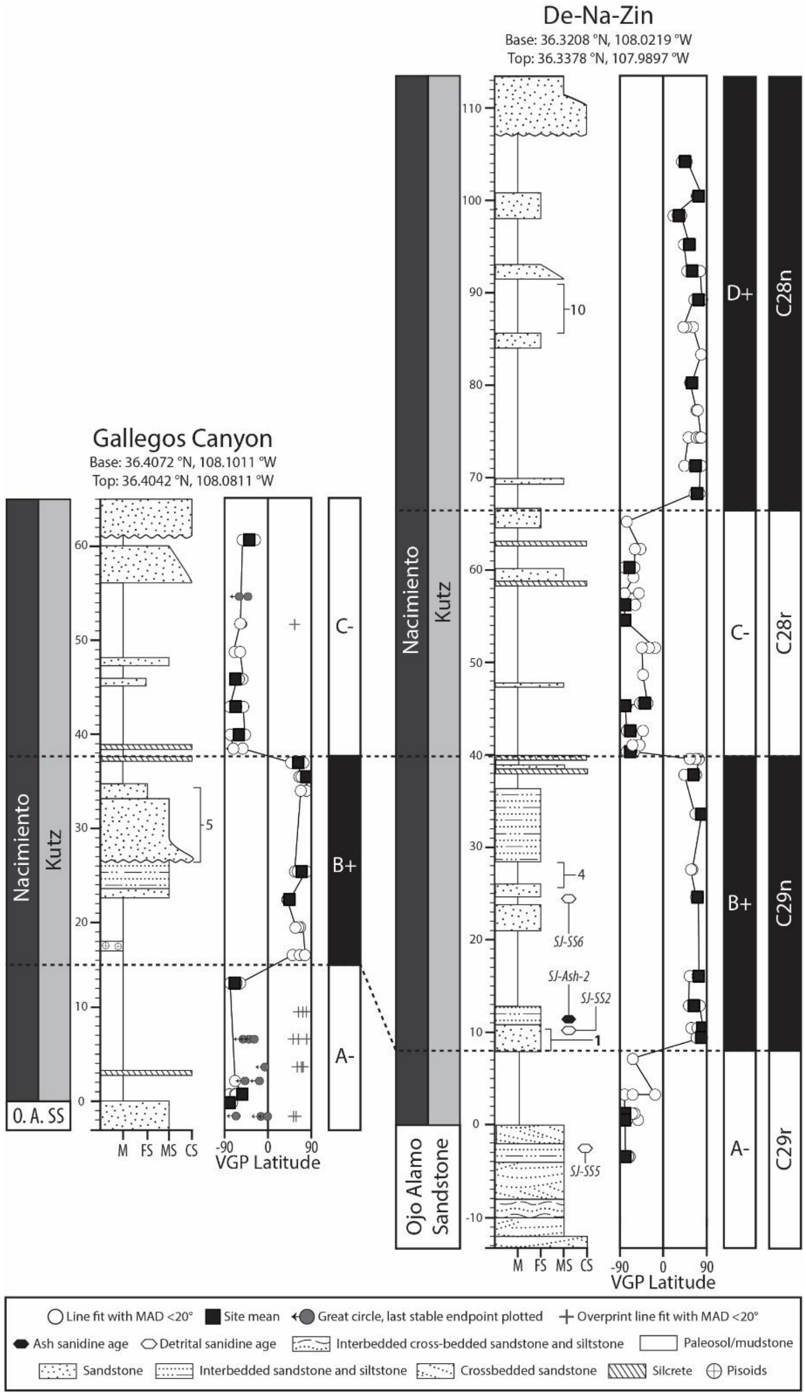

Figure 2.2. Measured sections from Gallegos Canyon and De-Na-Zin showing major lithologic units, vertebrate fossil horizons (described in Table 2.1), virtual geomagnetic pole (VGP) latitude, and interpreted polarity zonation. The base of local polarity zone C- was used as a datum. The decimal degree coordinates (NAD27 datum) of the section base and top are shown below section names. Grain sizes are located at the bottom of each section: M—mud, FS—fine sand, MS—medium sand, CS—coarse sand.

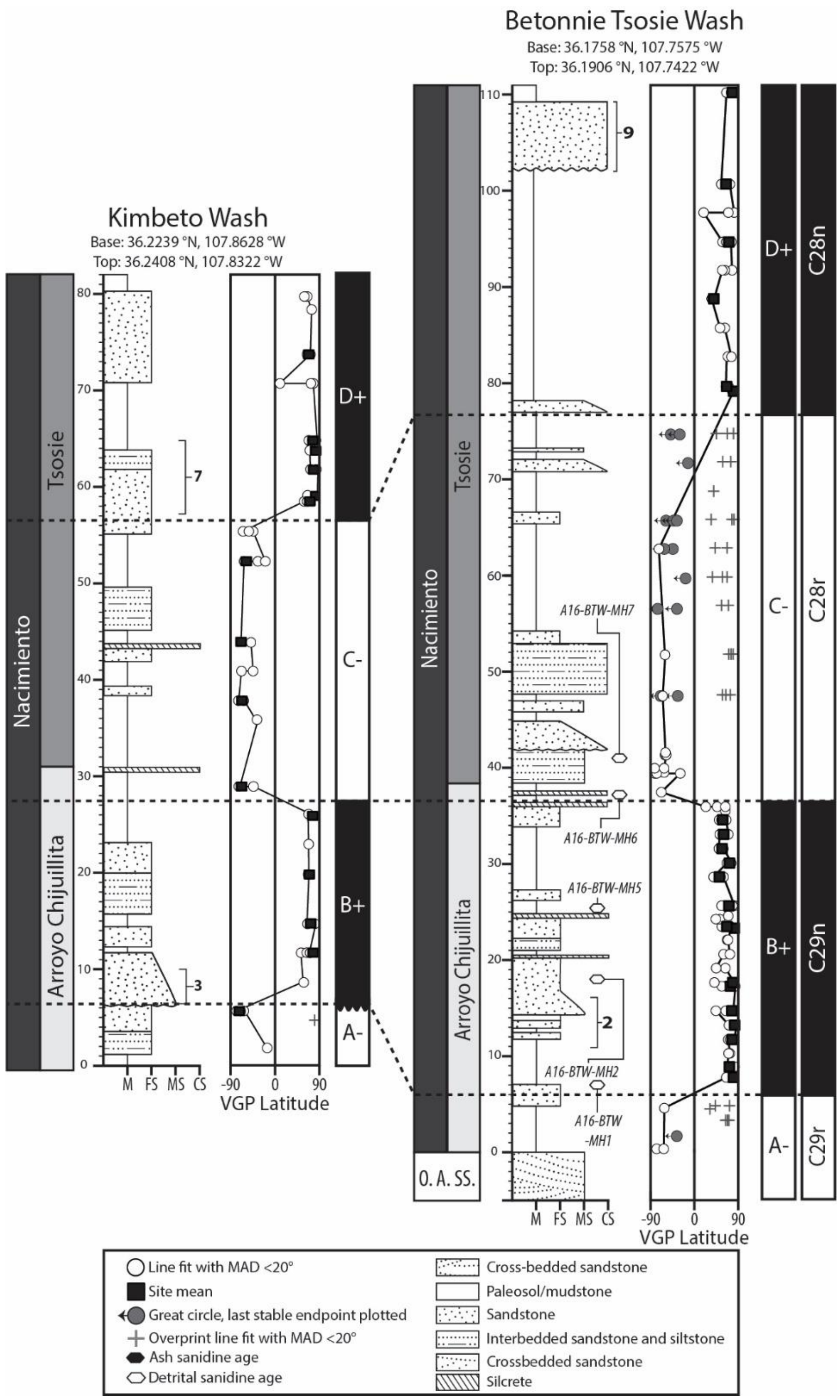

Figure 2.3. Measured sections from Kimbeto Wash and Betonnie Tsosie Wash showing major lithologic units, vertebrate fossil horizons (described in Table 2.1), virtual geomagnetic pole (VGP) latitude, and interpreted polarity zonation. The base of local polarity zone C- was used as a datum. The decimal degree coordinates (NAD27 datum) of the section base and top are shown below section names. Grain sizes are located at the bottom of each section: M—mud, FS—fine sand, MS—medium sand, CS—coarse sand.

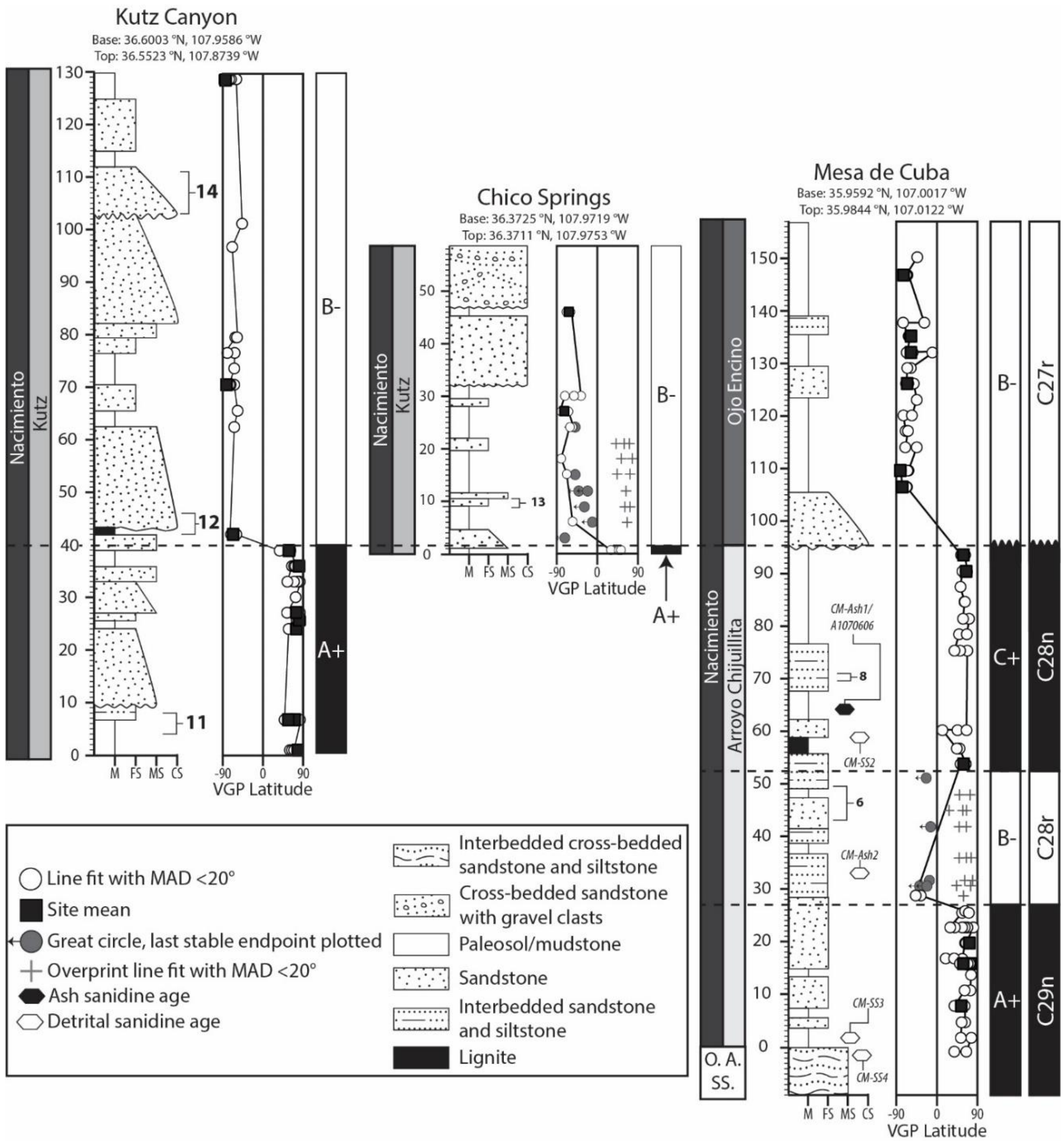

Figure 2.4. Measured sections from Kutz Canyon, Chico Springs, and Mesa de Cuba showing major lithologic units, vertebrate fossil horizons (described in Table 2.1), virtual geomagnetic pole (VGP) latitude, and interpreted polarity zonation. The base of local polarity zone C- was used as a datum. The decimal degree coordinates (NAD27 datum) of the section base and top are shown below section names. Grain sizes are located at the bottom of each section: M—mud, FS—fine sand, MS—medium sand, CS—coarse sand.

Principal component analysis (PCA) was used to determine the characteristic remanent magnetism for demagnetized samples (Kirschvink, 1980). A best fit line that was anchored to the origin was calculated for samples with at least three stable demagnetization steps that trended towards the origin and a had maximum angle of deviation (MAD) < 20° (Figs. 2.5A-E and 2.6A; Table A.2). Great circles were calculated for samples that did not have at least 3 stable demagnetization steps trending towards the origin but did trend towards the origin before complete demagnetization (Table A.4). Only great circles with a mean angular deviation (MAD) < 20° were used. Virtual geomagnetic pole directions for great circles were calculated using the last stable end point from the great circle calculation. Samples with erratic demagnetization trajectories were excluded from all further analyses (Fig. 2.5F). Site-mean directions were calculated from sampling horizons with three reliable sample directions using Fisher Statistics (Fig. 2.6A; Tables 2.2 and A.3) (Fisher, 1953). Any site means that did not pass the Watson (1956) test for randomness (i.e., a 95% confidence circle with an α_{95} > 35°) were excluded from additional analyses. Reversal boundaries were placed at the stratigraphic midpoint between samples with opposite polarity, except in cases where there was evidence for a depositional unconformity. In instances where an unconformity was interpreted, reversal boundaries were placed at the lithologic contact equivalent with the unconformity. The local polarity stratigraphy for each section was correlated with the geomagnetic polarity timescale (GPTS) (Ogg, 2012).

To determine the primary and secondary magnetic carriers in mixed mineralogy samples, a triaxial isothermal remanent magnetization (IRM) Lowrie test (Lowrie, 1990) was performed at Baylor University on 10 samples that represented the range of

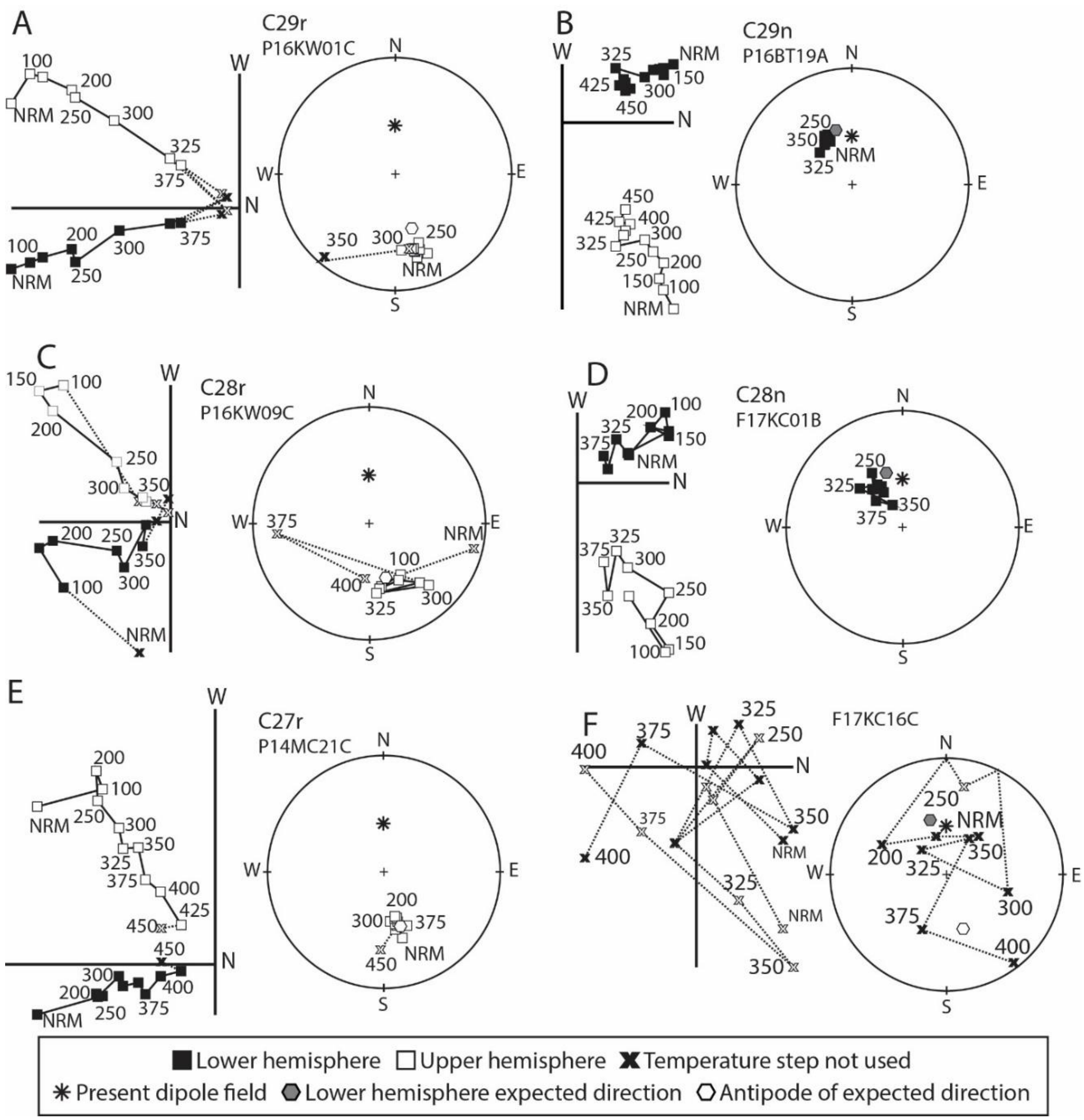

Figure 2.5. Representative orthogonal end vector demagnetization and equal area diagrams for each subset of data. (A-E) Demagnetization trajectories for reversed (A, C, E) and normal (B, D) polarity samples from C29r-C27r, which allowed line fitting to determine a characteristic direction. (F) Representative sample where line fitting was not possible due to erratic nature of data and was not used in any interpretations.

lithologies that occur within the Ojo Alamo Sandstone and lower Nacimiento Formation. A 1T, 300 mT, and 100 mT field was imparted along the X, Y, and Z axes, respectively, using an ASC pulse magnetizer. Samples were then thermally demagnetized in 25 °C increments from 100 °C to 200 °C and 50 °C increments from 200 °C to 700 °C using an ASC controlled atmosphere thermal demagnetizer in an N_2 atmosphere. The magnetization in the X, Y, and Z axes was measured at each temperature step using the 2G cryogenic DC-SQuID magnetometer.

Sediment accumulation rates were calculated for each complete chron (i.e., both the lower and upper reversal were present) in each measured section. Sediment accumulation rates were then used to estimate total section duration and interpolate the age of mammal fossil horizons (Tables 2.1, 2.3-2.5). We used the duration and uncertainty in anomaly thickness of each magnetic chron from Ogg (2012) and the stratigraphic thickness and associated measurement uncertainties (Table 2.3) to calculate sediment accumulation rates. Importantly, these sediment accumulation rates and the ages associated with them include only measurement errors associated with the position of the reversal boundary and thus may underestimate total uncertainties of the sediment accumulation rates. Additionally, these rates assume uniform sediment accumulation rates throughout the polarity zone, which is likely not the case but cannot be quantified. The rates are asymmetrical due to different stratal thicknesses and chron durations used in our calculations. The maximum sediment accumulation rates were calculated by dividing the maximum thickness and the minimum duration of the magnetic chron while the minimum sediment accumulation rates were calculated using the minimum thickness and the maximum duration of the magnetic chron (Table 2.4). We were able to calculate reliable sediment accumulation rates for C29n from De-Na-Zin and Betonnie Tsosie Wash, for C28r from De-Na-Zin, Kimbeto Wash, Betonnie Tsosie Wash, and Mesa de Cuba, and for C27r from Kutz Canyon (Table 2.4).

The duration of the Gallegos Canyon measured section was calculated by extrapolating the C29n and C28r sediment accumulation rates from De-Na-Zin and applying them to the measured C29r and C28r measured thickness, respectively (Table 2.5). The duration of the De-Na-Zin and Betonnie Tsosie Wash measured sections was calculated by extrapolating the C29n and C28r sediment accumulation rates from each location to the C29r and C28n measured section thickness, respectively (Table 2.5). The Kimbeto Wash measured section duration was calculated by extrapolating the average C29n sedimentation rate from De-Na-Zin and Betonnie Tsosie Wash to the C29r sediment thickness for the base of the section and extrapolating the C28r sediment accumulation rate from Kimbeto Wash to C28n sediment thickness (Table 2.5). The duration of the Kutz Canyon measured section was done by extrapolating the C27r sediment accumulation rate down to the C28n sediment thickness and applying the C27r sedimentation rate to the total thickness of C27r sediments within the measured section (Table 2.5). The duration of the Chico Springs measured section was calculated by extrapolating the C27r sediment accumulation rate from Kutz Canyon to the C28n and C27r sediment thickness (Table 2.5). The Mesa de Cuba Measured section duration was calculated by extrapolating the average C29n sedimentation rate from De-Na-Zin and Betonnie Tsosie Wash to the Mesa de Cuba C29n thickness and by correlating the “lower black mudstone” to the same lithologic marker bed from Torreon West (Leslie et al., 2018b) (Table 2.5).

^{40}Ar/^{39}Ar Geochronology

Fine- to medium-grained sandstones were collected from De-Na-Zin, Betonnie Tsosie, and Mesa de Cuba sections and prepared for ^{40}Ar/^{39}Ar detrital sanidine geochronology. The argon data are presented in Tables C.1-C.5 (see footnote 1); table footnotes provide information on calculation methods for maximum deposition ages (MDA), correction factor data, flux monitor, and decay constants. Recovery of sanidine evolved over the course of the project, however all samples were either gently crushed in a jaw crusher and ground in a disc grinder or hand crushed using a mortar and pestle. Samples were washed ultrasonically in dilute HCl until signs of calcite were no longer present, though most samples showed no evidence of calcite. Samples were further ultrasonically treated in distilled water and rinsed in acetone to expedite drying. Samples were then inspected for sanidine content under a petrographic microscope while immersed in wintergreen oil; based on this a grain size (typically between 45 mesh and 120 mesh) was chosen to maximize sanidine recovery. K-feldspar was concentrated by heavy liquid floatation and from this concentrate we initially picked for sanidine based on optical clarity under a standard binocular microscope. This method was not fully effective at distinguishing sanidine from clear plutonic and/or metamorphic K-feldspar, and we suggest that most detrital grain ages older than at least 500 Ma are likely not sanidine. To improve sanidine recovery for samples analyzed later in the study (i.e., Betonnie Tsosie section), K-feldspar concentrates were placed in a petri dish, covered in wintergreen oil and viewed under a polarizing binocular microscope with transmitted light. This allowed us to pick mostly sanidine by avoiding K-feldspars with microtextures that could not be easily observed under a standard binocular microscope. We evaluated for any hydrocarbon contamination potential created by immersion in wintergreen oil by immersing sanidines in standards and looking for any age bias, and finding that there was none. Wintergreen oil was removed from selected grains by ultrasonic cleaning in acetone.

A total of 13 detrital sanidine concentrates were irradiated in several packages at the U.S. Geologic Survey Triga reactor in Denver, Colorado, along with flux monitor standard Fish Canyon sanidine (FC-2). FC-2 was assigned an age of 28.201 Ma (Kuiper et al., 2008) and a total ^{40}K decay constant of 5.463e-10 /a was used (Min et al., 2000). Following irradiation, argon was extracted from single grains by either total fusion (SCLF) or low-resolution (2-6 step) incremental heating with a CO_2 laser. Typical heating was conducted for 30 seconds followed by gas cleanup for 30-180 seconds. Argon isotopes were measured on ARGUS VI mass spectrometers with various Faraday resistor configurations for masses 40, 39, 38, and 37, whereas mass 36 was measured with a compact discrete dynode (CDD) ion counter. Typically masses 40 and 39 were determined using 1E13 Ohm resistors whereas masses 38 and 37 were measured using 1E12 Ohm resistors. Procedural blanks, air standards, and calibration gas (enriched in radiogenic ^{40}Ar and ^{39}Ar) were measured numerous times during the course of data collection. These measurements were fit with a time-series analysis (typically averaged or fit with linear regression) and applied to the sample analysis to correct for blank, atmospheric argon and detector drift. Since our primary goal was to find Paleocene grains to define maximum deposition ages, many analyses were truncated during the data collection when the calculated age was substantially older than 66 Ma; thus, many of these older grains have overall lower precision due to shorter counting times in the mass spectrometer. Maximum deposition ages were calculated from the youngest mode of grain ages based on an inverse variance weighted mean (Taylor, 1982). In some cases, only one grain defines the youngest mode, and in these cases, the apparent age of the single grain is reported. All uncertainties are reported at 1σ.

Results

Magnetostratigraphy

Six-hundred-and-ninety samples from 241 sampling horizons -- 12 samples from four sampling horizons in the Ojo Alamo Sandstone and 678 samples from 237 sampling horizons from the Nacimiento Formation -- were analyzed during this study (see Table A.1 for detailed sampling data; see footnote 1). Most samples were fully demagnetized by 150 °C to 400 °C and their demagnetization trajectories trended towards the origin after few heating steps (Fig. 2.5A-E). All specimens with reliable demagnetization trajectories were characterized by line or great circle fits (Tables A.2-A.4). Reliable paleomagnetic directions using best-fit lines were generated for 473 samples (68.6%) from 195 sampling horizons (80.9%; Fig. 2.6A; Tables A.1-A.2). Great circles were calculated from 38 samples (5.5%) from 23 sampling horizons (9.5%; Tables A.1 and A.4). At stratigraphic sampling horizons with at least three reliable best-fit lines, site-means were calculated. Ninety-five of these sampling horizons (39.8% of total sampling horizons) passed the Watson (1956) test for randomness and were used for further analyses (Fig. 2.6B; Tables A.1 and A.3).

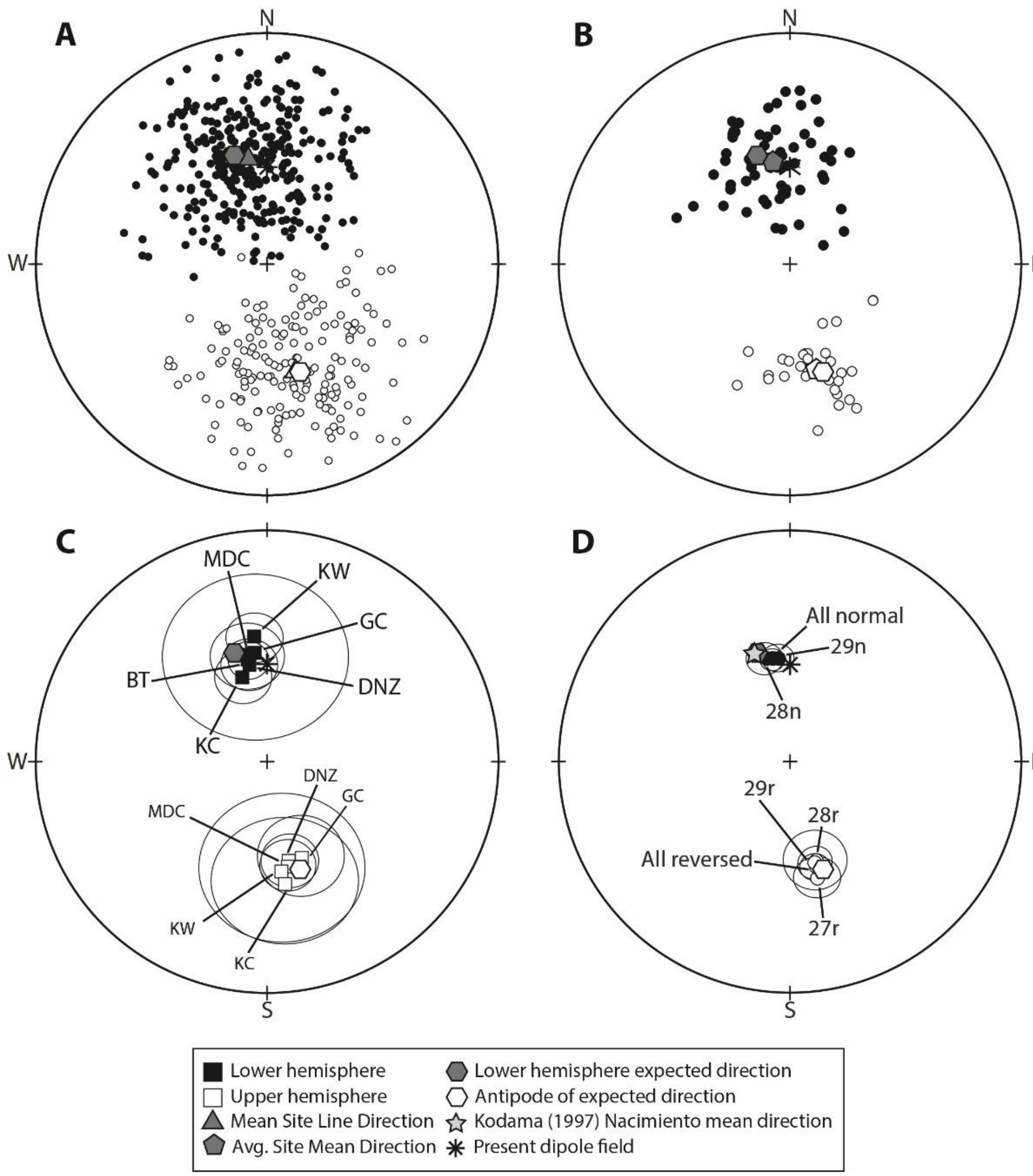

Figure 2.6. (A) Equal area plot shows all line-fitted characteristic magnetization directions obtained (see Table A.2 for full list). (B) Equal area plot shows all site-mean directions calculated from this study (see Table A.3 for full list). (C) Equal area plot shows all normal and reversed site-mean directions averaged by sections: KC—Kutz Canyon, DNZ—De-Na-Zin, KW—Kimbeto Wash, BT—Betonnie Tsosie Wash, GC—Gallegos Canyon, and MDC—Mesa de Cuba. The ellipse surrounding each mean direction represents the 95% confidence cone (see Table 2.2 for details) (Fisher, 1953). (D) Equal area plot shows the site-mean average for each magnetic chron (C29r–C27r) and total Ojo Alamo Sandstone and lower Nacimiento Formation mean normal and reversed directions. The mean Nacimiento Formation direction reported by Kodama (1997) is also shown. The ellipse surrounding each mean direction represents the 95% confidence cone (see Table 2.2 for details) (Fisher, 1953). The modern dipole, the expected early Paleocene direction recalculated from Torsvik et al. (2008), and the antipode of the early Paleocene expected direction are shown in each equal area plot.

The average normal and reversed site-mean for each section and basin-wide for each magnetic polarity chron was calculated (Fig. 2.5C-D). The site mean directions were then used to calculate paleomagnetic pole latitude and longitude for each magnetic chron and for all reversed and normal direction site means (Table 2.2). The average Ojo Alamo Sandstone and lower Nacimiento Formation normal site-mean direction was oriented at 349.9°, 52.9° (n = 66, α_{95} = 3.9°) and the average reversed site-mean direction was oriented at 164.9°, -51.1° (n = 29, α_{95} = 5.1°). The reversal test of McFadden and McElhinny (1990) returned a positive, class B reversal test, indicating that it is not possible to reject the hypothesis that the two distributions share a common mean direction at with 90% confidence (i.e., passed reversals test). These directions overlap within uncertainty with the expected early Paleocene (65.5 Ma) direction of 343.0°, 49.7° (recalculated from Torsvik et al., 2008)) and the mean characteristic remanent direction of 342.1°, 49.6° (n = 20, α_{95} = 7.1°) for the Nacimiento Formation from Kodama (1997) (Fig. 2.6D; Table 2.2). The mean virtual geomagnetic pole (VGP) latitude and longitude calculated from all normal polarity site means was 81.4 °N, 161.6 °E (N = 66, A_{95} = 5.8°) and for all reversed polarity site means was 76.9 °N, 152.7 °E (N = 29, A_{95} = 6.1°), which overlaps within uncertainty of the early Paleocene (65.5 Ma) expected paleopole of 74.7 °N, 190.6 °E (recalculated from Torsvik et al.,2008; Table 2.2). Reversal tests were also performed between each chron in each magnetostratigraphic section, for all normal and reversed site mean directions for each section, and between each chron for all sections across the basin, and the majority of these subsets of data passed the reversal tests (Table A.5; see footnote 1).

Table 2.2 – Mean Paleomagnetic Direction Data

Subset	*n*	D (°)	I (°)	k	a95 (°)	Pole (°N)	Pole (°E)	K	A95 (°)
Kutz Canyon normal sites	7	343.9	59.0	40.6	9.6	76.7	187.2	26.0	12.1
Kutz Canyon reversed sites	3	171.4	-45.9	27.34	24.0	79.2	116.0	45.7	18.4
Gallegos Canyon normal sites	4	353.7	51.1	9.8	31.0	87.6	169.3	6.6	38.7
Gallegos Canyon reversed sites	7	159.9	-53.8	17.9	14.7	72.5	166.9	11.4	18.7
Chico Springs normal sites	0	---	---	---	---	---	---	---	---
Chico Springs reversed sites	2	157.7	-37.1	---	---	65.4	130.9	---	---
De-Na-Zin normal sites	16	349.9	55.1	16.3	9.4	82.2	175.0	10.0	12.2
De-Na-Zin reversed sites	10	167.5	-54.1	26.0	9.7	79.7	164.1	16.2	12.4
Kimbeto normal sites	8	354.3	45.0	36.8	9.2	80.0	103.8	42.9	8.6
Kimbeto reversed sites	2	159.6	-45.4	---	---	70.4	141.1	---	---
Betonnie Tsosie normal sites	23	349.4	53.1	20.3	6.9	81.1	156.9	13.8	8.4
Betonnie Tsosie reversed sites	0	---	---	---	---	---	---	---	---
Mesa de Cuba normal sites	8	349.2	51.5	21.4	12.2	81.7	153.1	15.1	14.7
Mesa de Cuba reversed sites	5	168.6	-52.1	65.6	9.5	80.3	147.5	40.3	12.2
C29r sites	7	166.4	-53.2	109.3	5.8	78.9	156.4	72.1	7.2
C29n sites	34	353.5	53.0	22.5	5.3	83.7	161.2	8.3	9.1
C28r sites	12	162.2	-53.0	16.7	10.9	74.4	164.2	10.6	14.0
C28n sites	32	346.2	52.7	19.3	5.9	79.1	161.9	13.0	7.3
C27r sites	10	166.9	-47.3	42.5	7.5	77.3	134.4	43.0	7.4
All normal sites	66	349.9	52.9	20.8	3.9	81.4	161.6	10.2	5.8
All reversed sites	29	164.9	-51.1	29.0	5.1	76.9	152.7	20.2	6.1

Note: n – number of site means; D – declination; I – inclination; k – Fisher's (1953) precision parameter; a95 – radius of 95% confidence cone around mean (Fisher, 1953); pole N and E – mean virtual geomagnetic pole latitude and longitude calculated from each subset; K and A95 – Fisher (1953) statistics for virtual geomagnetic pole.

The lithostratigraphy, local polarity stratigraphy, specimen and site-mean polarity, and specimen and site-mean VGP latitude for the Gallegos Canyon and De-Na-Zin measured sections are shown in Figure 2.2. The lowermost sample from De-Na-Zin and the two lowermost samples from Gallegos Canyon are from the Ojo Alamo Sandstone; the remaining samples are from the Nacimiento Formation. The lowermost sample at De-Na-Zin and the lowermost two samples from Gallegos Canyon are in the Ojo Alamo. The A- and B+ local polarity reversal occurs above the Ojo Alamo Sandstone-Nacimiento Formation contact in both sections (Fig. 2.2). The reversal between local polarity zones B+ and C- is constrained to 1.5 m at Gallegos Canyon and 0.7m at De-Na-Zin (Fig. 2.2; Table 2.3). The reversal between local polarity zones A- and B+ is constrained to 3.0 m at Gallegos Canyon and 0.7 m at De-Na-Zin (Fig. 2.2; Table 2.3). The reversal between local polarity zones C- and D+ at De-Na-Zin is constrained to 3.0 m (Fig. 2.2; Table 2.3).

The Kimbeto Wash and Betonnie Tsosie Wash measured section lithostratigraphy, local polarity stratigraphy, specimen and site-mean polarity, and specimen and site-mean VGP latitude are shown in Figure 2.3. The reversal between local polarity zones A- and B+ is constrained to 1.5 m at both Kimbeto and Betonnie Tsosie Washes (Fig. 2.3, Table 2.3). The reversal between local polarity zones B+ and C- is constrained to 1.5 m at Kimbeto Wash and 0.55 m at Betonnie Tsosie Wash (Fig. 2.3, Table 2.3). The reversal between local polarity zones C- and D+ is constrained to 3.0 m at Kimbeto Wash and 4.5 m at Betonnie Tsosie Wash.

The measured sections from Kutz Canyon, Chico Springs, and Mesa de Cuba with their associated lithostratigraphy, local polarity stratigraphy, specimen and site-mean polarity, and specimen and site-mean VGP latitude are shown in Figure 2.4. The reversal in the

Chico Springs section is constrained to 3.0 m and is constrained in the Kutz Canyon section to 1.5 m (Fig. 2.4; Table 2.3). The reversal between local polarity zones A+ and B- at Mesa de Cuba is constrained to 1.5 m, the reversal between local polarity zones B- and C+ is constrained to 1.5 m, and the reversal between local polarity zones C+ and D- is constrained to 2.0 m (Fig. 2.4; Table 2.3). The reversal between local polarity zones C+ and D- is positioned at the base of a large channel complex that is presumed to represent an unconformity within the section; without conformity, the reversal is constrained to 9.0 m due to the presence of coarse-grained sandstones in this interval (Fig. 2.4).

Table 2.4 – Calculated Sediment Accumulation Rates

Chron	Chron Duration*	Kutz Canyon	De Na Zin	Kimbeto	Betonnie Tsosie	Mesa de Cuba
C29r	0.344 ± 0.033	N.A.†	N.A.†	N.A.†	N.A.†	N.A.†
C29n	0.730 ± 0.071	N.A.†	43.3 (+6.5, -5.4)	N.A.†	41.6 (+7.9, -6.5)	N.A.†
C28r	0.291 ± 0.028	N.A.†	92.3 (+16.9, -13.9)	101.0 (+22.2, -18.3)	138.8 (+14.8, -21.6)	92.8 (+15.6, -12.8)
C28n	1.173 ± 0.114	N.A.†	N.A.†	N.A.†	N.A.†	N.A.†
C27r	0.977 ± 0.135	121.8 (+24.8, -18.8)	N.A.†	N.A.†	N.A.†	N.A.†

Note: all sediment accumulation rates are in m/m.y.
*chron duration and uncertainty from Ogg (2012).
†N.A. = not applicable.

Table 2.3 – Stratigraphic Position of Polarity Zones

Chron	Location	Local polarity zone	Lowermost sample in Chron	Uppermost sample in chron	Strat. position of base (m)	Strat. position of top (m)	Chron thickness (m)	Uncertainty (m)
29r	Gallegos Canyon	A-	F19GJ01	F19GC05	-1.45	14.40	15.85	1.50
	De Na Zin	A-	P13OJ01	P13NZ06	-12.00	8.03	20.03	0.88
	Kimbeto	A-	P16KW14	P16KW01	0.00	6.15	6.15	0.75
	Betonnie Tsosie	A-	P16BT01	P16BT04	0.00	6.00	6.00	1.50
29n	Gallegos Canyon	B+	F19GC06	F19GP03	14.40	37.45	23.05	2.25
	De Na Zin	B+	P13NZ04	F19SZ01	8.03	39.65	31.62	1.23
	Kimbeto	B+	P16KW02	P16KW08	6.15	27.35	21.20	1.50
	Betonnie Tsosie	B+	P16BT05	P16BT23	6.00	36.38	30.38	2.28
	Mesa de Cuba	A+	P13LC01	P14MC02	0.00	28.15	28.15	1.50
28r	Gallegos Canyon	C-	F19GP04	F19GP11	37.45	60.7	23.25	0.75
	De Na Zin	C-	P10NZ06	F19BZ04	39.65	66.50	26.85	1.85
	Kimbeto	C-	P16KW09	F17KW07	27.35	56.75	29.40	3.00
	Betonnie Tsosie	C-	F19BW02	F19BW12	36.38	76.80	40.42	3.00
	Mesa de Cuba	B-	P14MC03	P14MC09	28.15	55.15	27.00	1.50
28n	Kutz Canyon	A+	F17KC01	F17KC09	0.00	40.00	40.00	0.75
	Chico Springs	A+	F19CS01	F19CS01	0.00	1.50	1.50	1.50
	De Na Zin	D+	F19BZ05	F19TZ12	66.50	104.00	37.50	1.50
	Kimbeto	D+	F17KW08	F17KW16	56.75	78.95	22.20	1.50
	Betonnie Tsosie	D+	F19BW13	F19BT09	76.80	110.00	33.20	2.25
	Mesa de Cuba	C+	P14MC10	P14MC19	55.15	94.15	39.00	9.00
27r	Kutz Canyon	B-	F17KC10	F17KC25	40.00	129.00	89.00	0.75
	Chico Springs	B-	F19CS02	F19CS12	1.50	58.00	56.50	1.50
	Mesa de Cuba	D-	P14MC20	P14MC32	94.15	152.65	58.50	3.50

Magnetic Mineralogy

The Triaxial IRM Lowrie tests for all samples indicated mixed mineralogy with the majority of IRM held by grains with coercivities of less than 100 mT (Fig. 2.7). In all samples there was a large drop in remanence between 100 °C and 200 °C in the low coercivity fraction. suggesting intermediate titanohematite (Sprain et al., 2016). In some samples, the remanence held from 100 – 300 mT dropped beginning at 100-200 °C and

was completely demagnetized by 400 °C, which indicates the presence of only intermediate titanohematite (Sprain et al., 2016) (sample P16BT06, Fig. 2.6D). In other samples, in addition to the drop in the remanence held from 100 – 300 mT from 100 - 400 °C, indicating intermediate titanohematite, some remanence was retained above 400 °C until it was fully demagnetized between 550 to 600 °C, which indicates the presence of (titano)magnetite (sample P14MC06, Fig. 2.7G) (Dunlop and Özdemir, 1997).

In addition to the presence of titanohematite and (titano)magnetite, the Triaxial IRM Lowrie Fuller tests indicated the occurrence of other magnetic minerals in some samples. Hematite and/or maghemite is likely present in samples P13NZ07 and P16BT19 due to the relatively high proportion of remanence held in the > 1T and 100-300 mT coercivities, loss of remanence at 700 °C, and the red coloring of the sample (Fig. 2.7A-B). We interpret the iron sulfide mineral greigite, which became magnetite upon heating at > 400 °C, to be present in sample P13OJ01 based on large drop in 0-300 mT coercivities between 200 °C and 350 °C and the presence of numerous sulfur bearing layers in samples of this this lithology (Fig. 2.7C) (Roberts, 1995).

Table 2.5 – Calculated Measured Section Duration

	Kutz Canyon	Chico Springs	Gallegos Canyon	De Na Zin	Kimbeto	Betonnie Tsosie	Mesa de Cuba
C29r Duration	N.A.*	N.A.*	0.37 (+0.07, -0.06)	0.46 (+0.09, -0.08)	0.13 (+0.02, -0.02)	0.14 (+0.07, -0.05)	N.A.*
C29n Duration	N.A.*	N.A.*	0.53 (+0.14, -0.12)	----†	0.51 (+0.14, -0.11)	----†	0.59 (+0.11, -0.08)
C28r Duration	N.A.*	N.A.*	0.25 (+0.05, -0.05)	----†	----†	----	----†
C28n Duration	0.33 (+0.07, -0.06)	0.01 (+0.02, -0.01)	N.A.*	0.41 (+0.08, -0.07)	0.22 (+0.05, -0.04)	0.24 (+0.06, -0.04)	0.42 (+0.07, -0.06)
C27r Duration	0.73 (+0.14, -0.13)	0.46 (+0.10, -0.09)	N.A.*	N.A.*	N.A.*	N.A.*	0.48 (+0.18, -0.14)
Age of Section Base	63.82 (+0.20, -0.20)	63.51 (+0.15, -0.15)	66.05 (+0.11, -0.08)	66.15 (+0.12, -0.15)	65.82 (+0.06, -0.09)	65.83 (+0.10, -0.12)	65.55 (+0.11, -0.08)
Age of Section Top	62.76 (+0.26, -0.28)	63.03 (+0.22, -0.23)	64.71 (+0.07,-0.08)	64.26 (+0.18,-0.20)	64.45 (+0.15, -0.18)	64.43 (+0.15, -0.16)	62.82 (+0.18, -0.14)
Total Duration	1.06 (+0.48, -0.46)	0.48 (+0.39, -0.37)	1.35 (+0.19, -0.21)	1.89 (+0.32, -0.30)	1.37 (+0.22, -0.24)	1.39 (+0.26, -0.24)	2.73 (+0.25, -0.26)

Notes: all measured section durations are in Myr

*N.A. = not applicable

†---- = entire chron was measured and no estimated duration calculated

At Chico Springs, Betonnie Tsosie Wash, and Mesa de Cuba, local polarity zones B-, C-, and B-, respectively, are dominated by samples with erratic demagnetization behavior and we were only able to calculate good directions for a small subset of samples within those intervals (Table A.1). We interpret these intervals to be reversed and to correlate to C28r at Betonnie Tsosie and Mesa de Cuba and to C27r at Chico Springs; however, a large subset of samples recording an overprint direction rather than the primary Paleocene direction (Figs. 2.3-2.4, Table A.1). We analyzed four samples from Mesa de Cuba that span the predominantly overprinted section that corresponds with the top of magnetozone A+, B-, and the bottom of C+ to assess the magnetic mineralogy of samples within and stratigraphically above and below the overprinted interval to try to determine the cause of this overprinted interval, (Fig. 2.7E-H; Table A.2-A.4). The analyzed samples and the demagnetization behavior of other samples from the same sampling horizon are as follows: sample P14MC02, from magnetozone A+, had a normal demagnetization trajectory characterized by a best-fit line (Fig. 2.7E); sample P14MC04, from magnetozone B-, had an incoherent demagnetization trajectory (Fig. 2.7F), sample P14MC06, from magnetozone B-, was characterized by a reversed great circle (Fig. 2.7G), and sample P14 MC12, from magnetozone C+, had a normal demagnetization trajectory characterized for best-fit lines and a reliable site mean (Fig. 2.7H). In all of these samples, the Triaxial IRM Lowrie tests indicated that intermediate titanohematite was the major remanence carrier. Titanohematite is easily reset, and as a result, it is frequently overprinted (Dunlop and Ozdemir, 1997; Sprain et al., 2016). In addition to the presence of titanohematite, all samples from Mesa de Cuba showed evidence of the occurrence of (titano)magnetite as well. Samples with a relatively high proportion of (titano)magnetite, (i.e., P14MC02, P14MC06, P14MC12; Fig. 2.7E and 2.7G-H) produced reliable magnetic directions, while samples with relatively small proportion of magnetite (P14MC04, Fig. 2.7F) produced incoherent directions. Thus, we hypothesize that while intermediate titanohematite is the most common magnetic mineral in these Chico Springs, Betonnie Tsosie, and Mesa de Cuba samples, magnetite is the characteristic remanent magnetization carrier. Based on this, we posit that in the overprinted interval the magnetic signature of samples with relatively small proportions of magnetite (e.g., P14MC04) was dominated by titanohematite which recorded either an overprint direction or produced erratic demagnetization behavior.

^{40}Ar/^{39}Ar Geochronology

The detrital sanidine (DS) results are presented on age probability plots arranged in stratigraphic order and separated into the three measured sections (Fig. 2.8). We also included the probability plot of sanidine from a minimally reworked volcanic ash (sample SJ-Ash-2) from the Da-Na-Zin section that is published in Cather et al. (2019) for comparison with the DS spectra. Sample A1070606 from Mesa de Cuba overall has individual crystal ages ranging from Paleocene and Precambrian with many grains being Late Cretaceous. Grains older than ca. 500 Ma are likely non-sanidine, whereas grains younger than 300 Ma are likely sanidine. Age spectrum analyses of single grains (Tables C.1-C.5) are generally flat and yield plateau ages equal to total gas ages, which supports the validity of the total fusion ages. Step-heating spectra commonly reveal climbing spectra in samples sufficiently high in precision and resolution. This is consistent with

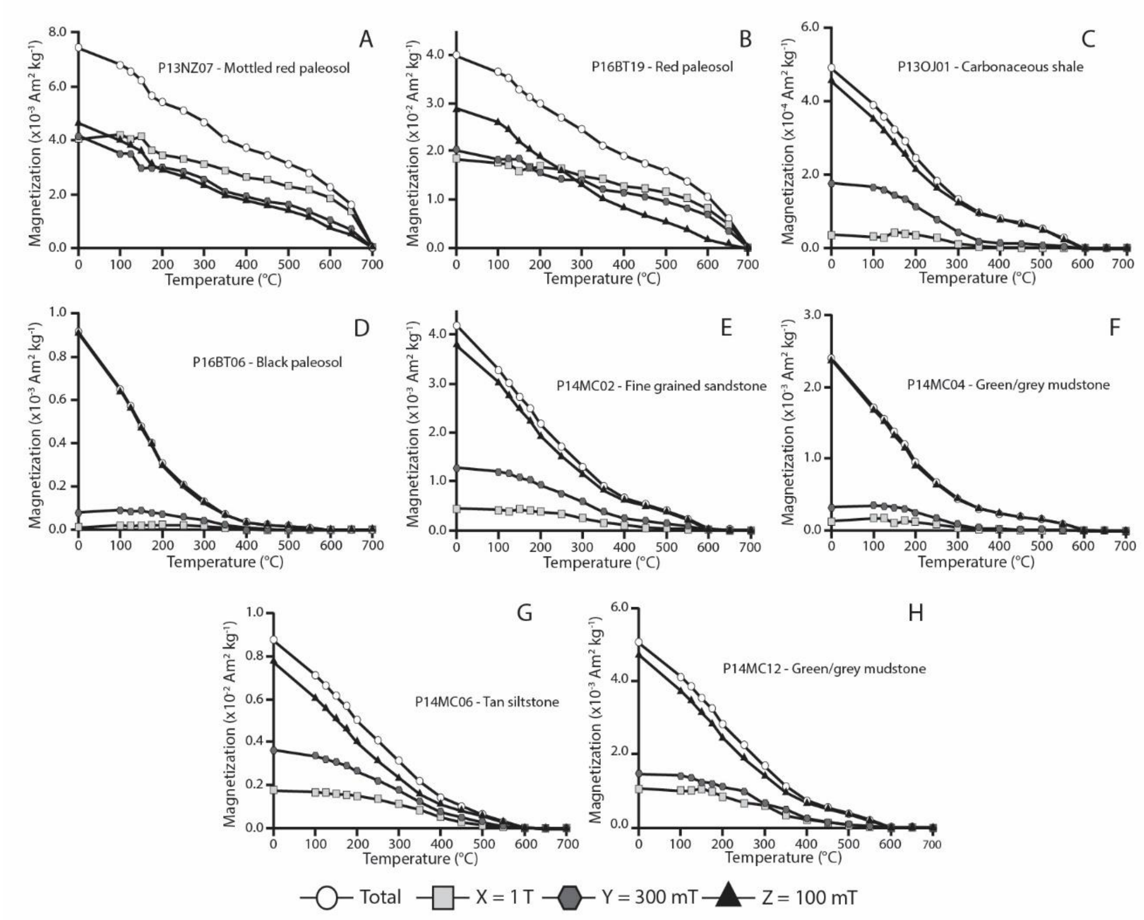

Figure 2.7. Thermal demagnetization curves of orthogonal isothermal remanent magnetization (IRM) imparted along the X, Y, and Z axes for eight samples (A-H) following the approach of Lowrie (1990). All samples had a mixed magnetic mineralogy with intermediate titano-hematite present in all samples. Samples with additional magnetic carriers (i.e., (titano)magnetite, maghemite, greigite) produced reliable directions, which indicates that these minerals are the primary characteristic remanence carriers.

recent studies (Phillips et al., 2017; Fleck et al., 2019) that suggest that climbing spectra for sanidine result from isotope fraction during heating, and therefore the total gas ages of these spectra remain the best representation of the crystal age. In several cases, the youngest group of grains used to define maximum deposition ages (MDA) is associated with an elevated mean square of weighted deviates (MSWD) value that indicates dispersion higher than that predicted by analytical error alone. Primarily this dispersion is related to neutron fluence gradients where no two single grains can occupy the same space in the irradiation package. Thus, slight differences in production of ^{39}Ar between crystals, coupled with high precision analyses, leads to measurable minor age dispersion. Dispersion can also be a result of choosing grains with ages from more than one population, but we err on the side of combining as many grains as is reasonable to represent the MDA even if the MDA is slightly skewed to be too old. All MDA results are reported at 1σ analytical error that includes the error in the J-factor and irradiation parameters. Errors associated with decay constants and the age of the flux monitor are propagated and reported in the data repositories (Tables C.1-C.5).

Two samples (SJ-SS5 and CM-SS4) from the Ojo Alamo Sandstone (one from De-Na-Zin and one from Mesa de Cuba) yield mostly Upper Cretaceous or older grains, which we interpret to represent reworking of older material (Fig. 2.8). A single grain from CM-SS4 is 65.69±0.09 Ma and represents the only Paleocene DS grain recovered from Ojo Alamo samples. For the Nacimiento Formation, a minor component of Paleocene grains was recovered from many of the samples and provides useful MDA (Fig. 2.8). Generally, the mode of youngest Paleocene grains consists of less than five grains; however, the Paleocene mode from A16-BTW-MH2 has 13 grains and CM-SS2 has seven. Three of the five samples from Betonnie Tsosie did not yield Paleocene grains but rather have a substantial component around 68 Ma as well as many older late Upper Cretaceous DS grains. In a single instance, a DS grain appears anomalously young based on other information that will be discussed below. This grain comes from sample A16-BTW-MH5 and yields an apparent age of 64.48±0.16 Ma and although the age is imprecise it is statistically younger than the preferred MDA of 65.17±0.06 Ma defined by three grains (Fig. 2.8, Table C.1).

Sample A1070606 is a recollection of what appears to be significantly reworked ash from Mesa de Cuba. Fassett et al. (2010) first reported an age of 64.5±0.2 Ma (1σ; and recalculated to an FCT standard of 28.201 Ma) for this unit. Our new analysis of this ash yields a more precise age of 64.60 ± 0.06 Ma (Fig. 2.8). CM-Ash-1 was collected at the same stratigraphic level as A1070606 but ~1 km to the west and analysis did not yield any Paleocene grains, perhaps reflecting the reworked nature of the unit. These “ash” samples have a significant component of microcline which is different from SJ-SS-2 ash that is dominated by sanidine with very minor inherited microcline.

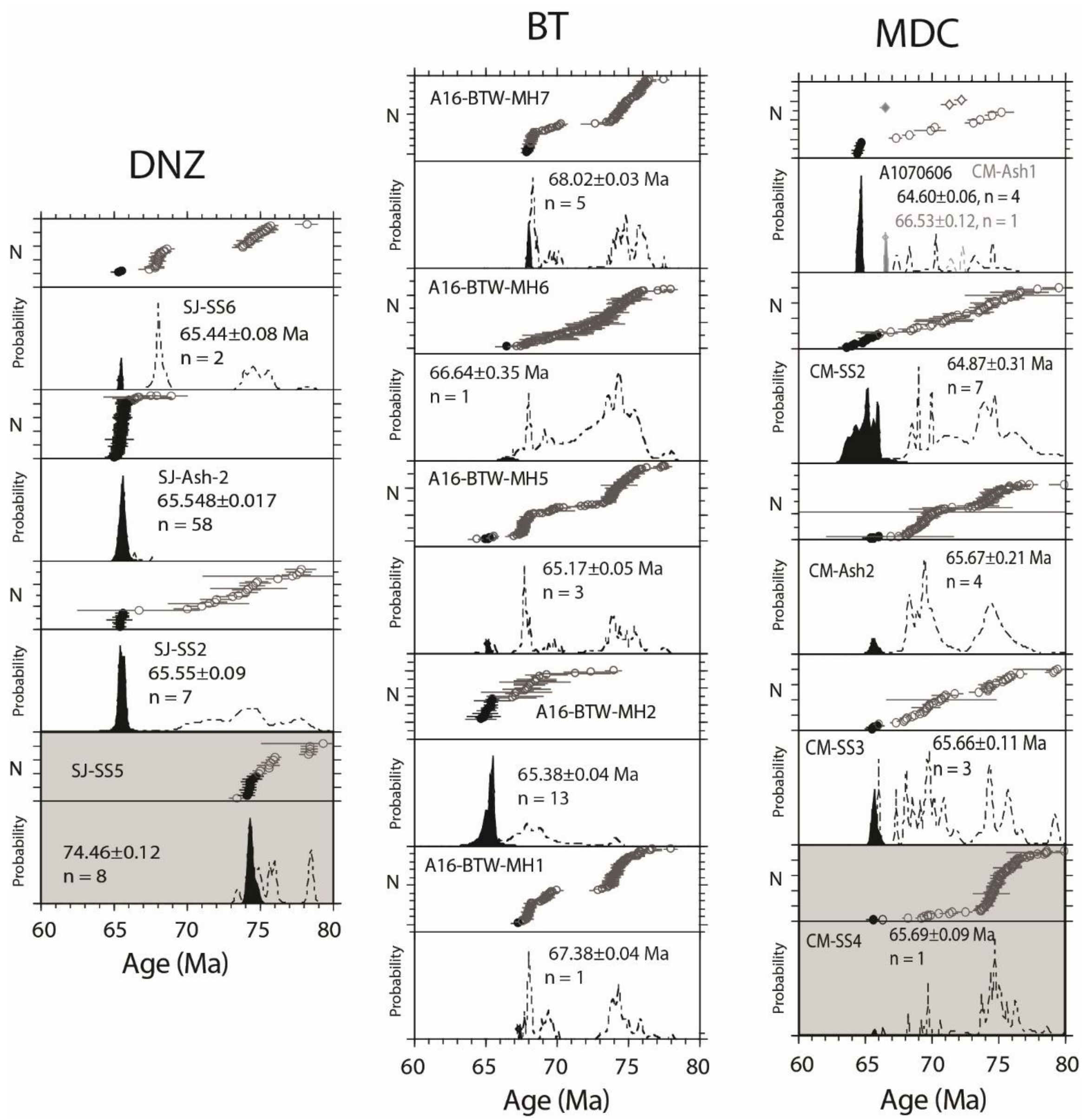

Figure 2.8. $^{40}Ar/^{39}Ar$ sanidine probability distribution diagrams. Apparent ages between 60 Ma and 80 Ma are shown, and solid symbols delineate dates used to determine maximum depositional ages. The data are arranged in stratigraphic order and divided into three dated stratigraphic sections. DNZ – De-Na-Zin section, BT – Betonnie Tsosie Wash section, MDC – Mesa de Cuba section. White shading indicates the Nacimiento Formation and gray indicates the Ojo Alamo Sandstone. Errors are reported at 1σ

.

Relationship of Polarity Stratigraphy to GPTS

Based on lithostratigraphic correlations between the sections, the similarity of the patterns and stratigraphic position of reversal boundaries, and the ash and detrital dates, we correlated the A-, B+, C- local polarity zones from Gallegos Canyon, De-Na-Zin, Kimbeto Wash, and Betonnie Tsosie Wash with C29r-C28r and local polarity zone D+ from De-Na-Zin, Kimbeto Wash, and Betonnie Tsosie Wash with C28n (Figs. 2.2-2.3). These correlations are the same as the interpretations from Butler and Lindsay (1985), though the stratigraphic position of the reversal boundaries is at much higher stratigraphic resolution. Using the polarity interpretations from Kutz Canyon of Leslie et al. (2018b) and Taylor and Butler (1980), which correlate to the top of our section, we correlate the local polarity zones A+ and B- from Kutz Canyon and Chico Springs to C28n and C27r (Fig. 2.4).

No polarity stratigraphy from Mesa de Cuba has previously been published. Our section contains A+, B-, C+, and D- magnetozones. Reworked ash sample A1070606 from an ash layer at 65 m in the section yields an $^{40}Ar/^{39}Ar$ age of 64.60 ± 0.06 Ma. This sample is within magnetozone C+, which indicates correlation with C28n (Fig. 2.3). Sample CM-SS3 is from ~3 m in the section and within magnetozone A+. The detrital sanidine MDA is 65.67 ± 0.08 Ma, and because there is a magnetically reversed interval between A1070606 and CM-SS3 we can confirm that the MDA of this sample places this interval within C29n. Thus, we correlate magnetozones A+, B-, C+, and D- at Mesa de Cuba to C29n-27r (Fig. 2.3).

We note that improvements and additions to the Ogg (2012) geologic time scale are ongoing, and there have been revisions to the geologic time scale since 2012, which could potentially affect our GPTS correlations based on detrital and ash dates. For example, Sprain et al. (2015) suggested an age of 64.931±0.072 Ma for the top of C28r. This date for the top of C28r is based on an age of Fish Canyon sanidine and decay constants recommended by Renne et al. (2011). Thus, using either the Ogg (2012) age (64.667 Ma) or Sprain et al. (2015) age (64.931 Ma) for the top of C28r, ash sample A1070606 falls within C28n supporting our correlation to that subchron (Fig. 2.3). Sprain et al. (2018) reported an age of 65.724±0.013 Ma for C29r/C29n boundary as compared with the Ogg (2012) C29r/C29n boundary of 65.668 Ma. Our MDA of 65.67±0.08 Ma for CM-SS3 is older than the Sprain et al. (2018) C29r/C29n chron boundary. However, because this is a MDA, our result -- combined with the local polarity stratigraphy at Mesa de Cuba, which is normal at, above, and below the CM-SS3 sampling interval -- demonstrates that CM-SS3, and thus the upper Ojo Alamo Sandstone at Mesa de Cuba, was most likely deposited within C29n.

Further, although we are confident of our placement of the detrital sanidine samples into specific chrons, many issues remain for accurately delineating the absolute age of the chron boundaries and durations. These include the choice of age for $^{40}Ar/^{39}Ar$ standards and ^{40}K decay constants, and, importantly, upon laboratory intercalibration, which prevent us from fully accounting for known and unknown uncertainties in the GPTS and our age determinations for the chron boundaries. For these reasons we do not attempt herein to use our magnetostratigraphic, detrital, and ash age determinations to revise the GPTS.

Sediment Accumulation Rates and Measured Section Duration

Sedimentation accumulation rates that we calculated for C29n from De-Na-Zin (43.3 +6.5/-5.4 m/m.y.) and Betonnie Tsosie Wash (41.6 +7.9/-6.5 m/m.y.) were nearly identical and overlap within uncertainty (Table 2.4). The C29n sediment accumulation rates from Gallegos Canyon (31.6 +6.8/-5.6 m/m.y.) and Kimbeto Wash (27.7 +7.5/-6.9 m/m.y.) overlap within uncertainty of each other and were approximately half the average sediment accumulation rates from De-Na-Zin and Betonnie Tsosie for C29n (Fig. 2.2 and 2.3; Table 2.4). The Gallegos Canyon section has an interval of significant channelization ~27 m above the Ojo Alamo Sandstone-Nacimiento contact. Additionally, the base of C29n at Kimbeto Wash occurs in a channelized sandstone complex (Fig. 2.2). Based on the sedimentology and sediment accumulation rates, we interpret unconformities to occur in Gallegos Canyon at the channelized interval (Fig. 2.2) and in the Kimbeto Wash section at the channelized sandstone complex (Fig. 2.3). The De-Na-Zin and Gallegos Canyon sections are geographically proximate (~10 km apart) and the lithostratigraphic units at both sections are remarkably similar (Fig. 2.2); thus, we applied the C29n sedimentation rate of 43.3 m/m.y. (+6.5/-5.4 m/m.y.) from De-Na-Zin to the Gallegos Canyon section. Using that sediment accumulation rate, we estimate that the duration of C29n sedimentation at Gallegos Canyon is 0.53 m.y. (+0.14/-0.12 m.y.), indicating an unconformity duration of ~0.2 m.y. We estimate that the unconformity occurs from approximately 65.4 – 65.2 Ma (Fig. 2.9, Table 2.5). The Betonnie Tsosie and Kimbeto sections are within ~10 km of each other, and the lithostratigraphy of the basal Nacimiento is nearly identical at both sections; thus we applied the C29n sedimentation rate from Betonnie Tsosie Wash of 41.6 m/m.y. (+7.9/-6.5 m/m.y.) to Kimbeto Wash.

Using the Betonnie Tsosie Wash sediment accumulation rate provides an estimate for the duration of C29n sedimentation at Kimbeto Wash of 0.51 m.y. (+0.14/-0.11 m.y.), indicating an estimated unconformity duration of ~0.2 m.y. between approximately 65.7 – 65.5 Ma (Fig. 2.9; Table 2.5).

Sedimentation accumulation rates calculated for C28r from De-Na-Zin (92.3 +16.9/-13.9 m/m.y.), Kimbeto Wash (101.0 +22.2/-18.3 m/m.y.), Betonnie Tsosie Wash (138.8 +14.8/-21.6 m/m.y.), and Mesa de Cuba (92.8 +15.6/-12.8 m/m.y.) are roughly double the sedimentation rates from C29n (Table 2.4). Further, the rates for 28r from De-Na-Zin, Kimbeto, and Mesa de Cuba are nearly identical and overlap with uncertainty (Table 2.4). These sections are all interpreted to represent more distal portions of the San Juan Basin during deposition of the Nacimiento (e.g., Cather et al., 2019). The Betonnie Tsosie section, which has been interpreted to have been near the basin center (i.e., The Tsosie Member, Cather et al., 2019), has notably higher sediment accumulation rates in C28r than in the other sections (Table 2.4).

The only measured section that constrains the lower and upper reversals of C28n is at Mesa de Cuba (Fig. 2.3). The calculated C28n mean sediment accumulation rate using the chron thickness from Mesa de Cuba was 39.6 m/m.y. (+12.8/-10.5 m/m.y.), which is significantly lower than the C28r sedimentation rates from the same section. The

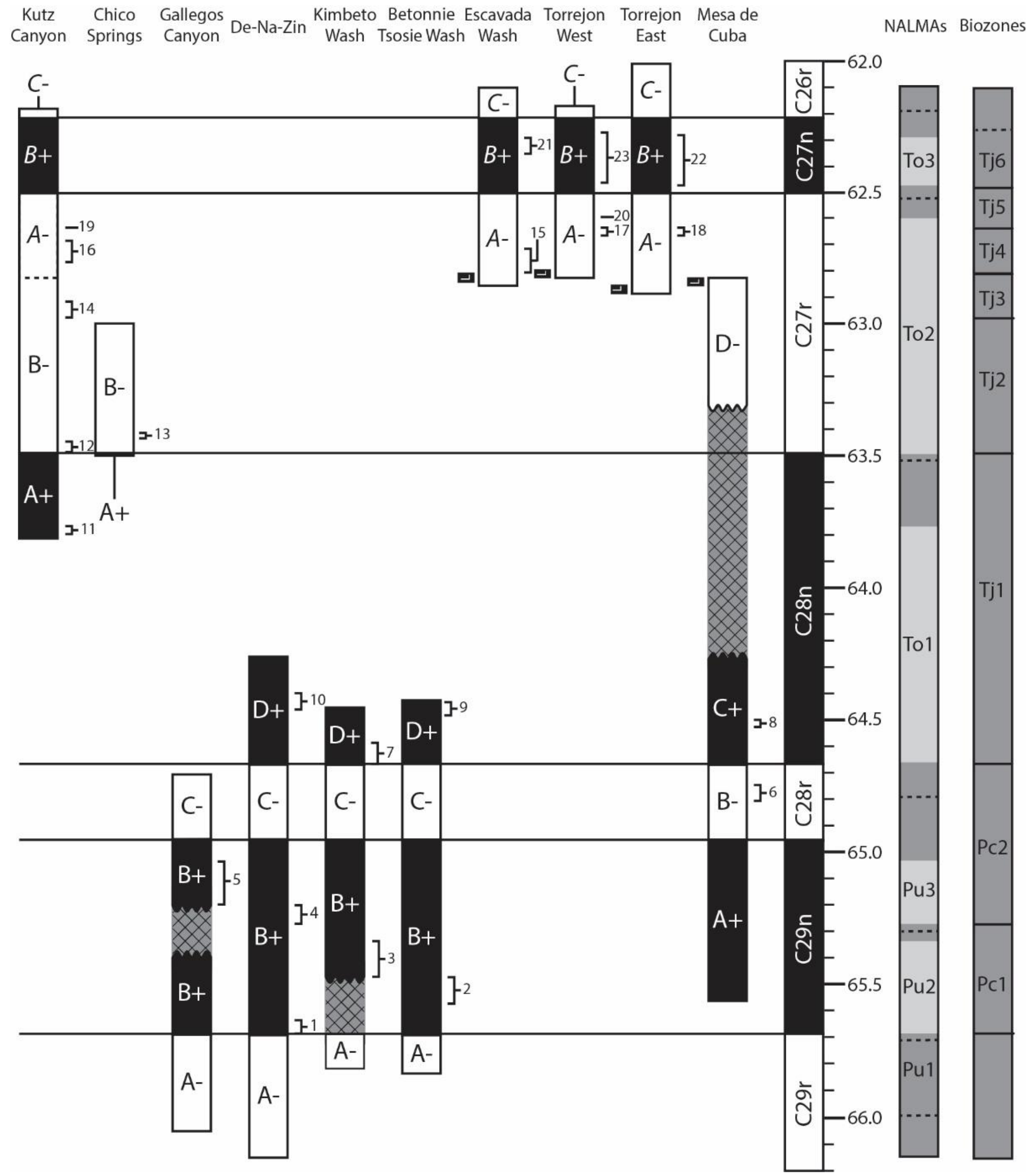

Figure 2.9. Chronostratigraphy of the Ojo Alamo Sandstone and Nacimiento Formation showing the age, calculated duration, and associated North American land mammal age (NALMA) intervals for the sections in this study (lower portion of Kutz Canyon, Gallegos Canyon, Chico Springs, De-Na-Zin, Kimbeto Wash, Betonnie Tsosie Wash, and Mesa de Cuba) and sections from Leslie et al. (2018a) (upper portion of Kutz Canyon, Escavada Wash, Torreon West, and Torreon East). Geomagnetic polarity time scale (GPTS) is from Ogg (2012). The estimated duration of unconformities is indicated by dark gray boxes. Fossil vertebrate horizons described in Table 2.1 are shown (1–14 this study, 15–23 Leslie et al., 2018b). Biozones following the biostratigraphic zonation of Williamson (1996) and duration of San Juan Basin (SJB) fossil horizons within each NALMA biochron are shown. The "lower black mudstone" lithology from Leslie et al. (2018b) is indicated beside the sections where it is present.

basal contact between magnetozone C+ and D- at Mesa de Cuba occurs at the base of a large channel sandstone complex that has an erosive basal contact (Fig. 2.3). Based on the erosive nature of the basal contact of the sandstone channel complex and the very low sediment accumulation rates, we infer the presence of an unconformity within C28n at Mesa de Cuba (Table 2.4). We placed the unconformity at the base of a large channel complex, which erosively overlies the last normal polarity points in C28n (Fig. 2.3). When the C28r sedimentation rate from Mesa de Cuba is applied to the C28n section thickness, the C28n duration at Mesa de Cuba is estimated to be 0.42 m.y. (+0.07/-0.06 m.y.) (Table 2.5).

Since the uppermost sample in the Kutz Canyon measured section presented in this paper (Fig. 2.4) is the lowermost sample in the Kutz Canyon section from Leslie et al. (2018b), we could estimate a total thickness for C27r. The C27r sedimentation accumulation rate calculated from Kutz Canyon is 121.8 m/m.y. (+24.8/-18.8 m/m.y.), which similar to the estimated C27r sediment accumulation rates from Taylor (1977) and nearly identical to those calculated by Leslie et al. (2018b) for C27n from the same location (Table 2.4).

Based on its lithology and polarity, we correlate the upper 3.0 m of the Mesa de Cuba measured section with the “lower black mudstone” from Leslie et al. (2018b). Using the age estimate of 62.82 Ma for the “lower black mudstone” from Torreon West in Leslie et al. (2018b) for the top of the Mesa de Cuba section and the C27r sediment accumulation rate from Kutz Canyon, the duration of C27r at Mesa de Cuba is estimated to be 0.48 m.y. (+0.09/-0.08 m.y.) and the base of the C27r portion of the section is estimated to be 63.30 Ma (Fig. 2.4, 2.9; Table 2.5). Thus, we estimate the total unconformity duration between C28n and C27r at Mesa de Cuba to be ~1.0 m.y. from ca. 64.3 – 63.3 Ma (Fig. 2.9; Table 2.5).

Discussion

San Juan Basin Evolution

Age and depositional model of the Ojo Alamo Sandstone. The age of the Ojo Alamo Sandstone has been contentious, with disagreements about the duration of the underlying unconformity with the Naashoibito Member and how far into the lower Paleocene the Ojo Alamo Sandstone extends (e.g., Sullivan and Lucas, 2003; Sullivan et al., 2005; Williamson et al., 2008; Fassett, 2009b) . Previous palynostratigraphy placed the Ojo Alamo Sandstone in the lower Paleocene palynostratigraphic zones P1 or P2 (Anderson, 1959; Williamson et al., 2008) and analyses of the megaflora also suggest an early Paleocene age (Flynn and Peppe, 2019). The Ojo Alamo Sandstone is an average of 12 m thick and varies from 5 – 17 m in De-Na-Zin. Using the average thickness for the Ojo Alamo and the C29n sediment accumulation rates of the overlying Nacimiento Formation, we estimate that the base of the Ojo Alamo is 66.15 Ma (+0.012/-0.15 m.y.), which is approximately 150 k.y. before the K/Pg boundary (Ogg, 2012). There are two important caveats to this age estimate. First there are dramatic sedimentological differences between the Ojo Alamo Sandstone and the Nacimiento Formation. Sediment accumulation rates were likely much higher during deposition of the Ojo Alamo Sandstone, which is a massive multi-storied channel complex (e.g., Baltz et al., 1966; Chapin and Cather, 1983; Cather, 2004; Flynn and Peppe, 2019), than during deposition of the Nacimiento Formation, which is comprised of paleosols, floodplain, overbank, back swamp, ponded deposits, and channels of varying sizes and dimensions (e.g., Cather et al., 2019; Davis et al., 2016; Williamson, 1996). Second, there is an erosive basal contact between the Ojo Alamo Sandstone and Naashoibito Member, which indicates that there is an unconformity between the Paleocene Ojo Alamo Sandstone and the Cretaceous Naashoibito. Thus, this method almost certainly overestimates the duration of the Ojo Alamo Sandstone and produces a maximum depositional age. Regardless, our analyses indicate that the onset of deposition of the Ojo Alamo Sandstone probably postdates the K/Pg boundary and the formation likely samples much of the lower Paleocene C29r.

When compared across the basin, the polarity stratigraphy, sediment accumulation rates, and a detrital sanidine date from the Ojo Alamo Sandstone indicate that the Ojo Alamo-Nacimiento formational contact is time transgressive from northwest to southeast (Figs. 2.2-2.4, Fig. A.1). The Ojo Alamo Sandstone-Nacimiento Formation contact is in C29r in Gallegos Canyon, De-Na-Zin, and Betonnie Tsosie Wash, but in C29n at Mesa de Cuba (Fig. A.1). Additionally, the C29r thickness of the Nacimiento Formation – 14.40 m in Gallegos Canyon, 8.03 m in De-Na-Zin, and 6.0 m in Betonnie Tsosie Wash - decreases from northwest to southeast, which indicates longer duration of Nacimiento deposition during C29r in the northwest portion of the basin (Fig. A.1). The C29n polarity interpretation for the Mesa de Cuba section is supported by a detrital sanidine $^{40}Ar/^{39}Ar$ date of 65.68 ± 0.09 Ma just below the Ojo Alamo-Nacimiento formational contact near Mesa de Cuba (Fig. 2.8). Based on these polarity interpretations and local sediment accumulation rates for C29n of the Nacimiento Formation, we constrain the maximum age of the Ojo Alamo Sandstone-Nacimiento Formation contact at Gallegos Canyon to be 66.02 Ma (+0.05/-0.04 m.y.), 65.87 Ma (+0.03/-0.02 m.y.) at De-Na-Zin, 65.83 Ma (+0.03/-0.02 m.y.) at Betonnie Tsosie Wash, and 65.63 Ma (+0.12/-0.11 m.y.) at Mesa de Cuba (Fig. 2.2-4). Using these age constraints for the formational contact, we interpret deposition of the Ojo Alamo Sandstone to have occurred during the first ~350 k.y. of the lower Paleocene in the northern parts of the basin and within the first ~500 k.y. of the lower Paleocene in the southern parts of the basin.

Based on the time transgressive nature of the contact and the sedimentology of the unit, we interpret the Ojo Alamo Sandstone to represent the progradational proximal deposits of a distributed fluvial system (DFS) (Weissmann et al., 2013; Hobbs, 2016) and the basal Nacimiento Formation to represent the distal deposits of a later DFS. Thus, we suggest that the time transgressive nature of the Ojo Alamo Sandstone-Nacimiento Formation contact is the result of basin infilling in the early Paleocene via the progradation of a large DFS.

Age and depositional model of the lower Nacimiento Formation. The calculated sediment accumulation rates for C29n were relatively low. which suggests limited available accommodation space in the SJB prior to and during C29n (Table 2.4). Interestingly, sediment accumulation rates roughly double in C28r and remain >90 m/m.y. for at least the succeeding ~2.75 m.y. (e.g., through C27n; Table 2.4; this study and Leslie et al., 2018b). Further, they are not equal across the basin; sedimentation rates are highest in the basin center at Betonnie Tsosie Wash and lowest in De-Na-Zin and Mesa de Cuba on the basin margin (Table 2.4, Fig. A.1). We interpret this increase in sedimentation rates, and variability of rates across the basin, to have been caused by a significant increase in accommodation created by increased subsidence rates in C28r through C27n.

Cather (2004) hypothesized a three-phase subsidence model for the Upper Cretaceous – Eocene deposits of the San Juan Basin. In particular, Cather (2004) argued for a phase of subsidence from ca. 74-67 Ma that allowed for the deposition of the Ojo Alamo Sandstone and Nacimiento Formations. Based on our age constraints for the Ojo Alamo Sandstone and Nacimiento Formation, we modify Cather's (2004) subsidence model. We propose that the initial onset of subsidence and creation of accommodation space in the Maastrichtian allowed the deposition of the Maastrichtian Naashoibito Member of the Kirtland/Fruitland Formations, the Ojo Alamo Sandstone, and the lower (C29r and C29n) portion of the Nacimiento Formation. Later, in C28r, a second pulse of increased subsidence created accommodation space, which allowed the deposition of the upper portion of the Nacimiento Formation before subsidence slowed in the middle Paleocene, ultimately creating the unconformity between the Nacimiento Formation and the overlying San Jose Formation. The third phase of subsidence then occurred at some point in the late Paleocene to early Eocene, allowing the deposition of the Eocene San Jose Formation. Determining the age of the third phase of subsidence will require precise dating of both the uppermost Escavada Member of the Nacimiento Formation and the San Jose Formation, which should be the focus of future work in the San Juan Basin.

Using this refined model of basin subsidence, we can make interpretations about the drivers of deposition of the Nacimiento Formation. The lower Nacimiento Formation, correlated with C29r and C29n, is dominated by poorly developed paleosols and pond deposits (Figs. 2-4) (Davis et al., 2016). Channels in this interval tend to be small and/or isolated, with an overall increase in channelization towards the end of C29n (Fig. 2.2-2.4). In C28r and C28n, channelization becomes more common and paleosols become better developed (Fig. 2.2-2.4). The approximate doubling of sedimentation rates in C28r agrees with the basin subsidence model of Cather et al. (2019), which argued for an increase in basin subsidence during the early Torrejonian and the development of the large Tsosie paleoriver during this time interval. The high degree of channelization during C28r, especially in the Kimbeto and Betonnie Tsosie Wash sections, likely reflects the emplacement of the Tsosie paleoriver (Cather et al., 2019). Towards the top of C28n in Kutz Canyon, large sheet sands become common (Fig. 2.4). In C27r, grain size is the greatest with a high amount of sheet sands near the basin center at Kutz Canyon, while smaller sheet sands and paleosols are present at the basin margin at Mesa de Cuba (Fig. 2.4). The presence of large-scale sheet sands in C27r suggests an accommodation minimum resulting in unconfined flow when the sediment transport capacity of the channel was exceeded, which is consistent with the conclusions of Leslie et al. (2018b) for the upper Nacimiento Formation. We hypothesize that the Nacimiento Formation represents a progradational DFS, overlying the previous Maastrichtian-earliest Paleocene DFS capped by the Ojo Alamo Sandstone, with the C29r/C29n deposits representing the distal portion of the DFS and the C27r deposits representing the more proximal part (e.g., Trendell et al., 2013; Weissmann et al., 2013). However, the sedimentological and mineralogical data needed to test this hypothesis fully is beyond the scope of this paper.

Age Constraints on San Juan Basin Mammalian Biozones

We constrained the age of Puercan and earliest Torrejonian vertebrate fossil horizons of the Nacimiento Formation within our measured sections (Table 2.2.1) using our estimated sediment accumulation rates (Table 2.4). Using our magnetostratigraphic correlations among sections and the age constraints for each fossil locality, we were able to calculate the ages and durations of the Nacimiento Formation mammalian biostratigraphic zones (Pc1, Pc2, Tj1-Tj5) (Fig. 2.9, Table 2.1). These results indicate that strata in which the Pc1 and Pc2 faunas have been found occur in C29n, Tj1 faunas occur only in C28n, and the Tj2 and Tj3 faunas occur in C27r (Fig. 2.9, Table 2.1). Combining our results with the work of Leslie et al. (2018b), which determined that Tj4 and Tj5 faunas occurred within C27r and the Tj6 faunas occurred within C27n, corroborates previous interpretations of the early Paleocene NALMA biochronologic interval zones for the SJB (e.g., Lofgren et al., 2004). Importantly it also provides more precise age constraints for the first and last occurrences and durations of the Puercan and Torrejonian equivalent biozones in the SJB. This has global implications for understanding mammal evolution after the end-Cretaceous mass extinction.

Because both Pc1 and Pc2 faunas (i.e., Pu2 and Pu3) in the SJB occur within C29n, the duration of each biozone was previously uncertain (Williamson and Lucas, 1992; Williamson, 1996). We constrained Pc1 fossil horizons from De-Na-Zin, Kimbeto Wash, and Betonnie Tsosie Wash to 65.68 – 65.34 Ma (+0.04/-0.01 m.y.) for a total duration of 340 ± 50 k.y. (Fig. 2.9, Table 2.2.1). This demonstrates that, at maximum, the Pc1 mammals occurred within 380 k.y. of the K-Pg boundary. We were also able to constrain the Pc2 fossil horizons from Gallegos Canyon and De-Na-Zin to 65.27 – 65.03

Ma (+0.03/-0.01 m.y.) for a total duration of 240 ± 40 k.y. (Fig. 2.9, Table 2.2.1). The only section where Pc1 and Pc2 are found in superposition is in De-Na-Zin (Fig. 2.9, Table 2.2.1). The duration in De-Na-Zin between strata with Pc1 and Pc2 faunas was 360 ± 70 k.y. (Table 2.2.1). However, the Pc1 fossil site in De-Na-Zin is the oldest horizon in the basin and if the full duration of Pc1 fossil-bearing interval is used, the gap between Pc1 and Pc2 fossil horizons was 70 ± 90 k.y. (Fig. 2.9, Table 2.2.1).

We were able to constrain the Tj1 fossil-bearing interval in the SJB to C28n from 64.66 – 63.76 Ma (+0.07/-0.09 m.y.) for a total duration of 900 k.y. (+70/-90 k.y.) (Fig. 2.9, Table 2.2.1). Interestingly, fossil horizon 5 (locality AMNH 230; Simpson, 1959) at Mesa de Cuba (Table 2.1) contains diagnostic Tj1 mammals, but unfortunately the stratigraphic position of the locality is uncertain. Using measurements and descriptions from Simpson (1959) for the locality (AMNH 230), we estimate that it most likely occurs between 40 m and 50 m in our Mesa de Cuba section, which would suggest an age of 64.80-64.74 Ma (+0.04/-0.02 m.y.) making the base of Tj1 considerably older. However, because we were unable to relocate the site, it was not used to determine either SJB mammal biozone or biochronologic interval zone boundaries (Fig. 2.9, Table 2.1). Even without the Simpson (1959) site, these results indicate that the base of the Tj1 biozone is potentially older than previously suggested (e.g., Williamson, 1996; Lofgren et al., 2004) and the duration of the ‘barren interval’ separating Pc2 and Tj1 is considerably shorter (Williamson, 1996). Using our revised chronology, we estimate the interval between Pc2 and Tj1 faunas (i.e., the “barren interval”) to be 380 k.y. (+120/-110 k.y.) in duration (Fig. 2.9, Table 2.1).

Combining our magnetostratigraphy with that of Leslie et al. (2018b) allowed us to determine that SJB biozones Tj2-5, which are equivalent to the To2 biochron of Lofgren et al. (2004), occur within C27r from 63.48 – 62.59 Ma (+0.03/-0.04 m.y.) for a total duration of 890 k.y. (+30/-40 k.y.) (Fig. 2.9, Table 2.1). Using the uppermost Tj1 horizon (vertebrate horizon 8; Table 2.1) and the lowermost Tj2 horizon (vertebrate horizon 9; Table 2.1), the transition between Tj1 and Tj2 faunas occurred over 280 k.y. (+80/-90 k.y.) (Table 2.1, Fig. 2.9).

Regional NALMA interval zone chronology comparison

The revised age model for SJB faunal zones has important implications for regional patterns of first and last occurrences of the biochronologic zones of Lofgren et al. (2004) across North America. It should be noted, though, that these biochrons are based on the first occurrences of consecutive taxa (interval zones) and that by definition each zone lasts until the first occurrence of the next younger index taxon. For this reason, the zones extend through unfossiliferous intervals in the SJB, which adds uncertainty about the placement of upper and lower boundaries. The magnitude of this uncertainty is dependent on the duration of the unfossiliferous interval (Fig. 2.9). We proceed by describing where the placement of zone boundaries occurs chronostratigraphically based solely on the occurences of fossils.

Our results indicate that biochrons Pu2 and Pu3 occur within C29n in the San Juan Basin, which is consistent with interpretations from the Williston Basin (LeCain et al., 2014; Sprain et al., 2015, 2018), Crazy Mountain Basin (Buckley, 2018), and the Wasatch Plateau (Tomida and Butler, 1980) (Fig. 2.10). Previous work from the

Williston and Denver Basins suggests that Pu2 mammals first occurred in upper C29r (Peppe et al., 2009; Lyson et al., 2019), which suggests that Pu2 mammals first occur in C29r across western North America (Fig. 2.10). No *in situ* vertebrate remains have been found in strata correlative to C29r in the SJB. The Ojo Alamo Sandstone, which has yet to yield any mammal fossils, comprises most of the C29r strata in the basin and the lowermost occurrence of Pu2 fossil in the SJB occurs within 2 m of the C29r-C29n boundary (Figs. 2.2, 2.9-2.10). Given the dramatic change in depositional environments between the Ojo Alamo Sandstone and the Nacimiento Formation, the lack of mammal fossils from C29r in the SJB is probably the result of taphonomic constraints.

Our results indicate that in the SJB the duration between Pu2 and Pu3 fossil localities was very short. Furthermore, age constraints for Pu1 localities from other basins (e.g., Eberle, 2003; Hicks et al., 2003; Peppe et al., 2009; Sprain et al., 2015, 2018) combined with either the maximum age of Pu2 fossil sites (i.e., in C29r, Peppe et al., 2009; Lyson et al., 2019), or the age of Pu2 sites from the SJB (65.68 Ma), also imply a rapid turnover between Pu1 and Pu2 faunas (Fig. 2.9). Both the Pu1-Pu2 and the Pu2-Pu3 turnovers are characterized by the extinction of important zone taxa (e.g., Lofgren et al., 2004). The short durations between Pu1-Pu2 and Pu2-Pu3 fossil sites suggest that the Puercan is characterized by the relatively rapid turnover of earliest Paleocene "disaster taxa" to more diverse recovery faunas (Smith et al., 2018a; Lyson et al., 2019).

The faunal transition marking the Puercan-Torrejonian boundary has been interpreted as nearly synchronous across North America, occurring in either late C28r or early C28n (Lofgren et al., 2004). Latest Puercan localities are found in upper C29n in the SJB, Denver Basin (Lyson et al., 2019), and Williston Basin (Sprain et al., 2018) but in C28r in the Wasatch Plateau, Utah (Tomida and Butler, 1980). However, To1 mammals occur in upper C29n in the Williston Basin of North Dakota and Montana (Peppe et al., 2009; Sprain et al., 2018) and the Crazy Mountain Basin of Montana (Buckley, 2018), in C28r in the Wasatch Plateau of Utah (Tomida and Butler, 1980), and in C28n in the San Juan Basin (this study) (Fig. 2.10). This suggests that the faunal change marking the Puercan-Torrejonian boundary may be diachronous across North America, with the boundary being older in the north and younger in the south (Fig. 2.10). The To2 and To3 faunas are constrained to C27r and C27n in the SJB as documented here and by Leslie et al. (2018b). However, much like in the Puercan, it is difficult to determine if the patterns of faunal change documented in the SJB during the Torrejonian are representative of local or regional phenomena because the SJB is the only basin in which faunas representing the entire Torrejonian occur in superposition (Fig. 2.10). Although there are collections of middle and late Torrejonian mammals from outside the SJB (e.g., Butler et al., 1987; Leslie et al., 2018a; Buckley, 2018), these faunas typically occur in isolation and are difficult to correlate precisely to the SJB record. Furthermore, in some cases, faunas have been recognized as being Torrejonian in age based on the occurrence of typical Torrejonian taxa but not the diagnostic index species for the biochrons (e.g., Hunter and Hartman, 2003). Thus, it is possible that these apparently older Torrejonian faunas may not be Torrejonian and instead document the transition between the Puercan and Torrejonian. Nonetheless, our data combined with previously published work suggest that the timing of the Puercan-Torrejonian boundary is unlikely to be time equivalent across North America and should be the focus of future work. Lastly, our work highlights the importance of the SJB faunas, which occur in

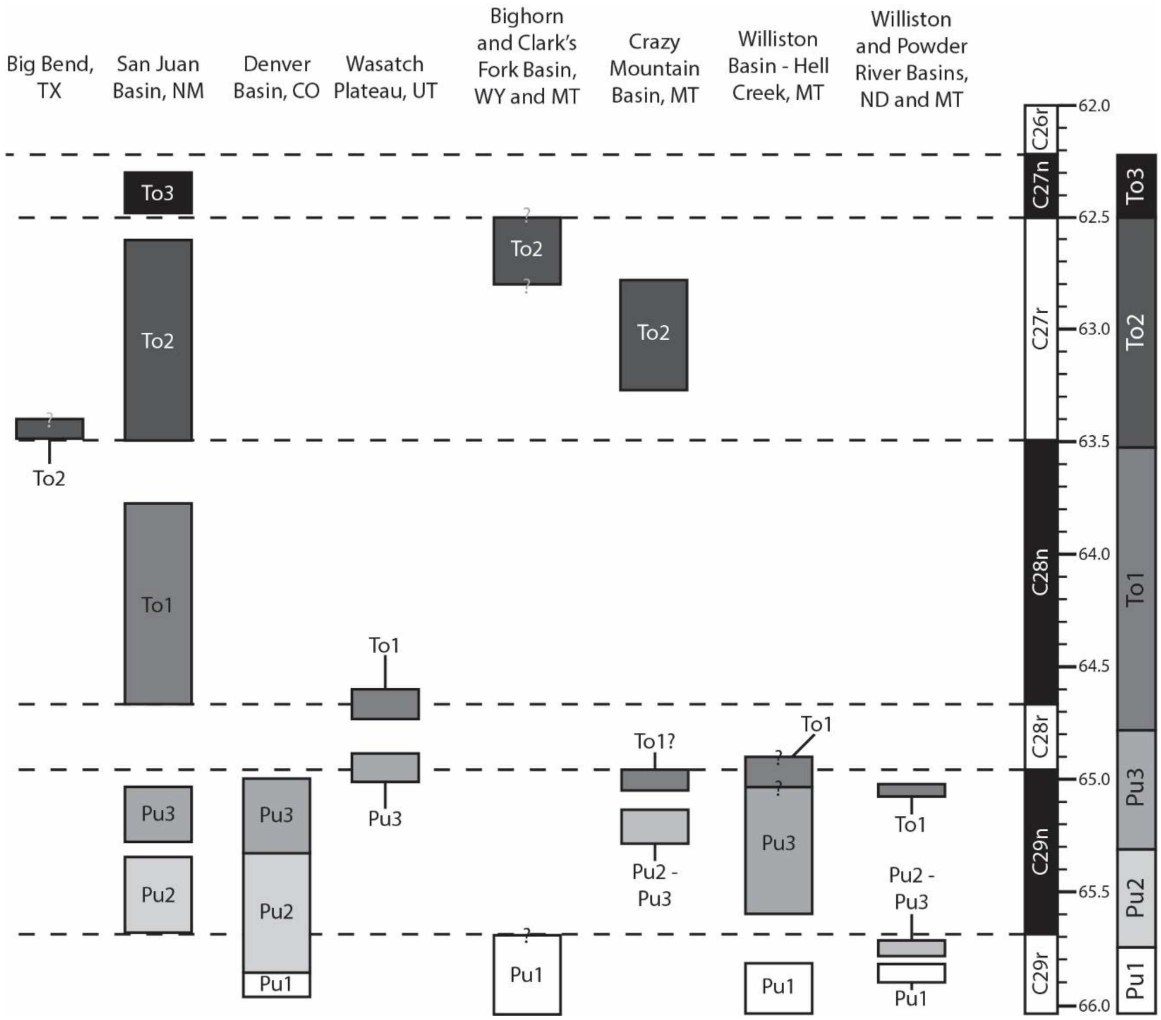

Figure 2.10. Regional comparison of North American land mammal age (NALMA) interval zones across western North America: Big Bend, Texas (Leslie et al., 2018a); San Juan Basin, New Mexico (this study; Leslie et al. 2018b); Denver Basin, Colorado (Eberle, 2003; Hicks et al., 2003; Dahlberg et al., 2016; Lyson et al., 2019); Wasatch Plateau, Utah (Tomida and Butler, 1980); Bighorn and Clark's Fork Basin, Wyoming and Montana (Butler et al., 1987); Crazy Mountain Basin, Montana (Buckley, 2018); Williston Basin, Montana (Sprain et al., 2018); and Williston and Powder River Basins, North Dakota (Peppe et al., 2009). NALMA zones from Lofgren et al. (2004) are indicated.

superposition across multiple localities and sample nearly the entirety of the Puercan and Torrejonian NALMAs, for understanding early Paleocene mammalian evolution following the K-Pg mass extinction.

Conclusions

We correlate the lower Paleocene Ojo Alamo Sandstone and lower Nacimiento Formation to magnetic chrons C29r-C27r of the GPTS based on seven measured sections across the SJB including the first magnetostratigraphy for the type section of the Nacimiento Formation at Mesa de Cuba. We identified the occurrence of intermediate titanohematite in all samples that were analyzed for rock magnetism (Fig. 2.7), which is similar to what has been found in previous work in the San Juan Basin and contemporaneous Laramide basins (Butler and Lindsay, 1985; Force et al., 2001; Sprain et al., 2016). In addition, we documented the presence of (titano)magnetite, hematite, and possibly greigite in some samples. We interpret that titanohematite and (titano)magnetite are the primary characteristic remanence carriers. However, in sections that are overprinted, we interpret (titano)magnetite to be the primary characteristic remanence carrier and find that the titanohematite present in those samples has been reset.

Our magnetostratigraphic results indicate relatively low sediment accumulation rates in C29r and C29n and a rough doubling of sedimentation rates in C28r, which remained consistently high through C27r and were similar to sedimentation rates reported by Leslie and others (2018a) for C27n. We amend the SJB basin evolution model of Cather (2004), and instead hypothesize that the onset of the middle phase of relatively slow subsidence started in the Maastrichtian. This phase allowed for deposition of the

Naashoibito Member, Ojo Alamo Sandstone, and the C29n portion of the Nacimiento Formation. This was followed by a pulse of high subsidence and likely development of the Tsosie paleo-river starting in C28r (Cather and others, 2019), which allowed for deposition of the remainder of the Nacimiento Formation. We find that the contact between the Ojo Alamo Sandstone and Nacimiento Formation is time transgressive, with the contact occurring in C29r in the northwestern part of the basin (Gallegos Canyon, De-Na-Zin, Kimbeto Wash, and Betonnie Tsosie Wash) and in C29n in the southeastern part of the basin (Mesa de Cuba). This time transgressive nature of the Ojo Alamo Sandstone indicates progradation from northwest to southeast during the early Paleocene. These results are consistent with the interpretation that the Ojo Alamo Sandstone and the Nacimiento Formation represent the proximal and distal deposits of two different distributive fluvial systems, respectively.

Our revised age model constrains the intervals in which Pu2 faunas occur in the SJB to 65.68 – 65.34 Ma (+0.04/-0.01 m.y.), Pu3 faunas to 65.27 – 65.03 Ma (+0.03/-0.01 m.y.), To1 faunas to 64.66 – 63.76 Ma (+0.07/-0.12 m.y.), and the To2 faunas to 63.48 – 62.59 Ma (+0.03/-0.04 m.y.). Our results indicate that Pu2 and Pu3 faunas are separated by ~70 k.y. and that Pu3 and To1 faunas in the SJB are separated by ~370 k.y. (+40 k.y./-30 k.y.). Further, comparisons of our age model for the SJB to other mammal fossil sites across North America suggest that the first appearance of To1 mammals may have been diachronous across North America, with the To1 mammals first appearing in the north (Montana and North Dakota) during C29n, then in the middle latitudes (Utah) in C28r, and lastly in southern North America (New Mexico) in C28n. These findings have broad implications for understanding the tempo of mammalian evolution after the end-Cretaceous extinction.

Acknowledgments

This work was supported by the National Science Foundation (EAR-132552 to Daniel J. Peppe, EAR 1325544 and DEB 1654952 to Thomas E. Williamson and Stephen L. Brusatte, EAR 1325612 to Ross Secord), the American Chemical Society Petroleum Research Fund (PRF#52822-DN18 to Daniel J. Peppe), The US Bureau of Land Management (Thomas E. Williamson and Stephen L. Brusatte), the Geological Society of America (Andrew G. Flynn), Dallas Paleontological Society (Andrew G. Flynn), and Baylor University Department of Geosciences' Dixon Fund (Andrew G. Flynn). Stephen L. Brusatte's work on mammal evolution is supported by a European Research Council Starting Grant (ERC StG 2017, 756226, PalM). We thank J. Robinson, H. Anderson, J. Geng, J. Milligan, P. Wright, A. Baumgartner, D. Futcher, U. Denetclaw, R. Williamson, and B. Abbuhl for their assistance in section measuring, sample collection, and sample preparation, and G. Brown and R. Skolnick for fossil preparation at the University of Nebraska State Museum. We also thank S. Atchley, S. Dworkin, B. Hockaday, and J. White, C. Sprain, and an anonymous reviewer for their helpful comments on previous versions of this manuscript and S. Shelley for her collaborative work on San Juan Basin mammals. Lastly, we thank the US Bureau of Land Management for issuing fossil collecting permits.

CHAPTER THREE

Early Paleocene Tropical Forest from the Ojo alamo Sandstone, San Juan Basin, New Mexico, USA

This chapter published as: Flynn, A.G and Peppe, D.J., 2019, Early Paleocene Tropical Forest from the Ojo alamo Sandstone, San Juan Basin, New Mexico, USA. *Paleobiology*, 45(4): 612-635.

Abstract

Earliest Paleocene megafloras from North America are hypothesized to be low diversity and dominated by long-lived cosmopolitan species following the Cretaceous/Paleogene (K/Pg) mass extinction. However, megafloras used to develop this hypothesis are from the Northern Great Plains (NGP) of North America, and relatively little is known about floras from southern basins. Here, we present a quantitative analysis of an earliest Paleocene megaflora (<350 kyr after K/Pg boundary) from the Ojo Alamo Sandstone in the San Juan Basin (SJB), New Mexico. The megaflora, comprising 53 morphotypes, was dominated by angiosperms, with accessory taxa composed of pteridophytes, lycophytes, and conifers. Diversity analyses indicate a species-rich, highly uneven, and laterally heterogeneous flora. Paleoclimate estimates using multivariate and univariate methods indicate warm temperatures and relatively high precipitation consistent with a modern tropical seasonal forest.

When compared with contemporaneous floras from the Denver Basin (DB) of Colorado and the Williston Basin (WB) of North Dakota, the SJB flora had significantly higher species richness but lower evenness. Paleoclimate estimates from the SJB were 7–

14°C warmer than the estimates for the DB and WB, indicating a shift from a temperate forest in the NGP to a tropical forest in the SJB. These results demonstrate the presence of a latitudinal floral diversity and paleoclimatic gradient during the earliest Paleocene in western North America. We hypothesize that the warm, wet conditions in the earliest Paleocene SJB drove rapid rates of speciation following the K/Pg boundary, resulting in a diverse and heterogeneous flora.

Introduction

The Cretaceous/Paleogene (K/Pg) boundary at ~66 Ma is perhaps best known for the extinction of nonavian dinosaurs (e.g., Schulte et al. 2010; Brusatte et al. 2015). However, there was also a major extinction of plant taxa across the K/Pg boundary, with ~50–60% and 15–30% of mega- and microfloral species becoming extinct, respectively (e.g., Wilf and Johnson 2004; Nichols and Johnson 2008; Vajda and Bercovici 2014). The best records of this extinction in plants are from North America (e.g., Nichols and Johnson, 2008). The post extinction North American record documents a major restructuring of terrestrial ecosystems, a destabilization of terrestrial food webs, and a prolonged recovery that extended at least into the middle Paleocene (Hickey 1980; Wing et al. 1995; McIver 1999; Dunn 2003; Wilf and Johnson 2004; Wilf et al. 2006; Peppe 2010; Blonder et al. 2014). Thus, reconstructions of patterns of plant community diversity and composition in the early Paleocene are necessary to fully understand both local and regional ecosystem recovery following the K/Pg mass extinction.

Extensive early Paleocene megafloral collections have been made in North America for over 150 years (e.g., Newberry 1868; Lesquereux 1878; Brown 1962;

Hickey 1980; Wolfe and Upchurch 1987; Wing et al. 1995; Johnson 2002; Barclay et al. 2003; Peppe 2010). The majority of these studies have focused on the Northern Great Plains (NGP) of North America (Fig. 3.1A) (e.g., Newberry 1868; Lesquereux 1878; Brown 1962; Hickey 1980; Barclay et al. 2003; Dunn 2003; Wilf and Johnson 2004; Peppe 2010), with large collections of floras from the first 300,000 years of the Paleocene being primarily from the Denver Basin (DB) of central Colorado (Barclay et al. 2003; Johnson et al. 2003) and the Williston Basin (WB) of North Dakota (e.g., Johnson 1989, 2002; Johnson and Hickey 1990; Wilf and Johnson 2004; Peppe 2010). Early Paleocene plant communities from the NGP are characterized by low diversity and are dominated by long-lived, cosmopolitan, mire-adapted taxa (Hickey 1980; Johnson 2002; Barclay et al. 2003; Peppe 2010). These floras were dominated by fast-growing angiosperms with high assimilation rates and low carbon investment, suggesting the K/Pg bolide impact selected against slower-growing evergreen species, leading to large-scale ecosystem restructuring (Blonder et al. 2014). These patterns of low floral diversity and relatively homogeneous floral composition have been documented across a distance of >1200 km from southern Alberta to central Colorado (e.g., Brown 1962; Hickey 1980; McIver and Basinger 1993; Johnson 2002; Barclay et al. 2003; Dunn 2003; Peppe 2010). Analyses of NGP floras through the Paleocene indicate that it took several million years for floras to fully recover and approach levels of floral diversity common in the Late Cretaceous (Hickey 1980; Wing et al. 1995; Dunn 2003; Wilf and Johnson 2004; Peppe 2010).

In contrast to the patterns from the NGP (e.g., Brown 1962; Johnson 2002; Barclay et al. 2003; Peppe 2010), fossil megafloral patterns from the first ~3.0 Myr of the Paleocene collected along the Colorado Front Range in the DB are considerably more diverse and comprise many species that are interpreted as endemic to the area (Johnson and Ellis 2002; Ellis et al. 2003; Johnson et al. 2003). While contemporaneous floras from the NGP had ~10–40 morphotypes (Hickey 1980; Wing et al. 1995; Johnson 2002; Dunn 2003; Wilf and Johnson 2004; Peppe 2010), the floras from the Colorado Front Range typically have >30 morphotypes and are the basis for suggestions that rapid floral recovery and high rates of speciation following the K/Pg boundary along the margins of the ancestral Rocky Mountains (Johnson and Ellis 2002; Ellis et al. 2003; Johnson et al. 2003). This pattern of recovery is in stark contrast to patterns of speciation and diversity documented across the NGP, including floras from <50 km to the east in the central DB (e.g., Wing et al. 1995; Barclay et al. 2003; Johnson et al. 2003; Wilf and Johnson 2004; Peppe, 2010), and suggests both latitudinal differences in diversity and/or the potential for local or regional diversity hotspots that resulted from rapid recovery after the K/Pg extinctions. Further, the high proportion of endemic megafloral taxa in the Colorado Front Range (Johnson and Ellis 2002; Ellis et al. 2003; Johnson et al. 2003) suggests that the early Paleocene flora is not as homogeneous as has been suggested, and instead that there are latitudinal differences in floral composition across North America. Studies of pollen and fossil wood from the latest Cretaceous and early Paleocene also support a latitudinal gradient in floral composition across North America and a clear differentiation in composition of floras from the mid- to low latitudes and floras from the NGP (Frederiksen 1987; Nichols et al. 1990; Lehman and Wheeler 2009). Nichols et al. (1990) found that floras from mid- to low latitudes had higher diversity and were more dominated by endemic taxa than floras from more northern provinces. However, relatively little research has been conducted on the fossil leaf floras from southern North

America, limiting comparisons of the megafloral record across latitudes and a comparison of the biogeographic patterns identified from both fossil wood and pollen to the megafloral record.

Here we describe a relatively diverse early Paleocene fossil megaflora from the San Juan Basin of New Mexico that occurred within the first ~350 kyr of the Paleogene (Figs. 3.1 – 3.2). We describe the composition and diversity of floral communities, examine differences in floral communities between depositional environments, and estimate mean annual temperature and precipitation within the San Juan Basin. Finally, we compare the earliest Paleocene San Juan Basin megaflora to contemporaneous megafloras from the NGP of North America to assess regional differences in floral diversity, composition, and paleoclimate during the earliest Paleocene.

Geologic Setting

The San Juan Basin (SJB), located in northwestern New Mexico and southwestern Colorado (Fig. 3.1A), is a foreland basin formed during the Laramide Orogeny (Chapin and Cather 1983; Williamson 1996). The basin preserves a relatively continuous succession of terrestrial sedimentary rocks spanning the Late Cretaceous (Campanian) through the early Paleocene (Baltz et al. 1966; O'Sullivan et al. 1972; Williamson 1996; Williamson et al. 2008). Fossil plant material for this study was collected from the earliest Paleocene Ojo Alamo Sandstone in the Bisti/De-Na-Zin (BDNZ) Wilderness Area (Fig. 3.1B,C), which varies from 10 to 15 m in thickness in the study area and is predominantly a gold to yellow-colored, cross-bedded, medium- to coarse-grained

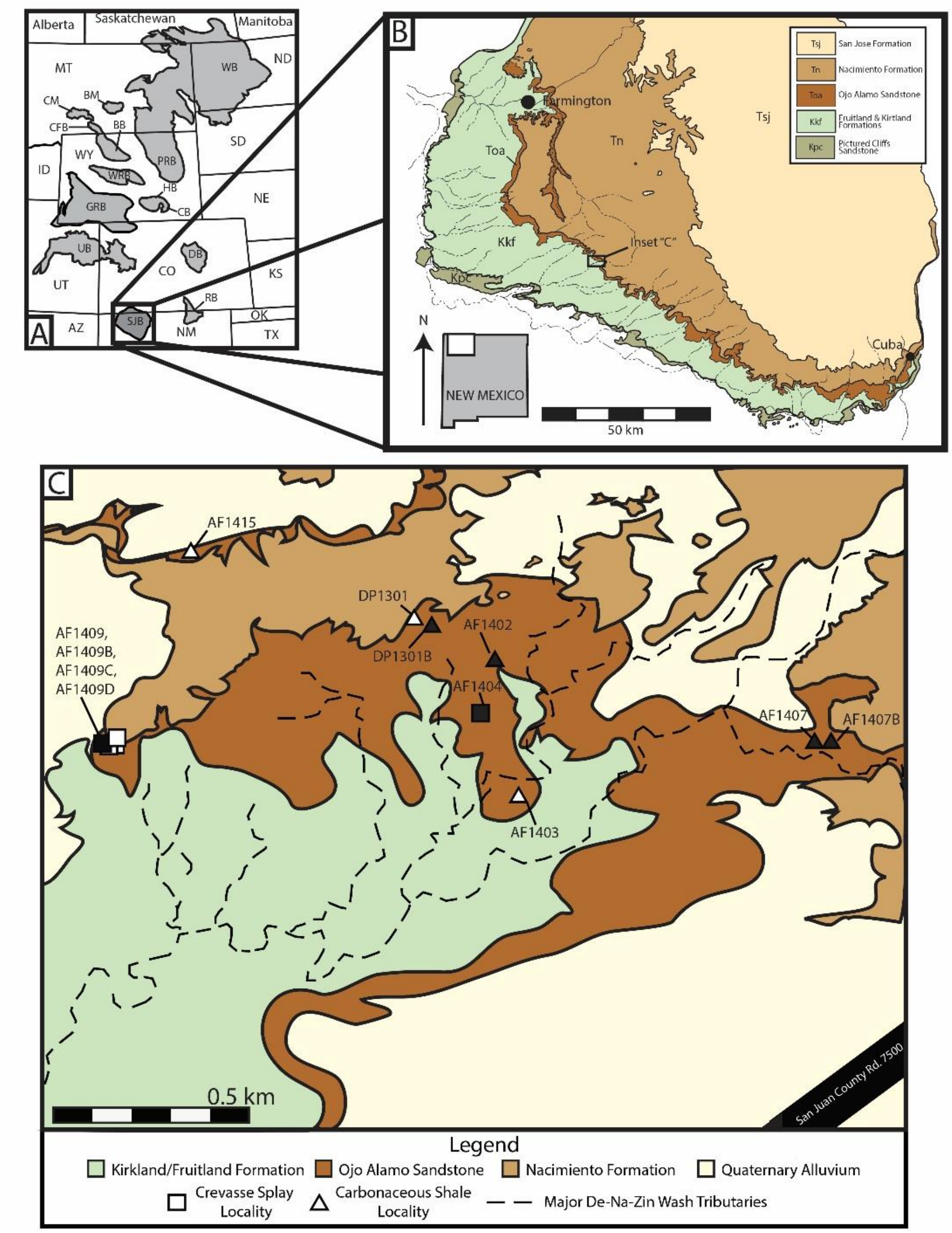

Figure 3.1. Regional basin map, San Juan Basin (SJB) geologic map, and map of the study area. A, Early Paleocene basins of western North America (modified from Peppe 2010) showing the location of the SJB. B, Geologic map of the southwestern SJB showing the geographic occurrences of Late Cretaceous–Eocene deposits and the study area (modified from Williamson et al. 2008). C, Geologic map of the Bisti/De-Na-Zin Wilderness Area with fossil leaf localities indicated (filled shapes, census collections; open shapes, voucher collections).

sandstone with interbedded sandstone and siltstone deposits and localized carbonaceous shale beds (Baltz et al. 1966; O'Sullivan et al. 1972). The Ojo Alamo Sandstone is thought to represent an alluvial plain with one or more sediment sources in the southern Rocky Mountains that was deposited during the onset of tectonism associated with basin development (Powell 1973; Chapin and Cather 1983; Sikkink 1987; Cather 2004). The amalgamated channel belts, low mud to sand ratio, and the presence of relatively high flow regime bedforms correspond with proximal deposits in a distributed fluvial system (Weissmann et al. 2013), which supports the hypothesis that the Ojo Alamo was deposited during a time of relatively limited accommodation space associated with the onset of basin subsidence in the latest Cretaceous and early Paleocene (Cather 2004). The Ojo Alamo Sandstone overlies the Maastrichtian Naashoibito Member of the Kirtland Formation and underlies the early Paleocene Nacimiento Formation (Baltz et al. 1966; Lindsay et al. 1978; Williamson 1996; Mason 2013; Peppe et al. 2013). The contact between the Ojo Alamo Sandstone and Nacimiento Formation is complex and regionally varies from being conformable with the basal paleosols of the Nacimiento weathering into the upper Ojo Alamo Sandstone to unconformable with evidence for the contact being erosive (e.g., Williamson and Lucas 1992; Williamson 1996; Davis et al. 2016). In the BDNZ, the contact between the Ojo Alamo Sandstone and Nacimiento Formation appears to generally be conformable (Williamson 1996; Davis et al. 2016).

Differences in nomenclature between the Ojo Alamo Sandstone and the Naashoibito Member of the Kirtland Formation have caused confusion when relating the two lithologic units (e.g., Sullivan et al. 2005; Williamson and Weil 2008; Fassett 2009). The Ojo Alamo Sandstone and Naashoibito Member have both been recognized as unique stratigraphic units in different formations (i.e., the Ojo Alamo Sandstone is its own formation and the Naashoibito is a member of the Kirtland Formation [e.g., Baltz et al. 1966; Williamson 1996; Williamson and Weil 2008; Williamson et al. 2008]) or as different members within the Ojo Alamo Formation (i.e., the Kimbeto Member and the Naashoibito Member [e.g., Sullivan et al. 2005; Fassett 2009]). Herein we use the definition of Baltz et al. (1966) for the Ojo Alamo Sandstone and recognize it as a unique stratigraphic formation. For clarity, this is equivalent to the Kimbeto Member of the Ojo Alamo Formation proposed by Sullivan et al. (2005).

In addition to confusion about the nomenclature of the Ojo Alamo Sandstone and the Naashoibito Member of the Kirtland Formation, the age of the units remains contentious. Some authors have claimed that both the Ojo Alamo Sandstone and Naashoibito Member of the Kirtland Formation are Paleocene (Fassett 2009), while others have interpreted the Naashoibito Member of the Kirtland Formation to be Late Cretaceous and the Ojo Alamo Sandstone to be early Paleocene (Sullivan and Lucas 2003; Sullivan et al. 2005; Williamson et al. 2008). Palynostratigraphy of the Ojo Alamo Sandstone and the Nacimiento Formation indicates that the Ojo Alamo Sandstone is earliest Paleocene (Anderson 1959; Williamson et al. 2008). Further, the occurrence of *Momipites inaequalis* in the Ojo Alamo Sandstone (Anderson 1959), suggests that it can be correlated to the North American Paleocene palynostratigraphic zones P1 or P2 (Nichols 2003). Mason (2013) used detrital sanidine dating to constrain the maximum depositional age of the Naashoibito Member of the Kirtland Formation to the late Maastrichtian and the Ojo Alamo Sandstone near Cuba, New Mexico, to early Paleocene in age. Magnetostratigraphy from the BDNZ Wilderness Area through the Naashoibito

Member of the Kirtland Formation, Ojo Alamo Sandstone, and lower Nacimiento Formation indicate that the upper Naashoibito Member of the Kirtland Formation, the entire Ojo Alamo Sandstone, and the basal 4 m of the Nacimiento Formation are all reversed polarity, indicating deposition within magnetic chron 29r (Peppe et al. 2013). Based on the Ojo Alamo Sandstone pollen assemblage and geochronology of the Naashoibito Member of the Kirtland Formation, Ojo Alamo Sandstone, and Nacimiento Formation, we interpret that the Ojo Alamo floras, which are the focus of this work, to have been deposited within C29r during the first ~350 kyr of the Paleocene (Fig. 3.2).

Methods

Collection and Classification

Plant fossils were collected from 12 localities from the Ojo Alamo Sandstone in the BDNZ Wilderness Area during field seasons in 2013–2016 (Fig. 3.1C). Because the upper and lower contacts of the Ojo Alamo are not flat lying, the stratigraphic position of each leaf locality was measured to both from the top of the underlying Naashoibito Member of the Kirtland Formation and to the base of the overlying Nacimiento Formation (Fig. 3.2). Localities ranged from 4.65 to 14.5 m above the base of the Ojo Alamo Sandstone and between 10.0 and 1.0 m below the Nacimiento Formation contact (Fig. 3.2). Localities were assigned a two-letter code for site discoverer, and a field locality number using a two-digit annual number indicating the year of collection and a sequential site number (e.g., AF1404 is the fourth site found by A.F. in 2014 and DP1301 is the first site found by D.P. in 2013); when more than one quarry was collected at a locality, sites were given an additional letter to denote different quarries (e.g., AF1409D is the fourth quarry from the ninth site found by A.F. in 2014). All collected specimens are stored in the Carlisle Geology Research Building at Baylor University in Waco, Texas, USA.

Fossil leaves were collected using the bench and quarry method in which large blocks of matrix were split along leaf-bearing bedding planes (following Johnson 1989). Fossil leaf quarries covered ~5–10 m^2 of surface area and generally contained multiple, relatively thin (~5–25 cm) leaf-bearing horizons. At all leaf quarries, the sedimentological features of the site were recorded, and sites were assigned to sedimentary facies.

Voucher collections were made at all fossil localities. These voucher collections were selectively collected based on preservation. In addition to collecting the best-preserved specimens, when making voucher collections, we also collected at least one specimen from each known morphotype and all reasonably well-preserved unidentified plant fossils. Census collections were made at six of these localities, in addition to the voucher collection. During census collections, we quantitatively counted all identifiable plant material. At least 300 identifiable specimens were tallied in the field during census collections, because modern taphonomic studies have shown that ≥300 specimens are needed to accurately reflect floral composition (Burnham et al. 1992). During census collections, a new quarry adjacent to the voucher collection site was dug, and a new collection was made for the census. Representative samples and/or well-preserved samples from each identifiable morphotype and all unknown fossil material were

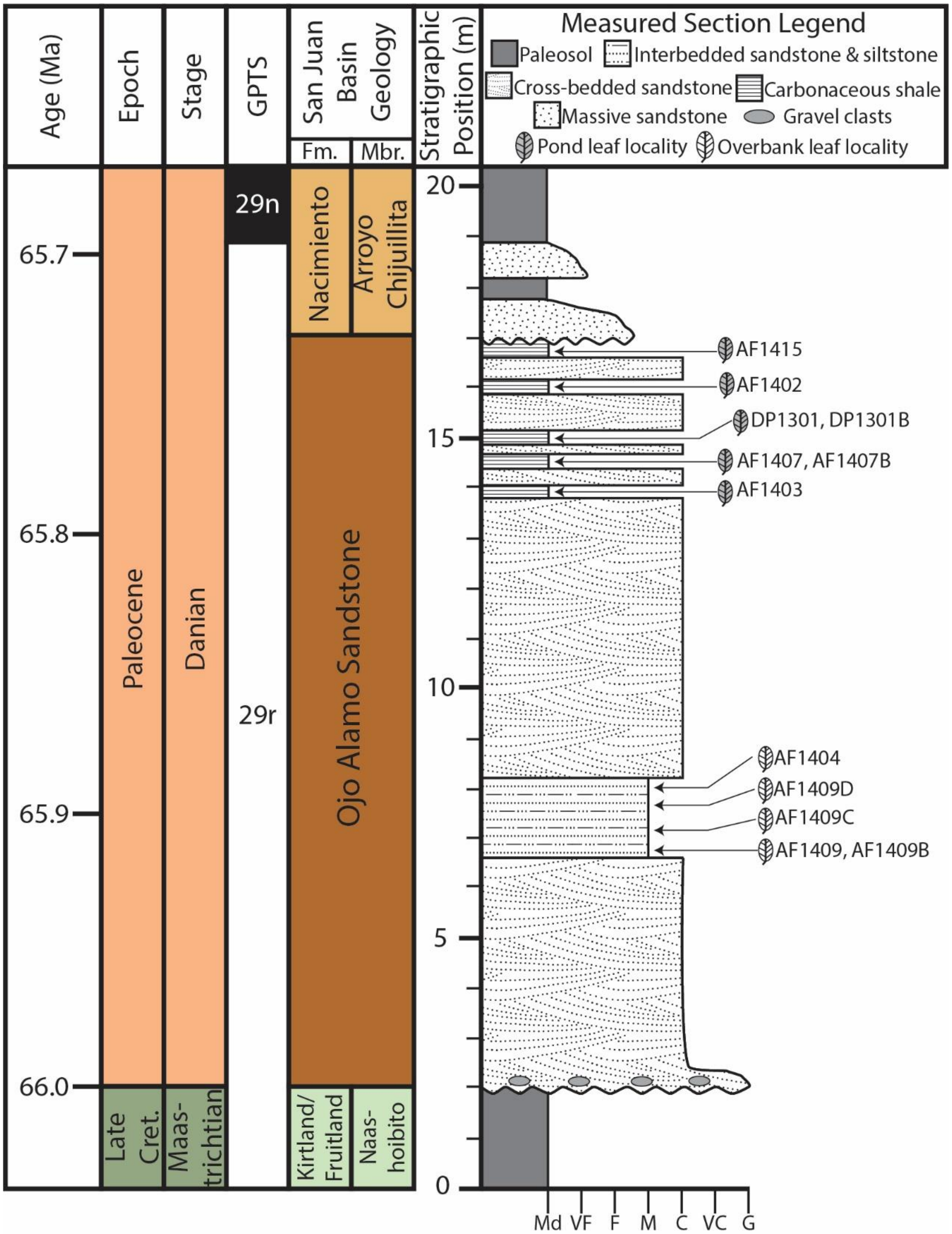

Figure 3.2. Generalized geochronology and measured section of latest Cretaceous Naashoibito Member and early Paleocene Ojo Alamo Sandstone and Nacimiento Formations. Age interpretations based on Mason (2013) and Peppe et al. (2013). North American Land Mammal Age (NALMA) and biozone (Pu1, Pu2) from Williamson (1996). The stratigraphic position and lithology of all fossil leaf–bearing horizons are shown.

collected. All collected specimens were given a unique site and specimen identification number (i.e., the sixth census morphotype from the site AF1404 census collection was labeled AF1404-C-006 with the “-C” denoting census collections from sites with voucher collections). After collection, all samples were wrapped in toilet paper, labeled, and shipped to Baylor University for additional analyses.

Fossil leaves are common in the Ojo Alamo Sandstone and were collected from two distinct lithologies, which we have interpreted as different depositional environments. The first fossil leaf–bearing lithology is interbedded medium- to fine-grained sandstone and siltstone beds. The interbeds generally dip at relatively low angles and pinch out laterally. Sedimentary structures, such as ripples and small-scale cross-bedding, occasionally occur. Well-preserved fossil leaves are common in the fine-grained interbeds and rare in the coarser-grained sandstone beds. Based on the physical characteristics, we interpret these deposits to be downstream accretionary bar forms in a braided river system with the finer-grained siltstones representing periodic flooding over the predominantly sand bar forms (Powell 1973; Miall 2010). We classified five leaf localities collected from this sedimentary facies as “overbank facies” (42% of sites; Figs. 3.1C and 3.2).

The second fossil leaf–bearing lithology is very fine grained, thinly laminated, carbonaceous shale beds with locally abundant sulfur and jarosite. The carbonaceous shales are often preserved as lenticular deposits ~15–25 m across and ~1–4 m in thickness. The beds are flat lying, and no additional sedimentary structures were observed. Fossil leaves generally occur in very dense leaf mats in these beds. We interpret the carbonaceous shale deposits to be low-lying, abandoned channel fills that were off axis from the major source of deposition in the braided stream, allowing ponding of water and very-fine-grained sediments to be deposited (Miall 2010). These deposits are analogous to oxbow lakes in meandering fluvial systems (Miall 2010). We classified seven leaf localities from this sedimentary facies as “pond facies” (58% of sites; Figs. 3.1C and 3.2).

In the lab at Baylor University, we assigned all identifiable plant material to SJB–wide morphotypes (morphotypes denoted by the prefix SJ- and their morphotype number, e.g., SJ-13). Morphotypes are distinct floral morphologies within a flora with no formal taxonomic assignment but are presumed to represent biological species (for review of morphotyping method, see Ash et al. [1999], Peppe et al. [2008], and Ellis et al. [2009]). When possible, morphotypes were also assigned to previously described Linnaean taxa for comparison to previously published collections (Table D.1). The majority of morphotypes from the Ojo Alamo Sandstone represent apparently previously undescribed species and are presumed to represent endemic taxa. Non-monocotyledonous angiosperm morphotypes (which will be referred to as dicotyledonous angiosperms or dicots for the remainder of the text following common convention) were described using the *Manual of Leaf Architecture* (Ellis et al. 2009). All other plant groups were described based on their morphology and distinctive traits. Brief descriptions and illustrations of all morphotypes are included in the Appendices, and a systematic list of morphotypes with their inferred taxonomy and species names is included in Table D.1.

Floral Diversity

The SJB megafloral diversity and composition were independently analyzed. These analyses were then compared with age-equivalent sites (i.e., early Paleocene localities within magnetic C29r) from the DB of central Colorado (Barclay et al. 2003) and the WB of western North Dakota and eastern Montana (Wilf and Johnson 2004; Peppe 2010) (Fig. 3.1A). These contemporaneous localities provided a tightly constrained interval spanning ~350 kyr after the K/Pg boundary (Ogg 2012). The geographic extent of collections made in the SJB (~5 km^2) is similar to the collection area in the DB (~1.5 km^2; Barclay et al. 2003). However, the WB material was collected over an area >100 km^2 (Wilf and Johnson 2004; Peppe 2010), which may have affected the diversity results of the WB when compared with the SJB and DB.

All diversity analyses were performed using the paleontological statistical program PAST 3.0 (Hammer et al. 2001). Rarefaction analyses were conducted on the six megafloral quantitative collections in the SJB, and all quantitative collections from sites within C29r in the DB and WB (Barclay et al. 2003; Wilf and Johnson 2004; Peppe 2010) using all vegetative (i.e., nonreproductive) morphotypes. Diversity analyses were performed using only vegetative morphotypes due uncertainty of taxonomic placement of reproductive organs and the possibility of double counting morphotypes. Rarefaction analyses for only dicot angiosperm leaves were also conducted for the quantitatively collected localities from the SJB, DB, and WB with ≥200 dicotyledonous angiosperm samples. Total basin rarefaction analyses, in which all census data from each basin were combined, were also calculated for all plant groups and only dicot angiosperms from the SJB, DB, and WB. Ecological diversity indices were calculated using the same quantitatively collected localities from the SJB, DB, and WB to compare the species richness, evenness, and dominance of the different floras. The differences in floral species richness was estimated using the Margalef diversity index (D_{mg}) (Margalef 1958; Magurran 2004). Floral evenness was assessed using Pielou's evenness index (J') (Pielou 1969). Floral dominance was assessed using the Berger-Parker index (d) (Berger and Parker 1970). All diversity indices were bootstrapped (N = 10,000) to generate confidence for site and basin comparisons.

In addition to species richness and diversity analyses, the influence of depositional facies, floral heterogeneity, and similarity was analyzed using the six SJB census collections. Detrended correspondence analysis (DCA) was used to assess the influence of depositional facies (i.e., landscape position) on floral composition. Cluster analysis was also performed using the Raup-Crick similarity index (Raup and Crick 1979) to identify groupings of localities with all analyses bootstrapped (N = 10,000). Floral heterogeneity between sites (i.e., β-diversity) was analyzed using the Bray-Curtis distance index (Bray and Curtis 1957) between all pairs of census localities. The total, within-facies, and between-facies results were then averaged to obtain total and facies-specific values of floral heterogeneity.

Paleoclimate and Paleoecology

Mean annual temperature (MAT) and mean annual precipitation (MAP) were reconstructed using leaf physiognomic methods. For the SJB material, digital leaf physiognomy (DiLP), a multivariate paleoclimate model that uses the size and shape of fossil leaves, was used to estimate the MAT and MAP (Huff et al. 2003; Royer et al.

2005; Peppe et al. 2011). All nonaquatic woody dicot angiosperm leaves were measured using the protocols of Peppe et al. (2011) and Royer et al. (2005), which are briefly summarized here (see Fig. E.2 for examples). Fossil leaf specimens were digitally extracted from the rock matrix using Adobe Photoshop (Adobe Systems, San Jose, CA). The leaf size was then reconstructed for sufficiently well-preserved specimens, and the inferred blade area, inferred major axis length, and inferred Feret's diameter were calculated for each specimen in this subset of fossil leaves. For any morphotypes with an entire margin (i.e., lacking leaf margin teeth) for which leaf size could not be reconstructed, only the margin state was recorded. Fragmentary toothed leaves were included if two or more consecutive teeth and at least 25% of the leaf area and margin were preserved. For fragmentary specimens, the damaged margin was removed and only the total number of teeth, undamaged perimeter length, and undamaged leaf area were recorded. For toothed leaves too fragmentary to measure for DiLP, only the margin state was scored.

Leaf margin analysis (LMA) (e.g., Wilf 1997; Miller et al. 2006; Peppe et al. 2018) and leaf area analysis (LAA) (e.g., Wilf et al. 1998; Peppe et al. 2018) were used to estimate MAT and MAP, respectively, for the SJB, DB, and WB to facilitate regional paleoclimate comparisons. LMA is a univariate climate model that uses the presence or absence of toothed woody dicot angiosperm leaves to estimate MAT (Wilf 1997; Miller et al. 2006; Peppe et al. 2018). The standard error for the LMA MAT estimate was calculated using the uncertainty equation of Miller et al. (2006). LAA is a univariate climate model that uses the average leaf size of a flora to estimate MAP (Wilf et al. 1998; Peppe et al. 2018). Each morphotype was scored to a Raunkiaer-Webb leaf size class

(Webb 1959) to estimate leaf area. Site mean leaf area was calculated using the methods of Wilf et al. (1998).

Leaf mass per area (M_a) is a proxy for leaf life span (Wright et al. 2004; Royer et al. 2007, 2010; Riva et al. 2016), and the M_a threshold between deciduous and evergreen taxa is ~129 g m^{-2} (Wright et al. 2004; Royer et al. 2007, 2010). The M_a of fossil leaves was estimated following the methods of Royer et al. (2007) using the relationship between petiole width (PW) and leaf area (A) to M_a.

Results

San Juan Basin Floral Description

Megafloral collections from the SJB yielded 55 morphotypes: 5 pteridophytes (9.43% of the morphotypes), 1 lycophyte (1.89% of morphotypes), 2 conifers (3.77%), 7 monocotyledonous (monocot) angiosperms (13.21%), and 38 dicot angiosperms (71.70%) (Table 3.1). The 6 census collections produced 2939 specimens composed of 4.86% pteridophytes, 0.71% lycophytes, 3.27% conifers, 4.83% monocots, and 86.33% dicots (Table 3.1). The majority of the morphotypes have not been previously described (69.81%) and may represent taxa endemic to the SJB during the early Paleocene (Table D.1).

San Juan Basin Floral Diversity

The average site rarefied richness from the six Ojo Alamo census localities was 12.99 ± 0.86 morphotypes (downsampled to 300 specimens per locality; Fig. 3.3, Table

F.1). With the exception of site AF1402, the site rarefaction curves were not asymptotic, indicating that total species richness at most sites has not been fully

Table 3.1 – Ojo Alamo Sandstone floral composition

Higher taxon or organ		Morphotypes	Specimens	% Morphotypes	% Specimens
Pteridophytes					
	Leaves	4	142	7.55	4.83
	Reproductive structures	1	1	1.89	0.03
Lycophytes		1	21	1.89	0.71
Conifers		2	96	3.77	3.27
Monocotyledonous angiosperms					
	Leaves	6	141	11.32	4.80
	Reproductive structures	1	1	1.89	0.03
Dicotyledonous angiosperms					
	Leaves	35	2533	66.04	86.19
	Reproductive structures	3	4	5.66	0.14
Total		53	2939		

sampled (Fig. 3.3) (Foote 1992; Hammer et al. 2001). The rarefied richness for the entire Ojo Alamo flora was 34.52 ± 2.17 morphotypes (downsampled to 1000 specimens), Table F.1), and the rarefied richness for only dicot leaves was 21.79 ± 1.90 morphotypes (downsampled to 900 specimens).

There was a strong facies effect on floral composition and diversity within the SJB flora. The pond and overbank floras had a similar number of total morphotypes, 28 and 32 morphotypes, respectively (Table 3.2). However, the taxonomic composition of the floras from each facies is notably different. Floras from both facies share 12 morphotypes despite being located within a relatively small geographic area (~5 km^2; Fig. 3.1). DCA indicated that composition and relative abundance of morphotypes was considerably

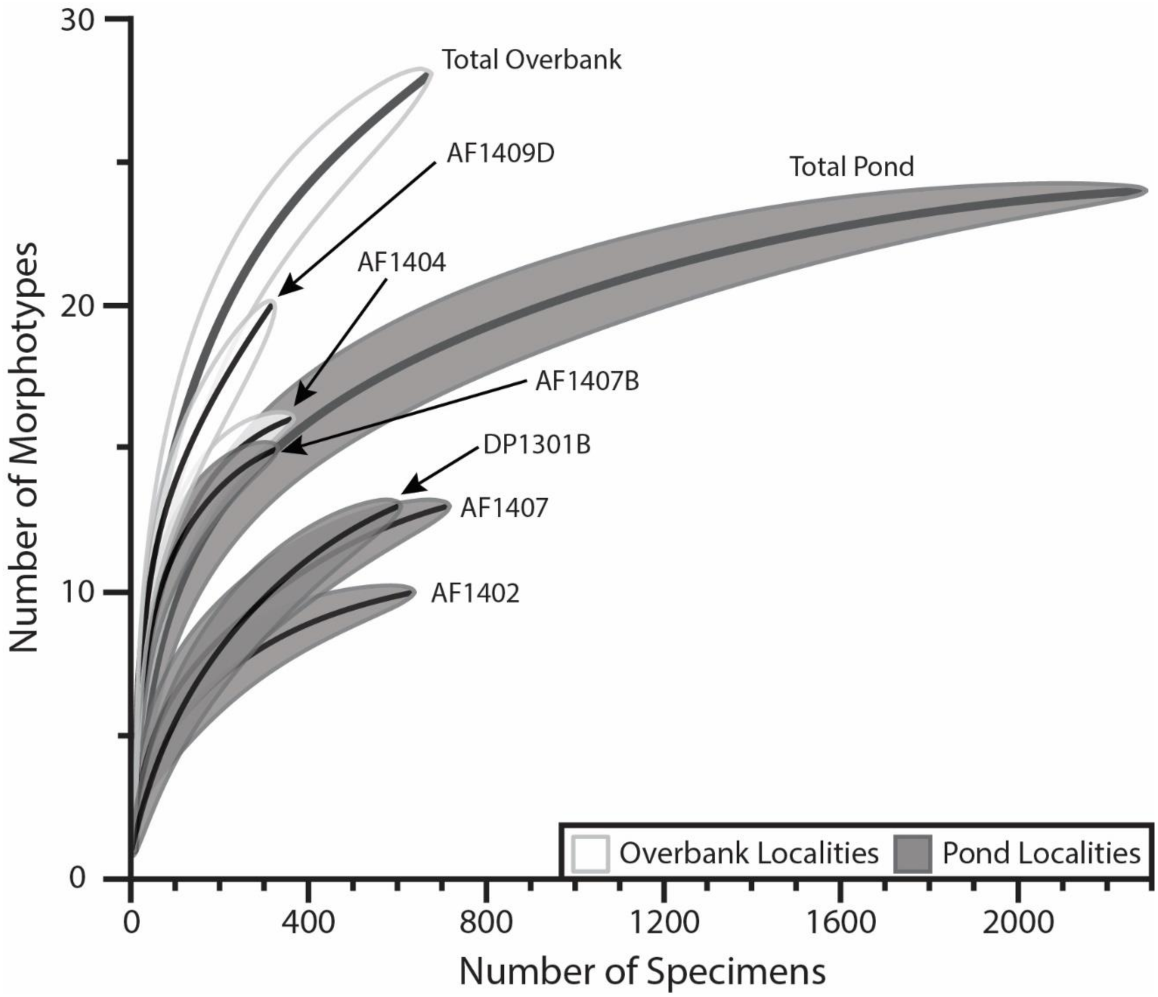

Figure 3.3. Rarefaction curves using all identified vegetative plant organs from the six census localities in the early Paleocene Ojo Alamo Sandstone; envelopes indicate 95% confidence intervals. Dark gray curves indicate pond localities and light gray curves indicate overbank localities. Overbank localities have greater rarefied richness at both the site and study area scales, indicating facies effect on floral species richness.

Table 3.2 – Comparison of total # of morphotypes, # of specimens, Margalef's Diversity Index (D_{mg}) (Margalef 1958), Pielou's Evenness Index (J') (Pielou 1969), and Berger-Parker Dominance Index (d) (Berger and Parker 1970) for each floral facies and total flora. The pond flora had fewer morphotypes, lower diversity and evenness compared to the overbank flora. Additionally, the pond flora was more strongly dominated by the most common morphotype. Error indicates 95% confidence interval for estimates.

Facies	# of Morphotypes	# of Specimens	Margalef's Diversity Index (D_{mg})	Pielou's Evenness (J')	Berger-Parker Dominance (d)
Total	53	2941	5.386	0.4488 ± 0.0164	0.6282 ± 0.0176
Pond	27	2275	2.976	0.3327 ± 0.0200	0.7755 ± 0.0174
Overbank	31	666	4.157	0.6985 ± 0.0287	0.1858 ± 0.0219

different between the pond and overbank facies (Fig. 3.4A). Raup-Crick cluster analysis resulted in two major clusters corresponding to the overbank and pond localities (Fig. 3.4B), and the clustering of overbank and pond localities into separate groups occurred 100% of the time, indicating the difference in floral composition between facies is highly significant. Cluster analysis also indicated that overbank localities were less similar to each other than the pond localities, with the two overbank localities having a 0.25 similarity index, while the four pond localities had a similarity index >0.9 (Fig. 3.4B). The overall mean Bray-Curtis distance between localities was 0.278, indicating considerable compositional differences between the censused floras (Table 3.3). The average Bray-Curtis distance was 0.571 between pond localities and 0.396 between overbank localities, indicating that the pond localities were more similar to one another than the overbank localities. Additionally, the mean Bray-Curtis distance was 0.154 between facies and 0.588 within facies. These results are statistically significant (t = 4.312, p = 0.008, df = 13), indicating that the β-diversity between different facies was

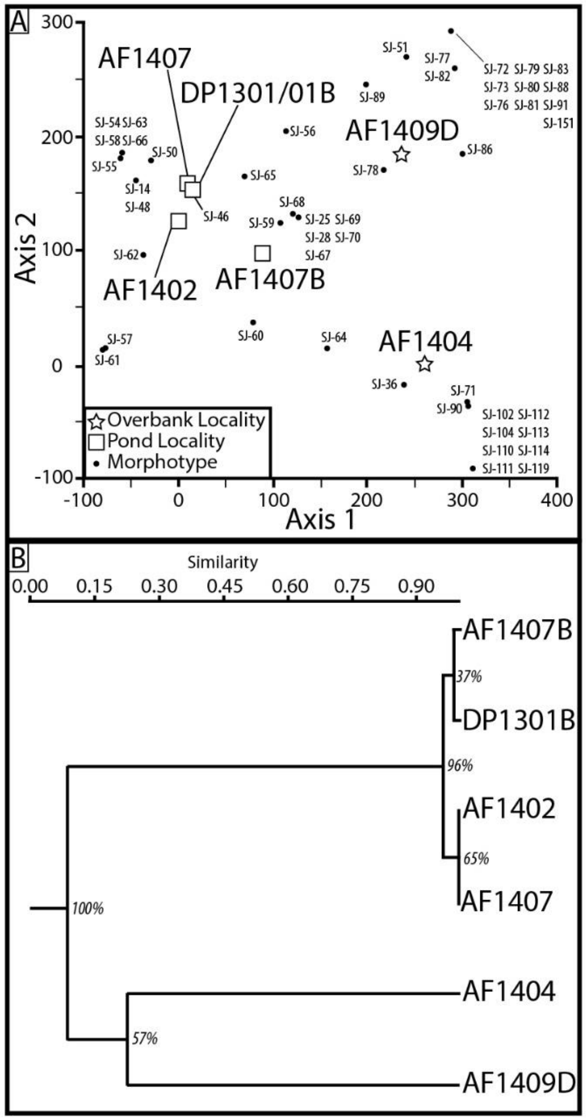

Figure 3.4. A, Detrended correspondence analysis scatter plot of all San Juan Basin (SJB) census localities and morphotypes (axis 1 eigenvalue = 0.7338; axis 2 eigenvalue = 0.1302). Localities clustered by their floral facies with the pond floras located on the left side of the plot and the overbank facies in the upper right. There was a closer relationship between morphotypes found in individual overbank facies localities compared with pond facies localities. B, Dendrogram of six SJB census localities showing two major clusters of localities (Cohen correlation = 0.9702). Dendrogram generated using the Raup-Crick index (Raup and Crick 1979). Localities clustered together based on their depositional facies. Percentages at each branching point indicate percentage of 10,000 iterations in which that branching point appeared. In 100% of runs, the two overbank and four pond localities formed separate clusters.

Table 3.3 - Bray-Curtis Index of Similarity: Beta Diversity Proxy. Mean distance – 0.278. Within facies (0.588) is greater than between facies (0.154) and is statistically significant ($t = 4.312$, $df = 13$, $p = 0.0008$). Average between pond localities (0.571) is greater than average between overbank localities (0.396) indicating pond facies had more similar floral composition.

	DP1301/01B	AF1402	AF1404	AF1407	AF1407B	AF1409D
DP1301/01B	---					
AF1402	0.788	---				
AF1404	0.090	0.069	---			
AF1407	0.883	0.721	0.081	---		
AF1407B	0.350	0.366	0.292	0.316	---	
AF1409D	0.158	0.126	0.396	0.133	0.279	---

significantly greater than within facies. The diversity and species richness of the pond and overbank floras were also significantly different. When all plant groups were included, the overbank flora had a greater site-based rarefied richness at 300 specimens than the pond flora (17.70 ± 0.51 morphotypes [$n = 2$] for the overbank vs. 10.63 ± 1.04 morphotypes [$n = 4$] for the pond; Fig. 3.4). Further, when all sites from each facies were combined, the overbank flora had significantly greater rarefied richness than the pond flora (Fig. 3.4). The total overbank flora also had a significantly greater D_{mg} value than the total pond flora (overbank flora: 4.157; pond flora: 2.976), indicating greater species richness (Table 3.2). The overbank flora was also significantly more even (overbank J': 0.6985 ± 0.0287; pond J': 0.3327 ± 0.0200) and less dominated by the most common morphotype than the pond flora (overbank d: 0.1858 ± 0.0219; pond d: 0.7755 ± 0.0174) (Table 3.2). Taken together, these results demonstrate that the overbank floras and pond floras are taxonomically distinct, and the overbank floras are more diverse and species rich than the pond floras.

San Juan Basin Paleoclimate and Paleoecology

The estimated MAT using DiLP with all measurable dicot angiosperm morphotypes from the Ojo Alamo Sandstone was 27.4 ± 4.0°C (*n* = 30 morphotypes) and using LMA it was 23.5 ± 2.5°C (*n* = 33 morphotypes) (Table 3.4, Table E.1). The estimated MAP using DiLP for the Ojo Alamo Sandstone was 154.4 cm/yr (+126.9/−69.6cm/yr, *n* =30 morphotypes), and using LAA it was 192.8 cm/yr (+83.3/−58.2cm/yr, *n* = 33 morphotypes) (Table 3.4). DiLP is likely underestimating MAP, because large fossil leaves within our collection were often fragmentary and impossible to include in DiLP analysis (see further discussion of this general point in Peppe et al. [2018]). When leaf area estimate from LAA was used in the DiLP model, the MAP estimate was 201.0 cm/yr (+165.3/−90.7 cm/yr), which likely represents a more reasonable approximation of MAP.

Table 3.4 – San Juan Basin paleoclimate estimates using digital leaf physiognomy (DiLP) (Peppe et al. 2011), leaf margin analysis (LMA) (Miller et al. 2006), leaf area analysis (LAA) (Wilf et al. 1998), and leaf mass per area (M_a) (Royer et al. 2007) for the total flora and each floral facies. Error indicates 95% confidence intervals for each estimate.

Site/Facies	DiLP MAT (°C)	LMA MAT (°C)	DiLP MAP (cm/yr)	LAA MAP (cm/yr)	M_a (g/m^2)
Total Ojo Alamo	27.4 ± 4.0	24.3 ± 2.3	154.4 +126.9/-69.6	192.8 +83.3/-58.2	78.1 +113.9/-55.2
Pond Flora	23.6 ± 4.0	24.5 ± 2.8	156.3 +128.5/-70.5	142.3 +61.5/-42.9	74.5 +107.5/-51.6
Overbank Flora	27.3 ± 4.0	22.4 ± 3.0	174.3 +143.3/-78.6	243.0 +104.9/-73.3	79.3 +113.4/-55.5

To assess the effect of facies on paleoclimate estimates, the DiLP MAT and MAP were calculated separately for the overbank and pond floras. The two different data sets used to calculate these estimates had very little overlap in their morphotype composition (Table E.1), yet their paleoclimate estimates were similar and overlap within uncertainty. The MAT estimated using DiLP was 23.6 ± 4.0°C for the pond flora and 27.3 ± 4.0°C for the overbank flora (Table 3.4, Table E.1). The MAP estimated using DiLP was 156.3 cm/yr (+128.5/−70.5 cm/yr) for the pond flora and 174.3 cm/yr (+143.3/−78.6 cm/yr) for the overbank flora (Table 3.4, Table E.1). These similar estimates for MAT and MAP for the overbank and pond facies indicate that despite differences in the taxonomic composition, there is no obvious facies effect with respect to paleoclimate estimates.

The M_a estimate for the total Ojo Alamo Sandstone was 78.1 g/m^2 (+113.9/−55.2 g/m^2, n = 11 morphotypes; Table 3.4), and only one morphotype had an M_a greater than 129 g/m^2. These results demonstrate that the majority of Ojo Alamo morphotypes had a leaf life span <12 months and were deciduous (Wright et al. 2004; Royer et al. 2007). This distribution of M_a is most similar to the distribution found in riparian habitats in temperate rain forests and tropical seasonal forests (Fig. 3.5).

Regional Floral Diversity and Paleoclimate

All species richness indices indicate that the SJB had a higher species richness than contemporaneous floras in the NGP. The SJB flora had greater species richness (n = 55 morphotypes) than contemporaneous floras from the DB (n = 49 morphotypes [Barclay et al. 2003]) and the WB (n = 33 morphotypes [Wilf and Johnson 2004]; n = 24 morphotypes [Peppe 2010]) (Table F.1). The mean site rarefied richness at 300

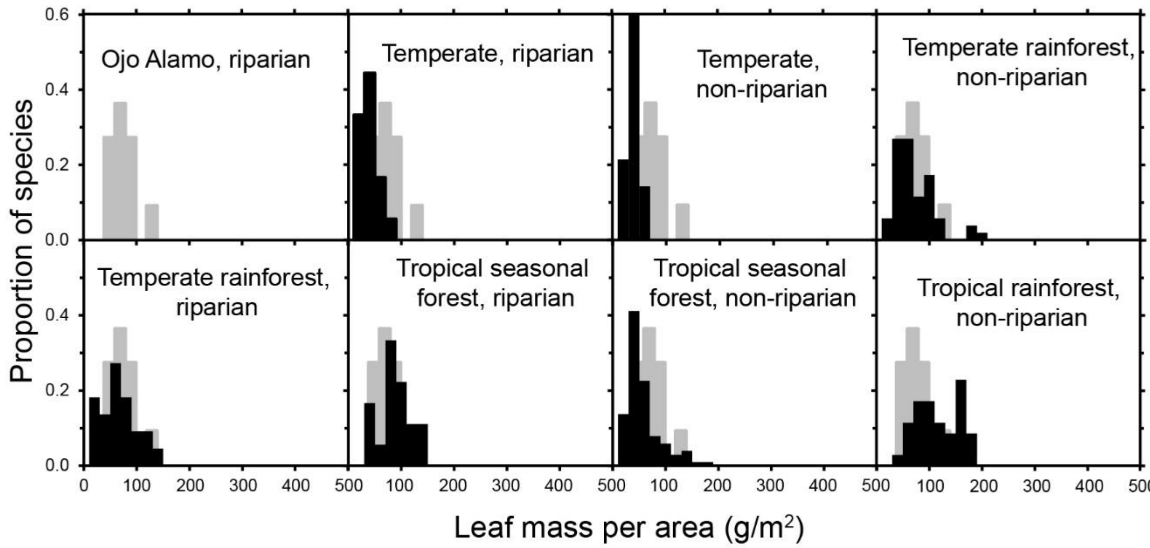

Figure 3.5. Comparison of Ojo Alamo Sandstone floral leaf mass per area distribution with representative modern sites with different biomes/environments (modern biome data from Peppe et al. 2011). The leaf mass per area distribution of the SJB flora is most similar to riparian tropical seasonal forests, in agreement with the paleoclimate estimates, which indicate a tropical seasonal forest.

specimens from the SJB (12.99 ± 0.86) was greater than what has been reported for the DB (11.50 ± 0.58 [Barclay et al. 2003]) and the WB (7.64 ± 0.73 [Wilf and Johnson 2004];11.06 ± 0.59 [Peppe 2010]), indicating greater α-diversity in the SJB than in floras from the NGP (Fig. 3.6A, Table F.1). The basin-wide rarefied richness downsampled to 1000 specimens was also greater in the SJB (34.52 ± 2.17) than what has been reported for the DB (22.53 ± 1.30 [Barclay et al. 2003]) and the WB (20.52 ± 1.47 [Wilf and Johnson 2004]; 18.95 ± 0.20 [Peppe 2010]) (Fig. 3.6C, Table F.1). The difference in both site and basin-wide rarefied richness is smaller, but still distinct, when using only dicot angiosperm leaves (Fig. 3.6B–D), because the SJB flora had a higher proportion of non-angiosperm morphotypes, in particular pteridophytes, when compared with the DB and

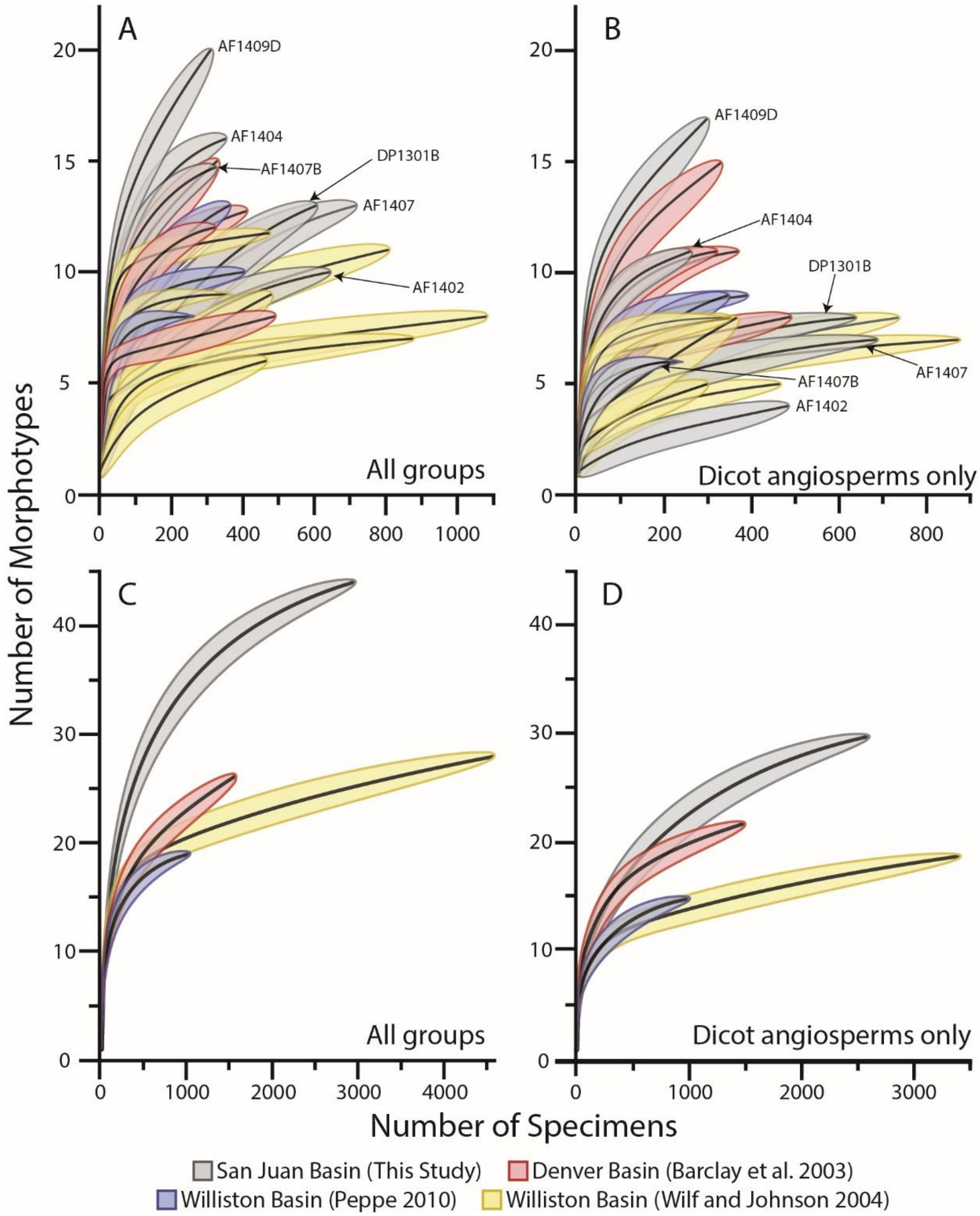

Figure 3.6. Regional rarefaction comparison between the San Juan Basin (SJB) (this study), the Denver Basin (DB) (Barclay et al. 2003), and the Williston Basin (WB) (Wilf and Johnson 2004; Peppe 2010) using plant vegetative organs with envelopes indicating 95% confidence intervals. A, All census localities using all groups; B, all census localities using dicot angiosperms only; C, basin-wide using all groups; and D, basin-wide using only dicot angiosperms. At both the site and basin-wide levels, the SJB flora has greater rarefied richness than the DB and WB floras, but the difference is smaller when only dicot angiosperms are included, due to the high diversity and abundance of non-dicot angiosperm taxa in the SJB flora.

WB floras. The D_{mg} for the SJB (5.386) was greater than what has been reported for the DB (3.268 [Barclay et al. 2003]) and the WB (3.205 [Wilf and Johnson 2004]; 2.596 [Peppe 2010]), indicating greater species richness, similar to the pattern observed from the rarefaction analysis (Fig. 3.7A, Table F.1). The differences between the SJB and the DB and WB were significant (p = 0.0027 to <0.0001), but there was no significant difference between the DB and WB (p = 0.9509 to 0.2217) (Table F.2A).

Diversity indices indicate that while the SJB floras had higher species richness than contemporaneous floras, it was less even and more dominated by the most common morphotype than floras from the DB and the WB. The J' value for the SJB (0.4488 ± 0.0164) was lower than what has been reported for the DB (0.6583 ± 0.0139 [Barclay et al. 2003]) and the WB (0.6425 ± 0.0089 [Wilf and Johnson 2004]; 0.6746 ± 0.0205 [Peppe 2010]), indicating the SJB flora is less even (Fig. 3.7B, Table F.1). This difference was significant (p < 0.0001) when the J' permutations from the SJB were compared to those of the DB and WB, but there was no significant difference between the DB and WB (p = 0.8309 to 0.9974) (Table F.2B). Finally, the d value for the SJB (0.6282 ± 0.0176) was greater than what has been reported for the DB (0.2332 ± 0.0184 [Barclay 2003]) and WB (0.3167 ± 0.0136 [Wilf and Johnson 2004]; 0.2917 ± 0.0273 [Peppe 2010]), indicating the SJB flora was more strongly dominated by the most common morphotype (Fig. 3.7C, Table F.1). The difference in d values between the SJB and the DB and WB was significant when the permutations between the SJB and the other basins were calculated ($p \leq 0.0001$). Additionally, the d value of the DB flora was also significantly different than both WB floras ($p \leq 0.0001$), but there was no significant difference between both WB floras (p = 0.1031) (Table F.2C).

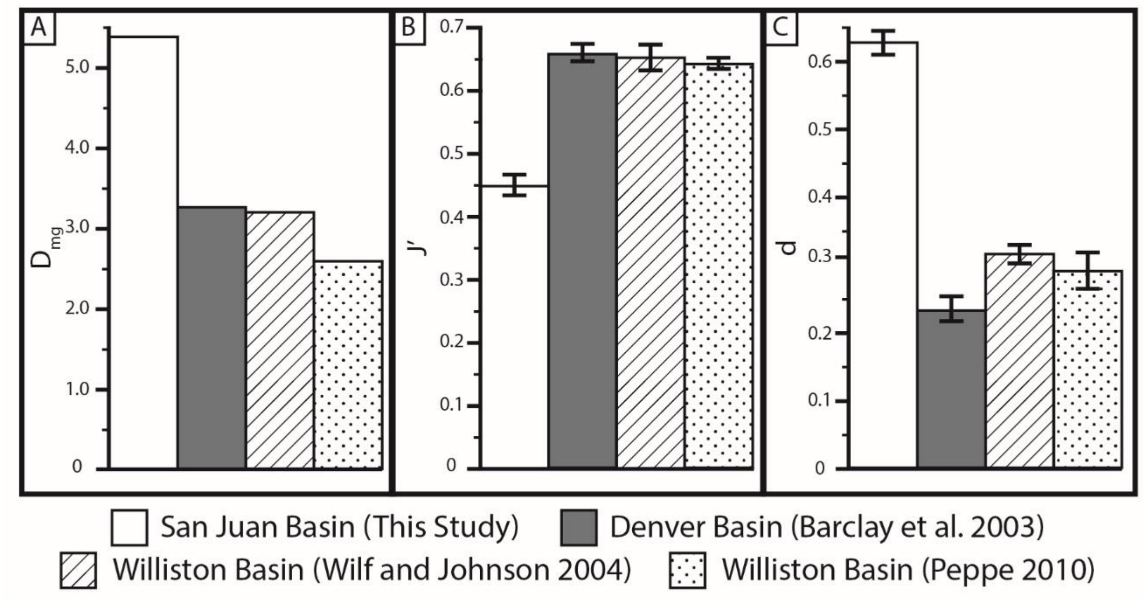

Figure 3.7. Diversity comparison between the San Juan Basin (SJB) (this study), Denver Basin (DB) (Barclay et al. 2003), and Williston Basin (WB) (Wilf and Johnson 2004; Peppe 2010). A, Margalef's index (D_{mg}), B, Pielou's evenness (J'), and C, Berger-Parker index (d). The SJB D_{mg} value for the SJB flora was significantly higher than for both the DB and WB floras, indicating greater species richness. The J' value was significantly lower and the *d* value was significantly greater for the SJB compared with the DB and WB, indicating the SJB flora was significantly less even and more heavily dominated by the most common taxa. Bars indicate 95% confidence intervals. For absolute values and pairwise comparisons, see Table F.1-F.2.

Paleoclimate estimates therefore indicate that then SJB was warmer and wetter than the DB and WB. MAT estimates using LMA for the SJB are >6°C warmer than estimates for the DB and >14°C warmer than those for the WB (Table 3.5, Fig. 3.8). The estimated MAP using LAA from the SJB is >35 cm/yr wetter than MAP estimates for the DB and WB, though these differences are within the uncertainty of the estimates (Table 3.5, Fig. 3.8).

In addition to these LMA and LAA paleoclimate estimates, there are estimates for MAT and MAP from the WB using DiLP (Peppe et al. 2011) that can be compared with the ones for the SJB flora. There are no DiLP MAT or MAP estimates for the DB. MAT using DiLP is 27.4 ± 4.0°C for the SJB and 15.7 ± 4.0°C for the WB (Peppe et al. 2011), considerably warmer than LMA estimates for the same floras (3.1°C and 5.5°C warmer for the SJB and the WB, respectively). The large difference in MAT between DiLP and LMA is probably related to the freshwater margin effect, wherein toothed leaves are more common in environments with seasonal water availability because leaf teeth allow for more rapid leaf growth (Peppe et al. 2011), which can cause LMA to underestimate MAT. Thus, we interpret the DiLP MAT estimates to be a more accurate reconstruction of climate. However, the magnitude of difference in MAT between the SJB and WB is similar using LMA and DiLP (14.1°C and 11.7°C, respectively), suggesting that the magnitude of differences in LMA MAT estimates between the basins are reasonable. The DiLP estimated MAP for the SJB (154.4 cm/yr +126.9/−69.6 cm/yr) is lower than estimates for the WB (175.0 cm/yr +144.0/−79.0 cm/yr [Peppe et al. 2011]). However, as discussed earlier the DiLP MAP estimates are probably too low, and when the average leaf size from LAA is used in DiLP, the MAP estimates for the SJB are >25 cm wetter than those for the WB. The MAP estimates using LAA and DiLP for the SJB and WB overlap within uncertainty, suggesting that both are reasonable approximations of MAP.

Table 5 – Comparison of San Juan Basin (this study), Denver Basin (Barclay et al. 2003), and Williston Basin (Peppe 2010) MAT estimates using leaf margin analysis (Miller et al. 2006) and MAP using leaf area analysis (Wilf et al. 1998). Error indicates 95% confidence interval.

Basin	MAT (°C)	MAP (cm/yr)
San Juan	24.3 ± 2.3	192.8 +83.3/-58.2
Denver	17.6 ± 3.0	155.0 +66.9/-46.8
Williston	10.2 ± 4.0	154.4 +66.7/-46.6

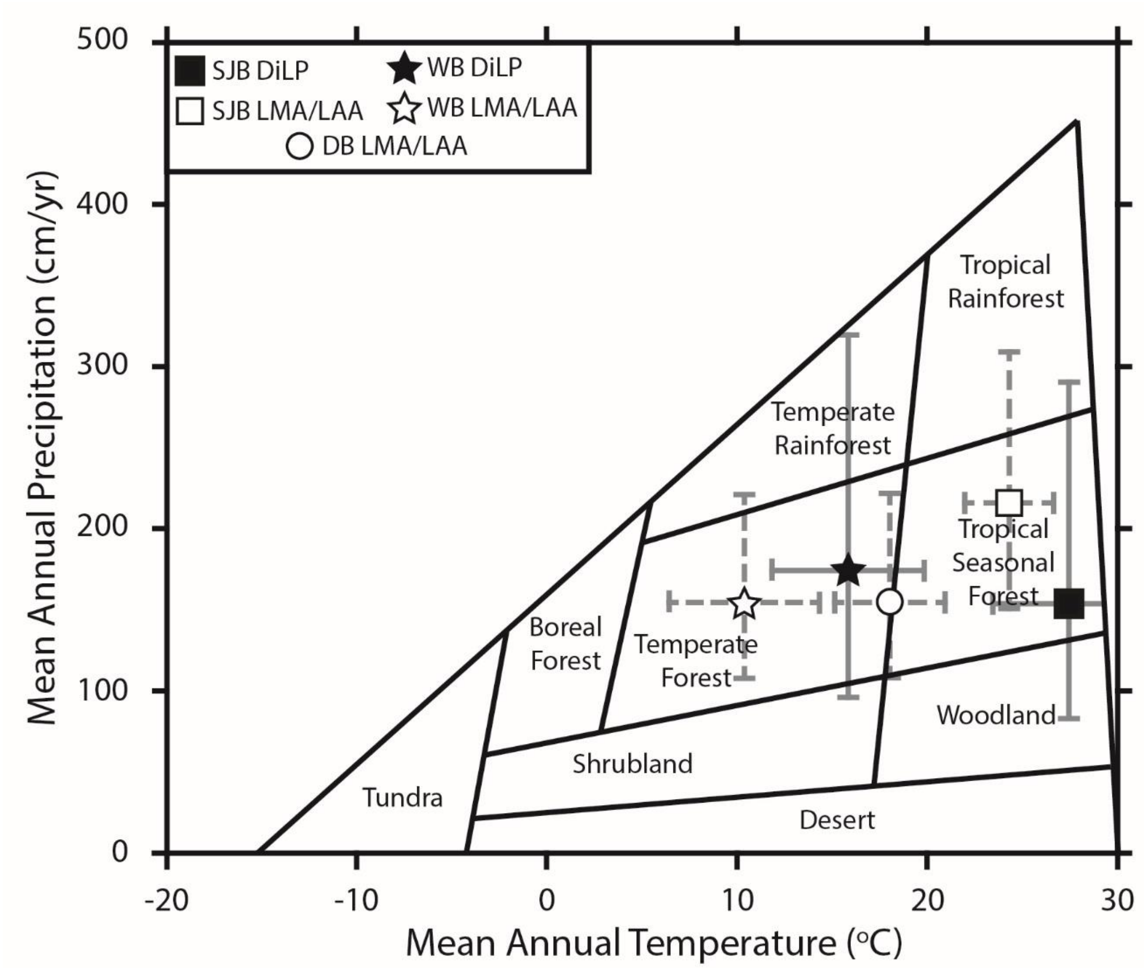

Figure 3.8. Modern ecosystem plots with paleoclimate variables. The San Juan Basin (SJB) flora corresponded with modern tropical seasonal forests using both digital leaf physiognomy (DiLP) and leaf margin analysis (LMA) + leaf area analysis (LAA). Both the Denver Basin (DB) and Williston Basin (WB) corresponded with warm and cool temperate forests, respectively, indicating the SJB represents a different biome than previously studied localities. The 95% confidence intervals for all paleoclimate estimates are shown by gray bars.

Discussion

San Juan Basin Flora

San Juan Basin Floral Composition. The early Paleocene SJB flora is dominated by dicot angiosperms, which account for 66.04% of morphotypes and 86.19% of specimens collected during censuses (Table 3.1), similar to observed patterns in early Paleocene floras from across North America (e.g., Brown 1962; Barclay et al. 2003; Dunn 2003; Wilf and Johnson 2004; Peppe 2010). The majority of dicot angiosperm leaves were interpreted to be woody plants (i.e., trees or shrubs; 94.24%) consistent with modern taphonomic studies (Ellis and Johnson 2013). Interestingly, pteridophytes are relatively common (9.09% of morphotypes and 4.86% of specimens; Table 3.1) and conifers are relatively rare (3.64% of morphotypes and 3.26 % of specimens; Table 3.1), which is a different pattern than observed in contemporaneous floras from the NGP (i.e., Barclay et al. 2003; Wilf and Johnson 2004; Peppe 2010; Table 3.1).

Landscape Floral Heterogeneity. There is significant facies effect on the Ojo Alamo floral composition and diversity (Figs. 3.3 – 3.4, Tables 3.2 – 3.3). Our interpretation for the depositional facies (pond vs. overbank) is based on the sedimentological features of the sites and is qualitatively supported by the floral composition of each facies. For example, the pond flora is more strongly dominated by non-angiosperm morphotypes than the overbank facies. The modern nearest living relatives of the majority of these non-angiosperm morphotypes, such as the ferns *Onoclea sensibilis* (SJ-56) and the cupressaceous conifer *Cupressinocladus interruptus* (SJ-68), are commonly found in water-saturated environments such as ponds and/or swamps (e.g., Mehltreter et al. 2010; Pittermann et al. 2012). In comparison, the overbank facies is more strongly dominated by dicot angiosperms and the modern relatives of common overbank morphotypes such as *Platanites marginata* (SJ-71) and *Browneia serrata* (SJ-78) that commonly inhabit disturbed lake and streamside environments (Stromberg 2001; Manchester and Hickey 2007), as would be expected in downstream and lateral bar forms in a braided stream.

The strong facies effect on diversity could be explained by taphonomic differences between the facies or lateral heterogeneity in the floral communities between the environments. If taphonomy caused the observed facies effect, we would expect the overbank facies to have higher species richness than the pond facies due to a larger catchment area "collecting" multiple depositional environments (Ellis and Johnson 2013). Additionally, we would expect that because the overbank facies incorporated morphotypes from other facies, paleoclimate estimates between facies might differ due to the incorporation of allochthonous morphotypes. However, while the overbank facies did have higher species richness than the pond facies (Table 3.2), the two facies shared relatively few morphotypes. Only 12 morphotypes (22.64%) are found in both the pond and overbank facies, and the majority of the shared morphotypes, such as *Platanites raynoldsii* (SJ-36) and *Averrhoites affinis* (SJ-46), occur at the majority of SJB sites and also have widespread distributions throughout the Western Interior of North America during the early Paleocene (e.g., Johnson 2002; Barclay et al. 2003; Dunn 2003; Peppe 2010). Conversely, most facies-restricted morphotypes have only been identified in the SJB. Further, while the pond floras are relatively homogeneous, there is a large difference in species composition between the overbank sites, indicating a considerable variability in floral composition within the higher-disturbance overbank facies (Figs. 3.3A-B and 3.4). Within groups, the overbank localities were more dissimilar to each other than the pond localities (Table 3.3), which suggests considerable variability in the floral composition between overbank facies localities and between the pond and overbank facies. Conversely, two pond localities that were collected along a transect from the same carbonaceous shale deposits and are separated by the shortest geographical distance (AF1407 and AF1407B; Fig. 3.1C) have a relatively low Bray-Curtis similarity (0.316; Table 3.3), indicating the occurrence of spatial heterogeneity within the plant community even within the facies that is more likely to preserve relatively autochthonous flora. Anecdotally, the overbank deposits preserve many complete compound leaves of *P. raynoldsii* (SJ-36) and *P. marginata* (SJ-71), as well as many relatively complete branches of *C. interruptus* (SJ-68), which are delicate and are unlikely to have been preserved over long transport distances, suggesting the overbank deposits primarily sampled an autochthonous or parautochthonous flora. Thus, there is no evidence to suggest that the overbank facies sampled taxa from the pond facies. Finally, DiLP paleoclimate estimates for the two facies were nearly identical, which suggests both facies were sampling relatively autochthonous or parautochthonous floras (Table 3.4). Based on the differences in floral composition between the pond and overbank facies, differences between floras collected from the overbank facies, and the similar paleoclimate estimates between facies, it is unlikely that the facies effect that we document is the result of differences in taphonomy between the overbank and pond facies.

Instead, we interpret the facies effect to be the result of landscape heterogeneity in the Ojo Alamo Sandstone plant communities. This strong facies effect, in which the overbank floras have higher species richness and diversity than the pond floras, is best explained by the intermediate disturbance hypothesis, which predicts the highest species diversity occurs in areas of intermediate disturbance (Connell 1978). In tropical forest communities, disturbance creates holes in the canopy that allow a succession of plant species to colonize the newly available growing area, leading to greater species richness (e.g., Brokaw and Busing 2000; Molino 2001). The overbank flora was deposited in more active parts of the depositional system, and thus underwent more disturbance, which in turn likely resulted in greater floral diversity. The overbank facies had clear evidence of repeated depositional events, likely from flooding and high water, which would have regularly disturbed the landscape and likely killed some of the standing vegetation. The modern relatives of common SJB overbank flora species (e.g., *P. raynoldsii,* SJ-36) are commonly pioneer species (Stromberg 2001), supporting our hypothesis that episodic disturbance in these localities created canopy breaks that allowed colonization by pioneer species. In comparison, the lower-diversity pond flora was deposited in a restricted and less active area of the depositional system that encountered relatively little disturbance, which may have allowed a few species (i.e., *A. affinis*, SJ-46) to become dominant. The effect of disturbance on diversity is also highlighted by the pond flora being significantly less even and more dominated by a single morphotype when compared with the overbank flora (Table 3.2). These results indicate considerable landscape heterogeneity in the SJB flora and suggest that if a larger spatial area was collected, the species richness and diversity would likely increase.

Paleoclimate and Paleoecology. The Ojo Alamo Sandstone has been interpreted to represent a braided stream system on an alluvial plain subject to seasonal precipitation (Powell 1973; Fassett 1985; Sikkink 1987). Our MAT and MAP estimates indicate that the climate of the SJB flora is most similar to a tropical seasonal forest biome (Fig. 3.8), which is typified by environments with a pronounced dry season (Whittaker 1975), supporting the interpretation of seasonal precipitation. The M_a estimates for the Ojo Alamo Sandstone flora also suggest seasonal precipitation. Deciduous taxa are commonly found in disturbed environments and in environments with marked differences between seasons in rainfall and/or temperature (e.g., Whittaker 1975; Reich et al. 1992; Lavorel et al. 1997; Yoshifuji et al. 2006; Poorter et al. 2009). Further, in tropical forest ecosystems, the degree of deciduousness in plant communities is controlled by the amount of precipitation and the length and magnitude of the dry season (Condit et al. 2000; Pyke et al. 2001), and modern tropical forests dominated by deciduous species are marked by a long dry season with little to no precipitation and a short but intense wet season (Bullock and Solis-Magallanes 1990). The distributions of M_a for the Ojo Alamo flora indicate that it sampled a riparian temperate rain forest/tropical seasonal forest (Figs. 3.5 and 3.8), which also suggests that precipitation during the deposition of the Ojo Alamo Sandstone was seasonal with a pronounced dry season. This interpretation is further supported by fossil wood anatomy from the early Paleocene SJB that exhibited variations in vessel density and diameter that may correspond with seasonal variations in precipitation (Wheeler et al. 1995). Taken together, the sedimentological and paleontological evidence from the Ojo Alamo indicates that it was deposited in a tropical seasonal forest biome with a considerable dry season.

Regional Patterns of Vegetation and Paleoclimate

Regional Patterns in Floral Composition. Previous research on early Paleocene floras from North America has suggested that they are relatively similar across the continent (e.g., Brown 1962; Johnson 2002; Johnson et al. 2003; Barclay et al. 2003; Peppe 2010) and are dominated by diagnostic "FU1 taxa" (sensu Johnson and Hickey 1990; Johnson 2002). In the SJB, the FU1 taxa *P. raynoldsii*, *B. serrata* (SJ-78), *"Populus" nebrascensis* (SJ-13), and *Paranymphaea crassfolia* (SJ-51) are present. However, the majority of FU1 taxa, such as the dicot angiosperms *Quereuxia angulata*, *Mciveraephyllum nebrascense*, and *Zizophoides flabella* and the taxodiaceous conifers *Glyptostrobus europaeus* and *Metasequoia occidentalis*, are absent. Further, with the exception of *P. raynoldsii* (SJ-36), the FU1 taxa present in the SJB are very rare, while accessory taxa from the NGP, such as *A. affinis* (SJ-46) and *Ditaxocladus catenulatus* (SJ-102), are common in the SJB. Further, *Gingko adiantoides*, which is also common in the NGP (Johnson 2002; Peppe 2010) is notably absent from the SJB flora. The SJB was likely too warm for *G. adiantoides* and the taxodiaceous conifers *M. occidentalis* and *G. europaeus*, as their nearest living relatives are primarily restricted to temperate climates in latitudes above ~35°N (e.g., Tralau 1967; Ziegler et al. 1996; Liu et al. 2007).

Though markedly different, the floral composition and relative abundance of morphotypes between the SJB and contemporaneous localities in the NGP have some similarities. For example, the most common SJB morphotype (*A. affinis*, SJ-46) is relatively uncommon or absent in floras from North Dakota and Montana (Johnson 2002; Peppe 2010) but is a common morphotype in the West Bijou Site from the DB (Barclay et al. 2003). Additionally, the most common morphotype found by Johnson (2002) in the

WB flora was *P. raynoldsii* (SJ-36), which is a common morphotype from the SJB, but relatively rare in the DB (Barclay et al. 2003). Conversely, the most abundant morphotype in the DB (*M. nebrascense*; Barclay et al. 2003) is also common in the WB (Peppe 2010), but absent in the SJB. This suggests some plant species had extensive ranges during the early Paleocene, while others, such as the most common constituents of the FU1 flora from the NGP, were restricted to more northern latitudes.

The greater diversity and abundance of pteridophyte morphotypes in the SJB were likely linked to the warmer and wetter climate compared to contemporaneous localities and the transition from temperate to tropical forests (Figs. 3.6B–D and 3.8, Table 3.5) (Barclay et al. 2003; Wilf and Johnson 2004; Peppe 2010). This suggests a latitudinal difference in pteridophyte diversity and abundance across North America in the early Paleocene. The greater abundance and diversity of pteridophytes may have been driven by higher rate of speciation in tropical ecosystems compared with temperate forests, a pattern that has been well documented in modern fern communities (Haufler et al. 2000). Additionally, the climate of the SJB was likely better suited to pteridophytes than the climate of the more northern basins (Mehltreter et al. 2010; Table 3.5). There is evidence that the SJB, in addition to being warmer and wetter than other basins, experienced seasonal precipitation (e.g., Wheeler et al. 1995; Davis et al. 2016). The modern relatives of the most common pteridophyte morphotype found in the SJB (SJ-57, cf. *Anemia*) are drought tolerant and are often found in seasonally dry and warm habitats (Tryon and Tryon 1982) similar to those predicted for the SJB based on the paleoclimate estimates. Additionally, fossil relatives of SJ-57 (cf. *Anemia*) from the Lower Cretaceous Crato Formation in Brazil have been interpreted to be ground cover in dry, sunny areas with adaptations to survive drought stress (Mohr et al. 2015). Taken together, the lack of many diagnostic FU1 flora species and the relatively high abundance of pteridophytes in the SJB flora suggest significant latitudinal variation in floral composition across western North America immediately following the K/Pg boundary.

Palynological work from the latest Cretaceous and earliest Paleocene (e.g., Frederiksen 1987; Nichols et al. 1990) also supports this latitudinal compositional gradient found in the megaflora. Frederiksen (1987) found different palynological floral provinces during the latest Cretaceous along the continental margin and the Western Interior. Interestingly, he found that the SJB palynological assemblage shared a higher percentage of palynomorphs with the continental margin than with other localities in the continental interior, suggesting that the SJB was composed of a different floral assemblage than other Western Interior basins. Using palynological collections from the earliest Paleocene, Nichols et al. (1990) found three pollen-based floral clusters that roughly correspond to the southern, mid-, and high latitudes of North America. The southern group, including the SJB and DB, had greater species richness and greater endemism than the mid- and northern groups, which include the WB (Nichols et al. 1990). A "southern" floristic province is also supported by fossil wood collections from Mexico, Texas, and New Mexico, which suggest that the vegetation across these areas was similar from the Campanian through the Paleocene (e.g., Wheeler et al. 1995; Lehman and Wheeler 2009). When combined, our megafloral analyses and the palynology and fossil wood record from the Late Cretaceous and early Paleocene all suggest latitudinal variation in floral compositions across North America and a marked difference in the SJB flora compared with floras in of the NGP of North America in the early Paleocene, and also possibly in the Late Cretaceous.

Regional Patterns of Floral Diversity. The species richness of the SJB flora is 10–55% higher than those of contemporaneous floras from North America (Table F.1). The SJB flora also has ~15–20% higher rarefied richness at the site level and ~35–40% higher rarefied richness at the basin-wide level (Table 3.5). The increased relative difference in rarefied richness at the basin-wide level is driven by the predominance of non-dicot angiosperm taxa and the large amount of lateral heterogeneity in the SJB (Fig. 3.6B–D, Table F.1). However, while the SJB flora was more species rich, it was significantly less even and more strongly dominated by common morphotypes than contemporaneous NGP floras (Fig. 3.7B-C, Table F.1). While the most common taxa make up between 21.54 and 33.19% of samples from the DB and WB, the most common taxa make up 62.67% of samples collected in the SJB (Table 3.5). The high richness but uneven flora runs counter to the hypothesis that the earliest Paleocene floras had low species richness and were relatively even (e.g., Hickey 1980; Johnson and Ellis 2002; Barclay et al. 2003; Wilf and Johnson 2004). This suggests notably different patterns in floral diversity across North America after the K/Pg extinction event, with the floras from the NGP being relatively even and homogeneous on the landscape, but low in species richness, while the floras from the SJB, and potentially other areas in southern North America, were uneven but species rich and very heterogeneous. These differences may have been driven by climate in the earliest Paleocene, in which the warm temperatures in southern North America allowed more rapid speciation following the K/Pg extinction event. Additionally, the latitudinal gradient in floral species richness in the early

Paleocene documented here is consistent with a relatively steep mammalian latitudinal diversity gradient in the early Paleocene (Marcot et al. 2016), suggesting that they may be related.

Interestingly, early Paleocene fossil floras from Patagonia (Iglesias et al. 2007; Comer et al. 2015) had species richness similar to the SJB floras (rarefied richness using only dicot angiosperm leaves downsampled to 2000 specimens: SJB = 28.28 ± 1.18 morphotypes; Salamanca Flora = 32.47 ± 0.67 morphotypes). The high species richness in Patagonia has been linked to lower rates of extinction than in North America and dispersal of refugia taxa following the K/Pg boundary (Donovan et al. 2016). Similar to the SJB flora, the early Paleocene megaflora from the Salamanca Formation in Argentina (64.67–63.49 Ma) had >50% more species than comparable North American localities (Iglesias et al. 2007). This suggests that the pattern in macrofloral diversity found in the SJB could be more similar to South American floras than to floras from the NGP in North America, but further work will need to be done to test this hypothesis.

Regional Patterns of Paleoclimate and Paleoecology. Paleoclimate estimates for the SJB, DB, and WB indicate that climate in the SJB was markedly warmer and somewhat wetter than contemporaneous basins in western North America (Table 3.5, Fig. 3.8). MAT in the SJB is reconstructed to be >6°C warmer than in the DB and >11°C warmer than in the WB (Table 3.5, Fig. 3.8), and the paleolatitudes of the SJB, DB, and WB were ~42°N, ~44°N, and ~51°N, respectively (reconstructed based on Torsvik et al. [2008]). This difference in MAT and the latitudinal differences between the sites implies that continental latitudinal temperature gradients across the Western Interior of North America were at least as steep in the early Paleocene as in the modern (e.g., North et al.

1981). Further, when compared with modern biomes (Whittaker 1975), the DB and WB climate estimates indicate a temperate deciduous forest biome, while the SJB is reconstructed as a tropical seasonal forest (Fig. 3.8). Today, tropical seasonal forests are primarily restricted to north and south latitudes <30° (Murphy and Lugo 1986; Mooney et al. 1995; Dupuy et al. 1999). Thus, the climate and ecosystem reconstructions for the SJB, DB, and WB indicate greater latitudinal expansion of tropical biomes and the transition between tropical and temperate forests in the earliest Paleocene compared with the present.

In modern ecosystems, there is a strong latitudinal diversity gradient, and tropical forests have higher α- and β-diversity than temperate forests (e.g., Givnish 1999; Phillips and Miller 2002; Leigh et al. 2004; Kraft et al. 2011; Brown 2014). In our comparison between contemporaneous floras across North America, we document a similar pattern of increasing species richness with decreasing latitude (Figs. 3.6 - 3.7, Table F.1). This demonstrates that in the earliest Paleocene, there was a strong latitudinal diversity gradient, suggesting that it was either maintained across the K/Pg boundary or that it was rapidly reestablished within the first ~350 kyr of the earliest Paleocene. Our results, which document considerable differences in climate and species richness between the SJB, DB, and WB, support the concept that the latitudinal diversity gradient is linked to climate and has been through much of Earth's history (e.g., see review by Brown [2014]). Thus, we hypothesize that the differences in floral diversity and composition across North America in the earliest Paleocene were driven by differences in climate that caused the latitudinal transition from temperate forests in the NGP to paratropical forests in the SJB.

Conclusion

The Ojo Alamo Sandstone preserves a species-rich, heterogeneous, and uneven megaflora in the SJB deposited within 350 kyr of the Cretaceous/Paleogene boundary. The SJB flora is dominated by dicot angiosperms with pteridophytes, conifers, and monocot angiosperms as common accessory taxa. There is a strong facies effect on floral diversity and composition in the SJB: (1) an overbank flora found on riparian margins has higher species richness, is more even, and appears to have been dominated by fast-growing pioneer dicot angiosperms species and (2) a pond flora found in swamps or low-lying areas has lower species richness and is less even, and non-dicot angiosperm morphotypes appear to have been more common within this flora. The majority of morphotypes found in the SJB flora have not been previously described, suggesting that a large proportion of species may be endemic to the SJB. Paleoclimate estimates from the SJB indicate a very warm and wet climate consistent with a modern tropical seasonal forest biome.

When compared with contemporaneous floras from North America, the SJB flora has ~10–55% greater species richness, but is significantly less even. While taxa common in the NGP are present in the SJB flora, only *P. raynoldsii* is common, whereas accessory taxa in the NGP are important parts of the SJB flora. The SJB had a greater proportion and abundance of pteridophyte morphotypes than contemporaneous collections, likely linked the warm and wet climate. The pattern of laterally heterogeneous, species-rich, but uneven flora found in the SJB runs is different than the pattern found in the NGP (e.g., Johnson and Hickey 1990; Johnson 2002; Peppe 2010), but potentially more similar to floras from the front range of the Rocky Mountains in Colorado (Johnson and Ellis 2002;

Johnson et al. 2003). Additionally, the SJB paleoclimate estimates indicate a warmer and wetter environment than previously studied localities farther north (Barclay et al. 2003; Peppe 2010). Taken together, these results demonstrate that the early Paleocene flora in the SJB is markedly different from floras in the NGP and that there were significant differences in species composition and diversity along a north–south gradient in North America in the earliest Paleocene. The latitudinal differences in megaflora observed in this study are similar to those found in the microflora (i.e., Fredericksen 1987; Nichols et al. 1990) and fossil wood (Lehman and Wheeler 2009). We hypothesize that the warm, wet conditions in the SJB drove rapid rates of speciation following the K/Pg boundary, resulting in a heterogeneous, endemic flora in the earliest Paleocene. These results indicate that the floral response to the K/Pg boundary likely varied regionally across North America and was influenced by latitudinal differences in paleoclimate and paleoecology.

Acknowledgments

This work was supported by the National Science Foundation (EAR-132552), the American Chemical Society Petroleum Research Fund (PRF#52822-DN18), the Geological Society of America, Dallas Paleontological Society, and Baylor University Department of Geosciences' Dixon Fund. We thank T. Williamson for significant logistical support for this research project; B. Abbuhl, P. Wright, J. Milligan, R. Secord, S. Brusatte, U. Denenclaw, C. Leslie, A. Davis, S. Atchley, A. Baumgartner, and A. Weil for assistance in the field and lab; and R. Dunn, S. Manchester, and E. Currano for their assistance identifying morphotypes. We would also like to thank S. Atchley, S. Dworkin,

B. Hockaday, and J. White, two anonymous reviewers, associate editor K. Boyce, and editor C. Jaramillo for their helpful comments on previous versions of this article.

CHAPTER FOUR

Terrestrial Ecosystem Instability Following the Cretaceous-Paleogene Boundary

Introduction

The Cretaceous-Paleogene (K-Pg) mass extinction ~66 Ma caused a dramatic restructuring of terrestrial ecosystems and a major destabilization of terrestrial food webs (e.g., McIver, 1999; Wilf and Johnson, 2004; Wilf et al., 2006; Blonder et al., 2014; Smith et al., 2018). The terrestrial ecosystem upheaval at the K-Pg boundary included the extinction of nonavian dinosaurs and the subsequent radiation of mammals (e.g., Wilson, 2014; Brusatte et al., 2015; Grossnickle and Newham, 2016), decrease insect herbivore diversity (e.g., Labandeira et al., 2002; Donovan et al., 2016), and the extinction of ~50-80% of megafloral and ~15-30% of microfloral species respectively (e.g., Wilf and Johnson, 2004; Nichols and Johnson, 2008; Barreda et al., 2012; Vajda and Bercovici, 2014; Lyson et al., 2019). Marine planktonic ecosystems experienced high volatility for the first ~1.8 million years of the Paleocene before stabilizing (Alvarez et al., 2019) but whether terrestrial ecosystems, and in particular plant communities, experienced similar volatility during the early Paleocene is unclear. The most voluminous phase of Deccan Traps (DT) volcanism erupted during the first ~1 Myr of the Paleocene (Renne et al., 2015; Schoene et al., 2019; Sprain et al., 2019) and may have impacted contemporaneous ecosystem recovery and contributed to the sustained instability in marine records. Thus, understanding patterns in floral community diversity and structure is critical to understanding how unstable early Paleocene terrestrial ecosystems recovered following the K-Pg boundary.

Extensive early Paleocene megafloral collections have been made in North America for over 150 years (e.g., Newberry, 1868; Lesquereux, 1878; Brown, 1962; Hickey, 1980; Wing et al., 1995; Johnson, 2002; Barclay et al., 2003; Peppe, 2010; Flynn and Peppe, 2019). Early Paleocene plant communities from the Northern Great Plains of North America (NGP) are characterized by low diversity and are dominated by long-lived, cosmopolitan, fast-growing taxa (Hickey, 1980; Johnson, 2002; Barclay et al., 2003; Peppe, 2010; Blonder et al., 2014; Lyson et al., 2019). Analyses of these floras indicate relative stability in floral diversity and low diversity floral communities persisted until the middle to late Paleocene in the NGP (Hickey, 1980; Wing et al., 1995; Dunn, 2003; Peppe, 2010). In contrast, megafloras from the mid- to low latitudes of North America and Patagonia are considerably more diverse than their NGP counterparts and there is a clear differentiation between fossil wood and pollen from mid- to low latitudes and the NGP potentially indicating differential latitudinal and regional response to the K-Pg boundary (Frederiksen, 1987; Nichols et al., 1990; Iglesias et al., 2007; Lehman and Wheeler, 2009; Comer et al., 2015; Flynn and Peppe, 2019; Lyson et al., 2019). Paleoclimate estimates from the early Paleocene indicate climate cooling across the K-Pg boundary and overall ~1-2 °C warming during the first 600 Kyr of the Paleocene imprinted on a longer term trend of modest cooling (Hickey, 1980; Wilf et al., 2003; Peppe, 2010; Hull et al., 2020). There is tentative evidence for short term warming events during the early Paleocene at ~65.8 Ma (Danian C2) and ~65.3 Ma (Lower C29n Event) from marine and lacustrine records (Coccioni et al., 2010; Gilmour et al., 2013; Barnet et al., 2019) and potential link between early Paleocene hyperthermal events and floral diversity (Lyson et al., 2019).

Here we present a record of early Paleocene megafloral diversity dynamics spanning 66.0 – 64.5 Ma from the three well dated localities in western North America - (1) San Juan Basin, New Mexico, (2) Denver Basin, Colorado, and (3) Williston Basin, Montana and North Dakota – to investigate how terrestrial ecosystem recovered following the K/Pg mass extinction (Fig. 4.1). We used Capture-Mark-Recapture (CMR) models to simultaneously estimate interval-to-interval extinction, origination, and sampling probabilities while also estimating net diversification rates. We correlate the megafloral diversity results with coeval leaf physiognomic paleoclimate estimates and a new terrestrial bulk organic $\delta^{13}C$ record from the San Juan Basin. These results have important implications for understanding how terrestrial ecosystems recovered following the K-Pg boundary and drivers of early Paleocene ecosystem instability.

Materials and Methods

Megafloral samples spanning the latest Cretaceous to early Paleocene from the western interior of North America were used to estimate floral turnover and paleoclimate parameters from the (1) the San Juan Basin (SJB), New Mexico (66.0 – 63.5 Ma; 56 localities; 147 morphotypes; Table H.1) (Flynn and Peppe, 2019, this study), (2) the Denver Basin (DB), Colorado (66.5-65.0 Ma; 65 localities; 192 morphotypes; Table H.2) (Lyson et al., 2019), and (3) the Williston Basin (WB), North Dakota and Montana (67.5

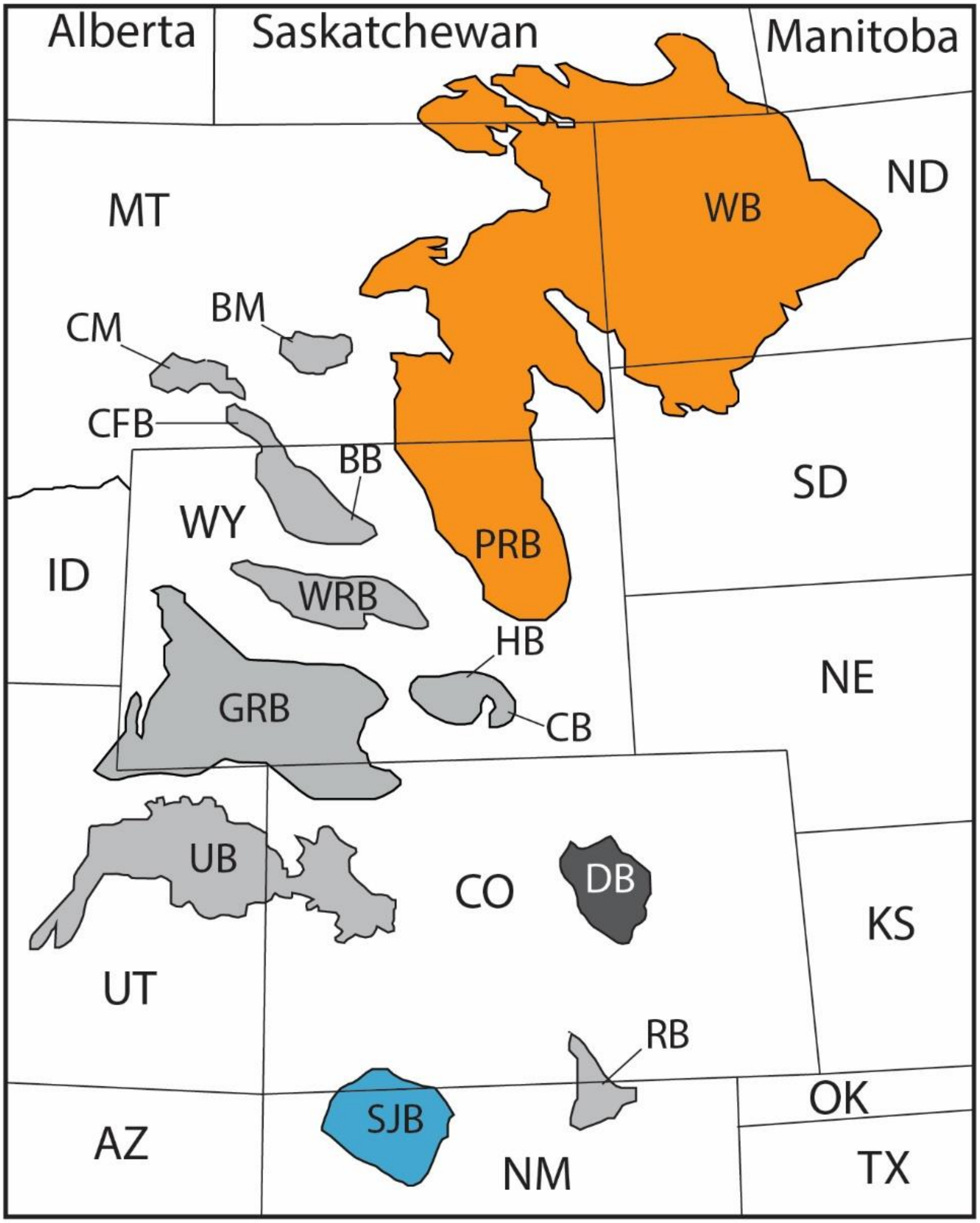

Figure 4.1. Early Paleocene basins of western North America showing the location of the SJB, DB, and WB (modified from Peppe 2010).

– 63.5 Ma; 239 localities; 399 morphotypes; Table H.3) (Fig. 4.1) (Wilf and Johnson, 2004; Peppe, 2010). Due to the problematic nature of assigning fossil leaves to Linnaean taxa, all leaves were assigned to basin-wide morphotypes. Morphotypes are distinct floral morphologies with no formal taxonomic but are presumed to represent biological species (for review of morphotyping method, see Ash et al., 1999; Ellis et al., 2009). Floral occurrences were sorted into 100 Kyr time bins using previously published magnetostratigraphic age models for each basin and recalibrated, if necessary, to the 2012 Geomagnetic Polarity Timescale (Flynn et al., in press; Hicks et al., 2002; Peppe et al., 2009; Ogg, 2012; Lyson et al., 2019). We focus this study on the interval from 66.2 – 64.5 Ma but use occurrence data from outside this interval in paleoclimate and floral diversity analyses (see below). Any intervals with no occurrence data were skipped and the time period between sampling was adjusted for analyses.

We used the Pradel seniority CMR model (Pradel, 1996) (hereafter referred to as the Pradel model) to simultaneously estimate origination, extinction, and net diversification rates while concurrently estimating sampling probabilities using the program MARK (White and Burnham, 1999) for the SJB, DB, and WB (Fig. 4.2-4.3). CMR models were originally developed by statistical ecologists to address the issue where the observation probability in any ecological sample is never 100% and this can have an outsized effect on estimates of survivorship and recruitment (e.g., Cormack, 1964; Jolly, 1965; Lebreton et al., 1992; Pradel, 1996). Recently, CMR models have been successfully applied to a variety of paleontological datasets, including mammals (Liow and Finarelli, 2014), marine fish (Sibert et al., 2018), and marine invertebrates (e.g., Connolly and Miller, 2001; Liow et al., 2015).

Here we briefly summarize important characteristics and assumptions of the Pradel model necessary to understand our results (see Liow and Finarelli, 2015 for details about the Pradel model and its assumptions). In CMR literature, each individual is given a "capture history" which indicates time intervals when the individual was alive and sampled; we applied this to fossil leaf morphotypes as a "sampling history" which refers to time intervals during which the morphotype was extant and sampled (Liow and Nichols, 2010). The forward-time probability of a given sampling history for each morphotype can be expressed in terms of the sampling probability (*p*; probability that a morphotype present at time *i* was also sampled at time *i*) and sampling probability (φ; probability that a morphotype present at time *i* will also be present at time *i+1*). Extinction probability is the complement of survival probability ($1 – φ_i$; probability that a morphotype present at time *i* did not survive to time *i+1*). Alternatively, the reverse-time sampling history of a given morphotype can be expressed in terms of *p* and seniority probability (γ; the probability that a morphotype present at time *i* was also present at time *i-1*). Similar to extinction probability, the origination probability is the complement of survival probability ($1 – γ_i$; probability a morphotype present at time *i* was not present at time *i-1*). The extinction and origination probabilities can then be used to derive the species growth rate from time *i* to *i+1* (λ; the ratio of taxa in successive time intervals). The net *per capita* diversification rate can then be estimated (i.e., the relative change in diversity from time *i* to time *i+1*) can be estimated as $λ_i – 1$; a net diversification rate > 0 ($λ_i > 1$) implies increasing diversity and vice versa. We compared 9 models from the SJB, DB, and WB, where φ, *p*, and λ were either constant for the whole sampling duration or time-varied for each bin, and focus on the fully time varying model since we fell it best represents the nature of paleontological collections (see Table G.1 for summary of model results). Estimates with large uncertainties were excluded from further analyses.

Floral occurrence data from the SJB, DB, and WB was used to estimate two mean annual temperature (MAT) data sets using leaf margin analysis (LMA) (Miller et al., 2006) (Fig. 4.4). LMA is a univariate climate model that uses the presence or absence of toothed woody dicot angiosperm leaves (e.g., Wilf, 1997; Miller et al., 2006; Peppe et al., 2011); the standard error for LMA MAT estimates was calculated using the uncertainty equation of Miller et al. (2006). The first dataset are individual floral localities with at least 15 unique dicot morphotypes that have previously published MAT estimates, which were used for MAT estimates from specific time intervals (Fig. 4.4) (Wilf et al., 2003; Wilf and Johnson, 2004; Peppe et al., 2011; Flynn and Peppe, 2019; Lyson et al., 2019). The second dataset applies LMA to the standing diversity of dicot leaves in each time bin (i.e., all leaf morphotypes that occur within that time plus all those that occur both before and after the time bin but not found in it) to calculate a range through MAT on all time bins with at least 15 unique dicot morphotypes. The range through approach enables MAT estimates from intervals with little or no site-specific estimates and allows for a more complete temporal pattern in MAT.

The $\delta^{13}C$ of bulk organic carbon was measured from lower Nacimiento Formation sediment samples collected from Bisti/De-Na-Zin Wilderness Area in the SJB (Fig. 4.1). These samples are from ~65.85 to ~64.25 Ma and the age of $\delta^{13}C$ samples estimated from Flynn et al. (*in press*) (complete results are in Table I.1) (Fig. 4.4). A 1-10g sample of rock was crushed and acidified using 1 *M* HCl to remove inorganic carbon. The $\delta^{13}C$ values of bulk organic carbon were measured at Baylor University's Stable Isotope Laboratory.

Results

The average extinction probability per 100 Kyr bin for early Paleocene macrofloras, not including the interval directly following the K-Pg boundary (i.e., 65.9-64.5 Ma), for the SJB was 0.158 (s.e. = 0.094), 0.204 (s.e. = 0.071) for the DB, and 0.174 (s.e. = 0.081) for the WB (Fig. 4.3A, Table G.2-G.4). The average origination probability over the same interval was 0.106 (s.e. = 0.010) for the SJB, 0.114 (s.e. = 0.071) for the DB, and 0.084 (s.e. = 0.072) for the WB (Fig. 4.3B, Table G.2-G.4). The comparatively higher extinction rate resulted in overall decreasing net macrofloral diversity change of -0.030 (s.e. = 0.172) for the SJB, -0.071 (s.e. = 0.147) for the DB, and -0.064 (s.e. = 0.191) for the WB per 100 Kyr time bin (Fig. 4.3C, Table G.2-G.4). These results agree with previously work which found overall decreasing macrofloral diversity during the early to middle Paleocene in western North America (e.g., Hickey, 1980; Wing et al., 1995; Dunn, 2003; Peppe, 2010). Range through LMA estimates indicate significantly higher MAT in the SJB and DB compared to the WB indicating the presence of a latitudinal temperature gradient during the early Paleocene (Fig. 4.4). This difference in temperature suggests latitudinal differences in biomes supported by the taxonomic similarity between contemporaneous macrofloras from the SJB and DB compared to the

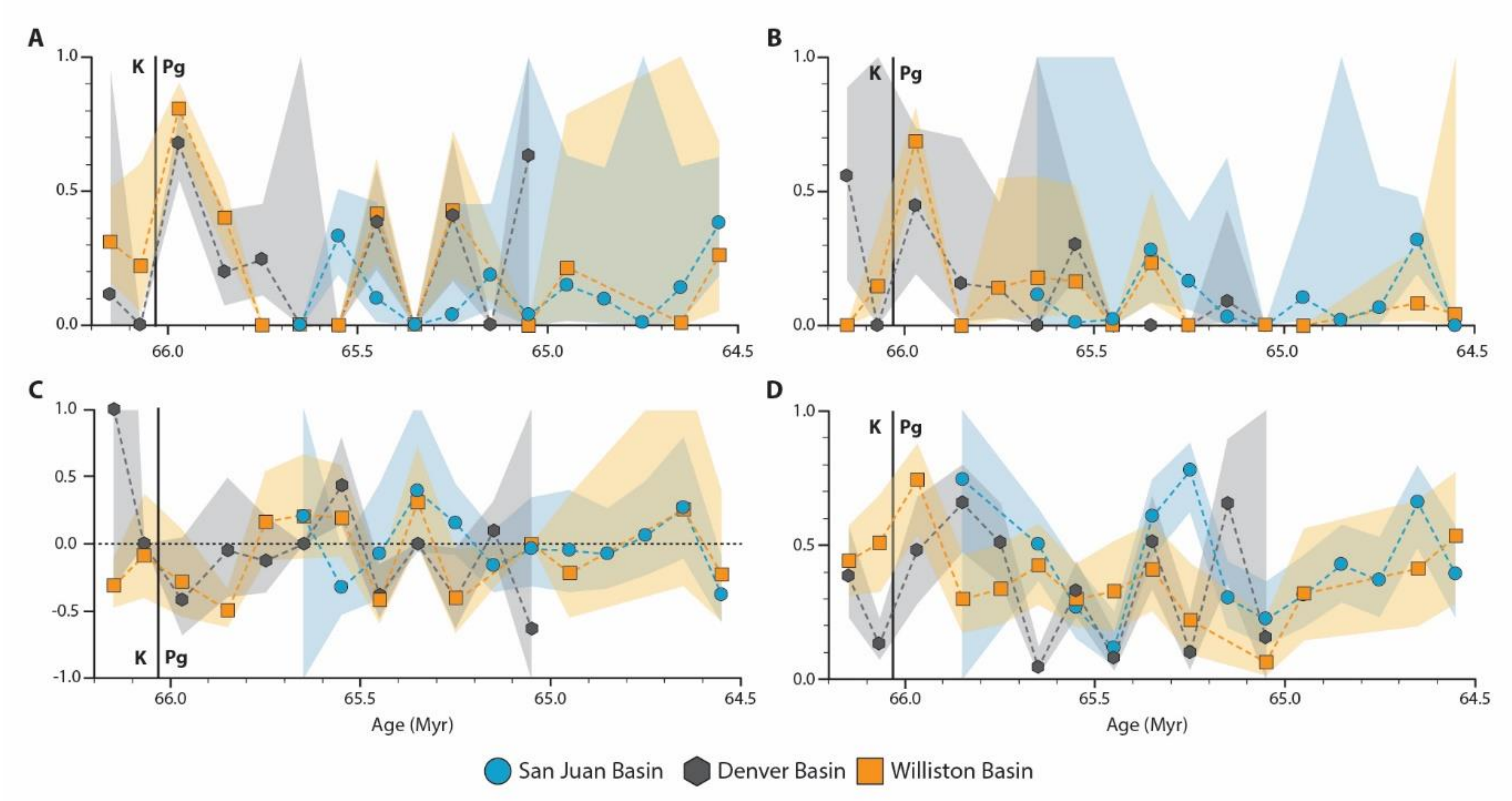

Figure 4.2. The megafloral (a) extinction probability, (b) origination probability, (c) net diversification rate (dashed line shows net zero diversification), and (d) sampling probability from the SJB, DB, and WB using the fully time varying model. Shaded areas indicate 95% confidence intervals. *Note:* the estimates from A-C are plotted time interval to the next whereas estimates from D are for the time interval itself. All points plotted at midpoint.

WB (Barclay et al., 2003; Flynn and Peppe, 2019). A slight cooling of ~1.5-2.5 °C through the first 1.5 Myr of the Paleocene consistent with previous early Paleocene MAT estimates (Peppe, 2010).

There are three notable intervals of net decreasing megafloral diversity during the early Paleocene which are coeval across western North America (Fig. 4.2C). The first is the interval immediately following the K-Pg boundary where both the DB and WB see a net decrease of 40-50% in species (Fig. 4.2C). Both locations have an estimated extinction rate of 70-80% (Fig. 4.2A) which is similar to previous macrofloral extinction estimates from western North America (Wilf and Johnson, 2004; Lyson et al., 2019). Additionally, origination rates immediately following the K-Pg boundary are relatively high, approximately 45% in the DB and approximately 70% in the WB (Fig. 4.2B), indicating onset of mass extinction radiation was relatively rapid. The second interval is from ~65.5-65.4 Ma (EI2) where the estimated net floral diversity from the SJB, DB, and WB all decrease by ~30-40% (Fig. 4.2C). This interval is associated with moderately high extinction rates and low origination rates which is significantly different than the extinction pattern seen at the K-Pg boundary (Fig. 4.2A-B). The final interval of low net floral diversity was initiated ~65.3-65.2 Ma (EI3) and is associated with a ~15% decrease in floral diversity in the SJB and ~40% decrease in the DB and WB (Fig. 4.2C). This interval is followed by a prolonged period until ~64.7 Ma with near zero net floral diversity change and relatively low extinction and origination rates (Fig. 4.2A-C). This period of static floral diversity is associated with significant increases in sediment accumulation rates in the SJB and WB (Flynn et al., in press; Peppe et al., 2009) and a basin-wide unconformity in the DB (Hicks et al., 2003; Fuentes et al., 2019). Similar to

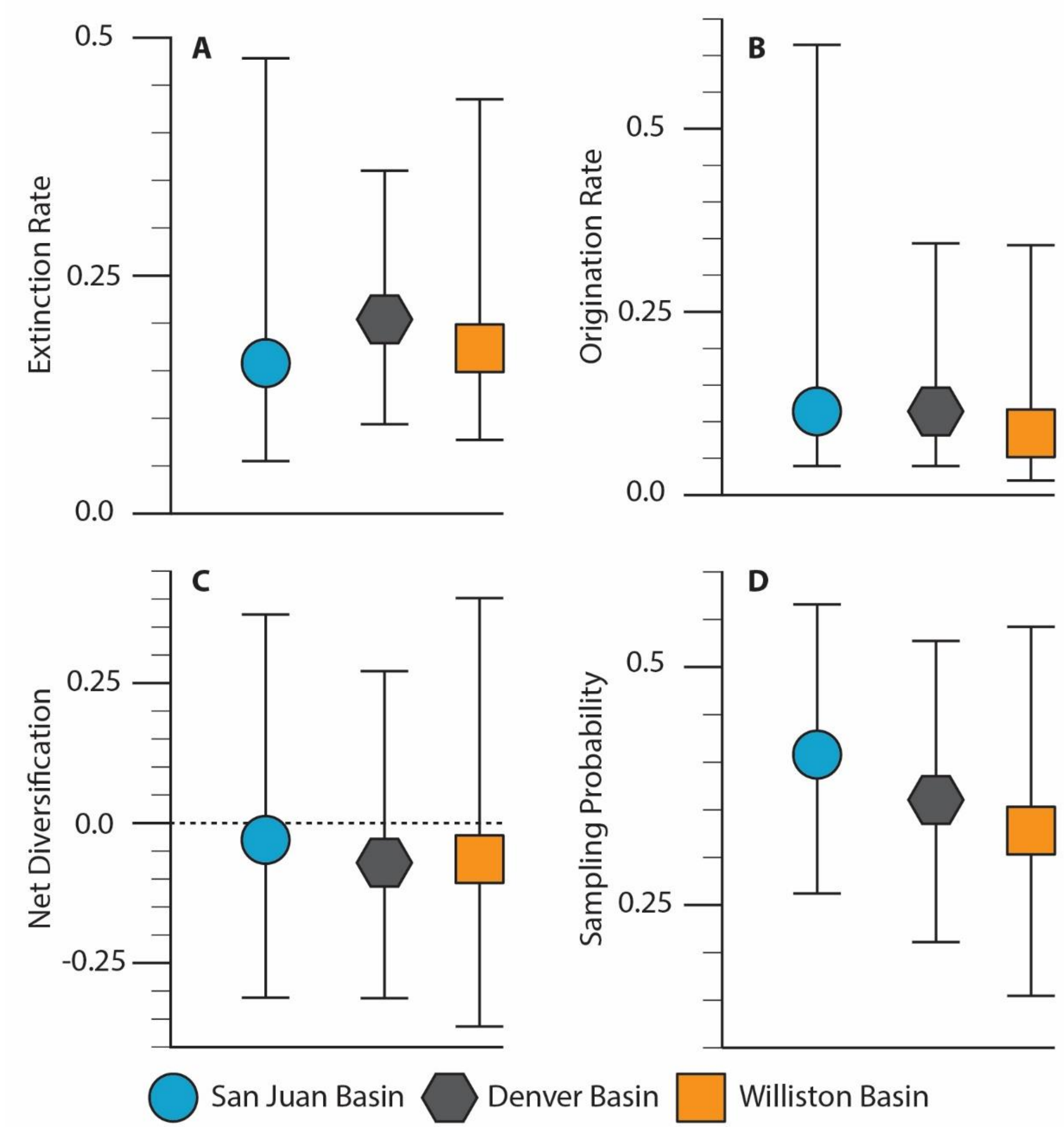

Figure 4.3. Comparison of the average megafloral (a) extinction probability, (b) origination probability, (c) net diversification rate, and (d) sampling probability from the SJB, DB, and WB using the fully time varying model. Bars indicate 95% confidence intervals.

EI2, this interval had moderately high extinction rates but very low origination rates (Fig. 4.2A-B). Both EI2 and EI3 are associated with a -1.5-2.5 ‰ $\delta^{13}C$ isotope excursion suggesting a regional driver in floral diversity during the early Paleocene (Fig. 4.4C; Table I.1).

There are three intervals of increasing floral diversity from approximately 65.8-65.5 Ma, 65.4-65.3 Ma, and 64.7-64.5 Ma (Fig. 4.2C). The first interval (OI1) corresponds with initial radiation following the K-Pg boundary with the greatest net floral diversification occurring at ~65.6 Ma approximately contemporaneous with the proposed Danian C2 hyperthermal event (Quillévéré et al., 2008; Gilmour et al., 2013). The second interval (OI2) corresponds with the Pu2-Pu3 transition in the SJB and DB (Flynn et al., in press), the first appearance of legumes (Lyson et al., 2019), and the appearance of large bodied mammals in western North America (Williamson, 1996). The final interval (OI3) of increased floral diversity corresponds with the Puercan-Torrejonian transition and the dominance of Juglandaceae floras in SJB (Flynn et al., in press, 2018; Williamson, 1996), the transition between WBI and WBII floras in the WB (Peppe, 2010), a tentative transient warming pulse in the DB (Lyson et al., 2019), and the Lower C29n Event in marine records (Barnet et al., 2019) (Fig. 4.2C).

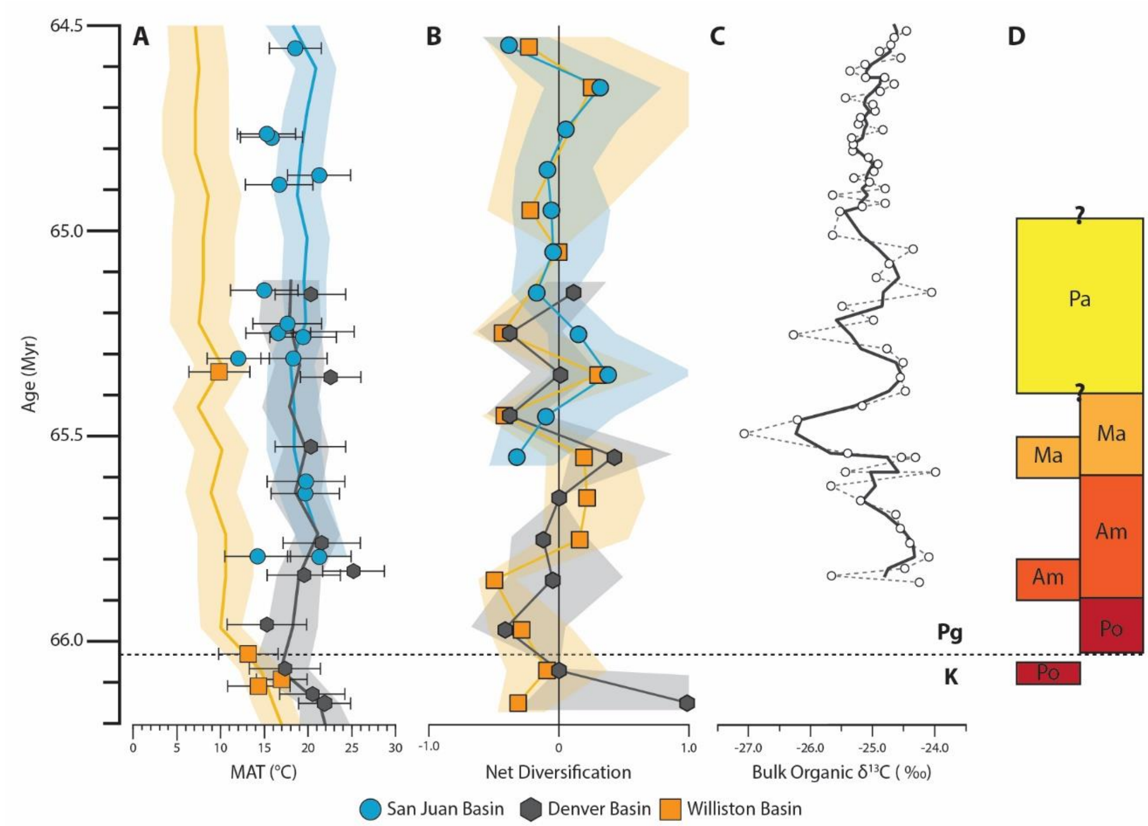

Figure 4. (A) range through and site LMA MAT estimates from the SJB (Flynn et al. 2019; this study), DB (Lyson et al., 2019), and WB (Wilf and Johnson, 2004; Peppe 2010). Shading and bars indicate 95% confidence interval. (B) Net floral diversification rate (dashed line shows net zero diversification). Shaded areas indicate 95% confidence intervals. (C) bulk organic $\delta^{13}C$ record from the SJB. Blank line is the 3 pt moving average and white circles are individual measurements. (D) DT Wai subgroup stratigraphy and geochronology from Schoene et al. 2019 and Sprain et al. 2019. Po – Poladpur Formation, Am – Ambenali Formation, Ma –Mahabaleshwar Formation, and Pa – Panhala Formation.

Discussion

These results show the volatile nature of early Paleocene macrofloral diversity dynamics, especially in the first ~800 Kyr following the K-Pg boundary, with at least two intervals with net *per capita* diversity reductions comparable to the K-Pg boundary (Fig. 4.2). This pattern is similar to marine phytoplankton who show high volatility for the first ~1.8 Myr of the Paleocene indicating the instability in both communities is likely related to the K-Pg mass extinction (Alvarez et al., 2019). The contemporaneous nature of floral turnover across western North America suggests an external driver in floral diversity during the early Paleocene, at least during intervals of floral community upheaval (Fig. 4.2). We hypothesize the terrestrial ecosystem instability reflected in the floral community changes is linked the final phase of DT volcanism. The study interval is coeval Wai subgroup DT basalts, the most voluminous phase of DT volcanism, which erupted over at least the initial 700 Kyr of the Paleocene (Renne et al., 2015; Schoene et al., 2019; Sprain et al., 2019). The Wai subgroup basalts are divided into four formations, from oldest to youngest, the (1) Poladpur, (2) Ambenali, (3) Mahabaleshwar, and (4) Panhala (Beane et al., 1986). There is disagreement if the Wai subgroup formations erupted relatively continuously with little temporal separation between adjacent formations or if each formation was erupted over short intervals (< 100 Kyr) and adjacent formations are separated by intervals of periods of relative inactivity (Schoene et al., 2019; Sprain et al., 2019). The eruption of the Ambenali formation began ~65.9 Ma with the main eruptive pulse lasting until at least ~65.8 Ma but may have continuously erupted until ~65.6 Ma (Schoene et al., 2019; Sprain et al., 2019). The Mahabaleshwar Formation began erupting ~65.6 Ma and the major eruptive pulse lasted until at least ~65.5 Ma ceasing by ~65.4 Ma (Schoene et al., 2019; Sprain et al., 2019). Age constraints on the uppermost Panhala Formation are imprecise due to poor exposure but it was emplaced during magnetochron 29n (Subbarao and Courtillot, 2017) constraining eruptions to ~65.4 – 64.9 Ma.

The emplacement the Mahadeshwar and potentially the Panhala Formations immediately precedes both EI2 and EI3 respectively (Fig. 4.4). The discrete and rapid floral diversity changes support pulses of relatively high eruptive activity followed by intervals of relative quintessence (Fig. 4.4). Net floral diversity increases or remains relatively constant in the interims between eruptive pulses and, after cessation of Wai subgroup emplacement before the C29n/C28r boundary ~64.96 Ma, net floral diversity remains relatively constant until OI3 (Fig. 4.4). Volatiles and aerosols released from these eruptions, particularly SO_2, would have caused short-term pronounced climate cooling and may have directly damage vegetation if S concentrations were high enough (Schmidt et al., 2016). While CO_2 is released during active eruptive phases, the majority of CO_2 outgassing occurs prior to eruption (Edmonds and Wallace, 2017); SO_2 and associated phases have a shorter resonance time in the atmosphere than CO_2 so the initial cooling from eruptions would likely be followed by intervals increased temperature but increased silicate weathering from exposed basalt may have mitigated these effects. Several earliest Paleocene hyperthermal events have been proposed from marine and lacustrine records (e.g., Quillévéré et al., 2008; Coccioni et al., 2010; Gilmour et al., 2013). The majority of Paleogene hyperthermal events occur at 405 Kyr eccentricity maxima and have a characteristic double peak due to the mobilization of isotopically light carbon reservoirs (Barnet et al., 2019). However, it is debated whether these earliest

Paleocene hyperthermal reflect true global events, regional differences in carbon cycling, or the depauperate planktonic communities following the K-Pg boundary (Barnet et al., 2019). The negative bulk organic $\delta^{13}C$ excursions from the SJB are out of phase with the 405 Kyr eccentricity maxima and lack the characteristic double peak (Fig. 4.4C). LMA estimates from the DB tentatively link the negative $\delta^{13}C$ intervals to increased temperatures (Lyson et al., 2019) and there is evidence of increased erosive unconformities in the SJB possibly linked to enhanced hydrological cycle due to higher temperatures (Flynn et al., in press; Carmichael et al., 2017). Paleogene hyperthermal events have been associated high floral turnover and increased floral diversity (e.g., Wing et al., 2005; Jaramillo et al., 2010; Wing and Currano, 2013) but these effects may be modulated by latitude (Harrington and Jaramillo, 2007).

We propose the timeline below for western North American terrestrial ecosystems following the K-Pg boundary. Following the bolide impact, there is a protracted net negative diversity interval from ~66.0 – 65.8 Ma and floral recovery is delayed due to the emplacement of the Poladpur and Ambenali Formations (Fig. 4.4). Floral diversity increases during OI1 after the main phase of Ambenali Formation volcanism from ~65.8-65.5 Ma with highest diversification rates in the DB and WB potentially associated with the Danian C2 hyperthermal event (Fig. 4.4). The emplacement of the Mahabaleshwar Formation causes a loss in floral diversity from ~65.5-65.4 Ma which is followed a short interval of increasing diversity at ~65.4-65.3 Ma after the main eruptive phase of Mahabaleshwar Formation (Fig. 4.4). The significant bulk organic $\delta^{13}C$ excursion in this interval may be the L. C29n Event (Coccioni et al., 2010) and/or related to the change in floral community. The initial emplacement of the Panhala Formation correlates with the last significant reduction in floral diversity at ~65.3 Ma which is followed by a period of relative floral community stability following the cessation of major DT volcanism before a final interval of increasing floral diversity at ~64.7-64.5 Ma (Fig. 4.4).

Conclusion

The similarity and volatility of early Paleocene megafloral diversity estimates presented here, particularly during the first 800 Kyr of the Paleocene, from the SJB, DB, and WB suggest widespread terrestrial ecosystem instability following the K-Pg mass extinction. We estimate ~70-80% of megafloral species went extinct at the K-Pg boundary in both the DB and WB (Fig. 4.2A). After the K-Pg boundary, the patterns in floral diversity appear to be strongly tied to DT volcanism. Two other intervals of comparable net diversity decrease to the K-Pg boundary were identified at ~65.5-65.4 Ma and ~65.3 Ma which are coeval with the onset of Mahabaleshwar and Panhala Formation DT basalts (Fig. 4.4) (Schoene et al., 2019; Sprain et al., 2019). Additionally, both of these periods are associated with a -1.5 to -2.5 $\delta^{13}C$ excursions which possibly reflect the first terrestrial evidence for the L. C29n Event and/or changes in plant community composition related to DT volcanism (Coccioni et al., 2010). Intervals of increasing floral diversity at ~65.6 and ~65.4-65.3 correlate with periods of relatively low eruptive flux between major formations in the Wai subgroup. Floral diversity dynamics become significantly less volatile after ~65.3 Ma perhaps reflecting either the recovery of terrestrial ecosystem function and/or cessation of major DT volcanism. These results have broad implications for understanding the tempo terrestrial ecosystem recovery following the K-Pg mass extinction and provides context for major early Paleocene evolutionary innovations in both plants and mammals.

Acknowledgments

This work was supported by the National Science Foundation (EAR-132552 to DP, EAR 1325544 and DEB 1654952 to TEW and SLB, EAR 1325612 to RS), the American Chemical Society Petroleum Research Fund (PRF#52822-DN18 to DP), The US Bureau of Land Management (TEW and SLB), the Geological Society of America (AF), Dallas Paleontological Society (AF), and Baylor University Department of Geosciences’ Dixon Fund (AF). SLB’s work on mammal evolution is supported by a European Research Council Starting Grant (ERC StG 2017, 756226, PalM). We thank J. Robinson, H. Anderson, J. Milligan, P. Wright, A. Baumgartner, A. Davis, C. Leslie, and M. Donahoo for their assistance in SJB sample collection and sample preparation and L. H. Liow for her assistance with CMR modeling. We would also like to thank S. Atchley, S. Dworkin, B. Hockaday, and J. White for their helpful comments on previous versions of this manuscript. Lastly, we thank the US Bureau of Land Management for issuing fossil collecting permits to TEW.

CHAPTER FIVE

Conclusions

Magnetostratigraphy from the early Ojo Alamo Sandstone and lower Nacimiento Formation from the San Juan Basin, New Mexico constrain the deposits to C29r-C27r of the GPTS. The Ojo Alamo Sandstone has time transgressive deposition being older in the northwest and youngest in the southeast areas of the basin. Sediment accumulation rates were low during C29r and C29n and similar from basin margin to basin center before roughly doubling in C28r and being highest in the basin center and lowest on the basin margin indicating an increase in basin subsidence near the C29n/C28r boundary and an increase in accommodation. Rock magnetic analysis indicates intermediate titanohematite as the major remanence carrier with (titano)magnetite, maghemite, and greigite present in some samples. This age model constrains Puercan 2 and Puercan 3 mammal localities to C29n, Torrejonian 1 to C28n, and Torrejonian 2 to C27r. When this work is combined with previous work by Leslie et al. (2018b), a basin wide chronostratigraphy can be constructed which contains the age of all major Puercan and Torrejonian mammal localities in the San Juan Basin. The revised age model for the SJB suggests that the first appearance of To1 mammals may have been diachronous across North America, with the Torrejonian 1 mammals first appearing in the north (Montana and North Dakota) during C29n, then in middle latitudes (Utah) in C28r, and lastly in southern North America (New Mexico) in C28n.

The fossil flora from the Ojo Alamo Sandstone was deposited < 350 Kyr after the Cretaceous-Paleogene boundary. The megaflora was comprised of 53 unique morphotypes and dominated by angiosperms with accessory taxa composed of pteridophytes, lycophytes, and conifers. Diversity analyses indicate that the Ojo Alamo Sandstone megaflora was species rich, highly uneven, and laterally heterogeneous with a more even and diverse flora on the more disturbed channel margins and a less even and diverse flora on the less disturbed pond deposits. Both multivariate and univariate leaf physiognomic climate estimates indicate warm temperatures and relatively high precipitation which, when combined with leaf mass per area estimates indicating all measured morphotypes were deciduous, is consistent with a modern tropical seasonal forest. When compared to coeval megafloras from the Denver Basin, Colorado and the Williston Basin, North Dakota, the San Juan Basin megaflora had significantly higher species richness but were significantly less even. Paleoclimate estimates from the San Juan Basin were 7-14 °C warmer than estimates from either the Denver or Williston Basins and show a shift from a temperate to tropical seasonal forest. This works highlights the presence of a latitudinal megafloral diversity and temperature gradient during the earliest Paleocene.

The Pradel Capture-Mark-Recapture model was used to investigate megafloral diversity dynamics using occurrence data from the San Juan Basin, Denver Basin, and Williston Basin during the first ~1.5 Myr of the Paleocene. These model results show megafloral diversity was volatile the first ~800 Kyr of the Paleocene before settling ~65 Ma suggesting prolonged recovery of terrestrial ecosystems. Model results indicate approximately 70-80% of megafloral species went extinct and a totally net loss of ~40%

of species at the Cretaceous-Paleogene boundary in the Denver and Williston Basins, consistent with estimates using other methods. Two additional intervals of sharply decreasing net diversity during the early Paleocene from all three basins were identified at ~65.6 Ma and ~65.2-64.8 Ma. These two intervals correspond with a proportional loss of megafloral species comparable to the Cretaceous-Paleogene boundary Both of these periods are associated with a -1.5 to -2.5 ‰ bulk organic carbon $\delta^{13}C$ excursion. Three intervals of sharply net increasing floral diversity across all basins at ~65.7, ~65.3, and ~64.6 Ma were also identified. The intervals of net decreasing floral diversity correspond with the onset of major eruptive phases of the Wai Subgroup basalts from the Deccan Traps. These results highlight the potential importance of Deccan Traps volcanism of terrestrial ecosystem renewal following the Cretaceous-Paleogene boundary and provides context for major early Paleocene evolutionary innovations in both plants and mammals.

APPENDICES

APPENDIX A

Ojo Alamo Sandstone and Lower Nacimiento Formation Paleomagnetic Data

Table A.1 - Ojo Alamo Sandstone and lower Nacimiento Formation paleomagnetic sampling information

Location/ Formation	# Sam. Hor.	# of Sam.	# Sam. Hor. w/ Line Fit	% Sam. Hor. w/ Line Fit	# Sam. w/ Line Fit	% Sam w/ Line Fit	# Sam. Hor. w/ Great Circle Fit	% Sam. Hor. w/ Great Circle Fit	# Sam. w/ Great Circle Fit	% Sam. w/ Great Circle Fit	# Sam. Hor. w/ Site Mean	% Sam. Hor. w/ Site Mean
Kutz Canyon	25	68	22	88.0	47	69.1	0	0.0	0	0.0	10	40.0
Chico Springs	12	36	8	66.7	17	47.2	5	41.7	7	19.4	2	16.7
Gallegos Canyon	24	73	18	75.0	48	65.8	7	29.2	13	17.8	12	50.0
De-Na-Zin	50	146	43	86.0	112	76.7	0	0.0	0	0.0	26	52.0
Kimbeto Wash	32	93	25	78.1	63	67.7	0	0.0	0	0.0	9	28.1
Betonnie Tsosie Wash	52	150	42	80.8	102	68.0	7	13.5	13	8.7	24	46.2
Mesa de Cuba	46	124	37	80.4	84	67.7	4	8.7	5	4.0	13	28.3
Ojo Alamo Sandstone	4	12	3	75.0	8	66.7	1	25.0	3	25.0	2	50.0
Nacimiento Formation	237	678	192	81.0	465	68.6	20	8.4	35	5.2	94	39.7
Total	241	690	195	80.9	473	68.6	23	9.5	38	5.5	96	39.8

Table A.2 - Ojo Alamo Sandstone and lower Nacimiento Formation paleomagnetic data: lines

Location	Sample	Strat Level (m)	Temp. Steps	Strat. Declination (°)	Strat inclination (°)	MAD*	Strat. VGP latitude (°N)	Strat. VGP longitude (°E)
Kutz Canyon	F17KC01A	0.0	300-350	7.9	33.1	7.1	70.2	49.3
Kutz Canyon	F17KC01B	0.0	325-375	325.6	68.9	19.9	61.2	206.1
Kutz Canyon	F17KC01D	0.0	200-300	334.5	47.0	11.3	67.0	148.0
Kutz Canyon	F17KC02A	6.0	300-350	321.1	59.6	17.7	59.6	181.3
Kutz Canyon	F17KC02B	6.0	325-375	318.8	39.3	19.0	51.7	151.7
Kutz Canyon	F17KC02D	6.0	200, 250, 325	327.1	68.1	5.4	62.5	204.5
Kutz Canyon	F17KC03A	6.0	250-325	1.0	51.9	14.2	85.8	60.3
Kutz Canyon	F17KC03B	6.0	300-350	311.2	48.6	13.5	48.9	166.8
Kutz Canyon	F17KC03D	6.0	150-250	343.9	42.6	16.9	71.8	125.7
Kutz Canyon	F17KC04A	23.5	250-325	346.3	57.8	16.9	79.0	175.8
Kutz Canyon	F17KC04C	23.5	350-400	335.7	25.7	9.7	58.3	121.6
Kutz Canyon	F17KC04D	23.5	250-325	9.0	43.6	10.4	76.5	34.9
Kutz Canyon	F17KC05A	25.0	100-200	345.7	51.3	20.0	77.3	144.7
Kutz Canyon	F17KC05C	25.0	100-200	347.9	52.5	8.2	79.5	146.1
Kutz Canyon	F17KC05D	25.0	100-200	5.2	59.2	10.7	84.7	300.7
Kutz Canyon	F17KC06B	26.5	150-250	355.6	52.9	15.0	85.2	122.3
Kutz Canyon	F17KC06C	26.5	300, 375, 400	350.1	66.9	13.0	75.2	226.1
Kutz Canyon	F17KC06D	26.5	250-325	336.3	79.4	10.4	54.7	237.9
Kutz Canyon	F17KC07B	29.5	350-400	340.6	54.1	15.8	74.1	160.6
Kutz Canyon	F17KC08A	32.5	250-325	10.4	47.2	13.8	78.0	22.3
Kutz Canyon	F17KC08C	32.5	150-250	355.4	53.7	13.6	85.6	131.2
Kutz Canyon	F17KC11A	32.5	250-325	335.0	59.3	5.7	70.2	179.8

Location	Sample	Strat Level (m)	Temp. Steps	Strat. Declination (°)	Strat inclination (°)	MAD*	Strat. VGP latitude (°N)	Strat. VGP longitude (°E)
Kutz Canyon	F17KC11C	32.5	200-300	314.9	66.0	5.9	55.3	196.2
Kutz Canyon	F17KC09A	35.5	350-400	335.0	70.0	14.9	65.5	215.1
Kutz Canyon	F17KC12A	35.5	250-325	6.9	71.0	1.3	70.6	263.8
Kutz Canyon	F17KC12B	35.5	250-325	19.6	64.2	5.0	72.6	303.3
Kutz Canyon	F17KC12C	35.5	250-325	335.7	50.8	5.4	69.3	154.9
Kutz Canyon	F17KC09C	38.5	300, 375, 400	285.0	73.2	5.2	38.2	212.6
Kutz Canyon	F17KC09D	38.5	300-350	31.1	71.9	5.9	61.1	287.7
Kutz Canyon	F17LL01A	41.5	100-300	176.5	-25.7	3.6	-66.7	260.6
Kutz Canyon	F17LL01B	41.5	100-300	175.9	-33.6	5.9	-71.4	264.3
Kutz Canyon	F17LL01C	41.5	100-400	159.8	-24.1	4.7	-59.9	294.3
Kutz Canyon	F17KC13B	62.3	150-250	173.7	-19.1	8.9	-62.6	265.6
Kutz Canyon	F17KC14C	65.3	100-200	215.2	-39.7	17.2	-56.6	177.0
Kutz Canyon	F17KC15A	70.3	200-300	162.3	-50.3	8.6	-74.3	326.5
Kutz Canyon	F17KC15B	70.3	200, 250, 325	167.5	-41.9	6.1	-73.6	296.3
Kutz Canyon	F17KC15D	70.3	250-325	193.4	-74.4	14.6	-64.3	87.1
Kutz Canyon	F17KC16D	73.3	250-325	212.7	-63.2	16.4	-64.1	133.5
Kutz Canyon	F17KC17B	76.3	250, 325, 350	179.2	-55.4	11.3	-89.1	296.3
Kutz Canyon	F17KC17C	76.3	250, 300, 350	185.6	-75.7	9.0	-63.4	77.7
Kutz Canyon	F17KC18B	79.3	150-250	157.8	-25.3	10.7	-59.4	298.2
Kutz Canyon	F17KC18C	79.3	300-350	153.8	-37.4	13.5	-62.3	314.7
Kutz Canyon	F17KC20C	96.5	250-325	186.8	-30.0	8.0	-68.6	233.8
Kutz Canyon	F17KC21B	101.0	150-250	235.3	-56.4	7.1	-46.4	144.2
Kutz Canyon	F17KC25B	129.0	300-350	141.6	-66.8	14.2	-59.6	19.1
Kutz Canyon	F17KC25C	129.0	325, 350, 400	197.2	-53.7	12.7	-75.8	166.5

Location	Sample	Strat Level (m)	Temp. Steps	Strat. Declination (°)	Strat inclination (°)	MAD*	Strat. VGP latitude (°N)	Strat. VGP longitude (°E)
Kutz Canyon	F17KC25D	129.0	350-400	173.0	-34.7	13.8	-71.4	273.2
Chico Springs	F19CS01A	0	225, 250, 325	283.4	60.2	19.8	31.9	193.4
Chico Springs	F19CS01B	0	275, 300, 325	337.6	9.6	15.1	52.6	111.7
Chico Springs	F19CS01C	0	250, 300, 325	332	11.4	5.6	50.3	120.0
Chico Springs	F19CS03D	6	375, 300, 250	147.7	-25.6	12.2	-53.3	313.4
Chico Springs	F19CS06A	15	375, 450, 475	154.3	-42.1	19.1	-65.0	322.3
Chico Springs	F19CS07A	18	325, 350, 375	191.1	-47.3	16.3	-78.0	198.7
Chico Springs	F19CS09A	24	325, 400, 450	154.7	-27.2	17.9	-58.7	305.9
Chico Springs	F19CS09C	24	425, 450, 475	153.2	-18.3	14	-53.9	302.1
Chico Springs	F19CS10A	27	325, 350, 375	158	-33.5	15.4	-63.7	306.5
Chico Springs	F19CS10C	27	250, 300, 325	166.1	-54	17.8	-78.6	339.7
Chico Springs	F19CS10D	27	200, 250, 475	158.9	-38.5	15.9	-66.7	310.8
Chico Springs	F19CS11B	30	325, 350, 520	126.8	-69.7	20	-49.5	25.8
Chico Springs	F19CS11C	30	400, 450, 500	120.1	-33.2	16.7	-34.6	341.0
Chico Springs	F19CS11D	30	225, 300, 400	177.1	-29.2	17.6	-69.4	261.0
Chico Springs	F19CS12A	46	225, 325, 350	151.5	-37.4	11.2	-60.9	319.5
Chico Springs	F19CS12C	46	200, 225, 250	163.6	-28	3.3	-64.3	292.0
Chico Springs	F19CS12D	46	100, 375, 450	150.2	-30.6	4.7	-57.1	314.4
Gallegos Canyon	F19GJ02A	0	250, 275, 325	162.8	-55.3	4.5	-76.1	344.7
Gallegos Canyon	F19GJ02B	0	150, 175, 200	176.1	-69.3	2.4	-73.3	63.7
Gallegos Canyon	F19GJ02D	0	225, 250, 275	170.4	-48.5	2.5	-79.4	303.9
Gallegos Canyon	F19GJ03B	0.9	125, 175, 325	136.6	-38.5	13.5	-49.7	332.7
Gallegos Canyon	F19GJ03C	0.9	325, 350, 375	151.5	-63.3	19.9	-66.9	12.2
Gallegos Canyon	F19GJ03D	0.9	275, 300, 325	187.5	-49.2	6.9	-81.1	205.0

Location	Sample	Strat Level (m)	Temp. Steps	Strat. Declination (°)	Strat inclination (°)	MAD*	Strat. VGP latitude (°N)	Strat. VGP longitude (°E)
Gallegos Canyon	F19GC01B	0.9	125, 200, 375	213.7	-61.6	8.9	-63.4	137.6
Gallegos Canyon	F19GJ04B	2.35	100, 200, 325	199.2	-69.9	10.5	-68.1	103.3
Gallegos Canyon	F19GC05A	12.9	225, 250, 275	148.7	-46.2	8.9	-62.2	332.4
Gallegos Canyon	F19GC05B	12.9	150, 175, 200	173.2	-46	15	-79.3	286.4
Gallegos Canyon	F19GC05C	12.9	150, 175, 200	142.5	-46.4	4.2	-57.3	337.4
Gallegos Canyon	F19GC06A	15.9	100, 125, 150	36.3	28.8	8.5	51.5	5.4
Gallegos Canyon	F19GC06B	15.9	100, 150, 175	23.7	42.1	13.8	66.3	6.0
Gallegos Canyon	F19GC06D	15.9	200, 225, 275	345	53.7	10.6	77.6	156.3
Gallegos Canyon	F19GC07A	18.9	200, 225, 250	344.5	17.5	8.4	59.2	102.9
Gallegos Canyon	F19GC07B	18.9	225, 250, 275	24	42.1	5.5	66.1	5.6
Gallegos Canyon	F19GC07D	18.9	200, 225, 275	27.9	29	3.4	57.6	14.7
Gallegos Canyon	F19GC08A	21.9	NRM, 275, 300	57.1	67.1	2.3	47.3	305.0
Gallegos Canyon	F19GC08B	21.9	200, 225, 250	72.4	68.8	11.8	38.2	299.9
Gallegos Canyon	F19GC08D	21.9	200, 250, 275	284.8	85	6.2	38.3	239.6
Gallegos Canyon	F19GC09A	24.9	200, 225, 250	2.9	25	12.2	66.6	64.8
Gallegos Canyon	F19GC09B	24.9	125, 150, 175	333.9	22.5	9.6	55.9	122.1
Gallegos Canyon	F19GC09C	24.9	100, 125, 200	1.7	46.8	15.6	81.5	61.7
Gallegos Canyon	F19GP01B	33.7	225, 250, 275	8.7	55	1.8	82.9	346.4
Gallegos Canyon	F19GP01C	33.7	225, 250, 275	11	32.3	7.9	68.8	41.7
Gallegos Canyon	F19GP02B	35.2	225, 250, 275	346.9	73.7	11.7	65.2	236.0
Gallegos Canyon	F19GP02C	35.2	150, 175, 200	16.4	44.4	4.8	72.6	13.7
Gallegos Canyon	F19GP02D	35.2	225, 250, 275	344	43.6	9.2	72.5	127.7
Gallegos Canyon	F19GP03A	36.7	225, 250, 275	344.5	35.1	6.9	68.2	114.7
Gallegos Canyon	F19GP03B	36.7	225, 250, 275	350.3	38.5	7.3	73.0	104.4

Location	Sample	Strat Level (m)	Temp. Steps	Strat. Declination (°)	Strat inclination (°)	MAD*	Strat. VGP latitude (°N)	Strat. VGP longitude (°E)
Gallegos Canyon	F19GP03C	36.7	250, 325, 350	321	25.2	12.7	48.1	138.5
Gallegos Canyon	F19GP04A	38.2	350, 375, 400	131.4	-72.3	18.2	-51.9	31.1
Gallegos Canyon	F19GP04B	38.2	150, 175, 200	161.7	-44.7	13.3	-71.5	314.2
Gallegos Canyon	F19GP05B	39.7	150, 175, 200	133.6	-65.9	1.3	-54.3	16.0
Gallegos Canyon	F19GP05C	39.7	150, 175, 200	168.6	-64.2	5.8	-77.2	33.7
Gallegos Canyon	F19GP05D	39.7	125, 150, 175	124.7	-58.4	3.1	-46.9	2.9
Gallegos Canyon	F19GP06A	42.7	150, 175, 200	198.8	-36.4	3.6	-67.0	201.3
Gallegos Canyon	F19GP06C	42.7	125, 150, 175	222.8	-39.9	6.5	-50.7	170.2
Gallegos Canyon	F19GP06D	42.7	200, 225, 250	188.2	-48.3	6.2	-80.1	205.5
Gallegos Canyon	F19GP07A	45.7	150, 175, 200	144.4	-30.4	6.7	-52.7	319.0
Gallegos Canyon	F19GP07B	45.7	150, 175, 200	176.1	-32	5.4	-70.6	263.2
Gallegos Canyon	F19GP07C	45.7	150, 175, 200	163	-42.9	5.1	-71.5	308.4
Gallegos Canyon	F19GP08B	48.7	150, 175, 200	140.7	-71.3	5.6	-57.2	30.9
Gallegos Canyon	F19GP08C	48.7	150, 175, 200	153.2	-57.4	11.7	-68.7	354.4
Gallegos Canyon	F19GP09B	51.7	200, 250, 275	162.7	-12.3	16.5	-55.9	283.7
Gallegos Canyon	F19GP11A	60.7	175, 200, 225	131.5	-58.2	12.4	-52.0	0.8
Gallegos Canyon	F19GP11B	60.7	150, 175, 200	113.2	-51.2	18.8	-35.6	358.1
Gallegos Canyon	F19GP11C	60.7	125, 150, 175	94.1	-62	10.8	-26.6	17.5
De-Na-Zin	P13OJ01A	-4	200-250	158.1	-66.5	6.2	-69.6	27.3
De-Na-Zin	P13OJ01B	-4	175-225	191	-58.5	5.2	-80.8	140.2
De-Na-Zin	P13OJ01C	-4	200, 250, 300	194	-40.8	11	-72.3	205.1
De-Na-Zin	P10NZ01A	0	175-300, 350-375	137.8	-42.4	10.9	-52.1	336.0
De-Na-Zin	P10NZ01B	0	250,300-325,375	190.2	-60.2	7.9	-80.7	127.7
De-Na-Zin	P10NZ01C	0	250-300, 325	190.5	-45.4	17.9	-77.0	205.6

Location	Sample	Strat Level (m)	Temp. Steps	Strat. Declination (°)	Strat inclination (°)	MAD*	Strat. VGP latitude (°N)	Strat. VGP longitude (°E)
De-Na-Zin	P13NZ01A	0.65	TT150-250	209.9	-74.5	5.2	-58.9	99.9
De-Na-Zin	P13NZ01B	0.65	250-300	150.3	-43.9	14	-62.6	327.7
De-Na-Zin	P13NZ01C	0.65	225-350	178.4	-50	9.5	-84.3	266.1
De-Na-Zin	P13NZ03B	3.15	AF100-125	151.1	-44.2	15.8	-63.3	327.3
De-Na-Zin	P13NZ03C	3.15	AF 100-125	190.1	-50.6	5	-80.3	189.7
De-Na-Zin	P13NZ03D	3.15	125-175	82.9	-57.3	16.5	-16.6	17.2
De-Na-Zin	P13NZ06B	7.15	175, 200, 225	166.3	-23.6	11.9	-63.3	284.0
De-Na-Zin	P13NZ07A	8.9	200-225,300-350	350.4	69.2	7.9	72.2	232.7
De-Na-Zin	P13NZ07B	8.9	100-125,150,200	354.6	52.7	13.7	84.6	129.3
De-Na-Zin	P13NZ07C	8.9	100-175	356.7	71.8	10.4	69.5	246.8
De-Na-Zin	P10NZ03A	10	175, 225, 275	321.8	53.4	10.2	58.9	169.1
De-Na-Zin	P10NZ03B	10	175-225	7.9	35	10.3	71.6	47.7
De-Na-Zin	P10NZ03D	10	300-350	8.9	54.4	13	82.6	350.1
De-Na-Zin	P13NZ09A	12.4	200-250, 350	35	43.4	4.9	58.2	352.3
De-Na-Zin	P13NZ09B	12.4	225-350	8.2	42.4	10.7	76.3	38.8
De-Na-Zin	P13N 09C	12.4	200-350	40.8	44.6	6	54.0	346.4
De-Na-Zin	P13NZ10A	15.65	225-300	22.7	62.5	2.9	71.1	311.4
De-Na-Zin	P13NZ10B	15.65	150, 200-225	38.6	43.3	6.4	55.3	349.6
De-Na-Zin	P13NZ10D	15.65	100, 150, 200	355.3	38.3	17.9	74.7	88.8
De-Na-Zin	F19PZ01A	24.4	300, 325, 350	344.1	48.2	7	75.0	140.6
De-Na-Zin	F19PZ01C	24.4	300, 325, 350	351.7	29.1	6.7	68.3	95.0
De-Na-Zin	F19PZ01D	24.4	300, 325, 350	342.7	47.9	8.1	73.8	142.1
De-Na-Zin	F19PZ02A	27.4	300, 325, 350	323.4	44.9	5.1	57.5	156.4
De-Na-Zin	F19PZ02C	27.4	150, 200, 250	5.1	10.4	5.8	58.9	63.1

Location	Sample	Strat Level (m)	Temp. Steps	Strat. Declination (°)	Strat inclination (°)	MAD*	Strat. VGP latitude (°N)	Strat. VGP longitude (°E)
De-Na-Zin	F19PZ02D	27.4	100, 150, 200	324.2	63.9	4.2	61.5	193.8
De-Na-Zin	F19PZ04A	33.4	250, 300, 325	28.2	64.1	11.8	66.7	309.3
De-Na-Zin	F19PZ04B	33.4	200, 250, 350	347.1	56	8.9	79.6	169.8
De-Na-Zin	F19PZ04C	33.4	300, 325, 350	339.7	40.7	12.2	68.3	132.6
De-Na-Zin	P10NZ 05B	37.5	100-200	4.9	68.8	10	73.7	262.8
De-Na-Zin	P10NZ 05C	37.5	250-275, 325	315.7	38.7	19.2	49.1	153.8
De-Na-Zin	P10NZ 05D	37.5	100-175	334.6	57.3	10.7	69.7	174.2
De-Na-Zin	F19SZ01B	39.3	300, 325, 350	346.8	9.2	9.2	56.4	97.3
De-Na-Zin	F19SZ01C	39.3	300, 325, 350	11.2	28.4	7.2	66.9	44.5
De-Na-Zin	F19SZ01D	39.3	200, 250, 300	340.4	52.8	16.1	73.7	159.5
De-Na-Zin	P10NZ06A	40	325-375	170.7	-34.9	16	-71.1	280.1
De-Na-Zin	P10NZ06B	40	325-375	153.1	-35.8	18.1	-61.3	314.3
De-Na-Zin	P10NZ06C	40	275, 350, 375	145.1	-36.9	7	-55.8	324.3
De-Na-Zin	F19SZ02A	40.8	300, 350, 400	198.1	-27.9	13.4	-63.4	211.0
De-Na-Zin	F19SZ02C	40.8	150, 325, 350	225.7	-40.5	20.1	-48.6	168.2
De-Na-Zin	F19SZ03B	42.3	150, 200, 250	151.5	-69.6	5.7	-63.6	33.1
De-Na-Zin	F19SZ03C	42.3	150, 200, 250	109.5	-77.4	6.6	-40.3	42.7
De-Na-Zin	F19SZ03D	42.3	250, 300, 325	163.8	-47.8	4.5	-74.6	320.0
De-Na-Zin	P10NZ 07A	45	150-175	191.1	-40.4	10.6	-73.6	213.0
De-Na-Zin	P10NZ 07C	45	200-250	191.2	-39.6	17.8	-73.1	213.9
De-Na-Zin	P10NZ 07D	45	AF75-TT100	191.4	-69	6.7	-71.9	94.8
De-Na-Zin	F19SZ04A	45.3	100, 150, 200	127.4	-54.1	11	-47.6	357.3
De-Na-Zin	F19SZ04C	45.3	100, 150, 200	107.7	-57.1	4	-33.6	8.1
De-Na-Zin	F19SZ04D	45.3	100, 150, 200	102.6	-61.6	9.6	-31.9	15.4

Location	Sample	Strat Level (m)	Temp. Steps	Strat. Declination (°)	Strat inclination (°)	MAD*	Strat. VGP latitude (°N)	Strat. VGP longitude (°E)
De-Na-Zin	F19SZ05D	48.3	325, 375, 400	138.2	-10.6	17.4	-40.9	314.5
De-Na-Zin	F19SZ06A	51.3	150, 200, 250	115.5	-26.1	17.5	-28.6	339.5
De-Na-Zin	F19SZ06B	51.3	100, 150, 250	144	-6.2	8.9	-43.3	306.7
De-Na-Zin	F19SZ06D	51.3	150, 200, 250	92.1	-45.4	11.4	-17.0	4.3
De-Na-Zin	F19SZ07A	54.3	250, 300, 325	194.6	-49.6	6.2	-76.6	183.4
De-Na-Zin	F19SZ07B	54.3	250, 300, 325	192.8	-50.7	5.9	-78.4	182.6
De-Na-Zin	F19SZ07C	54.3	250, 300, 325	185.6	-44.1	8.5	-78.8	226.2
De-Na-Zin	F19BZ01A	56	250, 300, 325	197.2	-52.3	19.8	-75.5	170.3
De-Na-Zin	F19BZ01B	56	100, 150, 300	137.2	-60.2	4.7	-56.5	5.0
De-Na-Zin	F19BZ01C	56	250, 300, 325	173.6	-53.2	10.1	-84.3	321.7
De-Na-Zin	F19SZ08A	57.15	250, 300, 325	131.2	-51	5.8	-49.7	351.5
De-Na-Zin	F19SZ08B	57.15	250, 300, 325	183.5	-50.2	9.1	-84.2	221.9
De-Na-Zin	F19BZ02B	59	100, 150, 200	156.3	-31.5	18.6	-61.7	307.2
De-Na-Zin	F19SZ09A	60.05	200, 250, 300	143.9	-49	16.8	-59.3	342.1
De-Na-Zin	F19SZ09B	60.05	200, 250, 300	176.8	-48	14.4	-82.5	275.1
De-Na-Zin	F19SZ09C	60.05	100, 150, 200	159.8	-21.2	16.4	-59.0	294.2
De-Na-Zin	F19BZ03B	62	100, 150, 250	156.2	-22.7	4.7	-57.7	300.6
De-Na-Zin	F19BZ03C	62	250, 300, 325	127.9	-51.6	8.2	-47.2	353.7
De-Na-Zin	F19BZ04D	65	250, 300, 350	178.6	-37.1	18.5	-74.7	258.0
De-Na-Zin	F19BZ05A	68	150, 200, 250	5.4	41.2	8.9	76.8	50.8
De-Na-Zin	F19BZ05B	68	200, 250, 300	7.1	22.2	6.4	64.7	56.5
De-Na-Zin	F19BZ05D	68	200, 250, 325	358.9	30.8	13	70.6	76.2
De-Na-Zin	F19BZ06C	71	250, 300, 325	4.4	26	4.4	67.4	61.8
De-Na-Zin	F19BZ06D	71	200, 250, 300	337.8	37.7	10.4	65.6	131.5

Location	Sample	Strat Level (m)	Temp. Steps	Strat. Declination (°)	Strat inclination (°)	MAD*	Strat. VGP latitude (°N)	Strat. VGP longitude (°E)
De-Na-Zin	F19TZ01B	71	200, 250, 300	333.3	54.5	6.1	68.3	168.3
De-Na-Zin	F19TZ01C	71	250, 300, 325	349.4	61.9	11.5	79.2	207.3
De-Na-Zin	F19TZ01D	71	250, 300, 325	318.9	83.9	15.6	44.6	241.9
De-Na-Zin	F19BZ07A	74	150, 200, 250	11	53	12.7	80.6	354.9
De-Na-Zin	F19BZ07B	74	200, 250, 300	34.1	30.5	11.1	54.0	6.9
De-Na-Zin	F19TZ02A	74	150, 200, 250	357.2	40.6	2.7	77.0	84.5
De-Na-Zin	F19TZ02C	74	100, 150, 200	2.2	71.5	5.1	69.7	256.5
De-Na-Zin	F19TZ03B	77	150, 200, 250	344.9	44.3	9.1	73.7	129.5
De-Na-Zin	F19TZ03D	77	200, 250, 300	353.6	35.1	7.7	72.4	93.4
De-Na-Zin	F19TZ04A	80	250, 300, 325	35	74.8	16.7	56.4	282.7
De-Na-Zin	F19TZ04B	80	150, 200, 250	5.6	75	3.3	63.9	259.0
De-Na-Zin	F19TZ04C	80	200, 250, 300	355.3	75.5	1.6	63.2	248.2
De-Na-Zin	F19TZ05C	83	100, 150, 200	1.7	44	11.2	79.7	64.4
De-Na-Zin	F19TZ06B	86	150, 200, 250	306.4	62.6	6.1	48.9	191.2
De-Na-Zin	F19TZ06C	86	100, 150, 200	60.8	59.5	14.7	42.9	318.4
De-Na-Zin	F19TZ06D	86	100, 150, 200	36	60.3	6.6	61.6	321.3
De-Na-Zin	F19TZ07B	89	250, 300, 325	349.8	55.8	5.4	81.8	168.4
De-Na-Zin	F19TZ07C	89	250, 300, 325	336.2	40.8	4.7	65.9	137.9
De-Na-Zin	F19TZ07D	89	250, 300, 325	341.7	47.9	5.7	73.1	143.6
De-Na-Zin	F19TZ08A	92	250, 300, 325	314.2	39.4	9.1	48.2	156.8
De-Na-Zin	F19TZ08B	92	200, 250, 300	353.6	42.6	4.8	77.4	100.7
De-Na-Zin	F19TZ08C	92	250, 300, 325	315.1	51.4	17.6	52.9	170.3
De-Na-Zin	F19TZ09B	95	250, 300, 325	300.8	57	8.9	43.4	183.5
De-Na-Zin	F19TZ09C	95	250, 300, 325	320.6	57.1	13.2	58.7	178.1

Location	Sample	Strat Level (m)	Temp. Steps	Strat. Declination (°)	Strat inclination (°)	MAD*	Strat. VGP latitude (°N)	Strat. VGP longitude (°E)
De-Na-Zin	F19TZ09D	95	250, 300, 325	330.1	26.6	12.5	55.4	131.4
De-Na-Zin	F19TZ10B	98	200, 250, 300	297.8	52.3	6.6	39.5	178.7
De-Na-Zin	F19TZ10C	98	250, 300, 325	282.4	36.7	13.4	21.6	173.2
De-Na-Zin	F19TZ10D	98	200, 250, 300	298.9	47.6	8.5	38.7	173.3
De-Na-Zin	F19TZ11A	100.25	250, 300, 325	351.8	45.3	4.7	78.5	112.5
De-Na-Zin	F19TZ11B	100.25	250, 300, 325	348.1	47.8	6	77.7	131.0
De-Na-Zin	F19TZ11D	100.25	250, 300, 325	359.8	29.6	3.3	69.9	73.6
De-Na-Zin	F19TZ12A	104	200, 250, 300	40.6	77.5	4.9	51.8	278.3
De-Na-Zin	F19TZ12B	104	150, 200, 250	61.8	69.7	3.1	44.4	300.2
De-Na-Zin	F19TZ12C	104	100, 150, 200	62.8	55.6	1	40.2	323.1
Kimbeto	P16KW15A	4.7	150-250	353.3	51.8	4.2	83.3	130.1
Kimbeto	P16KW15B	4.7	100, 150, 325	4.8	46.6	7.5	80.7	45.1
Kimbeto	P16KW15C	4.7	200-300	354.2	47.5	5.4	81.0	106.9
Kimbeto	P16KW01A	5.7	200-300	144.4	-56.6	6.3	-61.6	355.1
Kimbeto	P16KW01C	5.7	325, 375, 400	167.6	-34.8	1.8	-69.8	288.3
Kimbeto	P16KW01D	5.7	200, 300, 350	167.9	-45.8	15.7	-76.4	304.6
Kimbeto	P16KW02C	8.7	350-400	352.4	8.4	6.1	57.3	86.5
Kimbeto	P16KW02D	8.7	300-350	333.2	24.5	18.1	56.5	125.1
Kimbeto	P16KW03A	11.7	200-300	334.8	53.7	7.3	69.4	164.4
Kimbeto	P16KW03B	11.7	100, 150, 325	44.3	45.6	7.5	51.5	343.3
Kimbeto	P16KW03C	11.7	150, 200, 350	22.9	72.9	11.3	63.2	279.3
Kimbeto	P16KW04A	14.7	300, 350, 375	350.8	57.8	5.2	82.4	182.2
Kimbeto	P16KW04B	14.7	300, 350, 375	330.6	48.6	3.7	64.5	155.8
Kimbeto	P16KW04C	14.7	250-325	335.3	50.7	5.9	69.0	156.4

Location	Sample	Strat Level (m)	Temp. Steps	Strat. Declination (°)	Strat inclination (°)	MAD*	Strat. VGP latitude (°N)	Strat. VGP longitude (°E)
Kimbeto	P16KW06C	19.9	100-200	337.0	47.0	17.3	69.0	146.5
Kimbeto	P16KW06A	19.9	250, 300, 350	354.7	20.2	5.8	63.8	84.3
Kimbeto	P16KW06B	19.9	100-200	9.1	22.9	5.5	64.4	51.4
Kimbeto	P16KW07A	22.9	150-250	346.2	32.5	15.8	67.8	109.4
Kimbeto	P16KW08B	25.9	150-250	335.7	44.6	14.7	67.0	143.6
Kimbeto	P16KW08C	25.9	150-250	8.0	42.5	4.9	76.5	39.5
Kimbeto	P16KW08D	25.9	300, 250, 375	338.1	48.8	14.4	70.6	149.3
Kimbeto	P16KW09B	28.9	200, 325, 400	175.8	-33.6	14.6	-71.8	265.3
Kimbeto	P16KW09C	28.9	300-350	133.2	-26.4	15.5	-42.7	326.8
Kimbeto	P16KW09D	28.9	100, 200, 250	189.6	-31.5	12.6	-69.0	225.9
Kimbeto	P16KW11D	34.9	250, 325, 400	115.0	-48.1	9.8	-35.8	354.8
Kimbeto	P16KW12A	37.9	100, 150, 250	155.8	-40.1	7.7	-65.2	316.5
Kimbeto	P16KW12D	37.9	100-200	161.4	-60.7	9.9	-74.6	8.9
Kimbeto	P16KW12C	37.9	100-200	157.0	-33.1	12.6	-62.8	306.7
Kimbeto	P16KW13C	40.9	100, 150, 250	123.8	-52.5	14.9	-44.3	355.8
Kimbeto	P16KW13D	40.9	100, 150, 400	206.0	-50.8	13.0	-68.0	167.1
Kimbeto	F17KW01B	43.9	100-200	161.8	-69.6	6.0	-68.7	41.6
Kimbeto	F17KW01C	43.9	100, 200, 300	224.3	-38.6	11.6	-49.1	170.6
Kimbeto	F17KW01D	43.9	150-250	205.3	-52.0	7.4	-68.9	164.7
Kimbeto	F17KW04A	52.3	100-250	93.3	-49.4	7.6	-19.7	6.0
Kimbeto	F17KW04B	52.3	100-200	105.1	-63.3	13.6	-34.4	16.3
Kimbeto	F17KW04C	52.3	150-250	204.6	-36.4	10.5	-63.2	192.3
Kimbeto	F17KW05A	55.3	150-250	124.8	-49.2	20.0	-44.0	351.4
Kimbeto	F17KW05B	55.3	100-200	157.3	-37.5	8.1	-65.0	311.0

Location	Sample	Strat Level (m)	Temp. Steps	Strat. Declination (°)	Strat inclination (°)	MAD*	Strat. VGP latitude (°N)	Strat. VGP longitude (°E)
Kimbeto	F17KW07A	55.3	150-250	216.6	-35.5	12.2	-54.0	179.8
Kimbeto	F17KW08A	58.3	300-400	338.5	34.0	13.1	64.2	125.3
Kimbeto	F17KW08B	58.3	200-350	34.2	41.1	9.1	58.0	356.0
Kimbeto	F17KW08D	58.3	150-250	21.6	29.1	4.9	61.8	23.8
Kimbeto	F17KW09A	58.9	200-300	349.3	51.0	9.8	80.1	138.6
Kimbeto	F17KW09B	58.9	100, 150, 250	353.1	74.4	3.1	65.0	244.4
Kimbeto	F17KW09C	58.9	100-200	358.9	60.1	4.8	85.1	242.6
Kimbeto	F17KW10A	61.9	100-400	8.4	39.1	9.6	74.1	42.7
Kimbeto	F17KW10B	61.9	150, 250, 300	11.0	35.6	4.8	70.9	39.1
Kimbeto	F17KW10D	61.9	350, 350, 400	356.7	53.1	5.6	86.3	120.2
Kimbeto	F17KW06A	64.0	100-200	353.1	32.6	5.8	70.6	92.5
Kimbeto	F17KW06B	64.0	100-200, 300	15.2	58.2	6.2	77.7	325.3
Kimbeto	F17KW06C	64.0	100-250	5.8	69.4	8.4	72.7	264.1
Kimbeto	F17KW11A	64.9	100-250	339.3	40.4	7.4	67.8	131.8
Kimbeto	F17KW11B	64.9	100-200, 300	354.5	37.9	4.4	74.3	91.7
Kimbeto	F17KW11C	64.9	300-400	357.3	50.5	12.9	84.6	97.5
Kimbeto	F17KW13B	70.9	300-400	343.6	55.7	5.0	76.8	167.4
Kimbeto	F17KW13D	70.9	200-300	340.5	46.9	4.4	71.7	141.8
Kimbeto	F17KW14A	73.9	200, 250, 400	5.1	32.5	7.5	70.9	57.4
Kimbeto	F17KW14B	73.9	200, 250, 350	357.1	22.2	7.2	65.2	79.2
Kimbeto	F17KW14C	73.9	200-300	353.7	23.3	2.3	65.3	87.3
Kimbeto	F17KW15C	76.9	150-250	14.1	14.3	5.3	58.3	45.0
Kimbeto	F17KW15D	76.9	200-300	3.2	12.3	10.3	59.9	66.1
Kimbeto	F17KW16B	79.9	300-400	30.5	35.6	3.5	58.6	5.8

Location	Sample	Strat Level (m)	Temp. Steps	Strat. Declination (°)	Strat inclination (°)	MAD*	Strat. VGP latitude (°N)	Strat. VGP longitude (°E)
Kimbeto	F17KW16C	79.9	300-400	32.3	58.0	3.4	64.4	327.1
Betonnie Tsosie	P16BT01A	0	250, 325, 400	213.7	-54.1	4.8	-62.6	155.8
Betonnie Tsosie	P16BT01B	0	350-400	195.2	-58.4	10.2	-77.6	144.0
Betonnie Tsosie	P16BT04A	4.5	400, 425, 450	181.4	-13.2	15.4	-60.7	250.2
Betonnie Tsosie	P16BT05A	7.5	100-200	6.4	47.5	15	80.9	35.0
Betonnie Tsosie	P16BT05B	7.5	100-200	330.1	53.3	19.9	65.5	166.8
Betonnie Tsosie	P16BT05D	7.5	150-250	345.9	60.6	8.7	77.7	194.2
Betonnie Tsosie	P16BT06A	8.65	250-325	343.9	43	4.9	72.3	128.9
Betonnie Tsosie	P16BT06B	8.65	200, 300, 325	339.4	56.8	3.9	73.5	173.9
Betonnie Tsosie	P16BT06D	8.65	200, 250, 325	332.6	53.3	11	67.5	165.6
Betonnie Tsosie	P16BT07A	10	325-375	348.9	34.4	7.7	70.3	105.7
Betonnie Tsosie	P16BT07B	10	375-425	350.8	36.9	7	72.6	103.0
Betonnie Tsosie	P16BT08B	11.5	300-350	347.5	35.1	11.9	70.1	109.8
Betonnie Tsosie	P16BT08C	11.5	325-375	350.3	59.5	6.9	81.2	195.5
Betonnie Tsosie	P16BT08D	11.5	350-400	339.6	58.1	8.8	73.6	178.8
Betonnie Tsosie	P16BT09A	13	325-375	354.2	46.5	8.1	80.4	105.5
Betonnie Tsosie	P16BT09B	13	375-425	339	64.3	15.7	71.3	202.2
Betonnie Tsosie	P16BT09D	13	375-425	359.2	53.8	5.2	88.2	94.7
Betonnie Tsosie	P16BT10A	14.5	200-300	297.6	70.2	9.2	44.1	206.8
Betonnie Tsosie	P16BT10B	14.5	150-250	8.9	49.6	3.5	80.7	17.3
Betonnie Tsosie	P16BT10D	14.5	375-425	343.7	27.5	5.5	64.1	111.4
Betonnie Tsosie	FBW1501A	17.1	250-350	0.7	49.9	10.5	84.7	66.5
Betonnie Tsosie	FBW1501B	17.1	250-350	20.5	57.5	10.5	73.5	329.5
Betonnie Tsosie	FBW1501C	17.1	200-300	42.4	58	7	56.5	325.4

Location	Sample	Strat Level (m)	Temp. Steps	Strat. Declination (°)	Strat inclination (°)	MAD*	Strat. VGP latitude (°N)	Strat. VGP longitude (°E)
Betonnie Tsosie	P16BT11A	17.5	100-200	351.2	46.1	9.9	78.7	116.6
Betonnie Tsosie	P16BT11B	17.5	200-300	56	84.8	11.6	41.2	264.4
Betonnie Tsosie	P16BT11C	17.5	100, 150, 250, 300	354.1	61.5	5.8	81.9	220.3
Betonnie Tsosie	P16BT12C	19	300, 350, 400	300.2	65	11.8	45.0	196.5
Betonnie Tsosie	P16BT12D	19	100-200	333.1	40.9	12	63.6	142.0
Betonnie Tsosie	P16BT13B	20.5	300-350	328.4	72.2	9.5	60.1	218.4
Betonnie Tsosie	P16BT13C	20.5	150-250	348.4	39.4	6.7	73.0	112.5
Betonnie Tsosie	P16BT14A	22	300, 325, 400	3.3	29.3	13.3	69.5	63.9
Betonnie Tsosie	P16BT14B	22	250-325	9.5	28.7	2.8	67.6	48.3
Betonnie Tsosie	P16BT14C	22	250-325	357.1	18.6	14.2	63.4	79.4
Betonnie Tsosie	FBW1503A	23.2	150-250	349.1	46.5	10.4	77.6	124.4
Betonnie Tsosie	FBW1503C	23.2	200, 250, 400	348.3	60.8	9.4	79.2	199.2
Betonnie Tsosie	FBW1503D	23.2	200-300	7	44.9	12.7	78.8	38.9
Betonnie Tsosie	FBW1502A	23.4	250-350	4.8	38.1	10.6	74.8	55.7
Betonnie Tsosie	FBW1502B	23.4	250-350	4.6	32.1	13.3	71.0	59.4
Betonnie Tsosie	FBW1502D	23.4	250-350	15.8	14.9	3.5	58.1	42.3
Betonnie Tsosie	FBW1507A	24.2	300-400	325.6	27.2	6.9	52.4	136.9
Betonnie Tsosie	FBW1507C	24.2	200-300	318.2	20.5	11.3	44.5	139.7
Betonnie Tsosie	P16BT15C	24.5	100-200	335.1	57.2	12.3	70.1	175.7
Betonnie Tsosie	P16BT17B	25.6	150-250	12.2	49.2	4.9	78.2	9.6
Betonnie Tsosie	P16BT17C	25.6	250-325	34	34.9	13.6	55.8	3.1
Betonnie Tsosie	P16BT17D	25.6	300-350	9.5	53.4	2.2	82.0	355.0
Betonnie Tsosie	P16BT18A	28.6	150-250	323	54.4	11.3	60.0	172.0
Betonnie Tsosie	P16BT18C	28.6	250, 300, 350	293.8	61.1	10.4	39.5	191.4

Location	Sample	Strat Level (m)	Temp. Steps	Strat. Declination (°)	Strat inclination (°)	MAD*	Strat. VGP latitude (°N)	Strat. VGP longitude (°E)
Betonnie Tsosie	P16BT18D	28.6	200, 350, 325	314	58.2	4.2	53.7	181.7
Betonnie Tsosie	P16BT19A	30.1	400-450	331.5	53.5	5	66.7	166.6
Betonnie Tsosie	P16BT19B	30.1	400-450	344.1	50.8	4.2	76.1	148.8
Betonnie Tsosie	P16BT19C	30.1	400-450	338.7	62.8	3.7	71.8	196.4
Betonnie Tsosie	P16BT20A	31.6	150-250	37.6	71.5	8.7	57.7	292.4
Betonnie Tsosie	P16BT20C	31.6	400-450	38.1	54.7	6.2	59.2	333.0
Betonnie Tsosie	P16BT20D	31.6	250-325	51.7	63.6	4.1	50.4	313.1
Betonnie Tsosie	P16BT21A	33.1	400-450	322.7	49.6	10	58.5	163.7
Betonnie Tsosie	P16BT21B	33.1	400-450	335.5	61.3	7.6	70.0	189.2
Betonnie Tsosie	P16BT21C	33.1	400-450	314.2	51.9	6.1	52.3	171.4
Betonnie Tsosie	P16BT22A	34.6	325-375	341	71.7	5.1	65.8	227.0
Betonnie Tsosie	P16BT22B	34.6	375-425	310.7	55.9	8.6	50.7	178.8
Betonnie Tsosie	P16BT22D	34.6	300-350	316.7	68.6	4.4	55.7	204.4
Betonnie Tsosie	F19BW01A	35.55	125, 150, 400	305.8	55.7	16	46.8	180.1
Betonnie Tsosie	F19BW01D	35.55	175, 200, 225	281.4	44.2	14	23.6	178.8
Betonnie Tsosie	P16BT23A	35.6	200-300	20	30.6	6.9	63.6	25.5
Betonnie Tsosie	F19BW02B	37.15	125, 150, 200	155.7	-65.8	11.4	-68.4	24.5
Betonnie Tsosie	F19BW03A	39.15	200. 225, 250	169.7	-54.3	14.7	-81.5	338.1
Betonnie Tsosie	F19BW03B	39.15	200, 250, 300	285.4	-80.5	15.7	-29.3	93.5
Betonnie Tsosie	F19BW03C	39.15	200, 225, 250	176.1	-54.2	8.8	-86.6	322.4
Betonnie Tsosie	FBW1504C	39.6	300-400	214.9	-62.2	9.2	-62.4	136.5
Betonnie Tsosie	FBW1504D	39.6	250-350	187.3	-57.5	9.2	-83.8	140.8
Betonnie Tsosie	FBW1505A	41.3	250-350	187.1	-13.4	15.2	-60.1	238.8
Betonnie Tsosie	FBW1505D	41.3	200-300	197.8	-22	16.4	-60.6	215.3

Location	Sample	Strat Level (m)	Temp. Steps	Strat. Declination (°)	Strat inclination (°)	MAD*	Strat. VGP latitude (°N)	Strat. VGP longitude (°E)
Betonnie Tsosie	F19BW04D	47.25	400, 425, 540	211	-43.3	19.7	-61.4	176.4
Betonnie Tsosie	F19BW05B	51.55	425, 475, 520	190.1	-19.1	18	-62.3	231.2
Betonnie Tsosie	F19BW08D	62.55	375, 500, 520	167.8	-44.6	10.1	-75.7	303.3
Betonnie Tsosie	F19BW13A	79.05	300, 325, 350	343.2	53.4	7.7	76.1	159.4
Betonnie Tsosie	F19BW13B	79.05	350, 375, 400	340.6	47.4	4.7	72.0	144.0
Betonnie Tsosie	F19BW13C	79.05	350, 375, 400	2.5	51.3	6	85.5	45.1
Betonnie Tsosie	F19BT01A	79.5	225, 250, 275	330.6	39.1	5.3	61.0	142.5
Betonnie Tsosie	F19BT01B	79.5	225, 250, 275	343.7	39.7	5.7	70.5	123.9
Betonnie Tsosie	F19BT01C	79.5	150, 175, 200	336.5	32.9	9.7	62.5	128.2
Betonnie Tsosie	F19BT02B	82.5	225, 250, 275	15.7	55.5	7.1	77.3	338.2
Betonnie Tsosie	F19BT02D	82.5	225, 250, 275	24.9	63.1	6	69.3	310.9
Betonnie Tsosie	F19BT03C	85.5	NRM, 200, 225	320.9	37.4	7	52.8	149.9
Betonnie Tsosie	F19BT03D	85.5	150, 175, 200	333.5	38.6	6.8	62.9	138.5
Betonnie Tsosie	F19BT04B	88.5	175, 200, 225	289	70.5	18	39.2	208.2
Betonnie Tsosie	F19BT04C	88.5	100, 125, 150	301.1	34.1	11.5	35.8	161.0
Betonnie Tsosie	F19BT04D	88.5	225, 250, 275	306.4	43.8	6.1	43.4	165.8
Betonnie Tsosie	F19BT05B	91.5	175, 200, 225	21.3	21	7.4	58.3	30.2
Betonnie Tsosie	F19BT05C	91.5	225, 250, 275	348.8	75	11.5	63.2	241.2
Betonnie Tsosie	F19BT05D	91.5	225, 250, 275	346.3	51.9	5.7	78.2	149.9
Betonnie Tsosie	F19BT06A	94.5	100, 125, 150	31.3	38	6.1	59.1	2.7
Betonnie Tsosie	F19BT06B	94.5	150, 175, 200	27.2	65	14.9	67.0	306.0
Betonnie Tsosie	F19BT06C	94.5	150, 175, 200	355.6	66.7	13.6	76.4	240.7
Betonnie Tsosie	F19BT07A	97.5	175, 200, 225	353.3	59.9	14	82.9	207.3
Betonnie Tsosie	F19BT07B	97.5	225, 250, 275	336.4	51.6	6.7	70.2	159.0

Location	Sample	Strat Level (m)	Temp. Steps	Strat. Declination (°)	Strat inclination (°)	MAD*	Strat. VGP latitude (°N)	Strat. VGP longitude (°E)
Betonnie Tsosie	F19BT07C	97.5	200, 225, 250	260.4	63.6	3.3	18.8	205.8
Betonnie Tsosie	F19BT08A	100.5	125, 150, 175	350.9	38.9	5	73.9	104.9
Betonnie Tsosie	F19BT08B	100.5	200, 225, 250	339.4	39.7	19.3	67.6	131.6
Betonnie Tsosie	F19BT08C	100.5	NRM, 225, 250	331.2	25.9	6.2	55.9	129.5
Betonnie Tsosie	F19BT09A	110	150, 175, 200	25.8	48	19.5	67.2	353.4
Betonnie Tsosie	F19BT09B	110	225, 250, 275	359.5	40	4.3	76.8	75.0
Betonnie Tsosie	F19BT09D	110	225, 250, 275	5.1	47.3	1.9	81.3	41.9
Mesa de Cuba	P13LC01A	-2.7	100-200	308.7	36.0	8.1	42.5	157.6
Mesa de Cuba	P13LC01B	-2.7	100-175	344.0	42.4	5.3	72.1	127.6
Mesa de Cuba	P13LC02B	0.0	100-250	358.4	49.3	10.4	84.0	86.4
Mesa de Cuba	P13LC02C	0.0	125-250	334.4	27.4	5.9	58.6	126.4
Mesa de Cuba	P13LC03B	3.0	125-225	335.4	50.6	2.9	69.1	157.2
Mesa de Cuba	P13LC03C	3.0	100-225	324.0	66.9	2.2	60.7	201.8
Mesa de Cuba	P13LC04B	6.0	100-200	309.8	83.9	3.9	43.1	240.3
Mesa de Cuba	P13LC04C	6.0	100-150, 200, 225	27.7	76.9	1.8	56.6	273.9
Mesa de Cuba	P13LC04D	6.0	100-200	334.6	66.1	2.1	67.6	204.7
Mesa de Cuba	P13LC05A	9.0	150-250, 325	9.8	57.5	2.7	81.9	324.9
Mesa de Cuba	P13LC05B	9.0	150-200, 300	336.0	46.3	3.9	68.0	147.4
Mesa de Cuba	P13LC06A	12.0	125-275	3.1	49.2	2.9	83.5	48.4
Mesa de Cuba	P13LC06B	12.0	300-400	307.5	58.2	11.7	48.8	183.4
Mesa de Cuba	FMC1501A	14.0	250-350	19.1	42.4	13.1	70.0	12.6
Mesa de Cuba	FMC1501B	14.0	250-350	359.4	44.2	6.6	79.9	76.1
Mesa de Cuba	FMC1501D	14.0	250-350	342.1	54.4	7.5	75.4	164.1
Mesa de Cuba	FMC1504A	14.0	200-350	328.8	31.1	8.3	56.3	136.5

Location	Sample	Strat Level (m)	Temp. Steps	Strat. Declination (°)	Strat inclination (°)	MAD*	Strat. VGP latitude (°N)	Strat. VGP longitude (°E)
Mesa de Cuba	FMC1504B	14.0	150-250	345.0	27.6	13.9	64.8	109.0
Mesa de Cuba	FMC1504C	14.0	200-300	333.5	55.3	7.1	68.6	170.4
Mesa de Cuba	P13LC07A	15.0	125-225	336.7	32.9	12.6	62.6	127.9
Mesa de Cuba	P13LC07C	15.0	125-300, 350-400	23.8	86.6	9.1	42.1	256.7
Mesa de Cuba	P13LC08A	18.0	125-225	339.7	64.6	2.7	71.6	203.9
Mesa de Cuba	P13LC08C	18.0	125-400	15.1	58.0	3.1	77.7	326.0
Mesa de Cuba	P13LC08D	18.0	125-225	24.4	63.9	1.6	69.3	307.9
Mesa de Cuba	P13LC09B	21.0	125-200	15.6	48.8	12.7	75.5	4.2
Mesa de Cuba	P13LC09C	21.0	275-325	312.4	31.6	20.7	44.0	151.7
Mesa de Cuba	P14MC01A	21.0	325-375	331.8	39.2	8.7	61.9	141.3
Mesa de Cuba	P14MC01B	21.0	250-325	1.3	56.0	13.9	88.8	315.0
Mesa de Cuba	P14MC01C	21.0	325-375	333.5	51.2	6.9	67.7	160.1
Mesa de Cuba	FMC1502A	23.8	100, 200, 250	14.5	56.9	14.7	78.3	331.4
Mesa de Cuba	FMC1502C	23.8	200, 300, 400	339.3	27.8	17.1	61.8	119.4
Mesa de Cuba	P14MC02B	24.0	200-300	27.3	25.5	18.8	56.7	18.7
Mesa de Cuba	P14MC02C	24.0	100, 300, 325	14.1	70.3	8.5	69.2	276.5
Mesa de Cuba	P14MC03C	27.0	325, 400, 425	107.6	-79.7	11.4	-39.5	48.0
Mesa de Cuba	P14MC10A	54.0	150-300	327.0	38.3	6.5	57.9	145.3
Mesa de Cuba	P14MC10C	54.0	400-450	344.8	38.9	9.2	70.7	120.4
Mesa de Cuba	P14MC10D	54.0	300-350	340.4	35.6	1.9	66.3	124.8
Mesa de Cuba	P14MC12A	60.0	350-425	340.5	49.4	13.4	72.7	149.2
Mesa de Cuba	P14MC12B	60.0	325-375	50.5	70.7	15.0	51.0	297.6
Mesa de Cuba	P14MC13B	73.5	400-450	308.6	37.7	5.6	43.1	159.0
Mesa de Cuba	P14MC13C	73.5	150, 200, 375	324.4	74.1	8.6	56.8	221.3

Location	Sample	Strat Level (m)	Temp. Steps	Strat. Declination (°)	Strat inclination (°)	MAD*	Strat. VGP latitude (°N)	Strat. VGP longitude (°E)
Mesa de Cuba	P14MC13D	73.5	200, 250, 325	5.6	38.0	8.4	74.5	53.1
Mesa de Cuba	P14MC14C	76.5	375, 425, 450	329.6	24.7	8.3	54.3	130.6
Mesa de Cuba	P14MC14D	76.5	200-300	350.6	38.3	13.4	73.4	105.1
Mesa de Cuba	P14MC15B	79.5	150-250	28.7	68.7	17.6	64.1	295.6
Mesa de Cuba	P14MC15D	79.5	150-250	13.4	59.4	8.5	78.7	317.2
Mesa de Cuba	P14MC16A	82.5	150-250	338.7	44.0	7.6	69.1	139.6
Mesa de Cuba	P14MC16B	82.5	200, 325, 350	334.0	48.8	19.5	67.4	154.4
Mesa de Cuba	P14MC17B	85.5	200-300	319.6	67.0	9.9	57.9	200.9
Mesa de Cuba	P14MC18B	88.5	325-375	15.1	39.8	5.8	71.3	24.5
Mesa de Cuba	P14MC18C	88.5	325-375	30.2	45.0	8.1	62.7	354.6
Mesa de Cuba	P14MC18D	88.5	400-450	18.0	65.4	4.7	72.4	296.6
Mesa de Cuba	P14MC19A	91.5	150-250	336.7	48.1	5.3	69.3	150.3
Mesa de Cuba	P14MC19B	91.5	200-300	327.5	40.6	5.3	59.2	147.5
Mesa de Cuba	P14MC19D	91.5	200-300	341.7	29.1	3.4	63.8	116.3
Mesa de Cuba	P14MC20A	106.5	250-325	179.6	-49.9	10.5	-84.7	256.7
Mesa de Cuba	P14MC20C	106.5	250-325	175.0	-38.2	11.9	-74.8	271.1
Mesa de Cuba	P14MC20D	106.5	200-300	200.5	-60.3	5.9	-73.2	138.6
Mesa de Cuba	P14MC21A	109.5	350-400	205.6	-55.8	6.9	-69.4	154.4
Mesa de Cuba	P14MC21C	109.5	375-425	159.1	-49.3	7.0	-71.6	330.5
Mesa de Cuba	P14MC21D	109.5	325-425	181.4	-57.0	9.8	-88.1	107.7
Mesa de Cuba	P14MC22C	114.0	200-300	126.1	-65.8	8.4	-49.1	17.4
Mesa de Cuba	P14MC22D	114.0	150-250	173.3	-65.5	1.9	-77.3	52.0
Mesa de Cuba	P14MC23B	117.0	325-375	193.5	-63.4	11.2	-76.4	117.7
Mesa de Cuba	P14MC23D	117.0	400-450	158.2	-48.7	12.1	-70.7	330.1

Location	Sample	Strat Level (m)	Temp. Steps	Strat. Declination (°)	Strat inclination (°)	MAD*	Strat. VGP latitude (°N)	Strat. VGP longitude (°E)
Mesa de Cuba	P14MC24A	120.0	325-375	150.9	-39.2	7.0	-61.2	322.3
Mesa de Cuba	P14MC24C	120.0	150-250	172.1	-60.8	5.0	-81.5	28.8
Mesa de Cuba	P14MC25A	123.0	250, 375, 425	132.2	-77.7	10.7	-49.1	46.1
Mesa de Cuba	P14MC26A	126.0	200-300	184.8	-71.3	10.2	-69.8	80.8
Mesa de Cuba	P14MC26B	126.0	325-375	162.2	-55.1	13.0	-75.6	346.8
Mesa de Cuba	P14MC26C	126.0	250, 400, 425	145.0	-39.1	16.2	-56.6	328.1
Mesa de Cuba	P14MC27A	129.0	300-325	165.8	-40.3	18.1	-72.1	300.2
Mesa de Cuba	P14MC27B	129.0	300, 350, 400	185.0	-19.9	9.2	-63.9	241.8
Mesa de Cuba	P14MC28A	132.0	300-350	183.6	-36.6	15.1	-74.1	240.6
Mesa de Cuba	P14MC28C	132.0	200-300	219.1	-62.4	13.3	-59.3	136.3
Mesa de Cuba	P14MC29A	135.0	400-450	155.5	-49.4	3.1	-68.8	334.4
Mesa de Cuba	P14MC29B	135.0	325-375	159.5	-35.7	3.6	-65.8	306.4
Mesa de Cuba	P14MC29D	135.0	400-450	132.4	-50.2	4.2	-50.4	349.9
Mesa de Cuba	P14MC30B	138.0	350-400	183.4	-61.8	18.4	-82.5	92.5
Mesa de Cuba	P14MC30C	138.0	325-400	116.4	-42.1	18.3	-34.7	349.6
Mesa de Cuba	P14MC31A	147.0	375, 425, 450	161.6	-46.3	9.2	-72.3	319.9
Mesa de Cuba	P14MC31B	147.0	150-250	166.6	-64.9	12.2	-75.2	34.5
Mesa de Cuba	P14MC31D	147.0	375-425	183.9	-36.3	13.1	-73.8	239.8
Mesa de Cuba	P14MC32D	150.0	250, 300, 425	126.8	-43.2	16.0	-43.5	345.0

Note: *mean angular deviation

Table A.3 - Ojo Alamo Sandstone and lower Nacimiento Formation paleomagnetic data: site means

Location	Sample	Strat Level (m)	n*	Strat. Declination (°)	Strat inclination (°)	alpha-95	Strat. VGP latitude	Strat. VGP longitude
Kutz Canyon	F17KC02	6.0	3	321.4	55.8	23.1	59.2	173.3
Kutz Canyon	F17KC03	6.0	3	338.6	49.5	26.6	71.1	148.9
Kutz Canyon	F17KC04	23.5	3	349.4	43.3	32.4	75.5	113.5
Kutz Canyon	F17KC05	25.0	3	352.2	54.6	11.2	83.5	151.2
Kutz Canyon	F17KC06	26.5	3	350.8	66.5	21.0	75.9	226.5
Kutz Canyon	F17KC12	35.5	3	356.7	63.4	23.4	81.3	236.4
Kutz Canyon	F17KC09	38.5	3	338.0	76.2	23.0	59.7	232.9
Kutz Canyon	F17LL01	41.5	3	170.6	-28.0	15.1	-66.7	275.5
Kutz Canyon	F17KC15	70.3	3	169.6	-55.9	28.6	-81.6	344.0
Kutz Canyon	F17KC25	129.0	3	174.3	-53.5	34.6	-84.7	314.9
Chico Springs	F19CS12	46.0	3	155.3	-32.1	12.2	-61.3	309.2
Chico Springs	F19CS10	27.0	3	160.5	-42.0	17.1	-69.5	313.4
Gallegos Canyon	F19GJ02	0.0	3	168.9	-57.8	17.0	-80.3	357.6
Gallegos Canyon	F19GJ03	0.9	3	157.5	-52.5	33.3	-50.7	149.6
Gallegos Canyon	F19GC05	12.9	3	154.8	-47.0	17.2	-67.3	328.0
Gallegos Canyon	F19GC08	21.9	3	59.7	76.6	23.5	45.3	283.7
Gallegos Canyon	F19GC09	24.9	3	352.0	32.1	30.5	69.7	94.4
Gallegos Canyon	F19GP02	35.2	3	357.9	54.8	32.0	88.0	130.3
Gallegos Canyon	F19GP03	36.7	3	337.9	33.6	23.0	63.5	125.0
Gallegos Canyon	F19GP05	39.7	3	141.1	-64.1	17.1	-59.6	12.2
Gallegos Canyon	F19GP06	42.7	3	203.8	-42.4	22.3	-66.4	185.4
Gallegos Canyon	F19GP07	45.7	3	161.0	-35.8	23.1	-66.5	302.1
Gallegos Canyon	F19GP11	60.7	3	113.6	-58.0	17.0	-38.5	5.8
De-Na-Zin	P13OJ01	-4.0	3	184.7	-56.2	25.8	-86.2	153.7

Location	Sample	Strat Level (m)	n*	Strat. Declination (°)	Strat inclination (°)	alpha-95	Strat. VGP latitude	Strat. VGP longitude
De-Na-Zin	P10NZ01	0.0	3	170.8	-52.2	34.8	-81.7	319.9
De-Na-Zin	P13NZ01	0.7	3	170.9	-57.9	33.9	-82.4	2.1
De-Na-Zin	P13NZ07	8.9	3	353.9	64.6	16.0	78.8	229.8
De-Na-Zin	P10NZ03	10.0	3	354.9	49.6	32.0	82.8	109.4
De-Na-Zin	P13NZ09	12.4	3	27.9	44.4	19.4	64.2	357.4
De-Na-Zin	P13NZ10	15.7	3	17.7	49.6	31.4	74.1	358.6
De-Na-Zin	F19PZ01	24.4	3	346.7	41.8	17.8	73.5	120.6
De-Na-Zin	F19PZ04	33.4	3	353.7	55.3	28.8	84.9	163.0
De-Na-Zin	P10NZ05	37.5	3	332.1	56.4	31.3	67.7	172.1
De-Na-Zin	P10NZ06	40.0	3	156.4	-36.3	16.3	-63.8	310.4
De-Na-Zin	F19SZ03	42.3	3	151.3	-66.3	28.4	-65.5	23.2
De-Na-Zin	P10NZ07	45.0	3	191.2	-49.6	26.0	-79.0	191.0
De-Na-Zin	F19SZ04	45.3	3	113.4	-58.0	12.2	-38.2	7.3
De-Na-Zin	F19SZ07	54.3	3	190.8	-48.2	7.3	-78.7	196.7
De-Na-Zin	F19BZ01	56.0	3	171.8	-57.6	26.3	-83.1	4.3
De-Na-Zin	F19SZ09	60.1	3	160.2	-40.2	30.8	-68.4	311.1
De-Na-Zin	F19BZ05	68.0	3	3.8	31.5	15.6	70.7	61.9
De-Na-Zin	F19TZ01	71.0	3	338.5	67.0	24.7	69.3	210.9
De-Na-Zin	F19TZ04	80.0	3	12.1	75.7	8.0	62.0	264.7
De-Na-Zin	F19TZ07	89.0	3	341.9	48.3	13.4	73.4	144.4
De-Na-Zin	F19TZ08	92.0	3	327.9	46.0	26.7	61.5	154.5
De-Na-Zin	F19TZ09	95.0	3	319.5	47.6	31.6	55.3	162.7
De-Na-Zin	F19TZ10	98.0	3	292.3	45.8	16.0	32.8	174.8
De-Na-Zin	F19TZ11	100.3	3	353.8	41.0	16.7	76.4	97.9
De-Na-Zin	F19TZ12	104.0	3	58.3	67.8	18.1	46.4	304.3
Kimbeto	P16KW01	5.65	3	161.6	-46.2	21.6	-72.2	318.5

Location	Sample	Strat Level (m)	n*	Strat. Declination (°)	Strat inclination (°)	alpha-95	Strat. VGP latitude	Strat. VGP longitude
Kimbeto	P16KW03	11.65	3	15.0	61.3	38.7	76.9	309.6
Kimbeto	P16KW04	14.65	3	338.1	52.7	12.0	71.8	159.6
Kimbeto	P16KW08	25.85	3	347.6	46.3	20.2	76.4	126.6
Kimbeto	F17KW09	58.85	3	353.5	61.9	18.5	81.5	218.6
Kimbeto	F17KW10	61.85	3	6.2	42.7	16.4	77.4	45.7
Kimbeto	F17KW06	63.95	3	2.4	53.9	31.5	87.4	23.7
Kimbeto	F17KW11	64.85	3	350.0	43.2	14.9	76.0	113.0
Kimbeto	F17KW14	73.85	3	358.4	26.1	11.7	67.4	75.9
Betonnie Tsosie	P16BT05	7.5	3	348.4	54.8	19.8	80.6	160.3
Betonnie Tsosie	P16BT06	8.7	3	339.0	51.1	12.3	72.1	154.0
Betonnie Tsosie	P16BT08	11.5	3	346.0	51.1	21.7	77.6	145.4
Betonnie Tsosie	P16BT09	13.0	3	352.1	55.1	16.2	83.6	159.4
Betonnie Tsosie	P16BT10	14.5	3	344.8	51.7	46.1	76.9	149.5
Betonnie Tsosie	FBW1501	17.1	3	19.8	56.3	19.6	74.1	333.9
Betonnie Tsosie	P16BT11	17.5	3	356.2	64.9	33.3	79.0	238.5
Betonnie Tsosie	P16BT14	22.0	3	3.1	25.6	12.6	67.1	64.4
Betonnie Tsosie	FBW1503	23.2	3	355.6	51.0	17.0	84.2	112.5
Betonnie Tsosie	FBW1502	23.4	3	8.8	28.5	20.6	67.6	49.4
Betonnie Tsosie	P16BT17	25.6	3	20.0	46.4	21.1	71.1	3.2
Betonnie Tsosie	P16BT18	28.6	3	311.2	58.4	13.0	51.7	181.7
Betonnie Tsosie	P16BT19	30.1	3	338.2	55.8	11.2	72.5	169.2
Betonnie Tsosie	P16BT20	31.6	3	42.5	63.4	14.0	57.0	313.5
Betonnie Tsosie	P16BT21	33.1	3	323.2	54.5	13.2	60.2	171.0
Betonnie Tsosie	P16BT22	34.6	3	320.1	65.9	16.0	58.5	197.2
Betonnie Tsosie	F19BW13	79.1	3	348.6	51.1	12.5	79.6	142.3
Betonnie Tsosie	F19BT01	79.5	3	336.9	37.4	9.7	64.7	131.3

Location	Sample	Strat Level (m)	n*	Strat. Declination (°)	Strat inclination (°)	alpha-95	Strat. VGP latitude	Strat. VGP longitude
Betonnie Tsosie	F19BT04	88.5	3	301.0	49.5	30.4	41.1	173.3
Betonnie Tsosie	F19BT06	94.5	3	21.6	57.5	29.4	72.7	329.3
Betonnie Tsosie	F19BT08	100.5	3	340.0	35.1	17.3	65.7	123.8
Betonnie Tsosie	F19BW08	62.6	3	330.0	43.8	29.0	62.4	149.4
Betonnie Tsosie	F19BW11	71.6	3	337.4	65.3	20.6	69.8	204.2
Betonnie Tsosie	F19BT09	110.0	3	9.6	45.7	16.3	77.8	27.6
Mesa de Cuba	P13LC04	6.0	3	346.7	77.3	18.6	59.2	242.3
Mesa de Cuba	FMC1501	14.0	3	1.6	48.0	21.5	82.9	61.6
Mesa de Cuba	FMC1504	14.0	3	336.2	38.2	25.7	64.7	134.5
Mesa de Cuba	P13LC08	18.0	3	7.4	63.4	17.0	79.4	282.8
Mesa de Cuba	P14MC01	21.0	3	340.7	49.5	20.8	72.9	149.2
Mesa de Cuba	P14MC10	54.0	3	337.4	37.9	11.4	65.4	132.3
Mesa de Cuba	P14MC18	88.5	3	21.4	50.2	22.5	71.5	352.6
Mesa de Cuba	P14MC19	91.5	3	335.6	39.4	17.1	64.8	136.8
Mesa de Cuba	P14MC20	106.5	3	183.1	-49.9	21.2	-84.1	226.1
Mesa de Cuba	P14MC21	114.0	3	180.8	-55.6	22.0	-89.3	150.7
Mesa de Cuba	P14MC26	123.0	3	158.4	-56.1	29.7	-72.6	351.6
Mesa de Cuba	P14MC29	135.0	3	150.1	-45.7	20.0	-63.2	332.2
Mesa de Cuba	P14MC31	147.0	3	172.1	-49.6	25.7	-81.4	305.1

Note: *number of samples used in site mean calculation

Table A.4 – Ojo Alamo Sandstone and lower Nacimiento Formation paleomagnetic data: great circles

Location	Sample	Strat Level (m)	Temp. Step of LSEP* (°C)	Strat. Dec. of LSEP* (°)	Strat Incl. of LSEP* (°)	MAD† of LSEP*	Strat. VGP lat.of LSEP* (°)	Strat. VGP long. of LSEP* (°)	Temp. Steps for Great Circle (°C)	Strat. Dec. of Great Circle (°)	Strat Incl. of Great Circle (°)	MAD† of Great Circle
Chico Springs	F19CS02B-C	3	325	173.4	-39	10.7	-74.9	277.2	250, 275, 325	341.4	-39.5	18.1
Chico Springs	F19CS03B-C	6	350	72.5	-52.8	9.9	-6.9	19.7	300, 325, 350	112	31.3	3.7
Chico Springs	F19CS04A-C	9	450	100.4	-54.9	8.5	-27.4	8.5	350, 425, 450	58.6	26.7	5.8
Chico Springs	F19CS05A-C	12	520	160.1	17.6	9.8	-41.2	279.6	475, 500, 520	68.9	2.8	1.9
Chico Springs	F19CS05D-C	12	500	237.7	12.1	11.9	-21.5	188.4	425, 475, 500	327.3	-3.4	3.3
Chico Springs	F19CS06C-C	15	475	137.9	-28.1	6.8	-47	324.8	425, 450, 475	51.4	9.6	19
Chico Springs	F19CS09B-C	24	275	154	-3.1	15.1	-48	293.9	200, 225, 275	74.5	46.3	17.4
Gallegos Canyon	F19GJ01B-C	-1.5	275	158	20.1	12.6	-65.8	64	200, 225, 250, 275	61.5	17.1	0.9
Gallegos Canyon	F19GJ01C-C	-1.5	300	106.7	46.8	11.6	-14.7	60.9	100, 125, 150, 175, 200, 300	55.8	-34.1	10.9
Gallegos Canyon	F19GJ01D-C	-1.5	325	91.5	86	9.7	-0.2	8	275, 300, 325	32.7	-1.1	7
Gallegos Canyon	F19GJ04C-C	2.4	325	138.8	21.7	5.6	-47.6	73.2	225, 300, 325	50.1	17.1	12.7
Gallegos Canyon	F19GJ04D-C	2.4	375	107.4	-13.1	8.7	-17.3	97	325, 350, 375	16.3	-27.7	9
Gallegos Canyon	F19GC02A-C	3.9	325	165.7	87.2	3.8	-5.4	1.4	275, 300, 325	65.9	0.6	0.8
Gallegos Canyon	F19GC03A-C	6.9	350	128.3	-8.9	12.4	-38.2	95.7	300,325, 350	197	55.1	15.4

Location	Sample	Strat Level (m)	Temp. Step of LSEP* (°C)	Strat. Dec. of LSEP* (°)	Strat Incl. of LSEP* (°)	MAD† of LSEP*	Strat. VGP lat.of LSEP* (°)	Strat. VGP long. of LSEP* (°)	Temp. Steps for Great Circle (°C)	Strat. Dec. of Great Circle (°)	Strat Incl. of Great Circle (°)	MAD† of Great Circle
Gallegos Canyon	F19GC03B-C	6.9	325	120	33.2	11	-28.4	69.3	225, 300, 325	31.8	-2.1	1.1
Gallegos Canyon	F19GC03C-C	6.9	375	185.7	-57.4	17.3	-51.6	187.2	250, 350, 375	59.3	30.4	8.5
Gallegos Canyon	F19GP04C-C	38.2	150	166.3	34	12.7	-67	35.1	NRM, 100, 150	71.4	15.8	10.8
Gallegos Canyon	F19GP09B-C	51.7	200	153	-14.3	3.5	-62.1	105.7	100, 150, 200	99.1	62.1	9.2
Gallegos Canyon	F19GP10A-C	54.7	350	178	-50.3	7.8	-58.9	176.7	250, 275, 300, 325, 350	76.7	13.8	19.2
Gallegos Canyon	F19GP10B-C	54.7	250	144.5	54.7	6.3	-41.7	39.4	NRM, 225, 250	67.3	-14.6	15.8
Betonnie Tsosie	P16BT02B-C	1.5	300	132	-4.9	6.4	-34.5	317.2	350, 375, 300	207.8	64.7	8
Betonnie Tsosie	F19BW04B-C	47.3	425	238	-32.4	12.1	-35.9	166.7	325, 350, 435	344.1	-21.6	12.3
Betonnie Tsosie	F19BW04D-C	47.3	400	190.1	-39.1	7.4	-73.6	217.9	325, 275, 400	107	13.1	19.7
Betonnie Tsosie	F19BW06A-C	56.6	560	250.6	-58.1	3.5	-35.3	137.3	500, 520, 560	349.1	-11.8	10.3
Betonnie Tsosie	F19BW06B-C	56.6	560	172.4	-40.1	3.6	-75.3	281.7	500, 520, 560	45.4	-35.1	0.8
Betonnie Tsosie	F19BW07A-C	59.6	475	249.2	-7.6	9.7	-19	172.4	425, 450, 475	167.5	70.3	12.3
Betonnie Tsosie	F19BW08C-C	62.6	500	159.8	-49.2	4.3	-72.1	329.5	250, 275, 300, 500	123.4	39.3	9.2
Betonnie Tsosie	F19BW08D-C	62.6	500	134.3	-21	2.7	-41.7	323.4	300, 450, 475, 500	73	51.1	10.8
Betonnie Tsosie	F10BW09A-C	65.6	500	206.4	-72.6	7.4	-62	103.2	275, 300, 500	28.3	-17.3	1

Location	Sample	Strat Level (m)	Temp. Step of LSEP* (°C)	Strat. Dec. of LSEP* (°)	Strat Incl. of LSEP* (°)	MAD† of LSEP*	Strat. VGP lat.of LSEP* (°)	Strat. VGP long. of LSEP* (°)	Temp. Steps for Great Circle (°C)	Strat. Dec. of Great Circle (°)	Strat Incl. of Great Circle (°)	MAD† of Great Circle
Betonnie Tsosie	F19BW09B -C	65.6	450	142.1	-11.1	7.9	-43.8	311	350, 375, 425, 450	47.8	30.4	12.5
Betonnie Tsosie	F19BW09C -C	65.6	400	138.3	-1.1	10	-37.6	310.1	250, 325, 400	53.4	-2.9	12.2
Betonnie Tsosie	F19BW12A -C	74.6	350	324.8	-86.8	22.4	-30.7	77.3	300, 325, 350	53.4	2.8	8.3
Betonnie Tsosie	F19BW12D -C	74.6	425	209.9	-12	12.7	-49.4	203.4	350, 375, 425	308	-32.6	4.5
Mesa de Cuba	FMC1503A -C	29	300	170.9	12.1	7.1	-47	266.3	200, 250, 300	74.1	15.8	8.7
Mesa de Cuba	FMC1503D -C	29	400	234.5	2	9.3	-27.4	186.6	100, 300, 400	323.7	-26.6	1.4
Mesa de Cuba	P14MC04B -C	30	350	209.3	44.6	4.6	-21.9	224.8	200, 225, 250, 275, 300, 325, 350	106.9	5.8	7.4
Mesa de Cuba	P14MC06B -C	39	450	97.2	-43.1	6.6	-19.9	0.1	375, 425, 450	106	49.8	17.4
Mesa de Cuba	P14MC09C -C	51	425	93.3	-70.5	14.4	-30.4	31	325, 375, 425	10.8	-1.8	10.9

Notes: *last stable endpoint, †mean angular deviation

Table A.5 - Ojo Alamo Sandstone and lower Nacimiento Formation paleomagnetic reversal tests

Site	Chron	*n*	D* (°)	I (°)	k	a95 (°)	r	Pole (°N)	Pole (°E)	K	A95 (°)	R	Reversal Test Type
Kutz Canyon	28n	7	343.9	59.0	40.6	9.6	6.9	76.7	187.2	26.0	12.1	6.8	Class C
	27r	3	171.4	-45.9	27.3	24.0	2.9	79.2	116.0	45.7	18.4	3.0	
Gallegos Canyon	29r	3	159.8	-52.6	134.8	10.7	3.0	73.5	159.7	102.2	12.3	3.0	indeterminate
	29n	4	353.7	51.1	9.8	31.0	3.7	87.6	169.3	6.6	38.7	3.5	indeterminate
	28r	4	160.0	-54.8	9.4	31.7	3.7	71.5	172.5	6.0	41.1	3.5	
	All N	4	353.7	51.1	9.8	31.0	3.7	87.6	169.3	6.6	38.7	3.5	Class C
	All R	7	159.9	-53.8	17.9	14.7	6.7	72.5	166.9	11.4	18.7	6.5	
Chico Springs	28n	0	---	---	---	---	---	---	---	---	---	---	
	27r	2	157.7	-37.1	114.2	23.6	2.0	65.4	130.9	187.3	18.4	2.0	
De-Na-Zin	29r	3	175.4	-55.6	227.5	8.2	3.0	86.3	167.7	130.9	10.8	3.0	indeterminate
	29n	7	359.1	53.0	33.2	10.6	6.8	88.6	100.9	4.7	31.2	5.7	Class C
	28r	7	164.2	-53.3	18.6	14.4	6.7	76.6	163.4	11.8	18.4	6.5	indeterminate
	28n	9	341.7	56.2	11.9	15.6	8.3	76.2	182.4	7.2	20.6	7.9	
	All N	16	349.9	55.1	16.3	9.4	15.1	82.2	175.0	10.0	12.2	13.5	Class B
	All R	10	167.5	-54.1	26.0	9.7	9.7	79.7	164.1	16.2	12.4	9.4	
Kimbeto Wash	29r	1	161.6	-46.2	---	---	1.0	72.3	139.7	---	---	1.0	
	29n	3	348.0	43.4	39.4	19.9	2.9	75.2	123.2	51.1	17.4	3.0	
	28r	1	157.6	-44.6	---	---	1.0	68.6	142.2	---	---	1.0	
	28n	5	358.3	45.7	32.6	13.6	4.9	82.1	84.2	42.2	11.9	4.9	
	All N	8	354.3	45.0	36.8	9.2	7.8	80.0	103.8	42.9	8.6	7.8	Class B
	All R	2	159.6	-45.4	1257.0	7.0	2.0	70.4	141.1	912.5	8.0	2.0	
Betonnie Tsosie Wash	29r	0	---	---	---	---	---	---	---	---	---	---	

Site	Chron	*n*	D* (°)	I (°)	k	a95 (°)	r	Pole (°N)	Pole (°E)	K	A95 (°)	R	Reversal Test Type
	29n	15	353.5	54.4	20.7	8.6	14.3	84.1	167.3	14.1	10.5	14.0	
	28r	0	---	---	---	---	---	---	---	---	---	---	
	28n	8	342.3	50.3	19.5	12.9	7.6	75.2	152.6	13.0	16.0	7.5	
	All N	23	349.4	53.1	20.3	6.9	21.9	81.1	156.9	13.8	8.4	21.4	
	All R	0	---	---	---	---	---	---	---	---	---	---	
Mesa de Cuba	29n	5	349.2	55.9	22.6	16.5	4.8	81.6	185.6	15.7	19.9	4.7	
	28r	0	---	---	---	---	---	---	---	---	---	---	
	28n	3	349.1	44.3	17.7	60.2	2.9	77.3	116.3	11.9	37.5	2.8	indeterminate
	27r	5	168.6	-52.1	65.6	9.5	4.9	80.3	147.5	40.3	12.2	4.9	
	All N	8	349.2	51.5	21.4	12.2	7.7	81.7	153.1	15.1	14.7	7.5	indeterminate
	All R	5	168.6	-52.1	65.6	9.5	4.9	80.3	147.5	40.3	12.2	4.9	
C29r sites	29r	7	166.4	-53.2	109.3	5.8	6.9	78.9	156.4	72.1	7.2	6.9	Class B
C29n sites	29n	34	353.5	53.0	22.5	5.3	32.5	83.7	161.2	8.3	9.1	30.9	Class B
C28r sites	28r	12	162.2	-53.0	16.7	10.9	11.3	74.4	164.2	10.6	14.0	11.0	indeterminate
C28n sites	28n	32	346.2	52.7	19.3	5.9	30.4	79.1	161.9	13.0	7.3	29.6	class B
C27r sites	27r	10	166.9	-47.3	42.5	7.5	9.8	77.3	134.4	43.0	7.4	9.8	
All Normal	29n, 28n	66	349.9	52.9	20.8	3.9	62.9	81.4	161.6	10.2	5.8	60.4	Class B
All Reversed	29r, 28r, 27r	29	164.9	-51.1	29.0	5.1	28.0	76.9	152.7	20.2	6.1	27.6	
Ojo Alamo 29r	29r	2	177.0	-57.2	172.3	19.1	2.0	86.9	200.8	52.6	27.8	2.0	
Ojo Alamo 29n	29n	0	---	---	---	---	---	---	---	---	---	---	
Nacimiento 29r	29r	5	162.7	-51.3	150.1	6.3	5.0	75.4	152.9	111.0	7.3	5.0	class B
Nacimiento 29n	29n	34	353.5	53.0	22.5	5.3	32.5	83.7	161.2	8.3	9.1	30.9	class B
Nacimiento 28r	28r	12	162.2	-53.0	16.7	10.9	11.3	74.4	164.2	10.6	14.0	11.0	indeterminate
Nacimiento 28n	28n	32	346.2	52.7	19.3	5.9	30.4	79.1	161.9	13.0	7.3	29.6	class B

Site	Chron	*n*	D* (°)	I (°)	k	a95 (°)	r	Pole (°N)	Pole (°E)	K	A95 (°)	R	Reversal Test Type
Nacimiento 27r	27r	10	166.9	-47.3	42.5	7.5	9.8	77.3	134.4	43.0	7.4	9.8	

Note: Chron - interpreted magnetic chron(s), *n* – number of site means; D – declination; I – inclination; k – Fisher's (1953) precision parameter; a95 – radius of 95% confidence cone around mean (Fisher, 1953); r - sample correlation coefficient (Fisher, 1953) pole N and E – mean virtual geomagnetic pole latitude and longitude calculated from each subset; K, A95, and R – Fisher (1953) statistics for virtual geomagnetic pole; Reversal Test Type - class of reversal from McFadden and McElhinny (1990).

APPENDIX B

Ojo Alamo Sandstone and Lower Nacimiento Formation Mammal Fossil Locality Information

Table B.1 - Ojo Alamo Sandstone and lower Nacimiento Formation mammal fossil localities

Mammal Horizon*	Localities	Location	NALMA[†]	SJB Biozone[§]	Magnetic Chron	Stratigraphic Position (m)**	Estimated Age (Ma)
1	L-06342	De-Na-Zin	Pu2	H-T Zone	29n	8.0 - 10.5	65.68 - 65.63 (+0.01/-0.01)
	L-06343	De-Na-Zin	Pu2	H-T Zone	29n	8.0 - 10.5	65.68 - 65.63 (+0.01/-0.01)
	L-06344	De-Na-Zin	Pu2	H-T Zone	29n	8.0 - 10.5	65.68 - 65.63 (+0.01/-0.01)
	L-06346	De-Na-Zin	Pu2	H-T Zone	29n	8.0 - 10.5	65.68 - 65.63 (+0.01/-0.01)
	L-06347	De-Na-Zin	Pu2	H-T Zone	29n	8.0 - 10.5	65.68 - 65.63 (+0.01/-0.01)
	L-06348	De-Na-Zin	Pu2	H-T Zone	29n	8.0 - 10.5	65.68 - 65.63 (+0.01/-0.01)
	L-08342	De-Na-Zin	Pu2	H-T Zone	29n	8.0 - 10.5	65.68 - 65.63 (+0.01/-0.01)
	L-08343	De-Na-Zin	Pu2	H-T Zone	29n	8.0 - 10.5	65.68 - 65.63 (+0.01/-0.01)
	L-08344	De-Na-Zin	Pu2	H-T Zone	29n	8.0 - 10.5	65.68 - 65.63 (+0.01/-0.01)
	L-08601	De-Na-Zin	Pu2	H-T Zone	29n	8.0 - 10.5	65.68 - 65.63 (+0.01/-0.01)
	L-08865	De-Na-Zin	Pu2	H-T Zone	29n	8.0 - 10.5	65.68 - 65.63 (+0.01/-0.01)
	L-08866	De-Na-Zin	Pu2	H-T Zone	29n	8.0 - 10.5	65.68 - 65.63 (+0.01/-0.01)
	L-08867	De-Na-Zin	Pu2	H-T Zone	29n	8.0 - 10.5	65.68 - 65.63 (+0.01/-0.01)
	L-08868	De-Na-Zin	Pu2	H-T Zone	29n	8.0 - 10.5	65.68 - 65.63 (+0.01/-0.01)
	L-12078	De-Na-Zin	Pu2	H-T Zone	29n	8.0 - 10.5	65.68 - 65.63 (+0.01/-0.01)
2	L-00317	Betonnie Tsosie	Pu2	H-T Zone	29n	11.0 - 16.0	65.57 - 65.47 (+0.02/-0.04)
	L-00646	Betonnie Tsosie	Pu2	H-T Zone	29n	11.0 - 16.0	65.57 - 65.47 (+0.02/-0.04)

Mammal Horizon*	Localities	Location	NALMA†	SJB Biozone§	Magnetic Chron	Stratigraphic Position (m)**	Estimated Age (Ma)
	L-00686	Betonnie Tsosie	Pu2	H-T Zone	29n	11.0 - 16.0	65.57 - 65.47 (+0.02/-0.04)
	L-00844	Betonnie Tsosie	Pu2	H-T Zone	29n	11.0 - 16.0	65.57 - 65.47 (+0.02/-0.04)
	L-01122	Betonnie Tsosie	Pu2	H-T Zone	29n	11.0 - 16.0	65.57 - 65.47 (+0.02/-0.04)
	L-01123	Betonnie Tsosie	Pu2	H-T Zone	29n	11.0 - 16.0	65.57 - 65.47 (+0.02/-0.04)
	L-01124	Betonnie Tsosie	Pu2	H-T Zone	29n	11.0 - 16.0	65.57 - 65.47 (+0.02/-0.04)
	L-02550	Betonnie Tsosie	Pu2	H-T Zone	29n	11.0 - 16.0	65.57 - 65.47 (+0.02/-0.04)
	L-02551	Betonnie Tsosie	Pu2	H-T Zone	29n	11.0 - 16.0	65.57 - 65.47 (+0.02/-0.04)
	L-02552	Betonnie Tsosie	Pu2	H-T Zone	29n	11.0 - 16.0	65.57 - 65.47 (+0.02/-0.04)
	L-05444	Betonnie Tsosie	Pu2	H-T Zone	29n	11.0 - 16.0	65.57 - 65.47 (+0.02/-0.04)
	L-05445	Betonnie Tsosie	Pu2	H-T Zone	29n	11.0 - 16.0	65.57 - 65.47 (+0.02/-0.04)
	L-05446	Betonnie Tsosie	Pu2	H-T Zone	29n	11.0 - 16.0	65.57 - 65.47 (+0.02/-0.04)
	L-05447	Betonnie Tsosie	Pu2	H-T Zone	29n	11.0 - 16.0	65.57 - 65.47 (+0.02/-0.04)
	L-05448	Betonnie Tsosie	Pu2	H-T Zone	29n	11.0 - 16.0	65.57 - 65.47 (+0.02/-0.04)
	L-06142	Betonnie Tsosie	Pu2	H-T Zone	29n	11.0 - 16.0	65.57 - 65.47 (+0.02/-0.04)
	L-06143	Betonnie Tsosie	Pu2	H-T Zone	29n	11.0 - 16.0	65.57 - 65.47 (+0.02/-0.04)
	L-06144	Betonnie Tsosie	Pu2	H-T Zone	29n	11.0 - 16.0	65.57 - 65.47 (+0.02/-0.04)
	L-06145	Betonnie Tsosie	Pu2	H-T Zone	29n	11.0 - 16.0	65.57 - 65.47 (+0.02/-0.04)
	L-06146	Betonnie Tsosie	Pu2	H-T Zone	29n	11.0 - 16.0	65.57 - 65.47 (+0.02/-0.04)
	L-06147	Betonnie Tsosie	Pu2	H-T Zone	29n	11.0 - 16.0	65.57 - 65.47 (+0.02/-0.04)
	L-06209	Betonnie Tsosie	Pu2	H-T Zone	29n	11.0 - 16.0	65.57 - 65.47 (+0.02/-0.04)
	L-06210	Betonnie Tsosie	Pu2	H-T Zone	29n	11.0 - 16.0	65.57 - 65.47 (+0.02/-0.04)
	L-06211	Betonnie Tsosie	Pu2	H-T Zone	29n	11.0 - 16.0	65.57 - 65.47 (+0.02/-0.04)
	L-06271	Betonnie Tsosie	Pu2	H-T Zone	29n	11.0 - 16.0	65.57 - 65.47 (+0.02/-0.04)
	L-06248	Betonnie Tsosie	Pu2	H-T Zone	29n	11.0 - 16.0	65.57 - 65.47 (+0.02/-0.04)
	L-06352	Betonnie Tsosie	Pu2	H-T Zone	29n	11.0 - 16.0	65.57 - 65.47 (+0.02/-0.04)

Mammal Horizon*	Localities	Location	NALMA†	SJB Biozone§	Magnetic Chron	Stratigraphic Position (m)**	Estimated Age (Ma)
	L-06353	Betonnie Tsosie	Pu2	H-T Zone	29n	11.0 - 16.0	65.57 - 65.47 (+0.02/-0.04)
	L-06354	Betonnie Tsosie	Pu2	H-T Zone	29n	11.0 - 16.0	65.57 - 65.47 (+0.02/-0.04)
	L-06355	Betonnie Tsosie	Pu2	H-T Zone	29n	11.0 - 16.0	65.57 - 65.47 (+0.02/-0.04)
	L-06356	Betonnie Tsosie	Pu2	H-T Zone	29n	11.0 - 16.0	65.57 - 65.47 (+0.02/-0.04)
	L-06357	Betonnie Tsosie	Pu2	H-T Zone	29n	11.0 - 16.0	65.57 - 65.47 (+0.02/-0.04)
	L-06358	Betonnie Tsosie	Pu2	H-T Zone	29n	11.0 - 16.0	65.57 - 65.47 (+0.02/-0.04)
	L-06359	Betonnie Tsosie	Pu2	H-T Zone	29n	11.0 - 16.0	65.57 - 65.47 (+0.02/-0.04)
	L-06456	Betonnie Tsosie	Pu2	H-T Zone	29n	11.0 - 16.0	65.57 - 65.47 (+0.02/-0.04)
	L-06615	Betonnie Tsosie	Pu2	H-T Zone	29n	11.0 - 16.0	65.57 - 65.47 (+0.02/-0.04)
	L-06620	Betonnie Tsosie	Pu2	H-T Zone	29n	11.0 - 16.0	65.57 - 65.47 (+0.02/-0.04)
	L-07483	Betonnie Tsosie	Pu2	H-T Zone	29n	11.0 - 16.0	65.57 - 65.47 (+0.02/-0.04)
	L-08777	Betonnie Tsosie	Pu2	H-T Zone	29n	11.0 - 16.0	65.57 - 65.47 (+0.02/-0.04)
	L-09183	Betonnie Tsosie	Pu2	H-T Zone	29n	11.0 - 16.0	65.57 - 65.47 (+0.02/-0.04)
	L-09971	Betonnie Tsosie	Pu2	H-T Zone	29n	11.0 - 16.0	65.57 - 65.47 (+0.02/-0.04)
	L-09972	Betonnie Tsosie	Pu2	H-T Zone	29n	11.0 - 16.0	65.57 - 65.47 (+0.02/-0.04)
	L-10406	Betonnie Tsosie	Pu2	H-T Zone	29n	11.0 - 16.0	65.57 - 65.47 (+0.02/-0.04)
	L-10407	Betonnie Tsosie	Pu2	H-T Zone	29n	11.0 - 16.0	65.57 - 65.47 (+0.02/-0.04)
	L-10408	Betonnie Tsosie	Pu2	H-T Zone	29n	11.0 - 16.0	65.57 - 65.47 (+0.02/-0.04)
	L-10409	Betonnie Tsosie	Pu2	H-T Zone	29n	11.0 - 16.0	65.57 - 65.47 (+0.02/-0.04)
	L-10411	Betonnie Tsosie	Pu2	H-T Zone	29n	11.0 - 16.0	65.57 - 65.47 (+0.02/-0.04)
	L-10412	Betonnie Tsosie	Pu2	H-T Zone	29n	11.0 - 16.0	65.57 - 65.47 (+0.02/-0.04)
	L-10427	Betonnie Tsosie	Pu2	H-T Zone	29n	11.0 - 16.0	65.57 - 65.47 (+0.02/-0.04)
	L-10428	Betonnie Tsosie	Pu2	H-T Zone	29n	11.0 - 16.0	65.57 - 65.47 (+0.02/-0.04)
	L-10429	Betonnie Tsosie	Pu2	H-T Zone	29n	11.0 - 16.0	65.57 - 65.47 (+0.02/-0.04)
	L-10430	Betonnie Tsosie	Pu2	H-T Zone	29n	11.0 - 16.0	65.57 - 65.47 (+0.02/-0.04)

Mammal Horizon*	Localities	Location	NALMA†	SJB Biozone§	Magnetic Chron	Stratigraphic Position (m)**	Estimated Age (Ma)
	L-10446	Betonnie Tsosie	Pu2	H-T Zone	29n	11.0 - 16.0	65.57 - 65.47 (+0.02/-0.04)
	L-10447	Betonnie Tsosie	Pu2	H-T Zone	29n	11.0 - 16.0	65.57 - 65.47 (+0.02/-0.04)
	L-10448	Betonnie Tsosie	Pu2	H-T Zone	29n	11.0 - 16.0	65.57 - 65.47 (+0.02/-0.04)
	L-10449	Betonnie Tsosie	Pu2	H-T Zone	29n	11.0 - 16.0	65.57 - 65.47 (+0.02/-0.04)
	L-10450	Betonnie Tsosie	Pu2	H-T Zone	29n	11.0 - 16.0	65.57 - 65.47 (+0.02/-0.04)
	L-10451	Betonnie Tsosie	Pu2	H-T Zone	29n	11.0 - 16.0	65.57 - 65.47 (+0.02/-0.04)
	L-10455	Betonnie Tsosie	Pu2	H-T Zone	29n	11.0 - 16.0	65.57 - 65.47 (+0.02/-0.04)
3	L-00684	Kimbeto	Pu2	H-T Zone	29n	6.2 - 10.0	65.49 - 65.34 (+0.03/-0.03)
	L-00685	Kimbeto	Pu2	H-T Zone	29n	6.2 - 10.0	65.49 - 65.34 (+0.03/-0.03)
	L-01121	Kimbeto	Pu2	H-T Zone	29n	6.2 - 10.0	65.49 - 65.34 (+0.03/-0.03)
	L-05200	Kimbeto	Pu2	H-T Zone	29n	6.2 - 10.0	65.49 - 65.34 (+0.03/-0.03)
	L-05201	Kimbeto	Pu2	H-T Zone	29n	6.2 - 10.0	65.49 - 65.34 (+0.03/-0.03)
	L-05202	Kimbeto	Pu2	H-T Zone	29n	6.2 - 10.0	65.49 - 65.34 (+0.03/-0.03)
	L-05203	Kimbeto	Pu2	H-T Zone	29n	6.2 - 10.0	65.49 - 65.34 (+0.03/-0.03)
	L-05204	Kimbeto	Pu2	H-T Zone	29n	6.2 - 10.0	65.49 - 65.34 (+0.03/-0.03)
	L-06345	Kimbeto	Pu2	H-T Zone	29n	6.2 - 10.0	65.49 - 65.34 (+0.03/-0.03)
	L-06349	Kimbeto	Pu2	H-T Zone	29n	6.2 - 10.0	65.49 - 65.34 (+0.03/-0.03)
	L-08233	Kimbeto	Pu2	H-T Zone	29n	6.2 - 10.0	65.49 - 65.34 (+0.03/-0.03)
	L-08869	Kimbeto	Pu2	H-T Zone	29n	6.2 - 10.0	65.49 - 65.34 (+0.03/-0.03)
	L-08870	Kimbeto	Pu2	H-T Zone	29n	6.2 - 10.0	65.49 - 65.34 (+0.03/-0.03)
	L-09179	Kimbeto	Pu2	H-T Zone	29n	6.2 - 10.0	65.49 - 65.34 (+0.03/-0.03)
	L-09180	Kimbeto	Pu2	H-T Zone	29n	6.2 - 10.0	65.49 - 65.34 (+0.03/-0.03)
	L-09181	Kimbeto	Pu2	H-T Zone	29n	6.2 - 10.0	65.49 - 65.34 (+0.03/-0.03)
	L-09182	Kimbeto	Pu2	H-T Zone	29n	6.2 - 10.0	65.49 - 65.34 (+0.03/-0.03)
	L-09875	Kimbeto	Pu2	H-T Zone	29n	6.2 - 10.0	65.49 - 65.34 (+0.03/-0.03)

Mammal Horizon*	Localities	Location	NALMA†	SJB Biozone§	Magnetic Chron	Stratigraphic Position (m)**	Estimated Age (Ma)
	L-09894	Kimbeto	Pu2	H-T Zone	29n	6.2 - 10.0	65.49 - 65.34 (+0.03/-0.03)
	L-09895	Kimbeto	Pu2	H-T Zone	29n	6.2 - 10.0	65.49 - 65.34 (+0.03/-0.03)
	L-09899	Kimbeto	Pu2	H-T Zone	29n	6.2 - 10.0	65.49 - 65.34 (+0.03/-0.03)
	L-09976	Kimbeto	Pu2	H-T Zone	29n	6.2 - 10.0	65.49 - 65.34 (+0.03/-0.03)
	L-09977	Kimbeto	Pu2	H-T Zone	29n	6.2 - 10.0	65.49 - 65.34 (+0.03/-0.03)
4	L-00390	De-Na-Zin	Pu3	T-P Zone	29n	25.6 - 28.4	65.27 - 65.22 (+0.06/-0.06)
	L-00391	De-Na-Zin	Pu3	T-P Zone	29n	25.6 - 28.4	65.27 - 65.22 (+0.06/-0.06)
	L-00392	De-Na-Zin	Pu3	T-P Zone	29n	25.6 - 28.4	65.27 - 65.22 (+0.06/-0.06)
	L-00393	De-Na-Zin	Pu3	T-P Zone	29n	25.6 - 28.4	65.27 - 65.22 (+0.06/-0.06)
	L-00394	De-Na-Zin	Pu3	T-P Zone	29n	25.6 - 28.4	65.27 - 65.22 (+0.06/-0.06)
	L-00395	De-Na-Zin	Pu3	T-P Zone	29n	25.6 - 28.4	65.27 - 65.22 (+0.06/-0.06)
	L-00396	De-Na-Zin	Pu3	T-P Zone	29n	25.6 - 28.4	65.27 - 65.22 (+0.06/-0.06)
	L-00397	De-Na-Zin	Pu3	T-P Zone	29n	25.6 - 28.4	65.27 - 65.22 (+0.06/-0.06)
	L-00626	De-Na-Zin	Pu3	T-P Zone	29n	25.6 - 28.4	65.27 - 65.22 (+0.06/-0.06)
	L-00629	De-Na-Zin	Pu3	T-P Zone	29n	25.6 - 28.4	65.27 - 65.22 (+0.06/-0.06)
	L-00630	De-Na-Zin	Pu3	T-P Zone	29n	25.6 - 28.4	65.27 - 65.22 (+0.06/-0.06)
	L-00634	De-Na-Zin	Pu3	T-P Zone	29n	25.6 - 28.4	65.27 - 65.22 (+0.06/-0.06)
	L-00636	De-Na-Zin	Pu3	T-P Zone	29n	25.6 - 28.4	65.27 - 65.22 (+0.06/-0.06)
	L-00638	De-Na-Zin	Pu3	T-P Zone	29n	25.6 - 28.4	65.27 - 65.22 (+0.06/-0.06)
	L-00642	De-Na-Zin	Pu3	T-P Zone	29n	25.6 - 28.4	65.27 - 65.22 (+0.06/-0.06)
	L-00643	De-Na-Zin	Pu3	T-P Zone	29n	25.6 - 28.4	65.27 - 65.22 (+0.06/-0.06)
	L-00644	De-Na-Zin	Pu3	T-P Zone	29n	25.6 - 28.4	65.27 - 65.22 (+0.06/-0.06)
	L-00658	De-Na-Zin	Pu3	T-P Zone	29n	25.6 - 28.4	65.27 - 65.22 (+0.06/-0.06)
	L-00659	De-Na-Zin	Pu3	T-P Zone	29n	25.6 - 28.4	65.27 - 65.22 (+0.06/-0.06)
	L-00660	De-Na-Zin	Pu3	T-P Zone	29n	25.6 - 28.4	65.27 - 65.22 (+0.06/-0.06)

Mammal Horizon*	Localities	Location	NALMA†	SJB Biozone§	Magnetic Chron	Stratigraphic Position (m)**	Estimated Age (Ma)
	L-00661	De-Na-Zin	Pu3	T-P Zone	29n	25.6 - 28.4	65.27 - 65.22 (+0.06/-0.06)
	L-00662	De-Na-Zin	Pu3	T-P Zone	29n	25.6 - 28.4	65.27 - 65.22 (+0.06/-0.06)
	L-00663	De-Na-Zin	Pu3	T-P Zone	29n	25.6 - 28.4	65.27 - 65.22 (+0.06/-0.06)
	L-00664	De-Na-Zin	Pu3	T-P Zone	29n	25.6 - 28.4	65.27 - 65.22 (+0.06/-0.06)
	L-00665	De-Na-Zin	Pu3	T-P Zone	29n	25.6 - 28.4	65.27 - 65.22 (+0.06/-0.06)
	L-00666	De-Na-Zin	Pu3	T-P Zone	29n	25.6 - 28.4	65.27 - 65.22 (+0.06/-0.06)
	L-00667	De-Na-Zin	Pu3	T-P Zone	29n	25.6 - 28.4	65.27 - 65.22 (+0.06/-0.06)
	L-00675	De-Na-Zin	Pu3	T-P Zone	29n	25.6 - 28.4	65.27 - 65.22 (+0.06/-0.06)
	L-00676	De-Na-Zin	Pu3	T-P Zone	29n	25.6 - 28.4	65.27 - 65.22 (+0.06/-0.06)
	L-00699	De-Na-Zin	Pu3	T-P Zone	29n	25.6 - 28.4	65.27 - 65.22 (+0.06/-0.06)
	L-01115	De-Na-Zin	Pu3	T-P Zone	29n	25.6 - 28.4	65.27 - 65.22 (+0.06/-0.06)
	L-01117	De-Na-Zin	Pu3	T-P Zone	29n	25.6 - 28.4	65.27 - 65.22 (+0.06/-0.06)
	L-01217	De-Na-Zin	Pu3	T-P Zone	29n	25.6 - 28.4	65.27 - 65.22 (+0.06/-0.06)
	L-01219	De-Na-Zin	Pu3	T-P Zone	29n	25.6 - 28.4	65.27 - 65.22 (+0.06/-0.06)
	L-01220	De-Na-Zin	Pu3	T-P Zone	29n	25.6 - 28.4	65.27 - 65.22 (+0.06/-0.06)
	L-01224	De-Na-Zin	Pu3	T-P Zone	29n	25.6 - 28.4	65.27 - 65.22 (+0.06/-0.06)
	L-01225	De-Na-Zin	Pu3	T-P Zone	29n	25.6 - 28.4	65.27 - 65.22 (+0.06/-0.06)
	L-01288	De-Na-Zin	Pu3	T-P Zone	29n	25.6 - 28.4	65.27 - 65.22 (+0.06/-0.06)
	L-01400	De-Na-Zin	Pu3	T-P Zone	29n	25.6 - 28.4	65.27 - 65.22 (+0.06/-0.06)
	L-01409	De-Na-Zin	Pu3	T-P Zone	29n	25.6 - 28.4	65.27 - 65.22 (+0.06/-0.06)
	L-02306	De-Na-Zin	Pu3	T-P Zone	29n	25.6 - 28.4	65.27 - 65.22 (+0.06/-0.06)
	L-02308	De-Na-Zin	Pu3	T-P Zone	29n	25.6 - 28.4	65.27 - 65.22 (+0.06/-0.06)
	L-02309	De-Na-Zin	Pu3	T-P Zone	29n	25.6 - 28.4	65.27 - 65.22 (+0.06/-0.06)
	L-02340	De-Na-Zin	Pu3	T-P Zone	29n	25.6 - 28.4	65.27 - 65.22 (+0.06/-0.06)
	L-02394	De-Na-Zin	Pu3	T-P Zone	29n	25.6 - 28.4	65.27 - 65.22 (+0.06/-0.06)

Mammal Horizon*	Localities	Location	NALMA†	SJB Biozone§	Magnetic Chron	Stratigraphic Position (m)**	Estimated Age (Ma)
	L-02396	De-Na-Zin	Pu3	T-P Zone	29n	25.6 - 28.4	65.27 - 65.22 (+0.06/-0.06)
	L-03206	De-Na-Zin	Pu3	T-P Zone	29n	25.6 - 28.4	65.27 - 65.22 (+0.06/-0.06)
	L-03230	De-Na-Zin	Pu3	T-P Zone	29n	25.6 - 28.4	65.27 - 65.22 (+0.06/-0.06)
	L-03232	De-Na-Zin	Pu3	T-P Zone	29n	25.6 - 28.4	65.27 - 65.22 (+0.06/-0.06)
	L-03233	De-Na-Zin	Pu3	T-P Zone	29n	25.6 - 28.4	65.27 - 65.22 (+0.06/-0.06)
	L-03234	De-Na-Zin	Pu3	T-P Zone	29n	25.6 - 28.4	65.27 - 65.22 (+0.06/-0.06)
	L-03235	De-Na-Zin	Pu3	T-P Zone	29n	25.6 - 28.4	65.27 - 65.22 (+0.06/-0.06)
	L-03236	De-Na-Zin	Pu3	T-P Zone	29n	25.6 - 28.4	65.27 - 65.22 (+0.06/-0.06)
	L-03237	De-Na-Zin	Pu3	T-P Zone	29n	25.6 - 28.4	65.27 - 65.22 (+0.06/-0.06)
	L-03239	De-Na-Zin	Pu3	T-P Zone	29n	25.6 - 28.4	65.27 - 65.22 (+0.06/-0.06)
	L-03329	De-Na-Zin	Pu3	T-P Zone	29n	25.6 - 28.4	65.27 - 65.22 (+0.06/-0.06)
	L-04329	De-Na-Zin	Pu3	T-P Zone	29n	25.6 - 28.4	65.27 - 65.22 (+0.06/-0.06)
	L-04546	De-Na-Zin	Pu3	T-P Zone	29n	25.6 - 28.4	65.27 - 65.22 (+0.06/-0.06)
	L-05196	De-Na-Zin	Pu3	T-P Zone	29n	25.6 - 28.4	65.27 - 65.22 (+0.06/-0.06)
	L-05404	De-Na-Zin	Pu3	T-P Zone	29n	25.6 - 28.4	65.27 - 65.22 (+0.06/-0.06)
	L-05663	De-Na-Zin	Pu3	T-P Zone	29n	25.6 - 28.4	65.27 - 65.22 (+0.06/-0.06)
	L-05664	De-Na-Zin	Pu3	T-P Zone	29n	25.6 - 28.4	65.27 - 65.22 (+0.06/-0.06)
	L-05665	De-Na-Zin	Pu3	T-P Zone	29n	25.6 - 28.4	65.27 - 65.22 (+0.06/-0.06)
	L-05666	De-Na-Zin	Pu3	T-P Zone	29n	25.6 - 28.4	65.27 - 65.22 (+0.06/-0.06)
	L-05667	De-Na-Zin	Pu3	T-P Zone	29n	25.6 - 28.4	65.27 - 65.22 (+0.06/-0.06)
	L-05668	De-Na-Zin	Pu3	T-P Zone	29n	25.6 - 28.4	65.27 - 65.22 (+0.06/-0.06)
	L-05669	De-Na-Zin	Pu3	T-P Zone	29n	25.6 - 28.4	65.27 - 65.22 (+0.06/-0.06)
	L-05670	De-Na-Zin	Pu3	T-P Zone	29n	25.6 - 28.4	65.27 - 65.22 (+0.06/-0.06)
	L-05671	De-Na-Zin	Pu3	T-P Zone	29n	25.6 - 28.4	65.27 - 65.22 (+0.06/-0.06)
	L-05672	De-Na-Zin	Pu3	T-P Zone	29n	25.6 - 28.4	65.27 - 65.22 (+0.06/-0.06)

Mammal Horizon*	Localities	Location	NALMA[†]	SJB Biozone[§]	Magnetic Chron	Stratigraphic Position (m)**	Estimated Age (Ma)
	L-05673	De-Na-Zin	Pu3	T-P Zone	29n	25.6 - 28.4	65.27 - 65.22 (+0.06/-0.06)
	L-05674	De-Na-Zin	Pu3	T-P Zone	29n	25.6 - 28.4	65.27 - 65.22 (+0.06/-0.06)
	L-05675	De-Na-Zin	Pu3	T-P Zone	29n	25.6 - 28.4	65.27 - 65.22 (+0.06/-0.06)
	L-05676	De-Na-Zin	Pu3	T-P Zone	29n	25.6 - 28.4	65.27 - 65.22 (+0.06/-0.06)
	L-05817	De-Na-Zin	Pu3	T-P Zone	29n	25.6 - 28.4	65.27 - 65.22 (+0.06/-0.06)
	L-05818	De-Na-Zin	Pu3	T-P Zone	29n	25.6 - 28.4	65.27 - 65.22 (+0.06/-0.06)
	L-05819	De-Na-Zin	Pu3	T-P Zone	29n	25.6 - 28.4	65.27 - 65.22 (+0.06/-0.06)
	L-05820	De-Na-Zin	Pu3	T-P Zone	29n	25.6 - 28.4	65.27 - 65.22 (+0.06/-0.06)
	L-05821	De-Na-Zin	Pu3	T-P Zone	29n	25.6 - 28.4	65.27 - 65.22 (+0.06/-0.06)
	L-05822	De-Na-Zin	Pu3	T-P Zone	29n	25.6 - 28.4	65.27 - 65.22 (+0.06/-0.06)
	L-05823	De-Na-Zin	Pu3	T-P Zone	29n	25.6 - 28.4	65.27 - 65.22 (+0.06/-0.06)
	L-05824	De-Na-Zin	Pu3	T-P Zone	29n	25.6 - 28.4	65.27 - 65.22 (+0.06/-0.06)
	L-05825	De-Na-Zin	Pu3	T-P Zone	29n	25.6 - 28.4	65.27 - 65.22 (+0.06/-0.06)
	L-05826	De-Na-Zin	Pu3	T-P Zone	29n	25.6 - 28.4	65.27 - 65.22 (+0.06/-0.06)
	L-05827	De-Na-Zin	Pu3	T-P Zone	29n	25.6 - 28.4	65.27 - 65.22 (+0.06/-0.06)
	L-05828	De-Na-Zin	Pu3	T-P Zone	29n	25.6 - 28.4	65.27 - 65.22 (+0.06/-0.06)
	L-05829	De-Na-Zin	Pu3	T-P Zone	29n	25.6 - 28.4	65.27 - 65.22 (+0.06/-0.06)
	L-05830	De-Na-Zin	Pu3	T-P Zone	29n	25.6 - 28.4	65.27 - 65.22 (+0.06/-0.06)
	L-05831	De-Na-Zin	Pu3	T-P Zone	29n	25.6 - 28.4	65.27 - 65.22 (+0.06/-0.06)
	L-05832	De-Na-Zin	Pu3	T-P Zone	29n	25.6 - 28.4	65.27 - 65.22 (+0.06/-0.06)
	L-05833	De-Na-Zin	Pu3	T-P Zone	29n	25.6 - 28.4	65.27 - 65.22 (+0.06/-0.06)
	L-05834	De-Na-Zin	Pu3	T-P Zone	29n	25.6 - 28.4	65.27 - 65.22 (+0.06/-0.06)
	L-05835	De-Na-Zin	Pu3	T-P Zone	29n	25.6 - 28.4	65.27 - 65.22 (+0.06/-0.06)
	L-05836	De-Na-Zin	Pu3	T-P Zone	29n	25.6 - 28.4	65.27 - 65.22 (+0.06/-0.06)
	L-05837	De-Na-Zin	Pu3	T-P Zone	29n	25.6 - 28.4	65.27 - 65.22 (+0.06/-0.06)

Mammal Horizon*	Localities	Location	NALMA†	SJB Biozone§	Magnetic Chron	Stratigraphic Position (m)**	Estimated Age (Ma)
	L-05838	De-Na-Zin	Pu3	T-P Zone	29n	25.6 - 28.4	65.27 - 65.22 (+0.06/-0.06)
	L-05842	De-Na-Zin	Pu3	T-P Zone	29n	25.6 - 28.4	65.27 - 65.22 (+0.06/-0.06)
	L-05864	De-Na-Zin	Pu3	T-P Zone	29n	25.6 - 28.4	65.27 - 65.22 (+0.06/-0.06)
	L-05865	De-Na-Zin	Pu3	T-P Zone	29n	25.6 - 28.4	65.27 - 65.22 (+0.06/-0.06)
	L-06053	De-Na-Zin	Pu3	T-P Zone	29n	25.6 - 28.4	65.27 - 65.22 (+0.06/-0.06)
	L-06054	De-Na-Zin	Pu3	T-P Zone	29n	25.6 - 28.4	65.27 - 65.22 (+0.06/-0.06)
	L-06055	De-Na-Zin	Pu3	T-P Zone	29n	25.6 - 28.4	65.27 - 65.22 (+0.06/-0.06)
	L-06056	De-Na-Zin	Pu3	T-P Zone	29n	25.6 - 28.4	65.27 - 65.22 (+0.06/-0.06)
	L-06057	De-Na-Zin	Pu3	T-P Zone	29n	25.6 - 28.4	65.27 - 65.22 (+0.06/-0.06)
	L-06058	De-Na-Zin	Pu3	T-P Zone	29n	25.6 - 28.4	65.27 - 65.22 (+0.06/-0.06)
	L-06059	De-Na-Zin	Pu3	T-P Zone	29n	25.6 - 28.4	65.27 - 65.22 (+0.06/-0.06)
	L-06060	De-Na-Zin	Pu3	T-P Zone	29n	25.6 - 28.4	65.27 - 65.22 (+0.06/-0.06)
	L-06061	De-Na-Zin	Pu3	T-P Zone	29n	25.6 - 28.4	65.27 - 65.22 (+0.06/-0.06)
	L-06062	De-Na-Zin	Pu3	T-P Zone	29n	25.6 - 28.4	65.27 - 65.22 (+0.06/-0.06)
	L-06063	De-Na-Zin	Pu3	T-P Zone	29n	25.6 - 28.4	65.27 - 65.22 (+0.06/-0.06)
	L-06064	De-Na-Zin	Pu3	T-P Zone	29n	25.6 - 28.4	65.27 - 65.22 (+0.06/-0.06)
	L-06065	De-Na-Zin	Pu3	T-P Zone	29n	25.6 - 28.4	65.27 - 65.22 (+0.06/-0.06)
	L-06066	De-Na-Zin	Pu3	T-P Zone	29n	25.6 - 28.4	65.27 - 65.22 (+0.06/-0.06)
	L-06067	De-Na-Zin	Pu3	T-P Zone	29n	25.6 - 28.4	65.27 - 65.22 (+0.06/-0.06)
	L-06243	De-Na-Zin	Pu3	T-P Zone	29n	25.6 - 28.4	65.27 - 65.22 (+0.06/-0.06)
	L-06253	De-Na-Zin	Pu3	T-P Zone	29n	25.6 - 28.4	65.27 - 65.22 (+0.06/-0.06)
	L-06254	De-Na-Zin	Pu3	T-P Zone	29n	25.6 - 28.4	65.27 - 65.22 (+0.06/-0.06)
	L-06273	De-Na-Zin	Pu3	T-P Zone	29n	25.6 - 28.4	65.27 - 65.22 (+0.06/-0.06)
	L-06274	De-Na-Zin	Pu3	T-P Zone	29n	25.6 - 28.4	65.27 - 65.22 (+0.06/-0.06)
	L-06335	De-Na-Zin	Pu3	T-P Zone	29n	25.6 - 28.4	65.27 - 65.22 (+0.06/-0.06)

Mammal Horizon*	Localities	Location	NALMA†	SJB Biozone§	Magnetic Chron	Stratigraphic Position (m)**	Estimated Age (Ma)
	L-06341	De-Na-Zin	Pu3	T-P Zone	29n	25.6 - 28.4	65.27 - 65.22 (+0.06/-0.06)
	L-06360	De-Na-Zin	Pu3	T-P Zone	29n	25.6 - 28.4	65.27 - 65.22 (+0.06/-0.06)
	L-06423	De-Na-Zin	Pu3	T-P Zone	29n	25.6 - 28.4	65.27 - 65.22 (+0.06/-0.06)
	L-06424	De-Na-Zin	Pu3	T-P Zone	29n	25.6 - 28.4	65.27 - 65.22 (+0.06/-0.06)
	L-06425	De-Na-Zin	Pu3	T-P Zone	29n	25.6 - 28.4	65.27 - 65.22 (+0.06/-0.06)
	L-06426	De-Na-Zin	Pu3	T-P Zone	29n	25.6 - 28.4	65.27 - 65.22 (+0.06/-0.06)
	L-06427	De-Na-Zin	Pu3	T-P Zone	29n	25.6 - 28.4	65.27 - 65.22 (+0.06/-0.06)
	L-06428	De-Na-Zin	Pu3	T-P Zone	29n	25.6 - 28.4	65.27 - 65.22 (+0.06/-0.06)
	L-06429	De-Na-Zin	Pu3	T-P Zone	29n	25.6 - 28.4	65.27 - 65.22 (+0.06/-0.06)
	L-06430	De-Na-Zin	Pu3	T-P Zone	29n	25.6 - 28.4	65.27 - 65.22 (+0.06/-0.06)
	L-06431	De-Na-Zin	Pu3	T-P Zone	29n	25.6 - 28.4	65.27 - 65.22 (+0.06/-0.06)
	L-06432	De-Na-Zin	Pu3	T-P Zone	29n	25.6 - 28.4	65.27 - 65.22 (+0.06/-0.06)
	L-06433	De-Na-Zin	Pu3	T-P Zone	29n	25.6 - 28.4	65.27 - 65.22 (+0.06/-0.06)
	L-06487	De-Na-Zin	Pu3	T-P Zone	29n	25.6 - 28.4	65.27 - 65.22 (+0.06/-0.06)
	L-06621	De-Na-Zin	Pu3	T-P Zone	29n	25.6 - 28.4	65.27 - 65.22 (+0.06/-0.06)
	L-08238	De-Na-Zin	Pu3	T-P Zone	29n	25.6 - 28.4	65.27 - 65.22 (+0.06/-0.06)
	L-08336	De-Na-Zin	Pu3	T-P Zone	29n	25.6 - 28.4	65.27 - 65.22 (+0.06/-0.06)
	L-08337	De-Na-Zin	Pu3	T-P Zone	29n	25.6 - 28.4	65.27 - 65.22 (+0.06/-0.06)
	L-08338	De-Na-Zin	Pu3	T-P Zone	29n	25.6 - 28.4	65.27 - 65.22 (+0.06/-0.06)
	L-08339	De-Na-Zin	Pu3	T-P Zone	29n	25.6 - 28.4	65.27 - 65.22 (+0.06/-0.06)
	L-08340	De-Na-Zin	Pu3	T-P Zone	29n	25.6 - 28.4	65.27 - 65.22 (+0.06/-0.06)
	L-08348	De-Na-Zin	Pu3	T-P Zone	29n	25.6 - 28.4	65.27 - 65.22 (+0.06/-0.06)
	L-08349	De-Na-Zin	Pu3	T-P Zone	29n	25.6 - 28.4	65.27 - 65.22 (+0.06/-0.06)
	L-08350	De-Na-Zin	Pu3	T-P Zone	29n	25.6 - 28.4	65.27 - 65.22 (+0.06/-0.06)
	L-08351	De-Na-Zin	Pu3	T-P Zone	29n	25.6 - 28.4	65.27 - 65.22 (+0.06/-0.06)

Mammal Horizon*	Localities	Location	NALMA†	SJB Biozone§	Magnetic Chron	Stratigraphic Position (m)**	Estimated Age (Ma)
	L-08352	De-Na-Zin	Pu3	T-P Zone	29n	25.6 - 28.4	65.27 - 65.22 (+0.06/-0.06)
	L-08353	De-Na-Zin	Pu3	T-P Zone	29n	25.6 - 28.4	65.27 - 65.22 (+0.06/-0.06)
	L-08354	De-Na-Zin	Pu3	T-P Zone	29n	25.6 - 28.4	65.27 - 65.22 (+0.06/-0.06)
	L-08355	De-Na-Zin	Pu3	T-P Zone	29n	25.6 - 28.4	65.27 - 65.22 (+0.06/-0.06)
	L-08356	De-Na-Zin	Pu3	T-P Zone	29n	25.6 - 28.4	65.27 - 65.22 (+0.06/-0.06)
	L-08357	De-Na-Zin	Pu3	T-P Zone	29n	25.6 - 28.4	65.27 - 65.22 (+0.06/-0.06)
	L-08361	De-Na-Zin	Pu3	T-P Zone	29n	25.6 - 28.4	65.27 - 65.22 (+0.06/-0.06)
	L-08366	De-Na-Zin	Pu3	T-P Zone	29n	25.6 - 28.4	65.27 - 65.22 (+0.06/-0.06)
	L-08367	De-Na-Zin	Pu3	T-P Zone	29n	25.6 - 28.4	65.27 - 65.22 (+0.06/-0.06)
	L-08368	De-Na-Zin	Pu3	T-P Zone	29n	25.6 - 28.4	65.27 - 65.22 (+0.06/-0.06)
	L-08614	De-Na-Zin	Pu3	T-P Zone	29n	25.6 - 28.4	65.27 - 65.22 (+0.06/-0.06)
	L-08615	De-Na-Zin	Pu3	T-P Zone	29n	25.6 - 28.4	65.27 - 65.22 (+0.06/-0.06)
	L-08856	De-Na-Zin	Pu3	T-P Zone	29n	25.6 - 28.4	65.27 - 65.22 (+0.06/-0.06)
	L-08857	De-Na-Zin	Pu3	T-P Zone	29n	25.6 - 28.4	65.27 - 65.22 (+0.06/-0.06)
	L-08858	De-Na-Zin	Pu3	T-P Zone	29n	25.6 - 28.4	65.27 - 65.22 (+0.06/-0.06)
	L-08859	De-Na-Zin	Pu3	T-P Zone	29n	25.6 - 28.4	65.27 - 65.22 (+0.06/-0.06)
	L-08860	De-Na-Zin	Pu3	T-P Zone	29n	25.6 - 28.4	65.27 - 65.22 (+0.06/-0.06)
	L-08861	De-Na-Zin	Pu3	T-P Zone	29n	25.6 - 28.4	65.27 - 65.22 (+0.06/-0.06)
	L-08862	De-Na-Zin	Pu3	T-P Zone	29n	25.6 - 28.4	65.27 - 65.22 (+0.06/-0.06)
	L-08863	De-Na-Zin	Pu3	T-P Zone	29n	25.6 - 28.4	65.27 - 65.22 (+0.06/-0.06)
	L-08864	De-Na-Zin	Pu3	T-P Zone	29n	25.6 - 28.4	65.27 - 65.22 (+0.06/-0.06)
	L-08884	De-Na-Zin	Pu3	T-P Zone	29n	25.6 - 28.4	65.27 - 65.22 (+0.06/-0.06)
	L-08887	De-Na-Zin	Pu3	T-P Zone	29n	25.6 - 28.4	65.27 - 65.22 (+0.06/-0.06)
	L-10478	De-Na-Zin	Pu3	T-P Zone	29n	25.6 - 28.4	65.27 - 65.22 (+0.06/-0.06)
	L-10479	De-Na-Zin	Pu3	T-P Zone	29n	25.6 - 28.4	65.27 - 65.22 (+0.06/-0.06)

Mammal Horizon*	Localities	Location	NALMA†	SJB Biozone§	Magnetic Chron	Stratigraphic Position (m)**	Estimated Age (Ma)
	L-10480	De-Na-Zin	Pu3	T-P Zone	29n	25.6 - 28.4	65.27 - 65.22 (+0.06/-0.06)
	L-10481	De-Na-Zin	Pu3	T-P Zone	29n	25.6 - 28.4	65.27 - 65.22 (+0.06/-0.06)
	L-10482	De-Na-Zin	Pu3	T-P Zone	29n	25.6 - 28.4	65.27 - 65.22 (+0.06/-0.06)
	L-10483	De-Na-Zin	Pu3	T-P Zone	29n	25.6 - 28.4	65.27 - 65.22 (+0.06/-0.06)
	L-10484	De-Na-Zin	Pu3	T-P Zone	29n	25.6 - 28.4	65.27 - 65.22 (+0.06/-0.06)
	L-10485	De-Na-Zin	Pu3	T-P Zone	29n	25.6 - 28.4	65.27 - 65.22 (+0.06/-0.06)
	L-12076	De-Na-Zin	Pu3	T-P Zone	29n	25.6 - 28.4	65.27 - 65.22 (+0.06/-0.06)
	L-12077	De-Na-Zin	Pu3	T-P Zone	29n	25.6 - 28.4	65.27 - 65.22 (+0.06/-0.06)
5	L-00633	Gallegos Canyon	Pu3	T-P Zone	29n	26.5 - 34.5	65.20 - 65.03 (+0.03/-0.01)
	L-00647	Gallegos Canyon	Pu3	T-P Zone	29n	26.5 - 34.5	65.20 - 65.03 (+0.03/-0.01)
	L-00648	Gallegos Canyon	Pu3	T-P Zone	29n	26.5 - 34.5	65.20 - 65.03 (+0.03/-0.01)
	L-00649	Gallegos Canyon	Pu3	T-P Zone	29n	26.5 - 34.5	65.20 - 65.03 (+0.03/-0.01)
	L-00650	Gallegos Canyon	Pu3	T-P Zone	29n	26.5 - 34.5	65.20 - 65.03 (+0.03/-0.01)
	L-00651	Gallegos Canyon	Pu3	T-P Zone	29n	26.5 - 34.5	65.20 - 65.03 (+0.03/-0.01)
	L-00652	Gallegos Canyon	Pu3	T-P Zone	29n	26.5 - 34.5	65.20 - 65.03 (+0.03/-0.01)
	L-00653	Gallegos Canyon	Pu3	T-P Zone	29n	26.5 - 34.5	65.20 - 65.03 (+0.03/-0.01)
	L-00654	Gallegos Canyon	Pu3	T-P Zone	29n	26.5 - 34.5	65.20 - 65.03 (+0.03/-0.01)
	L-00655	Gallegos Canyon	Pu3	T-P Zone	29n	26.5 - 34.5	65.20 - 65.03 (+0.03/-0.01)
	L-00669	Gallegos Canyon	Pu3	T-P Zone	29n	26.5 - 34.5	65.20 - 65.03 (+0.03/-0.01)
	L-00670	Gallegos Canyon	Pu3	T-P Zone	29n	26.5 - 34.5	65.20 - 65.03 (+0.03/-0.01)
	L-00671	Gallegos Canyon	Pu3	T-P Zone	29n	26.5 - 34.5	65.20 - 65.03 (+0.03/-0.01)
	L-00673	Gallegos Canyon	Pu3	T-P Zone	29n	26.5 - 34.5	65.20 - 65.03 (+0.03/-0.01)
	L-00674	Gallegos Canyon	Pu3	T-P Zone	29n	26.5 - 34.5	65.20 - 65.03 (+0.03/-0.01)
	L-01225	Gallegos Canyon	Pu3	T-P Zone	29n	26.5 - 34.5	65.20 - 65.03 (+0.03/-0.01)
	L-01405	Gallegos Canyon	Pu3	T-P Zone	29n	26.5 - 34.5	65.20 - 65.03 (+0.03/-0.01)

Mammal Horizon*	Localities	Location	NALMA†	SJB Biozone§	Magnetic Chron	Stratigraphic Position (m)**	Estimated Age (Ma)
	L-02094	Gallegos Canyon	Pu3	T-P Zone	29n	26.5 - 34.5	65.20 - 65.03 (+0.03/-0.01)
	L-02095	Gallegos Canyon	Pu3	T-P Zone	29n	26.5 - 34.5	65.20 - 65.03 (+0.03/-0.01)
	L-02096	Gallegos Canyon	Pu3	T-P Zone	29n	26.5 - 34.5	65.20 - 65.03 (+0.03/-0.01)
	L-02097	Gallegos Canyon	Pu3	T-P Zone	29n	26.5 - 34.5	65.20 - 65.03 (+0.03/-0.01)
	L-02098	Gallegos Canyon	Pu3	T-P Zone	29n	26.5 - 34.5	65.20 - 65.03 (+0.03/-0.01)
	L-02504	Gallegos Canyon	Pu3	T-P Zone	29n	26.5 - 34.5	65.20 - 65.03 (+0.03/-0.01)
	L-02505	Gallegos Canyon	Pu3	T-P Zone	29n	26.5 - 34.5	65.20 - 65.03 (+0.03/-0.01)
	L-02506	Gallegos Canyon	Pu3	T-P Zone	29n	26.5 - 34.5	65.20 - 65.03 (+0.03/-0.01)
	L-02507	Gallegos Canyon	Pu3	T-P Zone	29n	26.5 - 34.5	65.20 - 65.03 (+0.03/-0.01)
	L-02508	Gallegos Canyon	Pu3	T-P Zone	29n	26.5 - 34.5	65.20 - 65.03 (+0.03/-0.01)
	L-02509	Gallegos Canyon	Pu3	T-P Zone	29n	26.5 - 34.5	65.20 - 65.03 (+0.03/-0.01)
	L-02510	Gallegos Canyon	Pu3	T-P Zone	29n	26.5 - 34.5	65.20 - 65.03 (+0.03/-0.01)
	L-02511	Gallegos Canyon	Pu3	T-P Zone	29n	26.5 - 34.5	65.20 - 65.03 (+0.03/-0.01)
6	L-08906	Mesa de Cuba	To1?	P-P Zone	28r	43.0 - 49.5	64.80 - 64.74 (+0.04/-0.02)
7	L-00680	Kimbeto	To1	P-P Zone	28n	57.2 - 64.8	64.66 - 64.58 (+0.02/-0.01)
	L-00681	Kimbeto	To1	P-P Zone	28n	57.2 - 64.8	64.66 - 64.58 (+0.02/-0.01)
	L-00682	Kimbeto	To1	P-P Zone	28n	57.2 - 64.8	64.66 - 64.58 (+0.02/-0.01)
	L-00687	Kimbeto	To1	P-P Zone	28n	57.2 - 64.8	64.66 - 64.58 (+0.02/-0.01)
	L-00688	Kimbeto	To1	P-P Zone	28n	57.2 - 64.8	64.66 - 64.58 (+0.02/-0.01)
	L-00689	Kimbeto	To1	P-P Zone	28n	57.2 - 64.8	64.66 - 64.58 (+0.02/-0.01)
	L-00690	Kimbeto	To1	P-P Zone	28n	57.2 - 64.8	64.66 - 64.58 (+0.02/-0.01)
	L-00691	Kimbeto	To1	P-P Zone	28n	57.2 - 64.8	64.66 - 64.58 (+0.02/-0.01)
	L-00693	Kimbeto	To1	P-P Zone	28n	57.2 - 64.8	64.66 - 64.58 (+0.02/-0.01)
	L-00694	Kimbeto	To1	P-P Zone	28n	57.2 - 64.8	64.66 - 64.58 (+0.02/-0.01)

Mammal Horizon*	Localities	Location	NALMA†	SJB Biozone§	Magnetic Chron	Stratigraphic Position (m)**	Estimated Age (Ma)
	L-00695	Kimbeto	To1	P-P Zone	28n	57.2 - 64.8	64.66 - 64.58 (+0.02/-0.01)
	L-00696	Kimbeto	To1	P-P Zone	28n	57.2 - 64.8	64.66 - 64.58 (+0.02/-0.01)
	L-01109	Kimbeto	To1	P-P Zone	28n	57.2 - 64.8	64.66 - 64.58 (+0.02/-0.01)
	L-01110	Kimbeto	To1	P-P Zone	28n	57.2 - 64.8	64.66 - 64.58 (+0.02/-0.01)
	L-02019	Kimbeto	To1	P-P Zone	28n	57.2 - 64.8	64.66 - 64.58 (+0.02/-0.01)
	L-02020	Kimbeto	To1	P-P Zone	28n	57.2 - 64.8	64.66 - 64.58 (+0.02/-0.01)
	L-02713	Kimbeto	To1	P-P Zone	28n	57.2 - 64.8	64.66 - 64.58 (+0.02/-0.01)
	L-06446	Kimbeto	To1	P-P Zone	28n	57.2 - 64.8	64.66 - 64.58 (+0.02/-0.01)
	L-06447	Kimbeto	To1	P-P Zone	28n	57.2 - 64.8	64.66 - 64.58 (+0.02/-0.01)
	L-06494	Kimbeto	To1	P-P Zone	28n	57.2 - 64.8	64.66 - 64.58 (+0.02/-0.01)
	L-06627	Kimbeto	To1	P-P Zone	28n	57.2 - 64.8	64.66 - 64.58 (+0.02/-0.01)
	L-08871	Kimbeto	To1	P-P Zone	28n	57.2 - 64.8	64.66 - 64.58 (+0.02/-0.01)
	L-08872	Kimbeto	To1	P-P Zone	28n	57.2 - 64.8	64.66 - 64.58 (+0.02/-0.01)
	L-08873	Kimbeto	To1	P-P Zone	28n	57.2 - 64.8	64.66 - 64.58 (+0.02/-0.01)
	L-08874	Kimbeto	To1	P-P Zone	28n	57.2 - 64.8	64.66 - 64.58 (+0.02/-0.01)
	L-09223	Kimbeto	To1	P-P Zone	28n	57.2 - 64.8	64.66 - 64.58 (+0.02/-0.01)
	L-09224	Kimbeto	To1	P-P Zone	28n	57.2 - 64.8	64.66 - 64.58 (+0.02/-0.01)
	L-09873	Kimbeto	To1	P-P Zone	28n	57.2 - 64.8	64.66 - 64.58 (+0.02/-0.01)
	L-09874	Kimbeto	To1	P-P Zone	28n	57.2 - 64.8	64.66 - 64.58 (+0.02/-0.01)
	L-09881	Kimbeto	To1	P-P Zone	28n	57.2 - 64.8	64.66 - 64.58 (+0.02/-0.01)
	L-09900	Kimbeto	To1	P-P Zone	28n	57.2 - 64.8	64.66 - 64.58 (+0.02/-0.01)
	L-10437	Kimbeto	To1	P-P Zone	28n	57.2 - 64.8	64.66 - 64.58 (+0.02/-0.01)
8	L-02715	Mesa de Cuba	To1	P-P Zone	28n	69.7 - 71.0	64.52 - 64.50 (+0.03/-0.02)
	L-06604	Mesa de Cuba	To1	P-P Zone	28n	69.7 - 71.0	64.52 - 64.50 (+0.03/-0.02)
	L-06605	Mesa de Cuba	To1	P-P Zone	28n	69.7 - 71.0	64.52 - 64.50 (+0.03/-0.02)

Mammal Horizon*	Localities	Location	NALMA†	SJB Biozone§	Magnetic Chron	Stratigraphic Position (m)**	Estimated Age (Ma)
	L-07565	Mesa de Cuba	To1	P-P Zone	28n	69.7 - 71.0	64.52 - 64.50 (+0.03/-0.02)
	L-07566	Mesa de Cuba	To1	P-P Zone	28n	69.7 - 71.0	64.52 - 64.50 (+0.03/-0.02)
	L-07567	Mesa de Cuba	To1	P-P Zone	28n	69.7 - 71.0	64.52 - 64.50 (+0.03/-0.02)
	L-07568	Mesa de Cuba	To1	P-P Zone	28n	69.7 - 71.0	64.52 - 64.50 (+0.03/-0.02)
	L-07569	Mesa de Cuba	To1	P-P Zone	28n	69.7 - 71.0	64.52 - 64.50 (+0.03/-0.02)
	L-08609	Mesa de Cuba	To1	P-P Zone	28n	69.7 - 71.0	64.52 - 64.50 (+0.03/-0.02)
9	L-06492	Betonnie Tsosie	To1	P-P Zone	28n	102 - 109.2	64.49 - 64.44 (+0.05/-0.01)
	L-06493	Betonnie Tsosie	To1	P-P Zone	28n	102 - 109.2	64.49 - 64.44 (+0.05/-0.01)
	L-0613	Betonnie Tsosie	To1	P-P Zone	28n	102 - 109.2	64.49 - 64.44 (+0.05/-0.01)
	L-09973	Betonnie Tsosie	To1	P-P Zone	28n	102 - 109.2	64.49 - 64.44 (+0.05/-0.01)
	L-09974	Betonnie Tsosie	To1	P-P Zone	28n	102 - 109.2	64.49 - 64.44 (+0.05/-0.01)
	L-09975	Betonnie Tsosie	To1	P-P Zone	28n	102 - 109.2	64.49 - 64.44 (+0.05/-0.01)
10	L-08345	De-Na-Zin	To1	P-P Zone	28n	85.6 - 91.0	64.46 - 64.40 (+0.05/-0.03)
	L-04345	De-Na-Zin	To1	P-P Zone	28n	85.6 - 91.0	64.46 - 64.40 (+0.05/-0.03)
	L-06429	De-Na-Zin	To1	P-P Zone	28n	85.6 - 91.0	64.46 - 64.40 (+0.05/-0.03)
	L-06448	De-Na-Zin	To1	P-P Zone	28n	85.6 - 91.0	64.46 - 64.40 (+0.05/-0.03)
	L-06489	De-Na-Zin	To1	P-P Zone	28n	85.6 - 91.0	64.46 - 64.40 (+0.05/-0.03)
	L-08341	De-Na-Zin	To1	P-P Zone	28n	85.6 - 91.0	64.46 - 64.40 (+0.05/-0.03)
11	L-02659	Kutz Canyon	To1	P-P Zone	28n	4.0 - 8.0	63.79 - 63.76 (+0.05/-0.08)
	L-02660	Kutz Canyon	To1	P-P Zone	28n	4.0 - 8.0	63.79 - 63.76 (+0.05/-0.08)
	L-06616	Kutz Canyon	To1	P-P Zone	28n	4.0 - 8.0	63.79 - 63.76 (+0.05/-0.08)
	L-06617	Kutz Canyon	To1	P-P Zone	28n	4.0 - 8.0	63.79 - 63.76 (+0.05/-0.08)
	L-06618	Kutz Canyon	To1	P-P Zone	28n	4.0 - 8.0	63.79 - 63.76 (+0.05/-0.08)
	L-06619	Kutz Canyon	To1	P-P Zone	28n	4.0 - 8.0	63.79 - 63.76 (+0.05/-0.08)

Mammal Horizon*	Localities	Location	NALMA†	SJB Biozone§	Magnetic Chron	Stratigraphic Position (m)**	Estimated Age (Ma)
	L-10435	Kutz Canyon	To1	P-P Zone	28n	4.0 - 8.0	63.79 - 63.76 (+0.05/-0.08)
	L-10436	Kutz Canyon	To1	P-P Zone	28n	4.0 - 8.0	63.79 - 63.76 (+0.05/-0.08)
12	L-00624	Kutz Canyon	To2	P-E Zone	27r	42.0 - 46.0	63.48 - 63.44 (+0.01/-0.01)
	L-00625	Kutz Canyon	To2	P-E Zone	27r	42.0 - 46.0	63.48 - 63.44 (+0.01/-0.01)
	L-00627	Kutz Canyon	To2	P-E Zone	27r	42.0 - 46.0	63.48 - 63.44 (+0.01/-0.01)
	L-00628	Kutz Canyon	To2	P-E Zone	27r	42.0 - 46.0	63.48 - 63.44 (+0.01/-0.01)
	L-00678	Kutz Canyon	To2	P-E Zone	27r	42.0 - 46.0	63.48 - 63.44 (+0.01/-0.01)
	L-00848	Kutz Canyon	To2	P-E Zone	27r	42.0 - 46.0	63.48 - 63.44 (+0.01/-0.01)
	L-01258	Kutz Canyon	To2	P-E Zone	27r	42.0 - 46.0	63.48 - 63.44 (+0.01/-0.01)
	L-01259	Kutz Canyon	To2	P-E Zone	27r	42.0 - 46.0	63.48 - 63.44 (+0.01/-0.01)
	L-01260	Kutz Canyon	To2	P-E Zone	27r	42.0 - 46.0	63.48 - 63.44 (+0.01/-0.01)
	L-01261	Kutz Canyon	To2	P-E Zone	27r	42.0 - 46.0	63.48 - 63.44 (+0.01/-0.01)
	L-01263	Kutz Canyon	To2	P-E Zone	27r	42.0 - 46.0	63.48 - 63.44 (+0.01/-0.01)
	L-01397	Kutz Canyon	To2	P-E Zone	27r	42.0 - 46.0	63.48 - 63.44 (+0.01/-0.01)
	L-02629	Kutz Canyon	To2	P-E Zone	27r	42.0 - 46.0	63.48 - 63.44 (+0.01/-0.01)
	L-02630	Kutz Canyon	To2	P-E Zone	27r	42.0 - 46.0	63.48 - 63.44 (+0.01/-0.01)
	L-02716	Kutz Canyon	To2	P-E Zone	27r	42.0 - 46.0	63.48 - 63.44 (+0.01/-0.01)
	L-02717	Kutz Canyon	To2	P-E Zone	27r	42.0 - 46.0	63.48 - 63.44 (+0.01/-0.01)
	L-02718	Kutz Canyon	To2	P-E Zone	27r	42.0 - 46.0	63.48 - 63.44 (+0.01/-0.01)
	L-02726	Kutz Canyon	To2	P-E Zone	27r	42.0 - 46.0	63.48 - 63.44 (+0.01/-0.01)
	L-04334	Kutz Canyon	To2	P-E Zone	27r	42.0 - 46.0	63.48 - 63.44 (+0.01/-0.01)
	L-05645	Kutz Canyon	To2	P-E Zone	27r	42.0 - 46.0	63.48 - 63.44 (+0.01/-0.01)
	L-05646	Kutz Canyon	To2	P-E Zone	27r	42.0 - 46.0	63.48 - 63.44 (+0.01/-0.01)
	L-05647	Kutz Canyon	To2	P-E Zone	27r	42.0 - 46.0	63.48 - 63.44 (+0.01/-0.01)
	L-05648	Kutz Canyon	To2	P-E Zone	27r	42.0 - 46.0	63.48 - 63.44 (+0.01/-0.01)

Mammal Horizon*	Localities	Location	NALMA†	SJB Biozone§	Magnetic Chron	Stratigraphic Position (m)**	Estimated Age (Ma)
	L-05649	Kutz Canyon	To2	P-E Zone	27r	42.0 - 46.0	63.48 - 63.44 (+0.01/-0.01)
	L-05650	Kutz Canyon	To2	P-E Zone	27r	42.0 - 46.0	63.48 - 63.44 (+0.01/-0.01)
	L-05651	Kutz Canyon	To2	P-E Zone	27r	42.0 - 46.0	63.48 - 63.44 (+0.01/-0.01)
	L-05866	Kutz Canyon	To2	P-E Zone	27r	42.0 - 46.0	63.48 - 63.44 (+0.01/-0.01)
	L-05867	Kutz Canyon	To2	P-E Zone	27r	42.0 - 46.0	63.48 - 63.44 (+0.01/-0.01)
	L-06268	Kutz Canyon	To2	P-E Zone	27r	42.0 - 46.0	63.48 - 63.44 (+0.01/-0.01)
	L-06422	Kutz Canyon	To2	P-E Zone	27r	42.0 - 46.0	63.48 - 63.44 (+0.01/-0.01)
	L-06510	Kutz Canyon	To2	P-E Zone	27r	42.0 - 46.0	63.48 - 63.44 (+0.01/-0.01)
	L-06511	Kutz Canyon	To2	P-E Zone	27r	42.0 - 46.0	63.48 - 63.44 (+0.01/-0.01)
	L-07853	Kutz Canyon	To2	P-E Zone	27r	42.0 - 46.0	63.48 - 63.44 (+0.01/-0.01)
	L-06998	Kutz Canyon	To2	P-E Zone	27r	42.0 - 46.0	63.48 - 63.44 (+0.01/-0.01)
	L-08876	Kutz Canyon	To2	P-E Zone	27r	42.0 - 46.0	63.48 - 63.44 (+0.01/-0.01)
	L-08877	Kutz Canyon	To2	P-E Zone	27r	42.0 - 46.0	63.48 - 63.44 (+0.01/-0.01)
	L-08878	Kutz Canyon	To2	P-E Zone	27r	42.0 - 46.0	63.48 - 63.44 (+0.01/-0.01)
	L-08879	Kutz Canyon	To2	P-E Zone	27r	42.0 - 46.0	63.48 - 63.44 (+0.01/-0.01)
	L-08880	Kutz Canyon	To2	P-E Zone	27r	42.0 - 46.0	63.48 - 63.44 (+0.01/-0.01)
	L-08881	Kutz Canyon	To2	P-E Zone	27r	42.0 - 46.0	63.48 - 63.44 (+0.01/-0.01)
	L-08882	Kutz Canyon	To2	P-E Zone	27r	42.0 - 46.0	63.48 - 63.44 (+0.01/-0.01)
	L-08883	Kutz Canyon	To2	P-E Zone	27r	42.0 - 46.0	63.48 - 63.44 (+0.01/-0.01)
	L-08885	Kutz Canyon	To2	P-E Zone	27r	42.0 - 46.0	63.48 - 63.44 (+0.01/-0.01)
	L-08886	Kutz Canyon	To2	P-E Zone	27r	42.0 - 46.0	63.48 - 63.44 (+0.01/-0.01)
	L-09883	Kutz Canyon	To2	P-E Zone	27r	42.0 - 46.0	63.48 - 63.44 (+0.01/-0.01)
	L-09884	Kutz Canyon	To2	P-E Zone	27r	42.0 - 46.0	63.48 - 63.44 (+0.01/-0.01)
	L-09898	Kutz Canyon	To2	P-E Zone	27r	42.0 - 46.0	63.48 - 63.44 (+0.01/-0.01)
	L-11788	Kutz Canyon	To2	P-E Zone	27r	42.0 - 46.0	63.48 - 63.44 (+0.01/-0.01)

Mammal Horizon*	Localities	Location	NALMA†	SJB Biozone§	Magnetic Chron	Stratigraphic Position (m)**	Estimated Age (Ma)
	L-11789	Kutz Canyon	To2	P-E Zone	27r	42.0 - 46.0	63.48 - 63.44 (+0.01/-0.01)
	L-11790	Kutz Canyon	To2	P-E Zone	27r	42.0 - 46.0	63.48 - 63.44 (+0.01/-0.01)
13	L-01225	Chico Springs	To2	P-E Zone	27r	8.9 - 10.5	63.44 - 63.42 (+0.01/-0.01)
	L-02513	Chico Springs	To2	P-E Zone	27r	8.9 - 10.5	63.44 - 63.42 (+0.01/-0.01)
	L-02543	Chico Springs	To2	P-E Zone	27r	8.9 - 10.5	63.44 - 63.42 (+0.01/-0.01)
	L-02544	Chico Springs	To2	P-E Zone	27r	8.9 - 10.5	63.44 - 63.42 (+0.01/-0.01)
	L-02545	Chico Springs	To2	P-E Zone	27r	8.9 - 10.5	63.44 - 63.42 (+0.01/-0.01)
	L-02546	Chico Springs	To2	P-E Zone	27r	8.9 - 10.5	63.44 - 63.42 (+0.01/-0.01)
	L-02547	Chico Springs	To2	P-E Zone	27r	8.9 - 10.5	63.44 - 63.42 (+0.01/-0.01)
	L-02548	Chico Springs	To2	P-E Zone	27r	8.9 - 10.5	63.44 - 63.42 (+0.01/-0.01)
	L-02549	Chico Springs	To2	P-E Zone	27r	8.9 - 10.5	63.44 - 63.42 (+0.01/-0.01)
	L-04549	Chico Springs	To2	P-E Zone	27r	8.9 - 10.5	63.44 - 63.42 (+0.01/-0.01)
	L-04550	Chico Springs	To2	P-E Zone	27r	8.9 - 10.5	63.44 - 63.42 (+0.01/-0.01)
	L-04552	Chico Springs	To2	P-E Zone	27r	8.9 - 10.5	63.44 - 63.42 (+0.01/-0.01)
	L-04553	Chico Springs	To2	P-E Zone	27r	8.9 - 10.5	63.44 - 63.42 (+0.01/-0.01)
	L-04641	Chico Springs	To2	P-E Zone	27r	8.9 - 10.5	63.44 - 63.42 (+0.01/-0.01)
	L-05847	Chico Springs	To2	P-E Zone	27r	8.9 - 10.5	63.44 - 63.42 (+0.01/-0.01)
	L-05870	Chico Springs	To2	P-E Zone	27r	8.9 - 10.5	63.44 - 63.42 (+0.01/-0.01)
	L-08235	Chico Springs	To2	P-E Zone	27r	8.9 - 10.5	63.44 - 63.42 (+0.01/-0.01)
	L-08236	Chico Springs	To2	P-E Zone	27r	8.9 - 10.5	63.44 - 63.42 (+0.01/-0.01)
	L-08347	Chico Springs	To2	P-E Zone	27r	8.9 - 10.5	63.44 - 63.42 (+0.01/-0.01)
	L-08365	Chico Springs	To2	P-E Zone	27r	8.9 - 10.5	63.44 - 63.42 (+0.01/-0.01)
14	L-00631	Kutz Canyon	To2	E-A Zone	27r	103.0 - 111.0	62.97 - 62.91 (+0.10/-0.08)
	L-01227	Kutz Canyon	To2	E-A Zone	27r	103.0 - 111.0	62.97 - 62.91 (+0.10/-0.08)

Mammal Horizon*	Localities	Location	NALMA†	SJB Biozone§	Magnetic Chron	Stratigraphic Position (m)**	Estimated Age (Ma)
	L-01228	Kutz Canyon	To2	E-A Zone	27r	103.0 - 111.0	62.97 - 62.91 (+0.10/-0.08)
	L-01229	Kutz Canyon	To2	E-A Zone	27r	103.0 - 111.0	62.97 - 62.91 (+0.10/-0.08)
	L-01230	Kutz Canyon	To2	E-A Zone	27r	103.0 - 111.0	62.97 - 62.91 (+0.10/-0.08)
	L-01234	Kutz Canyon	To2	E-A Zone	27r	103.0 - 111.0	62.97 - 62.91 (+0.10/-0.08)
	L-01235	Kutz Canyon	To2	E-A Zone	27r	103.0 - 111.0	62.97 - 62.91 (+0.10/-0.08)
	L-01236	Kutz Canyon	To2	E-A Zone	27r	103.0 - 111.0	62.97 - 62.91 (+0.10/-0.08)
	L-01237	Kutz Canyon	To2	E-A Zone	27r	103.0 - 111.0	62.97 - 62.91 (+0.10/-0.08)
	L-01262	Kutz Canyon	To2	E-A Zone	27r	103.0 - 111.0	62.97 - 62.91 (+0.10/-0.08)
	L-01264	Kutz Canyon	To2	E-A Zone	27r	103.0 - 111.0	62.97 - 62.91 (+0.10/-0.08)
	L-01270	Kutz Canyon	To2	E-A Zone	27r	103.0 - 111.0	62.97 - 62.91 (+0.10/-0.08)
	L-01274	Kutz Canyon	To2	E-A Zone	27r	103.0 - 111.0	62.97 - 62.91 (+0.10/-0.08)
	L-01275	Kutz Canyon	To2	E-A Zone	27r	103.0 - 111.0	62.97 - 62.91 (+0.10/-0.08)
	L-01276	Kutz Canyon	To2	E-A Zone	27r	103.0 - 111.0	62.97 - 62.91 (+0.10/-0.08)
	L-01277	Kutz Canyon	To2	E-A Zone	27r	103.0 - 111.0	62.97 - 62.91 (+0.10/-0.08)
	L-01278	Kutz Canyon	To2	E-A Zone	27r	103.0 - 111.0	62.97 - 62.91 (+0.10/-0.08)
	L-01279	Kutz Canyon	To2	E-A Zone	27r	103.0 - 111.0	62.97 - 62.91 (+0.10/-0.08)
	L-01395	Kutz Canyon	To2	E-A Zone	27r	103.0 - 111.0	62.97 - 62.91 (+0.10/-0.08)
	L-02524	Kutz Canyon	To2	E-A Zone	27r	103.0 - 111.0	62.97 - 62.91 (+0.10/-0.08)
	L-02586	Kutz Canyon	To2	E-A Zone	27r	103.0 - 111.0	62.97 - 62.91 (+0.10/-0.08)
	L-02587	Kutz Canyon	To2	E-A Zone	27r	103.0 - 111.0	62.97 - 62.91 (+0.10/-0.08)
	L-02635	Kutz Canyon	To2	E-A Zone	27r	103.0 - 111.0	62.97 - 62.91 (+0.10/-0.08)
	L-02650	Kutz Canyon	To2	E-A Zone	27r	103.0 - 111.0	62.97 - 62.91 (+0.10/-0.08)
	L-02651	Kutz Canyon	To2	E-A Zone	27r	103.0 - 111.0	62.97 - 62.91 (+0.10/-0.08)
	L-02652	Kutz Canyon	To2	E-A Zone	27r	103.0 - 111.0	62.97 - 62.91 (+0.10/-0.08)
	L-05868	Kutz Canyon	To2	E-A Zone	27r	103.0 - 111.0	62.97 - 62.91 (+0.10/-0.08)

Mammal Horizon*	Localities	Location	NALMA†	SJB Biozone§	Magnetic Chron	Stratigraphic Position (m)**	Estimated Age (Ma)
	L-04174	Kutz Canyon	To2	E-A Zone	27r	103.0 - 111.0	62.97 - 62.91 (+0.10/-0.08)
	L-04338	Kutz Canyon	To2	E-A Zone	27r	103.0 - 111.0	62.97 - 62.91 (+0.10/-0.08)
	L-06244	Kutz Canyon	To2	E-A Zone	27r	103.0 - 111.0	62.97 - 62.91 (+0.10/-0.08)
	L-06245	Kutz Canyon	To2	E-A Zone	27r	103.0 - 111.0	62.97 - 62.91 (+0.10/-0.08)
	L-06256	Kutz Canyon	To2	E-A Zone	27r	103.0 - 111.0	62.97 - 62.91 (+0.10/-0.08)
	L-06269	Kutz Canyon	To2	E-A Zone	27r	103.0 - 111.0	62.97 - 62.91 (+0.10/-0.08)
	L-06362	Kutz Canyon	To2	E-A Zone	27r	103.0 - 111.0	62.97 - 62.91 (+0.10/-0.08)
	L-06388	Kutz Canyon	To2	E-A Zone	27r	103.0 - 111.0	62.97 - 62.91 (+0.10/-0.08)
	L-06389	Kutz Canyon	To2	E-A Zone	27r	103.0 - 111.0	62.97 - 62.91 (+0.10/-0.08)
	L-06390	Kutz Canyon	To2	E-A Zone	27r	103.0 - 111.0	62.97 - 62.91 (+0.10/-0.08)
	L-06391	Kutz Canyon	To2	E-A Zone	27r	103.0 - 111.0	62.97 - 62.91 (+0.10/-0.08)
	L-06392	Kutz Canyon	To2	E-A Zone	27r	103.0 - 111.0	62.97 - 62.91 (+0.10/-0.08)
	L-06403	Kutz Canyon	To2	E-A Zone	27r	103.0 - 111.0	62.97 - 62.91 (+0.10/-0.08)
	L-06408	Kutz Canyon	To2	E-A Zone	27r	103.0 - 111.0	62.97 - 62.91 (+0.10/-0.08)
	L-06410	Kutz Canyon	To2	E-A Zone	27r	103.0 - 111.0	62.97 - 62.91 (+0.10/-0.08)
	L-06568	Kutz Canyon	To2	E-A Zone	27r	103.0 - 111.0	62.97 - 62.91 (+0.10/-0.08)
	L-06260	Kutz Canyon	To2	E-A Zone	27r	103.0 - 111.0	62.97 - 62.91 (+0.10/-0.08)
	L-06879	Kutz Canyon	To2	E-A Zone	27r	103.0 - 111.0	62.97 - 62.91 (+0.10/-0.08)
	L-06880	Kutz Canyon	To2	E-A Zone	27r	103.0 - 111.0	62.97 - 62.91 (+0.10/-0.08)
	L-06881	Kutz Canyon	To2	E-A Zone	27r	103.0 - 111.0	62.97 - 62.91 (+0.10/-0.08)
	L-06883	Kutz Canyon	To2	E-A Zone	27r	103.0 - 111.0	62.97 - 62.91 (+0.10/-0.08)
	L-08358	Kutz Canyon	To2	E-A Zone	27r	103.0 - 111.0	62.97 - 62.91 (+0.10/-0.08)
	L-08619	Kutz Canyon	To2	E-A Zone	27r	103.0 - 111.0	62.97 - 62.91 (+0.10/-0.08)
	L-08620	Kutz Canyon	To2	E-A Zone	27r	103.0 - 111.0	62.97 - 62.91 (+0.10/-0.08)
	L-08621	Kutz Canyon	To2	E-A Zone	27r	103.0 - 111.0	62.97 - 62.91 (+0.10/-0.08)

Mammal Horizon*	Localities	Location	NALMA†	SJB Biozone§	Magnetic Chron	Stratigraphic Position (m)**	Estimated Age (Ma)
	L-08623	Kutz Canyon	To2	E-A Zone	27r	103.0 - 111.0	62.97 - 62.91 (+0.10/-0.08)
	L-08624	Kutz Canyon	To2	E-A Zone	27r	103.0 - 111.0	62.97 - 62.91 (+0.10/-0.08)
	L-08772	Kutz Canyon	To2	E-A Zone	27r	103.0 - 111.0	62.97 - 62.91 (+0.10/-0.08)
	L-08773	Kutz Canyon	To2	E-A Zone	27r	103.0 - 111.0	62.97 - 62.91 (+0.10/-0.08)
	L-08875	Kutz Canyon	To2	E-A Zone	27r	103.0 - 111.0	62.97 - 62.91 (+0.10/-0.08)
	L-08776	Kutz Canyon	To2	E-A Zone	27r	103.0 - 111.0	62.97 - 62.91 (+0.10/-0.08)
	L-09184	Kutz Canyon	To2	E-A Zone	27r	103.0 - 111.0	62.97 - 62.91 (+0.10/-0.08)

Notes: *see table 1 for mammalian horizons, †NALMA zones from Lofgren et al. (2004), §SJB biozones from Williamson (1996), **Stratigraphic position within each measured section for that locality (see figs. 2-4).

APPENDIX C

Ojo Alamo Sandstone and Lower Nacimiento Formation $^{40}Ar/^{39}Ar$ Data

Table C.1 - Single crystal laser fusion $^{40}Ar/^{39}Ar$ data

ID	Power (Watts)	$^{40}Ar/^{39}Ar$	$^{37}Ar/^{39}Ar$	$^{36}Ar/^{39}Ar$ (x 10^{-3})	$^{39}Ar_K$ (x10^{-15} mol)	K/Ca	$^{40}Ar^*$ (%)	Age (Ma)	±1σ (Ma)
CM-SS4, Sanidine, J=0.0091944±0.01%, IC=1.051596±0.0010175, NM-258E, Lab#=61750, Argus VI									
53	4	3.983	0.0024	0.0073	0.827	216.9	100.0	65.682	0.092
66	4	4.213	0.0036	0.0117	1.320	143.0	99.9	69.401	0.059
07	4	4.399	0.0013	-0.0194	0.398	378.3	100.1	72.55	0.19
15	4	4.488	0.0009	0.0290	0.427	592.0	99.8	73.75	0.18
42	4	4.482	0.0042	0.0089	0.715	121.5	99.9	73.77	0.11
36	4	4.509	0.0034	0.0116	0.720	151.4	99.9	74.18	0.11
55	4	4.513	0.0068	0.0004	0.779	75.4	100.0	74.31	0.10
16	4	4.519	0.0045	0.0139	1.696	113.5	99.9	74.342	0.048
51	4	4.528	0.0043	0.0116	1.211	118.8	99.9	74.497	0.067
37	4	4.555	0.0033	0.0117	1.378	153.2	99.9	74.934	0.060
60	4	4.560	0.0043	0.0108	1.297	119.5	99.9	75.014	0.063
45	4	4.567	0.0036	0.0126	0.694	143.3	99.9	75.12	0.11
10	4	4.593	0.0119	0.0868	0.599	42.9	99.5	75.18	0.30
64	4	4.577	0.0045	0.0290	1.044	112.5	99.8	75.208	0.077
57	4	4.610	0.0122	0.0605	0.885	42.0	99.6	75.59	0.21
52	4	4.631	0.0108	0.0233	0.480	47.4	99.9	76.11	0.29
48	4	4.715	0.0111	0.0455	0.707	46.0	99.7	77.36	0.27

ID	Power (Watts)	$^{40}Ar/^{39}Ar$	$^{37}Ar/^{39}Ar$	$^{36}Ar/^{39}Ar$ (x 10^{-3})	$^{39}Ar_K$ (x10^{-15} mol)	K/Ca	$^{40}Ar^*$ (%)	Age (Ma)	±1σ (Ma)
54	4	4.775	0.0040	0.0206	0.981	126.1	99.9	78.43	0.19
30	4	4.791	0.0110	0.0335	1.574	46.2	99.8	78.63	0.14
27	4	4.853	0.0098	-0.0196	0.818	52.2	100.1	79.90	0.25
58	4	4.887	0.0121	0.0655	0.628	42.1	99.6	80.03	0.30
08	4	4.936	0.0038	-0.0171	0.832	134.0	100.1	81.22	0.26
13	4	4.970	0.0048	0.0412	0.420	107.2	99.8	81.48	0.42
18	4	5.945	-0.0052	-0.0335	0.674	-	100.2	97.46	0.31
43	4	6.114	-0.0023	0.0469	0.143	-	99.8	99.8	1.3
62	4	6.931	-0.0037	0.1120	0.880	-	99.5	112.43	0.27
17	4	7.930	-0.0140	0.2063	0.413	-	99.2	127.72	0.52
03	4	8.161	-0.0019	0.2821	0.975	-	99.0	131.01	0.29
09	4	8.962	0.0240	0.0384	0.326	21.3	99.9	144.68	0.90
44	4	9.335	-0.0021	0.0304	0.850	-	99.9	150.47	0.36
33	4	9.996	0.0102	0.0371	0.955	50.0	99.9	160.68	0.36
41	4	11.36	0.0000	0.0940	0.629	19775	99.8	181.30	0.46
61	4	11.70	-0.0074	0.2999	0.230	-	99.2	185.5	1.3
23	4	12.01	0.0087	0.0434	1.397	59.0	99.9	191.50	0.31
39	4	12.27	-0.0039	0.0718	0.842	-	99.8	195.22	0.44
11	4	12.30	0.0058	0.0915	1.095	87.3	99.8	195.54	0.36
25	4	12.81	0.0075	0.0912	0.288	68.4	99.8	203.2	1.1
20	4	13.18	-0.0026	0.1241	0.389	-	99.7	208.68	0.86
06	4	13.28	0.0188	0.0495	0.357	27.2	99.9	210.6	1.1
12	4	13.68	-0.0066	0.2088	0.611	-	99.5	215.78	0.58
68	4	13.93	-0.0022	0.0143	1.294	-	100.0	220.41	0.30
70	4	15.76	-0.0016	0.0592	1.196	-	99.9	247.34	0.39

ID	Power (Watts)	$^{40}Ar/^{39}Ar$	$^{37}Ar/^{39}Ar$	$^{36}Ar/^{39}Ar$ (x 10^{-3})	$^{39}Ar_K$ (x10^{-15} mol)	K/Ca	$^{40}Ar^*$ (%)	Age (Ma)	±1σ (Ma)
01	4	19.53	-0.0020	0.0772	0.813	-	99.9	301.85	0.67
26	4	31.23	0.0020	0.0103	1.135	255.9	100.0	461.92	0.61
49	4	31.56	-0.0070	0.1176	0.575	-	99.9	465.8	1.1
22	4	34.30	0.0031	0.1047	0.769	164.1	99.9	501.3	1.1
46	4	35.15	-0.0032	0.2107	0.374	-	99.8	511.8	1.8
29	4	42.91	0.0042	0.1680	0.755	120.9	99.9	608.1	1.2
69	4	44.75	0.0014	0.0498	1.008	361.8	100.0	630.58	0.86
04	4	47.52	-0.0086	0.1403	0.257	-	99.9	663.0	3.2
40	4	51.76	0.0150	0.0899	0.553	34.1	100.0	712.2	1.8
31	4	58.56	0.0129	0.0363	0.393	39.6	100.0	788.4	2.5
24	4	59.23	-0.0004	0.1568	0.747	-	99.9	795.3	1.5
50	4	60.54	0.0151	0.0615	0.719	33.7	100.0	809.8	1.3
59	4	60.57	-0.0288	0.0837	0.246	-	100.0	810.0	4.4
35	4	60.80	0.0007	0.0794	1.570	727.0	100.0	812.50	0.82
34	4	62.52	-0.0029	0.1895	0.428	-	99.9	830.6	2.5
02	4	63.35	0.0153	0.2672	0.514	33.4	99.9	839.3	1.7
21	4	64.01	-0.0056	0.2107	0.527	-	99.9	846.4	2.2
32	4	68.21	-0.0071	0.0306	0.758	-	100.0	891.0	1.4
47	4	69.63	0.0007	0.0373	0.986	774.4	100.0	905.6	1.3
05	4	79.47	-0.0005	0.0944	1.270	-	100.0	1003.7	1.1
63	4	80.76	0.0028	0.0881	1.673	182.3	100.0	1016.21	0.98
19	4	83.52	-0.0069	0.0604	0.791	-	100.0	1042.7	1.6
38	4	87.21	0.0038	0.0394	0.688	132.8	100.0	1077.7	2.1
56	4	92.92	0.0028	0.0241	0.950	184.8	100.0	1130.2	1.6
28	4	95.52	0.0066	0.1686	0.834	77.9	99.9	1153.3	1.8

ID	Power (Watts)	$^{40}Ar/^{39}Ar$	$^{37}Ar/^{39}Ar$	$^{36}Ar/^{39}Ar$ (x 10^{-3})	$^{39}Ar_K$ (x10^{-15} mol)	K/Ca	$^{40}Ar^*$ (%)	Age (Ma)	±1σ (Ma)
14	4	118.6	0.0101	-0.0143	0.771	50.5	100.0	1349.6	1.9
67	4	119.5	-0.0017	0.0694	0.769	-	100.0	1356.5	2.0
CM-SS4, Sanidine, J=0.0091461±0.01%, IC=1.055411±0.0001298, NM-258E, Lab#=61744, Argus VI									
99	4	4.393	-0.0160	0.0915	0.915	-	99.3	71.53	0.14
11	4	4.529	0.0236	0.0348	0.522	21.6	99.8	74.04	0.22
09	4	4.625	0.0849	0.0326	0.269	6.0	99.9	75.67	0.43
92	4	4.713	0.0316	0.0109	0.441	16.1	100.0	77.12	0.26
45	4	4.923	-0.2448	0.3657	0.042	-	97.4	78.5	2.6
46	4	5.557	0.0126	0.0917	0.177	40.5	99.5	90.20	0.73
80	4	5.942	-0.0023	0.1049	0.416	-	99.5	96.25	0.39
03	4	6.005	-0.0245	0.1301	0.328	-	99.3	97.10	0.43
04	4	6.114	0.0056	0.0387	0.758	90.9	99.8	99.30	0.16
86	4	6.315	0.0051	0.0512	0.791	100.9	99.8	102.43	0.18
26	4	6.598	0.0206	0.0636	0.703	24.7	99.7	106.87	0.23
05	4	6.913	-0.0045	0.0580	1.315	-	99.7	111.83	0.14
19	4	6.984	0.0672	0.2135	0.320	7.6	99.2	112.32	0.50
41	4	8.868	0.4325	0.4491	0.034	1.2	98.8	141.1	6.0
69	4	9.327	0.1062	0.0398	0.215	4.8	100.0	149.7	1.1
01	4	9.695	-0.0155	0.0906	0.722	-	99.7	154.97	0.29
78	4	9.935	0.0295	0.2200	0.610	17.3	99.4	158.13	0.39
75	4	10.11	0.0224	0.5827	0.456	22.8	98.3	159.11	0.45
87	4	10.18	0.0026	0.1356	0.851	200.0	99.6	162.17	0.33
44	4	10.30	-0.0083	-0.0016	0.364	-	100.0	164.61	0.70
24	4	10.34	0.0390	0.0543	0.352	13.1	99.9	165.02	0.55

ID	Power (Watts)	$^{40}Ar/^{39}Ar$	$^{37}Ar/^{39}Ar$	$^{36}Ar/^{39}Ar$ (x 10^{-3})	$^{39}Ar_K$ (x10^{-15} mol)	K/Ca	$^{40}Ar^*$ (%)	Age (Ma)	±1σ (Ma)
10	4	10.39	0.0154	0.0572	0.660	33.0	99.8	165.86	0.35
62	4	11.85	-0.0046	0.0540	0.672	-	99.9	188.07	0.46
95	4	12.27	-0.0193	1.158	0.414	-	97.2	189.36	0.71
51	4	12.07	0.0438	0.2078	0.582	11.6	99.5	190.72	0.41
18	4	12.14	0.0055	0.0652	0.771	92.9	99.8	192.29	0.37
35	4	12.17	-0.0523	0.0836	0.178	-	99.8	192.7	1.3
02	4	12.18	-0.0042	0.0909	0.889	-	99.8	192.75	0.31
25	4	12.22	-0.0069	0.0926	1.348	-	99.8	193.46	0.23
07	4	12.29	0.0086	0.0532	1.370	59.3	99.9	194.71	0.23
60	4	12.33	0.0110	0.1281	0.565	46.4	99.7	194.88	0.49
16	4	12.30	0.0030	0.0257	1.410	168.7	99.9	194.95	0.19
40	4	12.32	0.0319	0.0469	0.506	16.0	99.9	195.14	0.57
76	4	12.94	-0.0003	-0.0039	0.497	-	100.0	204.60	0.68
104	4	13.18	0.0011	0.0672	0.946	481.7	99.8	207.98	0.37
06	4	13.17	-0.0069	0.0241	0.847	-	99.9	208.01	0.34
84	4	13.31	0.0116	0.2138	0.761	44.0	99.5	209.17	0.38
12	4	13.37	-0.0444	0.2035	0.242	-	99.5	210.1	1.1
48	4	13.35	0.0125	0.0912	0.732	41.0	99.8	210.43	0.40
32	4	14.22	-0.0314	0.3230	0.099	-	99.3	222.2	2.8
22	4	16.70	-0.0049	0.5436	0.752	-	99.0	257.77	0.48
29	4	16.65	0.0246	0.1019	0.589	20.8	99.8	258.88	0.50
98	4	16.78	0.0282	0.0656	0.230	18.1	99.9	261.0	1.7
59	4	17.61	0.0212	0.1856	0.873	24.0	99.7	272.46	0.43
31	4	18.49	-0.0588	0.0625	0.282	-	99.9	285.5	1.3
74	4	19.11	-0.0438	0.0598	0.740	-	99.9	294.39	0.51

ID	Power (Watts)	$^{40}Ar/^{39}Ar$	$^{37}Ar/^{39}Ar$	$^{36}Ar/^{39}Ar$ (x 10^{-3})	$^{39}Ar_K$ (x10^{-15} mol)	K/Ca	$^{40}Ar^*$ (%)	Age (Ma)	±1σ (Ma)
102	4	19.38	0.0124	0.0514	0.906	41.2	99.9	298.34	0.45
91	4	19.79	-0.0057	-0.0006	1.013	-	100.0	304.40	0.41
53	4	19.85	-0.0033	0.0971	1.295	-	99.9	304.81	0.33
08	4	21.19	0.0014	0.0738	1.156	368.2	99.9	323.88	0.46
49	4	21.50	0.0198	0.4223	0.291	25.8	99.4	326.8	1.3
73	4	22.11	0.0237	0.0862	1.393	21.5	99.9	336.65	0.35
58	4	24.98	-0.0157	0.1038	0.506	-	99.9	376.17	0.92
23	4	26.64	0.0405	0.0551	0.399	12.6	100.0	398.8	1.5
94	4	27.43	0.0072	0.0427	1.001	70.5	100.0	409.47	0.50
13	4	29.05	0.0006	5.191	0.490	917.5	94.7	410.6	1.0
70	4	28.11	0.0001	0.1919	0.439	6516.0	99.8	418.0	1.2
37	4	28.36	-0.0011	0.0633	0.787	-	99.9	421.78	0.75
68	4	30.52	0.0144	3.838	0.298	35.4	96.3	435.6	2.1
14	4	29.47	0.0045	0.1139	1.008	114.3	99.9	436.26	0.62
79	4	32.80	0.0293	0.1005	0.523	17.4	99.9	479.8	1.3
20	4	33.40	-0.0202	0.2647	0.253	-	99.8	486.8	2.5
67	4	34.93	0.0048	0.1045	0.929	106.9	99.9	507.02	0.70
103	4	35.11	0.0165	0.0407	0.753	30.9	100.0	509.58	0.75
100	4	38.59	0.0200	0.0990	0.970	25.5	99.9	552.95	0.65
57	4	39.71	-0.0407	0.0935	0.388	-	99.9	566.6	1.7
55	4	41.10	-0.0155	0.1578	1.114	-	99.9	583.50	0.77
82	4	41.27	0.0297	0.0232	0.954	17.2	100.0	586.08	0.82
17	4	45.17	-0.0327	0.0539	0.852	-	100.0	632.67	0.92
89	4	46.59	-0.0194	0.1164	0.870	-	99.9	649.27	0.98
50	4	47.78	0.0219	2.343	1.086	23.3	98.5	655.47	0.70

ID	Power (Watts)	$^{40}Ar/^{39}Ar$	$^{37}Ar/^{39}Ar$	$^{36}Ar/^{39}Ar$ (x 10^{-3})	$^{39}Ar_K$ (x10^{-15} mol)	K/Ca	$^{40}Ar^*$ (%)	Age (Ma)	±1σ (Ma)
83	4	47.15	-0.0116	0.0726	0.899	-	100.0	655.93	0.93
42	4	48.79	0.0195	0.0807	0.635	26.1	100.0	675.0	1.3
38	4	49.03	0.0336	0.1806	0.502	15.2	99.9	677.5	1.6
65	4	49.11	0.0293	0.1167	0.234	17.4	99.9	678.6	3.4
39	4	49.30	0.0198	0.0878	0.244	25.8	99.9	680.9	3.2
54	4	49.61	-0.0056	0.0547	1.074	-	100.0	684.55	0.83
96	4	50.02	-0.0006	0.4005	0.888	-	99.8	688.15	0.94
93	4	50.26	0.0516	-0.0381	0.324	9.9	100.0	692.5	2.4
61	4	52.37	0.0711	0.0942	0.304	7.2	100.0	716.1	2.5
36	4	54.31	-0.0001	0.1180	0.251	-	99.9	737.7	3.2
72	4	59.11	-0.0025	0.0468	0.731	-	100.0	790.9	1.4
63	4	60.17	-0.0463	0.3006	0.168	-	99.8	801.4	5.8
88	4	64.40	0.0016	0.1171	0.630	310.7	99.9	847.3	1.5
52	4	64.60	0.0297	0.2861	0.334	17.2	99.9	848.8	2.7
43	4	69.45	0.0331	0.1427	0.463	15.4	99.9	899.7	1.7
85	4	71.81	0.0188	-0.0141	0.341	27.2	100.0	924.1	2.4
30	4	72.84	-0.0143	0.0441	0.681	-	100.0	934.3	1.4
101	4	75.85	0.0316	0.0952	0.569	16.2	100.0	964.2	2.1
47	4	78.39	-0.0230	0.1599	0.482	-	99.9	988.9	2.2
21	4	80.12	-0.0122	0.1531	1.039	-	99.9	1005.8	1.1
56	4	83.80	0.0057	0.0474	2.076	89.0	100.0	1041.26	0.84
15	4	84.49	0.0140	2.211	1.247	36.5	99.2	1041.75	0.99
28	4	84.17	0.0351	0.0833	0.675	14.5	100.0	1044.7	1.5
81	4	88.41	0.0105	0.0623	0.764	48.4	100.0	1084.4	1.5
34	4	90.46	0.0105	0.0416	1.023	48.7	100.0	1103.4	1.0

ID	Power (Watts)	$^{40}Ar/^{39}Ar$	$^{37}Ar/^{39}Ar$	$^{36}Ar/^{39}Ar$ (x 10^{-3})	$^{39}Ar_K$ (x10^{-15} mol)	K/Ca	$^{40}Ar^*$ (%)	Age (Ma)	±1σ (Ma)
90	4	91.48	0.0561	-0.0059	0.715	9.1	100.0	1112.9	1.8
27	4	92.66	-0.0057	0.1173	0.881	-	100.0	1123.2	1.1
77	4	99.80	-0.0229	0.1227	0.513	-	100.0	1186.8	2.2
97	4	113.9	-0.0016	0.1664	0.869	-	100.0	1306.3	1.8
33	4	123.8	0.0069	0.0365	0.823	73.6	100.0	1386.1	1.8
64	4	139.6	-0.0200	0.0252	0.811	-	100.0	1506.0	2.0
CM-SS4, Sanidine, J=0.0091373±0.01%, IC=1.055411±0.0001298, NM-258E, Lab#=61748, Argus VI									
33	4	4.374	0.0247	0.0595	0.383	20.7	99.6	71.36	0.32
32	4	4.537	-0.0223	0.0262	0.488	-	99.8	74.08	0.24
100	4	4.526	0.2213	-0.0316	0.119	2.3	100.6	74.52	0.98
47	4	4.606	0.0260	-0.0003	0.770	19.6	100.0	75.37	0.17
54	4	4.703	0.0582	0.0340	0.331	8.8	99.9	76.81	0.36
20	4	4.819	0.0071	0.0323	0.859	71.9	99.8	78.61	0.15
60	4	5.211	0.0137	0.0669	0.396	37.2	99.6	84.71	0.33
45	4	5.555	0.0123	0.0666	0.820	41.5	99.7	90.20	0.17
74	4	5.568	0.0139	0.0246	0.487	36.7	99.9	90.61	0.31
73	4	5.693	0.1268	0.3150	0.190	4.0	98.5	91.38	0.70
79	4	5.931	0.0547	0.0189	0.284	9.3	100.0	96.47	0.47
68	4	6.039	-0.0060	0.1114	0.213	-	99.4	97.67	0.66
08	4	6.176	-0.0178	0.0181	1.256	-	99.9	100.27	0.12
83	4	8.020	-0.0796	4.225	0.328	-	84.2	109.51	0.57
77	4	6.865	0.0111	0.0311	1.282	46.0	99.9	111.12	0.13
40	4	7.283	0.0172	0.0101	0.519	29.6	100.0	117.78	0.31
58	4	7.883	-0.0133	0.0455	0.645	-	99.8	126.98	0.27

ID	Power (Watts)	$^{40}Ar/^{39}Ar$	$^{37}Ar/^{39}Ar$	$^{36}Ar/^{39}Ar$ (x 10^{-3})	$^{39}Ar_K$ (x10^{-15} mol)	K/Ca	$^{40}Ar^*$ (%)	Age (Ma)	±1σ (Ma)
21	4	8.062	-0.0558	0.1518	0.308	-	99.4	129.21	0.53
71	4	8.143	0.0127	0.0713	1.400	40.3	99.8	130.94	0.15
87	4	8.598	0.0912	0.0482	0.343	5.6	99.9	138.22	0.57
10	4	9.010	-0.0145	0.0516	0.689	-	99.8	144.45	0.31
98	4	9.471	0.0236	0.2822	0.674	21.7	99.1	150.55	0.36
96	4	9.512	-0.0003	0.0834	0.735	-	99.7	152.05	0.28
63	4	10.04	0.0366	0.0441	1.205	13.9	99.9	160.32	0.21
61	4	10.10	-0.0014	0.0619	1.012	-	99.8	161.14	0.22
15	4	10.39	0.1666	0.0598	0.188	3.1	100.0	165.9	1.2
91	4	11.06	0.0314	0.0427	1.133	16.3	99.9	175.90	0.22
34	4	11.06	-0.0005	0.0148	1.503	-	100.0	176.12	0.17
102	4	11.81	-0.0023	0.7725	0.534	-	98.1	184.00	0.45
07	4	12.22	-0.0014	0.0547	1.874	-	99.9	193.39	0.17
51	4	12.53	-0.0056	0.0732	0.420	-	99.8	198.00	0.58
85	4	12.57	-0.0039	0.0700	0.595	-	99.8	198.53	0.49
16	4	12.97	0.0126	0.0378	0.523	40.4	99.9	204.78	0.53
103	4	13.26	0.0129	0.1002	0.698	39.7	99.8	208.77	0.41
12	4	13.67	0.3617	0.3976	0.069	1.4	99.4	214.2	3.3
06	4	14.16	0.0086	-0.0019	1.291	59.5	100.0	222.62	0.27
24	4	14.35	0.0149	0.0457	1.005	34.3	99.9	225.19	0.33
03	4	14.52	-0.0037	0.0603	1.355	-	99.9	227.72	0.27
52	4	15.61	0.0598	0.1738	0.195	8.5	99.7	243.3	1.5
17	4	15.94	0.0128	0.0187	0.901	39.9	100.0	248.68	0.43
97	4	17.23	0.0044	0.0205	2.058	115.8	100.0	267.39	0.22
11	4	18.54	-0.0592	0.1334	0.355	-	99.8	285.7	1.1

ID	Power (Watts)	$^{40}Ar/^{39}Ar$	$^{37}Ar/^{39}Ar$	$^{36}Ar/^{39}Ar$ (x 10^{-3})	$^{39}Ar_K$ (x10^{-15} mol)	K/Ca	$^{40}Ar^*$ (%)	Age (Ma)	±1σ (Ma)
104	4	18.97	-0.0315	0.0024	0.238	-	100.0	292.4	1.6
93	4	50.96	-0.3887	102.5	0.011	-	40.0	312.4	34.2
31	4	20.85	0.0153	0.0436	0.643	33.4	99.9	319.00	0.69
76	4	23.36	0.0264	0.0653	0.269	19.3	99.9	353.8	1.7
81	4	24.68	0.0516	0.0014	0.293	9.9	100.0	372.2	1.5
44	4	25.13	0.0265	0.1797	0.178	19.3	99.8	377.5	2.4
78	4	25.32	0.0186	-0.0271	0.184	27.4	100.0	381.0	2.5
106	4	25.91	-0.0101	0.0222	0.953	-	100.0	388.69	0.58
46	4	26.27	0.0158	0.0777	0.460	32.3	99.9	393.4	1.1
42	4	27.49	-0.0019	0.0866	1.634	-	99.9	409.75	0.36
56	4	27.95	0.0090	0.0990	0.539	56.4	99.9	415.86	0.98
09	4	28.39	-0.0067	0.0738	0.997	-	99.9	421.78	0.48
29	4	32.40	0.0174	0.0789	0.740	29.3	99.9	474.32	0.91
70	4	33.04	0.0456	0.1382	0.191	11.2	99.9	482.4	2.7
02	4	39.02	0.0101	0.0977	1.079	50.4	99.9	557.78	0.70
13	4	40.99	-0.0039	0.0866	0.357	-	99.9	582.0	2.0
05	4	42.30	0.0051	0.0417	0.849	100.3	100.0	598.0	1.2
48	4	42.58	-0.0079	0.0147	0.188	-	100.0	601.4	3.7
22	4	45.54	0.0349	0.0989	0.500	14.6	99.9	636.4	1.3
107	4	46.06	-0.0133	-0.0499	0.325	-	100.0	643.1	2.7
18	4	46.20	0.0157	0.0620	0.363	32.4	100.0	644.3	1.8
69	4	48.28	-0.0372	0.1167	0.518	-	99.9	668.4	1.4
67	4	49.80	-0.0019	-0.0112	0.237	-	100.0	686.4	2.9
92	4	50.40	0.0125	0.1164	1.019	40.9	99.9	692.89	0.97
101	4	50.46	0.0211	0.2892	0.765	24.2	99.8	693.1	1.1

ID	Power (Watts)	$^{40}Ar/^{39}Ar$	$^{37}Ar/^{39}Ar$	$^{36}Ar/^{39}Ar$ (x 10^{-3})	$^{39}Ar_K$ (x10^{-15} mol)	K/Ca	$^{40}Ar^*$ (%)	Age (Ma)	±1σ (Ma)
82	4	51.32	0.0570	0.0674	0.418	8.9	100.0	703.7	1.9
59	4	51.73	0.0226	0.2288	0.834	22.6	99.9	707.68	0.89
53	4	52.44	-0.0121	0.0495	0.450	-	100.0	716.3	1.7
23	4	55.39	-0.0117	0.2474	0.457	-	99.9	748.8	1.8
62	4	57.74	0.0121	0.0956	1.469	42.2	100.0	775.23	0.84
65	4	57.78	-0.0087	0.0337	0.256	-	100.0	775.8	3.1
84	4	58.07	0.0253	0.0410	0.872	20.2	100.0	779.0	1.1
72	4	58.24	0.0538	0.1511	0.608	9.5	99.9	780.6	1.7
89	4	59.53	0.0637	0.0729	0.323	8.0	100.0	794.8	2.9
28	4	59.75	-0.0304	0.0455	0.221	-	100.0	797.1	4.6
25	4	60.19	0.0005	0.2716	0.727	1069.6	99.9	801.2	1.3
88	4	61.88	0.0289	0.0948	0.603	17.6	100.0	819.9	1.7
35	4	62.88	0.0086	0.0369	0.903	59.5	100.0	830.8	1.3
14	4	69.17	0.0004	0.0768	0.678	1428.7	100.0	896.3	1.6
64	4	69.54	0.0371	0.0333	0.400	13.8	100.0	900.3	2.5
39	4	71.32	-0.0208	0.2352	0.480	-	99.9	917.7	2.0
80	4	74.03	-0.0019	0.0653	1.098	-	100.0	945.47	0.92
49	4	74.24	-0.0074	0.0457	0.624	-	100.0	947.6	1.8
27	4	75.66	-0.0026	0.0451	0.551	-	100.0	961.8	1.8
41	4	75.70	0.0032	0.0263	0.555	159.8	100.0	962.2	1.8
50	4	75.80	-0.0446	0.1155	0.229	-	99.9	962.9	4.0
43	4	81.53	0.0340	0.2287	0.295	15.0	99.9	1018.4	3.6
01	4	84.18	0.0090	0.0087	0.204	57.0	100.0	1044.2	5.7
04	4	84.91	0.0209	0.0279	0.841	24.4	100.0	1051.1	1.4
36	4	85.88	0.0121	0.1198	0.868	42.2	100.0	1059.9	1.6

ID	Power (Watts)	$^{40}Ar/^{39}Ar$	$^{37}Ar/^{39}Ar$	$^{36}Ar/^{39}Ar$ (x 10^{-3})	$^{39}Ar_K$ (x10^{-15} mol)	K/Ca	$^{40}Ar^*$ (%)	Age (Ma)	±1σ (Ma)
26	4	86.90	-0.0238	0.2132	0.707	-	99.9	1069.2	1.5
90	4	87.72	0.0108	0.1162	1.612	47.4	100.0	1077.14	0.76
94	4	94.34	-0.0005	0.0447	0.840	-	100.0	1137.8	1.5
75	4	97.94	0.0075	0.0721	0.579	68.2	100.0	1169.7	2.3
30	4	100.5	-0.1027	0.0829	0.254	-	100.0	1192.1	4.0
19	4	105.6	-0.0179	-0.0248	0.508	-	100.0	1236.5	2.9
37	4	110.3	0.0435	0.1514	0.584	11.7	100.0	1275.8	2.4
99	4	115.6	0.0194	0.1763	0.418	26.3	100.0	1319.4	3.4
105	4	131.8	-0.0353	0.1111	0.272	-	100.0	1446.4	5.2
57	4	132.8	0.0300	-0.0124	1.024	17.0	100.0	1454.6	1.5
66	4	140.0	0.0413	0.2428	0.187	12.3	100.0	1507.4	8.5
38	4	203.6	0.0306	0.0055	0.493	16.7	100.0	1923.5	3.5
CM-SS4, Sanidine, J=0.009546±0.12%, IC=1.058206±0.0009102, NM-254E, Lab#=61414, Argus VI									
72B	3	4.368	0.0046	0.0250	2.336	110.7	99.8	74.518	0.067
29B	3	4.370	0.0049	0.0126	17.400	104.1	99.9	74.623	0.013
28B	3	4.370	0.0041	0.0104	10.204	125.4	99.9	74.632	0.019
49B	3	4.380	0.0041	0.0005	1.953	123.3	100.0	74.849	0.077
30B	3	4.410	0.0060	0.0477	2.965	84.9	99.7	75.120	0.055
64B	3	4.419	0.0069	0.0022	1.234	74.3	100.0	75.49	0.11
75B	3	4.470	0.0051	0.0029	2.565	100.3	100.0	76.348	0.061
50B	3	6.011	0.0064	0.0191	4.078	79.1	99.9	101.918	0.049
66B	3	11.82	0.0002	0.0011	3.342	2304.4	100.0	195.634	0.078
76B	3	64.17	0.0019	0.1049	3.356	261.9	100.0	874.28	0.26

ID	Power (Watts)	$^{40}Ar/^{39}Ar$	$^{37}Ar/^{39}Ar$	$^{36}Ar/^{39}Ar$ (x 10^{-3})	$^{39}Ar_K$ (x10^{-15} mol)	K/Ca	$^{40}Ar^*$ (%)	Age (Ma)	±1σ (Ma)
CM-SS3, Sanidine, J=0.0095261±0.12%, IC=1±0, NM-254E, Lab#=61413, Argus VI									
12	3	3.853	0.0051	-0.0115	0.585	100.0	100.1	65.92	0.21
14	3	4.126	0.0041	0.4587	1.123	123.8	96.7	68.15	0.13
27	3	4.082	0.0160	0.0055	0.184	31.8	100.0	69.69	0.64
07	3	4.488	0.0461	1.180	0.078	11.1	92.3	70.7	3.9
17	3	4.421	0.0113	0.1150	0.231	45.1	99.2	74.82	0.50
11	3	4.492	0.0319	-0.5586	0.194	16.0	103.8	79.4	2.9
16	3	4.836	-0.0099	0.4134	0.310	-	97.4	80.2	1.8
20	3	6.768	0.0074	0.1485	0.583	69.4	99.4	113.5	1.3
26	3	7.032	0.0108	0.7355	0.330	47.1	96.9	115.0	1.9
24	3	7.998	0.0480	0.4136	0.169	10.6	98.5	132.3	3.9
19	3	8.617	0.0032	0.2133	1.607	161.0	99.3	143.26	0.60
35	3	8.681	0.0106	0.4272	0.461	48.0	98.5	143.3	1.8
18	3	11.84	-0.0133	1.432	0.299	-	96.4	188.8	2.9
09	3	11.50	0.0090	0.0457	0.571	57.0	99.9	190.0	1.6
28	3	13.48	-0.0073	0.1058	0.336	-	99.8	220.6	2.9
04	3	13.81	0.0087	0.0595	1.127	58.5	99.9	225.9	1.1
15	3	18.02	-0.0114	0.2946	0.309	-	99.5	288.6	3.9
10	3	18.50	-0.0134	0.1628	0.345	-	99.7	296.3	3.5
03	3	21.31	0.0101	0.3045	0.494	50.6	99.6	336.9	3.5
47	3	22.80	0.0253	0.3505	0.232	20.2	99.5	358.2	5.1
23	3	23.71	-0.0418	0.2080	0.184	-	99.7	371.8	7.1
42	3	27.18	0.0113	0.1882	0.441	45.3	99.8	420.7	4.8
41	3	28.09	-0.0407	0.0732	0.239	-	99.9	433.5	5.9

ID	Power (Watts)	$^{40}Ar/^{39}Ar$	$^{37}Ar/^{39}Ar$	$^{36}Ar/^{39}Ar$ (x 10^{-3})	$^{39}Ar_K$ (x10^{-15} mol)	K/Ca	$^{40}Ar^*$ (%)	Age (Ma)	±1σ (Ma)
34	3	40.54	-0.0002	0.0961	1.276	-	99.9	597.3	2.8
06	3	51.89	-0.0099	0.0451	0.516	-	100.0	735.0	4.9
32	3	52.87	0.0194	0.0662	0.514	26.3	100.0	746.3	5.4
36	3	58.84	0.0026	-0.2266	0.398	196.7	100.1	815.3	7.3
08	3	59.48	-0.0101	-0.1966	0.554	-	100.1	822.2	6.6
44	3	65.86	-0.0167	0.3874	0.235	-	99.8	890.0	13.4
46	3	72.27	0.2841	5.397	0.026	1.8	97.8	942.4	89.8
45	3	74.72	0.0216	-0.1711	0.318	23.6	100.1	984.5	8.6
13	3	75.79	-0.0022	-0.1834	0.303	-	100.1	995.3	8.5
33	3	76.61	0.0028	0.1360	0.598	181.8	99.9	1002.7	7.1
40	3	80.48	0.0495	-0.3395	0.190	10.3	100.1	1042.7	17.1
02	3	81.53	0.0030	0.5994	1.451	172.0	99.8	1050.25	0.55
39	3	81.40	0.0058	-0.1275	0.505	87.8	100.0	1051.1	8.0
05	3	85.49	0.0213	0.5586	0.217	24.0	99.8	1088.9	14.1
31	3	90.11	0.0051	0.1748	0.304	101.0	99.9	1133.8	12.7
38	3	92.06	0.0182	0.1368	0.361	28.1	100.0	1152.2	9.1
21	3	94.47	0.0043	0.0039	0.217	117.9	100.0	1174.8	16.8
25	3	95.82	0.0139	0.1682	0.249	36.7	99.9	1186.6	12.0
01	3	102.2	0.0084	1.148	0.745	60.5	99.7	1241.4	4.8
37	3	110.2	0.0001	0.0970	0.488	6932.1	100.0	1313.8	8.4
CM-SS3, Sanidine, J=0.0091862±0.04%, IC=1.05445±0.0011591, NM-258C, Lab#=61734, Argus VI									
22	4	4.008	0.0027	0.0111	1.442	191.4	99.9	66.006	0.042
40	4	4.218	0.0054	0.2034	0.880	94.1	98.6	68.494	0.072
53	4	4.174	0.0138	0.0087	0.443	37.0	100.0	68.73	0.12

ID	Power (Watts)	$^{40}Ar/^{39}Ar$	$^{37}Ar/^{39}Ar$	$^{36}Ar/^{39}Ar$ (x 10^{-3})	$^{39}Ar_K$ (x10^{-15} mol)	K/Ca	$^{40}Ar^*$ (%)	Age (Ma)	±1σ (Ma)
02	4	4.302	0.0003	0.3618	0.902	1591.4	97.5	69.084	0.075
19	4	4.225	0.0015	-0.0016	0.902	349.7	100.0	69.595	0.064
15	4	4.256	-0.0025	0.0850	1.018	-	99.4	69.661	0.056
36	4	4.243	0.0049	0.0153	1.178	104.9	99.9	69.807	0.051
13	4	4.291	0.0081	0.1656	0.569	63.4	98.9	69.86	0.10
06	4	4.276	0.0119	0.0593	2.055	42.7	99.6	70.136	0.075
58	4	4.291	0.0173	0.0326	0.335	29.6	99.8	70.50	0.43
39	4	4.304	0.0037	-0.0108	1.554	139.1	100.1	70.91	0.12
55	4	4.360	0.0282	0.1643	0.274	18.1	98.9	71.00	0.61
44	4	4.360	0.0302	0.0056	0.684	16.9	100.0	71.78	0.23
08	4	4.513	-0.0015	0.0095	0.936	-	99.9	74.19	0.18
34	4	4.522	0.0071	0.0239	1.011	72.3	99.9	74.28	0.17
54	4	4.563	0.0168	0.1455	1.364	30.3	99.1	74.36	0.15
17	4	4.519	-0.0105	-0.0139	0.383	-	100.1	74.38	0.42
51	4	4.592	0.0170	-0.0094	0.730	29.9	100.1	75.58	0.22
35	4	4.662	0.0023	-0.0029	0.821	218.3	100.0	76.66	0.22
30	4	5.298	0.0023	1.093	0.863	222.9	93.8	81.64	0.31
01	4	6.130	0.0102	0.0517	0.693	50.1	99.8	99.92	0.26
47	4	6.893	0.0099	0.0498	1.482	51.8	99.8	112.05	0.16
27	4	8.500	0.0007	0.2694	3.247	709.3	99.1	136.25	0.10
14	4	10.07	0.0130	0.1970	1.053	39.1	99.4	160.97	0.26
52	4	12.12	-0.0027	0.1300	3.057	-	99.7	192.50	0.14
05	4	13.31	-0.0065	1.079	1.265	-	97.6	206.19	0.34
23	4	13.40	-0.0377	0.2639	0.492	-	99.4	211.20	0.58
33	4	14.50	-0.0079	0.0912	0.997	-	99.8	228.38	0.39

ID	Power (Watts)	$^{40}Ar/^{39}Ar$	$^{37}Ar/^{39}Ar$	$^{36}Ar/^{39}Ar$ (x 10^{-3})	$^{39}Ar_K$ (x10^{-15} mol)	K/Ca	$^{40}Ar^*$ (%)	Age (Ma)	±1σ (Ma)
32	4	14.80	-0.0053	0.1381	0.886	-	99.7	232.63	0.40
28	4	16.17	0.0241	0.0666	0.908	21.1	99.9	253.18	0.47
12	4	16.40	0.0045	0.0750	0.966	113.8	99.9	256.42	0.43
31	4	19.77	0.0228	0.3688	0.640	22.4	99.5	303.90	0.77
60	4	22.28	-0.0093	0.1171	1.154	-	99.8	340.24	0.44
04	4	22.37	0.0147	0.0477	0.537	34.8	99.9	341.75	0.87
18	4	23.26	0.0044	0.0581	1.235	116.5	99.9	354.14	0.42
49	4	24.84	0.0231	-0.0370	0.775	22.1	100.1	376.34	0.64
26	4	24.97	0.0042	0.2134	1.149	121.6	99.7	377.02	0.50
16	4	27.07	0.0104	0.1640	0.705	49.0	99.8	405.73	0.75
09	4	27.67	0.0127	0.1551	1.515	40.1	99.8	413.87	0.41
37	4	27.86	-0.0015	0.0287	3.920	-	100.0	416.88	0.20
38	4	32.19	0.0082	0.0305	1.183	62.3	100.0	474.03	0.49
42	4	33.42	0.0217	0.1307	0.702	23.5	99.9	489.54	0.97
43	4	33.66	-0.0022	0.0410	0.699	-	100.0	492.95	0.97
07	4	38.67	0.0065	0.0639	2.260	78.7	100.0	556.15	0.33
25	4	51.43	0.0035	0.0143	2.414	144.9	100.0	708.15	0.42
48	4	53.01	0.0164	-0.0330	0.780	31.2	100.0	726.2	1.2
11	4	53.37	0.0106	0.7205	0.616	48.3	99.6	727.8	1.5
24	4	55.21	0.0109	0.0058	0.873	47.0	100.0	750.8	1.1
10	4	60.08	0.0038	0.1575	2.069	134.0	99.9	803.90	0.70
50	4	64.35	-0.0059	0.1808	0.755	-	99.9	849.5	1.3
21	4	70.15	0.0045	0.1391	2.379	114.0	99.9	909.91	0.60
20	4	70.46	0.0071	0.0692	1.625	72.0	100.0	913.38	0.76
46	4	71.69	-0.0077	0.4735	1.188	-	99.8	924.58	0.90

ID	Power (Watts)	$^{40}Ar/^{39}Ar$	$^{37}Ar/^{39}Ar$	$^{36}Ar/^{39}Ar$ (x 10^{-3})	$^{39}Ar_K$ (x10^{-15} mol)	K/Ca	$^{40}Ar^*$ (%)	Age (Ma)	±1σ (Ma)
56	4	71.95	0.1591	0.5456	0.057	3.2	99.8	927.2	16.8
29	4	81.74	0.0087	0.0453	1.984	58.8	100.0	1025.09	0.66
45	4	85.13	-0.0090	0.0365	1.247	-	100.0	1057.4	1.0
59	4	87.77	0.0014	0.3082	0.537	364.3	99.9	1081.4	2.3
03	4	98.71	-3.2274	26.93	0.005	-	91.6	1105.3	196.7
41	4	150.2	-0.0438	0.0614	0.538	-	100.0	1586.7	2.7
CM-SS3, Sanidine, J=0.0091634±0.02%, IC=1.05445±0.0011591, NM-258C, Lab#=61735, Argus VI									
34	4	3.999	0.0039	0.0127	0.702	131.7	99.9	65.691	0.081
28	4	4.141	0.0144	0.0273	0.641	35.4	99.8	67.935	0.090
12	4	4.644	0.0202	0.1011	0.888	25.3	99.4	75.71	0.19
08	4	4.651	0.0143	0.1098	0.481	35.7	99.3	75.77	0.33
03	4	4.834	0.0087	0.0211	0.853	58.5	99.9	79.13	0.19
43	4	5.424	-0.0199	0.1432	0.888	-	99.2	87.97	0.21
25	4	5.417	0.0102	0.0483	0.468	50.0	99.7	88.35	0.41
16	4	5.888	-0.0126	1.152	0.843	-	94.1	90.58	0.33
06	4	5.598	0.0209	-0.0063	0.447	24.4	100.1	91.51	0.36
09	4	5.748	-0.0438	0.1611	0.399	-	99.1	93.02	0.49
10	4	8.561	-0.0055	0.1650	0.772	-	99.4	137.35	0.32
59	4	8.575	0.0212	0.1445	0.834	24.1	99.5	137.70	0.31
57	4	11.34	0.1898	7.230	0.070	2.7	81.1	148.0	3.8
18	4	9.972	0.0110	2.548	1.093	46.5	92.4	148.26	0.39
39	4	9.626	0.0069	0.2835	4.294	74.3	99.1	153.32	0.10
19	4	11.63	0.0493	0.7104	0.284	10.3	98.2	182.1	1.1
29	4	14.08	0.0241	0.2045	1.026	21.2	99.6	221.16	0.32

ID	Power (Watts)	$^{40}Ar/^{39}Ar$	$^{37}Ar/^{39}Ar$	$^{36}Ar/^{39}Ar$ (x 10^{-3})	$^{39}Ar_K$ (x10^{-15} mol)	K/Ca	$^{40}Ar^*$ (%)	Age (Ma)	±1σ (Ma)
23	4	14.34	0.0057	0.1724	0.669	89.0	99.6	225.12	0.47
14	4	14.38	-0.0009	0.1114	2.901	-	99.8	225.94	0.17
40	4	15.03	-0.0057	1.088	0.915	-	97.8	231.32	0.43
24	4	16.01	-0.0081	0.0654	0.923	-	99.9	250.15	0.41
33	4	16.21	0.0257	0.3034	1.057	19.8	99.5	252.17	0.38
17	4	17.15	0.0171	1.396	1.201	29.8	97.6	261.07	0.39
35	4	17.41	0.0129	0.1949	1.053	39.5	99.7	270.04	0.40
13	4	18.90	0.0013	1.166	1.517	394.9	98.2	287.35	0.52
45	4	21.21	0.0036	0.0496	0.871	142.3	99.9	324.85	0.50
02	4	21.45	0.0031	0.4186	1.550	163.1	99.4	326.60	0.35
47	4	23.20	-0.0003	0.0556	0.654	-	99.9	352.53	0.74
58	4	25.33	-0.0135	0.0837	0.992	-	99.9	381.57	0.57
36	4	25.46	0.0167	0.2649	1.281	30.5	99.7	382.74	0.47
41	4	26.72	0.0663	0.3490	0.096	7.7	99.6	399.4	5.0
32	4	30.81	-0.0082	0.0058	1.303	-	100.0	455.07	0.58
07	4	36.51	0.0158	0.0050	0.914	32.2	100.0	528.20	0.74
01	4	37.40	0.0061	0.0739	1.371	83.9	99.9	539.03	0.59
38	4	38.32	0.0018	0.3275	1.927	277.5	99.7	549.55	0.49
31	4	39.34	0.0121	2.173	0.689	42.3	98.4	555.4	1.1
05	4	41.16	0.0075	0.1313	1.397	68.0	99.9	585.21	0.52
44	4	43.22	-0.0164	0.1149	1.149	-	99.9	610.21	0.78
51	4	52.03	0.0135	0.0088	0.983	37.7	100.0	713.6	1.1
20	4	55.36	0.0155	0.0624	0.773	32.8	100.0	750.8	1.4
54	4	61.81	0.0122	0.5257	0.819	42.0	99.7	819.7	1.2
56	4	65.93	-0.0308	0.3095	0.248	-	99.9	864.0	3.5

ID	Power (Watts)	$^{40}Ar/^{39}Ar$	$^{37}Ar/^{39}Ar$	$^{36}Ar/^{39}Ar$ (x 10^{-3})	$^{39}Ar_K$ (x10^{-15} mol)	K/Ca	$^{40}Ar^*$ (%)	Age (Ma)	±1σ (Ma)
42	4	68.94	-0.0027	0.6031	1.399	-	99.7	894.33	0.82
27	4	70.51	0.0192	0.0740	0.595	26.6	100.0	912.1	1.8
37	4	78.65	0.0130	0.4815	0.963	39.3	99.8	992.0	1.2
30	4	81.02	0.0168	0.2076	0.582	30.3	99.9	1015.8	2.2
48	4	81.72	0.0491	0.2187	0.756	10.4	99.9	1022.5	1.6
21	4	85.21	0.0163	0.8314	0.588	31.3	99.7	1054.0	2.2
15	4	85.51	0.0053	0.3664	1.097	97.1	99.9	1058.1	1.1
53	4	89.06	0.0227	0.2535	0.868	22.5	99.9	1091.5	1.3
52	4	95.23	0.0041	0.2878	1.488	125.7	99.9	1147.50	0.98
26	4	103.1	0.0110	0.1728	1.506	46.5	100.0	1217.0	1.0
11	4	104.0	0.0018	0.1239	1.203	282.8	100.0	1225.0	1.2
55	4	107.9	-0.0682	0.4734	0.214	-	99.9	1256.7	5.8
04	4	129.6	0.0066	0.7106	1.623	77.5	99.8	1431.56	0.93
CM-SS3, Sanidine , J=0.0091716±0.01%, IC=1.05445±0.0011591, NM-258C, Lab#=61726, Argus VI									
45	4	4.062	-0.0028	0.2746	0.502	-	98.0	65.51	0.12
17	4	4.126	0.0036	0.1199	1.074	142.3	99.1	67.294	0.057
34	4	4.138	0.0103	0.0058	1.244	49.6	100.0	68.054	0.048
35	4	4.234	-0.0032	0.0388	0.747	-	99.7	69.419	0.080
28	4	4.316	0.0153	0.0499	0.917	33.3	99.7	70.72	0.19
24	4	4.504	0.0331	0.1105	0.544	15.4	99.3	73.49	0.32
30	4	4.541	0.0075	0.0510	0.930	67.8	99.7	74.33	0.18
33	4	4.600	0.0013	0.0306	0.584	406.5	99.8	75.37	0.29
44	4	4.623	0.0251	0.0058	0.686	20.4	100.0	75.90	0.24
21	4	4.846	0.0001	0.0437	0.992	5533.7	99.7	79.28	0.20

ID	Power (Watts)	$^{40}Ar/^{39}Ar$	$^{37}Ar/^{39}Ar$	$^{36}Ar/^{39}Ar$ (x 10^{-3})	$^{39}Ar_K$ (x10^{-15} mol)	K/Ca	$^{40}Ar^*$ (%)	Age (Ma)	±1σ (Ma)
25	4	4.961	-0.0151	0.0710	0.285	-	99.5	80.97	0.63
52	4	5.596	-0.0010	0.2280	1.123	-	98.8	90.41	0.22
08	4	6.520	0.0056	0.5669	1.197	91.2	97.4	103.52	0.21
53	4	7.203	0.0080	0.8299	0.717	63.5	96.6	113.09	0.33
65	4	8.750	-0.0913	0.7834	0.169	-	97.2	137.4	1.4
23	4	8.771	0.0166	0.0491	1.234	30.8	99.8	141.31	0.22
14	4	10.30	0.0001	0.2128	1.271	7096.0	99.4	164.21	0.21
56	4	10.45	0.0029	0.3487	1.156	174.9	99.0	165.80	0.25
58	4	12.33	0.0033	0.0304	1.923	154.5	99.9	195.85	0.21
26	4	12.80	0.0077	0.2503	1.012	65.8	99.4	201.95	0.33
36	4	13.15	-0.0077	0.1450	0.853	-	99.7	207.66	0.39
63	4	13.37	-0.0105	0.1613	1.284	-	99.6	210.85	0.32
57	4	13.75	0.0102	0.0035	1.190	49.9	100.0	217.28	0.29
41	4	14.63	0.0023	0.3490	1.058	217.9	99.3	228.83	0.36
27	4	17.55	-0.0205	0.1194	1.200	-	99.8	272.51	0.36
05	4	19.01	0.0071	0.3351	1.097	72.1	99.5	292.62	0.40
22	4	19.36	0.0120	0.0692	1.071	42.4	99.9	298.79	0.48
47	4	20.05	0.0037	0.0414	0.905	139.6	99.9	308.79	0.51
54	4	21.32	0.0095	0.0585	1.122	53.8	99.9	326.61	0.44
19	4	24.41	-0.0016	0.0562	1.890	-	99.9	369.52	0.34
15	4	25.27	0.0066	0.7970	0.381	76.9	99.1	378.2	1.4
03	4	28.76	-0.0096	0.0398	0.801	-	100.0	428.28	0.83
20	4	29.20	0.0489	0.0658	0.301	10.4	99.9	434.1	2.0
04	4	30.54	-0.0038	0.0009	1.399	-	100.0	451.92	0.43
31	4	32.01	-0.0014	0.0815	1.071	-	99.9	470.81	0.62

ID	Power (Watts)	$^{40}Ar/^{39}Ar$	$^{37}Ar/^{39}Ar$	$^{36}Ar/^{39}Ar$ (x 10^{-3})	$^{39}Ar_K$ (x10^{-15} mol)	K/Ca	$^{40}Ar^*$ (%)	Age (Ma)	±1σ (Ma)
38	4	34.70	-0.0028	0.0690	2.304	-	99.9	505.43	0.35
51	4	35.04	0.0028	0.0528	0.992	179.5	100.0	509.84	0.78
43	4	35.22	0.0101	0.0436	1.574	50.6	100.0	512.16	0.51
39	4	36.68	0.0224	0.4547	0.542	22.8	99.6	529.0	1.4
50	4	40.40	0.0025	0.0528	2.325	208.2	100.0	576.73	0.42
49	4	42.99	0.0089	0.1841	0.566	57.5	99.9	607.7	1.5
59	4	44.74	-0.0218	0.2284	1.025	-	99.8	628.49	0.77
13	4	46.98	0.0019	0.0428	0.848	273.2	100.0	655.7	1.0
60	4	49.01	0.0084	0.4353	1.044	60.7	99.7	677.89	0.73
10	4	50.82	-0.0176	0.0434	0.738	-	100.0	700.1	1.2
37	4	53.57	-0.0013	0.1763	2.776	-	99.9	730.86	0.43
48	4	54.56	-0.0065	0.7284	1.489	-	99.6	740.15	0.74
62	4	56.69	-0.0003	0.0228	1.485	-	100.0	766.18	0.73
46	4	59.25	-0.0047	0.1202	1.660	-	99.9	794.01	0.75
64	4	62.46	-0.0052	0.2421	1.875	-	99.9	828.21	0.61
06	4	63.32	-0.0184	0.1112	0.660	-	99.9	837.7	1.3
40	4	65.63	0.0092	0.4650	1.985	55.2	99.8	861.01	0.68
55	4	67.06	0.0046	0.1906	2.126	109.9	99.9	876.84	0.63
09	4	67.37	0.0134	0.0778	1.100	38.0	100.0	880.4	1.1
18	4	69.61	0.0033	0.1891	2.694	156.0	99.9	903.13	0.48
29	4	70.10	0.0118	0.2106	0.717	43.3	99.9	908.1	1.6
16	4	70.80	-0.0034	0.6439	0.991	-	99.7	913.9	1.2
01	4	75.17	-0.0115	0.4802	1.089	-	99.8	958.4	1.2
61	4	82.88	0.0073	0.5430	2.216	70.3	99.8	1033.37	0.63
42	4	84.41	-0.0036	0.6538	1.354	-	99.8	1047.56	0.98

ID	Power (Watts)	$^{40}Ar/^{39}Ar$	$^{37}Ar/^{39}Ar$	$^{36}Ar/^{39}Ar$ (x 10^{-3})	$^{39}Ar_K$ (x10^{-15} mol)	K/Ca	$^{40}Ar^*$ (%)	Age (Ma)	±1σ (Ma)
32	4	86.94	-0.0086	0.1887	1.217	-	99.9	1072.70	0.88
11	4	89.02	0.0212	0.1395	0.443	24.1	100.0	1092.1	2.7
07	4	92.14	0.0056	0.0782	1.709	91.3	100.0	1120.93	0.82
12	4	105.6	0.0056	0.1480	0.943	91.3	100.0	1239.7	1.5
CM-Ash2, Sanidine, J=0.0095068±0.28%, IC=1.056691±0.000774, NM-254E, Lab#=61412, Argus VI									
11	3	3.848	0.0046	0.0417	0.316	111.7	99.7	65.42	0.22
06	3	4.006	0.0026	0.0062	0.480	196.8	100.0	68.25	0.18
12	3	4.243	0.0073	0.4529	0.363	69.5	96.8	70.01	0.25
16	3	4.192	-0.0100	0.1413	0.124	-	99.0	70.67	0.75
02	3	4.504	0.0078	0.7379	0.274	65.1	95.1	73.0	1.3
03	3	4.409	0.0039	0.3032	0.311	130.3	98.0	73.5	1.2
10	3	4.388	0.0162	-0.0192	0.919	31.6	100.2	74.80	0.58
05	3	4.418	0.0092	-0.0940	1.559	55.6	100.7	75.65	0.39
17	3	4.603	0.0026	-0.7832	0.221	192.9	105.1	82.1	2.4
14	3	6.274	0.0021	-0.2447	0.450	248.6	101.2	107.1	1.2
15	3	9.033	0.0250	-0.0874	0.450	20.4	100.3	151.1	1.8
24	3	12.04	-0.0040	1.103	0.411	-	97.3	193.0	2.2
01	3	13.98	0.3765	4.226	0.080	1.4	91.2	209.4	21.8
08	3	34.60	-0.0033	0.1228	1.328	-	99.9	519.9	1.9
18	3	51.92	0.0068	0.9321	0.244	74.8	99.5	731.0	13.6
25	3	66.15	0.0210	0.0041	0.208	24.4	100.0	893.0	10.3
19	3	82.03	0.0040	0.2803	0.388	127.1	99.9	1054.4	8.1
20	3	84.90	-0.0316	-0.6235	0.257	-	100.2	1084.8	15.0
22	3	119.0	0.0020	0.0029	8.841	255.0	100.0	1385.1	2.5

ID	Power (Watts)	$^{40}Ar/^{39}Ar$	$^{37}Ar/^{39}Ar$	$^{36}Ar/^{39}Ar$ (x 10^{-3})	$^{39}Ar_K$ (x10^{-15} mol)	K/Ca	$^{40}Ar^*$ (%)	Age (Ma)	±1σ (Ma)
CM-Ash2, Sanidine, J=0.0091559±0.00%, IC=1.05521±0.0010653, NM-258C, Lab#=61736, Argus VI									
83	4	3.985	0.0112	-0.0246	0.614	45.5	100.2	65.61	0.13
13	4	4.001	0.0091	0.0131	0.859	55.9	99.9	65.68	0.19
51	4	4.018	0.0083	0.0051	0.827	61.6	100.0	66.00	0.19
37	4	4.121	-0.0093	0.0187	0.339	-	99.8	67.57	0.46
124	4	4.154	0.0248	0.0400	0.447	20.6	99.8	68.04	0.18
27	4	4.151	0.0041	0.0054	1.380	124.8	100.0	68.14	0.12
91	4	4.150	0.0037	-0.0074	0.622	138.5	100.1	68.18	0.14
94	4	4.155	0.0138	0.0079	0.888	36.9	100.0	68.209	0.095
152	4	4.160	0.0125	0.0039	0.752	40.8	100.0	68.31	0.11
138	4	4.221	0.0020	0.2037	0.643	251.4	98.6	68.31	0.13
140	4	4.161	0.0113	0.0019	0.627	45.2	100.0	68.33	0.13
05	4	4.164	0.0021	0.0078	1.118	244.4	99.9	68.33	0.15
77	4	4.166	0.0107	0.0048	0.818	47.7	100.0	68.393	0.100
149	4	4.183	0.0079	0.0381	0.945	64.8	99.7	68.497	0.092
141	4	4.178	0.0017	0.0010	0.911	292.5	100.0	68.584	0.092
74	4	4.183	0.0061	0.0105	0.605	83.2	99.9	68.64	0.14
128	4	4.194	0.0061	0.0174	0.788	83.2	99.9	68.78	0.11
150	4	4.203	0.0108	0.0261	0.987	47.2	99.8	68.878	0.089
76	4	4.193	0.0075	-0.0114	0.664	68.5	100.1	68.90	0.13
109	4	4.209	0.0122	0.0360	0.695	41.9	99.8	68.94	0.12
135	4	4.211	0.0189	0.0257	0.529	27.1	99.8	69.02	0.16
67	4	4.232	0.0064	0.0706	1.003	79.8	99.5	69.13	0.17
139	4	4.215	-0.0078	-0.0014	0.560	-	100.0	69.18	0.15

ID	Power (Watts)	$^{40}Ar/^{39}Ar$	$^{37}Ar/^{39}Ar$	$^{36}Ar/^{39}Ar$ (x 10^{-3})	$^{39}Ar_K$ (x10^{-15} mol)	K/Ca	$^{40}Ar^*$ (%)	Age (Ma)	±1σ (Ma)
47	4	4.232	0.0023	0.0591	0.575	225.4	99.6	69.19	0.28
125	4	4.223	0.0149	0.0146	0.818	34.2	99.9	69.268	0.100
21	4	4.218	0.0135	-0.0126	0.881	37.8	100.1	69.32	0.18
108	4	4.225	0.0048	0.0058	0.590	106.2	100.0	69.33	0.14
147	4	4.226	0.0076	0.0040	0.895	67.2	100.0	69.357	0.099
69	4	4.229	0.0054	0.0078	1.389	94.3	100.0	69.386	0.065
99	4	4.222	-0.0082	-0.0229	0.501	-	100.1	69.40	0.16
71	4	4.236	-0.0004	0.0260	0.824	-	99.8	69.41	0.11
62	4	4.237	0.0059	0.0266	1.227	86.7	99.8	69.43	0.14
145	4	4.232	0.0069	0.0029	1.738	74.4	100.0	69.464	0.052
133	4	4.238	0.0020	0.0096	1.415	254.9	99.9	69.528	0.061
72	4	4.237	-0.0023	-0.0002	0.634	-	100.0	69.55	0.14
123	4	4.242	0.0154	0.0135	0.657	33.1	99.9	69.58	0.13
73	4	4.232	0.0176	-0.0247	0.708	29.1	100.2	69.61	0.13
28	4	4.247	0.0026	-0.0057	0.902	196.5	100.0	69.74	0.18
134	4	4.279	0.0013	0.0986	0.297	391.7	99.3	69.75	0.36
85	4	4.252	-0.0057	-0.0052	0.526	-	100.0	69.81	0.40
40	4	4.246	0.0165	-0.0301	0.578	30.9	100.2	69.86	0.46
82	4	4.276	0.0100	0.0669	0.899	50.8	99.5	69.86	0.27
80	4	4.254	0.0067	-0.0152	0.683	76.3	100.1	69.89	0.13
127	4	4.266	0.0171	0.0151	1.197	29.8	99.9	69.96	0.15
111	4	4.257	0.0216	-0.0201	0.580	23.7	100.2	69.99	0.26
88	4	4.265	0.0026	0.0014	0.540	196.0	100.0	69.99	0.45
97	4	4.277	0.0281	0.0308	0.426	18.2	99.8	70.08	0.28
07	4	4.333	0.0060	0.1914	0.503	85.7	98.7	70.19	0.60

ID	Power (Watts)	$^{40}Ar/^{39}Ar$	$^{37}Ar/^{39}Ar$	$^{36}Ar/^{39}Ar$ (x 10^{-3})	$^{39}Ar_K$ (x10^{-15} mol)	K/Ca	$^{40}Ar^*$ (%)	Age (Ma)	±1σ (Ma)
87	4	4.283	0.0297	0.0181	0.961	17.2	99.9	70.24	0.29
89	4	4.298	0.0152	0.0233	1.158	33.7	99.9	70.43	0.20
22	4	4.273	0.0001	-0.0694	0.960	7765.7	100.5	70.46	0.32
68	4	4.411	0.0626	0.3599	0.074	8.1	97.7	70.7	2.1
106	4	4.331	0.0120	0.0289	0.885	42.5	99.8	70.93	0.33
93	4	4.331	0.0289	0.0210	0.346	17.7	99.9	71.00	0.72
30	4	4.383	-0.0348	0.0633	0.778	-	99.5	71.56	0.40
41	4	4.457	0.0065	-0.0214	1.119	78.7	100.2	73.20	0.28
100	4	4.507	0.0221	0.1511	1.412	23.1	99.0	73.21	0.19
35	4	4.500	-0.0113	0.0507	0.785	-	99.6	73.53	0.40
146	4	4.522	0.0467	0.1007	0.505	10.9	99.4	73.72	0.58
70	4	4.506	0.0100	0.0176	1.267	50.9	99.9	73.81	0.24
26	4	4.549	0.0187	0.1458	0.731	27.3	99.1	73.89	0.44
56	4	4.561	0.0247	0.1707	0.397	20.7	98.9	73.97	0.71
129	4	4.519	0.0354	0.0302	0.584	14.4	99.9	73.99	0.48
33	4	4.526	-0.0174	0.0344	0.775	-	99.7	74.02	0.41
90	4	4.533	0.0026	0.0362	1.315	196.1	99.8	74.14	0.19
116	4	4.585	0.0245	0.2178	0.503	20.8	98.6	74.15	0.54
107	4	4.548	0.0164	0.0645	0.794	31.1	99.6	74.26	0.37
101	4	4.535	0.0026	0.0059	1.328	195.8	100.0	74.32	0.23
104	4	4.585	0.0109	0.1762	0.566	47.0	98.9	74.33	0.42
112	4	4.535	0.0144	0.0069	1.084	35.4	100.0	74.34	0.27
25	4	4.532	-0.0042	-0.0104	1.445	-	100.1	74.35	0.22
63	4	4.556	0.0303	0.0746	0.571	16.8	99.6	74.36	0.53
113	4	4.573	0.0142	0.1155	0.625	35.9	99.3	74.43	0.46

ID	Power (Watts)	$^{40}Ar/^{39}Ar$	$^{37}Ar/^{39}Ar$	$^{36}Ar/^{39}Ar$ (x 10^{-3})	$^{39}Ar_K$ (x10^{-15} mol)	K/Ca	$^{40}Ar^*$ (%)	Age (Ma)	±1σ (Ma)
144	4	4.532	0.0074	-0.0253	0.785	68.5	100.2	74.43	0.34
29	4	4.547	0.0098	-0.0090	0.544	51.9	100.1	74.60	0.55
132	4	4.536	0.0260	-0.0523	0.624	19.6	100.4	74.64	0.37
11	4	4.584	-0.0005	0.0965	0.842	-	99.4	74.67	0.38
16	4	4.582	0.0205	0.0935	1.539	24.9	99.4	74.68	0.22
119	4	4.573	-0.0243	0.0372	0.453	-	99.7	74.76	0.57
118	4	4.575	0.0218	0.0226	0.440	23.4	99.9	74.91	0.58
20	4	4.573	-0.0080	0.0057	0.883	-	99.9	74.93	0.41
84	4	4.582	-0.0797	0.0133	0.284	-	99.8	74.94	0.90
31	4	4.563	0.0149	-0.0417	0.720	34.1	100.3	75.02	0.44
78	4	4.583	0.0445	0.0263	0.634	11.5	99.9	75.05	0.42
46	4	4.584	0.0198	0.0125	0.545	25.7	99.9	75.09	0.54
43	4	4.610	0.0167	0.0985	0.928	30.6	99.4	75.11	0.37
02	4	4.631	-0.0072	0.1238	1.100	-	99.2	75.28	0.33
15	4	4.590	0.0247	-0.0822	0.221	20.7	100.6	75.7	1.4
130	4	4.636	0.0275	0.0588	0.443	18.6	99.7	75.73	0.71
92	4	4.618	-0.0033	-0.0268	0.926	-	100.2	75.81	0.29
81	4	4.664	0.0352	0.1227	0.496	14.5	99.3	75.87	0.53
105	4	4.639	0.0592	0.0458	0.461	8.6	99.8	75.88	0.55
86	4	4.677	0.0265	0.0514	0.473	19.2	99.7	76.42	0.57
34	4	4.661	0.0023	-0.0415	0.603	226.1	100.3	76.57	0.46
18	4	4.658	0.0165	-0.0839	0.755	31.0	100.6	76.75	0.40
32	4	4.723	0.0149	0.0010	1.126	34.3	100.0	77.39	0.30
79	4	4.858	0.0698	-0.0574	0.347	7.3	100.5	79.91	0.74
60	4	5.233	0.0002	-0.0708	0.528	2826.6	100.4	85.89	0.61

ID	Power (Watts)	$^{40}Ar/^{39}Ar$	$^{37}Ar/^{39}Ar$	$^{36}Ar/^{39}Ar$ (x 10^{-3})	$^{39}Ar_K$ (x10^{-15} mol)	K/Ca	$^{40}Ar^*$ (%)	Age (Ma)	±1σ (Ma)
49	4	5.322	0.0108	0.0401	0.916	47.2	99.8	86.79	0.37
38	4	5.696	0.0019	-0.0086	0.738	264.3	100.0	92.98	0.49
10	4	6.930	0.0492	0.5682	0.238	10.4	97.6	109.9	1.5
148	4	8.189	0.0273	0.0597	0.715	18.7	99.8	131.99	0.63
03	4	8.225	-0.0126	0.0097	1.885	-	100.0	132.73	0.27
58	4	8.348	0.0111	0.0303	0.914	45.9	99.9	134.58	0.49
137	4	9.292	-0.0090	0.0359	0.707	-	99.9	149.16	0.67
24	4	10.26	-0.0141	0.0713	0.930	-	99.8	163.91	0.63
39	4	10.34	0.0002	0.0479	1.365	3143.6	99.9	165.25	0.38
59	4	10.71	-0.0183	0.0721	0.127	-	99.8	170.8	4.2
08	4	12.71	0.0159	0.0180	1.145	32.2	100.0	201.40	0.63
126	4	13.04	0.0273	0.0083	0.791	18.7	100.0	206.33	0.72
65	4	13.22	0.0254	0.0598	0.829	20.0	99.9	208.77	0.90
14	4	13.33	0.0182	0.1095	0.429	28.0	99.8	210.2	1.3
19	4	14.64	-0.0366	0.1885	0.476	-	99.6	229.3	1.4
44	4	14.81	-0.0038	0.0685	0.774	-	99.9	232.34	0.91
06	4	16.55	-0.0011	-0.0058	1.420	-	100.0	258.13	0.56
136	4	17.25	0.0154	0.1268	0.651	33.1	99.8	267.8	1.2
103	4	18.28	0.0064	0.0386	0.755	79.5	99.9	283.1	1.2
151	4	18.46	0.0525	0.0560	0.655	9.7	99.9	285.6	1.3
54	4	19.47	-0.0045	0.3598	0.660	-	99.4	298.6	1.3
102	4	22.11	-0.0202	0.0508	0.701	-	99.9	337.1	1.6
98	4	24.78	0.0340	0.0914	0.369	15.0	99.9	373.8	2.8
95	4	34.77	0.0219	-0.0190	0.625	23.3	100.0	505.9	2.1
110	4	37.78	0.0084	0.0334	0.466	60.8	100.0	543.6	2.9

ID	Power (Watts)	$^{40}Ar/^{39}Ar$	$^{37}Ar/^{39}Ar$	$^{36}Ar/^{39}Ar$ (x 10^{-3})	$^{39}Ar_K$ (x10^{-15} mol)	K/Ca	$^{40}Ar^*$ (%)	Age (Ma)	±1σ (Ma)
122	4	41.49	-0.0276	0.0818	0.442	-	99.9	589.0	3.3
96	4	47.68	0.0197	-0.0299	1.045	25.9	100.0	663.1	1.7
153	4	50.98	0.0254	0.0531	0.999	20.1	100.0	700.9	2.1
154	4	53.38	0.0370	-0.0859	0.603	13.8	100.1	728.7	3.7
53	4	57.47	0.0155	-0.0048	0.752	32.9	100.0	773.8	2.5
61	4	62.09	0.0196	0.0305	1.092	26.1	100.0	823.8	1.9
17	4	93.33	0.0007	0.0383	0.927	749.4	100.0	1130.4	2.5
120	4	102.9	0.0337	0.0923	0.801	15.2	100.0	1214.8	4.5
48	4	109.3	0.0238	-0.0588	1.039	21.4	100.0	1269.9	3.1
143	4	110.9	0.0227	0.0394	1.223	22.5	100.0	1282.8	2.6
121	4	111.5	0.0184	-0.0070	0.577	27.7	100.0	1287.8	5.3
23	4	120.6	-0.1182	-0.0189	0.256	-	100.0	1361.4	9.9
117	4	121.7	-0.0036	-0.0635	0.422	-	100.0	1370.5	7.7
CM-SS2, Sanidine, J=0.009459±0.37%, IC=1.057264±0.001044, NM-254E, Lab#=61411, Argus VI									
19	3	3.794	0.0047	0.0849	0.502	107.7	99.3	63.99	0.36
24	3	3.854	0.0030	0.0529	2.286	169.1	99.6	65.156	0.085
30	3	3.880	0.0062	0.0413	1.255	82.1	99.7	65.64	0.14
95	4	3.889	0.0020	0.0088	3.074	256.6	99.9	65.951	0.069
73	4	4.382	-0.0198	1.624	0.237	-	88.9	66.11	0.97
55	3	4.071	0.0038	0.0114	4.312	135.1	99.9	68.972	0.045
36	3	4.132	0.0053	0.0203	3.717	95.8	99.9	69.949	0.052
22	3	4.372	0.0224	0.0322	1.517	22.8	99.8	73.91	0.32
62	3	4.433	0.0053	0.1568	1.196	96.8	99.0	74.28	0.42
39	3	4.432	0.0178	0.1416	0.623	28.7	99.1	74.36	0.93

ID	Power (Watts)	$^{40}Ar/^{39}Ar$	$^{37}Ar/^{39}Ar$	$^{36}Ar/^{39}Ar$ (x 10^{-3})	$^{39}Ar_K$ (x10^{-15} mol)	K/Ca	$^{40}Ar^*$ (%)	Age (Ma)	±1σ (Ma)
26	3	4.436	0.0061	0.0832	10.415	84.1	99.5	74.70	0.13
77	4	4.479	0.0265	0.0659	0.436	19.2	99.6	75.5	1.1
59	3	4.497	-0.0190	-0.3782	0.477	-	102.5	78.0	1.1
04	3	4.755	0.0023	-0.1661	0.700	222.2	101.0	81.22	0.86
18	3	6.238	0.0074	-0.0094	2.415	68.8	100.1	104.86	0.33
85	4	6.608	0.0358	0.1787	0.381	14.3	99.2	110.0	1.6
78	4	6.861	0.0191	-0.0251	0.894	26.7	100.1	115.12	0.53
54	3	7.207	0.0008	0.1183	0.737	660.3	99.5	120.02	0.90
38	3	7.322	0.0068	0.1426	2.161	75.1	99.4	121.77	0.44
93	4	7.306	0.0774	0.0839	0.393	6.6	99.7	121.9	1.4
53	3	7.409	0.0080	0.1343	1.305	63.8	99.5	123.22	0.53
44	3	8.034	0.0010	0.9700	10.018	502.6	96.4	129.29	0.27
25	3	8.164	0.0029	0.2006	1.304	173.2	99.3	135.08	0.70
40	3	8.736	-0.0304	1.803	0.090	-	93.8	136.5	5.8
63	3	9.227	0.0030	0.1660	1.964	167.9	99.5	152.26	0.52
97	4	9.486	-0.0087	0.4454	0.487	-	98.6	155.0	1.3
46	3	9.835	0.0027	0.3297	4.733	186.5	99.0	161.15	0.45
81	4	9.908	0.0973	0.1165	0.460	5.2	99.7	163.5	1.6
28	3	10.95	0.0020	0.3330	2.910	256.3	99.1	178.74	0.46
90	4	11.32	-0.0126	0.2235	0.424	-	99.4	185.0	1.6
64	3	11.60	-0.0011	0.0511	1.385	-	99.9	190.20	0.78
96	4	12.07	0.0170	1.019	0.404	30.1	97.5	193.1	1.7
72	3	12.99	0.0009	0.5118	1.133	572.7	98.8	209.60	0.97
86	4	13.21	-0.0166	-0.0006	0.753	-	100.0	215.4	1.2
79	4	13.54	0.0521	0.2137	0.450	9.8	99.6	219.6	1.8

ID	Power (Watts)	$^{40}Ar/^{39}Ar$	$^{37}Ar/^{39}Ar$	$^{36}Ar/^{39}Ar$ (x 10^{-3})	$^{39}Ar_K$ (x10^{-15} mol)	K/Ca	$^{40}Ar^*$ (%)	Age (Ma)	±1σ (Ma)
87	4	13.90	-0.0065	-0.1323	0.409	-	100.3	226.5	1.7
65	3	14.00	-0.0129	0.1574	0.551	-	99.7	226.8	2.0
91	4	16.32	-0.0389	0.0879	0.405	-	99.8	262.2	2.5
89	4	16.42	-0.2105	-0.5612	0.054	-	100.9	266.3	11.8
32	3	17.23	0.0008	0.0716	5.964	608.1	99.9	275.90	0.65
70	3	18.95	0.0191	0.0356	0.385	26.7	100.0	301.6	3.3
41	3	20.11	-0.0026	0.3267	0.697	-	99.5	317.2	1.9
75	4	20.83	0.0590	1.430	0.284	8.6	98.0	323.1	3.4
33	3	20.98	0.0444	1.487	0.222	11.5	97.9	325.0	5.0
58	3	20.69	-0.0110	-0.0402	0.475	-	100.1	327.3	3.0
47	3	22.07	-0.0016	0.0876	1.671	-	99.9	346.6	1.3
98	4	22.30	0.0329	0.3166	0.323	15.5	99.6	348.9	3.3
88	4	24.18	-0.1741	0.3922	0.056	-	99.5	375.0	18.4
69	3	27.18	-0.0042	0.0796	1.121	-	99.9	418.4	1.9
01	3	27.70	-0.0025	0.3146	1.038	-	99.7	424.5	2.8
35	3	27.84	-0.0004	0.5432	0.237	-	99.4	425.6	6.2
100	4	28.41	0.0444	-0.9093	0.272	11.5	101.0	439.3	5.2
23	3	29.76	0.0012	0.3473	0.558	437.3	99.7	452.5	3.8
71	3	29.90	0.0014	0.0441	1.834	368.1	100.0	455.6	1.5
51	3	30.07	-0.0011	0.0526	0.773	-	99.9	457.9	2.6
67	3	31.22	-0.0082	0.2894	0.630	-	99.7	472.4	3.4
31	3	32.44	-0.0101	0.8215	0.582	-	99.2	486.5	3.3
80	4	36.56	0.0487	-0.1122	0.344	10.5	100.1	544.1	3.5
74	4	36.83	-0.0451	0.3227	0.445	-	99.7	545.7	3.7
52	3	38.64	0.0037	0.0381	0.844	139.8	100.0	570.0	3.2

ID	Power (Watts)	$^{40}Ar/^{39}Ar$	$^{37}Ar/^{39}Ar$	$^{36}Ar/^{39}Ar$ (x 10^{-3})	$^{39}Ar_K$ (x10^{-15} mol)	K/Ca	$^{40}Ar^*$ (%)	Age (Ma)	±1σ (Ma)
06	3	39.10	-0.0091	0.2307	0.797	-	99.8	575.0	3.2
07	3	39.14	-0.0056	0.1135	0.312	-	99.9	576.0	5.3
09	3	40.49	0.0072	0.0281	1.521	71.3	100.0	593.4	2.0
15	3	42.67	0.0025	0.2642	4.229	207.9	99.8	619.6	2.6
68	3	43.15	0.0017	0.0942	1.071	301.2	99.9	626.1	3.0
57	3	43.39	0.0036	0.0542	1.295	140.7	100.0	629.2	2.3
05	3	50.57	0.0035	0.1173	1.752	144.0	99.9	715.1	2.4
13	3	51.38	0.0030	0.2057	0.827	170.3	99.9	724.3	4.0
37	3	51.99	-0.0012	0.2624	1.299	-	99.8	731.1	3.3
34	3	54.92	0.0005	0.0641	3.366	973.5	100.0	765.5	2.1
60	3	57.32	0.0005	0.2827	1.602	934.8	99.9	792.0	2.6
29	3	59.68	0.0027	0.1388	2.288	187.0	99.9	818.8	3.0
99	4	60.94	-0.0207	-0.0643	0.174	-	100.0	833.3	8.5
49	3	61.84	0.0015	0.2981	1.637	340.2	99.9	841.9	2.3
42	3	61.90	-0.0001	0.1736	1.590	-	99.9	843.0	2.8
83	4	71.49	-0.3456	-2.9946	0.028	-	101.2	954.3	74.8
82	4	73.58	-0.0203	0.1117	0.423	-	100.0	966.5	6.5
21	3	73.94	0.0089	0.0075	0.914	57.6	100.0	970.6	3.6
76	4	74.59	-0.0012	0.0548	3.039	-	100.0	977.0	1.2
03	3	78.17	0.0036	0.2988	2.814	140.1	99.9	1012.3	2.2
56	3	80.15	0.0020	0.4353	5.485	256.9	99.8	1031.5	2.2
48	3	82.77	0.0132	0.2840	1.943	38.7	99.9	1057.6	4.4
92	4	83.88	0.0142	0.2464	0.763	35.9	99.9	1068.5	3.7
17	3	86.39	0.0006	0.2072	3.469	796.0	99.9	1092.6	2.3
11	3	94.67	0.0002	0.0245	1.638	2454.1	100.0	1170.4	2.9

ID	Power (Watts)	$^{40}Ar/^{39}Ar$	$^{37}Ar/^{39}Ar$	$^{36}Ar/^{39}Ar$ (x 10^{-3})	$^{39}Ar_K$ (x10^{-15} mol)	K/Ca	$^{40}Ar^*$ (%)	Age (Ma)	±1σ (Ma)
02	3	96.80	-0.0051	2.985	0.236	-	99.1	1181.8	16.2
27	3	102.4	0.0034	0.1852	3.203	150.7	99.9	1239.0	2.1
43	3	103.2	0.0030	1.006	4.244	169.0	99.7	1244.2	2.0
50	3	103.2	0.0032	0.0420	3.369	157.5	100.0	1246.5	2.2
94	4	105.9	-0.0122	0.5958	0.315	-	99.8	1268.4	9.4
66	3	106.9	0.0080	0.8092	0.616	63.6	99.8	1276.6	8.3
20	3	107.6	-0.0040	0.1615	0.890	-	100.0	1284.8	4.7
12	3	107.8	0.0067	0.3563	0.494	76.1	99.9	1285.7	9.5
45	3	125.3	0.0039	0.1642	1.207	132.2	100.0	1430.2	4.1
14	3	151.8	0.0242	0.3671	0.526	21.1	99.9	1629.2	11.4
16	3	267.3	0.0271	0.8217	0.075	18.8	99.9	2306.9	73.2
CM-SS2, Sanidine, J=0.009459±0.37%, IC=1.065671±0.0002916, NM-254E, Lab#=61411, Argus VI									
221	4	3.790	0.0176	0.1486	0.384	29.0	98.9	63.62	0.27
270	4	3.803	0.0115	0.0609	0.543	44.3	99.5	64.28	0.19
103	4	3.879	-0.0002	0.2025	0.975	-	98.4	64.82	0.23
138	4	3.823	0.0043	-0.0135	0.606	117.9	100.1	64.96	0.36
134	4	3.898	0.0104	0.1888	0.644	49.2	98.6	65.21	0.34
153	4	4.102	0.0090	0.2190	0.744	56.8	98.4	68.46	0.15
140	4	4.303	-0.0144	0.8491	0.360	-	94.1	68.65	0.62
233	4	4.133	0.0467	0.0162	0.379	10.9	100.0	70.05	0.98
172	4	4.153	0.0186	-0.0830	0.673	27.5	100.6	70.84	0.59
136	4	4.167	-0.0312	-0.0633	0.239	-	100.4	70.9	1.9
104	4	4.337	0.0001	0.4873	0.255	6102.9	96.6	71.0	1.8
234	4	4.292	0.0000	0.3070	0.316	-	97.9	71.2	1.1

ID	Power (Watts)	$^{40}Ar/^{39}Ar$	$^{37}Ar/^{39}Ar$	$^{36}Ar/^{39}Ar$ (x 10^{-3})	$^{39}Ar_K$ (x10^{-15} mol)	K/Ca	$^{40}Ar^*$ (%)	Age (Ma)	±1σ (Ma)
125	4	4.295	0.0190	0.2421	0.516	26.8	98.4	71.59	0.99
231	4	4.308	0.0128	0.2141	0.572	39.9	98.5	71.94	0.61
264	4	4.321	-0.1150	0.0766	0.307	-	99.2	72.6	1.4
217	4	4.395	0.0533	0.1874	0.523	9.6	98.8	73.56	0.79
281	4	4.437	-0.0156	0.2967	1.886	-	98.0	73.63	0.31
152	4	4.390	0.0395	0.0865	0.538	12.9	99.5	73.95	0.65
215	4	4.371	-0.0457	-0.0679	0.634	-	100.4	74.29	0.56
205	4	4.539	-0.0070	0.2874	0.400	-	98.1	75.39	0.86
207	4	4.556	0.0393	0.2545	0.915	13.0	98.4	75.89	0.48
165	4	4.644	-0.0369	0.4504	0.096	-	97.1	76.3	3.4
265	4	4.450	0.0389	-0.2420	0.436	13.1	101.7	76.61	0.75
154	4	4.467	0.1406	-0.1658	0.225	3.6	101.4	76.7	1.8
149	4	4.541	0.0322	0.0421	0.610	15.9	99.8	76.67	0.62
158	4	4.683	0.0079	-0.0610	0.550	64.8	100.4	79.52	0.81
144	4	4.818	0.1628	-0.0141	0.229	3.1	100.4	81.7	1.9
115	4	4.993	0.0027	-0.3072	0.087	188.9	101.8	85.8	5.2
166	4	5.122	0.0182	0.1162	0.477	28.0	99.4	85.94	0.88
135	4	5.217	0.0050	0.2673	0.664	102.7	98.5	86.73	0.59
147	4	5.375	0.0252	0.0799	1.241	20.2	99.6	90.29	0.39
167	4	5.854	0.0673	-0.0778	0.568	7.6	100.5	99.00	0.76
181	4	6.109	-0.0339	0.0564	0.531	-	99.7	102.37	0.77
110	4	6.236	0.0600	-0.0991	0.251	8.5	100.5	105.3	1.8
124	4	6.690	-0.0283	1.145	0.306	-	94.9	106.6	2.0
225	4	7.216	0.0358	0.0005	0.590	14.3	100.0	120.78	0.70
118	4	7.215	0.0250	-0.2432	0.359	20.4	101.0	121.9	1.5

ID	Power (Watts)	$^{40}Ar/^{39}Ar$	$^{37}Ar/^{39}Ar$	$^{36}Ar/^{39}Ar$ (x 10^{-3})	$^{39}Ar_K$ (x10^{-15} mol)	K/Ca	$^{40}Ar^*$ (%)	Age (Ma)	±1σ (Ma)
274	4	7.336	-0.0127	-0.0621	0.669	-	100.2	122.96	0.75
189	4	7.531	0.0280	-0.2223	0.124	18.2	100.9	126.9	3.8
127	4	7.805	-0.0469	0.0460	0.180	-	99.8	130.0	2.9
117	4	7.956	-0.0290	0.2553	0.334	-	99.0	131.4	1.7
202	4	7.978	-0.2346	0.1255	0.172	-	99.3	132.1	2.8
220	4	8.180	-0.0364	0.0761	0.325	-	99.7	135.8	1.6
119	4	8.159	0.0729	-0.0788	0.424	7.0	100.4	136.4	1.4
209	4	8.315	-0.1172	0.2727	0.422	-	98.9	137.0	1.2
183	4	8.311	-0.1269	0.0494	0.217	-	99.7	138.0	2.4
133	4	8.703	0.0233	0.3447	0.708	21.9	98.8	143.07	0.82
132	4	9.222	0.0156	0.2104	0.549	32.8	99.3	152.0	1.0
244	4	9.279	-0.0098	-0.0033	0.890	-	100.0	153.88	0.62
195	4	9.402	0.0284	0.1851	0.927	17.9	99.4	154.99	0.63
250	4	9.518	-0.0313	0.2997	1.115	-	99.0	156.21	0.60
194	4	9.518	0.0822	-0.0218	0.193	6.2	100.1	157.9	3.3
237	4	9.769	0.0181	0.1926	0.347	28.1	99.4	160.8	1.5
267	4	10.01	0.0190	0.0269	0.399	26.9	99.9	165.3	1.4
262	4	10.30	-0.0535	0.3061	0.594	-	99.1	168.59	0.93
141	4	13.01	0.0034	7.924	0.154	150.5	81.9	175.6	4.9
148	4	11.15	-0.0007	0.1321	0.955	-	99.6	182.79	0.71
284	4	11.23	0.0209	0.0984	0.255	24.4	99.8	184.2	2.3
236	4	11.56	0.0772	0.9585	0.168	6.6	97.6	185.6	3.2
126	4	11.58	-0.2030	0.4812	0.179	-	98.6	187.7	4.1
170	4	11.35	-0.2162	-0.3960	0.178	-	100.9	188.1	7.8
102	4	11.51	0.0311	-0.1923	0.310	16.4	100.5	190.1	2.1

ID	Power (Watts)	$^{40}Ar/^{39}Ar$	$^{37}Ar/^{39}Ar$	$^{36}Ar/^{39}Ar$ (x 10^{-3})	$^{39}Ar_K$ (x10^{-15} mol)	K/Ca	$^{40}Ar^*$ (%)	Age (Ma)	±1σ (Ma)
261	4	12.22	-0.0225	0.5052	0.458	-	98.8	197.7	1.6
258	4	12.24	-0.0073	0.1264	0.994	-	99.7	199.75	0.71
137	4	12.13	0.0615	-0.2115	0.442	8.3	100.6	199.8	1.5
206	4	12.55	0.2233	0.4206	0.127	2.3	99.2	203.5	5.1
185	4	12.55	0.0030	0.0635	4.881	167.5	99.9	204.93	0.19
203	4	12.64	-0.0757	0.2726	0.368	-	99.3	205.2	1.7
288	4	12.60	-0.1368	0.1140	0.440	-	99.6	205.2	1.7
116	4	12.92	0.1611	0.1673	0.442	3.2	99.7	210.4	1.6
279	4	12.94	0.0354	0.0586	0.375	14.4	99.9	211.0	2.1
156	4	13.74	-0.2977	1.038	0.078	-	97.6	218.3	8.4
142	4	13.64	0.0606	0.4731	0.166	-	99.0	220.0	4.5
257	4	13.51	0.1229	0.0288	0.312	4.2	100.0	220.0	2.5
107	4	13.77	0.0017	-0.2007	0.291	307.2	100.4	224.9	2.2
155	4	14.23	0.0321	0.1342	0.469	15.9	99.7	230.4	1.9
122	4	14.31	0.0463	0.0532	0.399	11.0	99.9	232.1	1.9
123	4	14.29	0.2977	-0.2487	0.168	1.7	100.7	233.5	3.8
278	4	14.51	-0.0383	-0.0432	0.422	-	100.1	235.5	1.6
150	4	14.67	-0.0151	-0.0078	0.679	-	100.0	237.8	1.3
178	4	15.33	0.0204	0.1078	0.856	25.0	99.8	247.24	1.00
213	4	15.61	0.0874	0.3633	0.306	5.8	99.3	250.4	2.3
263	4	15.56	-0.0122	-0.1460	0.573	-	100.3	251.9	1.3
255	4	15.87	-0.0720	0.4487	0.302	-	99.1	253.8	2.6
216	4	15.85	-0.0444	0.0888	0.257	-	99.8	255.1	2.2
199	4	15.71	0.0297	-0.4605	0.370	17.2	100.9	255.6	1.8
151	4	15.93	-0.0103	0.1547	0.399	-	99.7	256.1	1.7

ID	Power (Watts)	$^{40}Ar/^{39}Ar$	$^{37}Ar/^{39}Ar$	$^{36}Ar/^{39}Ar$ (x 10^{-3})	$^{39}Ar_K$ (x10^{-15} mol)	K/Ca	$^{40}Ar^*$ (%)	Age (Ma)	±1σ (Ma)
146	4	16.11	0.0511	0.1739	0.244	10.0	99.7	258.8	2.9
101	4	16.62	0.0103	-0.0190	0.708	49.6	100.0	267.3	1.6
196	4	19.24	-0.3311	8.168	0.022	-	87.2	269.4	40.7
198	4	16.94	-0.0062	0.0475	0.742	-	99.9	271.7	1.3
208	4	16.91	0.1245	-0.1669	0.199	4.1	100.3	272.4	4.0
230	4	17.54	0.0063	0.1677	0.855	80.9	99.7	280.09	1.00
245	4	17.81	0.0259	0.1370	0.763	19.7	99.8	284.3	1.3
168	4	18.25	-0.0321	0.0036	0.555	-	100.0	291.3	1.9
197	4	18.38	-0.0776	0.2334	0.445	-	99.6	292.2	1.8
182	4	18.74	-0.0113	0.2334	0.852	-	99.6	297.55	0.87
173	4	19.00	0.0095	0.3137	0.805	53.8	99.5	301.0	1.1
112	4	19.00	-0.1657	-0.0260	0.189	-	100.0	302.3	5.2
260	4	19.30	-0.0230	0.0938	0.433	-	99.8	306.3	1.9
273	4	19.77	-0.0136	0.4276	0.257	-	99.4	311.8	2.7
188	4	21.20	-0.0057	-0.0133	0.610	-	100.0	334.5	1.7
161	4	21.55	0.0145	0.2652	0.485	35.1	99.6	338.4	1.7
214	4	21.93	-0.0336	0.0156	1.486	-	100.0	344.83	0.89
128	4	22.32	0.0877	-0.0011	0.137	5.8	100.0	350.7	7.7
259	4	22.39	0.0159	-0.0897	0.811	32.0	100.1	351.9	1.4
111	4	23.76	0.0521	-0.0211	0.446	9.8	100.0	371.2	2.6
192	4	18.07	2.816	-19.9778	0.007	0.18	134.2	378.3	150.4
113	4	25.49	-0.0275	-0.2598	0.071	-	100.3	396.3	15.0
204	4	25.65	-0.0227	-0.1678	0.174	-	100.2	398.2	5.3
162	4	26.85	-0.0399	-0.0218	0.732	-	100.0	414.2	1.9
211	4	26.97	0.0065	-0.0390	1.036	78.8	100.0	415.9	1.2

ID	Power (Watts)	$^{40}Ar/^{39}Ar$	$^{37}Ar/^{39}Ar$	$^{36}Ar/^{39}Ar$ (x 10^{-3})	$^{39}Ar_K$ (x10^{-15} mol)	K/Ca	$^{40}Ar^*$ (%)	Age (Ma)	±1σ (Ma)
266	4	27.77	-0.1548	0.8531	0.048	-	99.0	423.1	24.6
145	4	27.56	0.0064	-0.0128	0.520	80.2	100.0	424.0	2.0
226	4	28.52	0.0345	0.1718	0.466	14.8	99.8	436.5	2.9
256	4	28.57	0.0110	0.1190	0.914	46.5	99.9	437.3	1.6
253	4	28.92	-0.1456	0.5376	0.267	-	99.4	440.2	4.1
238	4	29.32	0.0127	0.2487	0.443	40.0	99.8	447.0	2.5
143	4	29.39	0.0619	0.1615	0.168	8.2	99.9	448.3	6.6
106	4	29.57	-0.0210	0.1539	0.298	-	99.8	450.7	4.1
254	4	30.15	0.0412	0.0399	0.890	12.4	100.0	459.1	1.5
251	4	31.74	-0.0340	0.2296	0.885	-	99.8	479.5	1.8
169	4	32.25	0.0068	0.2906	0.902	74.7	99.7	486.1	1.9
130	4	33.98	0.0859	0.4845	0.230	5.9	99.6	508.3	5.2
174	4	34.82	0.0057	0.0843	3.008	89.2	99.9	520.68	0.63
249	4	36.13	0.0006	0.0378	0.459	922.9	100.0	537.9	3.6
224	4	38.95	0.1556	0.1583	0.239	3.3	99.9	573.7	6.3
248	4	41.05	-0.0006	-0.0044	0.841	-	100.0	600.5	1.8
190	4	41.72	0.0498	0.1597	0.435	10.3	99.9	608.3	3.3
235	4	46.48	-0.1055	0.2137	0.243	-	99.8	666.0	6.0
129	4	49.19	-0.0255	0.1469	0.315	-	99.9	698.7	3.9
157	4	49.72	0.0224	0.0527	0.557	22.8	100.0	705.4	3.7
272	4	50.00	-0.0028	0.1546	1.148	-	99.9	708.2	1.7
222	4	50.01	0.0316	-0.0153	0.486	16.2	100.0	709.0	3.4
200	4	54.03	-0.0056	0.0499	0.402	-	100.0	755.4	5.2
287	4	54.97	-0.0361	0.0708	0.558	-	100.0	766.0	3.4
269	4	56.74	-0.0525	0.0123	0.609	-	100.0	786.3	2.8

ID	Power (Watts)	$^{40}Ar/^{39}Ar$	$^{37}Ar/^{39}Ar$	$^{36}Ar/^{39}Ar$ (x 10^{-3})	$^{39}Ar_K$ (x10^{-15} mol)	K/Ca	$^{40}Ar^*$ (%)	Age (Ma)	±1σ (Ma)
164	4	57.13	0.0278	0.0929	0.474	18.3	100.0	790.4	3.2
271	4	60.39	0.0173	0.1116	0.712	29.5	99.9	826.7	2.9
210	4	62.25	-0.0151	0.1215	0.723	-	99.9	847.0	3.2
179	4	64.65	-0.0343	0.0404	0.516	-	100.0	873.2	3.9
243	4	68.34	0.0143	2.204	0.182	35.6	99.0	905.7	11.9
223	4	69.25	0.0811	-0.1663	0.413	6.3	100.1	922.8	5.1
201	4	69.43	-0.0357	-0.1545	0.313	-	100.1	924.5	8.0
242	4	70.19	-0.0051	-0.0876	0.607	-	100.0	932.2	4.1
120	4	70.66	0.0770	0.2867	0.369	6.6	99.9	936.1	6.1
285	4	70.90	0.0974	0.1321	0.319	5.2	100.0	939.0	6.6
241	4	72.86	-0.0012	1.448	0.122	-	99.4	955.1	19.0
232	4	73.46	0.0758	0.1504	0.372	6.7	99.9	965.3	6.3
114	4	75.07	0.0163	-0.1558	0.558	31.4	100.1	982.5	4.8
180	4	75.71	-0.0233	0.8182	0.428	-	99.7	986.0	6.6
239	4	78.32	0.0087	0.0821	0.776	58.8	100.0	1014.5	3.1
212	4	79.49	0.0117	-0.1003	0.493	43.6	100.0	1026.6	4.2
121	4	79.79	0.0615	0.0146	0.415	8.3	100.0	1029.3	6.2
139	4	80.69	-0.0507	0.0183	0.479	-	100.0	1038.0	5.3
171	4	81.02	0.0202	0.2162	0.895	25.3	99.9	1040.7	2.5
177	4	83.69	0.0553	0.1801	0.328	9.2	99.9	1066.9	7.0
276	4	84.28	-0.0055	0.2076	0.726	-	99.9	1072.4	3.6
176	4	85.09	0.0140	0.1467	0.546	36.5	100.0	1080.5	4.8
186	4	85.19	0.0152	0.0821	0.870	33.6	100.0	1081.6	2.8
159	4	85.74	0.0351	-0.0016	0.646	14.5	100.0	1087.1	4.7
280	4	85.75	-0.1316	-0.2640	0.116	-	100.1	1087.7	17.9

ID	Power (Watts)	$^{40}Ar/^{39}Ar$	$^{37}Ar/^{39}Ar$	$^{36}Ar/^{39}Ar$ (x 10^{-3})	$^{39}Ar_K$ (x10^{-15} mol)	K/Ca	$^{40}Ar^*$ (%)	Age (Ma)	±1σ (Ma)
286	4	87.18	-0.1066	0.0402	0.356	-	100.0	1100.5	5.6
105	4	87.69	0.0012	0.0740	0.294	440.5	100.0	1105.4	8.2
227	4	87.78	0.0254	-0.0779	0.306	20.1	100.0	1106.7	7.8
277	4	88.31	-0.0649	-0.1111	0.238	-	100.0	1111.7	9.6
268	4	90.16	-0.0398	0.2723	0.376	-	99.9	1128.0	6.6
252	4	93.01	0.0044	0.1922	1.542	116.6	99.9	1154.7	1.7
240	4	93.86	0.0339	0.8083	0.310	15.0	99.7	1160.9	7.9
282	4	94.61	0.0240	0.2270	0.707	21.3	99.9	1169.4	4.7
187	4	94.80	0.0346	-0.0216	0.509	14.8	100.0	1171.8	4.9
229	4	98.34	0.1116	-0.1335	0.395	4.6	100.0	1204.2	6.7
163	4	99.26	-0.0162	1.778	0.637	-	99.5	1207.2	3.5
131	4	100.3	-0.0180	-0.1310	0.441	-	100.0	1221.7	6.5
283	4	100.3	-0.0360	-0.2455	0.330	-	100.1	1222.2	8.9
246	4	107.0	-0.0332	0.3373	0.337	-	99.9	1279.1	8.2
108	4	108.8	0.0523	0.4306	0.160	9.7	99.9	1294.5	15.5
228	4	113.8	-0.0404	-0.0347	0.612	-	100.0	1337.0	4.9
191	4	117.9	0.0780	0.1732	0.325	6.5	100.0	1371.0	7.3
160	4	118.1	0.0326	-0.2372	0.678	15.7	100.1	1373.4	4.3
184	4	127.6	0.0192	0.1994	1.203	26.5	100.0	1448.6	3.0
CM-Ash1, Sanidine, J=0.0095388±0.18%, IC=1.057651±0.0003232, NM-254E, Lab#=61410, Argus VI									
05	3	4.001	0.0045	0.3772	5.664	112.7	97.2	66.532	0.048
24	3	4.211	0.0024	0.1157	0.974	209.5	99.2	71.39	0.19
18	3	5.159	0.0161	3.150	2.893	31.8	81.8	72.14	0.11
02	3	5.575	0.0050	0.3098	0.975	101.2	98.3	93.19	0.68

ID	Power (Watts)	$^{40}Ar/^{39}Ar$	$^{37}Ar/^{39}Ar$	$^{36}Ar/^{39}Ar$ (x 10^{-3})	$^{39}Ar_K$ (x10^{-15} mol)	K/Ca	$^{40}Ar^*$ (%)	Age (Ma)	±1σ (Ma)
26	3	5.773	0.0019	0.1648	2.281	267.9	99.2	97.17	0.37
14	3	6.395	0.0044	0.1917	2.226	116.8	99.1	107.32	0.41
35	3	7.434	-0.0072	0.8433	0.374	-	96.6	121.2	1.5
37	3	7.367	-0.0028	0.1844	1.786	-	99.3	123.28	0.66
20	3	7.736	0.0038	0.1653	3.979	133.2	99.4	129.39	0.27
03	3	9.761	0.0099	0.2804	1.835	51.5	99.2	161.51	0.68
33	3	10.89	0.0050	0.2917	6.517	102.4	99.2	179.35	0.34
11	3	11.23	-0.0023	0.2308	1.954	-	99.4	185.09	0.55
07	3	11.56	-0.0022	1.020	1.974	-	97.4	186.59	0.85
15	3	11.87	0.0032	0.7145	6.018	159.8	98.2	192.81	0.65
25	3	11.84	-0.0012	0.5276	0.273	-	98.7	193.3	3.1
10	3	12.95	0.0023	0.4715	4.343	226.2	98.9	210.91	0.41
27	3	16.67	0.0109	0.9593	0.951	46.7	98.3	265.7	1.2
23	3	18.19	0.0019	0.2330	2.540	267.9	99.6	291.76	0.69
09	3	19.33	0.0029	0.3297	0.856	174.8	99.5	308.2	1.7
08	3	21.83	0.0012	0.0740	2.057	439.4	99.9	345.81	0.95
22	3	25.28	0.0016	0.0535	4.247	316.9	99.9	395.1	1.3
31	3	28.61	0.0039	0.5590	2.064	130.4	99.4	439.3	2.3
13	3	29.18	0.0025	0.2355	2.943	205.1	99.8	448.47	0.98
30	3	30.26	0.0033	0.2889	0.981	154.9	99.7	462.9	2.6
17	3	36.59	0.0020	0.2756	12.878	259.3	99.8	546.81	0.65
16	3	38.58	0.0057	1.231	11.771	89.1	99.1	568.8	1.4
38	3	45.31	0.0036	0.1990	7.531	140.0	99.9	656.7	1.5
36	3	49.93	0.0012	0.5057	2.385	420.4	99.7	711.1	1.8
21	3	49.96	0.0081	0.1441	0.928	63.2	99.9	712.8	2.8

ID	Power (Watts)	$^{40}Ar/^{39}Ar$	$^{37}Ar/^{39}Ar$	$^{36}Ar/^{39}Ar$ (x 10^{-3})	$^{39}Ar_K$ (x10^{-15} mol)	K/Ca	$^{40}Ar^*$ (%)	Age (Ma)	±1σ (Ma)
28	3	56.32	0.0022	0.3361	6.463	233.8	99.8	785.9	1.6
32	3	57.54	0.0005	0.3068	5.359	1118.1	99.8	799.8	1.8
12	3	66.80	0.0026	0.7594	13.909	197.1	99.7	899.9	1.7
19	3	70.11	0.0019	0.2847	11.810	274.6	99.9	936.4	2.9
29	3	71.26	0.0037	0.9900	3.908	137.2	99.6	946.2	1.4
04	3	74.14	0.0038	0.5824	4.802	132.7	99.8	977.2	1.5
06	3	82.11	0.0087	1.129	1.514	58.3	99.6	1055.4	3.5
34	3	86.30	-0.0012	0.0696	1.900	-	100.0	1099.1	2.6
01	3	170.6	0.0337	1.652	0.227	15.1	99.7	1765.2	18.9
A1070606, Sanidine, J=0.0091618±0.01%, IC=1.049587±0.0004276, NM-258G, Lab#=61757, Argus VI									
08	4	3.921	0.0044	0.0089	1.762	116.1	99.9	64.439	0.056
22	4	3.930	0.0066	0.0133	1.238	76.8	99.9	64.578	0.079
04	4	3.931	0.0043	-0.0006	2.274	117.9	100.0	64.648	0.045
65	4.5	3.941	0.0070	0.0204	1.677	72.4	99.9	64.709	0.054
64	4.5	4.101	0.0126	0.0156	1.856	40.5	99.9	67.33	0.15
05	4	4.163	0.0041	0.0220	0.950	123.9	99.9	68.30	0.10
28	4	4.471	-0.0088	0.7251	0.118	-	95.2	69.88	0.88
53	4	4.285	0.0030	0.0181	1.381	171.1	99.9	70.289	0.073
33	4	4.472	0.0122	0.0536	0.705	41.9	99.7	73.14	0.21
59	4.5	4.944	0.0254	1.557	0.753	20.1	90.6	73.55	0.48
13	4	4.541	0.0053	-0.0088	1.497	97.1	100.1	74.542	0.088
76	4.5	4.583	0.0258	-0.0048	0.410	19.8	100.1	75.23	0.63
15	4	5.203	0.0053	0.0329	1.294	97.2	99.8	84.97	0.13
51	4	6.320	0.0008	0.8822	1.592	626.8	95.8	98.739	0.088

ID	Power (Watts)	$^{40}Ar/^{39}Ar$	$^{37}Ar/^{39}Ar$	$^{36}Ar/^{39}Ar$ (x 10^{-3})	$^{39}Ar_K$ (x10^{-15} mol)	K/Ca	$^{40}Ar^*$ (%)	Age (Ma)	±1σ (Ma)
62	4.5	7.824	0.2388	5.256	0.057	2.1	80.2	102.3	5.7
40	4	6.362	0.0001	0.1991	1.758	8603.8	99.1	102.643	0.069
69	4.5	7.637	-0.0016	0.1062	1.666	-	99.6	123.17	0.28
36	4	7.926	0.0046	0.1638	0.743	110.3	99.4	127.44	0.18
30	4	8.420	0.0093	0.9546	0.674	54.7	96.6	131.48	0.19
37	4	8.982	0.0084	0.4622	0.697	60.9	98.5	142.51	0.32
41	4	9.528	0.0004	0.5377	1.607	1268.5	98.3	150.604	0.091
75	4.5	9.426	0.0617	0.1086	0.389	8.3	99.7	151.1	1.2
47	4	9.987	0.0016	0.3732	1.572	312.3	98.9	158.435	0.096
58	4.5	11.47	-0.0194	0.2028	1.438	-	99.5	181.85	0.43
14	4	11.51	0.0013	0.0996	1.652	402.2	99.7	182.93	0.18
10	4	11.86	0.0004	0.3965	1.120	1413.3	99.0	186.98	0.15
07	4	11.79	0.0005	0.0511	2.465	1055.7	99.9	187.448	0.070
61	4.5	12.21	-0.0903	0.4975	0.487	-	98.7	191.6	1.2
38	4	12.30	0.0007	0.0636	3.048	728.1	99.8	195.027	0.069
54	4	12.45	0.0006	0.1345	1.712	879.4	99.7	196.93	0.10
44	4	13.02	-0.0006	0.1296	1.955	-	99.7	205.538	0.092
73	4.5	13.13	-0.0073	0.1612	0.806	-	99.6	207.04	0.83
55	4	13.18	0.0007	0.0667	1.338	759.0	99.8	208.28	0.13
45	4	13.99	0.0046	0.0342	0.891	110.6	99.9	220.49	0.19
67	4.5	14.09	-0.0059	0.2262	0.809	-	99.5	221.08	0.71
25	4	14.09	0.0014	0.1067	1.405	372.8	99.8	221.64	0.13
32	4	14.29	0.0028	0.0283	1.473	185.1	99.9	224.98	0.12
17	4	14.69	0.0025	0.1705	1.401	202.5	99.7	230.24	0.34
35	4	14.93	0.0030	0.0299	0.773	168.3	99.9	234.40	0.22

ID	Power (Watts)	$^{40}Ar/^{39}Ar$	$^{37}Ar/^{39}Ar$	$^{36}Ar/^{39}Ar$ (x 10^{-3})	$^{39}Ar_K$ (x10^{-15} mol)	K/Ca	$^{40}Ar^*$ (%)	Age (Ma)	±1σ (Ma)
31	4	14.98	0.0002	0.0567	0.774	2532.0	99.9	235.08	0.23
23	4	15.52	-0.0003	0.1439	0.896	-	99.7	242.63	0.21
77	4.5	15.94	-0.0130	0.5488	0.895	-	99.0	246.95	0.82
56	4	15.92	0.0004	0.1958	0.991	1422.0	99.6	248.28	0.19
06	4	16.00	0.0028	0.1685	0.825	184.7	99.7	249.58	0.22
74	4.5	16.51	0.0383	0.2519	0.261	13.3	99.6	256.7	2.5
66	4.5	16.57	0.0156	0.2431	1.020	32.6	99.6	257.61	0.90
43	4	17.00	0.0021	0.1391	0.892	247.9	99.8	264.23	0.21
46	4	18.50	0.0081	0.2224	0.669	62.8	99.6	285.49	0.31
16	4	19.06	0.0009	0.0302	1.927	541.3	100.0	294.38	0.21
11	4	19.38	0.0006	0.1219	3.103	893.1	99.8	298.525	0.077
34	4	24.41	0.0069	0.2337	0.394	73.4	99.7	368.42	0.61
27	4	24.49	0.0022	0.1365	1.213	232.6	99.8	369.84	0.21
63	4.5	26.32	0.0148	0.9611	0.797	34.6	98.9	391.5	1.4
01	4	30.66	0.0030	0.1243	1.345	169.7	99.9	452.65	0.23
78	4.5	31.11	-0.0263	0.1978	0.369	-	99.8	458.1	3.0
72	4.5	31.27	0.0148	0.1239	1.119	34.4	99.9	460.6	1.2
12	4	32.46	-0.0001	0.1243	1.015	-	99.9	476.05	0.68
60	4.5	32.64	-0.0291	0.1298	0.477	-	99.9	478.2	2.7
26	4	33.22	-0.0031	0.1375	0.635	-	99.9	485.70	0.47
20	4	33.61	0.0037	0.0778	0.601	137.2	99.9	491.06	0.87
42	4	34.10	0.0062	0.5140	0.679	82.9	99.6	495.67	0.47
21	4	35.50	0.0016	0.2792	1.142	320.5	99.8	514.36	0.31
50	4	36.26	0.0074	0.2920	0.316	68.9	99.8	523.8	1.1
48	4	38.32	-0.0013	0.1406	0.702	-	99.9	550.19	0.50

ID	Power (Watts)	$^{40}Ar/^{39}Ar$	$^{37}Ar/^{39}Ar$	$^{36}Ar/^{39}Ar$ (x 10^{-3})	$^{39}Ar_K$ (x10^{-15} mol)	K/Ca	$^{40}Ar^*$ (%)	Age (Ma)	±1σ (Ma)
49	4	38.82	0.0049	0.1304	0.349	104.6	99.9	556.42	0.94
70	4.5	39.04	-0.0182	0.2867	0.430	-	99.8	558.6	2.8
24	4	39.81	0.0011	0.1486	0.896	458.2	99.9	568.55	0.42
52	4	51.09	0.0201	0.2116	0.224	25.4	99.9	702.1	1.8
39	4	51.08	0.0046	0.0538	2.046	110.1	100.0	702.45	0.68
57	4.5	58.23	-0.1567	1.652	0.073	-	99.1	777.0	21.8
09	4	62.55	-0.0018	0.6829	0.568	-	99.7	826.98	0.85
03	4	66.79	0.0019	0.1006	2.561	272.7	100.0	873.54	0.23
02	4	67.96	0.0037	0.1560	1.891	136.5	99.9	885.47	0.28
29	4	75.77	0.0042	0.1921	1.201	122.2	99.9	964.42	0.45
19	4	84.14	0.0023	0.0339	1.194	222.3	100.0	1045.89	0.96
18	4	84.67	0.0032	0.2139	2.266	159.6	99.9	1050.40	0.31
68	4.5	87.75	0.0046	3.439	0.524	110.0	98.8	1070.3	4.2
71	4.5	89.91	-0.0005	0.7197	1.925	-	99.8	1097.9	1.4
SJ-SS5, Sanidine, J=0.0095555±0.07%, IC=1.05962±0.0011331, NM-254D, Lab#=61405, Argus VI									
20B	3	4.347	0.0042	0.0121	2.730	122.9	99.9	74.30	0.12
37B	3	4.364	0.0018	0.0009	1.646	280.9	100.0	74.65	0.19
03B	3	4.462	0.0056	0.1019	3.149	90.7	99.3	75.80	0.10
35A	0.11	7.475	0.0075	0.1797	0.515	67.8	99.3	125.29	0.87
01	3	9.930	0.0070	0.0368	6.045	72.8	99.9	165.65	0.13
42B	3	11.78	0.0006	0.0188	4.333	812.9	100.0	195.032	0.090
41B	3	26.91	0.0054	0.0275	3.095	94.9	100.0	418.69	0.18
02	3	98.09	0.0027	0.2405	2.600	192.5	99.9	1209.8	1.1

ID	Power (Watts)	$^{40}Ar/^{39}Ar$	$^{37}Ar/^{39}Ar$	$^{36}Ar/^{39}Ar$ (x 10^{-3})	$^{39}Ar_K$ (x10^{-15} mol)	K/Ca	$^{40}Ar^*$ (%)	Age (Ma)	±1σ (Ma)
SJ-SS-2, Sanidine, J=0.0095494±0.11%, IC=1.05325±0.0019241, NM-254C, Lab#=61402, Argus VI									
27	4	3.848	-0.0013	0.1040	1.021	-	99.2	65.40	0.15
55	4	3.813	0.0007	-0.0125	1.761	691.1	100.1	65.403	0.087
09	4	3.832	0.0038	0.0444	1.484	132.8	99.7	65.43	0.11
02	4	3.825	0.0197	0.0174	0.677	25.9	99.9	65.48	0.47
35	4	3.863	-0.0042	0.1180	0.695	-	99.1	65.58	0.22
79	4	3.833	0.0043	0.0018	1.932	119.6	100.0	65.664	0.078
41	4	3.840	0.0090	0.0228	1.490	56.7	99.8	65.69	0.10
04	4	3.943	-0.1298	0.1070	0.129	-	98.8	66.7	3.8
20	4	4.075	0.0139	-0.0605	1.163	36.6	100.5	70.07	0.47
100	4	4.183	-0.0003	0.0946	1.109	-	99.3	71.09	0.51
24	4	4.607	0.0107	1.460	0.176	47.8	90.6	71.4	2.5
12	4	4.234	0.0206	0.0997	1.212	24.8	99.3	71.95	0.54
07	4	4.364	-0.0001	0.5227	1.153	-	96.4	71.99	0.77
40	4	4.332	0.0239	0.1918	0.855	21.3	98.7	73.14	0.68
47	4	4.329	-0.0034	0.0870	1.551	-	99.4	73.57	0.38
05	4	4.423	0.0240	0.3097	0.985	21.3	97.9	74.08	0.49
33	4	4.358	-0.0032	0.0648	1.100	-	99.6	74.18	0.60
22	4	4.105	0.0100	-0.8134	0.250	51.2	106.0	74.4	2.2
51	4	4.379	-0.0009	0.0605	1.396	-	99.6	74.56	0.45
46	4	4.357	-0.0183	-0.0482	0.817	-	100.3	74.70	0.74
01	4	4.389	0.0117	0.0322	0.906	43.7	99.8	74.88	0.35
48	4	4.502	0.0195	0.1371	1.530	26.2	99.1	76.27	0.43
42	4	3.911	0.2555	-1.9847	0.104	2.0	115.6	77.3	5.8
44	4	4.518	0.0007	-0.0733	0.982	754.6	100.5	77.55	0.56

ID	Power (Watts)	$^{40}Ar/^{39}Ar$	$^{37}Ar/^{39}Ar$	$^{36}Ar/^{39}Ar$ (x 10^{-3})	$^{39}Ar_K$ (x10^{-15} mol)	K/Ca	$^{40}Ar^*$ (%)	Age (Ma)	±1σ (Ma)
68	4	4.528	0.0146	-0.0718	0.981	34.8	100.5	77.72	0.58
14	4	4.492	0.0109	-0.2188	0.820	46.6	101.5	77.86	0.72
32	4	5.090	-0.2417	1.187	0.068	-	92.7	80.5	8.3
03	4	4.514	0.0918	-0.7124	0.080	5.6	104.9	80.8	5.7
45	4	4.871	0.0073	-0.0984	1.229	69.7	100.6	83.60	0.49
50	4	5.721	-0.0105	-0.0139	1.583	-	100.1	97.29	0.41
36	4	5.752	0.0174	0.0653	0.357	29.2	99.7	97.5	1.6
58	4	5.802	-0.0033	0.0797	1.443	-	99.6	98.18	0.45
29	4	5.818	-0.0055	0.0979	1.572	-	99.5	98.35	0.44
77	4	5.776	0.0045	-0.0457	1.160	113.8	100.2	98.36	0.55
78	4	5.931	0.0290	0.2226	0.571	17.6	98.9	99.7	1.0
84	4	5.873	0.0124	-0.0417	1.283	41.0	100.2	99.98	0.52
63	4	7.152	0.0093	0.0642	2.022	54.7	99.7	120.50	0.43
23	4	7.574	-0.0134	0.3469	0.638	-	98.6	126.0	1.2
72	4	8.901	0.0003	0.0262	0.950	1466.9	99.9	149.06	0.77
43	4	9.014	-0.0023	-0.0173	1.147	-	100.1	151.10	0.69
53	4	9.839	0.0067	0.0391	2.066	76.2	99.9	164.08	0.45
90	4	10.30	0.0422	0.4487	0.878	12.1	98.7	169.47	0.96
88	4	11.23	-0.0423	-0.2243	0.114	-	100.6	187.3	7.3
92	4	11.36	-0.0034	0.2078	1.019	-	99.5	187.49	0.80
75	4	11.34	-0.0116	0.0511	0.704	-	99.9	187.9	1.3
80	4	11.58	0.0075	0.0360	1.366	67.7	99.9	191.64	0.74
73	4	11.59	0.0122	0.0928	1.898	41.8	99.8	191.67	0.46
103	4	11.63	0.0063	-0.0207	1.161	81.0	100.1	192.80	0.67
62	4	11.69	0.0004	0.1520	1.498	1400.9	99.6	192.96	0.60

ID	Power (Watts)	$^{40}Ar/^{39}Ar$	$^{37}Ar/^{39}Ar$	$^{36}Ar/^{39}Ar$ (x 10^{-3})	$^{39}Ar_K$ (x10^{-15} mol)	K/Ca	$^{40}Ar^*$ (%)	Age (Ma)	±1σ (Ma)
94	4	11.72	0.0096	0.1228	1.537	53.3	99.7	193.58	0.61
39	4	11.74	-0.0087	0.0733	1.203	-	99.8	194.07	0.73
19	4	11.85	-0.0077	-0.0131	1.871	-	100.0	196.23	0.57
56	4	11.97	-0.0087	0.0217	0.662	-	99.9	197.8	1.4
37	4	12.31	0.0270	0.0159	0.838	18.9	100.0	203.2	1.1
86	4	12.89	-0.0033	0.0837	0.933	-	99.8	212.0	1.2
30	4	12.84	-0.0012	-0.1884	1.562	-	100.4	212.40	0.67
17	4	13.41	-0.1601	0.8559	0.032	-	98.0	216.3	30.2
21	4	13.55	0.0505	0.8051	0.191	10.1	98.3	219.0	4.8
61	4	14.42	0.0028	-0.1194	1.397	184.3	100.2	236.59	0.73
57	4	14.52	0.0009	0.1001	1.538	543.3	99.8	237.14	0.81
06	4	15.22	-0.0230	-0.0703	0.627	-	100.1	248.6	1.7
99	4	16.18	-0.0065	0.0950	1.764	-	99.8	262.43	0.67
18	4	18.38	0.0221	-0.0008	1.150	23.1	100.0	296.0	1.1
16	4	18.89	0.0030	0.0958	0.612	171.9	99.9	303.1	2.1
91	4	19.72	-0.0163	-0.3596	0.171	-	100.5	317.2	6.9
74	4	20.95	0.0005	0.4845	0.570	948.9	99.3	331.6	2.3
08	4	23.02	-0.0204	0.1481	0.428	-	99.8	363.0	3.3
97	4	29.19	0.0019	0.1127	1.712	263.7	99.9	449.51	0.95
81	4	33.36	-0.0012	0.1785	2.036	-	99.8	505.4	1.2
89	4	34.51	-0.0254	0.1115	0.644	-	99.9	520.9	2.5
15	4	35.68	0.0182	-0.0967	0.793	28.1	100.1	537.0	1.9
69	4	39.00	0.0013	0.1318	2.068	407.7	99.9	578.88	0.99
65	4	39.59	0.0076	0.0155	2.828	66.9	100.0	586.90	0.90
28	4	40.28	-0.0154	0.2601	1.325	-	99.8	594.6	1.9

ID	Power (Watts)	$^{40}Ar/^{39}Ar$	$^{37}Ar/^{39}Ar$	$^{36}Ar/^{39}Ar$ (x 10^{-3})	$^{39}Ar_K$ (x10^{-15} mol)	K/Ca	$^{40}Ar^*$ (%)	Age (Ma)	±1σ (Ma)
67	4	46.63	-0.0101	0.1253	0.884	-	99.9	673.7	2.9
93	4	47.85	-0.0082	-0.0185	2.214	-	100.0	688.8	1.4
10	4	50.98	0.0067	0.1630	2.463	76.0	99.9	725.4	1.0
64	4	52.40	0.0002	-0.0310	1.829	2393.1	100.0	742.7	1.3
82	4	53.39	-0.0490	1.597	0.101	-	99.1	748.5	22.4
98	4	53.87	0.0182	0.0141	1.094	28.0	100.0	759.6	2.7
70	4	55.87	-0.0005	-0.0793	2.090	-	100.0	782.9	1.3
34	4	56.99	-0.0019	-0.1436	1.092	-	100.1	795.7	2.5
87	4	61.85	0.0026	-0.0777	1.746	193.4	100.0	849.7	1.6
26	4	62.88	0.0020	0.1432	1.745	250.2	99.9	860.3	1.8
102	4	64.78	0.0055	0.0386	2.585	92.2	100.0	881.3	1.1
96	4	64.88	0.0357	-0.0966	0.636	14.3	100.0	882.9	4.2
76	4	66.80	0.0111	0.0147	1.412	45.9	100.0	903.1	1.9
52	4	74.68	0.0056	-0.2234	1.291	90.6	100.1	986.1	2.2
38	4	82.90	-0.0028	-0.0577	1.686	-	100.0	1067.5	1.6
95	4	100.9	0.0102	-0.0783	1.384	50.2	100.0	1235.6	2.7
54	4	103.2	0.0114	-0.0017	1.171	44.8	100.0	1255.3	3.0
13	4	107.8	-0.0001	0.0700	1.312	-	100.0	1295.1	2.9
11	4	110.0	-0.0242	-0.0806	0.939	-	100.0	1314.1	4.6
49	4	115.4	-0.0166	0.0204	0.963	-	100.0	1359.8	3.8
59	4	116.6	0.0019	0.1271	0.884	267.8	100.0	1369.2	4.9
71	4	183.5	-0.0078	-0.0485	0.409	-	100.0	1853.2	11.4
MDA			n=7	MSWD=8.4				64.9	0.3

SJ-SS6, Sanidine, J=0.0095337±0.08%, IC=1.05325±0.0019241, NM-254D, Lab#=61406, Argus VI

ID	Power (Watts)	$^{40}Ar/^{39}Ar$	$^{37}Ar/^{39}Ar$	$^{36}Ar/^{39}Ar$ (x 10^{-3})	$^{39}Ar_K$ (x10^{-15} mol)	K/Ca	$^{40}Ar^*$ (%)	Age (Ma)	±1σ (Ma)
32B	3	3.981	0.0009	0.0158	2.936	553.2	99.9	67.975	0.054
01A	3	4.036	0.0029	0.1947	5.153	177.3	98.6	68.006	0.070
35B	3	3.984	0.0028	0.0030	2.084	183.2	100.0	68.101	0.069
17B	3	4.075	0.0085	-0.0113	5.645	59.7	100.1	69.71	0.12
20B	3	4.354	-0.0205	-0.0147	1.276	-	100.1	74.36	0.46
02A	3	4.390	0.0079	0.0168	1.167	64.3	99.9	74.85	0.27
31B	3	4.378	0.0089	-0.0261	1.828	57.0	100.2	74.86	0.34
19B	3	4.419	0.0061	-0.0389	4.183	83.5	100.3	75.60	0.17
A16-BTW-MH1, DetritalSanidine, J=0.0018994±0.03%, IC=1.002462±0.0008806, NM-293D, Lab#=65992, Argus VI									
91	2.25	19.80	0.0039	0.1704	2.149	129.8	99.7	67.378	0.028
92	2.25	20.01	0.0039	0.5842	1.759	129.8	99.1	67.674	0.033
25	2.25	19.90	0.0037	0.1941	2.248	137.2	99.7	67.689	0.030
24	2.25	24.32	0.0036	14.91	1.220	140.9	81.7	67.813	0.068
77	2.25	19.91	0.0047	0.0559	1.607	108.4	99.9	67.864	0.034
79	2.25	19.95	0.0037	0.0983	1.611	136.5	99.9	67.940	0.023
09	2.25	20.00	0.0030	0.2682	1.675	167.7	99.6	67.943	0.034
105	2.25	19.94	0.0032	0.0604	3.054	158.2	99.9	67.966	0.021
62	2.25	19.96	0.0045	0.1236	2.362	112.9	99.8	67.970	0.023
66	2.25	19.96	0.0032	0.0753	1.790	160.5	99.9	68.000	0.021
87	2.25	19.96	0.0041	0.0662	3.347	125.4	99.9	68.009	0.019
51	2.25	19.98	0.0053	0.0974	1.720	95.8	99.9	68.041	0.032
04	2.25	20.01	0.0030	0.2000	1.407	170.4	99.7	68.048	0.040
85	2.25	19.97	0.0028	0.0813	1.544	179.6	99.9	68.049	0.037
53	2.25	19.99	0.0031	0.0908	1.112	162.3	99.9	68.090	0.047

ID	Power (Watts)	$^{40}Ar/^{39}Ar$	$^{37}Ar/^{39}Ar$	$^{36}Ar/^{39}Ar$ (x 10^{-3})	$^{39}Ar_K$ (x10^{-15} mol)	K/Ca	$^{40}Ar^*$ (%)	Age (Ma)	±1σ (Ma)
48	2.25	19.98	0.0039	0.0635	3.854	131.6	99.9	68.101	0.020
34	2.25	20.01	0.0151	0.1499	2.037	33.7	99.8	68.103	0.029
68	2.25	20.11	0.0134	0.4436	2.209	38.1	99.3	68.139	0.019
115	2.25	20.01	0.0039	0.0684	4.427	129.9	99.9	68.174	0.012
109	2.25	20.01	0.0029	0.0472	3.015	176.6	99.9	68.190	0.022
64	2.25	20.01	0.0029	0.0468	2.321	175.9	99.9	68.200	0.028
122	2.25	20.02	0.0040	0.0390	3.736	128.0	99.9	68.241	0.013
112	2.25	20.02	0.0038	0.0278	3.601	132.5	100.0	68.253	0.018
106	2.25	20.03	0.0037	0.0497	2.101	136.1	99.9	68.262	0.026
73	2.25	20.05	0.0046	0.1149	1.481	110.3	99.8	68.269	0.038
101	2.25	20.07	0.0036	0.1004	4.439	142.2	99.9	68.356	0.016
113	2.25	20.21	0.0034	0.0301	2.270	150.7	100.0	68.883	0.033
69	2.25	20.27	0.0049	0.1557	2.250	103.6	99.8	68.981	0.077
14	2.25	20.44	0.0108	0.6570	1.185	47.1	99.0	69.04	0.13
11	2.25	20.36	0.0050	0.2834	1.735	102.1	99.6	69.136	0.070
60	2.25	20.38	0.0019	0.3362	0.767	275.5	99.5	69.15	0.20
50	2.25	20.36	0.0042	0.1720	3.652	122.5	99.7	69.252	0.083
13	2.25	20.38	0.0069	0.1182	1.772	74.0	99.8	69.36	0.10
57	2.25	20.46	0.0087	0.4079	1.195	58.4	99.4	69.37	0.14
110	2.25	20.38	0.0048	0.1141	4.770	105.7	99.8	69.368	0.047
42	2.25	20.43	0.0022	0.2276	1.224	235.4	99.7	69.43	0.13
06	2.25	20.41	0.0041	0.1154	2.551	125.2	99.8	69.475	0.070
97	2.25	20.51	0.0064	0.3384	1.024	79.5	99.5	69.59	0.20
111	2.25	20.55	0.0057	0.4367	1.794	90.0	99.4	69.624	0.100
63	2.25	20.49	0.0040	0.1592	1.608	127.4	99.8	69.69	0.11

ID	Power (Watts)	$^{40}Ar/^{39}Ar$	$^{37}Ar/^{39}Ar$	$^{36}Ar/^{39}Ar$ (x 10^{-3})	$^{39}Ar_K$ (x10^{-15} mol)	K/Ca	$^{40}Ar^*$ (%)	Age (Ma)	±1σ (Ma)
104	2.25	20.52	0.0042	0.2386	6.194	121.2	99.7	69.711	0.065
16	2.25	20.57	0.0045	0.0698	4.987	113.0	99.9	70.067	0.047
90	2.25	21.48	0.0097	0.1982	1.095	52.4	99.7	72.98	0.13
78	2.25	21.57	0.0124	0.1995	1.564	41.2	99.7	73.29	0.15
49	2.25	21.62	0.0104	0.3327	1.074	48.9	99.5	73.30	0.19
114	2.25	21.66	0.0069	0.1041	2.462	73.6	99.9	73.666	0.085
36	2.25	21.74	0.0104	0.2959	0.802	49.0	99.6	73.76	0.22
41	2.25	21.72	0.0113	0.2157	1.481	45.3	99.7	73.77	0.14
08	2.25	21.73	0.0071	0.2001	0.844	71.6	99.7	73.80	0.24
84	2.25	21.75	0.0069	0.2504	1.312	73.4	99.7	73.81	0.15
02	2.25	21.75	0.0101	0.2553	1.202	50.3	99.7	73.81	0.15
26	2.25	21.79	0.0095	0.3979	0.696	53.7	99.5	73.82	0.24
120	2.25	21.71	0.0032	0.1131	1.219	161.5	99.8	73.83	0.16
37	2.25	21.87	0.0055	0.6250	1.293	93.2	99.2	73.85	0.16
107	2.25	21.75	0.0044	0.2131	1.417	115.9	99.7	73.85	0.18
44	2.25	21.76	0.0062	0.2133	1.537	82.5	99.7	73.91	0.13
71	2.25	21.81	0.0117	0.3704	1.161	43.6	99.5	73.92	0.17
17	2.25	21.82	0.0127	0.3646	0.743	40.2	99.5	73.93	0.24
35	2.25	21.79	0.0056	0.2422	1.233	90.6	99.7	73.98	0.16
21	2.25	21.76	0.0151	0.1318	1.711	33.7	99.8	73.98	0.11
86	2.25	21.85	0.0093	0.3693	1.611	55.1	99.5	74.04	0.13
05	2.25	21.82	0.0103	0.2265	1.190	49.8	99.7	74.10	0.14
38	2.25	21.80	0.0075	0.0628	2.235	67.7	99.9	74.19	0.11
89	2.25	21.84	0.0124	0.1921	1.779	41.2	99.7	74.20	0.13
30	2.25	21.92	0.0055	0.3961	2.969	93.2	99.5	74.239	0.068

ID	Power (Watts)	$^{40}Ar/^{39}Ar$	$^{37}Ar/^{39}Ar$	$^{36}Ar/^{39}Ar$ (x 10^{-3})	$^{39}Ar_K$ (x10^{-15} mol)	K/Ca	$^{40}Ar^*$ (%)	Age (Ma)	±1σ (Ma)
19	2.25	21.84	0.0020	0.0872	2.333	258.0	99.9	74.275	0.098
54	2.25	21.86	0.0052	0.1627	2.528	97.2	99.8	74.280	0.085
27	2.25	21.85	0.0055	0.1069	1.813	93.1	99.9	74.31	0.12
76	2.25	21.88	0.0074	0.1834	3.016	68.5	99.8	74.323	0.062
33	2.25	21.86	0.0047	0.1321	3.116	109.0	99.8	74.324	0.072
12	2.25	21.85	0.0038	0.0902	5.662	133.9	99.9	74.33	0.12
03	2.25	21.89	0.0141	0.1980	1.879	36.3	99.7	74.36	0.12
96	2.25	21.89	0.0068	0.1273	4.304	74.8	99.8	74.401	0.052
72	2.25	21.88	0.0062	0.0648	3.581	81.8	99.9	74.455	0.083
58	2.25	21.94	0.0135	0.2462	1.131	37.9	99.7	74.47	0.16
94	2.25	21.94	0.0069	0.1919	1.808	74.4	99.7	74.51	0.13
74	2.25	21.95	0.0097	0.1631	1.930	52.4	99.8	74.57	0.10
121	2.25	21.95	0.0049	0.0815	2.548	103.6	99.9	74.66	0.10
10	2.25	21.97	0.0067	0.1039	1.434	76.5	99.9	74.72	0.13
83	2.25	22.04	0.0106	0.3036	2.573	48.3	99.6	74.733	0.074
47	2.25	21.99	0.0052	0.0599	4.859	98.0	99.9	74.824	0.061
07	2.25	22.07	0.0062	0.1488	2.970	82.1	99.8	74.994	0.054
15	2.25	22.13	0.0009	0.3097	0.863	596.4	99.6	75.04	0.24
52	2.25	22.12	0.0055	0.2555	2.205	93.0	99.7	75.052	0.079
29	2.25	22.16	0.0024	0.2548	1.113	214.9	99.7	75.18	0.17
56	2.25	22.21	0.0110	0.3233	0.652	46.2	99.6	75.30	0.22
28	2.25	22.29	0.0068	0.1905	1.197	75.2	99.7	75.70	0.17
119	2.25	22.30	0.0046	0.1277	1.468	111.6	99.8	75.77	0.12
117	2.25	22.29	0.0056	0.0827	2.568	90.5	99.9	75.779	0.084
88	2.25	22.38	0.0121	0.4182	1.197	42.2	99.4	75.78	0.16

ID	Power (Watts)	$^{40}Ar/^{39}Ar$	$^{37}Ar/^{39}Ar$	$^{36}Ar/^{39}Ar$ (x 10^{-3})	$^{39}Ar_K$ (x10^{-15} mol)	K/Ca	$^{40}Ar^*$ (%)	Age (Ma)	±1σ (Ma)
59	2.25	22.32	0.0072	0.1113	2.933	70.5	99.9	75.862	0.063
23	2.25	22.36	0.0071	0.1497	2.344	72.0	99.8	75.975	0.093
98	2.25	22.75	0.0255	0.9124	0.344	20.0	98.8	76.53	0.50
22	2.25	22.62	0.0083	0.3175	1.418	61.6	99.6	76.66	0.17
31	2.25	22.69	0.0023	0.4410	0.637	218.8	99.4	76.76	0.32
108	2.25	22.97	0.0091	0.1354	1.682	56.4	99.8	78.02	0.10
81	2.25	24.46	0.0063	0.2063	1.538	81.2	99.8	82.88	0.15
103	2.25	28.40	0.0062	0.2176	1.748	82.4	99.8	95.92	0.14
118	2.25	58.86	0.0081	0.6535	0.962	62.9	99.7	193.35	0.42
39	2.25	59.63	0.0070	1.987	1.823	73.1	99.0	194.52	0.31
95	2.25	80.80	-0.0001	0.9651	2.155	-	99.6	260.46	0.56
43	2.25	97.20	0.0048	1.668	1.146	107.0	99.5	308.63	0.63
99	2.25	111.1	0.0023	0.6927	2.609	219.6	99.8	349.89	0.85
18	2.25	145.7	0.0017	0.7709	1.536	304.2	99.8	446.4	1.2
61	2.25	152.5	0.0228	2.289	1.068	22.4	99.6	463.7	2.9
01	2.25	156.7	-0.0061	0.6200	1.153	-	99.9	476.4	2.3
67	2.25	174.2	0.0037	1.770	1.417	138.1	99.7	521.7	1.1
82	2.25	177.2	0.0259	1.327	0.964	19.7	99.8	530.0	3.4
45	2.25	178.6	0.0038	1.001	1.249	135.8	99.8	533.8	2.4
75	2.25	187.0	0.0116	0.9553	0.916	43.9	99.8	555.5	2.1
20	2.25	257.1	0.0115	1.467	0.811	44.3	99.8	726.9	4.5
100	2.25	263.1	0.0056	0.7976	1.020	91.6	99.9	741.3	2.7
40	2.25	283.2	0.0036	2.461	0.606	139.8	99.7	786.2	5.2
70	2.25	307.3	-0.0121	2.797	0.130	-	99.7	839.6	8.2
116	2.25	321.0	0.0420	1.772	0.098	12.2	99.8	870.2	10.6

ID	Power (Watts)	$^{40}Ar/^{39}Ar$	$^{37}Ar/^{39}Ar$	$^{36}Ar/^{39}Ar$ (x 10^{-3})	$^{39}Ar_K$ (x10^{-15} mol)	K/Ca	$^{40}Ar^*$ (%)	Age (Ma)	±1σ (Ma)
80	2.25	331.2	-0.0037	2.612	0.656	-	99.8	891.7	4.8
93	2.25	339.1	0.0483	1.134	0.107	10.6	99.9	909.4	10.7
65	2.25	388.9	0.0200	1.048	0.549	25.5	99.9	1011.8	5.7
102	2.25	392.4	0.0145	0.2143	0.726	35.2	100.0	1019.3	4.8
55	2.25	401.8	0.0312	0.7278	0.689	16.4	99.9	1037.6	4.0
46	2.25	435.4	0.0052	4.278	0.587	97.4	99.7	1100.7	6.3
32	2.25	625.3	0.0233	0.4764	0.136	21.9	100.0	1432.7	12.8
MDA			n=1					67.378	0.028
A16-BTW-MH2, DetritalSanidine, J=0.001882±0.03%, IC=1.002513±0.0006418, NM-293F, Lab#=66036, Argus VI									
62	4	19.48	0.0186	1.192	0.054	27.5	98.2	64.72	0.71
50	4	19.28	-0.0081	0.3190	0.198	-	99.5	64.90	0.20
57	4	25.20	0.0045	20.31	0.070	113.5	76.2	64.95	0.77
23	3	19.33	0.0005	0.3239	0.261	1076.6	99.5	65.055	0.099
27	3	19.62	0.0072	1.283	0.114	70.5	98.1	65.09	0.47
35	3	19.38	0.0112	0.4533	0.141	45.4	99.3	65.12	0.29
04	3	19.40	0.0030	0.3145	1.615	170.1	99.5	65.295	0.030
10	3	19.41	0.0146	0.3625	0.291	34.8	99.5	65.30	0.21
11	3	19.41	0.0035	0.2087	0.833	146.3	99.7	65.430	0.033
08	3	19.43	-0.0009	0.2206	0.502	-	99.7	65.481	0.085
05	3	19.41	0.0048	0.1442	1.180	105.6	99.8	65.491	0.039
54	4	19.86	-0.0021	1.644	0.052	-	97.6	65.53	0.94
01	3	19.41	-0.0014	0.1139	0.491	-	99.8	65.549	0.087
36	4	20.33	0.0690	1.839	0.081	7.4	97.4	66.9	1.3
34	3	20.20	0.0134	1.187	0.055	38.2	98.3	67.1	1.7

ID	Power (Watts)	$^{40}Ar/^{39}Ar$	$^{37}Ar/^{39}Ar$	$^{36}Ar/^{39}Ar$ (x 10^{-3})	$^{39}Ar_K$ (x10^{-15} mol)	K/Ca	$^{40}Ar^*$ (%)	Age (Ma)	±1σ (Ma)
19	3	20.07	-0.0070	0.7137	0.157	-	98.9	67.13	0.28
28	3	20.82	0.0191	3.156	0.026	26.8	95.5	67.2	2.1
59	4	20.18	-0.0099	0.3475	0.291	-	99.5	67.86	0.18
71	4	20.57	0.0783	1.586	0.053	6.5	97.8	68.0	1.3
89	4	20.30	0.0184	0.5616	0.072	27.7	99.2	68.05	0.50
22	3	20.46	0.0223	0.9566	0.142	22.9	98.6	68.20	0.67
60	4	20.44	-0.0312	0.8023	0.158	-	98.8	68.26	0.77
82	4	20.75	0.0647	1.654	0.048	7.9	97.7	68.5	2.2
44	4	20.67	0.1737	1.329	0.049	2.9	98.2	68.6	1.0
16	3	20.66	0.0125	1.168	0.552	40.8	98.3	68.6	1.0
02	3	20.44	0.0018	0.2231	0.777	287.1	99.7	68.83	0.21
42	4	20.77	0.0530	0.8285	0.087	9.6	98.8	69.4	1.1
86	4	21.77	0.0554	2.203	0.067	9.2	97.0	71.3	2.1
72	4	22.14	0.0805	2.356	0.104	6.3	96.9	72.4	1.5
03	3	22.03	0.0042	0.2523	0.762	122.5	99.7	74.10	0.20
69	4	28.71	0.1216	3.569	0.075	4.2	96.4	92.9	2.4
17	3	32.50	0.0505	1.538	0.199	10.1	98.6	107.19	1.00
38	4	34.26	0.0368	1.853	0.059	13.9	98.4	112.6	2.8
48	4	45.59	0.0901	2.310	0.095	5.7	98.5	148.5	2.9
78	4	46.89	0.1229	2.464	0.070	4.2	98.5	152.5	4.2
64	4	49.08	0.2649	4.148	0.046	1.9	97.6	157.9	6.5
46	4	54.21	0.0201	3.690	0.112	25.4	98.0	174.4	2.6
56	4	57.15	0.1123	5.124	0.046	4.5	97.4	182.3	7.2
93	4	58.75	0.1616	2.206	0.077	3.2	98.9	190.0	4.7
90	4	63.14	-0.0193	1.018	0.151	-	99.5	204.6	2.4

ID	Power (Watts)	$^{40}Ar/^{39}Ar$	$^{37}Ar/^{39}Ar$	$^{36}Ar/^{39}Ar$ (x 10^{-3})	$^{39}Ar_K$ (x10^{-15} mol)	K/Ca	$^{40}Ar^*$ (%)	Age (Ma)	±1σ (Ma)
30	3	64.90	0.0794	3.063	0.090	6.4	98.6	208.2	4.0
45	4	67.95	0.0591	0.5394	0.076	8.6	99.8	219.8	5.3
66	4	70.62	0.0127	2.378	0.106	40.2	99.0	226.3	3.2
29	3	72.05	0.1393	2.382	0.082	3.7	99.0	230.7	5.7
52	4	77.85	-0.0923	1.907	0.091	-	99.3	248.5	5.7
94	4	80.18	-0.0662	2.288	0.055	-	99.2	255.2	9.1
77	4	84.89	0.1160	2.524	0.086	4.4	99.1	269.1	5.7
24	3	84.52	0.0583	1.054	0.222	8.8	99.6	269.3	2.5
67	4	99.28	0.1925	5.726	0.071	2.6	98.3	308.7	7.6
06	3	108.7	0.0001	0.9090	0.741	4777.2	99.8	339.92	0.85
21	3	108.9	0.0151	1.208	0.372	33.8	99.7	340.2	2.1
58	4	127.4	0.0239	3.449	0.143	21.4	99.2	390.5	5.1
84	4	149.5	0.0971	2.529	0.081	5.3	99.5	451.9	11.0
83	4	174.6	0.0800	1.665	0.089	6.4	99.7	518.9	10.5
73	4	191.8	-0.0032	2.097	0.079	-	99.7	562.6	8.7
20	3	193.6	0.0103	1.256	0.195	49.5	99.8	567.8	6.7
65	4	211.5	0.0241	1.567	0.105	21.2	99.8	612.1	9.0
92	4	230.2	-0.0584	2.568	0.054	-	99.7	656.9	17.2
47	4	240.0	-0.0375	1.382	0.105	-	99.8	681.2	11.7
18	3	253.0	0.0180	0.5593	0.429	28.3	99.9	712.6	2.8
95	4	300.2	0.0519	2.927	0.067	9.8	99.7	817.9	25.6
95	4	300.2	0.0519	2.927	0.067	9.8	99.7	818.0	25.6
31	3	312.0	0.2468	4.494	0.053	2.1	99.6	842.9	20.7
39	3	407.6	0.1413	1.304	0.087	3.6	99.9	1041.5	18.2
87	4	433.0	0.3098	2.880	0.047	1.6	99.8	1089.7	31.3

ID	Power (Watts)	$^{40}Ar/^{39}Ar$	$^{37}Ar/^{39}Ar$	$^{36}Ar/^{39}Ar$ (x 10^{-3})	$^{39}Ar_K$ (x10^{-15} mol)	K/Ca	$^{40}Ar^*$ (%)	Age (Ma)	±1σ (Ma)
88	4	442.1	0.1372	2.439	0.044	3.7	99.8	1107.0	33.2
MDA			n=13	MSWD=3.53				65.38	0.04
A16-BTW-MH5, DetritalSanidine, J=0.0018926±0.02%, IC=1.002498±0.0007094, NM-293D, Lab#=65995, Argus VI									
144	2.5	19.40	0.0167	1.506	0.316	30.5	97.7	64.48	0.16
08	2.25	19.16	0.0047	0.0686	1.741	107.6	99.9	65.099	0.031
39	2.25	19.19	0.0038	0.0721	1.495	133.1	99.9	65.199	0.035
123	3	19.46	0.0099	0.8868	0.677	51.8	98.6	65.307	0.054
85	3	19.36	0.0038	0.2765	1.840	135.5	99.6	65.552	0.029
104	3	19.35	0.0037	0.2712	2.274	138.1	99.6	65.553	0.026
127	3	19.40	0.0026	0.3403	1.620	195.9	99.5	65.653	0.034
120	3	20.07	0.0145	1.163	0.789	35.1	98.3	67.06	0.17
106	3	20.07	0.0006	0.9398	0.817	864.3	98.6	67.28	0.18
119	3	20.08	0.0013	0.8347	0.795	378.9	98.8	67.43	0.17
67	2.25	19.91	0.0022	0.2048	0.607	226.8	99.7	67.48	0.12
131	3	20.09	0.0073	0.7259	1.122	70.1	98.9	67.55	0.13
05	2.25	19.93	0.0037	0.1029	1.682	137.0	99.8	67.629	0.023
60	2.25	19.94	0.0023	0.1480	0.757	224.1	99.8	67.632	0.060
23	2.25	19.93	0.0060	0.1014	1.186	85.7	99.9	67.634	0.057
20	2.25	19.93	0.0063	0.0917	2.226	80.9	99.9	67.657	0.054
11	2.25	19.92	0.0025	0.0528	1.671	204.6	99.9	67.669	0.035
59	2.25	19.92	0.0057	0.0397	1.329	89.6	99.9	67.674	0.055
10	2.25	19.94	0.0039	0.0989	2.203	129.6	99.9	67.684	0.080
46	2.25	19.93	0.0047	0.0539	2.002	108.1	99.9	67.685	0.030
36	2.25	19.94	0.0051	0.1045	1.283	99.9	99.8	67.691	0.062

ID	Power (Watts)	$^{40}Ar/^{39}Ar$	$^{37}Ar/^{39}Ar$	$^{36}Ar/^{39}Ar$ (x 10^{-3})	$^{39}Ar_K$ (x10^{-15} mol)	K/Ca	$^{40}Ar^*$ (%)	Age (Ma)	±1σ (Ma)
33	2.25	19.97	0.0052	0.1704	0.632	97.4	99.7	67.697	0.070
138	2.5	20.15	0.0139	0.8079	0.719	36.7	98.8	67.70	0.15
32	2.25	19.96	0.0044	0.1646	2.029	115.3	99.8	67.700	0.058
101	3	20.08	0.0064	0.5253	1.549	80.1	99.2	67.71	0.13
12	2.25	19.95	0.0044	0.0767	3.133	116.9	99.9	67.727	0.033
51	2.25	19.96	0.0044	0.1115	1.244	115.3	99.8	67.734	0.086
74	2.25	19.95	0.0052	0.0869	1.607	97.4	99.9	67.738	0.078
61	2.25	19.95	0.0037	0.0721	1.323	136.8	99.9	67.739	0.042
17	2.25	19.97	0.0056	0.1344	3.824	91.8	99.8	67.750	0.038
126	3	20.08	0.0090	0.5003	1.881	56.8	99.3	67.75	0.11
43	2.25	19.95	0.0056	0.0417	2.294	91.2	99.9	67.760	0.047
42	2.25	20.01	0.0031	0.2389	2.882	166.4	99.6	67.764	0.063
117	3	20.01	0.0066	0.2185	3.445	77.6	99.7	67.802	0.064
29	2.25	19.98	0.0040	0.0761	1.009	129.1	99.9	67.839	0.085
70	2.25	19.98	0.0047	0.0405	3.846	109.7	99.9	67.860	0.047
145	2.5	20.02	0.0030	0.1489	4.128	171.4	99.8	67.886	0.033
37	2.25	20.02	0.0113	0.1489	1.383	45.1	99.8	67.89	0.12
58	2.25	20.05	0.0028	0.1833	0.542	181.2	99.7	67.956	0.098
143	2.5	20.08	-0.0002	0.2448	1.882	-	99.6	68.012	0.067
129	3	20.15	0.0005	0.4491	1.783	1047.0	99.3	68.04	0.11
134	2.5	20.10	0.0000	0.2383	2.420	24767.2	99.6	68.064	0.055
28	2.25	20.04	0.0038	0.0486	5.163	134.6	99.9	68.070	0.035
90	3	20.19	0.0027	0.5235	1.298	186.1	99.2	68.079	0.042
81	2.25	20.07	0.0057	0.1408	0.910	88.9	99.8	68.08	0.14
92	3	20.17	0.0036	0.4343	1.776	141.5	99.4	68.107	0.030

ID	Power (Watts)	$^{40}Ar/^{39}Ar$	$^{37}Ar/^{39}Ar$	$^{36}Ar/^{39}Ar$ (x 10^{-3})	$^{39}Ar_K$ (x10^{-15} mol)	K/Ca	$^{40}Ar^*$ (%)	Age (Ma)	±1σ (Ma)
89	3	20.16	0.0042	0.3801	5.133	120.4	99.4	68.141	0.015
84	3	20.11	0.0036	0.1802	3.213	141.0	99.7	68.162	0.020
73	2.25	20.19	0.0079	0.1345	1.766	64.8	99.8	68.48	0.11
65	2.25	20.41	0.0306	0.5647	0.284	16.7	99.2	68.80	0.36
72	2.25	20.35	0.0040	0.0873	3.483	127.9	99.9	69.073	0.071
69	2.25	20.47	0.0082	0.1247	2.815	62.4	99.8	69.417	0.074
52	2.25	20.48	0.0057	0.1330	1.717	89.0	99.8	69.443	0.082
109	3	20.67	0.0004	0.6890	1.069	1308.6	99.0	69.53	0.18
107	3	20.67	0.0089	0.4796	1.606	57.1	99.3	69.74	0.11
63	2.25	20.90	0.0220	1.251	0.106	23.2	98.2	69.7	1.2
62	2.25	20.59	0.0033	0.1589	1.419	154.4	99.8	69.786	0.094
25	2.25	20.57	0.0025	0.0766	4.823	207.8	99.9	69.810	0.041
111	3	20.65	0.0089	0.1675	3.257	57.0	99.8	69.978	0.056
115	3	20.77	0.0066	0.4938	1.684	77.2	99.3	70.06	0.16
93	3	20.81	0.0033	0.4248	1.432	156.5	99.4	70.272	0.038
113	3	20.89	0.0035	0.4317	1.554	146.0	99.4	70.52	0.11
132	3	21.78	0.0312	2.219	0.345	16.4	97.0	71.72	0.55
47	2.25	21.40	0.0075	0.5765	0.481	68.1	99.2	72.09	0.33
128	3	21.77	0.0127	1.633	0.356	40.3	97.8	72.25	0.51
18	2.25	21.46	0.0050	0.2547	0.861	102.4	99.6	72.60	0.18
04	2.25	21.55	0.0198	0.3301	1.233	25.8	99.6	72.81	0.46
125	3	21.76	0.0126	0.5166	1.545	40.6	99.3	73.33	0.13
30	2.25	21.70	0.0143	0.3086	0.662	35.7	99.6	73.34	0.22
21	2.25	21.64	0.0081	0.0746	3.539	63.1	99.9	73.387	0.056
38	2.25	21.80	0.0323	0.5767	0.344	15.8	99.2	73.43	0.45

ID	Power (Watts)	$^{40}Ar/^{39}Ar$	$^{37}Ar/^{39}Ar$	$^{36}Ar/^{39}Ar$ (x 10^{-3})	$^{39}Ar_K$ (x10^{-15} mol)	K/Ca	$^{40}Ar^*$ (%)	Age (Ma)	±1σ (Ma)
57	2.25	21.66	0.0064	0.0724	2.134	79.8	99.9	73.431	0.075
27	2.25	21.82	0.0182	0.5564	0.385	28.1	99.2	73.50	0.33
53	2.25	21.81	0.0116	0.3577	0.627	44.0	99.5	73.65	0.20
91	3	21.96	0.0080	0.7950	0.761	63.8	98.9	73.711	0.074
07	2.25	21.76	0.0054	0.0873	2.509	94.6	99.9	73.763	0.086
75	2.25	21.76	0.0028	0.0950	1.836	185.3	99.9	73.768	0.078
26	2.25	21.78	0.0080	0.1353	1.645	63.5	99.8	73.77	0.11
116	3	22.02	0.0091	0.9163	1.422	56.0	98.8	73.79	0.14
64	2.25	21.76	0.0029	0.0700	2.429	177.4	99.9	73.791	0.097
22	2.25	21.77	0.0083	0.1012	1.164	61.2	99.9	73.80	0.12
140	2.5	21.85	0.0051	0.3192	1.502	101.0	99.6	73.824	0.090
19	2.25	21.81	0.0064	0.1758	1.594	80.1	99.8	73.83	0.12
15	2.25	21.78	0.0038	0.0681	4.284	132.9	99.9	73.840	0.049
56	2.25	21.84	0.0120	0.2115	0.892	42.5	99.7	73.92	0.17
88	3	21.85	0.0075	0.1850	3.171	68.0	99.8	73.966	0.021
66	2.25	21.83	0.0082	0.1224	1.872	62.0	99.8	73.974	0.096
31	2.25	21.85	0.0025	0.1537	1.872	203.0	99.8	73.977	0.087
105	3	21.89	0.0067	0.3026	2.201	75.7	99.6	73.997	0.098
137	2.5	21.90	0.0070	0.3081	1.475	73.2	99.6	74.008	0.080
48	2.25	21.83	0.0059	0.0795	1.422	86.2	99.9	74.01	0.13
68	2.25	21.83	0.0108	0.0730	1.450	47.1	99.9	74.01	0.13
100	3	21.94	0.0088	0.4107	1.963	57.8	99.4	74.04	0.10
98	3	22.02	0.0031	0.6149	1.043	164.4	99.2	74.10	0.18
80	2.25	21.86	0.0058	0.0571	3.552	87.5	99.9	74.137	0.045
02	2.25	21.93	0.0059	0.2201	3.308	86.6	99.7	74.19	0.19

ID	Power (Watts)	$^{40}Ar/^{39}Ar$	$^{37}Ar/^{39}Ar$	$^{36}Ar/^{39}Ar$ (x 10^{-3})	$^{39}Ar_K$ (x10^{-15} mol)	K/Ca	$^{40}Ar^*$ (%)	Age (Ma)	±1σ (Ma)
135	2.5	22.35	0.0648	1.635	0.289	7.9	97.8	74.21	0.37
77	2.25	22.00	0.0054	0.4363	0.513	94.1	99.4	74.22	0.35
142	2.5	22.32	0.0407	1.477	0.315	12.5	98.0	74.28	0.35
139	2.5	22.03	0.0092	0.4374	1.191	55.8	99.4	74.314	0.088
97	3	21.98	0.0043	0.2081	2.554	118.9	99.7	74.388	0.025
118	3	22.10	0.0096	0.5894	1.392	53.4	99.2	74.41	0.14
112	3	22.05	0.0051	0.3852	1.575	99.9	99.5	74.42	0.13
01	2.25	22.21	0.0027	0.8888	0.557	187.5	98.8	74.46	0.92
16	2.25	22.05	0.0070	0.2626	1.647	72.5	99.6	74.55	0.13
79	2.25	22.04	0.0081	0.1547	1.039	63.0	99.8	74.63	0.16
121	3	22.08	0.0086	0.2816	2.088	59.4	99.6	74.649	0.097
41	2.25	22.09	0.0132	0.2676	0.814	38.7	99.6	74.67	0.22
49	2.25	22.13	-0.0064	0.3710	0.534	-	99.5	74.71	0.28
24	2.25	22.18	0.0224	0.4863	0.469	22.8	99.4	74.78	0.30
44	2.25	22.13	0.0086	0.2300	1.174	59.1	99.7	74.85	0.13
95	3	22.18	0.0035	0.4029	1.392	144.7	99.5	74.859	0.040
78	2.25	22.13	0.0012	0.1755	1.110	420.2	99.8	74.89	0.11
87	3	22.17	0.0029	0.3346	1.695	174.4	99.6	74.889	0.037
86	3	22.29	0.0071	0.4992	1.063	71.5	99.3	75.126	0.052
103	3	22.46	0.0309	1.015	0.688	16.5	98.7	75.19	0.22
14	2.25	22.23	0.0104	0.1625	2.046	49.1	99.8	75.260	0.088
102	3	22.38	0.0208	0.6607	1.185	24.5	99.1	75.26	0.14
34	2.25	22.26	0.0055	0.2142	1.166	92.4	99.7	75.31	0.15
108	3	22.35	0.0035	0.4180	1.609	147.7	99.4	75.39	0.11
54	2.25	22.26	0.0044	0.1141	2.001	115.2	99.8	75.403	0.088

ID	Power (Watts)	$^{40}Ar/^{39}Ar$	$^{37}Ar/^{39}Ar$	$^{36}Ar/^{39}Ar$ (x 10^{-3})	$^{39}Ar_K$ (x10^{-15} mol)	K/Ca	$^{40}Ar^*$ (%)	Age (Ma)	±1σ (Ma)
96	3	22.35	0.0051	0.3834	1.661	99.8	99.5	75.420	0.035
94	3	22.33	0.0054	0.3104	1.947	94.3	99.6	75.449	0.033
50	2.25	22.29	0.0108	0.1463	1.303	47.2	99.8	75.47	0.13
06	2.25	22.32	0.0084	0.1769	1.159	60.7	99.8	75.54	0.15
110	3	22.49	0.0182	0.7070	0.803	28.1	99.1	75.57	0.25
130	3	22.42	0.0118	0.4553	1.189	43.4	99.4	75.59	0.16
09	2.25	22.43	0.0089	0.4710	1.881	57.4	99.4	75.615	0.089
141	2.5	22.44	0.0158	0.4269	1.109	32.2	99.4	75.68	0.10
45	2.25	22.34	0.0081	0.1006	1.537	62.7	99.9	75.687	0.094
13	2.25	22.35	0.0076	0.1330	1.586	66.9	99.8	75.687	0.099
40	2.25	22.39	0.0091	0.1026	1.530	56.3	99.9	75.83	0.10
83	2.25	22.43	0.0055	0.0749	3.118	93.5	99.9	75.998	0.074
114	3	22.53	0.0076	0.3318	1.900	67.5	99.6	76.07	0.13
99	3	22.59	0.0086	0.2897	2.624	59.0	99.6	76.308	0.077
122	3	23.07	0.0257	0.8771	0.779	19.8	98.9	77.35	0.22
76	2.25	22.88	0.0107	0.0724	1.296	47.8	99.9	77.50	0.11
124	3	23.04	0.0056	0.5630	1.254	91.6	99.3	77.53	0.19
55	2.25	22.96	0.0105	0.1878	1.179	48.4	99.8	77.65	0.14
35	2.25	23.85	0.0079	0.1331	2.565	65.0	99.8	80.651	0.060
146	2.5	24.22	-0.0020	0.8620	0.693	-	98.9	81.15	0.18
82	2.25	26.97	0.0150	0.1291	1.155	33.9	99.9	90.98	0.16
03	2.25	29.68	0.0064	1.121	1.372	79.8	98.9	98.91	0.60
71	2.25	36.07	0.0222	0.3509	0.523	23.0	99.7	120.53	0.55
MDA			n=3	MSWD=6.16				65.17	0.06

ID	Power (Watts)	$^{40}Ar/^{39}Ar$	$^{37}Ar/^{39}Ar$	$^{36}Ar/^{39}Ar$ (x 10^{-3})	$^{39}Ar_K$ (x10^{-15} mol)	K/Ca	$^{40}Ar^*$ (%)	Age (Ma)	±1σ (Ma)
A16-BTW-MH6, DetritalSanidine, J=0.0018989±0.03%, IC=1.001373±0.0009222, NM-293D, Lab#=65994, Argus VI									
58	2.25	20.11	0.0024	2.022	0.117	214.2	97.0	66.54	0.35
78	2.25	20.08	0.0175	1.236	0.209	29.1	98.2	67.25	0.21
79	2.25	20.17	0.0008	1.214	0.227	616.6	98.2	67.57	0.19
37	2.25	21.44	-0.0084	5.355	0.045	-	92.6	67.69	0.60
65	2.25	19.98	0.0040	0.2662	1.148	128.0	99.6	67.875	0.057
49	2.25	20.00	0.0037	0.2470	1.608	136.5	99.6	67.945	0.092
47	2.25	19.99	0.0053	0.2187	1.725	96.5	99.7	67.967	0.025
03	2.25	20.02	0.0049	0.2211	1.217	104.2	99.7	68.037	0.074
12	2.25	20.04	-0.0002	0.2661	1.102	-	99.6	68.08	0.11
01	2.25	20.10	0.0027	0.3908	0.841	189.6	99.4	68.155	0.090
99	2.25	20.74	0.0357	2.339	0.099	14.3	96.7	68.37	0.66
109	2.25	20.41	0.0169	0.8425	0.279	30.2	98.8	68.75	0.25
80	2.25	20.33	0.0014	0.1955	1.892	363.9	99.7	69.099	0.082
66	2.25	20.44	0.0148	0.5504	0.651	34.4	99.2	69.14	0.26
81	2.25	21.41	-0.0388	3.529	0.112	-	95.1	69.40	0.86
113	2.25	22.45	-0.0002	6.966	0.028	-	90.8	69.5	1.8
72	2.25	20.56	0.0108	0.4977	1.394	47.1	99.3	69.58	0.14
61	2.25	21.46	0.0195	3.417	0.126	26.2	95.3	69.7	1.4
04	2.25	21.68	0.0573	4.142	0.087	8.9	94.3	69.7	1.2
115	2.25	21.09	0.0913	2.174	0.129	5.6	97.0	69.7	1.3
08	2.25	21.02	0.0257	1.702	0.225	19.9	97.6	69.92	0.74
118	2.25	21.26	0.0058	2.487	0.192	88.6	96.5	69.93	0.86
21	2.25	22.06	0.0404	5.206	0.070	12.6	93.0	69.9	1.8
98	2.25	21.38	-0.0164	2.633	0.161	-	96.3	70.19	0.78

ID	Power (Watts)	$^{40}Ar/^{39}Ar$	$^{37}Ar/^{39}Ar$	$^{36}Ar/^{39}Ar$ (x 10^{-3})	$^{39}Ar_K$ (x10^{-15} mol)	K/Ca	$^{40}Ar^*$ (%)	Age (Ma)	±1σ (Ma)
62	2.25	21.68	0.0803	3.482	0.089	6.4	95.2	70.4	1.4
112	2.25	21.29	-0.0281	2.123	0.125	-	97.0	70.41	0.89
60	2.25	22.66	0.0093	6.466	0.041	55.1	91.5	70.7	1.5
45	2.25	21.73	0.0274	3.183	0.093	18.6	95.6	70.8	1.4
09	2.25	21.64	0.0359	2.827	0.134	14.2	96.1	70.9	1.1
73	2.25	21.48	0.0612	2.312	0.143	8.3	96.8	70.88	0.94
114	2.25	21.66	0.0165	2.450	0.157	30.9	96.6	71.3	1.1
89	2.25	21.34	-0.0152	1.185	0.243	-	98.3	71.50	0.65
121	2.25	21.62	0.0366	1.955	0.151	14.0	97.3	71.7	1.1
122	2.25	21.55	-0.0074	1.639	0.189	-	97.7	71.74	0.93
120	2.25	21.30	0.0321	0.7999	0.519	15.9	98.9	71.78	0.30
35	2.25	21.77	0.0190	2.188	0.173	26.8	97.0	71.95	0.76
117	2.25	22.13	0.0659	3.403	0.122	7.7	95.4	71.9	1.1
94	2.25	21.64	0.0189	1.690	0.183	27.0	97.7	72.00	0.83
07	2.25	21.75	0.0194	1.982	0.203	26.3	97.3	72.08	0.74
91	2.25	22.12	0.0237	3.057	0.134	21.5	95.9	72.2	1.1
70	2.25	21.47	0.0102	0.8724	0.454	50.1	98.8	72.25	0.44
84	2.25	21.65	-0.0065	1.469	0.290	-	98.0	72.27	0.45
101	2.25	21.74	0.0235	1.561	0.252	21.7	97.9	72.48	0.48
96	2.25	22.61	0.0258	4.278	0.062	19.8	94.4	72.7	1.7
75	2.25	21.94	0.0378	1.969	0.268	13.5	97.3	72.74	0.63
24	2.25	21.93	0.0123	1.886	0.230	41.4	97.4	72.78	0.65
10	2.25	21.90	0.0544	1.749	0.188	9.4	97.6	72.83	0.72
22	2.25	22.30	0.0363	3.058	0.126	14.0	95.9	72.9	1.2
56	2.25	21.82	-0.0126	1.403	0.217	-	98.1	72.88	0.73

ID	Power (Watts)	$^{40}Ar/^{39}Ar$	$^{37}Ar/^{39}Ar$	$^{36}Ar/^{39}Ar$ (x 10^{-3})	$^{39}Ar_K$ (x10^{-15} mol)	K/Ca	$^{40}Ar^*$ (%)	Age (Ma)	±1σ (Ma)
104	2.25	21.82	0.0255	1.328	0.296	20.0	98.2	72.96	0.55
57	2.25	21.83	0.0274	1.327	0.297	18.6	98.2	73.00	0.51
38	2.25	21.64	0.0004	0.6451	0.553	1276.5	99.1	73.03	0.25
67	2.25	21.65	0.0040	0.5730	0.719	129.1	99.2	73.14	0.29
93	2.25	21.96	0.0434	1.600	0.200	11.7	97.8	73.17	0.74
52	2.25	21.94	0.0240	1.475	0.207	21.2	98.0	73.23	0.68
119	2.25	21.74	0.0222	0.6705	0.375	23.0	99.1	73.36	0.50
107	2.25	21.94	0.0180	1.308	0.267	28.4	98.2	73.41	0.68
14	2.25	21.74	0.0026	0.6142	1.121	195.1	99.2	73.42	0.18
02	2.25	21.65	0.0061	0.2054	2.119	84.3	99.7	73.504	0.099
92	2.25	21.76	0.0049	0.5626	0.399	104.0	99.2	73.53	0.35
85	2.25	21.76	0.0077	0.5666	0.949	66.4	99.2	73.53	0.18
68	2.25	21.96	0.0148	1.158	0.312	34.5	98.4	73.62	0.53
05	2.25	21.72	0.0064	0.2694	1.608	79.7	99.6	73.70	0.11
110	2.25	22.40	0.0027	2.510	0.139	188.4	96.7	73.71	0.98
63	2.25	21.74	0.0108	0.3243	1.390	47.2	99.6	73.71	0.16
83	2.25	21.75	0.0073	0.3166	0.870	70.2	99.6	73.75	0.19
39	2.25	21.92	0.0379	0.6764	0.375	13.5	99.1	73.96	0.43
17	2.25	22.20	0.0116	1.539	1.220	43.9	97.9	74.02	0.15
108	2.25	21.91	0.0035	0.5818	0.430	147.5	99.2	74.02	0.36
30	2.25	21.88	0.0067	0.3416	1.603	76.5	99.5	74.16	0.12
31	2.25	21.97	0.0075	0.5919	0.519	68.2	99.2	74.19	0.32
11	2.25	21.88	0.0076	0.2884	1.273	67.2	99.6	74.20	0.14
25	2.25	21.88	0.0100	0.2884	1.741	51.0	99.6	74.21	0.10
87	2.25	22.03	0.0196	0.7669	0.483	26.0	99.0	74.24	0.30

ID	Power (Watts)	$^{40}Ar/^{39}Ar$	$^{37}Ar/^{39}Ar$	$^{36}Ar/^{39}Ar$ (x 10^{-3})	$^{39}Ar_K$ (x10^{-15} mol)	K/Ca	$^{40}Ar^*$ (%)	Age (Ma)	±1σ (Ma)
32	2.25	21.88	0.0044	0.2166	1.905	116.5	99.7	74.27	0.12
46	2.25	22.01	0.0067	0.5962	1.534	76.1	99.2	74.343	0.097
106	2.25	22.01	0.0169	0.5278	0.670	30.1	99.3	74.39	0.25
55	2.25	21.94	0.0060	0.2758	1.726	85.2	99.6	74.420	0.090
123	2.25	22.11	0.0150	0.7545	0.667	33.9	99.0	74.50	0.28
69	2.25	22.04	0.0102	0.5351	0.768	50.2	99.3	74.51	0.19
33	2.25	21.95	0.0051	0.1974	1.775	100.7	99.7	74.51	0.12
28	2.25	21.96	0.0075	0.2502	1.437	68.2	99.7	74.52	0.12
90	2.25	22.21	0.0232	1.047	0.312	22.0	98.6	74.56	0.60
42	2.25	22.18	0.0154	0.9040	0.425	33.1	98.8	74.58	0.41
50	2.25	22.11	0.0020	0.4245	0.689	256.8	99.4	74.83	0.28
43	2.25	22.15	0.0101	0.5288	0.609	50.7	99.3	74.88	0.21
53	2.25	22.05	0.0049	0.1840	1.983	103.6	99.8	74.89	0.12
29	2.25	22.44	-0.0080	1.387	0.261	-	98.2	74.97	0.61
27	2.25	22.20	0.0126	0.4632	0.746	40.5	99.4	75.09	0.26
71	2.25	22.35	0.0053	0.9262	0.353	96.4	98.8	75.14	0.52
34	2.25	22.43	0.0022	1.201	0.927	236.6	98.4	75.14	0.17
103	2.25	22.42	-0.0370	1.141	0.161	-	98.5	75.1	1.2
77	2.25	22.56	0.0405	1.615	0.192	12.6	97.9	75.15	0.90
116	2.25	22.33	0.0229	0.8302	0.275	22.3	98.9	75.18	0.63
105	2.25	22.27	0.0081	0.4168	0.870	63.1	99.4	75.38	0.15
88	2.25	22.32	0.0075	0.5724	0.609	68.0	99.2	75.39	0.30
13	2.25	22.27	0.0119	0.3891	0.928	42.9	99.5	75.41	0.20
59	2.25	22.37	0.0131	0.7003	1.040	38.9	99.1	75.42	0.23
74	2.25	22.44	0.0186	0.9329	0.430	27.4	98.8	75.44	0.41

ID	Power (Watts)	$^{40}Ar/^{39}Ar$	$^{37}Ar/^{39}Ar$	$^{36}Ar/^{39}Ar$ (x 10^{-3})	$^{39}Ar_K$ (x10^{-15} mol)	K/Ca	$^{40}Ar^*$ (%)	Age (Ma)	±1σ (Ma)
48	2.25	22.68	0.0018	1.677	0.604	283.2	97.8	75.49	0.28
44	2.25	22.40	0.0195	0.6903	0.613	26.1	99.1	75.55	0.32
54	2.25	22.39	0.0069	0.5095	0.866	74.1	99.3	75.69	0.18
15	2.25	22.44	0.0185	0.5857	0.426	27.6	99.2	75.78	0.31
64	2.25	22.36	0.0092	0.2616	1.380	55.3	99.7	75.82	0.15
41	2.25	22.56	0.0159	0.6857	0.508	32.0	99.1	76.08	0.37
06	2.25	22.44	0.0064	0.2108	1.545	79.2	99.7	76.15	0.15
26	2.25	23.24	0.0023	1.931	0.204	218.6	97.5	77.10	0.70
36	2.25	22.90	0.0088	0.2995	1.070	58.3	99.6	77.59	0.19
40	2.25	23.17	0.0172	0.7641	1.455	29.6	99.0	78.05	0.14
18	2.25	25.17	0.0095	1.694	0.470	53.6	98.0	83.75	0.40
76	2.25	25.88	0.0126	2.741	0.130	40.4	96.8	85.1	1.3
16	2.25	26.72	0.0026	0.8934	0.514	193.7	99.0	89.70	0.31
20	2.25	30.02	0.0359	1.598	0.207	14.2	98.4	99.90	0.95
100	2.25	32.53	0.0273	3.167	0.142	18.7	97.1	106.6	1.5
51	2.25	41.10	0.1237	7.742	0.054	4.1	94.4	130.1	3.7
23	2.25	42.98	0.0170	2.623	0.155	30.1	98.2	141.1	1.9
97	2.25	57.17	0.0298	2.174	0.203	17.1	98.9	186.6	1.5
86	2.25	57.90	0.0342	2.220	0.213	14.9	98.9	188.9	2.0
82	2.25	59.26	-0.0127	2.365	0.143	-	98.8	193.0	2.2
102	2.25	73.97	0.1292	4.091	0.074	3.9	98.4	236.9	5.7
111	2.25	79.98	0.0170	2.393	0.154	30.1	99.1	256.6	3.3
95	2.25	86.58	-0.0015	4.760	0.257	-	98.4	274.3	2.8
19	2.25	97.87	0.0349	16.32	0.045	14.6	95.0	297.7	13.6
124	2.25	500.3	0.0471	4.284	0.108	10.8	99.7	1220.2	17.2

ID	Power (Watts)	$^{40}Ar/^{39}Ar$	$^{37}Ar/^{39}Ar$	$^{36}Ar/^{39}Ar$ (x 10^{-3})	$^{39}Ar_K$ (x10^{-15} mol)	K/Ca	$^{40}Ar^*$ (%)	Age (Ma)	±1σ (Ma)
MDA			n=1					66.54	0.35
A16-BTW-MH7, DetritalSanidine, J=0.001903±0.03%, IC=1.002462±0.0008806, NM-293D, Lab#=65993, Argus VI									
22	2.25	19.89	0.0037	0.0436	3.391	137.4	99.9	67.927	0.018
08	2.25	19.91	0.0049	0.0502	1.937	104.7	99.9	68.010	0.028
21	2.25	19.91	0.0048	0.0508	2.595	106.9	99.9	68.011	0.025
17	2.25	19.94	0.0048	0.0944	4.922	106.5	99.9	68.038	0.015
16	2.25	19.92	0.0028	0.0254	3.918	180.6	100.0	68.046	0.013
57	2.25	20.17	0.0054	0.8443	4.481	94.3	98.8	68.089	0.041
71	2.25	19.98	0.0033	0.1792	2.516	153.4	99.7	68.111	0.034
43	2.25	19.95	0.0028	0.0308	3.518	184.1	100.0	68.132	0.024
60	2.25	19.95	0.0038	0.0190	2.081	133.3	100.0	68.151	0.033
38	2.25	19.95	0.0044	0.0188	2.745	115.4	100.0	68.157	0.028
46	2.25	19.97	0.0034	0.0379	3.364	148.3	99.9	68.197	0.029
72	2.25	19.97	0.0033	0.0456	2.752	157.0	99.9	68.208	0.032
73	2.25	19.97	0.0058	0.0214	1.966	87.6	100.0	68.226	0.031
02	2.25	19.98	0.0034	0.0395	3.323	148.9	99.9	68.251	0.020
67	2.25	19.99	0.0040	0.0356	2.656	126.2	99.9	68.275	0.034
75	2.25	19.99	0.0036	0.0233	3.367	141.0	100.0	68.284	0.041
03	2.25	19.99	0.0039	-0.0003	3.571	129.6	100.0	68.298	0.018
28	2.25	20.01	0.0038	0.0508	1.785	135.0	99.9	68.335	0.041
93	2.25	20.01	0.0025	0.0233	4.755	205.5	100.0	68.341	0.032
24	2.25	20.01	0.0045	0.0336	2.814	113.7	100.0	68.349	0.037
13	2.25	20.02	0.0031	0.0461	2.405	163.6	99.9	68.366	0.042
79	2.25	20.03	0.0045	0.0474	3.051	112.5	99.9	68.395	0.039

ID	Power (Watts)	$^{40}Ar/^{39}Ar$	$^{37}Ar/^{39}Ar$	$^{36}Ar/^{39}Ar$ (x $10^{-3)}$	$^{39}Ar_K$ (x10^{-15} mol)	K/Ca	$^{40}Ar^*$ (%)	Age (Ma)	±1σ (Ma)
49	2.25	20.04	0.0041	0.0470	1.596	124.9	99.9	68.429	0.055
34	2.25	20.04	0.0065	0.0404	2.601	78.2	99.9	68.446	0.065
59	2.25	20.05	0.0042	0.0563	2.739	121.0	99.9	68.456	0.041
10	2.25	20.09	0.0047	0.0299	4.454	109.4	100.0	68.609	0.016
62	2.25	20.21	0.0035	0.0399	2.233	146.4	99.9	69.017	0.073
27	2.25	20.28	0.0021	0.0448	2.059	243.8	99.9	69.24	0.10
56	2.25	20.35	0.0032	0.0698	3.046	158.9	99.9	69.444	0.052
31	2.25	20.38	0.0041	0.1176	2.917	125.3	99.8	69.495	0.058
37	2.25	20.40	0.0029	0.0440	2.615	176.3	99.9	69.642	0.070
81	2.25	20.44	0.0045	0.0279	3.486	112.5	100.0	69.799	0.039
40	2.25	20.52	0.0058	0.0329	1.496	88.0	100.0	70.05	0.11
69	2.25	20.55	0.0041	0.0808	3.242	123.3	99.9	70.112	0.053
96	2.25	20.77	0.0064	0.7050	2.107	80.3	99.0	70.224	0.082
80	2.25	20.60	0.0076	0.0223	1.556	67.2	100.0	70.33	0.10
88	2.25	21.55	0.0192	0.7942	0.174	26.6	98.9	72.77	0.59
86	2.25	21.58	0.0028	0.0436	3.696	181.1	99.9	73.584	0.043
58	2.25	21.78	0.0033	0.4418	3.538	153.5	99.4	73.880	0.052
20	2.25	21.67	0.0025	0.0487	1.928	204.1	99.9	73.901	0.094
61	2.25	21.73	0.0100	0.2145	0.943	51.0	99.7	73.92	0.15
55	2.25	21.71	0.0061	0.1038	4.109	83.0	99.9	73.965	0.049
84	2.25	21.70	0.0047	0.0438	2.495	108.5	99.9	73.994	0.067
92	2.25	21.76	0.0079	0.1576	1.024	64.2	99.8	74.08	0.13
32	2.25	21.78	0.0049	0.0977	1.537	104.1	99.9	74.22	0.10
74	2.25	21.81	0.0027	0.1824	2.005	188.9	99.8	74.239	0.086
97	2.25	21.77	0.0057	0.0506	2.958	90.2	99.9	74.240	0.055

ID	Power (Watts)	$^{40}Ar/^{39}Ar$	$^{37}Ar/^{39}Ar$	$^{36}Ar/^{39}Ar$ (x 10^{-3})	$^{39}Ar_K$ (x10^{-15} mol)	K/Ca	$^{40}Ar^*$ (%)	Age (Ma)	±1σ (Ma)
64	2.25	21.77	0.0049	0.0277	4.633	105.1	100.0	74.243	0.040
91	2.25	21.78	0.0060	0.0393	1.623	84.9	99.9	74.27	0.11
39	2.25	21.78	0.0070	0.0462	1.838	72.7	99.9	74.272	0.092
35	2.25	21.82	0.0050	0.0402	4.739	101.3	99.9	74.395	0.037
53	2.25	21.85	0.0042	0.0883	1.462	120.1	99.9	74.44	0.11
90	2.25	21.89	0.0046	0.2531	2.196	112.0	99.7	74.443	0.092
23	2.25	21.89	0.0053	0.1024	2.549	96.8	99.9	74.564	0.076
76	2.25	21.87	0.0058	0.0472	3.443	87.3	99.9	74.567	0.057
30	2.25	21.89	0.0041	0.0437	3.487	124.3	99.9	74.628	0.054
85	2.25	21.92	0.0074	0.1061	1.774	68.5	99.9	74.67	0.11
65	2.25	21.91	0.0047	0.0230	3.593	108.0	100.0	74.714	0.055
68	2.25	21.93	0.0072	0.0836	1.392	70.7	99.9	74.71	0.10
26	2.25	21.99	0.0215	0.2440	2.906	23.8	99.7	74.769	0.065
07	2.25	21.95	0.0059	0.0880	1.945	85.8	99.9	74.789	0.091
11	2.25	21.97	0.0050	0.1463	4.076	102.8	99.8	74.809	0.041
87	2.25	21.96	0.0047	0.0827	3.223	108.2	99.9	74.847	0.066
42	2.25	21.97	0.0061	0.1009	5.735	83.9	99.9	74.851	0.068
33	2.25	21.96	0.0068	0.0550	3.678	74.5	99.9	74.874	0.064
45	2.25	21.98	0.0057	0.0547	3.628	89.8	99.9	74.917	0.052
94	2.25	22.00	0.0034	0.0229	2.104	148.9	100.0	75.011	0.082
41	2.25	22.06	0.0054	0.0462	3.062	94.4	99.9	75.208	0.055
15	2.25	22.08	0.0070	0.0769	1.182	73.2	99.9	75.24	0.13
83	2.25	22.09	0.0064	0.0613	3.132	79.5	99.9	75.291	0.078
95	2.25	22.15	0.0082	0.0666	1.470	62.2	99.9	75.48	0.11
14	2.25	22.19	0.0053	0.0658	2.882	96.2	99.9	75.614	0.073

ID	Power (Watts)	$^{40}Ar/^{39}Ar$	$^{37}Ar/^{39}Ar$	$^{36}Ar/^{39}Ar$ (x 10^{-3})	$^{39}Ar_K$ (x10^{-15} mol)	K/Ca	$^{40}Ar^*$ (%)	Age (Ma)	±1σ (Ma)
04	2.25	22.19	0.0066	0.0364	2.597	76.9	100.0	75.634	0.063
78	2.25	22.19	0.0110	0.0365	1.146	46.3	100.0	75.64	0.14
82	2.25	22.22	0.0050	0.0902	1.340	102.7	99.9	75.71	0.14
09	2.25	22.25	0.0142	0.1573	1.357	35.9	99.8	75.73	0.13
70	2.25	22.23	0.0075	0.0799	2.532	67.6	99.9	75.750	0.063
66	2.25	22.24	0.0059	0.0480	1.200	85.8	99.9	75.79	0.13
18	2.25	22.27	0.0058	0.1347	1.692	88.0	99.8	75.81	0.11
29	2.25	22.27	0.0091	0.1531	1.626	56.3	99.8	75.81	0.11
12	2.25	22.30	0.0083	0.2492	1.059	61.7	99.7	75.81	0.16
52	2.25	22.30	0.0100	0.1587	1.177	50.9	99.8	75.91	0.15
48	2.25	22.28	0.0079	0.0653	1.973	64.2	99.9	75.912	0.082
63	2.25	22.30	0.0056	0.0804	2.807	90.9	99.9	75.970	0.058
44	2.25	22.37	0.0091	0.2380	0.851	56.2	99.7	76.04	0.15
25	2.25	22.34	0.0118	0.1116	1.973	43.2	99.9	76.070	0.078
50	2.25	22.37	0.0066	0.1483	2.430	76.8	99.8	76.139	0.070
54	2.25	22.36	0.0051	0.1028	2.660	99.1	99.9	76.153	0.095
47	2.25	22.37	0.0067	0.0825	1.969	76.3	99.9	76.208	0.093
51	2.25	22.37	0.0048	0.0258	3.557	106.2	100.0	76.271	0.058
89	2.25	22.39	0.0081	0.0563	1.200	63.0	99.9	76.29	0.16
05	2.25	22.46	0.0033	0.0923	1.005	152.9	99.9	76.48	0.14
77	2.25	22.46	0.0116	0.0325	1.330	43.9	100.0	76.57	0.12
01	2.25	22.75	0.0062	0.0595	3.130	82.1	99.9	77.504	0.051
36	2.25	27.59	0.0051	0.0495	2.423	100.1	99.9	93.602	0.099
MDA			n=5	MSWD=7.85				68.01	0.03

Notes:

ID	Power (Watts)	$^{40}Ar/^{39}Ar$	$^{37}Ar/^{39}Ar$	$^{36}Ar/^{39}Ar$ (x 10^{-3})	$^{39}Ar_K$ (x10^{-15} mol)	K/Ca	$^{40}Ar^*$ (%)	Age (Ma)	±1σ (Ma)

Isotopic ratios corrected for blank, radioactive decay, and mass discrimination, not corrected for interfering reactions.

Errors quoted for individual analyses include analytical error only, without interfering reaction or J uncertainties.

MDA (maximum deposition age) is weighted mean age (Taylor, 1982). MDA error is weighted error follows Taylor (1982), multiplied by the squareroot of the MSWD where MSWD>1, and also incorporates uncertainty in J factor and irradiation correction factor uncertainties.

Isotopic abundances after Steiger and Jäger (1977).

X preceding sample ID denotes analyses included for MDA calculations.

Ages calculated relative to FC-2 Fish Canyon Tuff sanidine interlaboratory standard at 28.201 Ma (Kuiper et al., 2008)

Decay Constant (LambdaK (total)) = $5.463e^{-10}$/a (Min et al., 2000)

- indciates no measurable 37Ar above blank value to determine K/Ca

IC = $^{40}Ar/^{36}Ar$ of air standard divided by 295.5

Table C.2 – Summary of $^{40}Ar/^{39}Ar$ step heating results

Sample	FM	Sect.	L#	Irrad	min	analysis	Preferred Age n	$\%^{39}Ar$	MSWD	K/Ca	±	2σ	Age (Ma)	±	1σ	Integrated Age n	Age (Ma)	±	1σ
CM-SS4	OA	MDC	61414-63	NM-254E	Sanidine	Plateau	5	100.0	4.1	42.9	±	3.5	66.27	±	0.12	5	66.34	±	0.09
CM-SS4	OA	MDC	61414-19	NM-254E	Sanidine	Plateau	4	100.0	14.3	144.2	±	30.1	68.13	±	0.11	4	68.21	±	0.09
CM-SS4	OA	MDC	61414-13	NM-254E	Sanidine	Plateau	4	96.6	18.6	122.4	±	11.8	69.13`	±	0.12	5	69.22	±	0.09
CM-SS4	OA	MDC	61414-39	NM-254E	Sanidine	Step B	1	82.3	NA	155.5	±	0.0	69.599	±	0.023	2	69.93	±	0.12
CM-SS4	OA	MDC	61414-15	NM-254E	Sanidine	Plateau	5	100.0	145.5	113.8	±	47.0	69.67	±	0.15	5	69.76	±	0.09
CM-SS4	OA	MDC	61414-04	NM-254E	Sanidine	Plateau	5	100.0	31.5	117.5	±	17.6	69.71	±	0.11	5	69.70	±	0.09
CM-SS4	OA	MDC	61414-40	NM-254E	Sanidine	Plateau	2	91.3	13.9	243.0	±	65.9	71.04	±	0.13	3	70.60	±	0.09
CM-SS4	OA	MDC	61414-12	NM-254E	Sanidine	Plateau	4	95.3	22.8	126.3	±	18.7	73.58	±	0.11	5	73.69	±	0.09
CM-SS4	OA	MDC	61414-58	NM-254E	Sanidine	Plateau	2	100.0	0.0	95.5	±	40.7	73.87	±	0.09	2	73.88	±	0.10
CM-SS4	OA	MDC	61414-17	NM-254E	Sanidine	Plateau	4	100.0	34.1	122.3	±	57.1	73.99	±	0.26	4	73.99	±	0.10
CM-SS4	OA	MDC	61414-60	NM-254E	Sanidine	Plateau	2	100.0	7.0	147.7	±	30.2	74.06	±	0.14	2	74.29	±	0.13
CM-SS4	OA	MDC	61414-10	NM-254E	Sanidine	Plateau	4	92.8	39.1	142.3	±	28.0	74.08	±	0.13	5	74.26	±	0.09
CM-SS4	OA	MDC	61414-08	NM-254E	Sanidine	Plateau	5	100.0	90.5	116.0	±	32.2	74.16	±	0.13	5	74.12	±	0.09
CM-SS4	OA	MDC	61414-14	NM-254E	Sanidine	Plateau	3	83.2	51.0	120.9	±	5.3	74.22	±	0.15	5	74.33	±	0.10
CM-SS4	OA	MDC	61414-07	NM-254E	Sanidine	Plateau	5	100.0	47.2	178.1	±	550.3	74.22	±	0.15	5	74.24	±	0.09
CM-SS4	OA	MDC	61414-37	NM-254E	Sanidine	Step B	1	90.4	NA	124.2			74.232	±	0.030	2	73.79	±	0.12

							Preferred Age									Integrated Age			
Sample	FM	Sect.	L#	Irrad	min	analysis	n	%^{39}Ar	MSWD	K/Ca	±	2σ	Age (Ma)	±	1σ	n	Age (Ma)	±	1σ
CM-SS4	OA	MDC	61414-31	NM-254E	Sanidine	Plateau	2	100.0	3.5	146.2	±	2.2	74.32	±	0.11	2	74.55	±	0.16
CM-SS4	OA	MDC	61414-23	NM-254E	Sanidine	Plateau	2	100.0	0.3	138.8	±	22.1	74.48	±	0.11	2	74.40	±	0.18
CM-SS4	OA	MDC	61414-47	NM-254E	Sanidine	Plateau	2	100.0	4.1	110.8	±	14.1	74.51	±	0.14	2	74.80	±	0.17
CM-SS4	OA	MDC	61414-06	NM-254E	Sanidine	Plateau	4	97.3	6.6	116.1	±	29.5	74.56	±	0.10	5	74.42	±	0.09
CM-SS4	OA	MDC	61414-74	NM-254E	Sanidine	Plateau	2	100.0	5.2	110.2	±	6.8	74.61	±	0.19	2	75.05	±	0.22
CM-SS4	OA	MDC	61414-54	NM-254E	Sanidine	Plateau	2	100.0	0.2	122.7	±	0.0	74.63	±	0.10	2	74.60	±	0.12
CM-SS4	OA	MDC	61414-25	NM-254E	Sanidine	Plateau	2	100.0	6.9	110.3	±	26.4	74.66	±	0.27	2	74.92	±	0.17
CM-SS4	OA	MDC	61414-79	NM-254E	Sanidine	Plateau	2	100.0	1.1	111.4	±	5.4	74.71	±	0.23	2	74.94	±	0.31
CM-SS4	OA	MDC	61414-48	NM-254E	Sanidine	Plateau	2	100.0	0.0	122.1	±	29.6	74.72	±	0.10	2	74.71	±	0.11
CM-SS4	OA	MDC	61414-34	NM-254E	Sanidine	Plateau	2	100.0	6.2	118.8	±	33.9	74.73	±	0.09	2	74.69	±	0.09
CM-SS4	OA	MDC	61414-05	NM-254E	Sanidine	Plateau	4	93.9	30.9	113.7	±	11.2	74.73	±	0.13	5	74.69	±	0.09
CM-SS4	OA	MDC	61414-42	NM-254E	Sanidine	Plateau	2	100.0	1.3	152.3	±	44.0	74.75	±	0.11	2	74.57	±	0.19
CM-SS4	OA	MDC	61414-44	NM-254E	Sanidine	Plateau	2	100.0	8.4	167.5	±	66.2	74.76	±	0.13	2	74.52	±	0.13
CM-SS4	OA	MDC	61414-65	NM-254E	Sanidine	Plateau	2	100.0	0.2	92.2	±	10.4	74.81	±	0.13	2	74.73	±	0.23
CM-SS4	OA	MDC	61414-09	NM-254E	Sanidine	Plateau	4	93.3	11.0	116.0	±	13.1	74.90	±	0.12	5	74.38	±	0.10
CM-SS4	OA	MDC	61414-68	NM-254E	Sanidine	Plateau	2	100.0	2.9	160.1	±	46.9	74.91	±	0.16	2	75.06	±	0.15
CM-SS4	OA	MDC	61414-55	NM-254E	Sanidine	Plateau	2	100.0	0.1	921.4	±	1463.0	74.99	±	0.13	2	75.03	±	0.18
CM-SS4	OA	MDC	61414-81	NM-254E	Sanidine	Plateau	2	100.0	1.0	78.4	±	38.3	75.11	±	0.10	2	75.00	±	0.15

							Preferred Age									Integrated Age			
Sample	FM	Sect.	L#	Irrad	min	analysis	n	%^{39}Ar	MSWD	K/Ca	±	2σ	Age (Ma)	±	1σ	n	Age (Ma)	±	1σ
CM-SS4	OA	MDC	61414-21	NM-254E	Sanidine	Plateau	3	96.3	15.5	102.5	±	8.9	75.12	±	0.11	5	74.81	±	0.09
CM-SS4	OA	MDC	61414-45	NM-254E	Sanidine	Plateau	2	100.0	0.5	131.5	±	93.0	75.15	±	0.15	2	75.37	±	0.31
CM-SS4	OA	MDC	61414-18	NM-254E	Sanidine	Plateau	5	100.0	14.6	142.4	±	55.7	75.17	±	0.11	5	75.18	±	0.10
CM-SS4	OA	MDC	61414-82	NM-254E	Sanidine	Plateau	2	97.2	8.6	121.2	±	87.4	75.24	±	0.29	3	74.97	±	0.16
CM-SS4	OA	MDC	61414-11	NM-254E	Sanidine	Plateau	4	93.8	7.6	100.6	±	3.1	75.42	±	0.10	5	75.60	±	0.10
CM-SS4	OA	MDC	61414-51	NM-254E	Sanidine	Step B	1	76.6	NA	122.3			75.447	±	0.016	2	75.63	±	0.11
CM-SS4	OA	MDC	61414-38	NM-254E	Sanidine	Plateau	2	100.0	0.1	91.1	±	17.8	75.61	±	0.11	2	75.65	±	0.15
CM-SS4	OA	MDC	61414-59	NM-254E	Sanidine	Step B	1	36.1	NA	107.1			75.64	±	0.12	2	77.97	±	0.23
CM-SS4	OA	MDC	61414-41	NM-254E	Sanidine	Step B	1	47.9	NA	91.9	±	0.0	75.860	±	0.036	2	76.32	±	0.16
CM-SS4	OA	MDC	61414-52	NM-254E	Sanidine	Plateau	2	100.0	0.9	92.9	±	18.2	76.04	±	0.14	2	76.17	±	0.19
CM-SS4	OA	MDC	61414-62	NM-254E	Sanidine	Step B	1	63.7	NA	65.8			76.086	±	0.049	2	76.65	±	0.16
CM-SS4	OA	MDC	61414-24	NM-254E	Sanidine	Plateau	2	100.0	1.1	66.8	±	14.7	76.12	±	0.10	2	76.21	±	0.13
CM-SS4	OA	MDC	61414-61	NM-254E	Sanidine	Plateau	2	100.0	1.9	69.3	±	44.7	76.13	±	0.11	2	76.25	±	0.13
CM-SS4	OA	MDC	61414-22	NM-254E	Sanidine	Plateau	2	100.0	0.7	88.0	±	0.0	76.20	±	0.10	2	76.24	±	0.11
CM-SS4	OA	MDC	61414-27	NM-254E	Sanidine	Plateau	2	100.0	8.0	98.2	±	31.9	76.25	±	0.23	2	76.47	±	0.14
CM-SS4	OA	MDC	61414-78	NM-254E	Sanidine	Step B	1	96.3	NA	65.4			76.303	±	0.099	2	77.47	±	0.28
CM-SS4	OA	MDC	61414-36	NM-254E	Sanidine	Plateau	2	100.0	6.1	100.1	±	79.1	76.31	±	0.10	2	76.36	±	0.10
CM-SS4	OA	MDC	61414-56	NM-254E	Sanidine	Plateau	2	100.0	12.0	96.6	±	9.7	76.40	±	0.27	2	76.10	±	0.15

Sample	FM	Sect.	L#	Irrad	min	analysis	n	%^{39}Ar	MSWD	K/Ca	±	2σ	Age (Ma)	±	1σ	n	Age (Ma)	±	1σ
							Preferred Age									Integrated Age			
CM-SS4	OA	MDC	61414-35	NM-254E	Sanidine	Plateau	2	100.0	2.6	124.5	±	7.7	76.41	±	0.14	2	76.26	±	0.15
CM-SS4	OA	MDC	61414-43	NM-254E	Sanidine	Plateau	2	100.0	2.1	144.0	±	85.1	76.59	±	0.36	2	75.73	±	0.68
CM-SS4	OA	MDC	61414-46	NM-254E	Sanidine	Step B	1	94.4	NA	160.5			81.852	±	0.032	2	84.63	±	0.13
CM-SS4	OA	MDC	61414-33	NM-254E	Sanidine	Step B	1	61.8	NA	104.5	±		82.717	±	0.022	2	82.96	±	0.12
CM-SS4	OA	MDC	61414-80	NM-254E	Sanidine	Step B	1	66.0	NA	84.1			86.900	±	0.075	2	83.82	±	0.23
CM-SS4	OA	MDC	61414-26	NM-254E	Sanidine	Step B	1	97.2	NA	145.7			102.493	±	0.049	2	103.26	±	0.18
CM-SS4	OA	MDC	61414-77	NM-254E	Sanidine	Plateau	2	100.0	1.5	23.2	±	1.8	153.25	±	0.35	2	153.78	±	0.52
CM-SS4	OA	MDC	61414-70	NM-254E	Sanidine	Plateau	2	100.0	0.2	190.0	±	121.9	161.93	±	0.20	2	161.86	±	0.25
CM-SS4	OA	MDC	61414-73	NM-254E	Sanidine	Step B	1	98.6	NA	416.9			178.429	±	0.064	2	179.48	±	0.27
CM-SS4	OA	MDC	61414-67	NM-254E	Sanidine	TGA	2	100.0	NA	156.0			189.96	±	0.51	2	189.96	±	0.51
CM-SS4	OA	MDC	61414-85	NM-254E	Sanidine	Plateau	2	100.0	17.2	212.7	±	183.6	193.40	±	0.49	2	194.98	±	0.45
CM-SS4	OA	MDC	61414-32	NM-254E	Sanidine	Plateau	2	100.0	13.3	197.0	±	77.9	193.97	±	0.32	2	194.70	±	0.31
CM-SS4	OA	MDC	61414-84	NM-254E	Sanidine	Plateau	2	100.0	0.0	375.9	±	0.0	194.62	±	0.29	2	194.64	±	0.39
CM-SS4	OA	MDC	61414-16	NM-254E	Sanidine	Plateau	2	13.1	1.6	84.6	±	0.0	205.84	±	1.88	5	215.97	±	0.93
CM-SS4	OA	MDC	61414-53	NM-254E	Sanidine	TGA	2	100.0	NA	66.6			374.42	±	0.51	2	374.42	±	0.51
CM-SS4	OA	MDC	61414-86	NM-254E	Sanidine	TGA	2	100.0	NA	45.6			387.36	±	1.84	2	387.36	±	1.84
CM-SS4	OA	MDC	61414-57	NM-254E	Sanidine	Plateau	2	100.0	287.4	492.4	±	0.0	639.24	±	4.64	2	637.51	±	0.93
CM-SS4	OA	MDC	61414-69	NM-254E	Sanidine	Plateau	2	100.0	NA	214.0			691.35	±	1.40	2	691.35	±	1.40

Sample	FM	Sect.	L#	Irrad	min	analysis	n	%^{39}Ar	MSWD	K/Ca	±	2σ	Age (Ma)	±	1σ	n	Age (Ma)	±	1σ
							Preferred Age									Integrated Age			
CM-SS4	OA	MDC	61414-87	NM-254E	Sanidine	TGA	2	100.0	NA	105.1			879.34	±	1.21	2	879.34	±	1.21
CM-SS4	OA	MDC	61414-71	NM-254E	Sanidine	TGA	2	100.0	NA				929.8	±	1.4	2	929.82	±	1.43
CM-SS4	OA	MDC	61414-20	NM-254E	Sanidine	TGA	2	100.0	NA	110.0	±	0.0	1299.44	±	1.47	2	1299.44	±	1.47
SJ-SS5	OA	DNZ	61405-39	NM-254D	Sanidine	Plateau	2	100.0	0.3	125.2	±	0.0	73.39	±	0.11	2	73.45	±	0.15
SJ-SS5	OA	DNZ	61405-32	NM-254D	Sanidine	Plateau	2	100.0	0.1	113.8	±	0.0	74.15	±	0.12	2	74.18	±	0.15
SJ-SS5	OA	DNZ	61405-05	NM-254D	Sanidine	Plateau	2	100.0	0.1	165.0	±	0.0	74.26	±	0.11	2	74.23	±	0.15
SJ-SS5	OA	DNZ	61405-18	NM-254D	Sanidine	Plateau	2	100.0	0.1	28.7	±	0.0	74.32	±	0.15	2	74.33	±	0.15
SJ-SS5	OA	DNZ	61405-27	NM-254D	Sanidine	Plateau	2	100.0	10.0	117.2	±	38.4	74.34	±	0.44	2	74.37	±	0.15
SJ-SS5	OA	DNZ	61405-21	NM-254D	Sanidine	Plateau	2	100.0	0.1	114.2	±	39.8	74.35	±	0.08	2	74.33	±	0.11
SJ-SS5	OA	DNZ	61405-14	NM-254D	Sanidine	Plateau	2	100.0	2.4	152.1	±	0.0	74.76	±	0.25	2	74.94	±	0.20
SJ-SS5	OA	DNZ	61405-06	NM-254D	Sanidine	Plateau	2	100.0	0.4	347.5	±	297.0	74.78	±	0.16	2	74.76	±	0.17
SJ-SS5	OA	DNZ	61405-25	NM-254D	Sanidine	Plateau	2	100.0	0.7	195.0	±	5.4	75.05	±	0.15	2	75.00	±	0.16
SJ-SS5	OA	DNZ	61405-10	NM-254D	Sanidine	Plateau	2	100.0	0.7	0.0	±	0.0	75.53	±	0.41	2	75.65	±	0.43
SJ-SS5	OA	DNZ	61405-17	NM-254D	Sanidine	Plateau	2	100.0	1.1	355.3	±	322.3	75.60	±	0.09	2	75.63	±	0.09
SJ-SS5	OA	DNZ	61405-08	NM-254D	Sanidine	Plateau	2	100.0	0.1	68.7	±	44.8	76.00	±	0.11	2	76.04	±	0.16
SJ-SS5	OA	DNZ	61405-23	NM-254D	Sanidine	Plateau	2	100.0	1.9	371.1	±	303.5	76.02	±	0.12	2	75.96	±	0.11
SJ-SS5	OA	DNZ	61405-04	NM-254D	Sanidine	Plateau	2	100.0	0.9	72.2	±	27.0	78.30	±	0.16	2	78.35	±	0.17

							Preferred Age										Integrated Age			
Sample	FM	Sect.	L#	Irrad	min	analysis	n	%^{39}Ar	MSWD	K/Ca	±	2σ	Age (Ma)	±	1σ	n	Age (Ma)	±	1σ
SJ-SS5	OA	DNZ	61405 -11	NM-254D	Sanidine	Plateau	2	100.0	0.5	65.5	±	17.7	78.46	±	0.14	2	78.49	±	0.15
SJ-SS5	OA	DNZ	61405 -12	NM-254D	Sanidine	Plateau	2	100.0	0.0	80.5	±	4.2	78.49	±	0.13	2	78.49	±	0.13
SJ-SS5	OA	DNZ	61405 -24	NM-254D	Sanidine	Step B	1	41.0	NA	64.8	±	0.0	81.08	±	0.23	2	78.47	±	0.16
SJ-SS5	OA	DNZ	61405 -13	NM-254D	Sanidine	Plateau	2	100.0	2.6	226.0	±	32.7	98.93	±	0.14	2	98.99	±	0.11
SJ-SS5	OA	DNZ	61405 -38	NM-254D	Sanidine	Plateau	2	100.0	2.1	57.8	±	0.0	162.60	±	0.45	2	163.05	±	0.44
SJ-SS5	OA	DNZ	61405 -26	NM-254D	Sanidine	Plateau	2	100.0	0.4	59.5	±	40.7	164.86	±	0.29	2	164.79	±	0.30
SJ-SS5	OA	DNZ	61405 -47	NM-254D	Sanidine	TGA	2	100.0	NA	122.8			170.30	±	0.17	2	170.30	±	0.17
SJ-SS5	OA	DNZ	61405 -31	NM-254D	Sanidine	Plateau	2	100.0	10.1	1315.6	±	0.0	194.04	±	0.53	2	194.49	±	0.25
SJ-SS5	OA	DNZ	61405 -40	NM-254D	Sanidine	Plateau	2	100.0	1.0	0.0	±	0.0	194.70	±	0.20	2	194.88	±	0.27
SJ-SS5	OA	DNZ	61405 -16	NM-254D	Sanidine	TGA	2	100.0	NA	1036.8			235.35	±	0.21	2	235.35	±	0.21
SJ-SS5	OA	DNZ	61405 -49	NM-254D	Sanidine	TGA	2	100.0	NA	695.6			357.64	±	0.42	2	357.64	±	0.42
SJ-SS5	OA	DNZ	61405 -07	NM-254D	Sanidine	TGA	2	100.0	NA	197.8			567.15	±	0.44	2	567.15	±	0.44
SJ-SS5	OA	DNZ	61405 -34	NM-254D	Sanidine	TGA	2	100.0	NA	163.9			593.42	±	0.91	2	593.42	±	0.91
SJ-SS5	OA	DNZ	61405 -45	NM-254D	Sanidine	TGA	2	100.0	NA	548.1			747.68	±	0.60	2	747.68	±	0.60
SJ-SS5	OA	DNZ	61405 -46	NM-254D	Sanidine	TGA	2	100.0	NA	69.6			751.84	±	1.44	2	751.84	±	1.44
SJ-SS5	OA	DNZ	61405 -33	NM-254D	Sanidine	TGA	2	100.0	NA	163.9			752.76	±	0.51	2	752.76	±	0.51
SJ-SS5	OA	DNZ	61405 -51	NM-254D	Sanidine	TGA	2	100.0	NA	821.6			807.56	±	0.96	2	807.56	±	0.96
SJ-SS5	OA	DNZ	61405 -44	NM-254D	Sanidine	TGA	2	100.0	NA	46.4			861.12	±	1.57	2	861.12	±	1.57

							Preferred Age									Integrated Age			
Sample	FM	Sect.	L#	Irrad	min	analysis	n	%^{39}Ar	MSWD	K/Ca	±	2σ	Age (Ma)	±	1σ	n	Age (Ma)	±	1σ
SJ-SS5	OA	DNZ	61405-43	NM-254D	Sanidine	TGA	2	100.0	NA	324.0			867.36	±	0.88	2	867.36	±	0.88
SJ-SS5	OA	DNZ	61405-30	NM-254D	Sanidine	TGA	2	100.0	NA	163.9			883.71	±	0.71	2	883.71	±	0.71
SJ-SS5	OA	DNZ	61405-28	NM-254D	Sanidine	TGA	2	100.0	NA				1039.12	±	1.08	2	1039.12	±	1.08
SJ-SS5	OA	DNZ	61405-19	NM-254D	Sanidine	TGA	2	100.0	NA	154.1			1043.91	±	0.97	2	1043.91	±	0.97
SJ-SS5	OA	DNZ	61405-29	NM-254D	Sanidine	TGA	2	100.0	NA	411.1			1141.14	±	0.69	2	1141.14	±	0.69
SJ-SS5	OA	DNZ	61405-50	NM-254D	Sanidine	TGA	2	100.0	NA	225.5			1322.08	±	1.23	2	1322.08	±	1.23
SJ-SS6	NAC	DNZ	61406-41	NM-254D	Sanidine	Plateau	4	100.0	7.0	150.9	±	77.9	65.37	±	0.09	4	65.37	±	0.07
SJ-SS6	NAC	DNZ	61406-28	NM-254D	Sanidine	Plateau	4	100.0	9.5	133.6	±	89.5	65.51	±	0.12	4	65.50	±	0.06
SJ-SS6	NAC	DNZ	61406-06	NM-254D	Sanidine	Plateau	4	100.0	0.5	115.9	±	55.3	67.90	±	0.10	4	67.89	±	0.27
SJ-SS6	NAC	DNZ	61406-12	NM-254D	Sanidine	Plateau	3	100.0	1.0	135.2	±	76.2	67.91	±	0.07	3	67.94	±	0.08
SJ-SS6	NAC	DNZ	61406-24	NM-254D	Sanidine	Step B	1	88.5	NA	183.7			67.921	±	0.017	2	68.00	±	0.06
SJ-SS6	NAC	DNZ	61406-25	NM-254D	Sanidine	Plateau	2	100.0	0.0	107.4	±	68.8	67.93	±	0.07	2	67.93	±	0.16
SJ-SS6	NAC	DNZ	61406-26	NM-254D	Sanidine	Plateau	2	100.0	7.9	173.5	±	121.1	67.96	±	0.26	2	68.46	±	0.20
SJ-SS6	NAC	DNZ	61406-04	NM-254D	Sanidine	Plateau	2	100.0	2.0	141.0	±	0.0	67.97	±	0.07	2	68.11	±	0.11
SJ-SS6	NAC	DNZ	61406-27	NM-254D	Sanidine	Plateau	2	100.0	0.2	124.3	±	4.8	68.05	±	0.08	2	68.06	±	0.09
SJ-SS6	NAC	DNZ	61406-03	NM-254D	Sanidine	Plateau	4	100.0	5.1	164.4	±	92.0	68.08	±	0.15	4	68.26	±	0.11
SJ-SS6	NAC	DNZ	61406-38	NM-254D	Sanidine	Plateau	2	100.0	0.2	65.4	±	4.1	68.14	±	0.11	2	68.05	±	0.21

Sample	FM	Sect.	L#	Irrad	min	analysis	n	%^{39}Ar	MSWD	K/Ca	±	2σ	Age (Ma)	±	1σ	n	Age (Ma)	±	1σ
							Preferred Age									Integrated Age			
SJ-SS6	NAC	DNZ	61406-23	NM-254D	Sanidine	Step B	1	84.5	NA	127.7			68.172	±	0.034	2	68.47	±	0.12
SJ-SS6	NAC	DNZ	61406-36	NM-254D	Sanidine	Plateau	2	100.0	3.7	150.6	±	106.6	68.22	±	0.10	2	68.62	±	0.20
SJ-SS6	NAC	DNZ	61406-34	NM-254D	Sanidine	Plateau	2	100.0	0.1	76.4	±	51.7	68.32	±	0.08	2	68.27	±	0.25
SJ-SS6	NAC	DNZ	61406-30	NM-254D	Sanidine	Plateau	2	100.0	11.9	140.7	±	78.8	68.32	±	0.14	2	68.23	±	0.07
SJ-SS6	NAC	DNZ	61406-07	NM-254D	Sanidine	Plateau	2	100.0	0.0	231.1	±	164.6	73.83	±	0.24	2	73.84	±	0.32
SJ-SS6	NAC	DNZ	61406-15	NM-254D	Sanidine	Plateau	2	100.0	0.8	112.8	±	36.2	73.86	±	0.11	2	73.86	±	0.11
SJ-SS6	NAC	DNZ	61406-33	NM-254D	Sanidine	Plateau	2	100.0	0.4	59.2	±	0.0	74.08	±	0.25	2	73.99	±	0.29
SJ-SS6	NAC	DNZ	61406-29	NM-254D	Sanidine	Plateau	2	100.0	1.4	81.0	±	0.0	74.16	±	0.24	2	74.17	±	0.21
SJ-SS6	NAC	DNZ	61406-21	NM-254D	Sanidine	Plateau	2	100.0	0.1	53.9	±	25.2	74.36	±	0.27	2	74.31	±	0.35
SJ-SS6	NAC	DNZ	61406-09	NM-254D	Sanidine	Plateau	2	100.0	0.0	43.7	±	24.2	74.45	±	0.12	2	74.44	±	0.16
SJ-SS6	NAC	DNZ	61406-08	NM-254D	Sanidine	Plateau	2	100.0	2.8	160.8	±	114.4	74.49	±	0.25	2	74.66	±	0.18
SJ-SS6	NAC	DNZ	61406-10	NM-254D	Sanidine	Plateau	3	100.0	0.5	72.1	±	42.7	74.66	±	0.21	3	74.61	±	0.30
SJ-SS6	NAC	DNZ	61406-42	NM-254D	Sanidine	Plateau	2	100.0	2.3	20.7	±	0.0	74.96	±	0.60	2	75.26	±	0.45
SJ-SS6	NAC	DNZ	61406-43	NM-254D	Sanidine	Plateau	2	100.0	0.6	27.3	±	17.2	75.25	±	0.37	2	75.49	±	0.47
SJ-SS6	NAC	DNZ	61406-37	NM-254D	Sanidine	Plateau	2	100.0	2.0	91.8	±	45.7	75.33	±	0.32	2	75.59	±	0.30
SJ-SS6	NAC	DNZ	61406-40	NM-254D	Sanidine	Plateau	2	100.0	4.5	62.9	±	43.8	75.35	±	0.53	2	75.40	±	0.25
SJ-SS6	NAC	DNZ	61406-16	NM-254D	Sanidine	Plateau	2	100.0	0.2	66.2	±	46.8	75.64	±	0.17	2	75.70	±	0.22
SJ-SS6	NAC	DNZ	61406-22	NM-254D	Sanidine	Plateau	2	100.0	0.0	0.2	±	0.0	78.27	±	0.27	2	78.22	±	0.40

							Preferred Age										Integrated Age			
Sample	FM	Sect.	L#	Irrad	min	analysis	n	%^{39}Ar	MSWD	K/Ca	±	2σ	Age (Ma)	±	1σ	n	Age (Ma)	±	1σ
SJ-SS6	NAC	DNZ	61406 -13	NM-254D	Sanidine	Plateau	2	100.0	3.6	46.2	±	24.5	95.70	±	1.60	2	96.04	±	0.86
SJ-SS6	NAC	DNZ	61406 -14	NM-254D	Sanidine	Plateau	2	100.0	1.7	84.2	±	56.4	1371.93	±	2.41	2	1373.32	±	2.15

Notes:

FM - formation (OA: Ojo Alamo Sandstone, NAC: Nacimiento Formation)

Section - sample location (DNZ: De-Na-Zin, MDC: Mesa de Cuba)

L# - sample number | Irrad - irradation run | min - mineralogy of sample

n - number of measurements used | analysis - type of analysis used for preferred age

Preferred Age - age estimate using only samples included in plateau calculations

Isotopic ratios corrected for blank, radioactive decay, and mass discrimination, not corrected for interfering reactions.

Errors quoted for individual analyses include analytical error only, without interfering reaction or J uncertainties.

Integrated age calculated by summing isotopic measurements of all steps.

Integrated age error calculated by quadratically combining errors of isotopic measurements of all steps.

Plateau age is inverse-variance-weighted mean of selected steps.

Plateau age error is inverse-variance-weighted mean error (Taylor, 1982) times root MSWD where MSWD>1.

Isotopic abundances after Steiger and Jäger (1977).

Italicized sample ID denotes analyses excluded from plateau age calculations.

Ages calculated relative to FC-2 Fish Canyon Tuff sanidine interlaboratory standard at 28.201 Ma (Kuiper et al., 2008)

Decay Constant (LambdaK (total)) = 5.463e^{-10}/a (Min et al., 2000)

Table C.3 – Single grain step-heating $^{40}Ar/^{39}Ar$ data

ID	Power (Watts)	$^{40}Ar/^{39}Ar$	$^{37}Ar/^{39}Ar$	$^{36}Ar/^{39}Ar$ (x 10^{-3})	$^{39}Ar_K$ (x 10^{-15} mol)	K/Ca	$^{40}Ar^*$ (%)	^{39}Ar (%)	Age (Ma)	±1σ (Ma)
		CM-SS4, Sanidine, J=0.009546±0.12%, IC=1.058206±0.0009102, NM-254E, Lab#=61414-04, Argus VI								
A	0.1	4.073	0.0047	0.0148	7.878	109.6	99.9	27.2	69.617	0.022
B	0.2	4.067	0.0041	0.0032	7.452	125.2	100.0	53.0	69.571	0.023
C	0.3	4.080	0.0044	-0.0008	9.950	116.5	100.0	87.4	69.820	0.017
D	0.5	4.095	0.0037	0.0135	2.534	136.3	99.9	96.1	69.993	0.057
E	3.0	4.071	0.0057	0.0454	1.120	89.6	99.7	100.0	69.43	0.13
Integrated age ± 1s			n=5		28.935				69.701	0.086
Plateau ± 1s		steps A-E	n=5	MSWD=31.51	28.935			100.0	69.71	0.106
		CM-SS4, Sanidine, J=0.009546±0.12%, IC=1.058206±0.0009102, NM-254E, Lab#=61414-05, Argus VI								
A	*0.1*	*4.298*	*0.0092*	*0.0247*	*1.109*	*55.7*	*99.8*	*6.1*	*73.35*	*0.13*
B	0.2	4.368	0.0041	0.0040	8.536	123.7	100.0	53.0	74.626	0.019
C	0.3	4.384	0.0050	0.0098	4.373	102.2	99.9	77.0	74.874	0.036
D	0.5	4.392	0.0048	0.0047	3.421	107.0	100.0	95.7	75.025	0.043
E	3.0	4.397	0.0052	0.0692	0.776	98.2	99.5	100.0	74.80	0.18
Integrated age ± 1s			n=5		18.216				74.691	0.093
Plateau ± 1s		steps B-E	n=4	MSWD=30.86	17.106			93.9	74.73	0.126
		CM-SS4, Sanidine, J=0.009546±0.12%, IC=1.058206±0.0009102, NM-254E, Lab#=61414-06, Argus VI								
A	0.1	4.360	0.0043	0.0036	5.836	119.3	100.0	40.5	74.493	0.027
B	0.2	4.357	0.0032	-0.0064	1.859	161.4	100.0	53.3	74.489	0.078
C	0.3	4.366	0.0055	-0.0022	3.250	92.5	100.0	75.9	74.632	0.045
D	0.6	4.375	0.0047	0.0103	3.083	107.6	99.9	97.3	74.714	0.048

ID	Power (Watts)	$^{40}Ar/^{39}Ar$	$^{37}Ar/^{39}Ar$	$^{36}Ar/^{39}Ar$ (x 10^{-3})	$^{39}Ar_K$ (x 10^{-15} mol)	K/Ca	$^{40}Ar^*$ (%)	^{39}Ar (%)	Age (Ma)	±1σ (Ma)
E	*3.0*	*4.065*	*0.0112*	*0.0904*	*0.395*	*45.5*	*99.4*	*100.0*	*69.11*	*0.34*
Integrated age ± 1s			n=5		14.424				74.424	0.094
Plateau ± 1s		steps A-D	n=4	MSWD=6.64	14.029			97.3	74.56	0.10
CM-SS4, Sanidine, J=0.009546±0.12%, IC=1.058206±0.0009102, NM-254E, Lab#=61414-07, Argus VI										
A	0.1	4.334	0.0044	0.0434	2.077	116.0	99.7	12.3	73.864	0.066
B	0.2	4.335	0.0037	0.0047	6.950	137.7	100.0	53.4	74.065	0.024
C	0.3	4.349	0.0047	0.0051	2.385	109.5	100.0	67.5	74.301	0.059
D	0.6	4.359	0.0037	-0.0046	4.844	138.1	100.0	96.2	74.527	0.031
E	3.0	4.407	0.0004	0.0577	0.651	1355	99.6	100.0	75.01	0.20
Integrated age ± 1s			n=5		16.907				74.243	0.093
Plateau ± 1s		steps A-E	n=5	MSWD=47.20	16.907			100.0	74.22	0.149
CM-SS4, Sanidine, J=0.009546±0.12%, IC=1.058206±0.0009102, NM-254E, Lab#=61414-08, Argus VI										
A	0.1	3.969	0.0105	0.0556	0.261	48.5	99.6	0.7	67.68	0.51
B	0.2	4.358	0.0056	0.0082	6.426	91.9	100.0	18.1	74.449	0.025
C	0.3	4.331	0.0043	-0.0006	10.179	119.4	100.0	45.6	74.025	0.018
D	0.5	4.341	0.0043	0.0031	9.820	119.8	100.0	72.2	74.176	0.017
E	3.0	4.339	0.0041	0.0052	10.280	125.8	100.0	100.0	74.127	0.017
Integrated age ± 1s			n=5		36.966				74.123	0.091
Plateau ± 1s		steps A-E	n=5	MSWD=90.45	36.966			100.0	74.16	0.126
CM-SS4, Sanidine, J=0.009546±0.12%, IC=1.058206±0.0009102, NM-254E, Lab#=61414-09, Argus VI										
A	0.1	4.416	0.0050	0.0101	1.250	101.6	99.9	11.6	75.40	0.11
B	0.2	4.375	0.0044	-0.0026	3.657	116.4	100.0	45.4	74.780	0.040

ID	Power (Watts)	$^{40}Ar/^{39}Ar$	$^{37}Ar/^{39}Ar$	$^{36}Ar/^{39}Ar$ (x 10^{-3})	$^{39}Ar_K$ (x 10^{-15} mol)	K/Ca	$^{40}Ar^*$ (%)	^{39}Ar (%)	Age (Ma)	±1σ (Ma)
C	0.3	4.385	0.0044	-0.0006	4.408	116.5	100.0	86.1	74.929	0.033
D	0.5	4.407	0.0038	0.0235	0.771	133.7	99.8	93.3	75.18	0.18
E	*3.0*	*3.928*	*0.0016*	*0.1627*	*0.729*	*321.6*	*98.8*	*100.0*	*66.43*	*0.19*
Integrated age ± 1s			n=5		10.815				74.380	0.095
Plateau ± 1s		steps A-D	n=4	MSWD=10.95	10.086			93.3	74.90	0.122
		CM-SS4, Sanidine, J=0.009546±0.12%, IC=1.058206±0.0009102, NM-254E, Lab#=61414-10, Argus VI								
A	*0.1*	*4.453*	*0.0039*	*0.0264*	*1.535*	*131.2*	*99.8*	*7.2*	*75.936*	*0.091*
B	0.2	4.330	0.0031	0.0051	10.238	163.0	100.0	55.2	73.984	0.017
C	0.3	4.338	0.0038	0.0037	4.118	135.5	100.0	74.5	74.121	0.036
D	0.5	4.366	0.0051	0.0310	1.081	100.2	99.8	79.6	74.46	0.12
E	3.0	4.355	0.0046	0.0107	4.358	110.5	99.9	100.0	74.379	0.035
Integrated age ± 1s			n=5		21.330				74.256	0.092
Plateau ± 1s		steps B-E	n=4	MSWD=39.09	19.795			92.8	74.08	0.126
		CM-SS4, Sanidine, J=0.009546±0.12%, IC=1.058206±0.0009102, NM-254E, Lab#=61414-11, Argus VI								
A	*0.1*	*4.535*	*0.0057*	*0.0298*	*0.896*	*89.0*	*99.8*	*6.2*	*77.30*	*0.15*
B	0.2	4.644	-0.0176	0.2542	0.225	-	98.3	7.7	78.0	2.1
C	0.3	4.411	0.0051	0.0008	7.374	99.4	100.0	58.5	75.366	0.021
D	0.5	4.420	0.0049	-0.0007	3.607	104.8	100.0	83.4	75.518	0.039
E	3.0	4.426	0.0052	0.0044	2.408	97.9	100.0	100.0	75.591	0.058
Integrated age ± 1s			n=5		14.510				75.601	0.100
Plateau ± 1s		steps B-E	n=4	MSWD=7.61	13.614			93.8	75.42	0.104
		CM-SS4, Sanidine, J=0.009546±0.12%, IC=1.058206±0.0009102, NM-254E, Lab#=61414-12, Argus VI								

ID	Power (Watts)	$^{40}Ar/^{39}Ar$	$^{37}Ar/^{39}Ar$	$^{36}Ar/^{39}Ar$ (x 10^{-3})	$^{39}Ar_K$ (x 10^{-15} mol)	K/Ca	^{40}Ar* (%)	^{39}Ar (%)	Age (Ma)	±1σ (Ma)
A	*0.1*	*4.400*	*0.0050*	*0.0058*	*1.097*	*101.7*	*100.0*	*4.7*	*75.15*	*0.12*
B	0.2	4.300	0.0040	0.0028	9.731	126.9	100.0	46.6	73.499	0.016
C	0.3	4.313	0.0050	0.0012	2.827	102.2	100.0	58.7	73.717	0.051
D	0.5	4.320	0.0035	0.0053	2.707	147.9	100.0	70.4	73.818	0.052
E	3.0	4.316	0.0040	0.0208	6.884	126.9	99.9	100.0	73.671	0.023
Integrated age ± 1s			n=5		23.246				73.692	0.091
Plateau ± 1s		steps B-E	n=4	MSWD=22.83	22.148			95.3	73.582	0.108
		CM-SS4, Sanidine, J=0.009546±0.12%, IC=1.058206±0.0009102, NM-254E, Lab#=61414-13, Argus VI								
A	*0.1*	*4.199*	*0.0064*	*0.0234*	*0.461*	*80.2*	*99.8*	*3.4*	*71.69*	*0.28*
B	0.2	4.035	0.0039	0.0034	6.037	130.0	100.0	47.3	69.032	0.025
C	0.3	4.027	0.0050	-0.0106	1.750	101.8	100.1	60.0	68.979	0.075
D	0.5	4.044	0.0043	0.0127	1.035	118.9	99.9	67.5	69.15	0.13
E	3.0	4.054	0.0042	0.0102	4.461	121.1	99.9	100.0	69.323	0.032
Integrated age ± 1s			n=5		13.744				69.218	0.088
Plateau ± 1s		steps B-E	n=4	MSWD=18.62	13.283			96.6	69.130	0.117
		CM-SS4, Sanidine, J=0.009546±0.12%, IC=1.058206±0.0009102, NM-254E, Lab#=61414-14, Argus VI								
A	*0.1*	*4.609*	*-0.0012*	*-0.0855*	*0.244*	-	*100.6*	*1.2*	*79.1*	*2.2*
B	*0.2*	*4.365*	*0.0045*	*0.0137*	*3.151*	*112.2*	*99.9*	*16.8*	*74.526*	*0.046*
C	0.3	4.348	0.0044	0.0021	5.189	115.3	100.0	42.4	74.295	0.028
D	0.5	4.354	0.0042	0.0056	5.382	120.4	100.0	68.9	74.389	0.029
E	3.0	4.334	0.0041	0.0124	6.298	126.0	99.9	100.0	74.021	0.025
Integrated age ± 1s			n=5		20.264				74.329	0.096
Plateau ± 1s		steps C-E	n=3	MSWD=50.97	16.868			83.2	74.22	0.145

ID	Power (Watts)	$^{40}Ar/^{39}Ar$	$^{37}Ar/^{39}Ar$	$^{36}Ar/^{39}Ar$ (x 10^{-3})	$^{39}Ar_K$ (x 10^{-15} mol)	K/Ca	$^{40}Ar^*$ (%)	^{39}Ar (%)	Age (Ma)	±1σ (Ma)
		CM-SS4, Sanidine, J=0.009546±0.12%, IC=1.058206±0.0009102, NM-254E, Lab#=61414-15, Argus VI								
A	0.1	4.369	0.0519	-0.7116	0.148	9.8	104.9	0.5	78.3	3.4
B	0.2	4.101	0.0043	0.0003	2.962	118.2	100.0	10.9	70.160	0.046
C	0.3	4.063	0.0041	0.0041	11.057	123.1	100.0	49.7	69.505	0.015
D	0.5	4.062	0.0048	0.0068	5.817	105.2	100.0	70.2	69.470	0.025
E	3.0	4.104	0.0047	0.0395	8.503	107.8	99.7	100.0	70.015	0.021
Integrated age ± 1s			n=5		28.488				69.765	0.088
Plateau ± 1s		steps A-E	n=5	MSWD=145.54	28.488			100.0	69.67	0.155
		CM-SS4, Sanidine, J=0.009546±0.12%, IC=1.058206±0.0009102, NM-254E, Lab#=61414-16, Argus VI								
A	*0.1*	*10.58*	*-0.7030*	*8.901*	*0.009*	-	*74.4*	*0.1*	*132.5*	*52.6*
B	*0.2*	*7.113*	*0.0213*	*0.0432*	*0.328*	*24.0*	*99.8*	*5.0*	*119.9*	*1.5*
C	*0.3*	*13.60*	*0.0010*	*-0.0053*	*5.460*	*487.9*	*100.0*	*86.9*	*223.3*	*1.1*
D	0.5	12.70	-0.0016	0.1931	0.319	-	99.5	91.7	208.4	2.6
E	3.0	12.42	0.0060	0.1085	0.554	84.6	99.7	100.0	204.5	1.8
Integrated age ± 1s			n=5		6.670				215.97	0.93
Plateau ± 1s		steps D-E	n=2	MSWD=1.55	0.873			13.1	205.84	1.878
		CM-SS4, Sanidine, J=0.009546±0.12%, IC=1.058206±0.0009102, NM-254E, Lab#=61414-17, Argus VI								
B	0.2	4.372	0.0056	-0.0131	0.561	90.5	100.1	9.9	74.79	0.22
C	0.3	4.340	0.0048	0.0124	2.873	106.2	99.9	60.8	74.112	0.049
D	0.5	4.359	0.0024	0.0324	0.937	213.9	99.8	77.4	74.34	0.14
E	3.0	4.282	0.0049	0.0207	1.277	105.2	99.9	100.0	73.10	0.10
Integrated age ± 1s			n=4		5.648				73.99	0.10

ID	Power (Watts)	$^{40}Ar/^{39}Ar$	$^{37}Ar/^{39}Ar$	$^{36}Ar/^{39}Ar$ (x 10^{-3})	$^{39}Ar_K$ (x 10^{-15} mol)	K/Ca	$^{40}Ar^*$ (%)	^{39}Ar (%)	Age (Ma)	±1σ (Ma)
Plateau ± 1s		steps B-E	n=4	MSWD=34.12	5.648			100.0	73.99	0.256
		CM-SS4, Sanidine, J=0.009546±0.12%, IC=1.058206±0.0009102, NM-254E, Lab#=61414-18, Argus VI								
A	0.1	-0.9273	0.0258	5.749	0.007	19.8	284.3	0.0	-47.1	65.6
B	0.2	4.549	0.0040	-0.4484	0.170	127.3	103.0	1.0	79.9	3.2
C	0.3	4.404	0.0034	0.0064	8.448	149.6	100.0	51.3	75.225	0.019
D	0.5	4.412	0.0032	-0.0080	2.035	158.1	100.1	63.4	75.432	0.065
E	3.0	4.394	0.0040	0.0090	6.155	127.8	99.9	100.0	75.040	0.025
Integrated age ± 1s			n=5		16.815				75.18	0.10
Plateau ± 1s		steps A-E	n=5	MSWD=14.61	16.815			100.0	75.169	0.108
		CM-SS4, Sanidine, J=0.009546±0.12%, IC=1.058206±0.0009102, NM-254E, Lab#=61414-19, Argus VI								
A	0.1	3.997	0.0032	0.0206	3.349	157.5	99.9	25.5	68.302	0.041
B	0.2	3.976	0.0033	0.0010	7.275	152.4	100.0	80.8	68.062	0.021
C	0.3	3.999	0.0050	0.0133	1.428	102.4	99.9	91.6	68.374	0.097
D	3.0	4.027	0.0049	0.0572	1.102	103.7	99.6	100.0	68.64	0.17
Integrated age ± 1s			n=4		13.155				68.206	0.087
Plateau ± 1s		steps A-D	n=4	MSWD=14.29	13.155			100.0	68.13	0.109
		CM-SS4, Sanidine, J=0.009546±0.12%, IC=1.058206±0.0009102, NM-254E, Lab#=61414-20, Argus VI								
A	*0.1*	*94.75*	*0.0599*	*0.6422*	*0.122*	*8.5*	*99.8*	*4.0*	*1177*	*19*
B	*3.0*	*108.9*	*0.0023*	*-0.0090*	*2.923*	*218.7*	*100.0*	*100.0*	*1304.35*	*0.36*
Integrated age ± 1s			n=2		3.045				1299.4	1.5
Plateau ± 1s		no plateau								

ID	Power (Watts)	$^{40}Ar/^{39}Ar$	$^{37}Ar/^{39}Ar$	$^{36}Ar/^{39}Ar$ (x 10^{-3})	$^{39}Ar_K$ (x 10^{-15} mol)	K/Ca	$^{40}Ar^*$ (%)	^{39}Ar (%)	Age (Ma)	±1σ (Ma)
		CM-SS4, Sanidine, J=0.009546±0.12%, IC=1.058206±0.0009102, NM-254E, Lab#=61414-21, Argus VI								
A	*0.1*	*3.054*	*0.0073*	*0.2151*	*0.253*	*69.6*	*97.9*	*1.5*	*51.39*	*0.48*
B	*0.2*	*4.498*	*0.0076*	*0.1118*	*0.358*	*67.5*	*99.3*	*3.7*	*76.27*	*0.36*
C	0.3	4.394	0.0053	-0.0003	8.702	96.9	100.0	57.0	75.081	0.019
D	0.5	4.391	0.0053	0.0178	1.290	96.9	99.9	64.9	74.95	0.10
E	3.0	4.409	0.0045	0.0070	5.729	112.3	100.0	100.0	75.305	0.038
Integrated age ± 1s			n=5		16.332				74.811	0.094
Plateau ± 1s		steps C-E	n=3	MSWD=15.47	15.721			96.3	75.12	0.112
		CM-SS4, Sanidine, J=0.009546±0.12%, IC=1.058206±0.0009102, NM-254E, Lab#=61414-22, Argus VI								
A	0.1	4.739	-0.0335	0.4589	0.120	-	97.1	1.6	78.5	2.9
B	3.0	4.462	0.0058	0.0046	7.190	88.0	100.0	100.0	76.200	0.025
Integrated age ± 1s			n=2		7.310				76.24	0.11
Plateau ± 1s		steps A-B	n=2	MSWD=0.66	7.310			100.0	76.20	0.096
		CM-SS4, Sanidine, J=0.009546±0.12%, IC=1.058206±0.0009102, NM-254E, Lab#=61414-23, Argus VI								
A	0.1	4.356	0.0041	0.0264	2.698	123.6	99.8	51.2	74.32	0.30
B	3.0	4.359	0.0033	0.0014	2.567	154.8	100.0	100.0	74.489	0.057
Integrated age ± 1s			n=2		5.264				74.40	0.18
Plateau ± 1s		steps A-B	n=2	MSWD=0.31	5.264			100.0	74.48	0.107
		CM-SS4, Sanidine, J=0.009546±0.12%, IC=1.058206±0.0009102, NM-254E, Lab#=61414-24, Argus VI								
A	0.1	4.490	0.0099	0.0449	1.595	51.4	99.7	25.9	76.47	0.34
B	3.0	4.459	0.0071	0.0133	4.551	72.2	99.9	100.0	76.113	0.037
Integrated age ± 1s			n=2		6.146	65.3			76.21	0.13

ID	Power (Watts)	$^{40}Ar/^{39}Ar$	$^{37}Ar/^{39}Ar$	$^{36}Ar/^{39}Ar$ (x 10^{-3})	$^{39}Ar_K$ (x 10^{-15} mol)	K/Ca	$^{40}Ar^*$ (%)	^{39}Ar (%)	Age (Ma)	±1σ (Ma)
Plateau ± 1s		steps A-B	n=2	MSWD=1.09	6.146	66.765±14.688		100.0	76.12	0.101
		CM-SS4, Sanidine, J=0.009546±0.12%, IC=1.058206±0.0009102, NM-254E, Lab#=61414-25, Argus VI								
A	0.1	4.396	0.0043	0.0099	3.846	119.4	99.9	75.6	75.06	0.18
B	3.0	4.368	0.0062	0.0309	1.240	82.1	99.8	100.0	74.49	0.12
Integrated age ± 1s			n=2		5.086	107.5			74.92	0.17
Plateau ± 1s		steps A-B	n=2	MSWD=6.92	5.086	110.303±26.369		100.0	74.66	0.274
		CM-SS4, Sanidine, J=0.009546±0.12%, IC=1.058206±0.0009102, NM-254E, Lab#=61414-26, Argus VI								
A	*0.1*	*7.182*	*0.0837*	*-1.7894*	*0.090*	*6.1*	*107.6*	*2.8*	*130.1*	*5.1*
B	*3.0*	*6.048*	*0.0012*	*0.0238*	*3.161*	*418.4*	*99.9*	*100.0*	*102.493*	*0.049*
Integrated age ± 1s			n=2		3.251	145.7			103.26	0.18
Step B			N=1		3.161			97.2	102.493	0.049
		CM-SS4, Sanidine, J=0.009546±0.12%, IC=1.058206±0.0009102, NM-254E, Lab#=61414-27, Argus VI								
A	0.1	4.492	0.0046	0.0276	4.930	110.1	99.8	73.7	76.59	0.14
B	3.0	4.472	0.0078	0.0577	1.763	65.0	99.6	100.0	76.117	0.087
Integrated age ± 1s			n=2		6.693	93.1			76.47	0.14
Plateau ± 1s		steps A-B	n=2	MSWD=8.04	6.693	98.243±31.874		100.0	76.25	0.231
		CM-SS4, Sanidine, J=0.009546±0.12%, IC=1.058206±0.0009102, NM-254E, Lab#=61414-31, Argus VI								
A	0.1	4.383	0.0035	0.0246	4.874	147.7	99.8	52.9	74.77	0.25
B	3.0	4.351	0.0035	0.0104	4.340	144.6	99.9	100.0	74.307	0.036
Integrated age ± 1s			n=2		9.214	146.2			74.55	0.16
Plateau ± 1s		steps A-B	n=2	MSWD=3.51	9.214	146.227±2.220		100.0	74.32	0.113

ID	Power (Watts)	^{40}Ar/^{39}Ar	^{37}Ar/^{39}Ar	^{36}Ar/^{39}Ar (x 10^{-3})	^{39}Ar$_K$ (x 10^{-15} mol)	K/Ca	^{40}Ar* (%)	^{39}Ar (%)	Age (Ma)	±1σ (Ma)
CM-SS4, Sanidine, J=0.009546±0.12%, IC=1.058206±0.0009102, NM-254E, Lab#=61414-32, Argus VI										
A	0.1	11.89	0.0044	-0.0026	2.136	116.1	100.0	26.5	196.74	0.76
B	3.0	11.72	0.0023	0.0064	5.911	226.3	100.0	100.0	193.955	0.059
	Integrated age ± 1s		n=2		8.047	180.7			194.70	0.31
Plateau ± 1s		steps A-B	n=2	MSWD=13.32	8.047	197.018±77.920		100.0	193.97	0.315
CM-SS4, Sanidine, J=0.009546±0.12%, IC=1.058206±0.0009102, NM-254E, Lab#=61414-33, Argus VI										
A	*0.1*	*4.888*	*0.0047*	*-0.0015*	*5.237*	*108.2*	*100.0*	*38.2*	*83.37*	*0.15*
B	3.0	4.851	0.0050	0.0039	8.460	102.3	100.0	100.0	82.717	0.022
	Integrated age ± 1s		n=2		13.697	104.5			82.96	0.12
Step B			n=1		8.460			61.8	82.717	0.022
CM-SS4, Sanidine, J=0.009546±0.12%, IC=1.058206±0.0009102, NM-254E, Lab#=61414-34, Argus VI										
A	0.1	4.216	0.0071	-0.0973	0.467	71.8	100.7	1.9	72.59	0.86
B	3.0	4.374	0.0043	0.0040	24.769	119.7	100.0	100.0	74.727	0.010
	Integrated age ± 1s		n=2		25.236	118.3			74.687	0.093
Plateau ± 1s		steps A-B	n=2	MSWD=6.16	25.236	118.841±33.859		100.0	74.73	0.095
CM-SS4, Sanidine, J=0.009546±0.12%, IC=1.058206±0.0009102, NM-254E, Lab#=61414-35, Argus VI										
A	0.1	4.466	0.0040	0.0346	2.715	129.2	99.8	57.5	76.12	0.19
B	3.0	4.479	0.0043	0.0136	2.008	118.2	99.9	100.0	76.448	0.071
	Integrated age ± 1s		n=2		4.723	124.3			76.26	0.15
Plateau ± 1s		steps A-B	n=2	MSWD=2.55	4.723	124.515±7.715		100.0	76.41	0.141

ID	Power (Watts)	$^{40}Ar/^{39}Ar$	$^{37}Ar/^{39}Ar$	$^{36}Ar/^{39}Ar$ (x 10^{-3})	$^{39}Ar_K$ (x 10^{-15} mol)	K/Ca	$^{40}Ar^*$ (%)	^{39}Ar (%)	Age (Ma)	±1σ (Ma)
CM-SS4, Sanidine, J=0.009546±0.12%, IC=1.058206±0.0009102, NM-254E, Lab#=61414-36, Argus VI										
A	0.1	4.508	0.0025	0.0019	2.146	203.2	100.0	7.8	76.99	0.27
B	3.0	4.468	0.0056	0.0032	25.327	91.4	100.0	100.0	76.311	0.011
Integrated age ± 1s			n=2		27.473	95.5			76.364	0.096
Plateau ± 1s		steps A-B	n=2	MSWD=6.12	27.473	100.121±79.078		100.0	76.31	0.097
CM-SS4, Sanidine, J=0.009546±0.12%, IC=1.058206±0.0009102, NM-254E, Lab#=61414-37, Argus VI										
A	*0.1*	*3.978*	*0.0122*	*-0.2947*	*0.636*	*41.8*	*102.2*	*9.6*	*69.59*	*0.70*
B	3.0	4.345	0.0032	0.0047	5.991	157.1	100.0	100.0	74.232	0.030
Integrated age ± 1s			n=2		6.627	124.2			73.79	0.12
Step B			n=1		5.991			90.4	74.232	0.030
CM-SS4, Sanidine, J=0.009546±0.12%, IC=1.058206±0.0009102, NM-254E, Lab#=61414-38, Argus VI										
A	0.1	4.427	0.0061	-0.0047	4.587	83.1	100.0	68.1	75.67	0.17
B	3.0	4.460	0.0047	0.1188	2.154	108.2	99.2	100.0	75.600	0.067
Integrated age ± 1s			n=2		6.741	89.7			75.65	0.15
Plateau ± 1s		steps A-B	n=2	MSWD=0.13	6.741	91.104±17.797		100.0	75.61	0.112
CM-SS4, Sanidine, J=0.009546±0.12%, IC=1.058206±0.0009102, NM-254E, Lab#=61414-39, Argus VI										
A	*0.1*	*4.176*	*0.0033*	*-0.0062*	*1.756*	*152.8*	*100.1*	*17.7*	*71.45*	*0.45*
B	3.0	4.069	0.0033	0.0052	8.147	155.5	100.0	100.0	69.599	0.023
Integrated age ± 1s			n=2		9.903	155.0			69.93	0.12
Step B			n=1		8.147			82.3	69.599	0.023
CM-SS4, Sanidine, J=0.009546±0.12%, IC=1.058206±0.0009102, NM-254E, Lab#=61414-40, Argus VI										

ID	Power (Watts)	$^{40}Ar/^{39}Ar$	$^{37}Ar/^{39}Ar$	$^{36}Ar/^{39}Ar$ (x 10^{-3})	$^{39}Ar_K$ (x 10^{-15} mol)	K/Ca	$^{40}Ar^*$ (%)	^{39}Ar (%)	Age (Ma)	±1σ (Ma)
A	*0.1*	*3.864*	*0.0047*	*0.0296*	*0.973*	*109.1*	*99.8*	*8.7*	*66.02*	*0.13*
B	0.2	4.149	0.0025	0.0020	5.668	201.6	100.0	59.5	70.957	0.034
C	0.3	4.165	0.0017	0.0177	4.517	294.9	99.9	100.0	71.140	0.035
Integrated age ± 1s			n=3		11.159	213.2			70.602	0.090
Plateau ± 1s		steps B-C	n=2	MSWD=13.87	10.186	242.979±65.927		91.3	71.04	0.126
		CM-SS4, Sanidine, J=0.009546±0.12%, IC=1.058206±0.0009102, NM-254E, Lab#=61414-41, Argus VI								
A	*0.1*	*4.492*	*0.0064*	*-0.0033*	*5.105*	*79.3*	*100.0*	*52.1*	*76.75*	*0.24*
B	3.0	4.443	0.0056	0.0101	4.689	91.9	99.9	100.0	75.860	0.036
Integrated age ± 1s			n=2		9.794	84.9			76.32	0.16
Step B			n=1		4.689			47.9	75.860	0.036
		CM-SS4, Sanidine, J=0.009546±0.12%, IC=1.058206±0.0009102, NM-254E, Lab#=61414-42, Argus VI								
A	0.1	4.353	0.0027	0.0203	2.043	190.0	99.9	39.5	74.29	0.40
B	3.0	4.384	0.0040	0.0323	3.134	127.7	99.8	100.0	74.755	0.052
Integrated age ± 1s			n=2		5.177	146.7			74.57	0.19
Plateau ± 1s		steps A-B	n=2	MSWD=1.33	5.177	152.320±44.049		100.0	74.75	0.109
		CM-SS4, Sanidine, J=0.009546±0.12%, IC=1.058206±0.0009102, NM-254E, Lab#=61414-43, Argus VI								
A	0.1	3.829	0.0154	0.0330	0.052	33.1	99.7	7.8	65.4	7.8
B	3.0	4.518	0.0033	0.1116	0.608	153.4	99.3	100.0	76.60	0.24
Integrated age ± 1s			n=2		0.660	119.4			75.73	0.68
Plateau ± 1s		steps A-B	n=2	MSWD=2.05	0.660	144.016±85.095		100.0	76.59	0.362
		CM-SS4, Sanidine, J=0.009546±0.12%, IC=1.058206±0.0009102, NM-254E, Lab#=61414-44, Argus VI								

ID	Power (Watts)	$^{40}Ar/^{39}Ar$	$^{37}Ar/^{39}Ar$	$^{36}Ar/^{39}Ar$ (x 10^{-3})	$^{39}Ar_K$ (x 10^{-15} mol)	K/Ca	$^{40}Ar^*$ (%)	^{39}Ar (%)	Age (Ma)	±1σ (Ma)
A	0.1	4.315	0.0021	-0.0003	1.539	238.4	100.0	24.3	73.76	0.35
B	3.0	4.379	0.0035	0.0123	4.790	144.8	99.9	100.0	74.771	0.033
Integrated age ± 1s			n=2		6.330	160.1			74.52	0.13
Plateau ± 1s		steps A-B	n=2	MSWD=8.39	6.330	167.548±66.161		100.0	74.76	0.131
CM-SS4, Sanidine, J=0.009546±0.12%, IC=1.058206±0.0009102, NM-254E, Lab#=61414-45, Argus VI										
A	0.1	5.603	0.3134	0.7047	0.016	1.6	97.0	1.3	92.5	23.6
B	3.0	4.418	0.0038	0.0661	1.231	133.1	99.6	100.0	75.15	0.12
Integrated age ± 1s			n=2		1.247	66.1			75.37	0.31
Plateau ± 1s		steps A-B	n=2	MSWD=0.54	1.247	131.492±92.995		100.0	75.15	0.148
CM-SS4, Sanidine, J=0.009546±0.12%, IC=1.058206±0.0009102, NM-254E, Lab#=61414-46, Argus VI										
A	*0.1*	*7.912*	*0.0040*	*0.4964*	*0.337*	*127.9*	*98.1*	*5.6*	*130.7*	*1.5*
B	3.0	4.801	0.0032	0.0078	5.672	160.5	100.0	100.0	81.852	0.032
Integrated age ± 1s			n=2		6.009	158.3			84.63	0.13
Step B			n=1		5.672			94.4	81.852	0.032
CM-SS4, Sanidine, J=0.009546±0.12%, IC=1.058206±0.0009102, NM-254E, Lab#=61414-47, Argus VI										
A	0.1	4.403	0.0043	0.0388	3.802	119.7	99.7	55.0	75.05	0.27
B	3.0	4.361	0.0051	0.0066	3.115	99.8	100.0	100.0	74.493	0.053
Integrated age ± 1s			n=2		6.917	109.8			74.80	0.17
Plateau ± 1s		steps A-B	n=2	MSWD=4.13	6.917	110.750±14.093		100.0	74.51	0.139
CM-SS4, Sanidine, J=0.009546±0.12%, IC=1.058206±0.0009102, NM-254E, Lab#=61414-48, Argus VI										
A	0.1	4.479	0.0062	0.3856	0.374	82.4	97.4	5.2	74.58	0.97

ID	Power (Watts)	$^{40}Ar/^{39}Ar$	$^{37}Ar/^{39}Ar$	$^{36}Ar/^{39}Ar$ (x 10^{-3})	$^{39}Ar_K$ (x 10^{-15} mol)	K/Ca	$^{40}Ar^*$ (%)	^{39}Ar (%)	Age (Ma)	±1σ (Ma)
B	3.0	4.373	0.0041	0.0025	6.848	124.2	100.0	100.0	74.717	0.026
Integrated age ± 1s			n=2		7.222	121.1			74.71	0.11
Plateau ± 1s		steps A-B	n=2	MSWD=0.02	7.222	122.082±29.611		100.0	74.72	0.095
		CM-SS4, Sanidine, J=0.009546±0.12%, IC=1.058206±0.0009102, NM-254E, Lab#=61414-51, Argus VI								
A	*0.1*	*4.465*	*0.0062*	*0.0104*	*4.223*	*82.6*	*99.9*	*23.4*	*76.23*	*0.26*
B	3.0	4.417	0.0042	0.0052	13.851	122.3	100.0	100.0	75.447	0.016
Integrated age ± 1s			n=2		18.075	110.0			75.63	0.11
Step B			n=1		13.851			76.6	75.447	0.016
		CM-SS4, Sanidine, J=0.009546±0.12%, IC=1.058206±0.0009102, NM-254E, Lab#=61414-52, Argus VI								
A	0.1	4.452	0.0060	-0.0385	2.514	84.6	100.3	67.6	76.25	0.24
B	3.0	4.443	0.0046	-0.0166	1.208	110.4	100.1	100.0	76.00	0.11
Integrated age ± 1s			n=2		3.722	91.5			76.17	0.19
Plateau ± 1s		steps A-B	n=2	MSWD=0.92	3.722	92.942±18.224		100.0	76.04	0.138
		CM-SS4, Sanidine, J=0.009546±0.12%, IC=1.058206±0.0009102, NM-254E, Lab#=61414-53, Argus VI								
A	*0.1*	*43.17*	*0.0081*	*0.0007*	*2.985*	*62.8*	*100.0*	*32.7*	*631.5*	*1.4*
B	3.0	14.36	0.0074	0.0084	6.138	68.6	100.0	100.0	234.987	0.063
Integrated age ± 1s			n=2		9.124	66.6			374.42	0.51
No Plateau										
		CM-SS4, Sanidine, J=0.009546±0.12%, IC=1.058206±0.0009102, NM-254E, Lab#=61414-54, Argus VI								
A	0.1	4.363	-0.0094	0.0955	0.268	-	99.3	5.2	74.1	1.4
B	3.0	4.368	0.0042	0.0046	4.910	122.7	100.0	100.0	74.626	0.035

ID	Power (Watts)	$^{40}Ar/^{39}Ar$	$^{37}Ar/^{39}Ar$	$^{36}Ar/^{39}Ar$ (x 10^{-3})	$^{39}Ar_K$ (x 10^{-15} mol)	K/Ca	$^{40}Ar^*$ (%)	^{39}Ar (%)	Age (Ma)	±1σ (Ma)
Integrated age ± 1s			n=2		5.178	147.6			74.60	0.12
Plateau ± 1s		steps A-B	n=2	MSWD=0.15	5.178	122.719±0.000		100.0	74.63	0.098
CM-SS4, Sanidine, J=0.009546±0.12%, IC=1.058206±0.0009102, NM-254E, Lab#=61414-55, Argus VI										
A	0.1	4.400	0.0031	0.0220	2.362	162.8	99.9	63.3	75.07	0.24
B	3.0	4.394	0.0002	0.0218	1.367	2231.9	99.9	100.0	74.97	0.11
Integrated age ± 1s			n=2		3.730	246.7			75.03	0.18
Plateau ± 1s		steps A-B	n=2	MSWD=0.14	3.730	921.414±1463.029		100.0	74.99	0.134
CM-SS4, Sanidine, J=0.009546±0.12%, IC=1.058206±0.0009102, NM-254E, Lab#=61414-56, Argus VI										
A	0.1	4.437	0.0050	0.0016	2.502	102.4	100.0	57.5	75.80	0.19
B	3.0	4.492	0.0058	0.0459	1.848	88.7	99.7	100.0	76.508	0.078
Integrated age ± 1s			n=2		4.350	96.1			76.10	0.15
Plateau ± 1s		steps A-B	n=2	MSWD=11.97	4.350	96.579±9.655		100.0	76.40	0.266
CM-SS4, Sanidine, J=0.009546±0.12%, IC=1.058206±0.0009102, NM-254E, Lab#=61414-57, Argus VI										
A	0.1	3.024	-0.0409	-2.5036	0.009	-	125.0	0.4	64.7	33.9
B	3.0	43.81	0.0010	0.0450	2.460	492.4	100.0	100.0	639.27	0.27
Integrated age ± 1s			n=2		2.468	576.0			637.51	0.93
Plateau ± 1s		steps A-B	n=2	MSWD=287.35	2.468	492.427±0.000		100.0	639.24	4.639
CM-SS4, Sanidine, J=0.009546±0.12%, IC=1.058206±0.0009102, NM-254E, Lab#=61414-58, Argus VI										
A	0.1	4.394	0.0127	0.2119	0.325	40.0	98.6	3.7	74.0	1.1
B	3.0	4.324	0.0052	0.0080	8.532	97.6	100.0	100.0	73.873	0.021
Integrated age ± 1s			n=2		8.857	92.7			73.88	0.10

ID	Power (Watts)	$^{40}Ar/^{39}Ar$	$^{37}Ar/^{39}Ar$	$^{36}Ar/^{39}Ar$ (x 10^{-3})	$^{39}Ar_K$ (x 10^{-15} mol)	K/Ca	$^{40}Ar^*$ (%)	^{39}Ar (%)	Age (Ma)	±1σ (Ma)
Plateau ± 1s		steps A-B	n=2	MSWD=0.02	8.857	95.485±40.715		100.0	73.87	0.093
		CM-SS4, Sanidine, J=0.009546±0.12%, IC=1.058206±0.0009102, NM-254E, Lab#=61414-59, Argus VI								
A	*0.1*	*4.659*	*0.0016*	*0.0478*	*2.250*	*327.1*	*99.7*	*63.9*	*79.28*	*0.32*
B	3.0	4.433	0.0048	0.0200	1.269	107.1	99.9	100.0	75.64	0.12
Integrated age ± 1s			n=2		3.519	187.9			77.97	0.23
Step B			n=1		1.269			36.1	75.64	0.12
		CM-SS4, Sanidine, J=0.009546±0.12%, IC=1.058206±0.0009102, NM-254E, Lab#=61414-60, Argus VI								
A	0.1	4.414	0.0046	-0.0375	0.625	111.5	100.3	15.3	75.60	0.58
B	3.0	4.334	0.0033	0.0047	3.472	154.2	100.0	100.0	74.055	0.041
Integrated age ± 1s			n=2		4.097	145.7			74.29	0.13
Plateau ± 1s		steps A-B	n=2	MSWD=6.96	4.097	147.694±30.231		100.0	74.06	0.142
		CM-SS4, Sanidine, J=0.009546±0.12%, IC=1.058206±0.0009102, NM-254E, Lab#=61414-61, Argus VI								
A	0.1	4.506	0.0737	-1.3664	0.058	6.9	109.2	1.5	83.9	5.7
B	3.0	4.457	0.0073	0.0012	3.826	70.2	100.0	100.0	76.132	0.041
Integrated age ± 1s			n=2		3.884	61.8			76.25	0.13
Plateau ± 1s		steps A-B	n=2	MSWD=1.86	3.884	69.261±44.744		100.0	76.13	0.109
		CM-SS4, Sanidine, J=0.009546±0.12%, IC=1.058206±0.0009102, NM-254E, Lab#=61414-62, Argus VI								
A	*0.1*	*4.533*	*0.0040*	*-0.0474*	*1.792*	*127.0*	*100.3*	*36.3*	*77.64*	*0.35*
B	3.0	4.455	0.0078	0.0060	3.144	65.8	100.0	100.0	76.086	0.049
Integrated age ± 1s			n=2		4.936	79.7			76.65	0.16
Step B			n=1		3.144			63.7	76.086	0.049

ID	Power (Watts)	$^{40}Ar/^{39}Ar$	$^{37}Ar/^{39}Ar$	$^{36}Ar/^{39}Ar$ (x 10^{-3})	$^{39}Ar_K$ (x 10^{-15} mol)	K/Ca	$^{40}Ar^*$ (%)	^{39}Ar (%)	Age (Ma)	±1σ (Ma)
CM-SS4, Sanidine, J=0.009546±0.12%, IC=1.058206±0.0009102, NM-254E, Lab#=61414-63, Argus VI										
A	0.1	3.869	0.0116	0.0124	2.347	43.8	99.9	38.4	66.204	0.058
B	0.2	3.866	0.0109	0.0148	1.559	46.8	99.9	63.9	66.150	0.084
C	0.3	3.879	0.0131	-0.0123	1.409	39.0	100.1	87.0	66.503	0.094
D	0.5	3.927	0.0121	0.0763	0.303	42.1	99.4	91.9	66.86	0.40
E	3.0	3.906	0.0133	0.0172	0.494	38.4	99.9	100.0	66.80	0.25
Integrated age ± 1s			n=5		6.111	42.7			66.340	0.094
Plateau ± 1s		steps A-E	n=5	MSWD=4.09	6.111	42.9 ±3.5		100.0	66.27	0.12
CM-SS4, Sanidine, J=0.009546±0.12%, IC=1.058206±0.0009102, NM-254E, Lab#=61414-65, Argus VI										
A	0.1	4.044	0.0048	-0.0120	0.023	106.7	100.1	1.4	69.3	13.8
B	3.0	4.380	0.0055	0.0088	1.669	92.0	100.0	100.0	74.806	0.089
Integrated age ± 1s			n=2		1.692	92.1			74.73	0.23
Plateau ± 1s		steps A-B	n=2	MSWD=0.16	1.692	92.160±10.431		100.0	74.81	0.127
CM-SS4, Sanidine, J=0.009546±0.12%, IC=1.058206±0.0009102, NM-254E, Lab#=61414-67, Argus VI										
A	*0.1*	*11.39*	*0.0031*	*0.0187*	*2.801*	*166.5*	*100.0*	*79.7*	*188.65*	*0.56*
B	*3.0*	*11.79*	*0.0041*	*-0.0088*	*0.713*	*124.5*	*100.0*	*100.0*	*195.11*	*0.28*
Integrated age ± 1s			n=2		3.514	155.8			189.96	0.51
No Plateau										
CM-SS4, Sanidine, J=0.009546±0.12%, IC=1.058206±0.0009102, NM-254E, Lab#=61414-68, Argus VI										
A	0.1	4.400	0.0038	-0.0024	3.158	135.0	100.0	62.2	75.19	0.18
B	3.0	4.380	0.0025	0.0000	1.918	201.4	100.0	100.0	74.851	0.081

ID	Power (Watts)	$^{40}Ar/^{39}Ar$	$^{37}Ar/^{39}Ar$	$^{36}Ar/^{39}Ar$ (x 10^{-3})	$^{39}Ar_K$ (x 10^{-15} mol)	K/Ca	$^{40}Ar^*$ (%)	^{39}Ar (%)	Age (Ma)	±1σ (Ma)
Integrated age ± 1s			n=2		5.076	154.2			75.06	0.15
Plateau ± 1s		steps A-B	n=2	MSWD=2.93	5.076	160.078±46.935		100.0	74.91	0.156
		CM-SS4, Sanidine, J=0.009546±0.12%, IC=1.058206±0.0009102, NM-254E, Lab#=61414-69, Argus VI								
A	*0.1*	*39.89*	*0.0025*	*0.1017*	*1.582*	*201.7*	*99.9*	*38.5*	*590.2*	*2.7*
B	*3.0*	*53.23*	*0.0023*	*0.0318*	*2.528*	*222.4*	*100.0*	*100.0*	*751.92*	*0.30*
Integrated age ± 1s			n=2		4.110	214.0			691.4	1.4
Plateau ± 1s		no plateau								
		CM-SS4, Sanidine, J=0.009546±0.12%, IC=1.058206±0.0009102, NM-254E, Lab#=61414-70, Argus VI								
A	0.1	9.675	0.0084	-0.0145	1.284	61.0	100.1	25.2	161.65	0.63
B	3.0	9.699	0.0022	0.0055	3.821	233.4	100.0	100.0	161.935	0.057
Integrated age ± 1s			n=2		5.105	136.4			161.86	0.25
Plateau ± 1s		steps A-B	n=2	MSWD=0.20	5.105	190.013±121.882		100.0	161.93	0.201
		CM-SS4, Sanidine, J=0.009546±0.12%, IC=1.058206±0.0009102, NM-254E, Lab#=61414-71, Argus VI								
A	*0.1*	*65.37*	*0.0187*	*0.6244*	*0.081*	*27.2*	*99.7*	*4.5*	*885.5*	*21.8*
B	*3.0*	*69.55*	*0.0000*	*0.0190*	*1.739*	-	*100.0*	*100.0*	*931.87*	*0.47*
Integrated age ± 1s			n=2		1.821				929.8	1.4
Plateau ± 1s		no plateau								
		CM-SS4, Sanidine, J=0.009546±0.12%, IC=1.058206±0.0009102, NM-254E, Lab#=61414-73, Argus VI								
A	*0.1*	*15.95*	*0.0387*	*1.077*	*0.048*	*13.2*	*98.0*	*1.4*	*254.6*	*13.6*
B	3.0	10.74	0.0012	0.0074	3.492	416.9	100.0	100.0	178.429	0.064
Integrated age ± 1s			n=2		3.540	294.8			179.48	0.27

ID	Power (Watts)	$^{40}Ar/^{39}Ar$	$^{37}Ar/^{39}Ar$	$^{36}Ar/^{39}Ar$ (x 10^{-3})	$^{39}Ar_K$ (x 10^{-15} mol)	K/Ca	^{40}Ar* (%)	^{39}Ar (%)	Age (Ma)	±1σ (Ma)
Step B			n=1		3.492			98.6	178.429	0.064
		CM-SS4, Sanidine, J=0.009546±0.12%, IC=1.058206±0.0009102, NM-254E, Lab#=61414-74, Argus VI								
A	0.1	4.432	0.0048	0.0601	2.510	105.9	99.6	55.4	75.42	0.37
B	3.0	4.364	0.0044	0.0013	2.017	115.5	100.0	100.0	74.574	0.073
Integrated age ± 1s			n=2		4.527	110.0			75.05	0.22
Plateau ± 1s		steps A-B	n=2	MSWD=5.17	4.527	110.196±6.776		100.0	74.61	0.187
		CM-SS4, Sanidine, J=0.009546±0.12%, IC=1.058206±0.0009102, NM-254E, Lab#=61414-77, Argus VI								
A	0.1	9.233	0.0213	0.0990	1.596	23.9	99.7	69.6	154.05	0.70
B	3.0	9.200	0.0238	0.1797	0.698	21.4	99.4	100.0	153.13	0.26
Integrated age ± 1s			n=2		2.294	23.1			153.78	0.52
Plateau ± 1s		steps A-B	n=2	MSWD=1.52	2.294	23.178±1.778		100.0	153.25	0.355
		CM-SS4, Sanidine, J=0.009546±0.12%, IC=1.058206±0.0009102, NM-254E, Lab#=61414-78, Argus VI								
A	*0.1*	*6.269*	*0.0365*	*-0.1535*	*0.060*	*14.0*	*100.8*	*3.7*	*107.1*	*7.3*
B	3.0	4.480	0.0078	0.0476	1.552	65.4	99.7	100.0	76.303	0.099
Integrated age ± 1s			n=2		1.613	57.5			77.47	0.28
Step B			n=1		1.552			96.3	76.303	0.099
		CM-SS4, Sanidine, J=0.009546±0.12%, IC=1.058206±0.0009102, NM-254E, Lab#=61414-79, Argus VI								
A	0.1	4.391	0.0045	-0.0118	1.298	113.8	100.1	67.9	75.10	0.43
B	3.0	4.370	0.0048	0.0168	0.613	106.2	99.9	100.0	74.60	0.23
Integrated age ± 1s			n=2		1.911	111.2			74.94	0.31
Plateau ± 1s		steps A-B	n=2	MSWD=1.05	1.911	111.365±5.395		100.0	74.71	0.229

ID	Power (Watts)	$^{40}Ar/^{39}Ar$	$^{37}Ar/^{39}Ar$	$^{36}Ar/^{39}Ar$ (x 10^{-3})	$^{39}Ar_K$ (x 10^{-15} mol)	K/Ca	$^{40}Ar^*$ (%)	^{39}Ar (%)	Age (Ma)	±1σ (Ma)
		CM-SS4, Sanidine, J=0.009546±0.12%, IC=1.058206±0.0009102, NM-254E, Lab#=61414-80, Argus VI								
A	*0.1*	*4.563*	*0.0016*	*0.0224*	*1.064*	*318.1*	*99.9*	*34.0*	*77.80*	*0.57*
B	3.0	5.104	0.0061	0.0119	2.069	84.1	99.9	100.0	86.900	0.075
Integrated age ± 1s			n=2		3.133	112.1			83.82	0.23
Step B			n=1		2.069			66.0	86.900	0.075
		CM-SS4, Sanidine, J=0.009546±0.12%, IC=1.058206±0.0009102, NM-254E, Lab#=61414-81, Argus VI								
A	0.1	4.307	0.0186	0.0771	0.213	27.4	99.5	5.8	73.3	1.8
B	3.0	4.399	0.0063	0.0140	3.433	81.6	99.9	100.0	75.107	0.045
Integrated age ± 1s			n=2		3.646	73.1			75.00	0.15
Plateau ± 1s		steps A-B	n=2	MSWD=1.03	3.646	78.408±38.322		100.0	75.11	0.102
		CM-SS4, Sanidine, J=0.009546±0.12%, IC=1.058206±0.0009102, NM-254E, Lab#=61414-82, Argus VI								
A	*0.1*	*4.172*	*0.0623*	*1.040*	*0.104*	*8.2*	*92.7*	*2.8*	*66.2*	*3.4*
B	0.2	4.389	0.0060	-0.0094	2.521	84.9	100.1	71.5	75.05	0.11
C	3.0	4.426	0.0024	-0.0036	1.046	208.5	100.0	100.0	75.63	0.16
Integrated age ± 1s			n=3		3.671	77.4			74.97	0.16
Plateau ± 1s		steps B-C	n=2	MSWD=8.60	3.567	121.174±87.402		97.2	75.24	0.285
		CM-SS4, Sanidine, J=0.009546±0.12%, IC=1.058206±0.0009102, NM-254E, Lab#=61414-84, Argus VI								
A	0.1	11.79	0.0010	0.0852	3.535	502.0	99.8	74.9	194.65	0.41
B	3.0	11.77	-0.0044	0.0187	1.185	-	100.0	100.0	194.62	0.19
Integrated age ± 1s			n=2		4.720	-1436.854			194.64	0.39
Plateau ± 1s		steps A-B	n=2	MSWD=0.00	4.720	375.948±0.000		100.0	194.62	0.289

ID	Power (Watts)	$^{40}Ar/^{39}Ar$	$^{37}Ar/^{39}Ar$	$^{36}Ar/^{39}Ar$ (x 10^{-3})	$^{39}Ar_K$ (x 10^{-15} mol)	K/Ca	$^{40}Ar^*$ (%)	^{39}Ar (%)	Age (Ma)	±1σ (Ma)
CM-SS4, Sanidine, J=0.009546±0.12%, IC=1.058206±0.0009102, NM-254E, Lab#=61414-85, Argus VI										
A	0.1	11.95	0.0097	-0.0070	1.697	52.6	100.0	38.3	197.6	1.0
B	3.0	11.70	0.0016	0.0593	2.730	312.2	99.8	100.0	193.35	0.11
Integrated age ± 1s			n=2		4.427	108.0			194.98	0.45
Plateau ± 1s		steps A-B	n=2	MSWD=17.21	4.427	212.720±183.579		100.0	193.40	0.494
CM-SS4, Sanidine, J=0.009546±0.12%, IC=1.058206±0.0009102, NM-254E, Lab#=61414-86, Argus VI										
A	*0.1*	*22.35*	*0.0101*	*-0.1276*	*0.595*	*50.8*	*100.2*	*75.4*	*354.5*	*2.1*
B	*3.0*	*31.78*	*0.0147*	*0.1180*	*0.195*	*34.7*	*99.9*	*100.0*	*484.4*	*1.8*
Integrated age ± 1s			n=2		0.790	45.6			387.4	1.8
Plateau ± 1s		no plateau								
CM-SS4, Sanidine, J=0.009546±0.12%, IC=1.058206±0.0009102, NM-254E, Lab#=61414-87, Argus VI										
A	0.1	8.807	0.0038	0.0318	0.760	135.2	99.9	19.0	147.49	0.94
B	3.0	77.74	0.0051	0.0320	3.230	99.8	100.0	100.0	1015.97	0.31
Integrated age ± 1s			n=2		3.990	105.1			879.3	1.2
Plateau ± 1s		no plateau								
SJ-SS5, Sanidine, J=0.0095555±0.07%, IC=1.05962±0.0011331, NM-254D, Lab#=61405-04, Argus VI										
A	0.1	4.595	0.0055	0.0032	1.571	92.3	100.0	47.3	78.51	0.27
B	3.0	4.572	0.0094	-0.0099	1.749	54.1	100.1	100.0	78.21	0.18
Integrated age ± 1s			n=2		3.320	67.3			78.35	0.17
Plateau ± 1s		steps A-B	n=2	MSWD=0.87	3.320			100.0	78.30	0.159

ID	Power (Watts)	$^{40}Ar/^{39}Ar$	$^{37}Ar/^{39}Ar$	$^{36}Ar/^{39}Ar$ (x 10^{-3})	$^{39}Ar_K$ (x 10^{-15} mol)	K/Ca	$^{40}Ar^*$ (%)	^{39}Ar (%)	Age (Ma)	±1σ (Ma)
		SJ-SS5, Sanidine, J=0.0095555±0.07%, IC=1.05962±0.0011331, NM-254D, Lab#=61405-05, Argus VI								
A	0.1	4.397	-0.0317	0.3007	0.214	-	97.9	6.2	73.7	1.8
B	3.0	4.341	0.0031	-0.0006	3.236	165.0	100.0	100.0	74.262	0.100
Integrated age ± 1s			n=2		3.450	546.4			74.23	0.15
Plateau ± 1s		steps A-B	n=2	MSWD=0.11	3.450			100.0	74.26	0.111
		SJ-SS5, Sanidine, J=0.0095555±0.07%, IC=1.05962±0.0011331, NM-254D, Lab#=61405-06, Argus VI								
A	0.1	4.383	0.0034	0.0618	1.781	149.5	99.6	52.9	74.66	0.24
B	3.0	4.373	0.0009	-0.0121	1.588	569.6	100.1	100.0	74.86	0.20
Integrated age ± 1s			n=2		3.369	229.2			74.76	0.17
Plateau ± 1s		steps A-B	n=2	MSWD=0.42	3.369			100.0	74.78	0.163
		SJ-SS5, Sanidine, J=0.0095555±0.07%, IC=1.05962±0.0011331, NM-254D, Lab#=61405-07, Argus VI								
A	*0.1*	*36.75*	*0.0028*	*0.0435*	*4.712*	*180.9*	*100.0*	*92.4*	*550.69*	*0.29*
B	*3.0*	*53.44*	*-0.0003*	*0.0152*	*0.390*	-	*100.0*	*100.0*	*755.0*	*1.9*
Integrated age ± 1s			n=2		5.102				567.15	0.44
Plateau ± 1s		no plateau								
		SJ-SS5, Sanidine, J=0.0095555±0.07%, IC=1.05962±0.0011331, NM-254D, Lab#=61405-08, Argus VI								
A	0.1	4.547	0.0707	0.1208	0.100	7.2	99.3	2.9	77.2	4.0
B	3.0	4.445	0.0072	0.0041	3.297	70.5	100.0	100.0	76.000	0.097
Integrated age ± 1s			n=2		3.397	56.1			76.04	0.16
Plateau ± 1s		steps A-B	n=2	MSWD=0.09	3.397			100.0	76.00	0.109
		SJ-SS5, Sanidine, J=0.0095555±0.07%, IC=1.05962±0.0011331, NM-254D, Lab#=61405-10, Argus VI								

ID	Power (Watts)	$^{40}Ar/^{39}Ar$	$^{37}Ar/^{39}Ar$	$^{36}Ar/^{39}Ar$ (x 10^{-3})	$^{39}Ar_K$ (x 10^{-15} mol)	K/Ca	$^{40}Ar^*$ (%)	^{39}Ar (%)	Age (Ma)	±1σ (Ma)
A	0.1	4.455	-0.0046	0.0038	0.486	-	100.0	36.4	76.16	0.87
B	3.0	4.537	-0.0015	0.4409	0.851	-	97.1	100.0	75.35	0.46
Integrated age ± 1s			n=2		1.338				75.65	0.43
Plateau ± 1s		steps A-B	n=2	MSWD=0.68	1.338			100.0	75.53	0.411
SJ-SS5, Sanidine, J=0.0095555±0.07%, IC=1.05962±0.0011331, NM-254D, Lab#=61405-11, Argus VI										
A	0.1	4.584	0.0097	-0.0478	1.805	52.6	100.3	48.4	78.60	0.23
B	3.0	4.593	0.0066	0.0225	1.924	77.6	99.9	100.0	78.39	0.17
Integrated age ± 1s			n=2		3.730	63.1			78.49	0.15
Plateau ± 1s		steps A-B	n=2	MSWD=0.53	3.730			100.0	78.46	0.145
SJ-SS5, Sanidine, J=0.0095555±0.07%, IC=1.05962±0.0011331, NM-254D, Lab#=61405-12, Argus VI										
A	0.1	4.591	0.0061	-0.0047	2.346	83.3	100.0	52.7	78.48	0.17
B	3.0	4.593	0.0066	-0.0011	2.104	77.3	100.0	100.0	78.50	0.15
Integrated age ± 1s			n=2		4.451	80.4			78.49	0.13
Plateau ± 1s		steps A-B	n=2	MSWD=0.01	4.451			100.0	78.49	0.126
SJ-SS5, Sanidine, J=0.0095555±0.07%, IC=1.05962±0.0011331, NM-254D, Lab#=61405-13, Argus VI										
A	0.1	5.854	0.0020	0.0718	3.268	250.5	99.6	47.1	99.14	0.15
B	3.0	5.823	0.0025	0.0287	3.666	204.2	99.9	100.0	98.853	0.091
Integrated age ± 1s			n=2		6.934	223.7			98.99	0.11
Plateau ± 1s		steps A-B	n=2	MSWD=2.62	6.934			100.0	98.93	0.143
SJ-SS5, Sanidine, J=0.0095555±0.07%, IC=1.05962±0.0011331, NM-254D, Lab#=61405-14, Argus VI										
A	0.1	4.394	-0.0030	-0.0882	0.732	-	100.6	27.9	75.60	0.57

ID	Power (Watts)	$^{40}Ar/^{39}Ar$	$^{37}Ar/^{39}Ar$	$^{36}Ar/^{39}Ar$ (x 10^{-3})	$^{39}Ar_K$ (x 10^{-15} mol)	K/Ca	$^{40}Ar^*$ (%)	^{39}Ar (%)	Age (Ma)	±1σ (Ma)
B	3.0	4.368	0.0034	0.0061	1.890	152.1	100.0	100.0	74.68	0.17
Integrated age ± 1s			n=2		2.622	321.5			74.94	0.20
Plateau ± 1s		steps A-B	n=2	MSWD=2.38	2.622			100.0	74.76	0.255
		SJ-SS5, Sanidine, J=0.0095555±0.07%, IC=1.05962±0.0011331, NM-254D, Lab#=61405-16, Argus VI								
A	*0.1*	*13.50*	*0.0001*	*0.0318*	*3.806*	*5967.3*	*99.9*	*58.4*	*221.87*	*0.23*
B	*3.0*	*15.61*	*0.0011*	*0.0562*	*2.708*	*479.7*	*99.9*	*100.0*	*254.14*	*0.15*
Integrated age ± 1s			n=2		6.514	1036.8			235.35	0.21
Plateau ± 1s		no plateau								
		SJ-SS5, Sanidine, J=0.0095555±0.07%, IC=1.05962±0.0011331, NM-254D, Lab#=61405-17, Argus VI								
A	0.1	4.430	0.0008	0.0063	3.340	610.4	100.0	44.1	75.72	0.13
B	3.0	4.420	0.0033	0.0078	4.242	154.5	100.0	100.0	75.557	0.077
Integrated age ± 1s			n=2		7.583	230.3			75.628	0.088
Plateau ± 1s		steps A-B	n=2	MSWD=1.10	7.583			100.0	75.60	0.086
		SJ-SS5, Sanidine, J=0.0095555±0.07%, IC=1.05962±0.0011331, NM-254D, Lab#=61405-18, Argus VI								
A	0.1	4.343	0.0087	-0.0156	1.750	58.5	100.1	49.1	74.38	0.22
B	3.0	4.357	-0.0002	0.0523	1.816	-	99.6	100.0	74.27	0.18
Integrated age ± 1s			n=2		3.566	121.6			74.33	0.15
Plateau ± 1s		steps A-B	n=2	MSWD=0.14	3.566			100.0	74.32	0.149
		SJ-SS5, Sanidine, J=0.0095555±0.07%, IC=1.05962±0.0011331, NM-254D, Lab#=61405-19, Argus VI								
A	*0.1*	*46.78*	*0.0243*	*0.2098*	*0.353*	*21.0*	*99.9*	*14.6*	*675.6*	*3.4*
B	*3.0*	*86.26*	*-0.0003*	*0.0340*	*2.058*	-	*100.0*	*100.0*	*1100.25*	*0.51*

ID	Power (Watts)	$^{40}Ar/^{39}Ar$	$^{37}Ar/^{39}Ar$	$^{36}Ar/^{39}Ar$ (x 10^{-3})	$^{39}Ar_K$ (x 10^{-15} mol)	K/Ca	$^{40}Ar^*$ (%)	^{39}Ar (%)	Age (Ma)	±1σ (Ma)
Integrated age ± 1s			n=2		2.411	154.1			1043.91	0.97
Plateau ± 1s		no plateau								
				SJ-SS5, Sanidine, J=0.0095555±0.07%, IC=1.05962±0.0011331, NM-254D, Lab#=61405-21, Argus VI						
A	0.1	4.367	0.0078	0.1102	0.708	65.3	99.3	13.2	74.15	0.57
B	3.0	4.346	0.0042	0.0009	4.658	121.6	100.0	100.0	74.355	0.070
Integrated age ± 1s			n=2		5.365	109.2			74.33	0.11
Plateau ± 1s		steps A-B	n=2	MSWD=0.13	5.365			100.0	74.35	0.085
				SJ-SS5, Sanidine, J=0.0095555±0.07%, IC=1.05962±0.0011331, NM-254D, Lab#=61405-23, Argus VI						
A	0.1	4.438	0.0053	0.0274	2.062	96.7	99.8	36.1	75.77	0.20
B	3.0	4.450	0.0010	0.0060	3.656	525.9	100.0	100.0	76.071	0.089
Integrated age ± 1s			n=2		5.718	202.2			75.96	0.11
Plateau ± 1s		steps A-B	n=2	MSWD=1.87	5.718			100.0	76.02	0.122
				SJ-SS5, Sanidine, J=0.0095555±0.07%, IC=1.05962±0.0011331, NM-254D, Lab#=61405-24, Argus VI						
A	*0.1*	*4.476*	*0.0042*	*-0.0255*	*2.035*	*120.6*	*100.2*	*59.0*	*76.66*	*0.21*
B	3.0	4.746	0.0079	-0.0033	1.414	64.8	100.0	100.0	81.08	0.23
Integrated age ± 1s			n=2		3.449	89.1			78.47	0.16
Plateau ± 1s		steps B-B	n=1	MSWD=0.00	1.414			41.0	81.08	0.23
				SJ-SS5, Sanidine, J=0.0095555±0.07%, IC=1.05962±0.0011331, NM-254D, Lab#=61405-25, Argus VI						
A	0.1	4.395	0.0026	0.0675	1.455	199.3	99.5	42.9	74.84	0.29
B	3.0	4.390	0.0027	-0.0070	1.933	191.7	100.1	100.0	75.12	0.17
Integrated age ± 1s			n=2		3.388	194.9			75.00	0.16

ID	Power (Watts)	$^{40}Ar/^{39}Ar$	$^{37}Ar/^{39}Ar$	$^{36}Ar/^{39}Ar$ (x 10^{-3})	$^{39}Ar_K$ (x 10^{-15} mol)	K/Ca	$^{40}Ar^*$ (%)	^{39}Ar (%)	Age (Ma)	±1σ (Ma)
Plateau ± 1s		steps A-B	n=2	MSWD=0.71	3.388			100.0	75.05	0.152
SJ-SS5, Sanidine, J=0.0095555±0.07%, IC=1.05962±0.0011331, NM-254D, Lab#=61405-26, Argus VI										
A	0.1	9.869	0.0164	0.0525	1.087	31.1	99.9	50.7	164.61	0.46
B	3.0	9.879	0.0058	0.0037	1.057	88.7	100.0	100.0	164.98	0.33
Integrated age ± 1s			n=2		2.144	45.7			164.79	0.30
Plateau ± 1s		steps A-B	n=2	MSWD=0.43	2.144			100.0	164.86	0.287
SJ-SS5, Sanidine, J=0.0095555±0.07%, IC=1.05962±0.0011331, NM-254D, Lab#=61405-27, Argus VI										
A	0.1	4.331	0.0035	0.0319	1.659	143.7	99.8	51.2	73.93	0.19
B	3.0	4.389	0.0057	0.0516	1.579	89.4	99.7	100.0	74.82	0.21
Integrated age ± 1s			n=2		3.239	110.9			74.37	0.15
Plateau ± 1s		steps A-B	n=2	MSWD=9.98	3.239			100.0	74.34	0.444
SJ-SS5, Sanidine, J=0.0095555±0.07%, IC=1.05962±0.0011331, NM-254D, Lab#=61405-28, Argus VI										
A	*0.1*	*84.04*	*-0.0019*	*0.0782*	*2.013*	*-*	*100.0*	*88.2*	*1078.73*	*0.98*
B	*3.0*	*49.72*	*0.0126*	*0.1958*	*0.268*	*40.6*	*99.9*	*100.0*	*710.8*	*2.8*
Integrated age ± 1s			n=2		2.282				1039.1	1.1
Plateau ± 1s		no plateau								
SJ-SS5, Sanidine, J=0.0095555±0.07%, IC=1.05962±0.0011331, NM-254D, Lab#=61405-29, Argus VI										
A	*0.1*	*87.35*	*0.0026*	*0.0320*	*3.231*	*198.0*	*100.0*	*46.7*	*1110.71*	*0.74*
B	*3.0*	*93.39*	*0.0001*	*0.0213*	*3.687*	*7196.1*	*100.0*	*100.0*	*1167.39*	*0.30*
Integrated age ± 1s			n=2		6.918	411.1			1141.14	0.69
Plateau ± 1s		no plateau								

ID	Power (Watts)	$^{40}Ar/^{39}Ar$	$^{37}Ar/^{39}Ar$	$^{36}Ar/^{39}Ar$ (x 10^{-3})	$^{39}Ar_K$ (x 10^{-15} mol)	K/Ca	$^{40}Ar^*$ (%)	^{39}Ar (%)	Age (Ma)	±1σ (Ma)
		SJ-SS5, Sanidine, J=0.0095555±0.07%, IC=1.05962±0.0011331, NM-254D, Lab#=61405-30, Argus VI								
A	*0.1*	*64.85*	*0.0010*	*0.0302*	*2.210*	*487.4*	*100.0*	*58.7*	*882.56*	*0.83*
B	*3.0*	*65.10*	*0.0061*	*-0.0024*	*1.553*	*84.3*	*100.0*	*100.0*	*885.34*	*0.54*
Integrated age ± 1s			n=2		3.763	163.9			883.71	0.71
Plateau ± 1s		no plateau								
		SJ-SS5, Sanidine, J=0.0095555±0.07%, IC=1.05962±0.0011331, NM-254D, Lab#=61405-31, Argus VI								
A	0.1	11.83	-0.0038	0.0246	0.964	-	99.9	30.2	195.85	0.59
B	3.0	11.71	0.0004	0.0235	2.230	1315.6	99.9	100.0	193.90	0.17
Integrated age ± 1s			n=2		3.194				194.49	0.25
Plateau ± 1s		steps A-B	n=2	MSWD=10.14	3.194			100.0	194.04	0.528
		SJ-SS5, Sanidine, J=0.0095555±0.07%, IC=1.05962±0.0011331, NM-254D, Lab#=61405-32, Argus VI								
A	0.1	4.339	0.0043	0.0175	3.033	119.7	99.9	95.1	74.15	0.10
B	3.0	4.347	-0.0126	-0.0686	0.156	-	100.4	100.0	74.7	2.0
Integrated age ± 1s			n=2		3.189				74.18	0.15
Plateau ± 1s		steps A-B	n=2	MSWD=0.07	3.189			100.0	74.15	0.116
		SJ-SS5, Sanidine, J=0.0095555±0.07%, IC=1.05962±0.0011331, NM-254D, Lab#=61405-33, Argus VI								
A	*0.1*	*27.07*	*0.0029*	*0.0236*	*1.559*	*173.6*	*100.0*	*26.7*	*420.97*	*0.59*
B	*3.0*	*62.80*	*0.0016*	*0.0247*	*4.274*	*323.0*	*100.0*	*100.0*	*860.24*	*0.23*
Integrated age ± 1s			n=2		5.832	262.6			752.76	0.51
Plateau ± 1s		no plateau								

ID	Power (Watts)	$^{40}Ar/^{39}Ar$	$^{37}Ar/^{39}Ar$	$^{36}Ar/^{39}Ar$ (x 10^{-3})	$^{39}Ar_K$ (x 10^{-15} mol)	K/Ca	$^{40}Ar^*$ (%)	^{39}Ar (%)	Age (Ma)	±1σ (Ma)
			SJ-SS5, Sanidine, J=0.0095555±0.07%, IC=1.05962±0.0011331, NM-254D, Lab#=61405-34, Argus VI							
A	*0.1*	*37.70*	*0.0032*	*0.0922*	*1.116*	*157.6*	*99.9*	*62.8*	*562.8*	*1.2*
B	*3.0*	*44.14*	*-0.0033*	*0.0428*	*0.662*	-	*100.0*	*100.0*	*643.97*	*1.00*
Integrated age ± 1s			n=2		1.778				593.42	0.91
Plateau ± 1s		no plateau								
			SJ-SS5, Sanidine, J=0.0095555±0.07%, IC=1.05962±0.0011331, NM-254D, Lab#=61405-38, Argus VI							
A	0.1	9.973	-0.0049	0.1306	0.205	-	99.6	15.2	165.9	2.3
B	3.0	9.727	0.0088	0.0066	1.142	57.8	100.0	100.0	162.54	0.30
Integrated age ± 1s			n=2		1.347				163.05	0.44
Plateau ± 1s		steps A-B	n=2	MSWD=2.14	1.347			100.0	162.60	0.452
			SJ-SS5, Sanidine, J=0.0095555±0.07%, IC=1.05962±0.0011331, NM-254D, Lab#=61405-39, Argus VI							
A	0.1	4.379	-0.0045	0.1926	0.471	-	98.7	12.0	73.93	0.91
B	3.0	4.307	0.0041	0.0608	3.458	125.2	99.6	100.0	73.386	0.096
Integrated age ± 1s			n=2		3.930				73.45	0.15
Plateau ± 1s		steps A-B	n=2	MSWD=0.34	3.930			100.0	73.39	0.107
			SJ-SS5, Sanidine, J=0.0095555±0.07%, IC=1.05962±0.0011331, NM-254D, Lab#=61405-40, Argus VI							
A	0.1	11.93	-0.0022	0.3673	0.476	-	99.1	17.1	195.8	1.2
B	3.0	11.76	-0.0019	0.0182	2.306	-	100.0	100.0	194.68	0.16
Integrated age ± 1s			n=2		2.782				194.88	0.27
Plateau ± 1s		steps A-B	n=2	MSWD=0.97	2.782			100.0	194.70	0.202
			SJ-SS5, Sanidine, J=0.0095555±0.07%, IC=1.05962±0.0011331, NM-254D, Lab#=61405-43, Argus VI							

ID	Power (Watts)	$^{40}Ar/^{39}Ar$	$^{37}Ar/^{39}Ar$	$^{36}Ar/^{39}Ar$ (x 10^{-3})	$^{39}Ar_K$ (x 10^{-15} mol)	K/Ca	$^{40}Ar^*$ (%)	^{39}Ar (%)	Age (Ma)	±1σ (Ma)
A	*0.1*	*62.35*	*-0.0001*	*0.2026*	*2.063*	*-*	*99.9*	*66.3*	*854.8*	*1.0*
B	*3.0*	*65.80*	*0.0048*	*0.3293*	*1.047*	*105.3*	*99.9*	*100.0*	*891.83*	*0.83*
Integrated age ± 1s			n=2		3.111	324.0			867.36	0.88
Plateau ± 1s		no plateau								
		SJ-SS5, Sanidine, J=0.0095555±0.07%, IC=1.05962±0.0011331, NM-254D, Lab#=61405-44, Argus VI								
A	*0.1*	*68.90*	*0.0174*	*-0.0666*	*0.811*	*29.3*	*100.0*	*63.2*	*926.1*	*2.3*
B	*3.0*	*52.51*	*0.0000*	*0.0394*	*0.473*	*-*	*100.0*	*100.0*	*744.1*	*1.5*
Integrated age ± 1s			n=2		1.284	46.4			861.1	1.6
Plateau ± 1s		no plateau								
		SJ-SS5, Sanidine, J=0.0095555±0.07%, IC=1.05962±0.0011331, NM-254D, Lab#=61405-45, Argus VI								
A	0.1	51.82	0.0031	0.0092	2.482	163.4	100.0	58.3	736.14	0.66
B	3.0	54.19	-0.0021	-0.0035	1.773	-	100.0	100.0	763.72	0.45
Integrated age ± 1s			n=2		4.255				747.68	0.60
Plateau ± 1s		no plateau								
		SJ-SS5, Sanidine, J=0.0095555±0.07%, IC=1.05962±0.0011331, NM-254D, Lab#=61405-46, Argus VI								
A	*0.1*	*40.34*	*0.0190*	*0.5286*	*0.259*	*26.8*	*99.6*	*22.6*	*594.8*	*4.4*
B	*3.0*	*57.02*	*0.0039*	*0.2106*	*0.886*	*130.8*	*99.9*	*100.0*	*795.34*	*0.90*
Integrated age ± 1s			n=2		1.146				751.8	1.4
Plateau ± 1s		no plateau								
		SJ-SS5, Sanidine, J=0.0095555±0.07%, IC=1.05962±0.0011331, NM-254D, Lab#=61405-47, Argus VI								
A	*0.1*	*8.490*	*0.0092*	*-0.0646*	*0.697*	*55.2*	*100.2*	*14.3*	*142.99*	*0.69*

ID	Power (Watts)	$^{40}Ar/^{39}Ar$	$^{37}Ar/^{39}Ar$	$^{36}Ar/^{39}Ar$ (x 10^{-3})	$^{39}Ar_K$ (x 10^{-15} mol)	K/Ca	$^{40}Ar^*$ (%)	^{39}Ar (%)	Age (Ma)	±1σ (Ma)
B	*3.0*	*10.50*	*0.0033*	*0.0159*	*4.181*	*154.2*	*100.0*	*100.0*	*174.814*	*0.088*
Integrated age ± 1s			n=2		4.878				170.30	0.17
Plateau ± 1s		no plateau								
		SJ-SS5, Sanidine, J=0.0095555±0.07%, IC=1.05962±0.0011331, NM-254D, Lab#=61405-49, Argus VI								
A	*0.1*	*22.10*	*-0.0006*	*-0.0109*	*3.098*	*-*	*100.0*	*90.1*	*350.67*	*0.36*
B	*3.0*	*26.98*	*0.0128*	*-0.1061*	*0.338*	*39.9*	*100.1*	*100.0*	*420.2*	*1.4*
Integrated age ± 1s			n=2		3.436				357.64	0.42
Plateau ± 1s		no plateau								
		SJ-SS5, Sanidine, J=0.0095555±0.07%, IC=1.05962±0.0011331, NM-254D, Lab#=61405-50, Argus VI								
A	*0.1*	*87.73*	*0.0000*	*-0.0303*	*0.434*	*-*	*100.0*	*18.1*	*1114.5*	*4.5*
B	*3.0*	*116.0*	*0.0028*	*0.0072*	*1.959*	*184.3*	*100.0*	*100.0*	*1365.02*	*0.65*
Integrated age ± 1s			n=2		2.393				1322.1	1.2
Plateau ± 1s		no plateau								
		SJ-SS5, Sanidine, J=0.0095555±0.07%, IC=1.05962±0.0011331, NM-254D, Lab#=61405-51, Argus VI								
A	*0.1*	*25.83*	*0.0054*	*0.5219*	*0.201*	*94.0*	*99.4*	*10.1*	*401.6*	*4.3*
B	*3.0*	*61.67*	*0.0001*	*0.0292*	*1.800*	*6066.6*	*100.0*	*100.0*	*847.81*	*0.49*
Integrated age ± 1s			n=2		2.001	821.6			807.56	0.96
Plateau ± 1s		no plateau								
		SJ-SS6, Sanidine, J=0.0095337±0.08%, IC=1.05325±0.0019241, NM-254D, Lab#=61406-03, Argus VI								
A	0.1	4.440	0.2681	-0.4854	0.093	1.9	103.8	1.1	78.6	6.1
B	0.2	3.980	0.0027	0.0127	4.253	191.7	99.9	51.7	67.983	0.076

ID	Power (Watts)	$^{40}Ar/^{39}Ar$	$^{37}Ar/^{39}Ar$	$^{36}Ar/^{39}Ar$ (x 10^{-3})	$^{39}Ar_K$ (x 10^{-15} mol)	K/Ca	$^{40}Ar^*$ (%)	^{39}Ar (%)	Age (Ma)	±1σ (Ma)
C	0.3	3.994	0.0027	0.0433	2.355	186.4	99.7	79.7	68.06	0.14
D	0.6	4.028	0.0068	0.0374	1.707	74.8	99.7	100.0	68.66	0.18
Integrated age ± 1s			n=4		8.408	78.8			67.28	0.11
Plateau ± 1s		steps A-D	n=4	MSWD=5.09	8.408			100.0	68.08	0.15
SJ-SS6, Sanidine, J=0.0095337±0.08%, IC=1.05325±0.0019241, NM-254D, Lab#=61406-04, Argus VI										
B	0.2	4.525	-0.1276	0.3873	0.124	-	97.2	1.9	75.1	5.0
C	3.0	3.979	0.0036	0.0094	6.354	141.0	99.9	100.0	67.971	0.027
Integrated age ± 1s			n=2		6.478				67.12	0.11
Plateau ± 1s		steps B-C	n=2	MSWD=1.99	6.478			100.0	67.97	0.067
SJ-SS6, Sanidine, J=0.0095337±0.08%, IC=1.05325±0.0019241, NM-254D, Lab#=61406-06, Argus VI										
B	0.2	3.686	-0.0602	-0.5973	0.101	-	104.8	3.1	66.0	5.5
C	0.3	3.972	0.0038	0.0004	2.696	135.0	100.0	85.2	67.909	0.081
D	0.6	3.959	-0.0989	-0.2909	0.296	-	102.0	94.2	69.0	2.1
E	3.0	4.070	0.0209	0.5461	0.191	24.4	96.1	100.0	66.9	1.1
Integrated age ± 1s			n=4		3.285				66.91	0.27
Plateau ± 1s		steps B-E	n=4	MSWD=0.45	3.285			100.0	67.904	0.097
SJ-SS6, Sanidine, J=0.0095337±0.08%, IC=1.05325±0.0019241, NM-254D, Lab#=61406-07, Argus VI										
B	0.2	4.707	0.1707	1.239	0.057	3.0	92.4	2.0	74.3	11.1
C	3.0	4.330	0.0022	0.0161	2.789	235.7	99.9	100.0	73.83	0.24
Integrated age ± 1s			n=2		2.846	92.5			72.77	0.32
Plateau ± 1s		steps B-C	n=2	MSWD=0.00	2.846			100.0	73.83	0.244

ID	Power (Watts)	$^{40}Ar/^{39}Ar$	$^{37}Ar/^{39}Ar$	$^{36}Ar/^{39}Ar$ (x 10^{-3})	$^{39}Ar_K$ (x 10^{-15} mol)	K/Ca	$^{40}Ar^*$ (%)	^{39}Ar (%)	Age (Ma)	±1σ (Ma)
			SJ-SS6, Sanidine, J=0.0095337±0.08%, IC=1.05325±0.0019241, NM-254D, Lab#=61406-08, Argus VI							
B	0.2	4.396	0.0946	-0.7894	0.218	5.4	105.5	4.0	79.1	2.7
C	3.0	4.360	0.0031	-0.0137	5.225	167.2	100.1	100.0	74.48	0.14
Integrated age ± 1s			n=2		5.443	76.0			73.58	0.18
Plateau ± 1s		steps B-C	n=2	MSWD=2.84	5.443			100.0	74.49	0.246
			SJ-SS6, Sanidine, J=0.0095337±0.08%, IC=1.05325±0.0019241, NM-254D, Lab#=61406-09, Argus VI							
B	0.2	4.359	0.0429	0.0331	0.440	11.9	99.8	6.9	74.3	1.5
C	3.0	4.362	0.0111	0.0014	5.917	46.1	100.0	100.0	74.46	0.11
Integrated age ± 1s			n=2		6.357	38.4			73.37	0.15
Plateau ± 1s		steps B-C	n=2	MSWD=0.01	6.357			100.0	74.45	0.123
			SJ-SS6, Sanidine, J=0.0095337±0.08%, IC=1.05325±0.0019241, NM-254D, Lab#=61406-10, Argus VI							
A	0.1	4.530	-0.4166	-1.6780	0.027	-	110.1	0.7	84.9	23.7
B	0.2	4.339	0.0037	0.1532	0.405	138.0	99.0	11.6	73.3	1.5
C	3.0	4.375	0.0080	-0.0008	3.295	64.0	100.0	100.0	74.69	0.20
Integrated age ± 1s			n=3		3.727				73.53	0.30
Plateau ± 1s		steps A-C	n=3	MSWD=0.48	3.727			100.0	74.66	0.21
			SJ-SS6, Sanidine, J=0.0095337±0.08%, IC=1.05325±0.0019241, NM-254D, Lab#=61406-12, Argus VI							
A	0.2	3.985	0.0029	-0.0070	1.543	176.4	100.1	19.0	68.15	0.19
C	0.3	3.984	0.0190	0.2329	0.078	26.8	98.3	19.9	67.0	2.6
D	3.0	3.978	0.0040	0.0213	6.515	126.7	99.8	100.0	67.898	0.038
Integrated age ± 1s			n=3		8.136	128.9			66.958	0.075
Plateau ± 1s		steps A-D	n=3	MSWD=0.97	8.136			100.0	67.908	0.066

ID	Power (Watts)	$^{40}Ar/^{39}Ar$	$^{37}Ar/^{39}Ar$	$^{36}Ar/^{39}Ar$ (x 10^{-3})	$^{39}Ar_K$ (x 10^{-15} mol)	K/Ca	$^{40}Ar^*$ (%)	^{39}Ar (%)	Age (Ma)	±1σ (Ma)
SJ-SS6, Sanidine, J=0.0095337±0.08%, IC=1.05325±0.0019241, NM-254D, Lab#=61406-13, Argus VI										
A	0.2	5.670	0.0087	0.3073	0.791	58.6	98.4	64.2	94.73	0.99
B	3.0	5.783	0.0213	-0.0426	0.441	24.0	100.3	100.0	98.4	1.6
Integrated age ± 1s			n=2		1.232	38.6			94.65	0.85
Plateau ± 1s		steps A-B	n=2	MSWD=3.58	1.232			100.0	95.70	1.602
SJ-SS6, Sanidine, J=0.0095337±0.08%, IC=1.05325±0.0019241, NM-254D, Lab#=61406-14, Argus VI										
A	0.2	117.1	0.0059	0.0586	3.108	86.8	100.0	96.7	1372	2
B	3.0	122.7	0.0726	0.4227	0.106	7.0	99.9	100.0	1417	34
Integrated age ± 1s			n=2		3.214	63.1			1353	2
Plateau ± 1s		steps A-B	n=2	MSWD=1.74	3.214			100.0	1372	2
SJ-SS6, Sanidine, J=0.0095337±0.08%, IC=1.05325±0.0019241, NM-254D, Lab#=61406-15, Argus VI										
A	0.2	4.330	0.0056	0.0255	7.501	91.5	99.8	58.5	73.79	0.12
B	3.0	4.335	0.0036	0.0091	5.329	142.7	99.9	100.0	73.95	0.13
Integrated age ± 1s			n=2		12.830	107.5			72.79	0.10
Plateau ± 1s		steps A-B	n=2	MSWD=0.81	12.830	112.783±36.238		100.0	73.86	0.106
SJ-SS6, Sanidine, J=0.0095337±0.08%, IC=1.05325±0.0019241, NM-254D, Lab#=61406-16, Argus VI										
A	0.2	5.437	1.168	2.014	0.030	0.44	90.7	0.7	84.0	21.1
B	3.0	4.439	0.0077	0.0214	4.318	66.7	99.9	100.0	75.64	0.16
Integrated age ± 1s			n=2		4.348	32.6			74.60	0.22
Plateau ± 1s		steps A-B	n=2	MSWD=0.16	4.348			100.0	75.64	0.175

ID	Power (Watts)	$^{40}Ar/^{39}Ar$	$^{37}Ar/^{39}Ar$	$^{36}Ar/^{39}Ar$ (x 10^{-3})	$^{39}Ar_K$ (x 10^{-15} mol)	K/Ca	$^{40}Ar^*$ (%)	^{39}Ar (%)	Age (Ma)	±1σ (Ma)
			SJ-SS6, Sanidine, J=0.0095337±0.08%, IC=1.05325±0.0019241, NM-254D, Lab#=61406-21, Argus VI							
A	0.2	4.339	0.0235	0.0757	0.261	21.7	99.6	9.7	73.8	2.6
B	3.0	4.370	0.0089	0.0443	2.430	57.4	99.7	100.0	74.37	0.26
Integrated age ± 1s			n=2		2.691	49.5			73.24	0.35
Plateau ± 1s		steps A-B	n=2	MSWD=0.05	2.691			100.0	74.36	0.270
			SJ-SS6, Sanidine, J=0.0095337±0.08%, IC=1.05325±0.0019241, NM-254D, Lab#=61406-22, Argus VI							
A	0.2	4.685	0.1327	0.5834	0.107	3.8	96.5	5.1	77.1	6.1
B	3.0	4.594	-0.0051	0.0091	1.989	-	99.9	100.0	78.28	0.27
Integrated age ± 1s			n=2		2.096				77.09	0.40
Plateau ± 1s		steps A-B	n=2	MSWD=0.03	2.096			100.0	78.27	0.275
			SJ-SS6, Sanidine, J=0.0095337±0.08%, IC=1.05325±0.0019241, NM-254D, Lab#=61406-23, Argus VI							
A	*0.2*	*4.157*	*0.0064*	*0.1818*	*0.886*	*79.3*	*98.7*	*15.5*	*70.10*	*0.69*
B	3.0	3.990	0.0040	0.0090	4.828	127.7	99.9	100.0	68.172	0.034
Integrated age ± 1s			n=2		5.714	116.6			67.48	0.12
Step B			n-1		4.828			84.5	68.172	0.034
			SJ-SS6, Sanidine, J=0.0095337±0.08%, IC=1.05325±0.0019241, NM-254D, Lab#=61406-24, Argus VI							
A	*0.2*	*4.009*	*0.0106*	*-0.0172*	*1.326*	*48.0*	*100.1*	*11.5*	*68.63*	*0.21*
B	3.0	3.975	0.0028	0.0065	10.220	183.7	100.0	100.0	67.921	0.017
Integrated age ± 1s			n=2		11.546	138.7			67.022	0.062
Step B			n=1		10.220			88.5	67.921	0.017
			SJ-SS6, Sanidine, J=0.0095337±0.08%, IC=1.05325±0.0019241, NM-254D, Lab#=61406-25, Argus VI							

ID	Power (Watts)	$^{40}Ar/^{39}Ar$	$^{37}Ar/^{39}Ar$	$^{36}Ar/^{39}Ar$ (x 10^{-3})	$^{39}Ar_K$ (x 10^{-15} mol)	K/Ca	$^{40}Ar^*$ (%)	^{39}Ar (%)	Age (Ma)	±1σ (Ma)
A	0.2	3.965	0.0396	0.0134	0.122	12.9	100.0	2.8	67.8	5.4
B	3.0	3.977	0.0046	0.0132	4.253	110.2	99.9	100.0	67.929	0.038
Integrated age ± 1s			n=2		4.376	91.0			66.95	0.16
Plateau ± 1s		steps A-B	n=2	MSWD=0.00	4.376			100.0	67.93	0.067
SJ-SS6, Sanidine, J=0.0095337±0.08%, IC=1.05325±0.0019241, NM-254D, Lab#=61406-26, Argus VI										
A	0.2	3.979	0.0028	0.0136	3.232	179.9	99.9	96.3	67.951	0.090
B	3.0	4.510	0.0594	-0.9507	0.125	8.6	106.4	100.0	81.7	4.9
Integrated age ± 1s			n=2		3.357	103.2			67.48	0.20
Plateau ± 1s		steps A-B	n=2	MSWD=7.87	3.357			100.0	67.96	0.258
SJ-SS6, Sanidine, J=0.0095337±0.08%, IC=1.05325±0.0019241, NM-254D, Lab#=61406-27, Argus VI										
A	0.2	3.985	0.0042	0.0112	3.242	121.8	99.9	63.7	68.072	0.091
B	3.0	3.994	0.0040	0.0518	1.849	128.6	99.6	100.0	68.022	0.084
Integrated age ± 1s			n=2		5.091	124.2			67.073	0.084
Plateau ± 1s		steps A-B	n=2	MSWD=0.17	5.091			100.0	68.05	0.083
SJ-SS6, Sanidine, J=0.0095337±0.08%, IC=1.05325±0.0019241, NM-254D, Lab#=61406-28, Argus VI										
A	0.2	3.820	0.0048	-0.0005	6.410	106.1	100.0	56.2	65.359	0.047
B	0.3	3.838	0.0035	0.0026	1.011	145.3	100.0	65.1	65.64	0.13
C	0.5	3.833	-0.0001	0.0067	2.093	-	99.9	83.5	65.531	0.071
D	3.0	3.857	0.0017	0.0232	1.883	301.5	99.8	100.0	65.843	0.080
Integrated age ± 1s			n=4		11.397	155.8			64.551	0.062
Plateau ± 1s		steps A-D	n=4	MSWD=9.48	11.397			100.0	65.506	0.118

ID	Power (Watts)	$^{40}Ar/^{39}Ar$	$^{37}Ar/^{39}Ar$	$^{36}Ar/^{39}Ar$ (x 10^{-3})	$^{39}Ar_K$ (x 10^{-15} mol)	K/Ca	$^{40}Ar^*$ (%)	^{39}Ar (%)	Age (Ma)	±1σ (Ma)
			SJ-SS6, Sanidine, J=0.0095337±0.08%, IC=1.05325±0.0019241, NM-254D, Lab#=61406-29, Argus VI							
A	0.2	4.337	0.0043	0.0052	3.197	118.2	100.0	68.5	74.01	0.24
B	3.0	4.369	-0.0027	0.0105	1.468	-	99.9	100.0	74.51	0.36
Integrated age ± 1s			n=2		4.665	242.8			73.10	0.20
Plateau ± 1s		steps A-B	n=2	MSWD=1.36	4.665			100.0	74.16	0.240
			SJ-SS6, Sanidine, J=0.0095337±0.08%, IC=1.05325±0.0019241, NM-254D, Lab#=61406-30, Argus VI							
A	0.2	3.983	0.0026	0.0033	3.706	194.8	100.0	51.5	68.077	0.080
B	3.0	4.000	0.0061	-0.0010	3.494	83.3	100.0	100.0	68.389	0.041
Integrated age ± 1s			n=2		7.201	118.1			67.244	0.071
Plateau ± 1s		steps A-B	n=2	MSWD=11.93	7.201			100.0	68.32	0.138
			SJ-SS6, Sanidine, J=0.0095337±0.08%, IC=1.05325±0.0019241, NM-254D, Lab#=61406-33, Argus VI							
A	0.2	4.288	-0.0550	-0.0194	0.407	-	100.0	12.7	73.2	1.5
B	3.0	4.337	0.0086	-0.0148	2.793	59.2	100.1	100.0	74.11	0.24
Integrated age ± 1s			n=2		3.200				72.93	0.28
Plateau ± 1s		steps A-B	n=2	MSWD=0.36	3.200			100.0	74.08	0.245
			SJ-SS6, Sanidine, J=0.0095337±0.08%, IC=1.05325±0.0019241, NM-254D, Lab#=61406-34, Argus VI							
A	0.2	3.969	0.0629	0.0842	0.170	8.1	99.5	6.6	67.5	3.7
B	3.0	4.004	0.0063	0.0249	2.411	81.2	99.8	100.0	68.322	0.062
Integrated age ± 1s			n=2		2.581	51.0			67.29	0.25
Plateau ± 1s		steps A-B	n=2	MSWD=0.05	2.581			100.0	68.32	0.083
			SJ-SS6, Sanidine, J=0.0095337±0.08%, IC=1.05325±0.0019241, NM-254D, Lab#=61406-36, Argus VI							

ID	Power (Watts)	$^{40}Ar/^{39}Ar$	$^{37}Ar/^{39}Ar$	$^{36}Ar/^{39}Ar$ (x 10^{-3})	$^{39}Ar_K$ (x 10^{-15} mol)	K/Ca	$^{40}Ar^*$ (%)	^{39}Ar (%)	Age (Ma)	±1σ (Ma)
A	0.2	4.908	0.3817	-5.2427	0.033	1.3	132.7	1.0	110.1	21.8
B	3.0	3.990	0.0034	-0.0022	3.446	152.0	100.0	100.0	68.216	0.046
Integrated age ± 1s			n=2		3.479	73.2			67.63	0.20
Plateau ± 1s		steps A-B	n=2	MSWD=3.70	3.479			100.0	68.22	0.104
SJ-SS6, Sanidine, J=0.0095337±0.08%, IC=1.05325±0.0019241, NM-254D, Lab#=61406-37, Argus VI										
A	0.2	4.442	0.0036	-0.2012	0.738	142.7	101.4	21.3	76.8	1.1
B	3.0	4.411	0.0065	0.0041	2.722	78.0	100.0	100.0	75.26	0.23
Integrated age ± 1s			n=2		3.460	86.4			74.50	0.29
Plateau ± 1s		steps A-B	n=2	MSWD=1.96	3.460			100.0	75.33	0.320
SJ-SS6, Sanidine, J=0.0095337±0.08%, IC=1.05325±0.0019241, NM-254D, Lab#=61406-38, Argus VI										
A	0.2	3.977	0.0083	0.0268	0.727	61.5	99.8	32.8	67.86	0.60
B	3.0	3.988	0.0076	0.0079	1.488	67.3	100.0	100.0	68.146	0.094
Integrated age ± 1s			n=2		2.215	65.3			67.07	0.21
Plateau ± 1s		steps A-B	n=2	MSWD=0.22	2.215			100.0	68.14	0.108
SJ-SS6, Sanidine, J=0.0095337±0.08%, IC=1.05325±0.0019241, NM-254D, Lab#=61406-40, Argus VI										
A	0.2	4.397	0.0064	-0.0047	2.619	80.2	100.0	72.0	75.06	0.28
B	3.0	4.428	0.0279	-0.1432	1.017	18.3	101.0	100.0	76.30	0.51
Integrated age ± 1s			n=2		3.636	41.2			74.32	0.25
Plateau ± 1s		steps A-B	n=2	MSWD=4.54	3.636			100.0	75.35	0.531
SJ-SS6, Sanidine, J=0.0095337±0.08%, IC=1.05325±0.0019241, NM-254D, Lab#=61406-41, Argus VI										
A	0.2	3.838	0.0055	0.0256	1.129	92.4	99.8	11.3	65.53	0.27

ID	Power (Watts)	$^{40}Ar/^{39}Ar$	$^{37}Ar/^{39}Ar$	$^{36}Ar/^{39}Ar$ (x 10^{-3})	$^{39}Ar_K$ (x 10^{-15} mol)	K/Ca	$^{40}Ar^*$ (%)	^{39}Ar (%)	Age (Ma)	±1σ (Ma)
B	0.3	3.819	0.0135	0.0678	0.388	37.7	99.5	15.2	65.02	0.36
C	0.5	3.815	0.0023	0.0104	3.569	223.4	99.9	50.8	65.218	0.043
D	3.0	3.827	0.0042	0.0018	4.921	120.6	100.0	100.0	65.465	0.034
Integrated age ± 1s			n=4		10.007	126.2			64.424	0.066
Plateau ± 1s		steps A-D	n=4	MSWD=7.04	10.007			100.0	65.369	0.089
SJ-SS6, Sanidine, J=0.0095337±0.08%, IC=1.05325±0.0019241, NM-254D, Lab#=61406-42, Argus VI										
A	0.2	4.379	0.0204	-0.0090	1.619	25.0	100.1	82.8	74.81	0.41
B	3.0	4.530	-0.0038	-0.0355	0.336	-	100.2	100.0	77.4	1.7
Integrated age ± 1s			n=2		1.956				74.18	0.44
Plateau ± 1s		steps A-B	n=2	MSWD=2.26	1.956			100.0	74.96	0.600
SJ-SS6, Sanidine, J=0.0095337±0.08%, IC=1.05325±0.0019241, NM-254D, Lab#=61406-43, Argus VI										
A	0.2	4.400	0.0185	-0.0260	1.818	27.6	100.2	98.7	75.25	0.37
B	3.0	4.322	0.1508	-4.1223	0.023	3.4	129.2	100.0	94.8	24.6
Integrated age ± 1s			n=2		1.842				74.41	0.46
Plateau ± 1s		steps A-B	n=2	MSWD=0.63	1.842			100.0	75.25	0.374

Notes:

Isotopic ratios corrected for blank, radioactive decay, and mass discrimination, not corrected for interfering reactions.

Errors quoted for individual analyses include analytical error only, without interfering reaction or J uncertainties.

Integrated age calculated by summing isotopic measurements of all steps.

Integrated age error calculated by quadratically combining errors of isotopic measurements of all steps.

Plateau age is inverse-variance-weighted mean of selected steps.

Plateau age error is inverse-variance-weighted mean error (Taylor, 1982) times root MSWD where MSWD>1.

Isotopic abundances after Steiger and Jäger (1977).

ID	Power (Watts)	$^{40}Ar/^{39}Ar$	$^{37}Ar/^{39}Ar$	$^{36}Ar/^{39}Ar$ (x 10^{-3})	$^{39}Ar_K$ (x 10^{-15} mol)	K/Ca	$^{40}Ar^*$ (%)	^{39}Ar (%)	Age (Ma)	±1σ (Ma)

Italicized sample ID denotes analyses excluded from plateau age calculations.

Ages calculated relative to FC-2 Fish Canyon Tuff sanidine interlaboratory standard at 28.201 Ma (Kuiper et al., 2008)

Decay Constant (LambdaK (total)) = $5.463e^{-10}$/a (Min et al., 2000)

Table C.4 - $^{40}Ar/^{39}Ar$ irradiation and correction factor information

Irradiation Run	Length (hours)	$(^{39}Ar/37Ar)_{Ca}$	$(^{36}Ar/^{37}Ar)_{Ca}$	$(^{40}Ar/^{39}Ar)_{K}$
NM-254	40	0.00698 ± 0.000008	0.00273 ± 0.0000002	0.008068 ± 0.00068
NM-258	40	0.00653 ± 0.000000	0.0002633 ± 0.0000003	0.007529 ± 0.000237
NM-293	8	0.000758 ± 0.000007	0.000286 ± 0.0000005	0.00873 ± 0.00017

Notes: all samples irradiated at the Triga Reactor, USGS, Denver, CO.

APPENDIX D

San Juan Basin Megafloral Collection Data

Table D.1 – San Juan Basin Megafloral Morphotype Systematic List: Aff = affinity in larger taxonomic category, PTE = pteridophyte, CON = conifer, CYD = cycad, MON = monocotyledonous angiosperm, DIC = non-monocotyledonous angiosperm, LYC = lycophyte, Margin = dicotyledonous angiosperm margin (T = toothed, U = Untoothed).

Morph.	Aff.	Order	Family	Organ	Margin	Taxonomic name
SJ-068	CON	Pinales	Cupressaceae	Leaf	N/A	*Cupressinocladus interruptis*
SJ-102	CON	Pinales	Cupressaceae	Leaf	N/A	*Ditaxocladus catenulatus*
SJ-097	CON	Pinales	Cupressaceae	Leaf	N/A	
SJ-126	CON	Pinales?	Incertae Sedis	Cone	N/A	
SJ-166	CYD	Incertae Sedis	-	Leaf	N/A	
SJ-185	CYD	Incertae Sedis	-	Cone	N/A	
SJ-078	DIC	Cornales	Nyssaceae	Leaf	T	*Browniea serrata*
SJ-124	DIC	Cornales	Nyssaceae	Leaf	T	*Davidia antiqua*
SJ-140	DIC	Cucurbitales	Cucurbitaceae	Leaf	T	*Cucurbitaciphyllum lobatum*
SJ-137	DIC	Fabales	Fabaceae	Leaf	U	
SJ-129	DIC	Fagales	Fagaceae	Leaf	T	*Fagopsophyllum groenlandicum*
SJ-019	DIC	Fagales	Juglandaceae	Leaf	T	*Juglandiphyllites glabra*
SJ-082	DIC	Gentianales	Apocynaceae	Leaf	U	
SJ-151	DIC	Laurales	Lauraceae	Leaf	U	*Artocarpus lessigiana*
SJ-150	DIC	Laurales	Lauraceae	Leaf	U	*Melastomites montanensis*
SJ-162	DIC	Malvales	Sterculiaceae	Leaf	T	
SJ-027	DIC	Malvales	Sterculiaceae	Leaf	U	*Penosphyllum cordatum*
SJ-088	DIC	Malvales?	Malvaceae?	Leaf	T	cf. *Tilia? sp.*

Morph.	Aff.	Order	Family	Organ	Margin	Taxonomic name
SJ-051	DIC	Nymphaeales	Nymphaeaceae	Leaf	U	*Paranymphaea crassfolia*
SJ-004	DIC	Proteales	Platanaceae	Leaf	U	
SJ-012	DIC	Proteales	Platanaceae	Leaf	T	*Macginitiea*
SJ-127	DIC	Proteales	Platanaceae	Leaf	T/U	*Macginitiea nobilis*
SJ-023	DIC	Proteales	Platanaceae	Leaf	T	*Macginitiea sp.*
SJ-173	DIC	Proteales	Platanaceae	Leaf	T	*Macginitiea sp.*
SJ-186	DIC	Proteales	Platanaceae	Leaf	T	*Macginitiea sp.*
SJ-071	DIC	Proteales	Platanaceae	Leaf	T	*Platanites marginata*
SJ-036	DIC	Proteales	Platanaceae	Leaf	T	*Platanites raynoldsii*
SJ-155	DIC	Rosales	Rhamnaceae	Leaf	U	*Rhamnites cleburnii*
SJ-080	DIC	Rosales	Rhamnaceae	Leaf	T/U	*Rhamnus goldiana*
SJ-125	DIC	Rosales	Rhamnaceae	Leaf	U	
SJ-175	DIC	Rosales	Rhamnaceae	Leaf	U	
SJ-113	DIC	Rosales	Rhamnaceae	Leaf	U	*Zizyphus fibrillosus*
SJ-046	DIC	Sapindales	Oxalidaceae	Leaf	U	*Averrhoites affinus*
SJ-007	DIC	Sapindales	Sapindaceae	Leaf	T	*Aesculus hickeyi*
SJ-013	DIC	Saxifragales	Cercidiphyllaceae	Leaf	T	*Archeampelos nebrascensis*
SJ-160	DIC	Saxifragales	Cercidiphyllaceae	Seed/Fruit	N/A	*Nyssidium arcticum*
SJ-163	DIC	Trochodendrales	Trochodendraceae	Leaf	T	*Zizyphoides flabella*
PB-25	DIC	Incertae Sedis	-	Flower	N/A	
SJ-002	DIC	Incertae Sedis	-	Leaf	T	
SJ-003	DIC	Incertae Sedis	-	Leaf	T	
SJ-005	DIC	Incertae Sedis	-	Leaf	U	
SJ-008	DIC	Incertae Sedis	-	Leaf	U	
SJ-009	DIC	Incertae Sedis	-	Leaf	Y	
SJ-011	DIC	Incertae Sedis	-	Leaf	U	
SJ-014	DIC	Incertae Sedis	-	Leaf	U	

Morph.	Aff.	Order	Family	Organ	Margin	Taxonomic name
SJ-015	DIC	Incertae Sedis	-	Leaf	U	
SJ-016	DIC	Incertae Sedis	-	Leaf	T	
SJ-017	DIC	Incertae Sedis	-	Leaf	U	
SJ-018	DIC	Incertae Sedis	-	Leaf	U	
SJ-020	DIC	Incertae Sedis	-	Leaf	U	
SJ-021	DIC	Incertae Sedis	-	Leaf	U	
SJ-022	DIC	Incertae Sedis	-	Leaf	U	
SJ-024	DIC	Incertae Sedis	-	Leaf	U	
SJ-025	DIC	Incertae Sedis	-	Leaf	U	
SJ-026	DIC	Incertae Sedis	-	Leaf	T	
SJ-028	DIC	Incertae Sedis	-	Leaf	U	
SJ-029	DIC	Incertae Sedis	-	Leaf	U	
SJ-030	DIC	Incertae Sedis	-	Leaf	U	
SJ-031	DIC	Incertae Sedis	-	Leaf	U	
SJ-033	DIC	Incertae Sedis	-	Leaf	U	
SJ-034	DIC	Incertae Sedis	-	Leaf	U	
SJ-035	DIC	Incertae Sedis	-	Leaf	U	
SJ-037	DIC	Incertae Sedis	-	Leaf	T	
SJ-039	DIC	Incertae Sedis	-	Leaf	U	
SJ-041	DIC	Incertae Sedis	-	Leaf	T	
SJ-042	DIC	Incertae Sedis	-	Leaf	U	
SJ-043	DIC	Incertae Sedis	-	Leaf	U	
SJ-044	DIC	Incertae Sedis	-	Leaf	U	
SJ-045	DIC	Incertae Sedis	-	Leaf	U	
SJ-048	DIC	Incertae Sedis	-	Leaf	U	
SJ-050	DIC	Incertae Sedis	-	Leaf	U	
SJ-053	DIC	Incertae Sedis	-	Leaf	U	

Morph.	Aff.	Order	Family	Organ	Margin	Taxonomic name
SJ-054	DIC	Incertae Sedis	-	Seed/Fruit	N/A	
SJ-055	DIC	Incertae Sedis	-	Leaf	U	
SJ-058	DIC	Incertae Sedis	-	Leaf	T	
SJ-063	DIC	Incertae Sedis	-	Leaf	U	
SJ-066	DIC	Incertae Sedis	-	Leaf	U	
SJ-069	DIC	Incertae Sedis	-	Leaf	N/A	
SJ-072	DIC	Incertae Sedis	-	Leaf	U	
SJ-073	DIC	Incertae Sedis	-	Leaf	U	
SJ-076	DIC	Incertae Sedis	-	Leaf	T	
SJ-077	DIC	Incertae Sedis	-	Leaf	T	
SJ-081	DIC	Incertae Sedis	-	Leaf	T/U	
SJ-083	DIC	Incertae Sedis	-	Leaf	U	*Dicotlophyllum horescreekium*
SJ-089	DIC	Incertae Sedis	-	Leaf	U	
SJ-090	DIC	Incertae Sedis	-	Leaf	U	
SJ-091	DIC	Incertae Sedis	-	Seed/Fruit	N/A	
SJ-092	DIC	Incertae Sedis	-	Leaf	U	
SJ-093	DIC	Incertae Sedis	-	Leaf	U	
SJ-094	DIC	Incertae Sedis	-	Leaf	U	
SJ-099	DIC	Incertae Sedis	-	Leaf	U	
SJ-100	DIC	Incertae Sedis	-	Seed/Fruit	N/A	
SJ-101	DIC	Incertae Sedis	-	Seed/Fruit	N/A	
SJ-103	DIC	Incertae Sedis	-	Leaf	T	
SJ-104	DIC	Incertae Sedis	-	Seed/Fruit	N/A	
SJ-105	DIC	Incertae Sedis	-	Leaf	U	
SJ-106	DIC	Incertae Sedis	-	Leaf	U	
SJ-107	DIC	Incertae Sedis	-	Leaf	T	
SJ-108	DIC	Incertae Sedis	-	Leaf	T	

Morph.	Aff.	Order	Family	Organ	Margin	Taxonomic name
SJ-109	DIC	Incertae Sedis	-	Seed/Fruit	N/A	
SJ-111	DIC	Incertae Sedis	-	Leaf	T	
SJ-112	DIC	Incertae Sedis	-	Leaf	U	
SJ-114	DIC	Incertae Sedis	-	Flower	N/A	
SJ-119	DIC	Incertae Sedis	-	Leaf	U	
SJ-121	DIC	Incertae Sedis	-	Leaf	T	
SJ-123	DIC	Incertae Sedis	-	Leaf	T	
SJ-128	DIC	Incertae Sedis	-	Leaf	U	
SJ-130	DIC	Incertae Sedis	-	Leaf	U	
SJ-131	DIC	Incertae Sedis	-	Leaf	T	
SJ-132	DIC	Incertae Sedis	-	Seed/Fruit	N/A	
SJ-133	DIC	Incertae Sedis	-	Leaf	T	
SJ-136	DIC	Incertae Sedis	-	Leaf	U	
SJ-138	DIC	Incertae Sedis	-	Leaf	T	
SJ-141	DIC	Incertae Sedis	-	Leaf	T	
SJ-142	DIC	Incertae Sedis	-	Leaf	U	
SJ-143	DIC	Incertae Sedis	-	Leaf	U	
SJ-144	DIC	Incertae Sedis	-	Leaf	T	
SJ-145	DIC	Incertae Sedis	-	Leaf	U	
SJ-146	DIC	Incertae Sedis	-	Leaf	U	
SJ-149	DIC	Incertae Sedis	-	Leaf	T	
SJ-152	DIC	Incertae Sedis	-	Leaf	T	
SJ-153	DIC	Incertae Sedis	-	Leaf	U	
SJ-154	DIC	Incertae Sedis	-	Leaf	U	
SJ-156	DIC	Incertae Sedis	-	Leaf	T	
SJ-157	DIC	Incertae Sedis	-	Leaf	U	
SJ-159	DIC	Incertae Sedis	-	Leaf	U	

Morph.	Aff.	Order	Family	Organ	Margin	Taxonomic name
SJ-161	DIC	Incertae Sedis	-	Leaf	U	
SJ-164	DIC	Incertae Sedis	-	Leaf	U	
SJ-165	DIC	Incertae Sedis	-	Seed/Fruit	N/A	
SJ-167	DIC	Incertae Sedis	-	Seed/Fruit	N/A	
SJ-168	DIC	Incertae Sedis	-	Leaf	U	
SJ-169	DIC	Incertae Sedis	-	Leaf	T	
SJ-170	DIC	Incertae Sedis	-	Leaf	T	
SJ-171	DIC	Incertae Sedis	-	Leaf	U	
SJ-172	DIC	Incertae Sedis	-	Leaf	T	
SJ-174	DIC	Incertae Sedis	-	Leaf	U	
SJ-176	DIC	Incertae Sedis	-	Seed/Fruit	N/A	
SJ-177	DIC	Incertae Sedis	-	Seed/Fruit	N/A	
SJ-178	DIC	Incertae Sedis	-	Leaf	T	
SJ-179	DIC	Incertae Sedis	-	Leaf	U	
SJ-180	DIC	Incertae Sedis	-	Leaf	T	
SJ-181	DIC	Incertae Sedis	-	Leaf	U	
SJ-182	DIC	Incertae Sedis	-	Leaf	U	
SJ-183	DIC	Incertae Sedis	-	Flower	N/A	
SJ-184	DIC	Incertae Sedis	-	Leaf	U	
SJ-187	DIC	Incertae Sedis	-	Leaf	T	
SJ-188	DIC	Incertae Sedis	-	Seed/Fruit	N/A	
SJ-189	DIC	Incertae Sedis	-	Leaf	U	
SJ-190	DIC	Incertae Sedis	-	Seed/Fruit	N/A	
SJ-095	LYC	Isoetales	Isoetaceae	Stem/Root	N/A	*Isoetes horridus*
SJ-096	LYC	Isoetales	Isoetaceae	Leaf	N/A	*Isoetes horridus*
SJ-059	LYC	Selaginellales	Selaginellaceae	Leaf	N/A	*Selaginella sp.*
SJ-062	MON	Alismatales	Araceae	Leaf	N/A	*Limnobiophyllum scutatum*

Morph.	Aff.	Order	Family	Organ	Margin	Taxonomic name
SJ-079	MON	Arecales	Areaceae	Leaf	N/A	*Sabalites sp.*
SJ-120	MON	Arecales	Areaceae	Seed/Fruit	N/A	*Sabalites sp.*
PB-24	MON	Arecales	Areaceae	Seed/Fruit	N/A	*Sabalites sp.*
SJ-070	MON	Arecales	Areaceae	Seed/Fruit	N/A	*Sabalites sp.*
SJ-086	MON	Arecales	Areaceae	Leaf	N/A	*Sabalites sp.*
SJ-117	MON	Arecales	Areaceae	Leaf	N/A	*Sabalites sp.*
SJ-135	MON	Arecales	Areaceae	Leaf	N/A	*Sabalites sp.*
SJ-190	MON	Arecales	Areaceae	Seed/Fruit	N/A	*Sabalites sp.*
SJ-065	MON	Zingiberales	Zingiberaceae	Leaf	N/A	*Zingiberopsis sp.*
SJ-115	MON	Zingiberales	Zingiberaceae	Leaf	N/A	*Zingiberopsis sp.*
SJ-060	MON	Incertae Sedis	-	Leaf	N/A	
SJ-110	MON	Incertae Sedis	-	Leaf	N/A	
SJ-067	PTE	Equisetales	Equisetaceae	Reproductive	N/A	*Equisetum*
SJ-064	PTE	Equisetales	Equisetaceae	Leaf	N/A	*Equisetum sp.*
PB-26	PTE	Equisetales	Equisetaceae	Leaf	N/A	*Equisetum sp.*
SJ-158	PTE	Polypodiales	Dryopteridaceae	Leaf	N/A	*Allantoidiopsis erosa*
SJ-134	PTE	Polypodiales	Dryopteridaceae	Leaf	N/A	*Dryopteris sp.*
SJ-056	PTE	Polypodiales	Onocleaceae	Leaf	N/A	*Onoclea sensibilis*
SJ-057	PTE	Schizaeales	Anemiaceae	Leaf	N/A	*Anemia sp.?*
SJ-098	PTE	Schizaeales	Anemiaceae	Leaf	N/A	*Anemia sp.?*
SJ-061	PTE	Polypodiales	Incertae Sedis	Leaf	N/A	
SJ-147	PTE	Polypodiales	Incertae Sedis	Leaf	N/A	
SJ-148	PTE	Polypodiales	Incertae Sedis	Leaf	N/A	

Table D.2 – San Just Basin Floral Locality and Specimen Count Information: Stratigraphic position (relative to formation contacts or paleomagnetic measured sections), depositional facies, location (NAD 27 datum), estimated age (Myr), and morphotype tallies for all floral collections. Affinity = major plant group (DIC = dicot angiosperms, MON = monocot angiosperms, PTE = ferns, EQU = horsetails, LYC = lycophytes, CON = conifers, CYD = cycads). Margin = dicot margin type (T = toothed, U = untoothed). Field tally = number of specimens tallied in the field for census collections. Lab tally = number of specimens tallied in the lab from voucher collections.

Locality	AF1409					
Location	De-Na-Zin					
Stratigraphic position above Naashoibito-Ojo Alamo Contact (m)	4.8					
Estimated Age (Myr)	66.0					
Depositional Facies	Overbank/Crevasse splay					
Location (UTM)	12 S 0767253 4023914					
Morphotype	**Name (if known)**	**Affinity**	**Margin**	**Field Tally**	**Lab Tally**	**Total**
SJ-036	*Platanites raynoldsii*	DIC	T	0	6	6
SJ-051	*Paranymphaea crassfolia*	DIC	U	0	1	1
SJ-078	*Browneia serrata*	DIC	T	0	1	1
SJ-079	*Sabalites sp.*	MON	-	0	1	1
SJ-080	*"Rhamnus" goldiana*	DIC	U	0	1	1
SJ-082		DIC	U	0	5	5
Total Morphotypes	6			0	15	15

Locality	AF1409B
Location	De-Na-Zin
Stratigraphic position above Naashoibito-Ojo Alamo Contact (m)	4.8
Estimated Age (Myr)	66.0
Depositional Facies	Overbank/Crevasse splay
Location (UTM)	12 S 0767154 4023382

Morphotype	**Name (if known)**	**Affinity**	**Margin**	**Field Tally**	**Lab Tally**	**Total**
SJ-013	*"Populus" nebrascensis*	DIC	T	0	1	1
SJ-036	*Platanites raynoldsii*	DIC	T	0	6	6
SJ-046	*Averrhoites affinis*	DIC	U	0	3	3
SJ-061		PTE	-	0	3	3
SJ-064	*Equisetum sp.*	EQU	-	0	2	2
SJ-071	*Platanites marginata*	DIC	T	0	1	1
SJ-080	*"Rhamnus" goldiana*	DIC	U	0	3	3
SJ-088		DIC	T	0	1	1
SJ-102	*Ditaxocladus catenulata*	CON	-	0	1	1
SJ-151	*"Artocarpus" lessigiana*	DIC	U	0	2	2
Total Morphotypes	10			0	23	23

Locality	AF1409C
Location	De-Na-Zin
Stratigraphic position above Naashoibito-Ojo Alamo Contact (m)	5.2
Estimated Age (Myr)	66.0
Depositional Facies	Overbank/Crevasse splay
Location (UTM)	12 S 0767154 4023382

Morphotype	**Name (if known)**	**Affinity**	**Margin**	**Field Tally**	**Lab Tally**	**Total**
SJ-036	*Platanites raynoldsii*	DIC	T	0	20	20
SJ-046	*Averrhoites affinis*	DIC	U	0	7	7
SJ-051	*Paranymphaea crassfolia*	DIC	U	0	2	2
SJ-062	*Limnobiophyllum scutatum*	MON	-	0	1	1
SJ-064	*Equisetum sp.*	EQU	-	0	3	3
SJ-068	*Cupressinocladus interruptis*	CON	-	0	27	27
SJ-071	*Platanites marginata*	DIC	T	0	1	1
SJ-077		DIC	T	0	4	4
SJ-080	*"Rhamnus" goldiana*	DIC	U	0	5	5
SJ-082		DIC	U	0	11	11
SJ-088		DIC	T	0	3	3
SJ-093		DIC	U	0	1	1
SJ-102	*Ditaxocladus catenulata*	CON	-	0	10	10
SJ-104		DIC	-	0	4	4
Total Morphotypes	14			0	99	99

Locality	AF1409D
Location	De-Na-Zin
Stratigraphic position above Naashoibito-Ojo Alamo Contact (m)	5.7
Estimated Age (Myr)	66.0
Depositional Facies	Overbank/Crevasse splay
Location (UTM)	12 S 0767140 4023368

Morphotype	Name (if known)	Affinity	Margin	Field Tally	Lab Tally	Total
SJ-036	*Platanites raynoldsii*	DIC	T	31	0	31
SJ-046	*Averrhoites affinis*	DIC	U	54	0	54
SJ-051	*Paranymphaea crassfolia*	DIC	U	6	0	6
SJ-056	*Onoclea sensibilus*	PTE	-	2	0	2
SJ-071	*Platanites marginata*	DIC	T	32	0	32
SJ-072		DIC	U	1	0	1
SJ-073		DIC	U	1	0	1
SJ-076		DIC	T	19	0	19
SJ-077		DIC	T	22	0	22
SJ-078	*Browneia serrata*	DIC	T	13	0	13
SJ-079		MON	-	10	0	10
SJ-080	*"Rhamnus" goldiana*	DIC	U	15	0	15
SJ-081		DIC	T	0	1	1
SJ-082		DIC	U	92	0	92
SJ-083		DIC	-	4	0	4
SJ-086	*Sabalites sp.*	MON	-	2	0	2
SJ-088		DIC	T	3	0	3
SJ-089		DIC	U	1	0	1
SJ-090		DIC	U	1	0	1
SJ-091		DIC	-	2	0	2
SJ-151	*"Artocarpus" lessigiana*	DIC	U	1	0	1
Total Morphotypes	21			312	1	313

Locality	AF1404
Location	De-Na-Zin
Stratigraphic position above Naashoibito-Ojo Alamo Contact (m)	6.0
Estimated Age (Myr)	66.0
Depositional Facies	Overbank/Crevasse splay
Location (UTM)	12 S 0768154 4023714

Morphotype	**Name (if known)**	**Affinity**	**Margin**	**Field Tally**	**Lab Tally**	**Total**
SJ-036	*Platanites raynoldsii*	DIC	T	92	17	109
SJ-046	*Averrhoites affinis*	DIC	U	27	2	29
SJ-048		DIC	U	0	1	1
SJ-051	*Paranymphaea crassfolia*	DIC	U	0	3	3
SJ-060		MON	-	2	0	2
SJ-064	*Equisetum sp.*	EQU	-	2	0	2
SJ-071	*Platanites marginata*	DIC	T	86	2	88
SJ-077		DIC	T	5	2	7
SJ-078	*Browneia serrata*	DIC	T	14	0	14
SJ-082		DIC	U	21	1	22
SJ-086	*Sabalites sp.*	MON	-	2	1	3
SJ-090		DIC	U	3	0	3
SJ-102	*Ditaxocladus catenulata*	CON	-	82	0	82
SJ-104		DIC	-	1	0	1
SJ-110		MON	-	5	0	5
SJ-111		DIC	T	1	0	1
SJ-112		DIC	U	5	0	5
SJ-113	*Zizyphus fibrillosus*	DIC	U	4	0	4
SJ-114		DIC	-	1	0	1
SJ-119		DIC	U	1	0	1
Total Morphotypes	20			354	29	383

Locality	AF1403
Location	De-Na-Zin
Stratigraphic position above Naashoibito-Ojo Alamo Contact (m)	11.9
Estimated Age (Myr)	65.9
Depositional Facies	Pond/Carbonaceous Shale
Location (UTM)	12 S 0768334 4023474

Morphotype	**Name (if known)**	**Affinity**	**Margin**	**Field Tally**	**Lab Tally**	**Total**
SJ-046	*Averrhoites affinis*	DIC	U	0	2	2
SJ-064	*Equisetum sp.*	EQU	-	0	10	10
SJ-065		MON	-	0	1	1
Total Morphotypes	3			0	13	13

Locality	AF1407
Location	De-Na-Zin
Stratigraphic position above Naashoibito-Ojo Alamo Contact (m)	12.5
Estimated Age (Myr)	65.9
Depositional Facies	Pond/Carbonaceous Shale
Location (UTM)	12 S 0769150 4023648

Morphotype	**Name (if known)**	**Affinity**	**Margin**	**Field Tally**	**Lab Tally**	**Total**
SJ-013	*"Populus" nebrascensis*	DIC	T	0	1	1
SJ-014		DIC	U	0	1	1
SJ-018		DIC	T	0	1	1
SJ-036	*Platanites raynoldsii*	DIC	T	0	7	7
SJ-046	*Averrhoites affinis*	DIC	U	594	176	770
SJ-050		DIC	U	57	2	59
SJ-051	*Paranymphaea crassfolia*	DIC	U	0	5	5
SJ-053		DIC	U	0	1	1
SJ-054		DIC	-	1	0	1
SJ-055		DIC	U	15	1	16
SJ-056	*Onoclea sensibilus*	PTE	-	1	1	2
SJ-057	cf. *Anemia*	PTE	-	1	6	7
SJ-058		DIC	U	2	0	2
SJ-059	*Selaginella sp.*	LYC	-	2	0	2
SJ-060		MON	-	2	6	8
SJ-062	*Limnobiophyllum scutatum*	MON	-	3	0	3
SJ-063		DIC	U	2	0	2
SJ-065		MON	-	15	2	17
SJ-066		DIC	U	1	0	1
SJ-068	*Cupressinocladus interruptis*	CON	-	0	2	2
SJ-071	*Platanites marginata*	DIC	T	0	1	1
SJ-078	*Browneia serrata*	DIC	T	15	8	23
SJ-082		DIC	U	0	1	1
SJ-093		DIC	U	0	2	2
SJ-094		DIC	U	0	1	1
Total Morphotypes	24			711	225	936

Locality	AF1407B
Location	De-Na-Zin
Stratigraphic position above Naashoibito-Ojo Alamo Contact (m)	12.5
Estimated Age (Myr)	65.9
Depositional Facies	Pond/Carbonaceous Shale
Location (UTM)	13S 0230696 4023960

Morphotype	**Name (if known)**	**Affinity**	**Margin**	**Field Tally**	**Lab Tally**	**Total**
SJ-025		DIC	U	5	0	5
SJ-028		DIC	T	2	0	2
SJ-036	*Platanites raynoldsii*	DIC	T	65	2	67
SJ-046	*Averrhoites affinis*	DIC	U	131	5	136
SJ-050		DIC	U	8	0	8
SJ-056	*Onoclea sensibilus*	PTE	-	2	0	2
SJ-057	cf. *Anemia*	PTE	-	1	0	1
SJ-059	*Selaginella sp.*	LYC	-	17	0	17
SJ-060		DIC	U	38	0	38
SJ-062	*Limnobiophyllum scutatum*	MON	-	1	1	2
SJ-064	*Equisetum sp.*	EQU	-	17	0	17
SJ-065				17	1	18
SJ-067		DIC	U	1	0	1
SJ-068	*Cupressinocladus interruptis*	CON	-	13	2	15
SJ-069		MON	-	2	0	2
SJ-070				1	0	1
SJ-078	*Browneia serrata*	DIC	T	3	0	3
SJ-092		MON	-	0	2	2
Total Morphotypes	18			324	13	337

Locality	DP1301
Location	De-Na-Zin
Stratigraphic position above Naashoibito-Ojo Alamo Contact (m)	13.0
Estimated Age (Myr)	65.9
Depositional Facies	Pond/Carbonaceous Shale
Location (UTM)	12S 0768124 4024321

Morphotype	**Name (if known)**	**Affinity**	**Margin**	**Field Tally**	**Lab Tally**	**Total**
SJ-046	*Averrhoites affinis*	DIC	U	0	31	31
SJ-050		DIC	U	0	1	1
SJ-057	cf. *Anemia*	PTE	-	0	2	2
SJ-062	*Limnobiophyllum scutatum*	MON	-	0	1	1
SJ-064	*Equisetum sp.*	EQU	-	0	1	1
SJ-065		MON	-	0	4	4
Total Morphotypes	3			0	40	40

Locality	DP1301B
Location	De-Na-Zin
Stratigraphic position above Naashoibito-Ojo Alamo Contact (m)	13.0
Estimated Age (Myr)	65.9
Depositional Facies	Pond/Carbonaceous Shale
Location (UTM)	12S 0768124 4024321

Morphotype	**Name (if known)**	**Affinity**	**Margin**	**Field Tally**	**Lab Tally**	**Total**
SJ-014		DIC	U	2	0	2
SJ-036	*Platanites raynoldsii*	DIC	T	11	0	11
SJ-046	*Averrhoites affinis*	DIC	U	561	0	561
SJ-048		DIC	U	2	0	2
SJ-050		DIC	U	10	0	10
SJ-051	*Paranymphaea crassfolia*	DIC	U	2	0	2
SJ-056	*Onoclea sensibilis*	PTE	-	1	0	1
SJ-060		MON	-	4	0	4
SJ-062	*Limnobiophyllum scutatum*	MON	-	1	0	1
SJ-065		MON	-	2	0	2
SJ-068	*Cupressinocladus interruptis*	CON	-	1	0	1
SJ-078	*Browneia serrata*	DIC	T	3	0	3
SJ-089		DIC	U	1	0	1
Total Morphotypes	13			601	0	601

Locality	AF1402
Location	De-Na-Zin
Stratigraphic position above Naashoibito-Ojo Alamo Contact (m)	14.0
Estimated Age (Myr)	65.9
Depositional Facies	Pond/Carbonaceous Shale
Location (UTM)	12S 0768330 4024210

Morphotype	**Name (if known)**	**Affinity**	**Margin**	**Field Tally**	**Lab Tally**	**Total**
SJ-036	*Platanites raynoldsii*	DIC	T	5	0	5
SJ-046	*Averrhoites affinis*	DIC	U	476	0	476
SJ-050		DIC	U	1	0	1
SJ-055		DIC	U	1	0	1
SJ-056	*Onoclea sensibilis*	PTE	-	2	0	2
SJ-057	cf. *Anemia*	PTE	-	111	0	111
SJ-059	*Selaginella sp.*	LYC	-	2	0	2
SJ-060		MON	-	33	0	33
SJ-061		PTE	-	3	0	3
SJ-062	*Limnobiophyllum scutatum*	MON	-	4	0	4
Total Morphotypes	10			638	0	638

Locality	AF1415
Location	De-Na-Zin
Stratigraphic position above Naashoibito-Ojo Alamo Contact (m)	14.7
Estimated Age (Myr)	65.9
Depositional Facies	Pond/Carbonaceous Shale
Location (UTM)	12S 0767362 4024540

Morphotype	**Name (if known)**	**Affinity**	**Margin**	**Field Tally**	**Lab Tally**	**Total**
SJ-036	*Platanites raynoldsii*	DIC	T	0	7	7
SJ-046	*Averrhoites affinis*	DIC	U	0	1	1
SJ-051	*Paranymphaea crassfolia*	DIC	U	0	1	1
SJ-071	*Platanites marginata*	DIC	T	0	1	1
SJ-079	*Sabalites sp.*	MON	-	0	1	1
SJ-104		DIC	-	0	1	1
Total Morphotypes	6			0	12	12

Locality	AF1518
Location	Betonnie Tsosie Wash
Stratigraphic position above Ojo Alamo Contact (m)	4.2
Estimated Age (Myr)	65.73
Depositional Facies	Overbank/Crevasse splay
GPS Location (UTM)	13 S 0251950 4007433

Morphotype	**Name (if known)**	**Affinity**	**Margin**	**Field Tally**	**Lab Tally**	**Total**
SJ-011		DIC	U	0	3	3
SJ-028		DIC	U	0	2	2
SJ-036	*Platanites rayndolsii*	DIC	T	0	6	6
SJ-080	*"Rhamnus" goldiana*	DIC	U	0	4	4
SJ-086	*Sabalites sp.*	MON	N/A	0	1	1
SJ-124	*Davidia antiqua*	DIC	U	0	1	1
SJ-144		DIC	T	0	1	1
Total Morphotypes	7			0	18	18

Locality	AF1406
Location	De-Na-Zin
Stratigraphic position relative to Ojo Alamo Sandstone-Nacimiento Formation contact (m)	7.9
Estimated Age (Myr)	65.69
Depositional Facies	Lacustrine, fine grained ss, ripple laminated
GPS Location (UTM)	12 S 0769311 4023845

Morphotype	**Name (if known)**	**Affinity**	**Margin**	**Field Tally**	**Lab Tally**	**Total**
SJ-036	*Platanites raynodlsii*	DIC	T	15	8	23
SJ-060		MON	N/A	1	0	1
SJ-070		MON	N/A	3	0	3
SJ-071	*Platanites marginata*	DIC	T	82	2	84
SJ-079	*Sabalites sp.*	MON	N/A	93	0	93
SJ-081		DIC	U	44	28	72
SJ-082		DIC	U	1	0	1
SJ-083	*Dicotylophyllum horsecreekium*	DIC	U	1	0	1
SJ-086	*Sabalites sp.*	MON	N/A	8	4	12
SJ-106		DIC	U	229	4	233
SJ-108		DIC	U	1	0	1
SJ-109		DIC	N/A	4	0	4
SJ-113	*"Zizyphus" fibrillosus*	DIC	U	1	0	1
SJ-117	*Sabalites sp.*	MON	N/A	0	1	1
SJ-119		DIC	U	11	0	11
SJ-120		MON	N/A	1	0	1
SJ-121		DIC	T	1	0	1
SJ-123		DIC	T	10	0	10
SJ-124	*Davidia antiqua*	DIC	T	0	1	1
Total Morphotypes	19			506	48	554

Locality	AF1408
Location	De-Na-Zin
Stratigraphic position relative to Ojo Alamo Sandstone-Nacimiento Formation contact (m)	9.2
Estimated Age (Myr)	65.66
Depositional Facies	Pond/swamp, carbonaceous shale
GPS Location (UTM)	12 S 0769176 4023523

Morphotype	**Name (if known)**	**Affinity**	**Margin**	**Field Tally**	**Lab Tally**	**Total**
SJ-036	*Platanites raynodlsii*	DIC	T	0	5	20
SJ-046	*"Anemia" sp.*	PTE	N/A	0	1	1
SJ-082		DIC	U	0	2	2
SJ-115	*Zingiberopsis sp.*	MON	N/A	0	1	1
SJ-127	*Macginitiea sp.*	DIC	T/U	0	1	1
Total Morphotypes	5			0	10	25

Locality	AF1408B
Location	De-Na-Zin
Stratigraphic position relative to Ojo Alamo Sandstone-Nacimiento Formation contact (m)	9.2
Estimated Age (Myr)	65.66
Depositional Facies	Pond/swamp, carbonaceous shale
GPS Location (UTM)	12 S 0769183 4023322

Morphotype	**Name (if known)**	**Affinity**	**Margin**	**Field Tally**	**Lab Tally**	**Total**
SJ-011		DIC	T	0	1	1
SJ-036	*Platanites raynodlsii*	DIC	T	0	20	20
SJ-046	*Averrhoites affinus*	DIC	U	0	4	4
SJ-064	*Equisetum sp.*	PTE	N/A	0	1	1
SJ-071	*Platanites marginata*	DIC	T	0	19	19
SJ-082		DIC	U	0	1	1
SJ-115	*Zingiberopsis sp.*	MON	N/A	0	4	4
SJ-127	*Macginitiea sp.*	DIC	T/U	0	3	3
Total Morphotypes	8			0	53	53

Locality	AF1405
Location	De-Na-Zin
Stratigraphic position relative to Ojo Alamo Sandstone-Nacimiento Formation contact (m)	9.5
Estimated Age (Myr)	65.65
Depositional Facies	Pond/swamp, carbonaceous shale
GPS Location (UTM)	12 S 0768808 4023911

Morphotype	**Name (if known)**	**Affinity**	**Margin**	**Field Tally**	**Lab Tally**	**Total**
SJ-013	*"Populus" nebrascensis*	DIC	T	1	1	2
SJ-028		DIC	U	5	0	5
SJ-033		DIC	U	6	0	6
SJ-036	*Platanites raynodlsii*	DIC	T	61	15	76
SJ-046	*Averrhoites affinus*	DIC	U	68	7	75
SJ-050		DIC	U	0	1	1
SJ-056	*Onoclea sensibilis*	PTE	N/A	0	2	2
SJ-057	*"Anemia" sp.*	PTE	N/A	139	6	145
SJ-071	*Platanites marginata*	DIC	T	5	8	13
SJ-073		DIC	U	0	8	8
SJ-078	*Browneia serrata*	DIC	T	6	1	7
SJ-079	*Sabalites sp.*	MON	N/A	1	0	1
SJ-081		DIC	U	9	1	10
SJ-082		DIC	U	36	8	44
SJ-086	*Sabalites sp.*	MON	N/A	11	1	12
SJ-095	*Isoetes horridus*	LYC	N/A	1	1	2
SJ-098		PTE	N/A	8	1	9
SJ-101		DIC	N/A	3	0	3
SJ-113	*"Zizyphus" fibrillosus*	DIC	U	8	0	8
SJ-115	*Zingiberopsis sp.*	MON	N/A	4	2	6
SJ-125	*"Rhamnus" sp.*	DIC	U	7	0	7
SJ-127	*Macginitiea sp.*	DIC	T/U	0	1	1
SJ-138	*Davidia antiqua*	DIC	T	0	1	1
Total Morphotypes	23			379	65	444

Locality	DP1109
Location	De-Na-Zin
Stratigraphic position relative to Ojo Alamo Sandstone-Nacimiento Formation contact (m)	11.0
Estimated Age (Myr)	65.62
Depositional Facies	Pond/swamp, carbonaceous shale
GPS Location (UTM)	12 S 0768789 4024502

Morphotype	**Name (if known)**	**Affinity**	**Margin**	**Field Tally**	**Lab Tally**	**Total**
SJ-012	*Macgenitea sp.*	DIC	T	2	0	2
SJ-033		DIC	U	4	0	4
SJ-035		DIC	U	2	0	2
SJ-036	*Platanites raynodlsii*	DIC	T	86	0	86
SJ-046	*Averrhoites affinus*	DIC	U	1036	0	1036
SJ-048		DIC	U	1	0	1
SJ-051	*Paranymphaea crassfolia*	DIC	N/A	20	0	20
SJ-056	*Onoclea sensibilis*	PTE	N/A	5	0	5
SJ-057	*"Anemia" sp.*	PTE	N/A	1187	0	1187
SJ-062	*Limnobiophyllum scutatum*	MON	N/A	1	0	1
SJ-064	*Equisetum sp.*	EQU	N/A	14	0	14
SJ-068	*Cupressinocladus interruptis*	CON	N/A	1	0	1
SJ-071	*Platanites marginata*	DIC	T	3	0	3
SJ-077		DIC	T	2	0	2
SJ-079	*Sabalites sp.*	MON	N/A	14	0	14
SJ-082		DIC	U	188	0	188
SJ-086	*Sabalites sp.*	MON	N/A	2	0	2
SJ-095	*Isoetes horridus*	LYC	N/A	32	0	32
SJ-096		DIC	N/A	1	0	1
SJ-097		CON	N/A	22	0	22
SJ-098		PTE	N/A	28	0	28
SJ-099	*Nelumbium montanum*	DIC	N/A	6	0	6
SJ-100		DIC	N/A	6	0	6
Total Morphotypes	23			2663	0	2663

Locality	AF1507
Location	Mesa de Cuba - Southside
Stratigraphic position relative to Ojo Alamo Sandstone-Nacimiento Formation contact (m)	-2.7
Estimated Age (Myr)	65.51
Depositional Facies	Braid plain overbank
GPS Location (UTM)	13 S 0319380 3981284

Morphotype	Name (if known)	Affinity	Margin	Field Tally	Lab Tally	Total
SJ-046	*Averrhoites affinus*	DIC	U	0	2	2
SJ-051	*Paranymphaea crassfolia*	DIC	-	0	1	1
SJ-077		DIC	T	0	3	3
SJ-078	*Browniea serrata*	DIC	T	0	1	1
SJ-082		DIC	U	0	5	5
SJ-086	*Sabalites sp.*	MON	-	0	2	2
SJ-141		DIC	T	0	2	2
Total Morphotypes	7			0	16	16

Locality	AF1508
Location	Mesa de Cuba - Southside
Stratigraphic position relative to Ojo Alamo Sandstone-Nacimiento Formation contact (m)	-0.5
Estimated Age (Myr)	65.47
Depositional Facies	Braid plain overbank
GPS Location (UTM)	13 S 0319629 3981321

Morphotype	Name (if known)	Affinity	Margin	Field Tally	Lab Tally	Total
SJ-011		DIC	U	0	1	1
SJ-013	*cf. Trochodendroides*	DIC	T	0	1	1
SJ-051	*Paranymphaea crassfolia*	DIC	-	0	1	1
SJ-080	*"Rhamnus" goldiana*	DIC	U	0	5	5
SJ-081		DIC	U	0	1	1
SJ-130		DIC	U	0	1	1
SJ-150	*Sassafrass sp.*	DIC	U	0	1	1
SJ-192		DIC	-	0	1	1
Total Morphotypes	8			0	12	12

Locality	AF1509
Location	Mesa de Cuba - Southside
Stratigraphic position relative to Ojo Alamo Sandstone-Nacimiento Formation contact (m)	-0.5
Estimated Age (Myr)	65.47
Depositional Facies	Braid plain overbank
GPS Location (UTM)	13 S 0319611 3981356

Morphotype	**Name (if known)**	**Affinity**	**Margin**	**Field Tally**	**Lab Tally**	**Total**
SJ-035		DIC	U	0	1	1
SJ-036	*Platanites raynoldsii*	DIC	T	0	1	1
SJ-077		DIC	T	0	1	1
SJ-078	*Browniea serrata*	DIC	T	0	1	1
SJ-080	*"Rhamnus" goldiana*	DIC	U	0	1	1
SJ-082		DIC	U	0	6	6
SJ-083	*Dicotylophyllum horsecreekium*	DIC	U	0	1	1
SJ-086	*Sabalites sp.*	MON	-	0	3	3
SJ-149		DIC	T	0	1	1
Total Morphotypes	9			0	16	16

Locality	AF1516
Location	Betonnie Tsosie Wash
Stratigraphic position relative to Ojo Alamo Sandstone-Nacimiento Formation contact (m)	15.2
Estimated Age (Myr)	65.47
Depositional Facies	Overbank/Crevasse splay
GPS Location (UTM)	13 S 0251634 4007499

Morphotype	**Name (if known)**	**Affinity**	**Margin**	**Field Tally**	**Lab Tally**	**Total**
SJ-036	*Platanites rayndolsii*	DIC	T	0	3	3
SJ-080	*"Rhamnus" goldiana*	DIC	U	0	9	9
SJ-081		DIC	T/U	0	1	1
SJ-127	*Macginitea sp.*	DIC	T/U	0	1	1
SJ-138		DIC	T	0	2	2
Total Morphotypes	5			0	16	16

Locality	AF1517
Location	Betonnie Tsosie Wash
Stratigraphic position relative to Ojo Alamo Sandstone-Nacimiento Formation contact (m)	17.1
Estimated Age (Myr)	65.42
Depositional Facies	Overbank/Crevasse splay
GPS Location (UTM)	13 S 0252544 4007155

Morphotype	**Name (if known)**	**Affinity**	**Margin**	**Field Tally**	**Lab Tally**	**Total**
PB-26	*Equisetum sp.*	PTE	N/A	0	2	2
SJ-080	*"Rhamnus" goldiana*	DIC	U	0	1	1
Total Morphotypes	2			0	3	3

Locality	AF1510
Location	Mesa de Cuba - Southside
Stratigraphic position relative to Ojo Alamo Sandstone-Nacimiento Formation contact (m)	3.9
Estimated Age (Myr)	65.38
Depositional Facies	Overbank/Crevasse splay
GPS Location (UTM)	13 S 0319572 3981678

Morphotype	**Name (if known)**	**Affinity**	**Margin**	**Field Tally**	**Lab Tally**	**Total**
PB-24		MON	N/A	0	1	1
SJ-005	*"Ficus" artocarpoides*	DIC	U	0	1	1
SJ-011		DIC	U	0	9	9
SJ-024		DIC	U	0	1	1
SJ-036	*Platanites raynoldsii*	DIC	T	0	17	17
SJ-070		MON	-	0	1	1
SJ-078	*Browniea serrata*	DIC	T	0	1	1
SJ-080	*"Rhamnus" goldiana*	DIC	U	0	94	94
SJ-081		DIC	U	0	4	4
SJ-082		DIC	U	0	2	2
SJ-086	*Sabalites sp.*	MON	-	0	3	3
SJ-100		DIC	-	0	1	1
SJ-141		DIC	T	0	1	1
SJ-143		DIC	U	0	1	1
SJ-150	*"Melastomites" montanensis*	DIC	U	0	1	1
SJ-151	*"Artocarpus" lessingiana*	DIC	U	0	4	4
SJ-158	*Allantoidiopsis erosa*	PTE	-	0	1	1
SJ-163		DIC	T	0	1	1
SJ-164		DIC	U	0	1	1
SJ-187		DIC	T	0	1	1
Total Morphotypes	20			0	146	146

Locality	AF1515
Location	Betonnie Tsosie Wash
Stratigraphic position relative to Ojo Alamo Sandstone-Nacimiento Formation contact (m)	20.2
Estimated Age (Myr)	65.35
Depositional Facies	Overbank/Crevasse splay
GPS Location (UTM)	13 S 0251530 4007807

Morphotype	**Name (if known)**	**Affinity**	**Margin**	**Field Tally**	**Lab Tally**	**Total**
SJ-070		MON	N/A	0	1	1
SJ-080	*"Rhamnus" goldiana*	DIC	U	0	1	1
SJ-135		MON	N/A	0	2	2
Total Morphotypes	3			0	4	4

Locality	AF1612
Location	Betonnie Tsosie Wash
Stratigraphic position relative to Ojo Alamo Sandstone-Nacimiento Formation contact (m)	20.2
Estimated Age (Myr)	65.35
Depositional Facies	Overbank/Crevasse splay
GPS Location (UTM)	13 S 0251489 4007526

Morphotype	**Name (if known)**	**Affinity**	**Margin**	**Field Tally**	**Lab Tally**	**Total**
SJ-011		DIC	U	0	1	1
SJ-019	*Juglandophyllites glabra*	DIC	T	0	2	2
SJ-036	*Platanites rayndolsii*	DIC	T	0	3	3
SJ-070		MON	N/A	0	1	1
SJ-078	*Browneia serrata*	DIC	T	0	1	1
SJ-080	*"Rhamnus" goldiana*	DIC	U	0	24	24
SJ-113	*"Zizyphus" fibrillosus*	DIC	U	0	4	4
SJ-114		DIC	N/A	0	2	2
SJ-121		DIC	T	0	1	1
SJ-141		DIC	T	0	1	1
SJ-143		DIC	U	0	1	1
SJ-151	*"Artocarpus" lessingiana*	DIC	U	0	1	1
SJ-166		CYD	N/A	0	11	11
Total Morphotypes	13			0	53	53

Locality	DP1304
Location	De-Na-Zin
Stratigraphic position relative to Ojo Alamo Sandstone-Nacimiento Formation contact (m)	23.5
Estimated Age (Myr)	65.33
Depositional Facies	Overbank, crevasse splays
GPS Location (UTM)	13 S 0230902 4024461

Morphotype	**Name (if known)**	**Affinity**	**Margin**	**Field Tally**	**Lab Tally**	**Total**
SJ-012	*Macgenitea sp.*	DIC	T	7	3	10
SJ-015		DIC	U	9	0	9
SJ-020		DIC	U	3	0	3
SJ-028		DIC	U	0	1	1
SJ-036	*Platanites raynodlsii*	DIC	T	347	17	364
SJ-046	*Averrhoites affinus*	DIC	U	88	11	99
SJ-051	*Paranymphaea crassfolia*	DIC	N/A	0	1	1
SJ-059		CON	N/A	1	4	5
SJ-060		MON	N/A	2	0	2
SJ-064	*Equisetum sp.*	EQU	N/A	1	0	1
SJ-071	*Platanites marginata*	DIC	T	74	17	91
SJ-080	*"Rhamnus" goldiana*	DIC	U	1	0	1
SJ-081		DIC	U	2	0	2
SJ-086	*Sabalites sp.*	MON	N/A	4	2	6
SJ-088		DIC	U	1	0	1
SJ-102	*Ditaxocladus catenulatus*	CON	N/A	79	5	84
SJ-103		DIC	T	1	0	1
SJ-109		DIC	N/A	10	0	10
SJ-113	*"Zizyphus" fibrillosus*	DIC	U	2	2	4
SJ-115	*Zingiberopsis sp.*	MON	N/A	12	1	13
SJ-119		DIC	U	1	0	1
SJ-124	*Davidia antiqua*	DIC	T	0	4	4
SJ-126		CON	N/A	0	1	1
SJ-127	*Macginitiea sp.*	DIC	T/U	0	1	1
SJ-132		DIC	N/A	0	1	1
SJ-137		DIC	U	0	1	1
SJ-158	*Allantoidiopsis erosa*	PTE	N/A	1	0	1
Total Morphotypes	27			646	72	718

Locality	AF1623
Location	De-Na-Zin
Stratigraphic position relative to Ojo Alamo Sandstone-Nacimiento Formation contact (m)	23.5
Estimated Age (Myr)	65.33
Depositional Facies	Overbank, crevasse splays
GPS Location (UTM)	13 S 0231135 4024236

Morphotype	**Name (if known)**	**Affinity**	**Margin**	**Field Tally**	**Lab Tally**	**Total**
SJ-012	*Macgenitea sp.*	DIC	T	2	0	2
SJ-019	*Julandiphyllites glabra*	DIC	T	2	0	2
SJ-036	*Platanites raynodlsii*	DIC	T	305	31	336
SJ-046	*Averrhoites affinus*	DIC	U	4	0	4
SJ-070		MON	N/A	1	0	1
SJ-071	*Platanites marginata*	DIC	T	45	12	57
SJ-078	*Browneia serrata*	DIC	T	5	0	5
SJ-079		MON	N/A	2	0	2
SJ-081		DIC	U	14	1	15
SJ-082		DIC	U	7	0	7
SJ-086	*Sabalites sp.*	MON	N/A	27	2	29
SJ-102	*Ditaxocladus catenulatus*	CON	N/A	53	2	55
SJ-103		DIC	T	4	0	4
SJ-109		DIC	N/A	1	0	1
SJ-119		DIC	U	7	2	9
SJ-121		DIC	T	3	0	3
SJ-124	*Davidia antiqua*	DIC	T	17	2	19
SJ-126		CON	N/A	7	1	8
SJ-127	*Macginitiea sp.*	DIC	T/U	11	4	15
SJ-128		DIC	U	32	1	33
SJ-129	*Fagopsiphyllum groenlandicum*	DIC	T	2	1	3
SJ-130	*"Ficus" subtruncata*	DIC	U	39	4	43
SJ-131		DIC	T	7	1	8
SJ-132		DIC	N/A	7	0	7
SJ-133		DIC	T	8	0	8
SJ-137		DIC	U	0	2	2
Total Morphotypes	26			612	66	678

Locality	AF1414
Location	Mesa de Cuba - Northside
Stratigraphic position relative to Ojo Alamo Sandstone-Nacimiento Formation contact (m)	14.0
Estimated Age (Myr)	65.29
Depositional Facies	VF sand, slight pedogenesis
GPS Location (UTM)	

Morphotype	**Name (if known)**	**Affinity**	**Margin**	**Field Tally**	**Lab Tally**	**Total**
SJ-036	*Platanites raynoldsii*	DIC	T	0	1	1
SJ-046	*Averrhoites affinus*	DIC	U	0	63	63
SJ-055		DIC	U	0	1	1
SJ-062	*Limnobiophyllum scutatum*	MON	-	0	1	1
SJ-064	*Equisetum sp.*	EQU	-	0	5	5
SJ-071	*Platanites marginata*	DIC	T	0	1	1
SJ-086	*Sabalites sp.*	MON	-	0	1	1
SJ-095	*Isoetes horridus*	LYC	-	0	1	1
SJ-096	*Isoetes horridus*	LYC	-	0	16	16
SJ-113	*Zizyphus fibrillosus*	DIC	U	0	1	1
SJ-177		DIC	-	0	1	1
Total Morphotypes	11			0	92	92

Locality	AF1521
Location	Betonnie Tsosie Wash
Stratigraphic position relative to Ojo Alamo Sandstone-Nacimiento Formation contact (m)	22.6
Estimated Age (Myr)	65.29
Depositional Facies	Overbank/Crevasse splay
GPS Location (UTM)	13 S 0252024 4007688

Morphotype	**Name (if known)**	**Affinity**	**Margin**	**Field Tally**	**Lab Tally**	**Total**
SJ-011		DIC	U	0	1	1
SJ-036	*Platanites raynoldsii*	DIC	T	0	1	1
SJ-080	*"Rhamnus" goldiana*	DIC	U	0	57	57
SJ-113	*"Zizyphus" fibrillosus*	DIC	U	0	2	2
SJ-138		DIC	T	0	1	1
SJ-144		DIC	U	0	1	1
SJ-151	*"Artocarpus" lessingiana*	DIC	U	0	12	12
SJ-158	*Allantoidiopsis erosa*	PTE	N/A	0	3	3
SJ-175	*Rhamnites sp.*	DIC	U	0	1	1
Total Morphotypes	9			0	79	79

Locality	DP1307
Location	Kimbeto Wash
Stratigraphic position above Base of Kimbeto Wash Pmag Section (m)	8.0
Estimated Age (Myr)	65.28
Depositional Facies	Overbank/Crevasse splay
GPS Location (UTM)	13 S 0242839 4012536

Morphotype	**Name (if known)**	**Affinity**	**Margin**	**Field Tally**	**Lab Tally**	**Total**
SJ-036	*Platanites raynoldsii*	DIC	T	0	2	2
SJ-080	*"Rhamnus" goldiana*	DIC	U	0	6	6
SJ-134		PTE	-	0	2	2
SJ-158	*Allantoidiopsis erosa*	PTE	-	0	1	1
SJ-166		CYD	-	0	7	7
SJ-185		CYD	-	0	1	1
Total Morphotypes	6			0	19	19

Locality	AF1526
Location	Kimbeto Wash
Stratigraphic position above Base of Kimbeto Wash Pmag Section (m)	8.0
Estimated Age (Myr)	65.28
Depositional Facies	Overbank/Crevasse splay
GPS Location (UTM)	

Morphotype	**Name (if known)**	**Affinity**	**Margin**	**Field Tally**	**Lab Tally**	**Total**
SJ-036	*Platanites raynoldsii*	DIC	T	0	1	1
SJ-046	*Averrhoites affinis*	DIC	U	0	1	1
SJ-059	*Selaginella sp.*	LYC	-	0	2	2
SJ-080	*"Rhamnus" goldiana*	DIC	U	0	11	11
SJ-086	*Sabalites sp.*	MON	-	0	1	1
SJ-127	*Macginitiea sp.*	DIC	T/U	0	1	1
SJ-135		MON	-	0	1	1
Total Morphotypes	7			0	18	18

Locality	AF1608
Location	Kimbeto Wash
Stratigraphic position above Base of Kimbeto Wash Pmag Section (m)	8.0
Estimated Age (Myr)	65.28
Depositional Facies	Overbank/Crevasse splay
GPS Location (UTM)	13 S 0242517 4012526

Morphotype	Name (if known)	Affinity	Margin	Field Tally	Lab Tally	Total
SJ-005		DIC	U	2	0	2
SJ-019	*Juglandiphyllites glabra*	DIC	T	10	3	13
SJ-036	*Platanites raynoldsii*	DIC	T	10	2	12
SJ-051	*Paranymphaea crassfolia*	DIC	N/A	0	1	1
SJ-056	*Onoclea sensibilis*	PTE	N/A	19	2	21
SJ-070		MON	N/A	1	0	1
SJ-071	*Platanites marginata*	DIC	T	0	1	1
SJ-080	*"Rhamnus" goldiana*	DIC	U	17	1	18
SJ-081		DIC	U	10	1	11
SJ-082		DIC	U	1	0	1
SJ-108		DIC	T	4	0	4
SJ-115	*Zingiberopsis sp.*	MON	N/A	38	2	40
SJ-119		DIC	U	8	0	8
SJ-124	*Davidia antiqua*	DIC	T	0	1	1
SJ-127	*Macginitiea sp.*	DIC	T/U	242	18	260
SJ-128		DIC	U	3	0	3
SJ-134		PTE	N/A	31	5	36
SJ-135	*Sabalites sp.*	MON	N/A	14	2	16
SJ-136		DIC	U	3	0	3
SJ-137		DIC	U	4	1	5
SJ-138		DIC	T	8	0	8
Total Morphotypes	21			425	40	465

Locality	AF1621
Location	De-Na-Zin
Stratigraphic position relative to Ojo Alamo Sandstone-Nacimiento Formation contact (m)	25.5
Estimated Age (Myr)	65.28
Depositional Facies	Overbank splays/partially ponded
GPS Location (UTM)	13 S 0231067 4023811

Morphotype	**Name (if known)**	**Affinity**	**Margin**	**Field Tally**	**Lab Tally**	**Total**
SJ-011		DIC	U	0	1	1
SJ-028		DIC	U	0	1	1
SJ-036	*Platanites raynodlsii*	DIC	T	0	3	3
SJ-046	*Averrhoites affinus*	DIC	U	0	1	1
SJ-062	*Limnobiophyllum scutatum*	MON	N/A	0	14	14
SJ-082		DIC	U	0	5	5
SJ-095	*Isoetes horridus*	LYC	N/A	0	5	5
SJ-112		DIC	U	0	1	1
SJ-115	*Zingiberopsis sp.*	MON	N/A	0	5	5
SJ-150	*Melastomites montanensis*	DIC	U	0	3	3
SJ-183		DIC	N/A	0	2	2
SJ-184		DIC	U	0	3	3
Total Morphotypes	12			0	44	44

Locality	AF1520
Location	Betonnie Tsosie Wash
Stratigraphic position relative to Ojo Alamo Sandstone-Nacimiento Formation contact (m)	23.2
Estimated Age (Myr)	65.27
Depositional Facies	Overbank/Crevasse splay
GPS Location (UTM)	13 S 0252153 4007648

Morphotype	**Name (if known)**	**Affinity**	**Margin**	**Field Tally**	**Lab Tally**	**Total**
SJ-036	*Platanites rayndolsii*	DIC	T	0	1	1
SJ-080	*"Rhamnus" goldiana*	DIC	U	0	3	3
SJ-121		DIC	T	0	1	1
SJ-146		DIC	U	0	1	1
SJ-148		PTE	N/A	0	4	4
SJ-151	*"Artocarpus" lessingiana*	DIC	U	0	1	1
SJ-153		DIC	U	0	1	1
Total Morphotypes	7			0	12	12

Locality	AF1520B
Location	Betonnie Tsosie Wash
Stratigraphic position relative to Ojo Alamo Sandstone-Nacimiento Formation contact (m)	23.2
Estimated Age (Myr)	65.27
Depositional Facies	Overbank/Crevasse splay
GPS Location (UTM)	13 S 0252126 4007668

Morphotype	**Name (if known)**	**Affinity**	**Margin**	**Field Tally**	**Lab Tally**	**Total**
SJ-016		DIC	T	0	1	1
SJ-036	*Platanites rayndolsii*	DIC	T	0	2	2
SJ-080	*"Rhamnus" goldiana*	DIC	U	0	9	9
SJ-086	*Sabalites sp.*	MON	N/A	0	3	3
SJ-127	*Macginitea sp.*	DIC	T/U	0	2	2
SJ-151	*"Artocarpus" lessingiana*	DIC	U	0	3	3
SJ-160		DIC	N/A	0	1	1
SJ-175	*Rhamnites sp.*	DIC	U	0	2	2
Total Morphotypes	8			0	23	23

Locality	AF1519
Location	Betonnie Tsosie Wash
Stratigraphic position relative to Ojo Alamo Sandstone-Nacimiento Formation contact (m)	23.4
Estimated Age (Myr)	65.27
Depositional Facies	Overbank/Crevasse splay
GPS Location (UTM)	13 S 0252204 4007575

Morphotype	**Name (if known)**	**Affinity**	**Margin**	**Field Tally**	**Lab Tally**	**Total**
PB-24		MON	N/A	0	1	1
SJ-011		DIC	U	0	2	2
SJ-036	*Platanites rayndolsii*	DIC	T	0	1	1
SJ-080	*"Rhamnus" goldiana*	DIC	U	0	34	34
SJ-081		DIC	U	0	1	1
SJ-086	*Sabalites sp.*	MON	N/A	0	4	4
SJ-113	*"Zizyphus" fibrillosus*	DIC	U	0	2	2
SJ-144		DIC	T	0	2	2
SJ-146		DIC	U	0	1	1
SJ-151	*"Artocarpus" lessingiana*	DIC	U	0	6	6
SJ-166		CYD	N/A	0	6	6
SJ-176		DIC	N/A	0	3	3
Total Morphotypes	12			0	63	63

Locality	AF1611
Location	Betonnie Tsosie Wash
Stratigraphic position relative to Ojo Alamo Sandstone-Nacimiento Formation contact (m)	23.4
Estimated Age (Myr)	65.27
Depositional Facies	Overbank/Crevasse splay
GPS Location (UTM)	13 S 0252084 4007102

Morphotype	Name (if known)	Affinity	Margin	Field Tally	Lab Tally	Total
SJ-015		DIC	U	21	0	21
SJ-016		DIC	T	8	0	8
SJ-019	*Juglandiphyllites glabra*	DIC	T	0	1	1
SJ-028		DIC	U	0	1	1
SJ-036	*Platanites rayndolsii*	DIC	T	27	0	27
SJ-051	*Paranymphaea crassfolia*	DIC	N/A	4	0	4
SJ-056	*Onoclea sensibilis*	PTE	N/A	1	0	1
SJ-070		MON	N/A	0	1	1
SJ-080	*"Rhamnus" goldiana*	DIC	U	147	27	174
SJ-081		DIC	U	17	0	17
SJ-107		DIC	T	1	0	1
SJ-113	*"Zizyphus" fibrillosus*	DIC	U	63	3	66
SJ-115	*Zingiberopsis sp.*	MON	N/A	6	0	6
SJ-117	*Sabalites sp.*	MON	N/A	29	1	30
SJ-127	*Macginitea sp.*	DIC	U/T	4	0	4
SJ-140	*Cucurbitaciphyllum lobatum*	DIC	T	1	0	1
SJ-141		DIC	T	5	0	5
SJ-142		DIC	U	1	0	1
SJ-143		DIC	U	8	0	8
SJ-144		DIC	T	4	1	5
SJ-145		DIC	U	4	0	4
SJ-146		DIC	U	27	3	30
SJ-147		DIC	N/A	1	0	1
SJ-148		PTE	N/A	6	7	13
SJ-149		DIC	T	1	0	1
SJ-151	*"Artocarpus" lessingiana*	DIC	U	27	3	30
Total Morphotypes	26			413	48	461

Locality	DP1303
Location	Betonnie Tsosie Wash
Stratigraphic position relative to Ojo Alamo Sandstone-Nacimiento Formation contact (m)	23.4
Estimated Age (Myr)	65.25
Depositional Facies	Overbank/Crevasse splay
GPS Location (UTM)	13 S 0251433 4006975

Morphotype	**Name (if known)**	**Affinity**	**Margin**	**Field Tally**	**Lab Tally**	**Total**
SJ-080	*"Rhamnus" goldiana*	DIC	U	0	20	20
SJ-086	*Sabalites sp.*	MON	N/A	0	1	1
SJ-138		DIC	T	0	3	3
SJ-144		DIC	T	0	1	1
SJ-151	*"Artocarpus" lessingiana*	DIC	U	0	8	8
Total Morphotypes	5			0	33	33

Locality	AF1524
Location	Betonnie Tsosie Wash
Stratigraphic position relative to Ojo Alamo Sandstone-Nacimiento Formation contact (m)	24.2
Estimated Age (Myr)	65.25
Depositional Facies	Overbank/Crevasse splay
GPS Location (UTM)	13 S 0251784 4007741

Morphotype	**Name (if known)**	**Affinity**	**Margin**	**Field Tally**	**Lab Tally**	**Total**
SJ-036	*Platanites rayndolsii*	DIC	T	46	7	53
SJ-060		MON	N/A	14	0	14
SJ-071	*Platanites marginata*	DIC	T	29	7	36
SJ-078	*Browneia serrata*	DIC	T	1	0	1
SJ-081		DIC	U	177	10	187
SJ-086	*Sabalites sp.*	MON	N/A	1	0	1
SJ-105		DIC	U	3	0	3
SJ-106		DIC	U	3	4	7
SJ-107		DIC	T	1	0	1
SJ-108		DIC	T	16	8	24
SJ-109		DIC	N/A	1	0	1
SJ-117	*Sabalites sp.*	MON	U	1	0	1
SJ-119		DIC	U	1	0	1
SJ-124	*Davidia antiqua*	DIC	T	16	6	22
SJ-130		DIC	U	0	2	2
SJ-150	*Melastomites montanensis*	DIC	U	0	1	1
Total Morphotypes	16			310	45	355

Locality	AF1524B
Location	Betonnie Tsosie Wash
Stratigraphic position relative to Ojo Alamo Sandstone-Nacimiento Formation contact (m)	24.2
Estimated Age (Myr)	65.25
Depositional Facies	Overbank/Crevasse splay
GPS Location (UTM)	13 S 0251655 4007225

Morphotype	Name (if known)	Affinity	Margin	Field Tally	Lab Tally	Total
SJ-011		DIC	U	0	1	1
SJ-036	*Platanites rayndolsii*	DIC	T	0	131	131
SJ-064	*Equisetum sp.*	EQU	N/A	0	6	6
SJ-070		MON	N/A	0	2	2
SJ-071	*Platanites marginata*	DIC	T	0	3	3
SJ-079	*Sabalites sp.*	MON	N/A	0	1	1
SJ-080	*"Rhamnus" goldiana*	DIC	U	0	1	1
SJ-081		DIC	U	0	2	2
SJ-101		DIC	N/A	0	1	1
SJ-107		DIC	T	0	6	6
SJ-108		DIC	T	0	3	3
SJ-113	*"Zizyphus" fibrillosus*	DIC	U	0	3	3
SJ-124	*Davidia antiqua*	DIC	T	0	3	3
SJ-151	*"Artocarpus" lessingiana*	DIC	U	0	10	10
SJ-153		DIC	U	0	1	1
SJ-154		DIC	U	0	3	3
SJ-160		DIC	N/A	0	1	1
SJ-166		CYD	N/A	0	1	1
SJ-171		DIC	U	0	14	14
SJ-172		DIC	T	0	1	1
SJ-173	*Macginitea sp.*	DIC	T	0	2	2
SJ-174		DIC	U	0	8	8
Total Morphotypes	22			0	204	204

Locality	AF1524C
Location	Betonnie Tsosie Wash
Stratigraphic position relative to Ojo Alamo Sandstone-Nacimiento Formation contact (m)	24.2
Estimated Age (Myr)	65.25
Depositional Facies	Overbank/Crevasse splay
GPS Location (UTM)	13 S 0251694 4007330

Morphotype	**Name (if known)**	**Affinity**	**Margin**	**Field Tally**	**Lab Tally**	**Total**
SJ-036	*Platanites rayndolsii*	DIC	T	0	14	14
SJ-071	*Platanites marginata*	DIC	T	0	1	1
SJ-080	*"Rhamnus" goldiana*	DIC	U	0	1	1
SJ-081		DIC	T/U	0	3	3
SJ-108		DIC	T	0	1	1
SJ-150	*"Artocarpus" lessingiana*	DIC	U	0	2	2
Total Morphotypes	6			0	22	22

Locality	AF1610
Location	Betonnie Tsosie Wash
Stratigraphic position above Ojo Alamo Contact (m)	27.4
Estimated Age (Myr)	65.17
Depositional Facies	Lacustrine/Overbank
GPS Location (UTM)	13 S 0252080 4007264

Morphotype	**Name (if known)**	**Affinity**	**Margin**	**Field Tally**	**Lab Tally**	**Total**
SJ-005		DIC	U	0	1	1
SJ-007	*Aeculus Hickeyi*	DIC	T	0	1	1
SJ-016		DIC	T	0	1	1
SJ-028		DIC	U	0	1	1
SJ-036	*Platanites rayndolsii*	DIC	T	0	1	1
SJ-062	*Limnobiophyllum scutatum*	MON	N/A	0	1	1
SJ-064	*Equisetum sp.*	EQU	N/A	0	1	1
SJ-071	*Platanites marginata*	DIC	T	0	1	1
SJ-080	*"Rhamnus" goldiana*	DIC	U	0	1	1
SJ-095	*Isoetes Horridus*	LYC	N/A	0	1	1
SJ-108		DIC	T	0	1	1
SJ-115	*Zingiberopsis sp.*	MON	N/A	0	1	1
SJ-124	*Davidia antiqua*	DIC	T	0	1	1
SJ-144		DIC	T	0	1	1
SJ-146		DIC	U	0	1	1
SJ-148		PTE	N/A	0	1	1
SJ-149		DIC	T	0	1	1
SJ-151	*"Artocarpus" lessingiana*	DIC	U	0	1	1
SJ-152		DIC	T	0	1	1
SJ-153		DIC	U	0	1	1
SJ-154		DIC	U	0	1	1
SJ-155	*Rhamnites cleburnii*	DIC	U	0	1	1
Total Morphotypes	22			0	22	22

Locality	DP1104
Location	De-Na-Zin
Stratigraphic position relative to Ojo Alamo Sandstone-Nacimiento Formation contact (m)	34.8
Estimated Age (Myr)	65.05
Depositional Facies	Overbank splays/channel fill
GPS Location (UTM)	13 S 0231015 4024887

Morphotype	Name (if known)	Affinity	Margin	Field Tally	Lab Tally	Total
SJ-011		DIC	U	0	1	1
SJ-030		DIC	U	0	1	1
SJ-036	*Platanites raynodlsii*	DIC	T	0	2	2
SJ-119		DIC	U	0	1	1
SJ-128		DIC	U	0	1	1
SJ-140		DIC	T	0	1	1
SJ-171		DIC	U	0	1	1
SJ-179		DIC	U	0	1	1
SJ-186	*Macginitiea sp.*	DIC	T	0	8	8
Total Morphotypes	9			0	17	17

Locality	AF1410
Location	Mesa de Cuba - Northside
Stratigraphic position Relative to Ojo Alamo/Nacimiento Contact (m)	24.0
Estimated Age (Myr)	64.99
Depositional Facies	VF sand, splays
GPS Location (UTM)	13 S 0318729 3983622

Morphotype	Name (if known)	Affinity	Margin	Field Tally	Lab Tally	Total
SJ-011		DIC	U	0	1	1
SJ-013	*cf. Trochodendroides*	DIC	T	0	4	4
SJ-036	*Platanites raynoldsii*	DIC	T	0	1	1
SJ-046	*Averrhoites affinus*	DIC	U	0	4	4
SJ-080	*"Rhamnus" goldiana*	DIC	U	0	8	8
SJ-086	*Sabalites sp.*	MON	T	0	2	2
SJ-151	*"Artocarpus" lessingiana*	DIC	U	0	1	1
SJ-164		DIC	U	0	1	1
Total Morphotypes	8			0	22	22

Locality	AF1513F
Location	Mesa de Cuba - Northside
Stratigraphic position relative to Ojo Alamo Sandstone-Nacimiento Formation contact (m)	37.9
Estimated Age (Myr)	64.90
Depositional Facies	Overbank/Crevasse splay
GPS Location (UTM)	13 S 0319260 3983784

Morphotype	**Name (if known)**	**Affinity**	**Margin**	**Field Tally**	**Lab Tally**	**Total**
SJ-011		DIC	U	33	4	37
SJ-013	*Archeampelos nebrascensis*	DIC	T	30	4	34
SJ-015		DIC	U	1	0	1
SJ-018		DIC	U	3	0	3
SJ-036	*Platanites raynoldsii*	DIC	T	100	0	100
SJ-070		MON	N/A	9	0	9
SJ-080	*"Rhamnus" goldiana*	DIC	U	7	0	7
SJ-086	*Sabalites sp.*	MON	N/A	77	8	85
SJ-106		DIC	U	1	0	1
SJ-113	*"Zizyphus" fibrillosus*	DIC	U	54	0	54
SJ-115	*Zingiberopsis sp.*	MON	N/A	1	0	1
SJ-128		DIC	U	0	1	1
SJ-131		DIC	T	9	0	9
SJ-138		DIC	T	20	1	21
SJ-146		DIC	U	15	0	15
SJ-151	*"Artocarpus" lessingiana*	DIC	U	0	1	1
SJ-153		DIC	U	10	0	10
SJ-158	*Allantoidiopsis erosa*	PTE	N/A	0	1	1
SJ-162		DIC	T	1	0	1
SJ-164		DIC	U	14	5	19
SJ-165		DIC	N/A	1	0	1
SJ-167		DIC	N/A	0	1	1
Total Morphotypes	22			386	26	412

Locality	AF1513B
Location	Mesa de Cuba - Northside
Stratigraphic position above Ojo Alamo Sandstone-Nacimiento Formation Contact (m)	39.4
Estimated Age (Myr)	64.89
Depositional Facies	Overbank/Crevasse splay
GPS Location (UTM)	13 S 0319401 3983934

Morphotype	**Name (if known)**	**Affinity**	**Margin**	**Field Tally**	**Lab Tally**	**Total**
SJ-011		DIC	U	0	19	19
SJ-013	*Archeampelos nebrascensis*	DIC	T	0	2	2
SJ-019	*Juglandiphyllites glabra*	DIC	T	0	1	1
SJ-046	*Averrhoites affinus*	DIC	U	0	1	1
SJ-080	*"Rhamnus" goldiana*	DIC	U	0	2	2
SJ-086	*Sabalites sp.*	MON	N/A	0	3	3
SJ-151	*"Artocarpus" lessingiana*	DIC	U	0	5	5
SJ-164		DIC	U	0	3	3
Total Morphotypes	8			0	36	36

Locality	AF1513E
Location	Mesa de Cuba - Northside
Stratigraphic position Relative to Ojo Alamo/Nacimiento Contact (m)	39.4
Estimated Age (Myr)	64.88
Depositional Facies	Overbank/Crevasse splay
GPS Location (UTM)	13 S 0319329 3983911

Morphotype	**Name (if known)**	**Affinity**	**Margin**	**Field Tally**	**Lab Tally**	**Total**
SJ-011		DIC	U	0	22	22
SJ-013	*cf. Trochodendroides*	DIC	T	0	1	1
SJ-079	*Sabalites sp.*	MON	N/A	0	8	8
SJ-080	*"Rhamnus" goldiana*	DIC	U	0	3	3
SJ-113	*"Zizyphus" fibrillosus*	DIC	U	0	1	1
SJ-158	*Allantoidiopsis erosa*	PTE	N/A	0	2	2
SJ-179		DIC	U	0	1	1
Total Morphotypes	7			0	38	38

Locality	AF1512
Location	Mesa de Cuba - Northside
Stratigraphic position relative to Ojo Alamo Sandstone-Nacimiento Formation contact (m)	6.6
Estimated Age (Myr)	64.89
Depositional Facies	Overbank/Crevasse splay
GPS Location (UTM)	13 S 0318755 3983982

Morphotype	**Name (if known)**	**Affinity**	**Margin**	**Field Tally**	**Lab Tally**	**Total**
SJ-011		DIC	U	1	14	15
SJ-013	*Archeampelos nebrascensis*	DIC	T	39	43	82
SJ-019	*Juglandiphyllites glabra*	DIC	T	4	0	4
SJ-020		DIC	U	0	1	1
SJ-035		DIC	U	11	0	11
SJ-036	*Platanites raynoldsii*	DIC	T	27	10	37
SJ-046	*Averrhoites affinus*	DIC	T	20	12	32
SJ-064	*Equisetum sp.*	EQU	N/A	1	2	3
SJ-080	*"Rhamnus" goldiana*	DIC	U	3	0	3
SJ-086	*Sabalites sp.*	MON	N/A	0	9	9
SJ-113	*"Zizyphus" fibrillosus*	DIC	U	4	0	4
SJ-124	*Davida antiqua*	DIC	T	0	1	1
SJ-127	*Macginieta sp.*	DIC	U/T	0	1	1
SJ-132		DIC	N/A	1	0	1
SJ-135	*Sabalites sp.*	MON	N/A	104	0	104
SJ-138		DIC	T	0	2	2
SJ-150	*"Melastomites" montanensis*	DIC	U	0	1	1
SJ-151	*"Artocarpus" lessingiana*	DIC	T	34	3	37
SJ-152		DIC	T	3	0	3
SJ-158	*Allantoidiopsis erosa*	PTE	N/A	0	3	3
SJ-162		DIC	T	0	2	2
SJ-163		DIC	T	1	0	1
SJ-164		DIC	U	0	1	1
SJ-167		DIC	N/A	129	0	129
SJ-172		DIC	T	0	2	2
SJ-178		DIC	T	9	6	15
SJ-179		DIC	U	0	6	6
Total Morphotypes	27			391	119	510

Locality	AF1631					
Location	Mesa de Cuba - Northside					
Stratigraphic position Relative to Ojo Alamo/Nacimiento Contact (m)	42.8					
Estimated Age (Myr)	64.84					
Depositional Facies	Overbank/Crevasse splay					
GPS Location (UTM)	13 S 0318727 3983798					
Morphotype	**Name (if known)**	**Affinity**	**Margin**	**Field Tally**	**Lab Tally**	**Total**
SJ-011		DIC	U	0	1	1
SJ-086	*Sabalites sp.*	MON	N/A	0	6	6
SJ-179		DIC	U	0	1	1
SJ-189		DIC	U	0	2	2
SJ-190	*Sabalites sp.?*	MON	N/A	0	4	4
Total Morphotypes	5			0	14	14

Locality	AF1528
Location	Kimbeto Wash
Stratigraphic position above Base of Kimbeto Wash Pmag Section (m)	44.9
Estimated Age (Myr)	64.80
Depositional Facies	Overbank/Crevasse splay
GPS Location (UTM)	13 S 0242613 4013602

Morphotype	**Name (if known)**	**Affinity**	**Margin**	**Field Tally**	**Lab Tally**	**Total**
SJ-005		DIC	U	5	0	5
SJ-007	*Aesculus hickeyi*	DIC	T	1	0	1
SJ-012	*Macginitiea sp.*	DIC	T	2	0	2
SJ-013	*Archeampelos nebrascensis*	DIC	T	39	8	47
SJ-019	*Juglandiphyllites glabra*	DIC	T	1	2	3
SJ-028		DIC	U	0	1	1
SJ-033		DIC	U	1	0	1
SJ-036	*Platanites raynoldsii*	DIC	T	249	62	311
SJ-070		MON	N/A	3	0	3
SJ-071	*Platanites marginata*	DIC	T	0	1	1
SJ-080	*"Rhamnus" goldiana*	DIC	U	9	3	12
SJ-081		DIC	U	0	1	1
SJ-088		DIC	T	0	1	1
SJ-101		DIC	N/A	5	0	5
SJ-113	*"Zizyphus" fibrillosus*	DIC	U	10	1	11
SJ-124	*Davidia antiqua*	DIC	T	33	8	41
SJ-136		DIC	U	0	2	2
SJ-138		DIC	T	32	8	40
SJ-150	*"Melastomites" montanensis*	DIC	U	0	1	1
SJ-151	*"Artocarpus" lessingiana*	DIC	U	9	1	10
SJ-153		DIC	U	0	1	1
SJ-160	*Nyssidium articum*	DIC	N/A	8	2	10
SJ-161		DIC	U	1	0	1
SJ-162		DIC	T	8	0	8
SJ-163	*Zizyphoides flabella*	DIC	T	3	4	3
SJ-164		DIC	U	0	2	3
SJ-180		DIC	T	0	2	3
SJ-181		DIC	U	0	1	3
Total Morphotypes	28			419	112	531

Locality	DP1313
Location	Kimbeto Wash
Stratigraphic position above Base of Kimbeto Wash Pmag Section (m)	58.6
Estimated Age (Myr)	64.65
Depositional Facies	Overbank/Crevasse splay
GPS Location (UTM)	13 S 0246044 4014038

Morphotype	**Name (if known)**	**Affinity**	**Margin**	**Field Tally**	**Lab Tally**	**Total**
SJ-011		DIC	U	0	4	4
SJ-013		DIC	T	0	27	27
SJ-016		DIC	T	0	1	1
SJ-019	*Juglandiphyllites glabra*	DIC	T	0	1	1
SJ-036	*Platanites raynoldsii*	DIC	T	0	3	3
SJ-046	*Averrhoites affinis*	DIC	U	0	23	23
SJ-080	*"Rhamnus" goldiana*	DIC	U	0	1	1
SJ-127	*Macginitiea sp.*	DIC	T/U	0	1	1
SJ-182		DIC	U	0	1	1
Total Morphotypes	9			0	62	62

Locality	AF1614
Location	Kimbeto Wash
Stratigraphic position above Base of Kimbeto Wash Pmag Section (m)	58.6
Estimated Age (Myr)	64.65
Depositional Facies	Overbank/Crevasse splay
GPS Location (UTM)	13 S 0246046 4013990

Morphotype	**Name (if known)**	**Affinity**	**Margin**	**Field Tally**	**Lab Tally**	**Total**
SJ-046	*Averrhoites affinis*	DIC	U	0	66	66
SJ-086	*Sabalites sp.*	MON	N/A	0	7	7
Total Morphotypes	2			0	73	73

Locality	AF1615B
Location	Kimbeto Wash
Stratigraphic position above Base of Kimbeto Wash Pmag Section (m)	58.6
Estimated Age (Myr)	64.65
Depositional Facies	Overbank/Crevasse splay
GPS Location (UTM)	13 S 0246232 4013760

Morphotype	**Name (if known)**	**Affinity**	**Margin**	**Field Tally**	**Lab Tally**	**Total**
SJ-013		DIC	T	0	1	1
SJ-036	*Platanites raynoldsii*	DIC	T	0	1	1
SJ-046	*Averrhoites affinis*	DIC	U	0	3	3
Total Morphotypes	3			0	5	5

Locality	AF1616
Location	Kimbeto Wash
Stratigraphic position above Base of Kimbeto Wash Pmag Section (m)	58.6
Estimated Age (Myr)	64.65
Depositional Facies	Overbank/Crevasse splay
GPS Location (UTM)	13 S 0246232 4013760

Morphotype	**Name (if known)**	**Affinity**	**Margin**	**Field Tally**	**Lab Tally**	**Total**
SJ-013		DIC	T	0	1	1
SJ-031		DIC	U	0	1	1
SJ-036	*Platanites raynoldsii*	DIC	T	0	5	5
SJ-143		DIC	U	0	1	1
SJ-144	*Averrhoites affinis*	DIC	U	0	1	1
Total Morphotypes	5			0	9	9

Locality	AF1617
Location	Kimbeto Wash
Stratigraphic position above Base of Kimbeto Wash Pmag Section (m)	58.6
Estimated Age (Myr)	64.65
Depositional Facies	Overbank/Crevasse splay
GPS Location (UTM)	13 S 0246232 4013760

Morphotype	**Name (if known)**	**Affinity**	**Margin**	**Field Tally**	**Lab Tally**	**Total**
SJ-013		DIC	T	0	3	3
SJ-024		DIC	U	0	1	1
SJ-036	*Platanites raynoldsii*	DIC	T	0	5	5
SJ-046	*Averrhoites affinis*	DIC	U	0	9	9
Total Morphotypes	4			0	18	18

Locality	AF1702
Location	Kimbeto Wash
Stratigraphic position above Base of Kimbeto Wash Pmag Section (m)	60.4
Estimated Age (Myr)	64.63
Depositional Facies	Overbank/Crevasse splay
GPS Location (UTM)	13 S 0244889 4014301

Morphotype	**Name (if known)**	**Affinity**	**Margin**	**Field Tally**	**Lab Tally**	**Total**
SJ-024		DIC	U	0	1	1
SJ-028		DIC	U	0	1	1
SJ-046	*Averrhoites affinis*	DIC	U	0	27	27
SJ-106		DIC	U	0	1	1
SJ-158	*Allantoidiopsis erosa*	PTE	-	0	1	1
SJ-166		CYD	-	0	5	5
Total Morphotypes	6			0	36	36

Locality	AF1618
Location	Kimbeto Wash
Stratigraphic position above Base of Kimbeto Wash Pmag Section (m)	62.0
Estimated Age (Myr)	64.62
Depositional Facies	Channel fill/ medium SS
GPS Location (UTM)	13 S 0245140 4014180

Morphotype	Name (if known)	Affinity	Margin	Field Tally	Lab Tally	Total
SJ-003		DIC	T	2	0	2
SJ-008		DIC	U	2	0	2
SJ-011		DIC	U	3	1	4
SJ-012	*Macginitiea sp.*	DIC	T	2	1	3
SJ-013	*Archeampelos nebrascensis*	DIC	T	28	0	28
SJ-016		DIC	T	4	0	4
SJ-017		DIC	U	0	2	2
SJ-019	*Juglandiphyllites glabra*	DIC	T	106	8	114
SJ-021		DIC	U	0	2	2
SJ-026		DIC	T	0	1	1
SJ-028		DIC	U	2	0	2
SJ-031		DIC	U	0	3	3
SJ-033		DIC	U	5	1	6
SJ-035		DIC	U	5	0	5
SJ-036	*Platanites raynoldsii*	DIC	T	140	27	167
SJ-070		MON	N/A	2	1	3
SJ-071	*Platanites marginata*	DIC	T	6	0	6
SJ-080	*"Rhamnus" goldiana*	DIC	U	0	3	3
SJ-082		DIC	U	0	1	1
SJ-117	*Sabalites sp.*	MON	N/A	93	5	98
SJ-127	*Macginitiea sp.*	DIC	T/U	18	0	18
SJ-130		DIC	U	6	0	6
SJ-136		DIC	U	3	1	4
SJ-151	*"Artocarpus" lessingiana*	DIC	U	3	0	3
SJ-156		DIC	T	14	0	14
SJ-157		DIC	U	19	0	19
Total Morphotypes	26			463	57	520

Locality	DP1309/10
Location	Kimbeto Wash
Stratigraphic position above Base of Kimbeto Wash Pmag Section (m)	63.5
Estimated Age (Myr)	64.60
Depositional Facies	Crevasse splay/overbank
GPS Location (UTM)	13 S 0245140 4014180

Morphotype	Name (if known)	Affinity	Margin	Field Tally	Lab Tally	Total
SJ-002		DIC	T	0	1	1
SJ-003		DIC	T	0	1	1
SJ-004		DIC	U	0	1	1
SJ-005		DIC	U	0	1	1
SJ-007	*Aesculus hickeyi*	DIC	T	0	1	1
SJ-008		DIC	U	0	1	1
SJ-009		DIC	T	0	1	1
SJ-011		DIC	U	0	1	1
SJ-012	*Macginitiea sp.*	DIC	T	0	1	1
SJ-015		DIC	U	0	1	1
SJ-016		DIC	T	0	1	1
SJ-017		DIC	U	0	1	1
SJ-018		DIC	U	0	1	1
SJ-019	*Juglandiphyllites glabra*	DIC	T	0	1	1
SJ-020		DIC	U	0	1	1
SJ-021		DIC	U	0	1	1
SJ-022		DIC	U	0	1	1
SJ-023	*Macginitiea sp.*	DIC	T	0	1	1
SJ-024		DIC	U	0	1	1
SJ-025		DIC	U	0	1	1
SJ-026		DIC	T	0	1	1
SJ-028		DIC	U	0	1	1
SJ-030		DIC	U	0	1	1
SJ-033		DIC	U	0	1	1
SJ-034		DIC	U	0	1	1
SJ-035		DIC	U	0	1	1
SJ-036	*Platanites raynoldsii*	DIC	T	0	1	1
SJ-037		DIC	T	0	1	1
SJ-039		DIC	U	0	1	1
SJ-046	*Averrhoites affinis*	DIC	U	0	1	1
Total Morphotypes	30			0	30	30

Locality	DP1311
Location	Kimbeto Wash
Stratigraphic position above Base of Kimbeto Wash Pmag Section (m)	63.5
Estimated Age (Myr)	64.60
Depositional Facies	Crevasse splay/overbank
GPS Location (UTM)	13 S 0245140 4014180

Morphotype	**Name (if known)**	**Affinity**	**Margin**	**Field Tally**	**Lab Tally**	**Total**
SJ-020		DIC	U	0	1	1
SJ-029		DIC	U	0	1	1
SJ-036	*Platanites raynoldsii*	DIC	T	0	1	1
SJ-042		DIC	U	0	1	1
SJ-046	*Averrhoites affinis*	DIC	U	0	1	1
Total Morphotypes	5			0	5	5

Locality	AF1701
Location	Kimbeto Wash
Stratigraphic position above Base of Kimbeto Wash Pmag Section (m)	70.8
Estimated Age (Myr)	64.53
Depositional Facies	Overbank/Crevasse splay
GPS Location (UTM)	13 S 0245141 4014320

Morphotype	**Name (if known)**	**Affinity**	**Margin**	**Field Tally**	**Lab Tally**	**Total**
SJ-007	*Aesculus hickeyi*	DIC	T	0	2	2
SJ-011		DIC	U	0	2	2
SJ-015		DIC	T	0	1	1
SJ-016		DIC	U	0	1	1
SJ-019	*Juglandiphyllites glabra*	DIC	T	0	5	5
SJ-036	*Platanites raynoldsii*	DIC	U	0	1	1
SJ-159		DIC	T	0	1	1
SJ-188		DIC	N/A	0	5	5
Total Morphotypes	8			0	18	18

Locality	AF1412
Location	Mesa de Cuba - Northside
Stratigraphic position relative to Ojo Alamo Sandstone-Nacimiento Formation contact (m)	62.8
Estimated Age (Myr)	64.52
Depositional Facies	Overbank/Crevasse splay
GPS Location (UTM)	13 S 0318731 3983848

Morphotype	**Name (if known)**	**Affinity**	**Margin**	**Field Tally**	**Lab Tally**	**Total**
SJ-011		DIC	U	0	4	4
SJ-019	*Juglandiphyllites glabra*	DIC	T	0	2	2
SJ-036	*Platanites raynoldsii*	DIC	T	0	4	4
SJ-046	*Averrhoites affinus*	DIC	U	0	4	4
SJ-079	*Sabalites sp.*	MON	-	0	19	19
SJ-080	*"Rhamnus" goldiana*	DIC	U	0	9	9
SJ-081		DIC	U	0	3	3
SJ-086	*Sabalites sp.*	MON	-	0	1	1
SJ-106		DIC	U	0	2	2
SJ-113	*Zizyphus fibrillosus*	DIC	U	0	2	2
SJ-150	*"Melastomites" montanensis*	DIC	U	0	1	1
SJ-151	*"Artocarpus" lessingiana*	DIC	U	0	3	3
SJ-168		DIC	U	0	7	7
SJ-169		DIC	T	0	3	3
SJ-170		DIC	T	0	1	1
Total Morphotypes	15			0	65	65

APPENDIX E

San Juan Basin Digital Leaf Physiognomy Measurements

Table E.1 – San Juan Basin Digital Leaf Physiognomy Measurements

Locality	Morph.	Specimen #	Margin	Petiole width (cm)	Petiole area (cm^2)	Inferred blade area (cm^2)	Raw blade area (cm^2)	Raw perimeter (cm)	Major length (cm)	Length of cut perimeter (cm)	Raw internal perimeter (cm)	Raw internal blade area (cm^2)	# 1° teeth	# 2° teeth	Tooth area (cm^2)
DP1309	SJ-003	DP1309-003	T			58.64	23.67	37.18	13.86	24.43	35.32	23.32	26.00		0.40
DP1310	SJ-005	DP1310-003	U			54.78			13.54						
DP1310	SJ-007	DP1310-007	T			17.99	11.66	26.61	7.89	13.62	25.17	11.55	49.00		0.15
DP1310	SJ-009	DP1310-001	T			12.88	3.01	15.62	6.67	11.21	14.49	2.93	20.00		0.09
DP1310	SJ-009	DP1310-036	T				3.42	12.13		8.15	11.18	3.36	14.00		0.08
AF1512	SJ-011	AF1512-044	U	0.12		27.54			9.88						
AF1513B	SJ-011	AF1513B-006	U	0.10	0.01	8.77			4.88						
AF1513B	SJ-011	AF1513B-020B	U	0.15	0.05	20.59			7.95						
AF1513F-C	SJ-011	AF1513F-C-040B	U			50.64			13.67						
AF1524B	SJ-011	AF1524B-007	U	0.10	0.01	54.72			12.80						
AF1612	SJ-011	AF1612-011	U	0.07		16.05			5.98						
DP1309/10	SJ-011	DP1309/10-023	U	0.18	0.03	47.56			12.13						
DP1310	SJ-011	DP1310-014	U	0.20	0.09	91.31			13.64						
AF1528-C	SJ-012	AF1528-C-039	T	0.08	0.02	5.80	4.64	11.52	3.54	4.48	10.91	4.60	5.00		0.05

Locality	Morph.	Specimen #	Margin	Petiole width (cm)	Petiole area (cm^2)	Inferred blade area (cm^2)	Raw blade area (cm^2)	Raw perimeter (cm)	Major length (cm)	Length of cut perimeter (cm)	Raw internal perimeter (cm)	Raw internal blade area (cm^2)	# 1° teeth	# 2° teeth	Tooth area (cm^2)
AF1618-C	SJ-012	AF1618-C-031	T			11.07	3.66	15.50	4.77	10.28	14.97	3.52	6.00		0.28
AF1618-C	SJ-012	AF1618-C-033	T			9.56	5.45	17.16	4.56	8.15	16.68	5.24	7.00		0.24
DP1304	SJ-012	DP1304-015	T	0.17	0.10	39.06	22.26	32.76	8.50	15.84	30.27	21.77	11.00		0.52
DP1304	SJ-012	DP1304-016	T			8.24	7.27	15.28	4.43	5.72	13.91	7.03	13.00		0.26
DP1304-C	SJ-012	DP1304-C-036	T	0.07		11.62	5.97	15.36	4.78	5.12	13.38	5.67	12.00		0.32
DP1309/10	SJ-012	DP1309/10-004	T	0.05		5.45	4.91	16.97	3.26	6.91	15.62	4.73	21.00		0.22
DP1310	SJ-012	DP1310-012	T	0.19	0.07	18.43	10.32	15.72	7.04	6.33	14.67	10.04	9.00		0.32
DP1310	SJ-012	DP1310-053	T			11.56	9.66	16.49	5.56	6.56	15.86	9.56	9.00		0.13
DP1310	SJ-012	DP1310-055	T			7.88	3.29	23.55	4.66	17.45	22.87	3.22	12.00		0.09
DP1310	SJ-012	DP1310-080	T	0.13		38.72			9.83						
DP1310	SJ-012	DP1310-082	T			19.15	13.55	36.33	6.42	24.67	35.47	13.40	14.00		0.17
AF1512	SJ-013	AF1512-037	T				16.36	49.40		42.83	47.75	16.15	16.00	9.00	0.23
AF1512	SJ-013	AF1512-043	T				17.77	27.41		21.53	26.45	17.53	11.00	6.00	0.31
AF1512	SJ-013	AF1512-048	T			52.18	24.84	62.53	11.13	46.90	60.18	24.49	42.00		0.39
AF1512	SJ-013	AF1512-068	T			40.86	38.37	36.96	9.79	9.32	30.73	37.58	77.00	32.00	0.89
AF1512	SJ-013	AF1512-069	T				14.90	33.78		21.37	31.09	14.49	32.00	14.00	0.48
AF1512-C	SJ-013	AF1512-C-005	T			17.72	2.95	19.05	7.08	12.27	17.03	2.66	13.00	2.00	0.32
AF1513F-C	SJ-013	AF1513F-C-014	T				14.50	18.32		8.01	15.75	14.18	19.00	12.00	0.35
AF1513F-C	SJ-013	AF1513F-C-018A	T				23.24	24.69		9.65	22.25	20.86	18.00	12.00	1.06
AF1528	SJ-013	AF1528-018	T	0.05		18.64	8.33	32.21	6.70	20.40	29.68	7.79	17.00	4.00	0.57
AF1528	SJ-013	AF1528-036	T	0.12	0.04	24.13	18.39	27.02	6.99	12.68	23.52	17.69	19.00	6.00	0.74
AF1528-C	SJ-013	AF1528-C-007	T	0.05		13.53	7.16	28.27	6.44	15.28	25.73	6.89	17.00	6.00	0.29
AF1528-C	SJ-013	AF1528-C-008	T	0.09	0.03	21.13	8.86	21.42	5.65	11.34	19.89	8.53	9.00	3.00	0.34
AF1407	SJ-014	AF1407-076	U			7.95			8.76						

Locality	Morph.	Specimen #	Margin	Petiole width (cm)	Petiole area (cm^2)	Inferred blade area (cm^2)	Raw blade area (cm^2)	Raw perimeter (cm)	Major length (cm)	Length of cut perimeter (cm)	Raw internal perimeter (cm)	Raw internal blade area (cm^2)	# 1° teeth	# 2° teeth	Tooth area (cm^2)
DP1310	SJ-015	DP1310-021	U	0.24		111.01			17.94						
DP1310	SJ-015	DP1310-032	U			32.88			9.24						
AF1610	SJ-016	AF1610-003	T			61.22	34.88	49.72	11.68	25.60	46.77	34.31	10.00		0.60
AF1610	SJ-016	AF1610-004A	T				15.28	43.26		24.38	38.46	14.75	16.00		0.56
DP1310	SJ-016	DP1310-010	T			32.66	12.96	24.54	8.01	14.62	24.18	12.87	6.00		0.10
DP1310	SJ-016	DP1310-026	T	0.22	0.03	29.85			7.85						
DP1310	SJ-017	DP1310-013	U			55.31			13.10						
AF1608-C	SJ-019	AF1608-C-071	T	0.08		21.31			9.00						
AF1618-C	SJ-019	AF1618-C-020	T				4.34	13.82		10.46	13.70	4.30	8.00		0.05
AF1623-C	SJ-019	AF1623-C-043	T	0.11	0.03		8.67	22.22		14.51	21.94	8.62	11.00		0.08
DP1309	SJ-019	DP1309-001	T	0.05		37.78	30.63	42.79	12.56	18.74	40.07	30.24	66.00		0.47
DP1309/10	SJ-019	DP1309/10-012	T			13.60	8.12	24.54	7.40	13.32	22.79	7.97	69.00		0.20
DP1310	SJ-019	DP1310-006	T				3.72	18.56		14.34	17.89	3.65	21.00		0.10
DP1310	SJ-019	DP1310-033	T			29.03	4.38	22.85	9.02	19.03	22.34	4.43	10.00		0.07
DP1310	SJ-019	DP1310-037	T				11.37	38.88		32.71	37.68	11.22	19.00		0.18
DP1310	SJ-019	DP1310-041	T				8.01	19.83		15.19	19.17	7.97	14.00		0.05
DP1310	SJ-019	DP1310-056	T			15.40	3.96	20.18	7.15	14.73	19.11	3.87	17.00		0.11
DP1310	SJ-019	DP1310-066	T				6.37	20.55		14.84	19.48	6.27	26.00		0.13
DP1310	SJ-019	DP1310-076	T				5.93	22.00		15.70	21.03	5.83	18.00		0.13
DP1310	SJ-020	DP1310-005	U			29.50			8.16						
DP1310	SJ-026	DP1310-004	T			103.68	8.58	25.76	13.30	22.72	25.04	8.53	11.00		0.06
DP1310	SJ-026	DP1310-030	T				11.46	17.88		5.91	17.07	11.40	12.00		0.07
AF1610	SJ-028	AF1610-016A	U	0.07		43.46			12.02						
AF1611	SJ-028	AF1611-016	U			28.51			12.02						
DP1310	SJ-028	DP1310-002	U			52.31			11.15						
JUM 8308	SJ-028	YPM47609	U			37.30			9.45						

Locality	Morph.	Specimen #	Margin	Petiole width (cm)	Petiole area (cm^2)	Inferred blade area (cm^2)	Raw blade area (cm^2)	Raw perimeter (cm)	Major length (cm)	Length of cut perimeter (cm)	Raw internal perimeter (cm)	Raw internal blade area (cm^2)	# 1° teeth	# 2° teeth	Tooth area (cm^2)
JUM 8308	SJ-028	YPM52251	U			11.72			4.56						
JUM 8308	SJ-028	YPM52264	U	0.13	0.02	12.91			5.25						
JUM 8308	SJ-028	YPM52304	U			4.42			5.49						
JUM 8308	SJ-028	YPM52319	U	0.06	0.07	19.10			6.68						
JUM 8308	SJ-028	YPM52322	U			23.24			6.63						
JUM 8308	SJ-028	YPM532296	U			33.71			9.05						
JUM 8308	SJ-028	YPM72527	U			25.77			7.14						
JUM 8308	SJ-028	YPM72528	U	0.15	0.03	8.80			4.13						
JUM 8308	SJ-028	YPM72529	U			13.13			6.63						
JUM 8308	SJ-028	YPM72531	U	0.19	0.14	23.53			8.03						
JUM 8308	SJ-028	YPM72541b	U	0.16	0.06	25.21			6.69						
JUM 8308	SJ-028	YPM72549a	U			66.20			11.09						
JUM 8308	SJ-028	YPM72560b	U	0.24	0.30	56.08			9.37						
JUM 8308	SJ-028	YPM72606	U			19.37			5.87						
JUM 8308	SJ-028	YPM75260a	U	0.25	0.21	56.59			9.46						
DP1310	SJ-030	DP1310-022	U			22.65			6.97						
DP1313	SJ-031	DP1313-004	U			14.22			8.21						
AF1405-C	SJ-033	AF1405-C-031	U			7.21			4.41						
DP1310	SJ-034	DP1310-017	U	0.16		31.15			8.83						
AF1404-C2	SJ-036	AF1404-C2-054	T	0.18	0.11	33.53	13.93	23.89	7.46	14.16	23.21	13.85	5.00		0.10
AF1404-C2	SJ-036	AF1404-C2-055	T	0.09	0.06	6.90	3.27	11.77	4.41	6.51	11.64	3.25	8.00		0.03
AF1405	SJ-036	AF1405-001	T	0.10		74.27	38.23	45.60	9.87	22.32	41.26	37.62	23.00		0.66
AF1405-C	SJ-036	AF1405-C-005	T			8.66	2.64	14.99	4.48	9.22	13.92	2.49	10.00		0.20
AF1406	SJ-036	AF1406-013	T	0.06		27.26	25.44	33.56	7.67	10.99	29.75	24.13	18.00		1.36
AF1407	SJ-036	AF1407-096B	T			34.49	14.80	31.84	9.74	16.71	30.97	14.67	5.00	2.00	0.14
AF1407B-C	SJ-036	AF1407B-C-022	T			7.36	4.03	16.10	4.46	9.56	15.23	3.96	10.00		0.08

Locality	Morph.	Specimen #	Margin	Petiole width (cm)	Petiole area (cm^2)	Inferred blade area (cm^2)	Raw blade area (cm^2)	Raw perimeter (cm)	Major length (cm)	Length of cut perimeter (cm)	Raw internal perimeter (cm)	Raw internal blade area (cm^2)	# 1° teeth	# 2° teeth	Tooth area (cm^2)
AF1407B-C	SJ-036	AF1407B-C-023	T			6.47	3.11	13.67	4.25	6.51	12.63	3.04	14.00		0.09
AF1409C	SJ-036	AF1409C-042	T	0.13	0.04	24.77	19.62	32.69	7.47	12.60	30.51	19.40	13.00		0.23
AF1409D	SJ-036	AF1409D-012	T			18.73	9.60	27.55	6.24	19.25	26.54	9.42	9.00		0.18
AF1409D	SJ-036	AF1409D-013	T				15.94	25.50		15.73	23.83	15.73	10.00		0.11
AF1409D	SJ-036	AF1409D-015	T				17.71	32.52		21.73	31.61	17.52	2.00	2.00	0.20
AF1409D	SJ-036	AF1409D-038	T				26.32	45.36		30.15	44.00	26.12	19.00		0.26
AF1409D	SJ-036	AF1409D-051	T			28.42	8.09	21.63	7.52	13.84	21.40	8.00	2.00		0.05
AF1409D	SJ-036	AF1409D-053	T				22.90	40.62		31.16	39.96	22.81	5.00		0.14
AF1512-C	SJ-036	AF1512-C-031	T			21.15	8.28	12.56	6.86	6.23	12.06	8.20	15.00		0.10
AF1513F-C	SJ-036	AF1513F-C-002	T	0.12		168.51	66.03	73.47	16.32	46.74	72.14	65.42	23.00		0.71
AF1513F-C	SJ-036	AF1513F-C-003	T	0.11	0.06	69.10	20.70	46.93	11.15	26.80	44.45	20.29	21.00	7.00	0.33
AF1513F-C	SJ-036	AF1513F-C-008B	T	0.05		12.23	9.81	15.45	6.14	8.96	20.05	9.60	16.00		0.24
AF1524	SJ-036	AF1524-028A	T	0.23	0.03	44.95	22.39	37.55	10.60	16.09	33.17	21.37	12.00	3.00	1.09
AF1524	SJ-036	AF1524-029B	T	0.16	0.15	129.80	74.22	72.11	15.23	38.97	66.31	72.88	21.00		1.43
AF1524B	SJ-036	AF1524B-003	T	0.26	0.24	105.69	31.65	64.51	13.05	49.51	61.16	30.98	13.00		0.73
AF1524B	SJ-036	AF1524B-008	T	0.09	0.06	7.55	4.49	18.45	4.35	9.32	17.79	4.41	10.00		0.11
AF1524B	SJ-036	AF1524B-037	T	0.09		15.15	10.19	24.91	5.46		22.49	9.67	19.00		0.58
AF1524B	SJ-036	AF1524B-054	T				7.33	15.06		4.82	12.70	6.51	6.00	4.00	0.86

Locality	Morph.	Specimen #	Margin	Petiole width (cm)	Petiole area (cm^2)	Inferred blade area (cm^2)	Raw blade area (cm^2)	Raw perimeter (cm)	Major length (cm)	Length of cut perimeter (cm)	Raw internal perimeter (cm)	Raw internal blade area (cm^2)	# 1° teeth	# 2° teeth	Tooth area (cm^2)
AF1610	SJ-036	AF1610-039	T				28.59	26.30			24.08	28.28	20.00		0.85
AF1610	SJ-036	AF1610-045B	T	0.17		143.53	123.64	50.67	19.02	13.93	46.01	122.62	46.00		1.29
AF1618-C	SJ-036	AF1618-C-011	T			69.15	19.65	45.94	10.57	34.61	43.82	19.21	13.00		0.69
AF1618-C	SJ-036	AF1618-C-014	T	0.22		175.64	62.97	59.02	18.42	38.00	57.93	61.97	7.00		1.04
AF1623	SJ-036	AF1623-010	T	0.22	0.09	127.95	50.74	60.45	15.02	38.56	58.06	50.13	32.00		0.75
AF1623-C	SJ-036	AF1623-C-046	T	0.21	0.09	30.01	10.24	39.20	7.46	26.49	37.34	9.98	26.00		0.30
DP1309	SJ-036	DP1309-004	T			148.17	44.25	49.89	16.75	30.64	45.08	43.61	15.00		0.69
DP1309	SJ-036	DP1309-011	T	0.12		101.61	54.01	60.52	14.12	34.97	58.41	53.60	22.00		0.49
DP1309/10	SJ-036	DP1309/10-013	T			48.37	23.55	30.75	8.66	15.56	28.40	23.10	24.00		0.50
DP1309/10	SJ-036	DP1309/10-020	T	0.18	0.20	44.92	22.85	32.02	8.30	13.56	30.34	22.42	23.00		0.48
DP1309/10	SJ-036	DP1309/10-022	T	0.25	0.22	107.93	102.73	46.54	13.35	8.18	41.92	101.38	31.00		1.51
DP1310	SJ-036	DP1310-016	T	0.15		115.24			15.15						
DP1310	SJ-036	DP1310-045	T	0.08		25.89	4.22	9.63	7.09	5.41	9.04	4.04	4.00		0.19
DP1310	SJ-036	DP1310-048	T	0.19	0.11	30.85	12.52	46.01	8.26	30.75	44.22	12.20	7.00		0.34
DP1310	SJ-036	DP1310-059	T	0.13	0.02	19.93	4.63	24.67	5.95	19.88	23.96	4.57	9.00		0.07
DP1310	SJ-036	DP1310-071	T				4.13	12.29		5.28	11.77	3.91	7.00		0.25
DP1310	SJ-036	DP1310-074	T				31.04	50.43		35.57	50.04	30.90	4.00		0.15
DP1310	SJ-036	DP1310-075	T	0.20	0.09	32.66	20.08	31.98	7.35	18.52	30.71	19.95	14.00	1.00	0.15
DP1311	SJ-036	DP1311-002	T			76.58	27.63	35.40	12.16	15.23	30.48	26.39	19.00	2.00	1.34
DP1311	SJ-036	DP1311-003	T	0.14	0.01	38.38	27.76	53.79	9.54	30.03	48.79	26.87	14.00	1.00	0.94
DP1311	SJ-036	DP1311-014	T	0.05		5.49	3.70	13.78	3.90	5.64	12.70	3.59	12.00		0.13
DP1311	SJ-036	DP1311-017	T	0.07	0.03	18.07	7.31	22.50	6.30	12.51	19.57	6.91	10.00	1.00	0.43
JUM8129	SJ-036	YPM68656	T										4.00		0.23
JUM8301	SJ-036	YPM47697a	T										3.00		0.22
JUM8301	SJ-036	YPM69802	T				16.09	50.27							

Locality	Morph.	Specimen #	Margin	Petiole width (cm)	Petiole area (cm^2)	Inferred blade area (cm^2)	Raw blade area (cm^2)	Raw perimeter (cm)	Major length (cm)	Length of cut perimeter (cm)	Raw internal perimeter (cm)	Raw internal blade area (cm^2)	# 1° teeth	# 2° teeth	Tooth area (cm^2)
JUM8310	SJ-036	YPM69949	T				1.24	9.62		6.80	8.94	1.10	3.00		0.14
DP1310	SJ-037	DP1310-008	T	0.12	0.10	28.09	6.74	22.88	7.91	14.22	22.10	6.58	7.00		0.18
AF1402	SJ-046	AF1402-008	U			7.33			6.22						
AF1404-C2	SJ-046	AF1404-C2-036B	U			31.85			11.33						
AF1404-C2	SJ-046	AF1404-C2-038	U	0.17	0.02	14.59			7.85						
AF1405	SJ-046	AF1405-014	U			6.37			5.42						
AF1405-C	SJ-046	AF1405-C-026	U			23.12			8.79						
AF1405-C	SJ-046	AF1405-C-028-1	U	0.07		11.16			6.49						
AF1405-C	SJ-046	AF1405-C-028-2	U	0.10		7.90			5.40						
AF1407	SJ-046	AF1407-002	U			5.32			5.82						
AF1407	SJ-046	AF1407-003	U	0.07		12.69			7.51						
AF1407	SJ-046	AF1407-006	U	0.12	0.03	3.78			4.39						
AF1407	SJ-046	AF1407-010	U			4.40			3.95						
AF1407	SJ-046	AF1407-017	U			4.29			3.33						
AF1407	SJ-046	AF1407-018	U			14.54			9.63						
AF1407	SJ-046	AF1407-020	U			14.20			6.82						
AF1407	SJ-046	AF1407-024	U	0.07		10.04			6.39						
AF1407	SJ-046	AF1407-026A	U			31.06			10.14						
AF1407	SJ-046	AF1407-037	U			37.73			10.53						
AF1407	SJ-046	AF1407-040	U			20.25			8.15						
AF1407	SJ-046	AF1407-049	U	0.03		4.91			5.08						
AF1407	SJ-046	AF1407-053	U	0.07	0.01	2.94			3.99						
AF1407	SJ-046	AF1407-056	U			22.94			8.68						
AF1407	SJ-046	AF1407-057	U			13.56			6.70						
AF1407	SJ-046	AF1407-058	U	0.10		13.07			6.09						
AF1407	SJ-046	AF1407-059	U	0.12		12.12			6.52						

Locality	Morph.	Specimen #	Margin	Petiole width (cm)	Petiole area (cm^2)	Inferred blade area (cm^2)	Raw blade area (cm^2)	Raw perimeter (cm)	Major length (cm)	Length of cut perimeter (cm)	Raw internal perimeter (cm)	Raw internal blade area (cm^2)	# 1° teeth	# 2° teeth	Tooth area (cm^2)
AF1409C	SJ-046	AF1409C-021A	U			7.32			6.85						
AF1409C	SJ-046	AF1409C-022A/B	U			7.96			6.57						
AF1409D	SJ-046	AF1409D-020	U			16.50			6.58						
AF1512	SJ-046	AF1512-062	U			32.08			9.60						
AF1512	SJ-046	AF1512-076	U			22.21			8.36						
AF1512-C	SJ-046	AF1512-C-030	U	0.06		14.41			6.62						
AF1702	SJ-046	AF1702-009A	U			28.26			7.84						
AF1702	SJ-046	AF1702-011	U	0.24	0.10	19.33			7.00						
AF1702	SJ-046	AF1702-013	U			41.99			10.45						
DP1108	SJ-046	DP1108-001A	U	0.16	0.08	12.53			7.65						
DP1301	SJ-046	DP1301-001	U	0.09		9.83			6.49						
DP1301	SJ-046	DP1301-002	U			12.83			6.45						
DP1301	SJ-046	DP1301-003	U			11.02			5.93						
DP1301	SJ-046	DP1301-004	U			13.02			6.53						
DP1301	SJ-046	DP1301-006	U	0.03		4.18			3.23						
DP1301B	SJ-046	DP1301B-001-A	U			10.64			6.85						
DP1301B	SJ-046	DP1301B-001-B	U	0.09		19.45			7.96						
DP1301B	SJ-046	DP1301B-002A	U			1.82			3.65						
DP1301B	SJ-046	DP1301B-003	U	0.08		15.42			7.46						
DP1301B	SJ-046	DP1301B-004	U			4.77			4.10						
DP1301B	SJ-046	DP1301B-007	U	0.08	0.02	14.14			6.36						

Locality	Morph.	Specimen #	Margin	Petiole width (cm)	Petiole area (cm^2)	Inferred blade area (cm^2)	Raw blade area (cm^2)	Raw perimeter (cm)	Major length (cm)	Length of cut perimeter (cm)	Raw internal perimeter (cm)	Raw internal blade area (cm^2)	# 1° teeth	# 2° teeth	Tooth area (cm^2)
DP1301B	SJ-046	DP1301B-008-A	U	0.05		5.58			4.86						
DP1301B	SJ-046	DP1301B-008-B	U			9.06			4.86						
DP1301B	SJ-046	DP1301B-009-A	U			2.09			2.50						
DP1301B	SJ-046	DP1301B-009-B	U			13.91			6.28						
DP1301B	SJ-046	DP1301B-010	U	0.12	0.03	8.41			5.24						
DP1301B	SJ-046	DP1301B-011	U			17.07			7.50						
DP1301B	SJ-046	DP1301B-012A-A	U	0.12		11.87			5.60						
DP1301B	SJ-046	DP1301B-012A-B	U			9.67			6.11						
DP1301B	SJ-046	DP1301B-012A-C	U			9.15			5.26						
DP1301B	SJ-046	DP1301B-012A-D	U	0.12		7.63			5.33						
DP1301B	SJ-046	DP1301B-012A-E	U			7.52			4.78						
DP1301B	SJ-046	DP1301B-012B-A	U	0.05		8.05			5.91						
DP1301B	SJ-046	DP1301B-012B-B	U			10.07			5.97						
DP1301B	SJ-046	DP1301B-012B-C	U			6.39			4.38						
DP1301B	SJ-046	DP1301B-012B-D	U	0.09		4.77			4.69						
DP1301B	SJ-046	DP1301B-013-A	U	0.07	0.03	12.18			7.90						
DP1301B	SJ-046	DP1301B-013-B	U			10.12			5.64						
DP1301B	SJ-046	DP1301B-013-C	U			9.29			5.85						

Locality	Morph.	Specimen #	Margin	Petiole width (cm)	Petiole area (cm^2)	Inferred blade area (cm^2)	Raw blade area (cm^2)	Raw perimeter (cm)	Major length (cm)	Length of cut perimeter (cm)	Raw internal perimeter (cm)	Raw internal blade area (cm^2)	# 1° teeth	# 2° teeth	Tooth area (cm^2)
DP1301B	SJ-046	DP1301B-014	U			16.10			6.83						
DP1301B	SJ-046	DP1301B-016	U			5.33			3.49						
DP1301B	SJ-046	DP1301B-017	U			11.74			6.70						
DP1301B	SJ-046	DP1301B-018	U			20.62			7.71						
DP1301B	SJ-046	DP1301B-019	U			11.40			6.37						
DP1301B	SJ-046	DP1301B-020	U			9.29			4.96						
DP1301B	SJ-046	DP1301B-023-A	U			6.33			4.03						
DP1301B	SJ-046	DP1301B-023-B	U	0.08		13.05			5.82						
DP1301B	SJ-046	DP1301B-023-C	U			10.91			6.53						
DP1301B	SJ-046	DP1301B-025-A	U			9.47			6.38						
DP1301B	SJ-046	DP1301B-025-B	U	0.09	0.04	9.11			5.38						
DP1301B	SJ-046	DP1301B-026-A	U			8.94			5.86						
DP1301B	SJ-046	DP1301B-026-B	U			7.97			4.54						
DP1301B	SJ-046	DP1301B-028-A	U	0.06		12.28			5.86						
DP1301B	SJ-046	DP1301B-028-B	U			8.32			4.87						
DP1301B	SJ-046	DP1301B-029-A	U			10.16			6.22						
DP1301B	SJ-046	DP1301B-029-B	U			7.10			4.44						
DP1301B	SJ-046	DP1301B-030	U			14.37			6.34						

Locality	Morph.	Specimen #	Margin	Petiole width (cm)	Petiole area (cm^2)	Inferred blade area (cm^2)	Raw blade area (cm^2)	Raw perimeter (cm)	Major length (cm)	Length of cut perimeter (cm)	Raw internal perimeter (cm)	Raw internal blade area (cm^2)	# 1° teeth	# 2° teeth	Tooth area (cm^2)
DP1301B	SJ-046	DP1301B-031	U			19.69			10.02						
DP1301B	SJ-046	DP1301B-032	U			10.44			7.30						
DP1301B	SJ-046	DP1301B-033	U			10.98			8.87						
DP1301B	SJ-046	DP1301B-035	U			19.01			7.98						
DP1301B	SJ-046	DP1301B-036	U			16.14			8.01						
DP1301B	SJ-046	DP1301B-041	U			5.10			3.74						
DP1301B	SJ-046	DP1301B-043-A	U	0.05		10.62			5.77						
DP1301B	SJ-046	DP1301B-043-B	U			11.57			5.63						
DP1301B	SJ-046	DP1301B-045	U			7.99			5.28						
DP1301B	SJ-046	DP1301B-047-A	U	0.03		0.55			1.58						
DP1301B	SJ-046	DP1301B-047-B	U			5.58			3.80						
DP1301B	SJ-046	DP1301B-048-A	U	0.07		7.45			5.65						
DP1301B	SJ-046	DP1301B-049	U			6.98			4.49						
DP1301B	SJ-046	DP1301B-051-A	U			1.26			2.08						
DP1301B	SJ-046	DP1301B-051-B	U			8.19			5.28						
DP1301B	SJ-046	DP1301B-052-A	U	0.08		9.88			6.28						
DP1301B	SJ-046	DP1301B-052-B	U			5.08			4.04						
DP1301B	SJ-046	DP1301B-052-C	U			13.20			5.80						

Locality	Morph.	Specimen #	Margin	Petiole width (cm)	Petiole area (cm^2)	Inferred blade area (cm^2)	Raw blade area (cm^2)	Raw perimeter (cm)	Major length (cm)	Length of cut perimeter (cm)	Raw internal perimeter (cm)	Raw internal blade area (cm^2)	# 1° teeth	# 2° teeth	Tooth area (cm^2)
DP1301B	SJ-046	DP1301B-054	U	0.07		7.90			4.99						
DP1301B	SJ-046	DP1301B-057	U	0.05		7.37			5.06						
DP1301B	SJ-046	DP1301B-058	U			4.98			4.02						
DP1301B	SJ-046	DP1301B-060	U			16.67			6.26						
DP1301B	SJ-046	DP1301B-063-A	U	0.15	0.02	4.33			3.39						
DP1301B	SJ-046	DP1301B-063-B	U			7.54			4.07						
DP1301B	SJ-046	DP1301B-065	U			5.23			3.81						
DP1301B	SJ-046	DP1301B-069-A	U			10.85			5.29						
DP1301B	SJ-046	DP1301B-069-B	U			8.22			5.75						
DP1301B	SJ-046	DP1301B-070-A	U			5.69			4.88						
DP1301B	SJ-046	DP1301B-072-A	U			11.52			6.19						
DP1301B	SJ-046	DP1301B-072-B	U	0.05		3.72			3.59						
DP1301B	SJ-046	DP1301B-074	U			13.26			7.53						
DP1301B	SJ-046	DP1301B-077	U			8.50			6.08						
DP1301B	SJ-046	DP1301B-078	U			16.11			7.59						
DP1301B	SJ-046	DP1301B-080	U			10.18			5.83						
DP1301B	SJ-046	DP1301B-082	U			10.52			6.63						
DP1301B	SJ-046	DP1301B-083-A	U			20.83			10.04						

Locality	Morph.	Specimen #	Margin	Petiole width (cm)	Petiole area (cm^2)	Inferred blade area (cm^2)	Raw blade area (cm^2)	Raw perimeter (cm)	Major length (cm)	Length of cut perimeter (cm)	Raw internal perimeter (cm)	Raw internal blade area (cm^2)	# 1° teeth	# 2° teeth	Tooth area (cm^2)
DP1301B	SJ-046	DP1301B-083-B	U	0.04	0.00	7.94			5.22						
DP1301B	SJ-046	DP1301B-083-C	U			8.99			5.07						
DP1301B	SJ-046	DP1301B-090-A	U	0.09		14.07			6.67						
DP1301B	SJ-046	DP1301B-090-B	U			12.45			6.95						
DP1301B	SJ-046	DP1301B-090-C	U			2.40			3.47						
DP1301B	SJ-046	DP1301B-090-D	U			12.31			7.71						
DP1301B	SJ-046	DP1301B-090-E	U	0.08		8.05			6.10						
DP1301B	SJ-046	DP1301B-090-F	U			6.36			4.37						
DP1301B	SJ-046	DP1301B-090-G	U			4.64			4.72						
DP1301B	SJ-046	DP1301B-090-H	U			7.61			4.89						
DP1304	SJ-046	DP1304-042A	U	0.07	0.01	9.30			5.89						
DP1304-C	SJ-046	DP1304-C-003	U	0.09		30.79			11.26						
DP1310	SJ-046	DP1310-020	U			27.16			10.87						
JUM 8308	SJ-046	YPM72622	U			5.19			4.08						
JUM8129	SJ-046	YPM68563	U			13.66			7.83						
JUM8129	SJ-046	YPM72819B	U												
JUM8301	SJ-046	YPM67123B	U			12.43			7.45						
JUM8301	SJ-046	YPM67803	U			8.91			6.07						
JUM8301	SJ-046	YPM67816	U			21.89			9.23						
JUM8301	SJ-046	YPM67932	U	0.11	0.03	5.74			4.41						
JUM8302B	SJ-046	YPM71197	U			31.72			12.05						
JUM8303	SJ-046	YPM70004	U			10.07			7.01						

Locality	Morph.	Specimen #	Margin	Petiole width (cm)	Petiole area (cm^2)	Inferred blade area (cm^2)	Raw blade area (cm^2)	Raw perimeter (cm)	Major length (cm)	Length of cut perimeter (cm)	Raw internal perimeter (cm)	Raw internal blade area (cm^2)	# 1° teeth	# 2° teeth	Tooth area (cm^2)
JUM8303	SJ-046	YPM70006	U			7.63			5.52						
JUM8310	SJ-046	YPM69917	U												
AF1402	SJ-050	AF1402-012-B	U			1.00			1.84						
DP1301B	SJ-050	DP1301B-084	U			2.59			3.11						
DP1301B	SJ-050	DP1301B-085	U			1.82			2.44						
AF1402	SJ-053	AF1402-012-A	U			8.86			4.18						
AF1407-C	SJ-053	AF1407-C-006	U	0.07		6.13			3.62						
AF1407-C	SJ-063	AF1407-C-002	U			25.15			8.18						
AF1404-C2	SJ-071	AF1404-C2-001A	T	0.13		35.43	22.59	38.51	9.56	18.14	37.08	22.37	8.00		0.24
AF1404-C2	SJ-071	AF1404-C2-003A	T				9.46	15.71		9.99	15.09	9.35	5.00		0.12
AF1404-C2	SJ-071	AF1404-C2-005	T			57.08	21.00	37.13	9.09	21.67	34.07	20.71	23.00		0.32
AF1404-C2	SJ-071	AF1404-C2-006	T				16.19	25.22		9.93	22.77	15.93	14.00	2.00	0.29
AF1404-C2	SJ-071	AF1404-C2-009A	T	0.07		15.29	10.70	18.68	6.65	6.04	16.82	10.76	12.00	3.00	0.22
AF1405	SJ-071	AF1405-026	T				10.52	24.74		9.01	20.12	9.86	24.00		0.70
AF1405-C	SJ-071	AF1405-C-032	T				4.40	17.10		15.33	16.75	4.38	5.00		0.03
AF1406	SJ-071	AF1406-011	T				16.56	18.42		9.11	16.87	16.08	6.00		0.51
AF1406-C	SJ-071	AF1406-C-013	T	0.12		20.72	9.64	20.43	7.31	9.62	18.72	9.24	13.00		0.43
AF1409D	SJ-071	AF1409-084	T	0.14	0.03	14.33	7.26	29.62	6.33	20.05	28.60	7.19	6.00		0.08
AF1409D	SJ-071	AF1409D-093	T				9.05	12.98		7.32	12.68	8.99	5.00		0.06
AF1409D	SJ-071	AF1409D-094	T	0.15		24.25	8.51	29.26	8.25	17.24	28.64	8.40	8.00		0.13

Locality	Morph.	Specimen #	Margin	Petiole width (cm)	Petiole area (cm^2)	Inferred blade area (cm^2)	Raw blade area (cm^2)	Raw perimeter (cm)	Major length (cm)	Length of cut perimeter (cm)	Raw internal perimeter (cm)	Raw internal blade area (cm^2)	# 1° teeth	# 2° teeth	Tooth area (cm^2)
AF1409D	SJ-071	AF1409D-106	T	0.19	0.04	41.88	15.32	32.73	8.90	21.00	32.22	15.23	5.00		0.10
AF1524-C	SJ-071	AF1524-C-005A	T	0.11	0.02	19.13	9.93	21.85	5.74	10.43	19.37	9.59	11.00		0.37
AF1623	SJ-071	AF1623-005A-1	T	0.21	0.25	44.45	17.83	19.24	8.09	8.66	17.40	17.37	11.00		0.49
AF1623	SJ-071	AF1623-005A-2	T	0.08	0.03	8.00	4.39	17.42	4.12	7.34	16.00	4.21	15.00		0.21
AF1623	SJ-071	AF1623-005A-3	T	0.08	0.01	5.04	2.49	9.23	3.48	5.19	8.31	2.38	11.00		0.13
AF1623-C	SJ-071	AF1623-C-040	T	0.13		27.44	14.18	33.78	6.86	22.93	31.09	13.80	19.00		0.42
AF1623-C	SJ-071	AF1623-C-042	T	0.13	0.06	20.91	11.03	22.91	5.33	7.78	19.91	10.50	23.00		0.60
DP1109	SJ-071	DP1109-001	T				11.21	20.30		7.84	17.88	10.88	29.00		0.38
DP1304	SJ-071	DP1304-001-1	T	0.27	0.12	51.33	50.24	47.90	9.76	7.75	37.37	48.78	44.00		1.67
DP1304	SJ-071	DP1304-001-2	T			25.00	18.71	31.40	7.93	9.62	24.75	17.79	22.00		1.04
DP1304	SJ-071	DP1304-001-3	T	0.15	0.05	17.83	14.12	30.29	6.73	14.45	26.87	13.59	16.00		0.61
DP1304	SJ-071	DP1304-020	T			20.56	9.88	22.50	7.17	11.48	20.57	9.64	11.00		0.27
DP1304-C	SJ-071	DP1304-C-021	T	0.08	0.01	19.67	4.78	23.74	7.48	13.32	21.18	4.35	9.00	2.00	0.47
JUM8129	SJ-071	YPM68656	T										4.00		0.23
JUM8301	SJ-071	YPM47696	T												
JUM8301	SJ-071	YPM67833	T				5.87	16.86		10.44	14.71	5.55			0.34
JUM8301	SJ-071	YPM67906	T										10.00		4.99
JUM8301	SJ-071	YPM69805	T			20.36	4.26	12.20	7.08	8.81	12.11	4.22	3.00		0.04
JUM8303	SJ-071	YPM70052	T				2.47	4.79		4.12	6.22	2.38	3.00		0.10
JUM8310	SJ-071	YPM69816	T				1.65	8.19		4.93	7.50	1.54	8.00		0.12
JUM8310	SJ-071	YPM69932	T												
AF1404-C2	SJ-072	AF1404-C2-039	U			1.14			2.15						

Locality	Morph.	Specimen #	Margin	Petiole width (cm)	Petiole area (cm^2)	Inferred blade area (cm^2)	Raw blade area (cm^2)	Raw perimeter (cm)	Major length (cm)	Length of cut perimeter (cm)	Raw internal perimeter (cm)	Raw internal blade area (cm^2)	# 1° teeth	# 2° teeth	Tooth area (cm^2)
AF1405	SJ-073	AF1405-022	U			22.70			12.40						
AF1409D	SJ-076	AF1409D-098	T			25.68	7.86	26.81	8.21	18.93	26.11	7.77	17.00		0.10
AF1409D	SJ-076	AF1409D-099	T	0.28	0.15	14.64	4.78	18.31	6.59	11.18	17.96	4.74	6.00	2.00	0.04
AF1409D	SJ-076	AF1409D-102	T	0.22	0.08	15.18	6.97	17.68	5.85	9.03	17.08	6.87	9.00		0.11
AF1409D	SJ-077	AF1409D-059	T	0.07	0.01	26.40	10.21	29.41	7.10	18.63	29.13	10.19	6.00		0.03
AF1404-C2	SJ-078	AF1404-C2-015A	T				18.68	34.52		23.69	33.24	18.49	35.00		0.22
AF1405	SJ-078	AF1405-043	T				8.55	17.54		13.36	17.40	8.51	11.00		0.37
AF1407	SJ-078	AF1407-080	T				6.52	25.97		21.81	25.76	6.49	9.00		0.04
AF1407	SJ-078	AF1407-081	T				6.23	10.50		7.71	10.16	6.19	9.00		0.05
AF1407-C	SJ-078	AF1407-C-012	T			89.92	19.64	39.32	12.70	31.44	39.96	19.54	10.00		0.12
AF1409D	SJ-078	AF1409D-009	T				15.51	36.59		30.71	35.85	15.39	9.00		0.10
AF1409D	SJ-078	AF1409D-028	T			46.25	19.95	46.94	13.45	34.67	44.94	19.73	40.00		0.26
AF1409D	SJ-078	AF1409D-030	T	0.30		90.54	31.57	56.10	14.62	40.78	54.06	31.30	30.00		0.35
AF1409D	SJ-078	AF1409D-073	T	0.13	0.01	21.22			7.38						
AF1409D	SJ-078	AF1409D-099	T				17.15	27.53		21.55	26.63	17.00	19.00		0.18
AF1612	SJ-078	AF1612-017	T				8.46	15.53		10.29	14.74	8.33	19.00		0.16
AF1409C	SJ-080	AF1409C-010	U	0.08	0.03	25.20			6.53						
AF1513F-C	SJ-080	AF1513F-C-048	U	0.05		22.54			9.24						
AF1521	SJ-080	AF1521-002	U	0.09	0.01	8.76			4.57						
AF1521	SJ-080	AF1521-014	U			7.76			5.69						
AF1528	SJ-080	AF1528-005	U			40.46			9.71						

Locality	Morph.	Specimen #	Margin	Petiole width (cm)	Petiole area (cm^2)	Inferred blade area (cm^2)	Raw blade area (cm^2)	Raw perimeter (cm)	Major length (cm)	Length of cut perimeter (cm)	Raw internal perimeter (cm)	Raw internal blade area (cm^2)	# 1° teeth	# 2° teeth	Tooth area (cm^2)
AF1528-C	SJ-080	AF1528-C-036	U	0.05		14.01			5.67						
AF1611	SJ-080	AF1611-002	U	0.16	0.08	51.67			10.93						
AF1611	SJ-080	AF1611-004	U	0.10		63.21			12.74						
AF1611-C	SJ-080	AF1611-C-018	U			11.65			5.72						
AF1612	SJ-080	AF1612-009	U			34.69			8.59						
AF1612	SJ-080	AF1612-020	U			18.14			6.97						
JUM 8308	SJ-080	YPM41857	U	0.16	0.09	9.98			6.64						
JUM 8308	SJ-080	YPM44813	U	0.15	0.15	26.63			7.03						
JUM 8308	SJ-080	YPM47610	U			26.40			7.03						
JUM 8308	SJ-080	YPM47619	U			37.12			9.11						
JUM 8308	SJ-080	YPM52187	U			13.83			5.54						
JUM 8308	SJ-080	YPM52212	U			37.75			8.58						
JUM 8308	SJ-080	YPM52218	U			15.43			5.47						
JUM 8308	SJ-080	YPM52218	U			16.60			6.12						
JUM 8308	SJ-080	YPM52219	U			40.28			8.75						
JUM 8308	SJ-080	YPM52221	U			33.62			7.11						
JUM 8308	SJ-080	YPM52223a	U			70.01			13.74						
JUM 8308	SJ-080	YPM52223b	U			64.21			12.38						
JUM 8308	SJ-080	YPM52224	U	0.13	0.04	10.78			5.06						
JUM 8308	SJ-080	YPM52230	U			23.81			7.20						
JUM 8308	SJ-080	YPM52249	U			12.37			6.22						
JUM 8308	SJ-080	YPM52272	U			135.96			19.89						
JUM 8308	SJ-080	YPM55241	U												
JUM 8308	SJ-080	YPM72582	U			24.09			8.59						
JUM 8308	SJ-080	YPM72584A	U			25.40			8.21						
JUM 8308	SJ-080	YPM72591	U			38.70			9.39						
AF1406	SJ-081	AF1406-003A	U	0.14		42.97			11.40						

Locality	Morph.	Specimen #	Margin	Petiole width (cm)	Petiole area (cm^2)	Inferred blade area (cm^2)	Raw blade area (cm^2)	Raw perimeter (cm)	Major length (cm)	Length of cut perimeter (cm)	Raw internal perimeter (cm)	Raw internal blade area (cm^2)	# 1° teeth	# 2° teeth	Tooth area (cm^2)
AF1406	SJ-081	AF1406-039	U			108.83			17.58						
AF1406-C	SJ-081	AF1406-C-033-1	U			39.19			9.95						
AF1406-C	SJ-081	AF1406-C-033-2	U	0.23		37.55			10.73						
AF1406-C	SJ-081	AF1406-C-033-3	U			93.61			15.51						
AF1406-C	SJ-081	AF1406-C-035B	U			57.40			13.51						
AF1406-C	SJ-081	AF1406-C-040	U	0.14		30.28			9.42						
JUM 8308	SJ-081	YPM41834	U			22.31			7.95						
JUM 8308	SJ-081	YPM72596	U			49.10			14.00						
AF1405-C	SJ-082	AF1405-C-007	U			14.59			7.26						
AF1405-C	SJ-082	AF1405-C-009	U			14.88			8.35						
AF1405-C	SJ-082	AF1405-C-010	U			8.48			5.66						
AF1409D	SJ-082	AF1409D-006	U			64.65			16.97						
JUM 8308	SJ-082	YPM52196	U			31.85			6.38						
AF1409C	SJ-088	AF1409C-025	T			42.62	13.54	49.06	7.66	38.17	48.32	14.67	9.00		0.04
AF1528	SJ-088	AF1528-088	T	0.05		29.67	14.99	26.58	8.05	14.53	25.14	14.62	19.00		0.40
DP1304-C	SJ-088	DP1304-C-007	T	0.11		25.52	18.41	43.76	7.25	28.60	41.56	18.23	45.00		0.24
AF1407	SJ-093	AF1407-086A/B	U	0.06		2.31			3.00						
AF1407	SJ-093	AF1407-087	U			4.24			4.00						
AF1623-C	SJ-103	AF1623-C-044	T			32.16	25.78	44.69	7.94	20.66	40.96	24.51	13.00	9.00	1.35
DP1304-C	SJ-103	DP1304-C-017	T			39.38	19.37	30.88	7.19	17.65	27.54	18.53	13.00	3.00	0.89

Locality	Morph.	Specimen #	Margin	Petiole width (cm)	Petiole area (cm^2)	Inferred blade area (cm^2)	Raw blade area (cm^2)	Raw perimeter (cm)	Major length (cm)	Length of cut perimeter (cm)	Raw internal perimeter (cm)	Raw internal blade area (cm^2)	# 1° teeth	# 2° teeth	Tooth area (cm^2)
AF1524-C	SJ-105	AF1524-C-032	U	0.14	0.11	39.70			9.49						
AF1406-C	SJ-106	AF1406-C-001A/B	U			315.98			24.94						
AF1524	SJ-108	AF1524-003	T				15.67	31.72		20.20	30.10	15.42	26.00		0.29
AF1524B	SJ-108	AF1524B-065A	T			28.30	4.75	17.82	12.02	14.07	17.43	4.66	11.00		0.11
AF1524-C	SJ-108	AF1524-C-015	T				3.70	12.01		8.49	11.74	3.61	15.00		0.10
AF1610	SJ-108	AF1610-032	T			29.07	15.16	23.13	10.11	10.32	21.23	14.87	40.00		0.36
AF1404-C2	SJ-111	AF1404-C2-032A	T	0.10		47.97	16.87	45.80	10.20	26.15	45.21	16.84	18.00		0.05
AF1404-C2	SJ-112	AF1404-C2-033A	U	0.17	0.10	30.69			6.58						
AF1405-C	SJ-113	AF1405-C-013	U			83.15			12.13						
DP1309/10	SJ-113	DP1309/10-003	U	0.09		36.21			8.10						
AF1406-C	SJ-119	AF1406-C-002	U	0.08		47.09			11.36						
AF1406-C	SJ-119	AF1406-C-043	U			49.01			11.63						
AF1623-C	SJ-119	AF1623-C-029	U	0.21	0.23	55.07			11.98						
AF1406	SJ-124	AF1406-012	T	0.15		46.65	22.60	35.20	9.64	19.77	33.49	22.25	18.00		0.40
AF1518	SJ-124	AF1518-003	T			39.29	12.93	40.29	8.09	29.32	37.85	12.30	12.00	3.00	0.57
AF1524B	SJ-124	AF1524B-018	T	0.09		20.98	9.23	26.06	6.31	16.69	24.81	9.00	15.00		0.26
AF1524B	SJ-124	AF1524B-043	T				13.21	26.79		13.02	22.88	12.88	37.00		0.39
AF1524-C	SJ-124	AF1524-C-033A	T												
AF1528-C	SJ-124	AF1528-C-014	T				21.97	23.55		12.49	22.74	21.75	12.00		0.25

Locality	Morph.	Specimen #	Margin	Petiole width (cm)	Petiole area (cm^2)	Inferred blade area (cm^2)	Raw blade area (cm^2)	Raw perimeter (cm)	Major length (cm)	Length of cut perimeter (cm)	Raw internal perimeter (cm)	Raw internal blade area (cm^2)	# 1° teeth	# 2° teeth	Tooth area (cm^2)
AF1623-C	SJ-124	AF1623-C-055	T				17.44	26.69		16.72	26.42	17.02	18.00	3.00	0.47
AF1623-C	SJ-124	AF1623-C-056	T	0.14	0.03	19.03	10.16	22.86	5.68	9.41	20.08	9.87	35.00	5.00	0.35
AF1405-C	SJ-125	AF1405-C-002	U			12.98			4.70						
AF1623	SJ-128	AF1623-019	U			25.36			9.71						
AF1623-C	SJ-128	AF1623-C-005	U			38.25			13.88						
AF1623-C	SJ-128	AF1623-C-011	U	0.07		31.63			11.28						
JUM 8308	SJ-128	YPM47605	U			38.00			10.34						
JUM 8308	SJ-128	YPM47616	U	0.16	0.23	23.68			8.26						
JUM 8308	SJ-128	YPM52195A	U			20.85			8.04						
JUM 8308	SJ-128	YPM52252	U												
AF1623	SJ-129	AF1623-001	T				9.02	13.07		8.12	11.96	8.52	5.00		0.50
AF1623-C	SJ-130	AF1623-C-019	U	0.18	0.05	32.02			7.69						
AF1623-C	SJ-133	AF1623-C-017	T	0.08		24.24	6.24	30.25	9.15	23.29	29.84	6.17	13.00		0.09
AF1608	SJ-137	AF1608-018	U	0.07		7.46			6.17						
AF1608-C	SJ-137	AF1608-C-036	U	0.07		12.94			7.49						
AF1623	SJ-137	AF1623-011	U	0.13	0.07	12.41			6.43						
DP1304	SJ-137	DP1304-006	U			17.24			7.05						
JUM 8308	SJ-137	YPM52207	U			21.85			8.89						
JUM 8308	SJ-137	YPM72529	U			13.62			6.57						
AF1521	SJ-138	AF1521-010	T	0.22	0.43	56.13	12.20	37.14	9.20	24.75	36.64	11.90	11.00		0.33
AF1528	SJ-138	AF1528-073	T	0.11		92.43	58.51	64.94	14.50	36.85	62.02	57.27	31.00		1.35
AF1519	SJ-141	AF1519-022	T			5.15	3.62	8.45	3.89	3.33	8.11	3.57	9.00		0.05
AF1611-C	SJ-143	AF1611-C-041	U	0.08	0.01	4.30			5.08						
AF1610	SJ-144	AF1610-012	T			23.07	15.86	28.47	9.37	13.78	27.09	15.63	16.00		0.27

Locality	Morph.	Specimen #	Margin	Petiole width (cm)	Petiole area (cm^2)	Inferred blade area (cm^2)	Raw blade area (cm^2)	Raw perimeter (cm)	Major length (cm)	Length of cut perimeter (cm)	Raw internal perimeter (cm)	Raw internal blade area (cm^2)	# 1° teeth	# 2° teeth	Tooth area (cm^2)
AF1611	SJ-144	AF1611-012	T			15.23	5.76	18.94	6.27	12.77	18.71	5.65	7.00		0.13
AF1611-C	SJ-144	AF1611-C-043	T				15.29	17.46		7.10	17.13	14.91	8.00		0.43
AF1611-C	SJ-145	AF1611-C-044A	U	0.09		24.53			6.20						
AF1610	SJ-149	AF1610-025A	T	0.20	1.07	31.52	24.14	37.37	10.54	17.81	35.36	23.76	52.00		0.47
AF1412	SJ-150	AF1412-002	U	0.09	0.05	23.67			7.86						
JUM8302B	SJ-150	YPM71136	U												
AF1513B	SJ-151	AF1513B-018A	U	0.15	0.19	86.18			15.13						
JUM 8308	SJ-151	YPM47611A	U			29.66			8.03						
JUM 8308	SJ-151	YPM52257	U	0.10	0.03	20.78			7.56						
AF1610	SJ-152	AF1610-035	T				15.66	36.25		18.47	30.03	14.96	49.00		0.78
AF1610	SJ-153	AF1610-047	U	0.19	0.08	71.63			10.41						
AF1524B	SJ-154	AF1524B-012	U			26.16			7.76						
AF1524B	SJ-154	AF1524B-055	U	0.15		50.69			11.32						
AF1610	SJ-155	AF1610-054	U	0.17	0.15	37.48			13.49						
AF1618-C	SJ-156	AF1618-C-056	T			20.08	8.12	30.39	8.68	22.97	29.74	8.00	32.00		0.15
AF1618-C	SJ-157	AF1618-C-060	U			7.19			4.29						
AF1528-C	SJ-162	AF1528-C-001	T	0.16		192.53	79.97	83.42	18.53	54.77	79.91	78.19	19.00		1.86
AF1528	SJ-163	AF1528-024	T			19.88	8.41	21.02	5.79	10.81	19.55	8.04	13.00		0.39
AF1528-C	SJ-163	AF1528-C-005	T	0.04		6.45	2.46	7.97	4.29	2.92	7.41	2.19	8.00		0.29
AF1512	SJ-164	AF1512-025	U			27.92			9.00						
AF1513F-C	SJ-164	AF1513F-C-057	U	0.09		36.00			10.72						
AF1412	SJ-169	AF1412-026	T	0.12		51.06	40.01	44.20	11.57	18.26	42.57	38.04	10.00		2.07

Locality	Morph.	Specimen #	Margin	Petiole width (cm)	Petiole area (cm^2)	Inferred blade area (cm^2)	Raw blade area (cm^2)	Raw perimeter (cm)	Major length (cm)	Length of cut perimeter (cm)	Raw internal perimeter (cm)	Raw internal blade area (cm^2)	# 1° teeth	# 2° teeth	Tooth area (cm^2)
AF1524B	SJ-171	AF1524B-051	U	0.09	0.24	90.88			16.54						
AF1524B	SJ-172	AF1524B-027A	T	0.14	0.10	59.27	27.32	55.00	16.79	38.92	54.30	26.86	20.00		0.36
AF1512-C	SJ-178	AF1512-C-036	T				23.48	33.62		23.03	31.55	22.80	16.00		0.73
JUM8301	SJ-180	YPM67978	U	0.39	0.20	32.77			7.99						
AF1528	SJ-181	AF1528-029A	U	0.11	0.01	14.29			4.92						

Figure E.2 – Digital Leaf Physiognomy Protocol

Examples of the 4 different types of leaves prepared for digital leaf physiognomy (DiLP) following the protocol of Peppe et al. 2011. All digital preparation was done using Adobe Photoshop.

A: entire margin leaf with majority of leaf preserved — A1: leaf is photographed, A2: leaf is digitally extracted from the rock matrix, A3: areas of damaged margin repaired to reconstruct leaf shape.

B: toothed margin leaf with majority of leaf preserved — B1: leaf is photographed, B2: leaf is digitally extracted from rock matrix, B3: A3: areas of damaged margin repaired to reconstruct leaf shape, B4: areas of damaged margin are removed by removing all leaf area between the damaged margin and the major vein along straight lines so only leaf area with undamaged margin is used, B5: teeth are cut from the leaf by connecting tooth sinuses between adjacent teeth.

C: toothed margin with only half of leaf preserved — C1: leaf is photographed, C2: leaf is digitally extracted from rock matrix, C3: damaged blade area removed and ½ of leaf of leaf area reconstructed (total leaf area estimated by multiplying ½ of reconstructed leaf area by 2), C4: areas of damaged margin are removed by removing all leaf area between the damaged margin and the major vein along straight lines so only leaf area with undamaged margin is used, C5: teeth are cut from the leaf by connecting tooth sinuses between adjacent teeth.

D: toothed margin with partial leaf persevered (no leaf area estimate) — D1: leaf is photographed, D2: leaf is digitally extracted from rock matrix, D3: areas of damaged margin are removed by removing all leaf area between the damaged margin and the major vein along straight lines so only leaf area with undamaged margin is used, D4: teeth are cut from the leaf by connecting tooth sinuses between adjacent teeth.

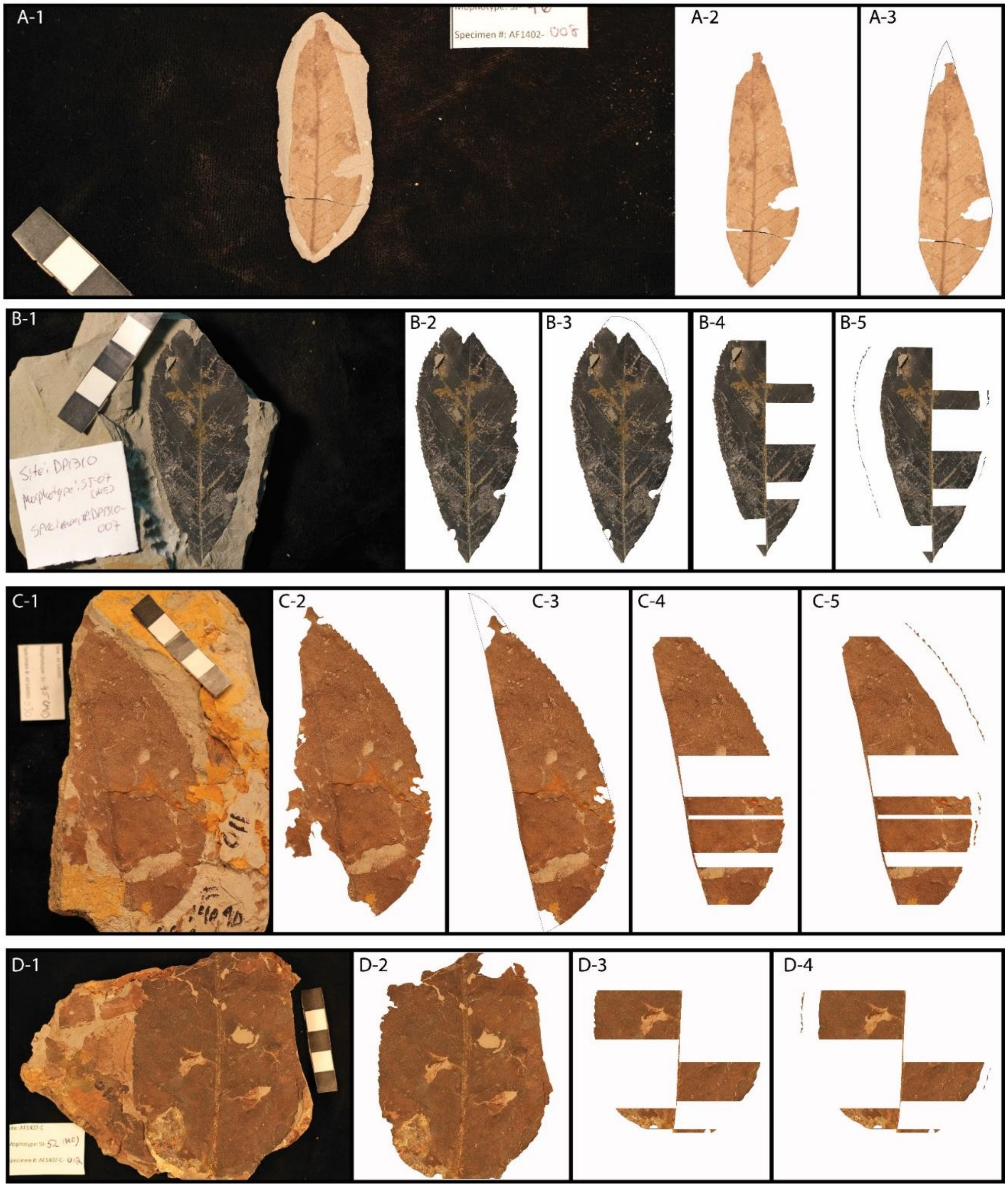
A-1
Specimen #: AF1402- 008
A-2
A-3
B-1
Site: DP1310
Morphotype: SS-07 (WE)
Specimen #: DP1310-007
B-2
B-3
B-4
B-5
C-1
C-2
C-3
C-4
C-5
D-1
Morphotype: SS-52 (WE)
D-2
D-3
D-4

APPENDIX F

Regional floral diversity indices data

Table F.1 – Regional Diversity Indices Results: Regional diversity comparison. Species richness is the total number of morphotypes found in each basin and the number in parentheses indicates the number of vegetative morphotypes found in quantitative collections used to calculate different diversity metrics. All rarefaction analysis and diversity indices calculated using PAST 3.0 (Hammer et al. 2001). 95% confidence intervals are shown where appropriate. Average site rarefied richness has been down sampled to 300 specimens. Total basin rarefied richness has been down sampled to 1000 specimens. D_{mg} - Margalef's Diversity Index, J' - Pielou's Evenness Index, d - Berger-Parker Dominance

	San Juan (This Study)	Denver (Barclay et al. 2003)	Williston (Wilf and Johnson 2004)	WIlliston (Peppe 2010)
Species Richness	53 (44)	49 (25)	33 (28)	24 (19)
Average Site Rarefied Richness	12.99 ± 0.86	11.50 ± 0.58	7.64 ± 0.73	11.06 ± 0.59
Total Basin Rarefied Richness	34.52 ± 2.17	22.53 ± 1.30	20.52 ± 1.47	18.95 ± 0.22
D_{mg}	5.386	3.268	3.205	2.596
J'	0.4488 ± 0.0164	0.6583 ± 0.0139	0.6425 ± 0.0089	0.6746 ± 0.0205
d	0.6282 ± 0.0176	0.2332 ± 0.0184	0.3167 ± 0.0136	0.2917 ± 0.0273

Table F.2 – Regional Floral Diversity Permutation Tests: calculated p-values for (**A**) Margalef Index (D_{mg}), (**B**) Pielou's Evenness (J'), and (**C**) Berger-Parker Index (d) for all San Juan Basin, Denver Basin, and Williston Basin diversity indice comparison. All statistics calculated using PAST 3.0 (Hammer et al. 2001) and bootstrapped 10,000 times.

A - D_{mg}	San Juan (This Study)	Denver (Barclay et al. 2003)	Williston (Wilf and Johnson 2004)	WIlliston (Peppe 2010)
San Juan (This Study)	------	------	------	------
Denver (Barclay et al. 2003)	0.0027	------	------	------
Williston (Wilf and Johnson 2004)	0.0003	0.9509	------	------
WIlliston (Peppe 2010)	< 0.0001	0.2217	0.4381	------
B - J'	**San Juan (This Study)**	**Denver (Barclay et al. 2003)**	**Williston (Wilf and Johnson 2004)**	**WIlliston (Peppe 2010)**
San Juan (This Study)	------	------	------	------
Denver (Barclay et al. 2003)	< 0.0001	------	------	------
Williston (Wilf and Johnson 2004)	< 0.0001	0.9609	------	------
WIlliston (Peppe 2010)	< 0.0001	0.8309	0.9974	------
C - d	**San Juan (This Study)**	**Denver (Barclay et al. 2003)**	**Williston (Wilf and Johnson 2004)**	**WIlliston (Peppe 2010)**
San Juan (This Study)	------	------	------	------
Denver (Barclay et al. 2003)	< 0.0001	------	------	------
Williston (Wilf and Johnson 2004)	< 0.0001	< 0.0001	------	------
WIlliston (Peppe 2010)	< 0.0001	< 0.0001	0.1031	------

APPENDIX G

Capture-Mark-Recapture Results

Table G.1 – Summary of Capture-Mark-Recapture Model Results

San Juan Basin - This Study							
Model #	Model Description	No. Params	AIC	AIC-Wt	Model Likelihood	Deviance	-2log(L)
1	φ(.) p(t) γ(t)	24	1754.4	1	1	596.045	1703.406
2	φ(t) p(t) γ(t)	34	1780.4	0	0	599.041	1706.402
3	φ(.) p(t) γ(.)	17	1797.5	0	0	654.6406	1762.002
4	φ(t) p(t) γ(.)	27	1811.2	0	0	646.0284	1753.39
5	φ(.) p(t) γ(t)	16	1840.6	0	0	699.9114	1807.273
6	φ(.) p(.) γ(t)	8	1866.2	0	0	742.5032	1849.864
7	φ(t) p(.) γ(.)	10	1915.2	0	0	787.2672	1894.628
8	φ(.) p(.) γ(.)	3	1952.7	0	0	839.2756	1946.637
Denver Basin (Corral Bluffs) - Lyson et al. 2019							
Model #	Model Description	No. Params	AIC	AIC-Wt	Model Likelihood	Deviance	-2log(L)
1	φ(t) p(t) γ(t)	27	1745.776	0.71564	1	357.8438	1687.406
2	φ(t) p(t) γ(.)	21	1747.622	0.28434	0.3973	373.4347	1702.997
3	φ(.) p(t) γ(t)	21	1768.227	0.00001	0	394.0394	1723.602
4	φ(.) p(t) γ(.)	16	1769.029	0.00001	0	405.9422	1735.505
5	φ(t) p(.) γ(t)	15	1852.549	0	0	491.6459	1821.208
6	φ(.) p(.) γ(t)	8	1892.189	0	0	546.2323	1875.795
7	φ(t) p(.) γ(.)	11	1933.395	0	0	581.1035	1910.666
8	φ(.) p(.) γ(.)	3	1972.737	0	0	637.11	1966.672
Williston Basin - Wilf and Johnson 2004; Peppe 2010							
Model #	Model Description	No. Params	AIC	AIC-Wt	Model Likelihood	Deviance	-2log(L)
1	φ(t) p(t) γ(t)	69	4883.921	1	1	1469.154	4734.141
2	φ(t) p(.) γ(t)	31	4940.42	0	0	1611.121	4876.108
3	φ(t) p(t) γ(.)	54	4944.429	0	0	1564.329	4829.316
4	φ(.) p(t) γ(t)	50	5002.206	0	0	1631.14	4896.127
5	φ(t) p(.) γ(.)	18	5110.395	0	0	1808.623	5073.61
6	φ(.) p(t) γ(.)	36	5151.339	0	0	1811.229	5076.216
7	φ(.) p(.) γ(t)	17	5154.739	0	0	1855.05	5120.037
8	φ(.) p(.) γ(.)	3	5537.127	0	0	2266.113	5531.1

Table G.2 – San Juan Basin Capture-Mark-Recapture Results: p – sampling probability, φ – survival probability, γ – seniority probability, and λ – net diversification. 95% confidence interval is shown in paraeneses.

Bin (Myr)	p	φ	γ	λ
66.0 - 65.7	0.742 (+0.258/-0.742)			
65.7 - 65.6	0.5 (+0.133/-0.133)	1 (+0/-0)	0.887 (+0.113/-0.887)	1.198 (+0.802/-1.196)
65.6 - 65.5	0.264 (+0.156/-0.113)	0.669 (+0.139/-0.176)	0.988 (+0.012/-0.988)	0.677 (+0.29/-0.203)
65.5 - 65.4	0.115 (+0.133/-0.066)	0.901 (+0.085/-0.358)	0.977 (+0.023/-0.977)	0.922 (+0.52/-0.332)
65.4 - 65.3	0.605 (+0.136/-0.154)	1 (+0/-0)	0.72 (+0.193/-0.334)	1.389 (+0.664/-0.449)
65.3 - 65.2	0.776 (+0.102/-0.152)	0.962 (+0.036/-0.41)	0.835 (+0.107/-0.223)	1.152 (+0.29/-0.231)
65.2 - 65.1	0.299 (+0.138/-0.109)	0.813 (+0.127/-0.266)	0.968 (+0.031/-0.592)	0.839 (+0.258/-0.197)
65.1 - 65.0	0.222 (+0.138/-0.096)	0.961 (+0.039/-0.958)	1 (+0/-0)	0.961 (+0.384/-0.275)
65 - 64.9	0.312 (+0.149/-0.118)	0.85 (+0.132/-0.484)	0.897 (+0.086/-0.327)	0.948 (+0.45/-0.305)
64.9 - 64.8	0.423 (+0.152/-0.138)	0.904 (+0.088/-0.492)	0.981 (+0.019/-0.98)	0.922 (+0.342/-0.25)
64.8 - 64.7	0.367 (+0.16/-0.135)	0.991 (+0.009/-0.991)	0.934 (+0.061/-0.455)	1.061 (+0.403/-0.292)
64.7 - 64.6	0.657 (+0.137/-0.169)	0.86 (+0.122/-0.452)	0.681 (+0.127/-0.16)	1.263 (+0.525/-0.371)
64.6 - 64.5	0.388 (+0.184/-0.156)	0.619 (+0.197/-0.245)	1 (+0/-0)	0.619 (+0.284/-0.195)

Table G.3 – Denver Basin Capture-Mark-Recapture Results: p – sampling probability, φ – survival probability, γ – seniority probability, and λ – net diversification. 95% confidence interval is shown in paraeneses.

Bin (Myr)	p	φ	γ	λ
66.5 - 66.4	0.316 (+0.461/-0.291)			
66.3 - 66.2	0.168 (+0.287/-0.121)	0.799 (+0.152/-0.35)	1 (+0/-1)	0.638 (+2.181/-0.494)
66.2 - 66.1	0.381 (+0.18/-0.153)	0.887 (+0.112/-0.835)	0.443 (+0.387/-0.328)	2.002 (+3.855/-1.318)
66.1 - 66.032	0.129 (+0.094/-0.058)	1 (+0/-0)	1 (+0/-1)	1 (+0.004/-0.004)
66.032 - 65.9	0.476 (+0.203/-0.196)	0.323 (+0.136/-0.112)	0.553 (+0.256/-0.288)	0.584 (+0.462/-0.258)
65.9 - 65.8	0.652 (+0.146/-0.181)	0.802 (+0.123/-0.231)	0.845 (+0.141/-0.543)	0.95 (+0.542/-0.345)
65.8 - 65.7	0.505 (+0.148/-0.15)	0.755 (+0.131/-0.206)	0.86 (+0.109/-0.315)	0.877 (+0.332/-0.24)
65.7 - 65.6	0.04 (+0.078/-0.027)	1 (+0/-1)	1 (+0/-1)	1 (+0.001/-0.001)
65.6 - 65.5	0.326 (+0.11/-0.096)	1 (+0/-0)	0.698 (+0.131/-0.174)	1.432 (+0.358/-0.286)
65.5 - 65.4	0.075 (+0.099/-0.045)	0.619 (+0.172/-0.208)	1 (+0/-0)	0.619 (+0.234/-0.169)
65.4 - 65.3	0.508 (+0.173/-0.173)	1 (+0/-0)	1 (+0/-0)	1 (+0/-0)
65.3 - 65.2	0.096 (+0.159/-0.061)	0.599 (+0.235/-0.292)	1 (+0/-0)	0.599 (+0.369/-0.228)
65.2 - 65.1	0.651 (+0.242/-0.294)	1 (+0/-0)	0.911 (+0.077/-0.342)	1.097 (+0.219/-0.182)
65.1 – 65.0	0.151 (+0.849/-0.151)	0.369 (+0.631/-0.369)	1 (+0/-0)	0.369 (+198.297/-0.368)

Table G.4 – Williston Basin Capture-Mark-Recapture Results: p – sampling probability, φ – survival probability, γ – seniority probability, and λ – net diversification. 95% confidence interval is shown in paraeneses.

Bin (Myr)	p	φ	γ	λ
67.6 - 67.5	0.162 (+0.833/-0.162)			
67.4 - 67.3	0.373 (+0.247/-0.195)	0.904 (+0.08/-0.302)	0.997 (+0.003/-0.997)	0.821 (+14.923/-0.778)
67.3 - 67.2	0.197 (+0.195/-0.112)	1 (+0/-0)	1 (+0/-0)	1 (+0/-0)
67.2 - 67.1	0.417 (+0.192/-0.17)	1 (+0/-0)	0.635 (+0.275/-0.405)	1.575 (+1.371/-0.733)
67.1 - 67	0.346 (+0.136/-0.115)	0.964 (+0.035/-0.657)	0.8 (+0.171/-0.477)	1.205 (+0.661/-0.427)
67 - 66.9	0.219 (+0.117/-0.084)	1 (+0/-0)	1 (+0/-0)	1 (+0/-0)
66.9 - 66.8	0.32 (+0.095/-0.082)	1 (+0/-0)	0.494 (+0.145/-0.144)	2.023 (+0.703/-0.522)
66.8 - 66.7	0.278 (+0.11/-0.089)	0.801 (+0.125/-0.236)	1 (+0/-1)	0.801 (+0.202/-0.161)
66.7 - 66.6	0.119 (+0.077/-0.049)	0.962 (+0.038/-0.925)	1 (+0/-0)	0.962 (+0.267/-0.209)
66.6 - 66.5	0.466 (+0.117/-0.113)	1 (+0/-0)	0.604 (+0.131/-0.148)	1.655 (+0.441/-0.348)
66.5 - 66.4	0.134 (+0.097/-0.06)	0.637 (+0.204/-0.27)	1 (+0/-1)	0.637 (+0.31/-0.209)
66.4 - 66.3	0.28 (+0.127/-0.099)	0.813 (+0.164/-0.503)	0.72 (+0.162/-0.25)	1.129 (+0.761/-0.454)
66.3 - 66.2	0.504 (+0.108/-0.108)	0.801 (+0.138/-0.288)	0.668 (+0.157/-0.207)	1.199 (+0.549/-0.376)
66.2 - 66.1	0.437 (+0.133/-0.125)	0.689 (+0.148/-0.199)	1 (+0/-0)	0.689 (+0.204/-0.157)
66.1 - 66.032	0.505 (+0.18/-0.181)	0.777 (+0.171/-0.381)	0.854 (+0.096/-0.212)	0.91 (+0.463/-0.307)
66.032 - 65.9	0.742 (+0.135/-0.204)	0.191 (+0.147/-0.092)	0.313 (+0.156/-0.123)	0.715 (+0.391/-0.253)
65.9 - 65.8	0.297 (+0.164/-0.124)	0.597 (+0.117/-0.129)	1 (+0/-0)	0.506 (+0.161/-0.122)
65.8 - 65.7	0.334 (+0.166/-0.133)	1 (+0/-0)	0.86 (+0.119/-0.408)	1.163 (+0.376/-0.284)
65.7 - 65.6	0.42 (+0.158/-0.143)	1 (+0/-0)	0.821 (+0.143/-0.377)	1.218 (+0.445/-0.326)
65.6 - 65.5	0.297 (+0.13/-0.104)	1 (+0/-0)	0.835 (+0.13/-0.355)	1.197 (+0.385/-0.291)
65.5 - 65.4	0.324 (+0.188/-0.145)	0.582 (+0.18/-0.205)	1 (+0/-0)	0.582 (+0.24/-0.17)
65.4 - 65.3	0.408 (+0.173/-0.153)	1 (+0/-0)	0.766 (+0.149/-0.268)	1.306 (+0.418/-0.317)
65.3 - 65.2	0.217 (+0.215/-0.125)	0.572 (+0.251/-0.294)	1 (+0/-0)	0.572 (+0.394/-0.233)
65.1 - 65	0.062 (+0.168/-0.048)	1 (+0/-0)	1 (+0/-0)	1 (+0/-0)

Bin (Myr)	p	φ	γ	λ
65 - 64.9	0.316 (+0.241/-0.171)	0.784 (+0.196/-0.571)	1 (+0/-0)	0.784 (+0.576/-0.332)
64.7 - 64.6	0.409 (+0.254/-0.213)	0.99 (+0.01/-0.99)	0.918 (+0.063/-0.206)	1.256 (+1.047/-0.571)
64.6 - 64.5	0.531 (+0.237/-0.251)	0.739 (+0.208/-0.427)	0.959 (+0.041/-0.955)	0.771 (+0.621/-0.344)
64.5 - 64.4	0.041 (+0.204/-0.035)	1 (+0/-0)	1 (+0/-1)	1 (+0.001/-0.001)
64.1 - 64	0.052 (+0.247/-0.045)	0.943 (+0.05/-0.268)	1 (+0/-1)	0.79 (+0.472/-0.295)
64 - 63.9	0.416 (+0.235/-0.202)	1 (+0/-0)	0.619 (+0.21/-0.266)	1.616 (+0.825/-0.546)
63.9 - 63.8	0.358 (+0.265/-0.2)	0.804 (+0.178/-0.571)	1 (+0/-1)	0.804 (+0.524/-0.317)
63.8 - 63.7	0.59 (+0.226/-0.272)	0.921 (+0.079/-0.911)	0.62 (+0.205/-0.259)	1.484 (+1.306/-0.695)
63.7 - 63.6	0.268 (+0.203/-0.137)	1 (+0/-0)	1 (+0/-0)	1 (+0/-0)
63.5 - 63.4	0.296 (+0.704/-0.296)	0.522 (+0.478/-0.522)	1 (+0/-0)	0.272 (+59.401/-0.271)

APPENDIX H

Binned Floral Occurrence Data

Table H.1 – San Juan Basin Binned Floral Occurrence Data

Morph	66.0 - 65.7	65.7 - 65.6	65.6 - 65.5	65.5 - 65.4	65.4 - 65.3	65.3 - 65.2	65.2 - 65.1	65.1 - 65.0	65 - 64.9	64.9 - 64.8	64.8 - 64.7	64.7 - 64.6	64.6 - 64.5	63.8- 63.7	63.4- 63.3
PB-026	0	0	0	1	0	1	0	0	0	0	0	0	0	0	0
SJ-002	0	0	0	0	0	0	0	0	0	0	0	1	0	0	0
SJ-003	0	0	0	0	0	0	0	0	0	0	0	1	0	1	0
SJ-004	0	0	0	0	0	0	0	0	0	0	0	1	0	1	0
SJ-005	0	0	0	0	1	1	1	0	0	0	1	1	0	1	0
SJ-007	0	0	0	0	0	0	1	0	0	0	1	1	1	1	1
SJ-008	0	0	0	0	0	0	0	0	0	0	0	1	0	0	0
SJ-009	0	0	0	0	0	0	0	0	0	0	0	1	0	0	0
SJ-011	1	1	1	0	1	1	0	1	1	1	0	1	1	1	0
SJ-012	0	1	0	0	1	0	0	0	0	0	1	1	0	0	0
SJ-013	1	1	1	0	0	1	0	1	1	1	1	1	0	0	1
SJ-014	1	0	0	0	0	0	0	0	0	0	0	1	0	0	1
SJ-015	0	0	0	0	1	1	0	0	1	0	0	1	1	0	1
SJ-016	0	0	0	0	0	1	1	0	0	0	0	1	1	1	0
SJ-017	0	0	0	0	0	0	0	0	0	0	0	1	0	0	0
SJ-018	0	0	0	0	0	0	0	0	1	0	0	1	0	1	0
SJ-019	0	0	0	0	1	1	0	0	0	1	1	1	1	1	1
SJ-020	0	0	0	0	1	0	0	0	0	1	0	1	0	1	0
SJ-021	0	0	0	0	0	0	0	0	0	0	0	1	0	0	0
SJ-022	0	0	0	0	0	0	0	0	0	0	0	1	0	0	0
SJ-023	0	0	0	0	0	0	0	0	0	0	0	1	0	0	0
SJ-024	0	0	0	0	1	0	0	0	0	0	0	1	0	0	0
SJ-025	1	0	0	0	0	0	0	0	0	0	0	1	0	0	0
SJ-026	0	0	0	0	0	0	0	0	0	0	0	1	0	0	0

Morph	66.0 - 65.7	65.7 - 65.6	65.6 - 65.5	65.5 - 65.4	65.4 - 65.3	65.3 - 65.2	65.2 - 65.1	65.1 - 65.0	65 - 64.9	64.9 - 64.8	64.8 - 64.7	64.7 - 64.6	64.6 - 64.5	63.8- 63.7	63.4- 63.3
SJ-027	0	0	0	0	0	0	0	0	0	0	0	1	0	0	0
SJ-028	1	1	0	0	1	1	1	1	0	0	1	1	0	1	1
SJ-029	0	0	0	0	0	0	0	0	0	0	0	1	0	0	0
SJ-030	0	0	0	0	0	0	0	0	0	0	0	1	0	0	0
SJ-031	0	0	0	0	0	0	0	0	0	0	0	1	0	0	0
SJ-033	0	1	0	0	0	0	0	0	0	0	1	1	0	0	0
SJ-034	0	0	0	0	0	0	0	0	0	0	0	1	0	0	0
SJ-035	0	1	1	0	0	0	0	0	0	1	0	1	0	0	0
SJ-036	1	1	1	1	1	1	1	1	1	1	1	1	1	1	1
SJ-037	0	0	0	0	0	0	0	0	0	0	0	1	0	1	0
SJ-039	0	0	0	0	0	0	0	0	0	0	0	1	0	0	0
SJ-042	0	0	0	0	0	0	0	0	0	0	0	1	0	0	0
SJ-046	1	1	0	0	1	1	0	1	1	1	0	1	1	0	1
SJ-048	1	1	0	0	0	0	0	0	0	0	0	0	0	0	0
SJ-050	1	1	0	0	0	0	0	0	0	0	0	0	0	0	0
SJ-051	1	1	1	0	1	1	0	0	0	0	0	0	0	0	0
SJ-053	1	0	0	0	0	0	0	0	0	0	0	0	0	0	0
SJ-055	1	0	0	0	0	0	0	0	0	0	0	0	0	0	0
SJ-056	1	1	0	0	0	1	0	0	0	0	0	0	0	0	0
SJ-057	1	1	0	0	0	0	0	0	0	0	0	0	0	0	0
SJ-058	1	0	0	0	0	0	0	0	0	0	0	0	0	0	0
SJ-059	1	0	0	0	1	1	0	0	0	0	0	0	0	0	0
SJ-060	1	1	0	0	1	1	0	0	0	0	0	0	0	0	0
SJ-061	1	0	0	0	0	0	0	0	0	0	0	0	0	0	0
SJ-062	1	1	0	0	0	1	1	1	0	0	0	0	0	0	0
SJ-063	1	0	0	0	0	0	0	0	0	0	0	0	0	0	0
SJ-064	1	1	0	0	1	1	1	0	0	1	0	0	0	0	1
SJ-065	1	0	0	0	0	0	0	0	0	0	0	0	0	0	0
SJ-066	1	0	0	0	0	0	0	0	0	0	0	0	0	0	0
SJ-068	1	1	0	0	0	0	0	0	0	0	0	0	0	0	0
SJ-069	1	0	0	0	0	0	0	0	0	0	0	0	0	0	0
SJ-071	1	1	0	0	1	1	1	0	0	0	1	1	0	0	0

Morph	66.0 - 65.7	65.7 - 65.6	65.6 - 65.5	65.5 - 65.4	65.4 - 65.3	65.3 - 65.2	65.2 - 65.1	65.1 - 65.0	65 - 64.9	64.9 - 64.8	64.8 - 64.7	64.7 - 64.6	64.6 - 64.5	63.8- 63.7	63.4- 63.3
SJ-072	1	0	0	0	0	0	0	0	0	0	0	0	0	0	0
SJ-073	1	1	0	0	0	0	0	0	0	0	0	0	0	0	0
SJ-076	1	0	0	0	0	0	0	0	0	0	0	0	0	0	0
SJ-077	1	1	1	0	0	0	0	0	0	0	0	0	0	0	0
SJ-078	1	1	1	0	1	1	0	0	0	0	0	0	0	0	0
SJ-079	1	1	0	0	1	1	0	0	0	1	0	0	1	0	0
SJ-080	1	0	1	1	1	1	1	1	1	1	1	1	1	0	0
SJ-081	1	1	1	1	1	1	0	0	0	0	1	0	1	0	0
SJ-082	1	1	1	0	1	1	0	1	0	0	0	1	0	0	0
SJ-083	1	1	1	0	0	0	0	0	0	0	0	0	0	0	0
SJ-086	1	1	1	0	1	1	0	1	1	1	0	1	1	0	0
SJ-088	1	0	0	0	1	0	0	0	0	0	1	0	0	0	0
SJ-089	1	0	0	0	0	0	0	0	0	0	0	0	0	0	0
SJ-090	1	0	0	0	0	0	0	0	0	0	0	0	0	0	0
SJ-092	1	0	0	0	0	0	0	0	0	0	0	0	0	0	0
SJ-093	1	0	0	0	0	0	0	0	0	0	0	0	0	0	0
SJ-094	1	0	0	0	0	0	0	0	0	0	0	0	0	0	0
SJ-097	0	1	0	0	0	0	0	0	0	0	0	0	0	0	0
SJ-098	0	1	0	0	0	0	0	0	0	0	0	0	0	0	0
SJ-099	0	1	0	0	0	0	0	0	0	0	0	0	0	0	0
SJ-102	1	0	0	0	1	0	0	0	0	0	0	0	0	0	0
SJ-103	0	0	0	0	1	0	0	0	0	0	0	0	0	0	0
SJ-105	0	0	0	0	0	1	0	0	0	0	0	0	0	0	0
SJ-106	0	1	0	0	0	1	0	0	1	0	0	1	1	0	0
SJ-107	0	0	0	0	0	1	0	0	0	0	0	0	0	0	0
SJ-108	0	1	0	0	0	1	1	0	0	0	0	0	0	0	0
SJ-110	1	0	0	0	0	0	0	0	0	0	0	0	0	0	0
SJ-111	1	0	0	0	0	0	0	0	0	0	0	0	0	0	0
SJ-112	1	0	0	0	0	1	0	1	0	0	0	0	0	0	0
SJ-113	1	1	0	0	1	1	0	0	1	1	1	0	1	0	0
SJ-115	0	1	0	0	1	1	1	1	1	0	0	0	0	0	1
SJ-117	0	1	0	0	0	1	0	0	0	0	0	1	0	1	1

Morph	66.0 - 65.7	65.7 - 65.6	65.6 - 65.5	65.5 - 65.4	65.4 - 65.3	65.3 - 65.2	65.2 - 65.1	65.1 - 65.0	65 - 64.9	64.9 - 64.8	64.8 - 64.7	64.7 - 64.6	64.6 - 64.5	63.8- 63.7	63.4- 63.3
SJ-119	1	1	0	0	1	1	0	0	0	0	0	0	0	0	0
SJ-121	0	1	0	0	1	1	0	0	0	0	0	0	0	0	0
SJ-123	0	1	0	0	0	0	0	0	0	0	0	0	0	0	0
SJ-124	1	1	0	0	1	1	1	0	0	1	1	0	0	0	0
SJ-125	0	1	0	0	0	0	0	0	0	0	0	0	0	0	0
SJ-127	0	1	0	1	1	1	0	0	0	1	0	1	0	1	0
SJ-128	0	0	0	0	1	1	0	0	1	0	0	0	0	0	0
SJ-129	0	0	0	0	1	0	0	0	0	0	0	0	0	0	0
SJ-130	0	0	1	0	1	1	0	0	0	0	0	1	0	0	0
SJ-131	0	0	0	0	1	0	0	0	1	0	0	0	0	0	0
SJ-133	0	0	0	0	1	0	0	0	0	0	0	0	0	0	0
SJ-134	0	0	0	0	0	1	0	0	0	0	0	0	0	0	0
SJ-135	0	0	0	0	1	1	0	0	0	1	0	0	0	0	0
SJ-136	0	0	0	0	0	1	0	0	0	0	1	1	0	0	0
SJ-137	0	0	0	0	1	1	0	0	0	0	0	0	0	0	0
SJ-138	0	1	0	1	0	1	0	0	1	1	1	0	0	1	0
SJ-140	0	0	0	0	0	1	0	0	0	0	0	0	0	0	0
SJ-141	0	0	0	0	1	1	0	0	0	0	0	0	0	0	0
SJ-142	0	1	0	0	0	1	0	0	0	0	0	0	0	0	0
SJ-143	0	0	0	0	1	1	0	0	0	0	0	1	0	0	0
SJ-144	1	0	0	0	0	1	1	0	0	0	0	1	0	0	0
SJ-145	0	0	0	0	0	1	0	0	0	0	0	0	0	0	0
SJ-146	0	0	0	0	0	1	1	0	1	0	0	0	0	0	0
SJ-147	0	0	0	0	0	1	0	0	0	0	0	0	0	0	0
SJ-148	0	0	0	0	0	1	1	0	0	0	0	0	0	0	0
SJ-149	0	0	1	0	0	1	1	0	0	0	0	0	0	0	0
SJ-150	0	0	1	0	1	1	0	1	0	1	1	0	1	0	0
SJ-151	1	0	0	0	1	1	1	1	1	1	1	1	1	1	1
SJ-152	0	0	0	0	0	0	1	0	0	1	0	0	0	0	1
SJ-153	0	0	0	0	0	1	1	0	1	0	1	0	0	0	0
SJ-154	0	0	0	0	0	1	1	0	0	0	0	0	0	0	0
SJ-155	0	0	0	0	0	0	1	0	0	0	0	0	0	0	0

Morph	66.0 - 65.7	65.7 - 65.6	65.6 - 65.5	65.5 - 65.4	65.4 - 65.3	65.3 - 65.2	65.2 - 65.1	65.1 - 65.0	65 - 64.9	64.9 - 64.8	64.8 - 64.7	64.7 - 64.6	64.6 - 64.5	63.8- 63.7	63.4- 63.3
SJ-156	0	0	0	0	0	0	0	0	0	0	0	1	0	0	1
SJ-157	0	0	0	0	0	0	0	0	0	0	0	1	0	0	0
SJ-158	0	0	0	0	1	1	0	0	1	1	0	1	0	1	0
SJ-159	0	0	0	0	0	0	0	0	0	0	0	0	1	1	0
SJ-161	0	0	0	0	0	0	0	0	0	0	1	0	0	0	0
SJ-162	0	0	0	0	0	0	0	0	1	1	1	0	0	0	0
SJ-163	0	0	0	0	1	0	0	0	0	1	1	0	0	0	0
SJ-164	0	0	0	0	1	0	0	0	1	1	1	0	0	0	0
SJ-166	0	0	0	0	1	1	0	0	0	0	0	1	0	0	0
SJ-168	0	0	0	0	0	0	0	0	0	0	0	0	1	0	0
SJ-169	0	0	0	0	0	0	0	0	0	0	0	0	1	0	0
SJ-170	0	0	0	0	0	0	0	0	0	0	0	0	1	0	0
SJ-171	0	0	0	0	0	1	0	0	0	0	0	0	0	0	0
SJ-172	0	0	0	0	0	1	0	0	0	1	0	0	0	0	0
SJ-173	0	0	0	0	0	1	0	0	0	0	0	0	0	0	0
SJ-174	0	0	0	0	0	1	0	0	0	0	0	0	0	0	0
SJ-175	0	0	0	0	0	1	0	0	0	0	0	0	0	0	0
SJ-178	0	0	0	0	0	0	0	0	0	1	0	0	0	0	0
SJ-179	0	0	0	0	0	0	0	0	0	1	0	0	0	0	0
SJ-180	0	0	0	0	0	0	0	0	0	0	1	0	0	0	0
SJ-181	0	0	0	0	0	0	0	0	0	0	1	0	0	0	0
SJ-182	0	0	0	0	0	0	0	0	0	0	0	1	0	0	0
SJ-183	0	0	0	0	0	1	0	1	0	0	0	0	0	0	0
SJ-184	0	0	0	0	0	1	0	1	0	0	0	0	0	0	0
SJ-186	0	0	0	0	0	0	0	0	1	0	0	0	0	0	0
SJ-187	0	0	0	0	1	0	0	0	0	0	0	0	0	0	0
SJ-189	0	0	0	0	0	0	0	0	0	1	0	0	0	0	0

Table H.2 – Denver Basin (Lyson et al. 2019) Binned Floral Occurrence Data

Morph	66.5 - 66.4	66.4 - 66.3	66.3 - 66.2	66.2 - 66.1	66.1 - 66.032	66.032 - 65.9	65.9 - 65.8	65.8 - 65.7	65.7 - 65.6	65.6 - 65.5	65.5 - 65.4	65.4 - 65.3	65.3 - 65.2	65.2 - 65.1	65.1 - 65.0
CS1	1	0	0	1	0	1	1	1	1	1	0	1	1	1	0
CS2	0	0	0	0	0	1	1	1	1	1	1	1	1	1	1
CS3	0	0	0	1	0	1	1	0	0	0	0	1	0	0	0
CS4	0	0	0	0	0	0	0	0	0	0	0	0	0	1	0
CS5	0	0	0	0	0	1	1	1	0	1	0	1	0	1	0
CS6	0	0	0	0	0	1	1	0	0	1	0	0	0	0	0
CS7	0	0	0	1	0	0	0	0	0	0	0	0	0	1	0
CS8	0	0	0	0	0	0	0	0	0	1	0	0	0	0	0
CS9	1	0	0	0	0	0	1	0	0	0	0	0	0	0	0
CS10	1	0	0	0	0	0	0	0	0	0	0	0	0	0	0
CS11	0	0	0	1	0	0	0	0	0	0	0	0	0	0	0
CS12	0	0	0	0	0	0	0	1	0	0	0	0	0	0	0
CS13	1	0	0	0	0	0	0	0	0	0	0	0	0	0	0
CS14	0	0	0	0	0	1	1	0	0	0	0	1	0	0	0
CS15	0	0	0	0	0	0	0	0	0	1	0	0	0	0	0
CS18	0	0	0	0	0	0	0	0	0	1	0	0	0	0	0
CS20	1	0	0	0	0	0	0	0	0	0	0	0	0	0	0
CS23	0	0	1	1	0	0	0	1	0	0	0	0	0	0	0
CS24	0	0	0	0	1	0	0	0	0	0	0	0	0	0	0
CS51	0	0	0	0	0	0	0	0	0	0	0	1	0	0	0
CS52	0	0	0	0	0	0	0	0	0	0	0	1	0	0	0
CS53	0	0	0	0	0	0	0	0	0	1	0	0	0	0	0
CS54	0	0	1	0	1	1	1	1	0	0	0	1	0	0	0
CS55	0	0	0	0	0	1	1	0	0	0	0	1	0	1	0
CS56	1	0	0	0	0	1	1	1	0	1	1	0	0	0	0
CS57	1	0	0	1	0	0	1	1	0	1	0	1	0	1	0
CS58	0	0	0	0	0	1	0	0	0	0	0	0	0	0	0

Morph	66.5 - 66.4	66.4 - 66.3	66.3 - 66.2	66.2 - 66.1	66.1 - 66.032	66.032 - 65.9	65.9 - 65.8	65.8 - 65.7	65.7 - 65.6	65.6 - 65.5	65.5 - 65.4	65.4 - 65.3	65.3 - 65.2	65.2 - 65.1	65.1 - 65.0
CS59	0	0	0	0	0	1	0	0	0	0	0	0	0	0	0
CS60	0	0	0	1	0	1	0	1	0	1	0	1	0	0	0
CS61	0	0	0	0	0	0	1	0	0	1	0	0	0	0	0
CS62	0	0	0	1	0	0	0	0	0	0	0	0	0	0	0
CS63	0	0	0	1	0	0	0	0	0	0	0	0	0	0	0
CS64	0	0	0	0	0	1	0	0	0	0	0	0	0	0	0
CS65	0	0	0	0	0	1	0	0	0	0	0	0	0	0	0
CS66	0	0	0	0	1	0	0	0	0	0	0	0	0	0	0
CS67	0	0	1	0	0	0	0	0	0	0	0	0	0	0	0
CS68	0	0	0	1	0	0	0	0	0	0	0	0	0	0	0
CS69	0	0	0	0	0	0	0	0	0	1	0	0	0	0	0
CS70	0	0	0	1	0	0	0	0	0	0	0	0	0	0	0
CS71	1	0	0	1	0	0	0	1	1	0	1	1	0	0	1
CS72	0	0	0	1	0	0	0	0	0	0	0	0	0	0	0
CS73	0	0	0	0	0	0	0	0	0	0	0	1	0	1	0
CS74	1	0	1	0	0	0	0	0	0	0	0	0	0	0	0
CS75	1	0	0	0	0	1	1	1	0	0	0	0	0	1	0
CS76	1	0	0	1	0	1	1	1	0	1	0	1	1	1	0
CS77	0	0	0	0	0	0	1	1	0	0	0	0	0	1	0
CS78	1	0	1	1	0	1	1	1	0	0	0	1	0	0	0
CS79	0	0	0	1	1	0	0	0	0	0	0	0	0	0	0
CS80	0	0	0	1	0	0	0	0	0	0	0	0	0	0	0
CS81	0	0	0	1	1	0	0	1	0	0	0	0	0	0	0
CS82	0	0	0	0	0	0	1	0	0	0	0	1	0	1	0
CS83	0	0	0	0	0	1	1	1	0	1	0	1	0	0	1
CS84	1	0	0	0	0	0	0	0	0	0	0	0	0	0	0
CS85	0	0	0	0	0	1	0	1	0	1	1	1	0	0	0

Morph	66.5 - 66.4	66.4 - 66.3	66.3 - 66.2	66.2 - 66.1	66.1 - 66.032	66.032 - 65.9	65.9 - 65.8	65.8 - 65.7	65.7 - 65.6	65.6 - 65.5	65.5 - 65.4	65.4 - 65.3	65.3 - 65.2	65.2 - 65.1	65.1 - 65.0
CS86	1	0	0	1	0	0	1	0	0	0	0	0	0	0	0
CS87	1	0	0	0	0	0	0	0	0	0	0	0	0	0	0
CS88	0	0	0	0	0	0	0	0	0	0	0	0	0	1	0
CS89	0	0	0	0	0	0	0	1	0	0	0	0	0	0	0
CS90	0	0	0	0	0	0	1	0	0	0	0	0	0	1	0
CS91	0	0	0	1	0	1	1	1	0	0	0	0	0	0	1
CS92	0	0	0	0	0	1	1	1	0	0	1	0	0	1	0
CS93	0	0	1	0	1	0	0	0	0	0	0	0	0	0	0
CS94	0	0	0	1	0	0	0	0	0	0	0	0	0	0	0
CS95	0	0	0	1	1	1	1	1	0	1	0	1	1	1	1
CS96	0	0	0	0	0	0	1	1	0	0	0	0	0	0	0
CS97	0	0	0	1	0	0	0	0	0	0	0	0	0	0	0
CS98	0	0	0	0	0	0	0	0	0	1	0	0	0	0	0
CS99	0	0	0	0	0	0	0	1	0	0	0	0	0	0	0
CS100	0	0	0	0	0	1	1	0	0	0	0	0	0	0	0
CS101	0	0	0	0	0	1	1	0	0	0	0	1	0	0	0
CS102	0	0	0	0	0	0	0	0	0	0	0	1	0	0	0
CS103	0	0	0	0	0	0	0	0	0	0	0	1	0	1	0
CS104	0	0	0	0	0	0	0	1	0	0	0	0	0	1	0
CS105	0	0	0	1	0	0	0	0	0	0	0	0	0	0	0
CS106	0	0	0	1	1	1	1	0	0	0	0	0	0	0	0
CS107	0	0	0	1	0	0	0	0	0	0	0	0	0	0	0
CS108	1	0	0	0	0	0	0	0	0	0	0	0	0	0	0
CS109	0	0	0	1	0	0	1	0	0	0	0	0	0	0	0
CS110	0	0	0	1	0	1	0	0	0	0	0	0	0	0	0
CS111	0	0	0	0	0	0	0	0	0	1	0	1	0	0	0
CS112	0	0	0	0	0	1	1	1	0	1	0	1	0	1	0

Morph	66.5 - 66.4	66.4 - 66.3	66.3 - 66.2	66.2 - 66.1	66.1 - 66.032	66.032 - 65.9	65.9 - 65.8	65.8 - 65.7	65.7 - 65.6	65.6 - 65.5	65.5 - 65.4	65.4 - 65.3	65.3 - 65.2	65.2 - 65.1	65.1 - 65.0
CS113	0	0	0	0	0	0	0	0	0	1	0	0	0	0	0
CS114	0	0	0	0	0	0	1	0	0	0	0	0	0	0	0
CS115	1	0	1	1	0	0	0	0	0	0	0	0	0	0	0
CS116	0	0	0	0	0	1	0	0	0	0	0	0	0	0	0
CS117	0	0	0	0	0	0	1	0	0	0	0	0	0	1	0
CS118	0	0	0	0	1	0	0	0	0	0	0	0	0	0	0
CS119	0	0	1	0	0	0	0	0	0	1	0	0	0	0	0
CS120	0	0	0	0	0	1	1	0	0	0	0	0	0	0	0
CS121	0	0	0	0	0	1	0	0	0	0	0	0	0	0	0
CS122	0	0	1	0	0	0	0	0	0	0	0	0	0	0	0
CS123	0	0	0	0	0	0	0	1	0	0	0	0	0	1	0
CS124	0	0	0	0	1	0	0	0	0	0	0	0	0	0	0
CS125	0	0	0	1	0	0	0	0	0	0	0	0	0	0	0
CS126	0	0	0	1	0	0	0	0	0	0	0	0	0	0	0
CS127	0	0	0	0	0	0	1	0	0	0	0	0	0	0	0
CS128	0	0	0	1	0	0	0	0	0	0	0	0	0	0	0
CS129	0	0	0	0	0	0	1	0	0	0	0	0	0	0	0
CS130	0	0	0	0	0	0	1	0	0	1	0	0	0	0	0
CS131	0	0	0	1	0	0	0	0	0	0	0	0	0	0	0
CS132	0	0	1	1	0	0	0	0	0	0	0	0	0	0	0
CS133	0	0	0	1	1	0	0	0	0	0	0	0	0	0	0
CS134	0	0	0	0	0	0	0	1	0	0	0	0	0	0	0
CS135	0	0	0	0	0	0	0	0	0	0	0	0	0	0	1
CS136	0	0	0	0	0	0	1	0	0	0	0	1	0	1	0
CS137	1	0	0	0	0	0	0	0	0	0	0	0	0	0	0
CS138	1	0	0	0	0	0	0	0	0	0	0	0	0	0	0
CS139	0	0	0	0	0	0	1	0	0	0	0	0	0	0	0

Morph	66.5 - 66.4	66.4 - 66.3	66.3 - 66.2	66.2 - 66.1	66.1 - 66.032	66.032 - 65.9	65.9 - 65.8	65.8 - 65.7	65.7 - 65.6	65.6 - 65.5	65.5 - 65.4	65.4 - 65.3	65.3 - 65.2	65.2 - 65.1	65.1 - 65.0
CS140	0	0	0	1	1	0	0	0	0	0	0	0	0	0	0
CS141	0	0	0	0	0	1	1	1	0	0	0	0	0	1	0
CS142	1	0	0	0	0	0	0	0	0	0	0	0	0	0	0
CS143	0	0	0	0	0	1	1	0	0	0	0	0	0	0	0
CS144	0	0	0	1	0	0	0	0	0	0	0	0	0	0	0
CS145	0	0	0	0	0	0	0	0	0	0	0	1	0	0	0
CS146	0	0	0	0	0	0	1	0	0	0	0	0	0	0	0
CS147	0	0	0	0	0	0	1	0	0	0	0	1	0	0	0
CS148	0	0	0	1	0	0	0	0	0	0	0	0	0	0	0
CS149	0	0	1	0	0	0	0	0	0	0	0	0	0	0	0
CS150	0	0	1	0	0	0	0	0	0	0	0	0	0	0	0
CS151	1	0	0	0	0	0	0	0	0	0	0	0	0	0	0
CS152	0	0	0	0	0	0	0	0	0	0	0	0	0	1	0
CS153	0	0	0	1	0	0	0	0	0	0	0	0	0	0	0
CS154	0	0	0	0	0	0	0	1	0	0	0	0	0	0	0
CS155	0	0	0	0	0	1	0	1	0	0	0	1	0	0	0
CS156	0	0	0	1	0	0	0	0	0	0	0	0	0	0	0
CS157	0	0	0	0	1	0	0	0	0	0	0	0	0	0	0
CS158	0	0	0	1	0	0	0	0	0	0	0	0	0	0	0
CS159	0	0	0	0	1	0	0	0	0	0	0	0	0	0	0
CS160	0	0	0	0	0	0	0	0	0	1	0	0	0	0	0
CS161	0	0	0	0	0	0	1	0	0	1	0	1	0	0	0
CS162	0	0	0	0	0	0	0	0	0	0	0	0	0	1	0
CS163	0	0	0	0	0	0	1	0	0	0	0	0	0	0	0
CS164	0	0	0	0	1	0	0	0	0	0	0	0	0	0	0
CS165	0	0	0	0	0	0	0	0	0	1	0	0	0	0	0
CS166	0	0	0	0	0	0	0	0	0	0	0	0	0	1	0

Morph	66.5 - 66.4	66.4 - 66.3	66.3 - 66.2	66.2 - 66.1	66.1 - 66.032	66.032 - 65.9	65.9 - 65.8	65.8 - 65.7	65.7 - 65.6	65.6 - 65.5	65.5 - 65.4	65.4 - 65.3	65.3 - 65.2	65.2 - 65.1	65.1 - 65.0
CS167	0	0	0	0	0	0	1	0	0	0	0	0	0	0	0
CS168	0	0	0	0	0	1	1	0	0	0	0	0	0	0	0
CS169	0	0	0	1	0	0	0	0	0	0	0	0	0	0	0
CS170	1	0	0	0	0	0	0	0	0	0	0	0	0	0	0
CS171	0	0	0	1	0	0	0	0	0	0	0	0	0	0	0
CS172	0	0	0	0	0	0	1	1	0	0	0	0	0	0	0
CS173	1	0	0	0	0	0	0	0	0	0	0	0	0	0	0
CS174	1	0	0	0	0	0	0	0	0	0	0	0	0	0	0
CS175	1	0	0	0	0	0	0	0	0	0	0	0	0	0	0
CS176	0	0	0	0	0	0	1	0	0	0	0	0	0	1	0
CS177	0	0	0	1	1	0	0	0	0	0	0	0	0	0	0
CS178	0	0	0	1	0	0	0	0	0	0	0	0	0	0	0
CS179	0	0	0	1	0	0	0	0	0	0	0	0	0	0	0
CS180	0	0	0	1	0	1	0	0	0	0	0	0	0	0	0
CS181	0	0	0	0	0	0	0	1	0	0	0	1	0	1	1
CS182	0	0	0	1	0	0	0	0	0	0	0	0	0	0	0
CS183	0	0	0	0	0	0	0	1	0	0	0	0	0	0	0
CS184	0	0	0	0	0	0	1	0	0	1	0	0	0	0	0
CS185	0	0	0	0	0	0	1	0	0	0	0	0	0	0	0
CS186	0	0	0	0	0	0	1	0	0	0	0	0	0	0	0
CS187	0	0	0	1	0	0	0	0	0	0	0	0	0	0	0
CS188	0	0	0	0	0	1	1	1	0	1	0	1	0	0	0
CS189	0	0	0	0	0	0	0	0	0	1	0	0	0	0	0
CS190	0	0	0	1	1	0	0	0	0	0	0	0	0	0	0
CS191	0	0	0	0	0	0	0	0	0	0	0	0	0	1	0
CS192	0	0	0	0	0	0	1	0	0	0	0	0	0	0	0
CS193	0	0	0	0	0	1	0	0	0	0	0	0	0	0	0

Morph	66.5 - 66.4	66.4 - 66.3	66.3 - 66.2	66.2 - 66.1	66.1 - 66.032	66.032 - 65.9	65.9 - 65.8	65.8 - 65.7	65.7 - 65.6	65.6 - 65.5	65.5 - 65.4	65.4 - 65.3	65.3 - 65.2	65.2 - 65.1	65.1 - 65.0
CS194	0	0	0	0	0	1	0	0	0	0	0	0	0	0	0
CS195	0	0	0	0	0	0	0	0	0	1	0	0	0	0	0
CS196	0	0	1	0	0	0	0	0	0	0	0	0	0	0	0
CS197	0	0	0	0	0	0	0	0	0	0	0	1	0	0	0
CS198	1	0	0	0	0	0	0	0	0	0	0	0	0	0	0
CS199	0	0	0	0	0	0	0	0	0	0	0	1	0	0	0
CS200	0	0	0	1	0	0	0	0	0	0	0	0	0	0	0
CS201	0	0	0	0	1	0	0	0	0	0	0	0	0	0	0
CS202	0	0	0	0	0	0	1	1	0	1	0	0	0	0	0
CS203	0	0	0	1	0	0	0	0	0	0	0	0	0	0	0
CS204	0	0	0	0	0	1	0	0	0	0	0	0	0	0	0
CS205	0	0	0	1	0	0	1	0	0	0	0	0	0	0	0
CS206	0	0	0	1	0	0	0	0	0	0	0	0	0	0	0
CS207	0	0	0	0	1	0	0	0	0	0	0	0	0	0	0
CS208	0	0	0	0	0	1	0	0	0	0	0	0	0	0	0
CS209	0	0	0	1	0	0	0	0	0	0	0	0	0	0	0
CS210	0	0	0	1	0	0	0	0	0	0	0	0	0	0	0
CS211	0	0	0	0	0	1	0	0	0	0	0	0	0	0	0
CS212	0	0	0	0	0	0	0	0	0	1	0	0	0	0	0
CS213	0	0	0	0	0	0	1	0	0	0	0	0	0	0	0
CS214	0	0	0	0	0	0	0	1	0	0	0	0	0	1	0
CS215	0	0	0	0	0	0	0	0	0	1	0	0	0	0	0
CS216	0	0	0	0	1	0	0	0	0	0	0	0	0	0	0
CS217	1	0	0	0	0	0	0	0	0	0	0	0	0	0	0
CS218	0	0	0	0	0	0	0	1	0	0	0	0	0	0	0
CS219	0	0	0	0	0	0	0	0	0	0	0	1	0	0	0
CS220	1	0	0	0	0	0	0	0	0	0	0	0	0	0	0

Morph	66.5 - 66.4	66.4 - 66.3	66.3 - 66.2	66.2 - 66.1	66.1 - 66.032	66.032 - 65.9	65.9 - 65.8	65.8 - 65.7	65.7 - 65.6	65.6 - 65.5	65.5 - 65.4	65.4 - 65.3	65.3 - 65.2	65.2 - 65.1	65.1 - 65.0
CS221	0	0	0	0	0	1	0	0	0	1	0	0	0	0	0
CS227	0	0	0	1	0	0	0	0	0	0	0	0	0	0	0
CS228	0	0	0	0	0	0	1	0	0	0	0	0	0	0	0
CS229	0	0	0	0	0	1	0	1	0	0	0	0	0	0	0
CS230	0	0	0	0	0	0	0	0	0	1	0	0	0	0	0
CS232	0	0	0	1	0	0	0	0	0	0	0	0	0	0	0
CS233	0	0	0	1	0	0	0	0	0	0	0	0	0	0	0

Table H.3 – Williston Basin (Wilf and Johnson, 2004; Peppe, 2010) Floral Occurrence Data

Morph	66.7 - 66.6	67.6 - 66.5	66.6 - 66.5	66.5 - 66.4	66.4 - 66.3	66.3 - 66.2	66.2 - 66.1	66.1 - 66.032	66.032 - 65.9	65.9 - 65.8	65.8 - 65.7	65.7 - 65.6	65.6 - 65.5	65.5 - 65.4	65.4 - 65.3	65.3 - 65.2	65.2 - 65.1	65.1 - 65	65 - 64.9	64.9 - 64.8	64.8 - 64.7	64.7 - 64.6	64.6 - 64.5	64.5 - 64.4	64.4 - 64.3	64.3 - 64.2	64.2 - 64.1	64.1 - 64	64 - 63.9	63.9 - 63.8	63.8 - 63.7	63.7 - 63.6	63.6 - 63.5	63.5 - 63.4
FU01	0	0	0	0	0	0	0	0	1	1	1	1	1	1	1	0	0	0	0	0	0	1	1	0	0	0	0	0	0	0	0	0	0	0
FU02	0	0	1	1	1	1	1	1	1	1	0	1	1	1	1	0	0	1	0	0	0	0	0	0	0	0	0	0	0	0	0	0	0	0
FU03	1	0	1	0	0	0	0	0	0	0	0	1	1	0	1	1	0	0	0	0	0	0	1	0	0	0	0	0	1	0	1	0	0	0
FU04	1	0	0	0	0	0	0	1	1	1	0	1	1	1	1	0	0	0	1	0	0	0	1	0	0	0	0	0	1	0	1	0	0	0
FU05	1	0	1	0	0	0	0	1	1	0	1	1	0	1	1	1	0	0	1	0	0	1	1	0	0	0	0	0	1	1	1	1	0	1
FU07	0	0	0	0	0	0	0	1	1	0	1	1	1	1	1	0	0	0	0	0	0	0	0	0	0	0	0	1	0	1	0	0	0	0
FU09	0	0	0	0	0	0	0	1	1	0	1	0	0	0	1	0	0	0	0	0	0	0	0	0	0	0	0	0	0	0	0	0	0	0
FU10	0	0	0	0	0	0	0	0	0	0	0	0	0	0	1	0	0	0	0	0	0	0	0	0	0	0	0	0	0	0	0	0	0	0
FU100	0	0	0	0	0	0	0	0	0	0	1	0	0	0	0	0	0	0	0	0	0	0	0	0	0	0	0	0	0	0	0	0	0	0
FU101	0	0	0	0	0	0	0	0	0	0	0	0	1	0	0	0	0	0	0	0	0	0	0	0	0	0	0	0	0	0	0	0	0	0
FU102	0	0	0	0	0	0	0	0	0	0	1	0	1	0	0	0	0	0	0	0	0	0	0	0	0	0	0	0	0	0	0	0	0	0
FU103	0	0	0	0	0	0	0	0	0	0	0	0	1	0	0	0	0	0	0	0	0	0	0	0	0	0	0	0	0	0	0	0	0	0
FU104	0	0	0	0	0	0	0	0	0	0	0	0	1	0	0	0	0	0	0	0	0	0	0	0	0	0	0	0	0	0	0	0	0	0
FU105	0	0	0	0	0	0	0	0	0	0	0	0	1	0	0	0	0	0	0	0	0	0	0	0	0	0	0	0	0	0	0	0	0	0
FU106	0	0	0	0	0	0	0	0	0	0	0	0	1	0	0	0	0	0	0	0	0	0	0	0	0	0	0	0	0	0	0	0	0	0
FU107	0	0	0	0	0	0	0	0	0	0	0	0	1	0	0	0	0	0	0	0	0	0	0	0	0	0	0	0	0	0	0	0	0	0
FU108	0	0	0	0	0	0	0	0	0	0	0	0	1	0	0	0	0	0	0	0	0	0	0	0	0	0	0	0	0	0	0	0	0	0
FU109	0	0	0	0	0	0	0	0	0	1	0	0	0	0	0	0	0	0	0	0	0	0	0	0	0	0	0	0	0	0	0	0	0	0
FU12	0	0	0	0	0	0	0	0	0	0	0	0	0	0	1	0	0	0	0	0	0	0	0	0	0	0	0	0	0	0	0	0	0	0
FU14	0	0	0	0	0	0	0	0	0	0	0	0	0	0	1	0	0	0	0	0	0	0	0	0	0	0	0	0	0	0	0	0	0	0
FU15	0	0	0	0	0	0	0	0	0	0	0	0	0	0	1	0	0	0	0	0	0	0	0	0	0	0	0	0	0	0	0	0	0	0
FU16	0	0	0	0	0	1	0	1	1	1	1	1	1	1	1	1	0	1	1	0	0	1	1	0	0	0	0	0	1	1	1	1	0	0
FU17	0	0	0	0	0	0	0	0	0	0	0	0	0	0	1	0	0	0	0	0	0	0	0	0	0	0	0	0	0	0	0	0	0	0
FU18	0	0	0	0	0	0	0	0	0	0	0	0	0	0	1	0	0	0	0	0	0	0	0	0	0	0	0	0	0	0	0	0	0	0

Morph	66.7 - 66.6	67.6 - 66.5	66.6 - 66.5	66.5 - 66.4	66.4 - 66.3	66.3 - 66.2	66.2 - 66.1	66.1 - 66.032	66.032 - 65.9	65.9 - 65.8	65.8 - 65.7	65.7 - 65.6	65.6 - 65.5	65.5 - 65.4	65.4 - 65.3	65.3 - 65.2	65.2 - 65.1	65.1 - 65	65 - 64.9	64.9 - 64.8	64.8 - 64.7	64.7 - 64.6	64.6 - 64.5	64.5 - 64.4	64.4 - 64.3	64.3 - 64.2	64.2 - 64.1	64.1 - 64	64 - 63.9	63.9 - 63.8	63.8 - 63.7	63.7 - 63.6	63.6 - 63.5	63.5 - 63.4
FU19	0	0	0	0	0	0	0	0	1	0	0	0	0	0	1	0	0	0	0	0	0	0	0	0	0	0	0	0	0	0	0	0	0	0
FU20	0	0	0	0	0	0	0	0	0	0	0	0	0	0	1	0	0	0	0	0	0	0	0	0	0	0	0	0	0	0	0	0	0	0
FU21	0	0	0	0	0	0	0	0	0	0	0	0	0	0	1	0	0	0	0	0	0	0	0	0	0	0	0	0	0	0	0	0	0	0
FU23	0	0	0	0	0	0	0	0	1	0	0	0	0	0	1	0	0	0	0	0	0	0	0	0	0	0	0	0	0	0	0	0	0	0
FU24	0	0	0	0	0	0	0	0	0	0	0	0	0	0	1	0	0	0	0	0	0	0	0	0	0	0	0	0	0	0	0	0	0	0
FU25	0	0	0	0	0	0	0	1	0	1	1	0	0	0	0	0	0	0	1	0	0	0	0	0	0	0	0	0	0	0	0	0	0	0
FU26	1	0	0	0	0	1	0	1	1	1	0	1	0	0	0	0	0	0	1	0	0	1	0	0	0	0	0	0	0	0	0	0	0	0
FU29	0	0	0	0	0	1	0	1	1	1	1	1	1	1	1	0	0	0	1	0	0	1	1	0	0	0	0	0	0	1	1	1	0	0
FU31	0	0	1	0	0	0	1	1	1	1	1	1	1	1	0	1	0	0	0	0	0	0	1	0	0	0	0	0	0	0	0	0	0	0
FU35	0	0	0	0	0	0	0	0	1	0	0	0	0	0	0	0	0	0	0	0	0	0	0	0	0	0	0	0	0	0	0	0	0	0
FU36	0	0	0	0	0	0	0	0	1	0	0	1	0	0	0	0	0	0	0	0	0	1	0	0	0	0	0	0	0	0	0	0	0	1
FU37	1	0	0	1	0	1	1	1	1	0	1	0	1	0	0	0	0	0	0	0	0	0	0	0	0	0	0	0	0	0	0	0	0	0
FU38	0	0	1	0	0	1	0	0	1	0	0	1	1	1	0	0	0	0	0	0	0	0	0	0	0	0	0	0	0	0	0	0	0	0
FU39	0	0	0	0	0	0	0	0	1	0	0	0	0	0	0	0	0	0	0	0	0	0	0	0	0	0	0	0	0	0	0	0	0	0
FU40	0	0	0	0	0	0	0	0	1	0	0	0	0	0	0	0	0	0	0	0	0	0	0	0	0	0	0	0	0	0	0	0	0	0
FU42	0	0	0	0	0	0	0	1	0	0	0	0	0	0	0	0	0	0	0	0	0	0	0	0	0	0	0	0	0	0	0	0	0	0
FU43	1	0	1	0	0	0	0	1	1	1	0	1	1	1	1	1	0	0	1	0	0	0	0	1	0	0	0	0	0	0	1	1	0	0
FU45	0	0	0	0	0	0	0	0	0	0	0	0	0	0	1	0	0	0	0	0	0	0	0	0	0	0	0	0	0	0	0	0	0	0
FU46	0	0	0	1	0	0	0	0	0	0	0	0	0	0	1	0	0	0	0	0	0	0	0	0	0	0	0	0	0	0	0	0	0	0
FU47	0	0	0	0	0	1	0	0	0	0	1	0	0	0	0	0	0	0	1	0	0	0	0	0	0	0	0	0	0	0	0	0	0	0
FU48	0	0	0	0	0	0	0	0	0	0	0	0	0	1	0	0	0	0	0	0	0	0	0	0	0	0	0	0	0	0	0	0	0	0
FU49	1	0	0	0	0	0	0	0	1	0	0	1	0	0	0	0	0	0	0	0	0	0	0	0	0	0	0	0	0	0	0	0	0	0
FU51	0	0	0	0	0	0	0	0	1	0	0	0	0	0	0	0	0	0	0	0	0	1	0	0	0	0	0	0	0	0	0	0	0	0
FU52	0	0	0	0	0	0	0	0	1	0	0	0	0	0	0	0	0	0	0	0	0	0	0	0	0	0	0	0	0	0	0	0	0	0
FU53	0	0	0	0	0	0	0	0	1	0	0	0	0	0	0	0	0	0	0	0	0	0	0	0	0	0	0	0	0	0	0	0	0	0
FU54	0	0	0	0	0	0	0	0	1	0	0	0	0	0	0	0	0	0	0	0	0	0	0	0	0	0	0	0	0	0	0	0	0	0
FU55	0	0	0	0	0	0	0	0	1	0	0	0	0	0	0	0	0	0	0	0	0	0	0	0	0	0	0	0	0	0	0	0	0	0
FU56	0	0	0	0	0	0	0	0	1	0	0	0	0	0	0	0	0	0	0	0	0	0	0	0	0	0	0	0	0	0	0	0	0	0

Morph	66.7 - 66.6	67.6 - 66.5	66.6 - 66.5	66.5 - 66.4	66.4 - 66.3	66.3 - 66.2	66.2 - 66.1	66.1 - 66.032	66.032 - 65.9	65.9 - 65.8	65.8 - 65.7	65.7 - 65.6	65.6 - 65.5	65.5 - 65.4	65.4 - 65.3	65.3 - 65.2	65.2 - 65.1	65.1 - 65	65 - 64.9	64.9 - 64.8	64.8 - 64.7	64.7 - 64.6	64.6 - 64.5	64.5 - 64.4	64.4 - 64.3	64.3 - 64.2	64.2 - 64.1	64.1 - 64	64 - 63.9	63.9 - 63.8	63.8 - 63.7	63.7 - 63.6	63.6 - 63.5	63.5 - 63.4
FU57	0	0	0	0	0	0	0	0	1	0	0	0	0	0	0	0	0	0	0	0	0	0	0	0	0	0	0	0	0	0	0	0	0	0
FU60	1	0	0	0	0	0	0	0	1	0	0	0	0	0	0	0	0	0	0	0	0	0	0	0	0	0	0	0	0	0	0	0	0	0
FU61	0	0	0	0	0	1	0	1	1	0	1	0	1	0	0	0	0	0	0	0	0	0	0	0	0	0	0	0	0	0	0	0	0	0
FU62	0	0	1	0	0	1	1	1	1	1	0	0	0	0	0	0	0	0	0	0	0	0	0	0	0	0	0	0	0	0	0	0	0	0
FU63	0	0	1	0	0	0	0	0	1	0	0	0	0	0	0	0	0	0	0	0	0	0	0	0	0	0	0	0	0	0	0	0	0	0
FU64	0	0	0	0	0	0	0	0	1	0	0	0	0	0	0	0	0	0	0	0	0	0	0	0	0	0	0	0	0	0	0	0	0	0
FU65	0	0	0	0	0	0	0	0	1	0	0	0	0	0	0	0	0	0	0	0	0	0	0	0	0	0	0	0	0	0	0	0	0	0
FU69	0	0	0	0	0	0	0	0	1	0	0	0	0	0	0	0	0	0	0	0	0	0	0	0	0	0	0	0	0	0	0	0	0	0
FU70	0	0	0	0	0	0	0	0	1	0	0	0	0	0	0	0	0	0	0	0	0	0	0	0	0	0	0	0	0	0	0	0	0	0
FU72	0	0	0	0	0	0	0	0	1	0	0	0	0	0	0	0	0	0	0	0	0	0	0	0	0	0	0	0	0	0	0	0	0	0
FU73	0	0	0	0	0	0	0	0	1	0	0	0	0	0	0	0	0	0	0	0	0	0	0	0	0	0	0	0	0	0	0	0	0	0
FU74	0	0	0	0	0	0	0	0	1	0	0	0	0	0	0	0	0	0	0	0	0	0	0	0	0	0	0	0	0	0	0	0	0	0
FU75	0	0	0	0	0	0	0	0	0	0	0	1	0	0	0	0	0	0	0	0	0	0	0	0	0	0	0	0	0	0	0	0	0	0
FU76	0	0	0	0	0	0	0	0	1	0	1	0	0	0	0	0	0	0	0	0	0	0	0	0	0	0	0	0	0	0	0	0	0	0
FU77	0	0	0	0	0	0	0	0	0	0	1	0	0	0	0	0	0	0	0	0	0	0	0	0	0	0	0	0	0	0	0	0	0	0
FU78	0	0	0	0	0	0	0	0	1	1	1	0	0	0	0	0	0	0	0	0	0	0	0	0	0	0	0	0	0	0	0	0	0	0
FU79	0	0	0	0	0	0	0	0	1	0	0	0	0	0	0	0	0	0	0	0	0	0	0	0	0	0	0	0	0	0	0	0	0	0
FU80	0	0	0	0	0	0	0	0	1	0	0	0	0	0	0	0	0	0	0	0	0	0	0	0	0	0	0	0	0	0	0	0	0	0
FU81	0	0	0	0	0	1	1	1	0	0	0	0	0	0	0	0	0	0	0	0	0	0	0	0	0	0	0	0	0	0	0	0	0	0
FU83	0	0	0	0	0	0	0	0	1	0	0	1	0	0	0	0	0	0	0	0	0	0	0	0	0	0	0	0	0	0	0	0	0	0
FU84	0	0	0	0	0	0	0	0	1	0	0	0	0	0	0	0	0	0	0	0	0	0	0	0	0	0	0	0	0	0	0	0	0	0
FU86	0	0	0	0	0	0	0	0	1	0	0	0	0	0	0	0	0	0	0	0	0	0	0	0	0	0	0	0	0	0	0	0	0	0
FU87	0	0	0	0	0	0	0	0	1	0	0	0	0	0	0	0	0	0	0	0	0	0	0	0	0	0	0	0	0	0	0	0	0	0
FU89	0	0	0	0	0	0	0	0	0	1	0	0	0	0	0	0	0	0	0	0	0	0	0	0	0	0	0	0	0	0	0	0	0	0
FU90	0	0	0	0	0	0	0	0	0	0	0	1	0	0	0	0	0	0	0	0	0	0	0	0	0	0	0	0	0	0	0	0	0	0
FU94	0	0	0	0	0	0	0	0	1	0	0	0	0	0	0	0	0	0	0	0	0	0	0	0	0	0	0	0	0	0	0	0	0	0
FU95	0	0	0	0	0	0	0	1	0	0	0	0	0	0	0	0	0	0	0	0	0	0	0	0	0	0	0	0	0	0	0	0	0	0
FU96	0	0	0	0	0	0	0	1	0	0	0	0	0	0	0	0	0	0	0	0	0	0	0	0	0	0	0	0	0	0	0	0	0	0

Morph	66.7 - 66.6	67.6 - 66.5	66.6 - 66.5	66.5 - 66.4	66.4 - 66.3	66.3 - 66.2	66.2 - 66.1	66.1 - 66.032	66.032 - 65.9	65.9 - 65.8	65.8 - 65.7	65.7 - 65.6	65.6 - 65.5	65.5 - 65.4	65.4 - 65.3	65.3 - 65.2	65.2 - 65.1	65.1 - 65	65 - 64.9	64.9 - 64.8	64.8 - 64.7	64.7 - 64.6	64.6 - 64.5	64.5 - 64.4	64.4 - 64.3	64.3 - 64.2	64.2 - 64.1	64.1 - 64	64 - 63.9	63.9 - 63.8	63.8 - 63.7	63.7 - 63.6	63.6 - 63.5	63.5 - 63.4
FU97	0	0	0	0	0	0	0	0	0	0	0	0	0	0	0	1	0	0	0	0	0	0	0	0	0	0	0	0	0	0	0	0	0	0
FU99	0	0	0	0	0	0	0	0	0	0	1	0	0	0	0	0	0	0	0	0	0	0	0	0	0	0	0	0	0	0	0	0	0	0
HC106	1	0	0	0	1	1	1	1	0	0	0	0	0	0	0	0	0	0	0	0	0	0	0	0	0	0	0	0	0	0	0	0	0	0
HC002	1	0	1	0	0	1	1	1	0	0	0	0	0	0	0	0	0	0	0	0	0	0	0	0	0	0	0	0	0	0	0	0	0	0
HC003	0	0	0	0	0	1	1	0	0	0	0	0	0	0	0	0	0	0	0	0	0	0	0	0	0	0	0	0	0	0	0	0	0	0
HC004	0	0	0	0	1	1	1	1	0	0	0	0	0	0	0	0	0	0	0	0	0	0	0	0	0	0	0	0	0	0	0	0	0	0
HC005	0	0	0	0	0	1	0	0	0	0	0	0	0	0	0	0	0	0	0	0	0	0	0	0	0	0	0	0	0	0	0	0	0	0
HC008	0	0	0	0	1	0	0	0	0	0	0	0	0	0	0	0	0	0	0	0	0	0	0	0	0	0	0	0	0	0	0	0	0	0
HC009	0	1	1	0	1	0	0	0	0	0	0	0	0	0	0	0	0	0	0	0	0	0	0	0	0	0	0	0	0	0	0	0	0	0
HC011	0	0	0	0	1	0	0	0	0	0	0	0	0	0	0	0	0	0	0	0	0	0	0	0	0	0	0	0	0	0	0	0	0	0
HC012	0	0	0	0	0	1	0	1	1	0	0	0	1	0	0	0	0	0	0	0	0	0	0	0	0	0	0	0	0	0	0	0	0	0
HC014	1	1	1	1	1	1	1	0	0	0	0	0	0	0	0	0	0	0	0	0	0	0	0	0	0	0	0	0	0	0	0	0	0	0
HC015	0	1	0	0	0	0	0	0	0	0	0	0	0	0	0	0	0	0	0	0	0	0	0	0	0	0	0	0	0	0	0	0	0	0
HC017	0	1	0	0	0	0	0	0	0	0	0	0	0	0	0	0	0	0	0	0	0	0	0	0	0	0	0	0	0	0	0	0	0	0
HC018	0	0	1	0	0	0	0	0	0	0	0	0	0	0	0	0	0	0	0	0	0	0	0	0	0	0	0	0	0	0	0	0	0	0
HC020	0	0	1	0	0	0	0	0	0	0	0	0	0	0	0	0	0	0	0	0	0	0	0	0	0	0	0	0	0	0	0	0	0	0
HC021	0	0	1	0	0	0	0	0	0	0	0	0	0	0	0	0	0	0	0	0	0	0	0	0	0	0	0	0	0	0	0	0	0	0
HC022	0	0	1	0	0	0	0	0	0	0	0	0	0	0	0	0	0	0	0	0	0	0	0	0	0	0	0	0	0	0	0	0	0	0
HC023	0	0	1	0	0	0	0	0	1	0	0	0	0	0	0	0	0	0	0	0	0	0	0	0	0	0	0	0	0	0	0	0	0	0
HC024	0	0	1	0	0	0	0	0	0	0	0	0	0	0	0	0	0	0	0	0	0	0	0	0	0	0	0	0	0	0	0	0	0	0
HC025	0	0	1	0	0	0	0	0	0	0	0	0	0	0	0	0	0	0	0	0	0	0	0	0	0	0	0	0	0	0	0	0	0	0
HC027	1	1	1	0	0	0	0	1	0	0	0	0	0	0	0	0	0	0	0	0	0	0	0	0	0	0	0	0	0	0	0	0	0	0
HC028	1	0	1	0	0	0	0	0	0	0	0	0	0	0	0	0	0	0	0	0	0	0	0	0	0	0	0	0	0	0	0	0	0	0
HC029	0	0	1	0	0	0	0	0	0	0	0	0	0	0	0	0	0	0	0	0	0	0	0	0	0	0	0	0	0	0	0	0	0	0
HC031	0	0	1	0	0	0	0	0	0	0	0	0	0	0	0	0	0	0	0	0	0	0	0	0	0	0	0	0	0	0	0	0	0	0
HC032	1	1	1	0	0	1	0	0	0	0	0	0	0	0	0	0	0	0	0	0	0	0	0	0	0	0	0	0	0	0	0	0	0	0
HC034	0	0	1	0	0	0	0	0	0	0	0	0	0	0	0	0	0	0	0	0	0	0	0	0	0	0	0	0	0	0	0	0	0	0
HC035	1	0	1	0	0	0	1	0	0	0	0	0	0	0	0	0	0	0	0	0	0	0	0	0	0	0	0	0	0	0	0	0	0	0

Morph	66.7 - 66.6	67.6 - 66.5	66.6 - 66.5	66.5 - 66.4	66.4 - 66.3	66.3 - 66.2	66.2 - 66.1	66.1 - 66.032	66.032 - 65.9	65.9 - 65.8	65.8 - 65.7	65.7 - 65.6	65.6 - 65.5	65.5 - 65.4	65.4 - 65.3	65.3 - 65.2	65.2 - 65.1	65.1 - 65	65 - 64.9	64.9 - 64.8	64.8 - 64.7	64.7 - 64.6	64.6 - 64.5	64.5 - 64.4	64.4 - 64.3	64.3 - 64.2	64.2 - 64.1	64.1 - 64	64 - 63.9	63.9 - 63.8	63.8 - 63.7	63.7 - 63.6	63.6 - 63.5	63.5 - 63.4
HC036	1	0	1	0	1	1	1	1	0	0	0	0	0	0	0	0	0	0	0	0	0	0	0	0	0	0	0	0	0	0	0	0	0	0
HC040	1	0	0	0	0	0	0	0	0	0	0	0	0	0	0	0	0	0	0	0	0	0	0	0	0	0	0	0	0	0	0	0	0	0
HC043	1	0	1	0	1	1	1	1	0	0	0	0	0	0	0	0	0	0	0	0	0	0	0	0	0	0	0	0	0	0	0	0	0	0
HC044	0	0	0	1	1	1	1	1	0	0	0	0	0	0	0	0	0	0	0	0	0	0	0	0	0	0	0	0	0	0	0	0	0	0
HC047	0	0	0	0	0	1	0	1	0	0	0	0	0	0	0	0	0	0	0	0	0	0	0	0	0	0	0	0	0	0	0	0	0	0
HC049	1	1	1	1	1	1	1	1	0	0	0	0	0	0	0	0	0	0	0	0	0	0	0	0	0	0	0	0	0	0	0	0	0	0
HC052	1	0	0	1	1	0	1	0	0	0	0	0	0	0	0	0	0	0	0	0	0	0	0	0	0	0	0	0	0	0	0	0	0	0
HC055	1	0	0	1	0	0	0	0	0	0	0	0	0	0	0	0	0	0	0	0	0	0	0	0	0	0	0	0	0	0	0	0	0	0
HC056	1	0	0	1	0	0	0	0	0	0	0	0	0	0	0	0	0	0	0	0	0	0	0	0	0	0	0	0	0	0	0	0	0	0
HC057	1	1	1	1	0	1	1	1	0	0	0	0	0	0	0	0	0	0	0	0	0	0	0	0	0	0	0	0	0	0	0	0	0	0
HC058	1	0	0	1	0	0	0	0	0	0	0	0	0	0	0	0	0	0	0	0	0	0	0	0	0	0	0	0	0	0	0	0	0	0
HC060	0	0	1	0	0	0	0	0	0	0	0	0	0	0	0	0	0	0	0	0	0	0	0	0	0	0	0	0	0	0	0	0	0	0
HC062	1	1	1	1	1	1	1	1	0	0	0	0	0	0	0	0	0	0	0	0	0	0	0	0	0	0	0	0	0	0	0	0	0	0
HC063	1	0	1	0	0	1	0	0	0	0	0	0	0	0	0	0	0	0	0	0	0	0	0	0	0	0	0	0	0	0	0	0	0	0
HC065	0	0	1	0	0	0	0	1	0	0	0	0	0	0	0	0	0	0	0	0	0	0	0	0	0	0	0	0	0	0	0	0	0	0
HC066	1	0	1	0	1	1	1	0	0	0	0	0	0	0	0	0	0	0	0	0	0	0	0	0	0	0	0	0	0	0	0	0	0	0
HC067	0	0	1	0	0	0	0	0	0	0	0	0	0	0	0	0	0	0	0	0	0	0	0	0	0	0	0	0	0	0	0	0	0	0
HC068	0	0	1	0	0	0	0	0	0	0	0	0	0	0	0	0	0	0	0	0	0	0	0	0	0	0	0	0	0	0	0	0	0	0
HC070	1	0	0	0	1	1	1	0	0	0	0	0	0	0	0	0	0	0	0	0	0	0	0	0	0	0	0	0	0	0	0	0	0	0
HC071	1	0	1	0	0	0	1	1	1	0	0	0	0	0	0	1	0	0	0	0	0	0	0	0	0	0	0	0	0	0	0	0	0	0
HC072	1	0	0	0	0	0	0	0	0	0	0	0	0	0	0	0	0	0	0	0	0	0	0	0	0	0	0	0	0	0	0	0	0	0
HC073	1	0	0	0	0	0	0	0	0	0	0	0	0	0	0	0	0	0	0	0	0	0	0	0	0	0	0	0	0	0	0	0	0	0
HC074	1	0	0	0	0	0	0	0	0	0	0	0	0	0	0	0	0	0	0	0	0	0	0	0	0	0	0	0	0	0	0	0	0	0
HC075	1	0	0	0	0	0	0	0	0	0	0	0	0	0	0	0	0	0	0	0	0	0	0	0	0	0	0	0	0	0	0	0	0	0
HC076	1	0	1	0	0	0	0	0	0	0	0	0	0	0	0	0	0	0	0	0	0	0	0	0	0	0	0	0	0	0	0	0	0	0
HC077	1	0	1	0	0	0	0	0	0	0	0	0	0	0	0	0	0	0	0	0	0	0	0	0	0	0	0	0	0	0	0	0	0	0
HC078	1	0	0	0	0	0	0	0	0	0	0	0	0	0	0	0	0	0	0	0	0	0	0	0	0	0	0	0	0	0	0	0	0	0
HC080	1	0	1	0	0	0	0	0	0	0	0	0	0	0	0	0	0	0	0	0	0	0	0	0	0	0	0	0	0	0	0	0	0	0

Morph	66.7 - 66.6	67.6 - 66.5	66.6 - 66.5	66.5 - 66.4	66.4 - 66.3	66.3 - 66.2	66.2 - 66.1	66.1 - 66.032	66.032 - 65.9	65.9 - 65.8	65.8 - 65.7	65.7 - 65.6	65.6 - 65.5	65.5 - 65.4	65.4 - 65.3	65.3 - 65.2	65.2 - 65.1	65.1 - 65	65 - 64.9	64.9 - 64.8	64.8 - 64.7	64.7 - 64.6	64.6 - 64.5	64.5 - 64.4	64.4 - 64.3	64.3 - 64.2	64.2 - 64.1	64.1 - 64	64 - 63.9	63.9 - 63.8	63.8 - 63.7	63.7 - 63.6	63.6 - 63.5	63.5 - 63.4
HC081	1	0	1	0	0	0	0	0	0	0	0	0	0	0	0	0	0	0	0	0	0	0	0	0	0	0	0	0	0	0	0	0	0	0
HC084	1	0	1	0	0	0	0	0	0	0	0	0	0	0	0	0	0	0	0	0	0	0	0	0	0	0	0	0	0	0	0	0	0	0
HC085	1	0	0	0	0	0	0	0	0	0	0	0	0	0	0	0	0	0	0	0	0	0	0	0	0	0	0	0	0	0	0	0	0	0
HC086	1	1	1	0	0	0	0	0	0	0	0	0	0	0	0	0	0	0	0	0	0	0	0	0	0	0	0	0	0	0	0	0	0	0
HC087	1	0	0	0	0	0	0	0	0	0	0	0	0	0	0	0	0	0	0	0	0	0	0	0	0	0	0	0	0	0	0	0	0	0
HC088	1	0	0	0	0	0	0	0	0	0	0	0	0	0	0	0	0	0	0	0	0	0	0	0	0	0	0	0	0	0	0	0	0	0
HC090	1	0	1	0	0	0	0	0	0	0	0	0	0	0	0	0	0	0	0	0	0	0	0	0	0	0	0	0	0	0	0	0	0	0
HC091	1	0	0	0	0	0	0	0	0	0	0	0	0	0	0	0	0	0	0	0	0	0	0	0	0	0	0	0	0	0	0	0	0	0
HC092	1	0	1	0	0	0	0	0	0	0	0	0	0	0	0	0	0	0	0	0	0	0	0	0	0	0	0	0	0	0	0	0	0	0
HC093	1	0	1	0	0	0	0	0	0	0	0	0	0	0	0	0	0	0	0	0	0	0	0	0	0	0	0	0	0	0	0	0	0	0
HC094	1	1	1	0	0	0	0	0	0	0	0	0	0	0	0	0	0	0	0	0	0	0	0	0	0	0	0	0	0	0	0	0	0	0
HC096	1	0	0	0	0	0	0	0	0	0	0	0	0	0	0	0	0	0	0	0	0	0	0	0	0	0	0	0	0	0	0	0	0	0
HC098	1	0	0	0	0	0	0	0	0	0	0	0	0	0	0	0	0	0	0	0	0	0	0	0	0	0	0	0	0	0	0	0	0	0
HC099	1	0	0	0	0	1	0	0	0	0	0	0	0	0	0	0	0	0	0	0	0	0	0	0	0	0	0	0	0	0	0	0	0	0
HC100	1	0	0	1	0	0	0	0	0	0	0	0	0	0	0	0	0	0	0	0	0	0	0	0	0	0	0	0	0	0	0	0	0	0
HC103	1	0	1	0	1	1	1	1	0	0	0	0	0	0	0	0	0	0	0	0	0	0	0	0	0	0	0	0	0	0	0	0	0	0
HC105	0	0	1	0	1	1	1	1	0	0	0	0	0	0	0	0	0	0	0	0	0	0	0	0	0	0	0	0	0	0	0	0	0	0
HC108	1	1	1	1	1	0	0	0	0	0	0	0	0	0	0	0	0	0	0	0	0	0	0	0	0	0	0	0	0	0	0	0	0	0
HC111	0	0	0	0	1	1	1	1	0	0	0	0	0	0	0	0	0	0	0	0	0	0	0	0	0	0	0	0	0	0	0	0	0	0
HC114	1	0	1	0	0	0	0	0	0	0	0	0	0	0	0	0	0	0	0	0	0	0	0	0	0	0	0	0	0	0	0	0	0	0
HC115	0	0	0	0	0	1	0	0	0	0	0	0	0	0	0	0	0	0	0	0	0	0	0	0	0	0	0	0	0	0	0	0	0	0
HC122	1	0	0	0	0	0	0	0	0	0	0	0	0	0	0	0	0	0	0	0	0	0	0	0	0	0	0	0	0	0	0	0	0	0
HC123	1	0	1	0	0	0	0	0	1	0	0	0	0	0	0	0	0	0	0	0	0	0	0	0	0	0	0	0	0	0	0	0	0	0
HC124	1	0	1	0	0	0	0	0	0	0	0	0	0	0	0	0	0	0	0	0	0	0	0	0	0	0	0	0	0	0	0	0	0	0
HC126	1	0	0	0	0	0	0	0	0	0	0	0	0	0	0	0	0	0	0	0	0	0	0	0	0	0	0	0	0	0	0	0	0	0
HC127	1	0	0	0	0	0	0	0	0	0	0	0	0	0	0	0	0	0	0	0	0	0	0	0	0	0	0	0	0	0	0	0	0	0
HC128	1	0	0	0	0	0	0	0	0	0	0	0	0	0	0	0	0	0	0	0	0	0	0	0	0	0	0	0	0	0	0	0	0	0
HC129	1	0	1	0	0	0	0	0	0	0	0	0	0	0	0	0	0	0	0	0	0	0	0	0	0	0	0	0	0	0	0	0	0	0

Morph	66.7 - 66.6	67.6 - 66.5	66.6 - 66.5	66.5 - 66.4	66.4 - 66.3	66.3 - 66.2	66.2 - 66.1	66.1 - 66.032	66.032 - 65.9	65.9 - 65.8	65.8 - 65.7	65.7 - 65.6	65.6 - 65.5	65.5 - 65.4	65.4 - 65.3	65.3 - 65.2	65.2 - 65.1	65.1 - 65	65 - 64.9	64.9 - 64.8	64.8 - 64.7	64.7 - 64.6	64.6 - 64.5	64.5 - 64.4	64.4 - 64.3	64.3 - 64.2	64.2 - 64.1	64.1 - 64	64 - 63.9	63.9 - 63.8	63.8 - 63.7	63.7 - 63.6	63.6 - 63.5	63.5 - 63.4
HC131	1	0	0	0	0	0	0	0	0	0	0	0	0	0	0	0	0	0	0	0	0	0	0	0	0	0	0	0	0	0	0	0	0	0
HC132	1	0	0	0	0	0	0	0	0	0	0	0	0	0	0	0	0	0	0	0	0	0	0	0	0	0	0	0	0	0	0	0	0	0
HC135	1	0	1	0	0	0	0	0	0	0	0	0	0	0	0	0	0	0	0	0	0	0	0	0	0	0	0	0	0	0	0	0	0	0
HC136	1	0	0	0	0	0	0	0	0	0	0	0	0	0	0	0	0	0	0	0	0	0	0	0	0	0	0	0	0	0	0	0	0	0
HC137	1	0	1	0	0	0	1	1	1	0	0	0	0	0	0	0	0	0	0	0	0	0	0	0	0	0	0	0	0	0	0	0	0	0
HC138	1	0	0	0	0	0	0	0	0	0	0	0	0	0	0	0	0	0	0	0	0	0	0	0	0	0	0	0	0	0	0	0	0	0
HC140	1	0	0	0	0	0	0	0	1	0	0	0	0	0	0	0	0	0	0	0	0	0	0	0	0	0	0	0	0	0	0	0	0	0
HC141	1	0	0	0	0	0	0	0	0	0	0	0	0	0	0	0	0	0	0	0	0	0	0	0	0	0	0	0	0	0	0	0	0	0
HC142	1	0	0	0	0	0	0	0	0	0	0	0	0	0	0	0	0	0	0	0	0	0	0	0	0	0	0	0	0	0	0	0	0	0
HC147	0	1	0	0	0	0	0	0	0	0	0	0	0	0	0	0	0	0	0	0	0	0	0	0	0	0	0	0	0	0	0	0	0	0
HC148	1	0	0	0	0	0	0	0	0	0	0	0	0	0	0	0	0	0	0	0	0	0	0	0	0	0	0	0	0	0	0	0	0	0
HC150	1	0	0	0	0	0	0	0	0	0	0	0	0	0	0	0	0	0	0	0	0	0	0	0	0	0	0	0	0	0	0	0	0	0
HC152	1	0	0	0	0	0	0	0	0	0	0	0	0	0	0	0	0	0	0	0	0	0	0	0	0	0	0	0	0	0	0	0	0	0
HC154	1	0	0	0	0	0	0	0	0	0	0	0	0	0	0	0	0	0	0	0	0	0	0	0	0	0	0	0	0	0	0	0	0	0
HC155	1	0	0	0	0	0	0	0	0	0	0	0	0	0	0	0	0	0	0	0	0	0	0	0	0	0	0	0	0	0	0	0	0	0
HC158	1	0	0	0	0	0	0	0	0	0	0	0	0	0	0	0	0	0	0	0	0	0	0	0	0	0	0	0	0	0	0	0	0	0
HC159	1	0	0	0	0	0	0	0	0	0	0	0	0	0	0	0	0	0	0	0	0	0	0	0	0	0	0	0	0	0	0	0	0	0
HC161	1	0	0	0	0	0	0	0	0	0	0	0	0	0	0	0	0	0	0	0	0	0	0	0	0	0	0	0	0	0	0	0	0	0
HC162	0	1	1	0	1	1	1	1	0	0	0	0	0	0	0	0	0	0	0	0	0	0	0	0	0	0	0	0	0	0	0	0	0	0
HC163	0	0	0	0	0	1	1	0	0	0	0	0	0	0	0	0	0	0	0	0	0	0	0	0	0	0	0	0	0	0	0	0	0	0
HC164	1	0	1	0	0	0	1	1	0	0	0	0	0	0	0	0	0	0	0	0	0	0	0	0	0	0	0	0	0	0	0	0	0	0
HC165	1	0	0	0	1	1	1	0	0	0	0	0	0	0	0	0	0	0	0	0	0	0	0	0	0	0	0	0	0	0	0	0	0	0
HC166	0	0	0	0	1	1	1	1	0	0	0	0	0	0	0	0	0	0	0	0	0	0	0	0	0	0	0	0	0	0	0	0	0	0
HC168	0	0	0	0	0	0	1	0	0	0	0	0	0	0	0	0	0	0	0	0	0	0	0	0	0	0	0	0	0	0	0	0	0	0
HC169	0	0	1	0	0	1	1	0	0	0	0	0	0	0	0	0	0	0	0	0	0	0	0	0	0	0	0	0	0	0	0	0	0	0
HC171	0	0	0	0	0	0	1	0	0	0	0	0	0	0	0	0	0	0	0	0	0	0	0	0	0	0	0	0	0	0	0	0	0	0
HC172	0	0	0	0	0	0	1	0	0	0	0	0	0	0	0	0	0	0	0	0	0	0	0	0	0	0	0	0	0	0	0	0	0	0
HC174	0	0	0	0	0	1	1	1	0	0	0	0	0	0	0	0	0	0	0	0	0	0	0	0	0	0	0	0	0	0	0	0	0	0

Morph	66.7 - 66.6	67.6 - 66.5	66.6 - 66.5	66.5 - 66.4	66.4 - 66.3	66.3 - 66.2	66.2 - 66.1	66.1 - 66.032	66.032 - 65.9	65.9 - 65.8	65.8 - 65.7	65.7 - 65.6	65.6 - 65.5	65.5 - 65.4	65.4 - 65.3	65.3 - 65.2	65.2 - 65.1	65.1 - 65	65 - 64.9	64.9 - 64.8	64.8 - 64.7	64.7 - 64.6	64.6 - 64.5	64.5 - 64.4	64.4 - 64.3	64.3 - 64.2	64.2 - 64.1	64.1 - 64	64 - 63.9	63.9 - 63.8	63.8 - 63.7	63.7 - 63.6	63.6 - 63.5	63.5 - 63.4
HC175	0	0	0	0	0	1	1	1	0	0	0	0	0	0	0	0	0	0	0	0	0	0	0	0	0	0	0	0	0	0	0	0	0	0
HC176	0	0	0	0	0	1	0	0	0	0	0	0	0	0	0	0	0	0	0	0	0	0	0	0	0	0	0	0	0	0	0	0	0	0
HC179	0	0	1	0	1	1	1	1	0	0	0	0	0	0	0	0	0	0	0	0	0	0	0	0	0	0	0	0	0	0	0	0	0	0
HC180	0	0	0	0	0	1	0	0	0	0	0	0	0	0	0	0	0	0	0	0	0	0	0	0	0	0	0	0	0	0	0	0	0	0
HC182	0	0	0	0	0	1	0	0	0	0	0	0	0	0	0	0	0	0	0	0	0	0	0	0	0	0	0	0	0	0	0	0	0	0
HC183	0	0	0	0	0	1	0	0	0	0	0	0	0	0	0	0	0	0	0	0	0	0	0	0	0	0	0	0	0	0	0	0	0	0
HC185	0	0	0	0	0	1	0	0	0	0	0	0	0	0	0	0	0	0	0	0	0	0	0	0	0	0	0	0	0	0	0	0	0	0
HC186	0	0	0	0	0	1	0	0	0	0	0	0	0	0	0	0	0	0	0	0	0	0	0	0	0	0	0	0	0	0	0	0	0	0
HC187	0	0	0	0	0	1	0	0	0	0	0	0	0	0	0	0	0	0	0	0	0	0	0	0	0	0	0	0	0	0	0	0	0	0
HC188	0	0	0	1	0	0	0	0	0	0	0	0	0	0	0	0	0	0	0	0	0	0	0	0	0	0	0	0	0	0	0	0	0	0
HC189	0	0	1	1	0	1	0	0	0	0	0	0	0	0	0	0	0	0	0	0	0	0	0	0	0	0	0	0	0	0	0	0	0	0
HC190	0	0	0	1	0	0	0	0	0	0	0	0	0	0	0	0	0	0	0	0	0	0	0	0	0	0	0	0	0	0	0	0	0	0
HC193	0	0	1	0	0	0	0	0	0	0	0	0	0	0	0	0	0	0	0	0	0	0	0	0	0	0	0	0	0	0	0	0	0	0
HC194	0	0	1	0	0	0	0	0	0	0	0	0	0	0	0	0	0	0	0	0	0	0	0	0	0	0	0	0	0	0	0	0	0	0
HC196	1	0	1	0	0	0	0	0	0	0	0	0	0	0	0	0	0	0	0	0	0	0	0	0	0	0	0	0	0	0	0	0	0	0
HC197	1	0	0	0	0	0	0	0	0	0	0	0	0	0	0	0	0	0	0	0	0	0	0	0	0	0	0	0	0	0	0	0	0	0
HC198	1	0	0	0	0	0	0	0	0	0	0	0	0	0	0	0	0	0	0	0	0	0	0	0	0	0	0	0	0	0	0	0	0	0
HC199	0	0	0	0	0	1	1	0	0	0	0	0	0	0	0	0	0	0	0	0	0	0	0	0	0	0	0	0	0	0	0	0	0	0
HC200	0	0	0	0	1	1	1	0	0	0	0	0	0	0	0	0	0	0	0	0	0	0	0	0	0	0	0	0	0	0	0	0	0	0
HC201	0	0	0	0	0	1	0	0	0	0	0	0	0	0	0	0	0	0	0	0	0	0	0	0	0	0	0	0	0	0	0	0	0	0
HC202	0	0	0	0	0	1	0	0	0	0	0	0	0	0	0	0	0	0	0	0	0	0	0	0	0	0	0	0	0	0	0	0	0	0
HC203	0	0	0	0	0	1	0	0	0	0	0	0	0	0	0	0	0	0	0	0	0	0	0	0	0	0	0	0	0	0	0	0	0	0
HC204	0	0	0	0	1	1	0	0	0	0	0	0	0	0	0	0	0	0	0	0	0	0	0	0	0	0	0	0	0	0	0	0	0	0
HC207	0	0	0	0	0	1	0	0	0	0	0	0	0	0	0	0	0	0	0	0	0	0	0	0	0	0	0	0	0	0	0	0	0	0
HC208	0	0	0	0	0	0	0	1	0	0	0	0	0	0	0	0	0	0	0	0	0	0	0	0	0	0	0	0	0	0	0	0	0	0
HC209	1	0	0	0	1	0	1	0	0	0	0	0	0	0	0	0	0	0	0	0	0	0	0	0	0	0	0	0	0	0	0	0	0	0
HC210	1	0	0	0	0	0	0	0	0	0	0	0	0	0	0	0	0	0	0	0	0	0	0	0	0	0	0	0	0	0	0	0	0	0
HC211	1	0	0	0	0	0	0	0	0	0	0	0	0	0	0	0	0	0	0	0	0	0	0	0	0	0	0	0	0	0	0	0	0	0

Morph	66.7 - 66.6	67.6 - 66.5	66.6 - 66.5	66.5 - 66.4	66.4 - 66.3	66.3 - 66.2	66.2 - 66.1	66.1 - 66.032	66.032 - 65.9	65.9 - 65.8	65.8 - 65.7	65.7 - 65.6	65.6 - 65.5	65.5 - 65.4	65.4 - 65.3	65.3 - 65.2	65.2 - 65.1	65.1 - 65	65 - 64.9	64.9 - 64.8	64.8 - 64.7	64.7 - 64.6	64.6 - 64.5	64.5 - 64.4	64.4 - 64.3	64.3 - 64.2	64.2 - 64.1	64.1 - 64	64 - 63.9	63.9 - 63.8	63.8 - 63.7	63.7 - 63.6	63.6 - 63.5	63.5 - 63.4
HC212	1	1	1	0	0	1	0	0	1	0	0	0	0	0	0	0	0	0	0	0	0	0	0	0	0	0	0	0	0	0	0	0	0	0
HC213	1	0	0	0	0	0	0	0	0	0	0	0	0	0	0	0	0	0	0	0	0	0	0	0	0	0	0	0	0	0	0	0	0	0
HC214	1	0	0	0	0	0	0	0	0	0	0	0	0	0	0	0	0	0	0	0	0	0	0	0	0	0	0	0	0	0	0	0	0	0
HC216	1	0	0	0	0	0	0	0	0	0	0	0	0	0	0	0	0	0	0	0	0	0	0	0	0	0	0	0	0	0	0	0	0	0
HC217	1	0	0	0	0	0	0	0	0	0	0	0	0	0	0	0	0	0	0	0	0	0	0	0	0	0	0	0	0	0	0	0	0	0
HC223	1	0	0	0	0	0	0	0	0	0	0	0	0	0	0	0	0	0	0	0	0	0	0	0	0	0	0	0	0	0	0	0	0	0
HC224	1	0	0	0	0	0	0	0	0	0	0	0	0	0	0	0	0	0	0	0	0	0	0	0	0	0	0	0	0	0	0	0	0	0
HC225	1	0	1	0	0	0	0	0	0	0	0	0	0	0	0	0	0	0	0	0	0	0	0	0	0	0	0	0	0	0	0	0	0	0
HC226	1	0	1	0	0	0	0	0	0	0	0	0	0	0	0	0	0	0	0	0	0	0	0	0	0	0	0	0	0	0	0	0	0	0
HC227	1	0	0	0	0	0	0	0	0	0	0	0	0	0	0	0	0	0	0	0	0	0	0	0	0	0	0	0	0	0	0	0	0	0
HC228	1	0	0	0	0	0	0	0	0	0	0	0	0	0	0	0	0	0	0	0	0	0	0	0	0	0	0	0	0	0	0	0	0	0
HC229	1	0	0	0	0	0	0	0	0	0	0	0	0	0	0	0	0	0	0	0	0	0	0	0	0	0	0	0	0	0	0	0	0	0
HC230	1	0	0	0	0	0	0	0	0	0	0	0	0	0	0	0	0	0	0	0	0	0	0	0	0	0	0	0	0	0	0	0	0	0
HC231	1	0	0	0	0	0	0	0	1	0	0	0	0	0	0	0	0	0	0	0	0	0	0	0	0	0	0	0	0	0	0	0	0	0
HC232	1	0	0	0	0	0	0	0	0	0	0	0	0	0	0	0	0	0	0	0	0	0	0	0	0	0	0	0	0	0	0	0	0	0
HC233	1	0	0	0	0	0	0	0	0	0	0	0	0	0	0	0	0	0	0	0	0	0	0	0	0	0	0	0	0	0	0	0	0	0
HC234	1	0	0	0	0	0	0	0	0	0	0	0	0	0	0	0	0	0	0	0	0	0	0	0	0	0	0	0	0	0	0	0	0	0
HC241	1	0	1	0	0	0	0	0	0	0	0	0	0	0	0	0	0	0	0	0	0	0	0	0	0	0	0	0	0	0	0	0	0	0
HC242	0	0	1	0	1	0	0	0	0	0	0	0	0	0	0	0	0	0	0	0	0	0	0	0	0	0	0	0	0	0	0	0	0	0
HC243	0	0	1	0	0	0	0	0	0	0	0	0	0	0	0	0	0	0	0	0	0	0	0	0	0	0	0	0	0	0	0	0	0	0
HC244	0	0	1	0	0	0	0	0	0	0	0	0	0	0	0	0	0	0	0	0	0	0	0	0	0	0	0	0	0	0	0	0	0	0
HC245	0	0	1	0	0	0	0	0	0	0	0	0	0	0	0	0	0	0	0	0	0	0	0	0	0	0	0	0	0	0	0	0	0	0
HC246	0	0	1	0	0	0	0	0	0	0	0	0	0	0	0	0	0	0	0	0	0	0	0	0	0	0	0	0	0	0	0	0	0	0
HC247	0	0	1	0	1	0	0	0	0	0	0	0	0	0	0	0	0	0	0	0	0	0	0	0	0	0	0	0	0	0	0	0	0	0
HC248	0	0	0	0	1	1	0	0	0	0	0	0	0	0	0	0	0	0	0	0	0	0	0	0	0	0	0	0	0	0	0	0	0	0
HC249	0	0	0	0	1	0	0	0	0	0	0	0	0	0	0	0	0	0	0	0	0	0	0	0	0	0	0	0	0	0	0	0	0	0
HC250	0	0	0	0	1	0	0	0	0	0	0	0	0	0	0	0	0	0	0	0	0	0	0	0	0	0	0	0	0	0	0	0	0	0
HC251	0	0	1	0	0	0	0	0	0	0	0	0	0	0	0	0	0	0	0	0	0	0	0	0	0	0	0	0	0	0	0	0	0	0

Morph	66.7 - 66.6	67.6 - 66.5	66.6 - 66.5	66.5 - 66.4	66.4 - 66.3	66.3 - 66.2	66.2 - 66.1	66.1 - 66.032	66.032 - 65.9	65.9 - 65.8	65.8 - 65.7	65.7 - 65.6	65.6 - 65.5	65.5 - 65.4	65.4 - 65.3	65.3 - 65.2	65.2 - 65.1	65.1 - 65	65 - 64.9	64.9 - 64.8	64.8 - 64.7	64.7 - 64.6	64.6 - 64.5	64.5 - 64.4	64.4 - 64.3	64.3 - 64.2	64.2 - 64.1	64.1 - 64	64 - 63.9	63.9 - 63.8	63.8 - 63.7	63.7 - 63.6	63.6 - 63.5	63.5 - 63.4
HC253	1	0	0	0	1	0	0	0	0	0	0	0	0	0	0	0	0	0	0	0	0	0	0	0	0	0	0	0	0	0	0	0	0	0
HC254	0	0	1	0	1	1	0	0	0	0	0	0	0	0	0	0	0	0	0	0	0	0	0	0	0	0	0	0	0	0	0	0	0	0
HC255	0	0	0	0	1	0	0	0	0	0	0	0	0	0	0	0	0	0	0	0	0	0	0	0	0	0	0	0	0	0	0	0	0	0
HC258	0	0	0	0	1	0	0	0	0	0	0	0	0	0	0	0	0	0	0	0	0	0	0	0	0	0	0	0	0	0	0	0	0	0
HC260	0	0	1	0	0	0	0	0	0	0	0	0	0	0	0	0	0	0	0	0	0	0	0	0	0	0	0	0	0	0	0	0	0	0
HC261	0	0	1	0	0	1	1	1	0	0	0	0	0	0	0	0	0	0	0	0	0	0	0	0	0	0	0	0	0	0	0	0	0	0
HC262	1	0	0	0	0	0	1	0	0	0	0	0	0	0	0	0	0	0	0	0	0	0	0	0	0	0	0	0	0	0	0	0	0	0
HC263	0	0	0	0	0	0	1	1	0	0	0	0	0	0	0	0	0	0	0	0	0	0	0	0	0	0	0	0	0	0	0	0	0	0
HC264	0	0	0	0	0	1	0	1	0	0	0	0	0	0	0	0	0	0	0	0	0	0	0	0	0	0	0	0	0	0	0	0	0	0
HC265	0	0	0	0	0	1	0	1	0	0	0	0	0	0	0	0	0	0	0	0	0	0	0	0	0	0	0	0	0	0	0	0	0	0
HC266	0	0	0	0	0	0	1	0	0	0	0	0	0	0	0	0	0	0	0	0	0	0	0	0	0	0	0	0	0	0	0	0	0	0
HC267	0	0	1	0	0	0	0	0	0	0	0	0	0	0	0	0	0	0	0	0	0	0	0	0	0	0	0	0	0	0	0	0	0	0
HC268	1	0	1	1	0	0	0	0	0	0	0	0	0	0	0	0	0	0	0	0	0	0	0	0	0	0	0	0	0	0	0	0	0	0
HC269	0	0	1	0	0	0	0	0	0	0	0	0	0	0	0	0	0	0	0	0	0	0	0	0	0	0	0	0	0	0	0	0	0	0
HC270	0	0	1	0	0	0	0	0	0	0	0	0	0	0	0	0	0	0	0	0	0	0	0	0	0	0	0	0	0	0	0	0	0	0
HC271	1	0	0	0	0	0	0	0	0	0	0	0	0	0	0	0	0	0	0	0	0	0	0	0	0	0	0	0	0	0	0	0	0	0
HC272	0	0	1	0	0	0	0	0	0	0	0	0	0	0	0	0	0	0	0	0	0	0	0	0	0	0	0	0	0	0	0	0	0	0
HC273	0	0	1	0	0	0	0	0	0	0	0	0	0	0	0	0	0	0	0	0	0	0	0	0	0	0	0	0	0	0	0	0	0	0
HC274	0	0	1	0	0	0	0	0	0	0	0	0	0	0	0	0	0	0	0	0	0	0	0	0	0	0	0	0	0	0	0	0	0	0
HC275	0	0	0	0	0	1	1	0	0	0	0	0	0	0	0	0	0	0	0	0	0	0	0	0	0	0	0	0	0	0	0	0	0	0
HC277	0	0	0	0	0	0	0	1	0	0	0	0	0	0	0	0	0	0	0	0	0	0	0	0	0	0	0	0	0	0	0	0	0	0
HC278	0	0	0	0	0	0	0	1	0	0	0	0	0	0	0	0	0	0	0	0	0	0	0	0	0	0	0	0	0	0	0	0	0	0
HC279	0	0	0	0	0	0	1	0	0	0	0	0	0	0	0	0	0	0	0	0	0	0	0	0	0	0	0	0	0	0	0	0	0	0
HC280	0	0	0	0	0	1	1	1	0	0	0	0	0	0	0	0	0	0	0	0	0	0	0	0	0	0	0	0	0	0	0	0	0	0
HC281	0	0	1	0	0	0	0	0	0	0	0	0	0	0	0	0	0	0	0	0	0	0	0	0	0	0	0	0	0	0	0	0	0	0
HC282	0	0	1	0	0	0	0	0	0	0	0	0	0	0	0	0	0	0	0	0	0	0	0	0	0	0	0	0	0	0	0	0	0	0
HC283	0	0	1	0	0	0	0	0	0	0	0	0	0	0	0	0	0	0	0	0	0	0	0	0	0	0	0	0	0	0	0	0	0	0
HC284	0	0	0	0	0	0	0	1	0	0	0	0	0	0	0	0	0	0	0	0	0	0	0	0	0	0	0	0	0	0	0	0	0	0

Morph	66.7 - 66.6	67.6 - 66.5	66.6 - 66.5	66.5 - 66.4	66.4 - 66.3	66.3 - 66.2	66.2 - 66.1	66.1 - 66.032	66.032 - 65.9	65.9 - 65.8	65.8 - 65.7	65.7 - 65.6	65.6 - 65.5	65.5 - 65.4	65.4 - 65.3	65.3 - 65.2	65.2 - 65.1	65.1 - 65	65 - 64.9	64.9 - 64.8	64.8 - 64.7	64.7 - 64.6	64.6 - 64.5	64.5 - 64.4	64.4 - 64.3	64.3 - 64.2	64.2 - 64.1	64.1 - 64	64 - 63.9	63.9 - 63.8	63.8 - 63.7	63.7 - 63.6	63.6 - 63.5	63.5 - 63.4
HC285	0	0	1	0	0	0	1	0	0	0	0	0	0	0	0	0	0	0	0	0	0	0	0	0	0	0	0	0	0	0	0	0	0	0
HC286	1	0	0	0	1	1	0	0	0	0	0	0	0	0	0	0	0	0	0	0	0	0	0	0	0	0	0	0	0	0	0	0	0	0
HC287	0	0	0	0	1	0	1	0	0	0	0	0	0	0	0	0	0	0	0	0	0	0	0	0	0	0	0	0	0	0	0	0	0	0
HC288	0	0	1	0	0	0	0	0	0	0	0	0	0	0	0	0	0	0	0	0	0	0	0	0	0	0	0	0	0	0	0	0	0	0
HC289	0	0	1	0	0	0	0	0	0	0	0	0	0	0	0	0	0	0	0	0	0	0	0	0	0	0	0	0	0	0	0	0	0	0
HC290	0	0	1	0	0	0	0	0	0	0	0	0	0	0	0	0	0	0	0	0	0	0	0	0	0	0	0	0	0	0	0	0	0	0
HC291	0	0	1	0	0	0	0	0	0	0	0	0	0	0	0	0	0	0	0	0	0	0	0	0	0	0	0	0	0	0	0	0	0	0
HC292	0	0	0	0	0	1	0	1	0	0	0	0	0	0	0	0	0	0	0	0	0	0	0	0	0	0	0	0	0	0	0	0	0	0
HC293	0	0	0	0	0	1	1	0	0	0	0	0	0	0	0	0	0	0	0	0	0	0	0	0	0	0	0	0	0	0	0	0	0	0
HC294	0	0	0	0	0	1	0	0	0	0	0	0	0	0	0	0	0	0	0	0	0	0	0	0	0	0	0	0	0	0	0	0	0	0
HC295	0	0	0	0	0	1	0	1	0	0	0	0	0	0	0	0	0	0	0	0	0	0	0	0	0	0	0	0	0	0	0	0	0	0
HC296	1	0	0	0	0	0	0	0	0	0	0	0	0	0	0	0	0	0	0	0	0	0	0	0	0	0	0	0	0	0	0	0	0	0
HC297	0	1	0	0	0	0	0	0	0	0	0	0	0	0	0	0	0	0	0	0	0	0	0	0	0	0	0	0	0	0	0	0	0	0
HC298	0	0	1	0	0	0	0	0	0	0	0	0	0	0	0	0	0	0	0	0	0	0	0	0	0	0	0	0	0	0	0	0	0	0
HC299	0	0	1	0	0	0	0	0	0	0	0	0	0	0	0	0	0	0	0	0	0	0	0	0	0	0	0	0	0	0	0	0	0	0
HC300	1	0	1	0	0	0	0	0	0	0	0	0	0	0	0	0	0	0	0	0	0	0	0	0	0	0	0	0	0	0	0	0	0	0
HC301	0	0	1	0	0	0	0	0	0	0	0	0	0	0	0	0	0	0	0	0	0	0	0	0	0	0	0	0	0	0	0	0	0	0
HC302	0	0	1	0	0	0	0	0	0	0	0	0	0	0	0	0	0	0	0	0	0	0	0	0	0	0	0	0	0	0	0	0	0	0
HC303	0	0	0	1	0	0	0	0	0	0	0	0	0	0	0	0	0	0	0	0	0	0	0	0	0	0	0	0	0	0	0	0	0	0
HC306	0	0	1	0	0	0	0	0	0	0	0	0	0	0	0	0	0	0	0	0	0	0	0	0	0	0	0	0	0	0	0	0	0	0
HC307	0	0	1	0	0	0	0	0	0	0	0	0	0	0	0	0	0	0	0	0	0	0	0	0	0	0	0	0	0	0	0	0	0	0
HC308	0	0	1	0	0	0	0	0	0	0	0	0	0	0	0	0	0	0	0	0	0	0	0	0	0	0	0	0	0	0	0	0	0	0
HC309	0	0	1	0	0	0	0	0	0	0	0	0	0	0	0	0	0	0	0	0	0	0	0	0	0	0	0	0	0	0	0	0	0	0
HC310	0	0	1	0	0	0	0	0	0	0	0	0	0	0	0	0	0	0	0	0	0	0	0	0	0	0	0	0	0	0	0	0	0	0
HC312	0	0	0	0	1	0	0	0	0	0	0	0	0	0	0	0	0	0	0	0	0	0	0	0	0	0	0	0	0	0	0	0	0	0
HC314	0	0	0	0	1	0	0	0	0	0	0	0	0	0	0	0	0	0	0	0	0	0	0	0	0	0	0	0	0	0	0	0	0	0
HC315	0	0	0	0	1	1	0	0	0	0	0	0	0	0	0	0	0	0	0	0	0	0	0	0	0	0	0	0	0	0	0	0	0	0
HC316	0	0	0	0	1	0	0	0	0	0	0	0	0	0	0	0	0	0	0	0	0	0	0	0	0	0	0	0	0	0	0	0	0	0

Morph	66.7 - 66.6	67.6 - 66.5	66.6 - 66.5	66.5 - 66.4	66.4 - 66.3	66.3 - 66.2	66.2 - 66.1	66.1 - 66.032	66.032 - 65.9	65.9 - 65.8	65.8 - 65.7	65.7 - 65.6	65.6 - 65.5	65.5 - 65.4	65.4 - 65.3	65.3 - 65.2	65.2 - 65.1	65.1 - 65	65 - 64.9	64.9 - 64.8	64.8 - 64.7	64.7 - 64.6	64.6 - 64.5	64.5 - 64.4	64.4 - 64.3	64.3 - 64.2	64.2 - 64.1	64.1 - 64	64 - 63.9	63.9 - 63.8	63.8 - 63.7	63.7 - 63.6	63.6 - 63.5	63.5 - 63.4
HC317	0	0	0	0	1	0	0	0	0	0	0	0	0	0	0	0	0	0	0	0	0	0	0	0	0	0	0	0	0	0	0	0	0	0
HC318	1	0	0	0	0	1	0	0	0	0	0	0	0	0	0	0	0	0	0	0	0	0	0	0	0	0	0	0	0	0	0	0	0	0
HC319	0	0	0	0	1	0	0	0	0	0	0	0	0	0	0	0	0	0	0	0	0	0	0	0	0	0	0	0	0	0	0	0	0	0
HC320	0	0	0	0	1	0	0	0	0	0	0	0	0	0	0	0	0	0	0	0	0	0	0	0	0	0	0	0	0	0	0	0	0	0
HC321	0	0	0	0	0	1	1	0	0	0	0	0	0	0	0	0	0	0	0	0	0	0	0	0	0	0	0	0	0	0	0	0	0	0
HC323	0	0	0	0	0	0	1	0	0	0	0	0	0	0	0	0	0	0	0	0	0	0	0	0	0	0	0	0	0	0	0	0	0	0
HC324	0	0	0	0	0	0	1	0	0	0	0	0	0	0	0	0	0	0	0	0	0	0	0	0	0	0	0	0	0	0	0	0	0	0
HC325	0	0	0	0	0	0	1	0	0	0	0	0	0	0	0	0	0	0	0	0	0	0	0	0	0	0	0	0	0	0	0	0	0	0
HC326	0	0	0	0	0	0	1	0	0	0	0	0	0	0	0	0	0	0	0	0	0	0	0	0	0	0	0	0	0	0	0	0	0	0
HC327	0	0	0	0	0	0	1	0	0	0	0	0	0	0	0	0	0	0	0	0	0	0	0	0	0	0	0	0	0	0	0	0	0	0
HC329	0	0	0	0	0	0	1	1	0	0	0	0	0	0	0	0	0	0	0	0	0	0	0	0	0	0	0	0	0	0	0	0	0	0
HC330	0	0	0	0	0	0	0	1	0	0	0	0	0	0	0	0	0	0	0	0	0	0	0	0	0	0	0	0	0	0	0	0	0	0
HC331	0	0	0	0	0	0	0	1	0	0	0	0	0	0	0	0	0	0	0	0	0	0	0	0	0	0	0	0	0	0	0	0	0	0
HC332	0	0	0	0	0	0	0	1	0	0	0	0	0	0	0	0	0	0	0	0	0	0	0	0	0	0	0	0	0	0	0	0	0	0
HC333	0	0	0	0	0	0	0	1	0	0	0	0	0	0	0	0	0	0	0	0	0	0	0	0	0	0	0	0	0	0	0	0	0	0
HC334	0	0	0	0	0	0	0	1	0	0	0	0	0	0	0	0	0	0	0	0	0	0	0	0	0	0	0	0	0	0	0	0	0	0
HC335	0	0	0	0	0	0	0	1	0	0	0	0	0	0	0	0	0	0	0	0	0	0	0	0	0	0	0	0	0	0	0	0	0	0
HC336	0	0	0	0	0	0	0	1	0	0	0	0	0	0	0	0	0	0	0	0	0	0	0	0	0	0	0	0	0	0	0	0	0	0
HC337	1	0	0	0	0	0	1	0	0	0	0	0	0	0	0	0	0	0	0	0	0	0	0	0	0	0	0	0	0	0	0	0	0	0
HC338	0	0	0	0	1	0	0	0	0	0	0	0	0	0	0	0	0	0	0	0	0	0	0	0	0	0	0	0	0	0	0	0	0	0
HC340	1	0	0	0	0	1	0	0	0	0	0	0	0	0	0	0	0	0	0	0	0	0	0	0	0	0	0	0	0	0	0	0	0	0
HC341	0	0	0	0	0	1	0	0	0	0	0	0	0	0	0	0	0	0	0	0	0	0	0	0	0	0	0	0	0	0	0	0	0	0
HC342	0	0	0	0	0	1	0	0	0	0	0	0	0	0	0	0	0	0	0	0	0	0	0	0	0	0	0	0	0	0	0	0	0	0
HC343	0	0	0	0	0	1	0	0	0	0	0	0	0	0	0	0	0	0	0	0	0	0	0	0	0	0	0	0	0	0	0	0	0	0
HC344	0	0	0	0	0	1	0	0	0	0	0	0	0	0	0	0	0	0	0	0	0	0	0	0	0	0	0	0	0	0	0	0	0	0
HC345	0	0	0	0	0	1	0	0	0	0	0	0	0	0	0	0	0	0	0	0	0	0	0	0	0	0	0	0	0	0	0	0	0	0
HC346	0	0	0	0	0	1	0	0	0	0	0	0	0	0	0	0	0	0	0	0	0	0	0	0	0	0	0	0	0	0	0	0	0	0
HC347	0	0	0	0	0	1	0	0	0	0	0	0	0	0	0	0	0	0	0	0	0	0	0	0	0	0	0	0	0	0	0	0	0	0

Morph	66.7 - 66.6	67.6 - 66.5	66.6 - 66.5	66.5 - 66.4	66.4 - 66.3	66.3 - 66.2	66.2 - 66.1	66.1 - 66.032	66.032 - 65.9	65.9 - 65.8	65.8 - 65.7	65.7 - 65.6	65.6 - 65.5	65.5 - 65.4	65.4 - 65.3	65.3 - 65.2	65.2 - 65.1	65.1 - 65	65 - 64.9	64.9 - 64.8	64.8 - 64.7	64.7 - 64.6	64.6 - 64.5	64.5 - 64.4	64.4 - 64.3	64.3 - 64.2	64.2 - 64.1	64.1 - 64	64 - 63.9	63.9 - 63.8	63.8 - 63.7	63.7 - 63.6	63.6 - 63.5	63.5 - 63.4
HC348	0	0	0	0	0	1	0	0	0	0	0	0	0	0	0	0	0	0	0	0	0	0	0	0	0	0	0	0	0	0	0	0	0	0
HC349	0	0	0	0	0	1	0	0	0	0	0	0	0	0	0	0	0	0	0	0	0	0	0	0	0	0	0	0	0	0	0	0	0	0
HC350	0	0	0	0	0	1	0	0	0	0	0	0	0	0	0	0	0	0	0	0	0	0	0	0	0	0	0	0	0	0	0	0	0	0
HC351	0	0	0	0	0	1	0	0	0	0	0	0	0	0	0	0	0	0	0	0	0	0	0	0	0	0	0	0	0	0	0	0	0	0
HC352	0	0	0	0	0	1	0	0	0	0	0	0	0	0	0	0	0	0	0	0	0	0	0	0	0	0	0	0	0	0	0	0	0	0
HC353	0	0	0	0	0	1	0	0	0	0	0	0	0	0	0	0	0	0	0	0	0	0	0	0	0	0	0	0	0	0	0	0	0	0
HC354	0	0	0	0	0	1	0	0	0	0	0	0	0	0	0	0	0	0	0	0	0	0	0	0	0	0	0	0	0	0	0	0	0	0
HC355	0	0	0	0	0	1	0	0	0	0	0	0	0	0	0	0	0	0	0	0	0	0	0	0	0	0	0	0	0	0	0	0	0	0
HC356	0	0	0	0	0	1	0	0	0	0	0	0	0	0	0	0	0	0	0	0	0	0	0	0	0	0	0	0	0	0	0	0	0	0
HC357	0	0	0	0	0	1	0	0	0	0	0	0	0	0	0	0	0	0	0	0	0	0	0	0	0	0	0	0	0	0	0	0	0	0
HC358	0	0	0	0	0	1	0	0	0	0	0	0	0	0	0	0	0	0	0	0	0	0	0	0	0	0	0	0	0	0	0	0	0	0
HC359	0	0	0	0	0	1	0	0	0	0	0	0	0	0	0	0	0	0	0	0	0	0	0	0	0	0	0	0	0	0	0	0	0	0
HC360	0	0	0	0	0	1	0	0	0	0	0	0	0	0	0	0	0	0	0	0	0	0	0	0	0	0	0	0	0	0	0	0	0	0
HC362	0	0	0	0	0	1	0	0	0	0	0	0	0	0	0	0	0	0	0	0	0	0	0	0	0	0	0	0	0	0	0	0	0	0
HC363	0	0	0	0	0	1	0	0	0	0	0	0	0	0	0	0	0	0	0	0	0	0	0	0	0	0	0	0	0	0	0	0	0	0
HC364	0	0	0	0	0	1	0	0	0	0	0	0	0	0	0	0	0	0	0	0	0	0	0	0	0	0	0	0	0	0	0	0	0	0
HC365	1	0	0	0	0	0	0	0	0	0	0	0	0	0	0	0	0	0	0	0	0	0	0	0	0	0	0	0	0	0	0	0	0	0
HC366	1	0	0	0	0	0	0	0	0	0	0	0	0	0	0	0	0	0	0	0	0	0	0	0	0	0	0	0	0	0	0	0	0	0
HC367	1	0	0	0	0	0	0	0	0	0	0	0	0	0	0	0	0	0	0	0	0	0	0	0	0	0	0	0	0	0	0	0	0	0
HC368	1	0	0	0	0	0	0	0	0	0	0	0	0	0	0	0	0	0	0	0	0	0	0	0	0	0	0	0	0	0	0	0	0	0
HC369	0	0	0	0	0	1	0	0	0	0	0	0	0	0	0	0	0	0	0	0	0	0	0	0	0	0	0	0	0	0	0	0	0	0
HC370	0	0	1	0	0	0	0	0	0	0	0	0	0	0	0	0	0	0	0	0	0	0	0	0	0	0	0	0	0	0	0	0	0	0
LM100	0	0	0	0	0	0	0	0	1	0	0	1	0	0	0	0	0	0	0	0	0	0	0	0	0	0	0	0	0	0	0	0	0	0
LM104	0	0	0	0	0	0	0	0	1	0	0	0	0	0	0	0	0	0	0	0	0	0	0	0	0	0	0	0	0	0	0	0	0	0
LM106	0	0	0	0	0	0	0	0	0	0	0	0	0	0	0	0	0	0	0	0	0	0	0	0	0	0	0	0	1	1	1	0	0	0
LM107	0	0	0	0	0	0	0	0	0	0	0	0	0	0	0	0	0	0	0	0	0	0	0	0	0	0	0	0	0	0	1	0	0	0
LM108	0	0	0	0	0	0	0	0	0	0	0	0	0	0	0	0	0	0	0	0	0	0	0	0	0	0	0	0	0	0	1	0	0	0
LM109	0	0	0	0	0	0	0	0	0	0	0	0	0	0	0	0	0	0	0	0	0	0	0	0	0	0	0	0	0	0	1	0	0	0

Morph	66.7 - 66.6	67.6 - 66.5	66.6 - 66.5	66.5 - 66.4	66.4 - 66.3	66.3 - 66.2	66.2 - 66.1	66.1 - 66.032	66.032 - 65.9	65.9 - 65.8	65.8 - 65.7	65.7 - 65.6	65.6 - 65.5	65.5 - 65.4	65.4 - 65.3	65.3 - 65.2	65.2 - 65.1	65.1 - 65	65 - 64.9	64.9 - 64.8	64.8 - 64.7	64.7 - 64.6	64.6 - 64.5	64.5 - 64.4	64.4 - 64.3	64.3 - 64.2	64.2 - 64.1	64.1 - 64	64 - 63.9	63.9 - 63.8	63.8 - 63.7	63.7 - 63.6	63.6 - 63.5	63.5 - 63.4
LM110	0	0	0	0	0	0	0	0	0	0	0	0	0	0	0	0	0	0	0	0	0	0	0	0	0	0	0	0	0	0	1	0	0	0
LM111	0	0	0	0	0	0	0	0	0	0	0	0	0	0	0	0	0	0	0	0	0	0	0	0	0	0	0	0	0	0	1	0	0	0
LM112	0	0	0	0	0	0	0	0	0	0	0	0	0	0	0	0	0	0	0	0	0	0	0	0	0	0	0	0	0	0	1	0	0	0
LM116	0	0	0	0	0	0	0	0	0	0	0	0	0	0	0	0	0	0	0	0	0	0	0	0	0	0	0	0	0	1	0	0	0	0
LM117	0	0	0	0	0	0	0	0	0	0	0	0	0	0	0	0	0	0	0	0	0	0	0	0	0	0	0	0	0	1	0	0	0	0
LM118	0	0	0	0	0	0	0	0	0	0	0	0	0	0	0	0	0	0	0	0	0	0	0	0	0	0	0	0	1	0	0	0	0	0
LM119	0	0	0	0	0	0	0	0	0	0	0	0	0	0	0	0	0	0	0	0	0	0	0	0	0	0	0	0	1	0	0	0	0	0
LM12	0	0	0	0	0	0	0	0	0	0	0	0	0	0	0	0	0	0	0	0	0	0	1	0	0	0	0	0	0	1	1	1	0	0
LM120	0	0	0	0	0	0	0	0	0	0	0	0	0	0	0	0	0	0	0	0	0	1	0	0	0	0	0	0	0	0	0	0	0	0
LM121	0	0	0	0	0	0	0	0	0	0	0	0	0	1	0	0	0	0	0	0	0	0	0	0	0	0	0	0	0	0	0	0	0	0
LM122	0	0	0	0	0	0	0	0	1	0	0	0	0	0	0	0	0	0	0	0	0	0	0	0	0	0	0	0	0	0	0	0	0	0
LM123	0	0	0	0	0	0	0	0	1	0	0	0	0	0	0	0	0	0	0	0	0	0	0	0	0	0	0	0	0	0	0	0	0	0
LM126	0	0	0	0	0	0	0	0	1	0	0	0	0	0	0	0	0	0	0	0	0	0	0	0	0	0	0	0	0	0	0	0	0	0
LM13	0	0	0	0	0	0	0	0	0	0	0	0	0	0	0	0	0	0	0	0	0	0	0	0	0	0	0	0	1	0	0	0	0	0
LM14	0	0	0	0	0	0	0	0	0	0	0	0	0	0	0	0	0	0	0	0	0	0	0	0	0	0	0	0	0	0	0	1	0	0
LM15	0	0	0	0	0	0	0	0	0	0	0	0	0	0	0	0	0	0	0	0	0	0	0	0	0	0	0	0	1	0	0	0	0	0
LM17	0	0	0	0	0	0	0	0	0	0	0	0	0	0	0	0	0	0	0	0	0	1	1	0	0	0	0	0	1	1	1	1	0	0
LM22	0	0	0	0	0	0	0	0	0	0	0	0	0	1	0	0	0	0	0	0	0	0	0	0	0	0	0	0	0	0	0	0	0	0
LM26	0	0	0	0	0	0	0	0	1	0	0	1	0	0	0	0	0	0	0	0	0	0	0	0	0	0	0	0	0	0	0	0	0	0
LM29	0	0	0	0	0	0	0	0	1	0	0	1	0	0	0	0	0	0	0	0	0	0	0	0	0	0	0	0	1	0	0	0	0	0
LM30	0	0	0	0	0	0	0	0	0	0	0	1	0	0	0	0	0	0	0	0	0	0	0	0	0	0	0	0	0	0	0	0	0	0
LM32	0	0	0	0	0	0	0	0	0	0	0	1	0	0	0	0	0	0	0	0	0	0	0	0	0	0	0	0	0	0	1	0	0	0
LM35	0	0	0	0	0	0	0	0	1	0	0	0	0	0	0	0	0	0	0	0	0	0	0	0	0	0	0	0	0	0	0	0	0	0
LM36	0	0	0	0	0	0	0	0	0	0	0	0	0	0	0	0	0	0	0	0	0	0	0	0	0	0	0	0	0	0	1	0	0	0
LM37	0	0	0	0	0	0	0	0	0	0	0	0	0	0	0	0	0	0	0	0	0	0	0	0	0	0	0	0	0	0	1	0	0	0
LM38	0	0	0	0	0	0	0	0	0	0	0	1	0	1	0	0	0	0	0	0	0	1	0	0	0	0	0	0	1	0	1	0	0	0
LM41	0	0	0	0	0	0	0	0	0	0	0	0	0	0	0	0	0	0	0	0	0	0	0	0	0	0	0	0	0	0	0	1	0	0
LM44	0	0	0	0	0	0	0	0	0	0	0	0	0	0	0	0	0	0	0	0	0	0	0	0	0	0	0	0	1	0	0	1	0	0

Morph	66.7 - 66.6	67.6 - 66.5	66.6 - 66.5	66.5 - 66.4	66.4 - 66.3	66.3 - 66.2	66.2 - 66.1	66.1 - 66.032	66.032 - 65.9	65.9 - 65.8	65.8 - 65.7	65.7 - 65.6	65.6 - 65.5	65.5 - 65.4	65.4 - 65.3	65.3 - 65.2	65.2 - 65.1	65.1 - 65	65 - 64.9	64.9 - 64.8	64.8 - 64.7	64.7 - 64.6	64.6 - 64.5	64.5 - 64.4	64.4 - 64.3	64.3 - 64.2	64.2 - 64.1	64.1 - 64	64 - 63.9	63.9 - 63.8	63.8 - 63.7	63.7 - 63.6	63.6 - 63.5	63.5 - 63.4
LM47	0	0	0	0	0	0	0	0	0	0	0	0	0	0	0	0	0	0	0	0	0	1	1	0	0	0	0	0	0	0	0	0	0	0
LM48	0	0	0	0	0	0	0	0	0	0	0	0	0	0	0	0	0	0	0	0	0	0	0	0	0	0	0	0	0	0	1	0	0	0
LM51	0	0	0	0	0	0	0	0	0	0	0	0	0	0	0	0	0	0	0	0	0	0	1	0	0	0	0	0	0	0	0	0	0	0
LM52	0	0	0	0	0	0	0	0	0	0	0	1	0	0	0	0	0	0	0	0	0	0	1	0	0	0	0	0	0	0	0	0	0	1
LM54	0	0	0	0	0	0	0	0	0	0	0	1	0	0	0	0	0	0	0	0	0	0	0	0	0	0	0	0	0	0	0	0	0	0
LM92	0	0	0	0	0	0	0	0	0	0	0	0	0	0	0	0	0	0	0	0	0	0	1	0	0	0	0	0	0	0	0	0	0	0
LM93	0	0	0	0	0	0	0	0	0	0	0	0	0	0	0	0	0	0	0	0	0	1	0	0	0	0	0	0	0	0	0	0	0	0
LM94	0	0	0	0	0	0	0	0	0	0	0	0	0	0	0	0	0	0	0	0	0	0	0	0	0	0	0	0	0	0	1	0	0	0
LM95	0	0	0	0	0	0	0	0	0	0	0	0	0	0	0	0	0	0	0	0	0	0	0	0	0	0	0	0	0	0	1	1	0	0
LM96	0	0	0	0	0	0	0	0	1	0	0	0	0	0	0	0	0	0	0	0	0	1	0	0	0	0	0	0	0	0	0	0	0	0
LM99	0	0	0	0	0	0	0	0	0	0	0	1	1	0	0	0	0	0	0	0	0	0	0	0	0	0	0	0	0	0	0	0	0	0

APPENDIX I

San Juan Basin Bulk Organic $\delta^{13}C$ Data

Table I.1 – San Juan Basin Bulk Organic $\delta^{13}C$ Data: all samples collected from De-Na-Zin Wilderness Area.

Sample #	Strat Pos. Relative to C29r/C29n Boundary	Age (Myr)	δ13C (‰)	3 Pt Moving Avg
BN15-BO-01	-7.2	-65.855	-24.2	
BN15-BO-02	-6.5	-65.839	-25.7	-24.7958
BN15-BO-03	-5.7	-65.820	-24.5	-24.7421
BN15-BO-04	-4.5	-65.793	-24.1	-24.3194
BN15-BO-05	-3.0	-65.758	-24.4	-24.3459
BN15-BO-06	-1.5	-65.723	-24.6	-24.5242
BN15-BO-07	0.0	-65.689	-24.6	-24.7899
BN15-BO-08	1.5	-65.654	-25.2	-25.1626
BN15-BO-09	3.0	-65.619	-25.7	-24.9502
BN15-BO-10	4.5	-65.585	-24.0	-25.033
BN15-BO-12	4.5	-65.585	-25.4	-24.5769
BN15-BO-11	6.0	-65.550	-24.3	-24.7608
BN15-BO-13	6.0	-65.550	-24.5	-24.749
BN15-BO-15	6.5	-65.539	-25.4	-25.6733
BN15-BO-16	8.5	-65.492	-27.1	-26.2351
BN15-BO-17	10.0	-65.458	-26.2	-26.155
BN15-BO-18	11.5	-65.423	-25.2	-25.2849
BN15-BO-19	13.0	-65.388	-24.5	-24.7293
BN15-BO-20	14.5	-65.354	-24.6	-24.5101
BN15-BO-21	16.0	-65.319	-24.5	-24.6116
BN15-BO-22	17.5	-65.285	-24.8	-25.1871
BN15-BO-23	19.0	-65.250	-26.3	-25.3448
BN15-BO-24	20.5	-65.215	-25.0	-25.5863
BN15-BO-25	22.0	-65.181	-25.5	-24.8393
BN15-BO-26	23.5	-65.146	-24.0	-24.8265
BN15-BO-27	25.0	-65.111	-24.9	-24.5709
BN15-BO-28	26.5	-65.077	-24.7	-24.6708
BN15-BO-29	28.0	-65.042	-24.3	-24.9066
BN15-BO-30	29.5	-65.007	-25.7	-25.1747

Sample #	Strat Pos. Relative to C29r/C29n Boundary	Age (Myr)	δ13C (‰)	3 Pt Moving Avg
BN15-BO-31	32.0	-64.950	-25.5	-25.4511
BN15-BO-32	1.9	-64.938	-25.2	-25.1649
BN15-BO-33	2.7	-64.929	-24.8	-25.2042
BN15-BO-34	4.4	-64.911	-25.7	-25.0808
BN15-BO-35	5.9	-64.895	-24.8	-25.1649
BN15-BO-36	7.4	-64.878	-25.0	-25.048
BN15-BO-37	8.4	-64.868	-25.3	-25.107
BN15-BO-38	9.9	-64.851	-25.0	-25.0631
BN15-BO-39	11.4	-64.835	-24.9	-24.9861
BN15-BO-40	12.9	-64.819	-25.1	-25.1027
BN15-BO-41	14.4	-64.803	-25.3	-25.2356
BN15-BO-42	15.9	-64.786	-25.3	-25.325
BN15-BO-43	17.4	-64.770	-25.3	-25.161
BN15-BO-44	19.2	-64.751	-24.8	-25.1331
BN15-BO-45	20.4	-64.738	-25.2	-25.086
BN15-BO-46	21.9	-64.721	-25.2	-25.1273
BN15-BO-47	23.4	-64.705	-25.0	-25.0497
BN15-BO-48	24.9	-64.689	-25.0	-25.1302
BN15-BO-49	26.4	-64.673	-25.4	-25.1037
BN15-BO-50	1.0	-64.656	-24.9	-24.9884
BN15-BO-51	2.5	-64.640	-24.7	-24.881
BN15-BO-52	4.0	-64.624	-25.1	-24.8568
BN15-BO-53	4.0	-64.624	-24.8	-25.0948
BN15-BO-54	5.5	-64.607	-25.4	-25.0971
BN15-BO-55	7.0	-64.591	-25.1	-25.0104
BN15-BO-56	8.5	-64.575	-24.5	-24.8496
BN15-BO-57	10.0	-64.559	-24.9	-24.7095
BN15-BO-58	11.5	-64.542	-24.7	-24.7463
BN15-BO-59	13.0	-64.526	-24.7	-24.6013
BN15-BO-60	14.5	-64.510	-24.4	-24.607
BN15-BO-61	16.0	-64.494	-24.7	-24.6532
BN15-BO-62	17.5	-64.477	-24.8	-24.6968
BN15-BO-63	19.0	-64.461	-24.6	-24.7724
BN15-BO-64	20.5	-64.445	-24.9	-24.739
BN15-BO-65	22.0	-64.429	-24.7	-24.6483
BN15-BO-66	23.5	-64.412	-24.3	-24.6755
BN15-BO-67	25.0	-64.396	-25.0	-24.7321
BN15-BO-68	26.5	-64.380	-24.9	-24.8785
BN15-BO-69	28.0	-64.364	-24.7	-24.9299
BN15-BO-70	29.5	-64.347	-25.2	-24.9404

Sample #	Strat Pos. Relative to C29r/C29n Boundary	Age (Myr)	δ13C (‰)	3 Pt Moving Avg
BN15-BO-71	30.5	-64.337	-24.9	-24.9968
BN15-BO-72	32.0	-64.320	-24.9	-25.0695
BN15-BO-73	33.5	-64.304	-25.4	-25.2692
BN15-BO-74	35.0	-64.288	-25.5	-25.5198
BN15-BO-75	36.5	-64.272	-25.7	-25.5496
BN15-BO-76	38.0	-64.255	-25.5	

BIBLIOGRAPHY

Alvarez, S.A., Gibbs, S.J., Bown, P.R., Kim, H., Sheward, R.M., and Ridgwell, A., 2019, Diversity decoupled from ecosystem function and resilience during mass extinction recovery: Nature, v. 574, p. 242–245, doi:10.1038/s41586-019-1590-8.

Anderson, R.Y., 1959, Cretaceous-Tertiary palynology, eastern side of the San Juan Basin, New Mexico [Ph.D. Dissertation]: Stanford University, 166 p.

Archibald, J.D., Clemens, W.A., Gingerich, P.D., Krause, D.W., and Lindsay, E.H., 1987, First North American land mammal ages of the Cenozoic Era, *in* Woodburne, M.O. ed., Cenozoic Mammals of North America, Berkley, University of California Press, p. 24–76.

Ash, A.W., Ellis, B., Hickey, L.J., Johnson, K.R., and Wilf, P., 1999, Manual of leaf architecture: morphological description and categorization of dicotyledons and net-veined monocotyledonous angiosperms: Washington D. C., Smithsonian Institution, 67 p.

Baltz, E.H., 1967, Stratigraphy and Regional Tectonic Implications of Part of Upper Cretaceous and Tertiary Rocks East-Central San Juan Basin New Mexico: Geological Survey Professional Paper 552, p. 101, doi:10.3133/pp552.

Baltz, E.H., Ash, S.R., and Anderson, R.Y., 1966, History of nomenclature and stratigraphy of rocks adjacent to the Cretaceous-Tertiary boundary, western San Juan Basin, New Mexico: United States Geological Survey Professional Paper 524-D, p. 1–23, doi:10.3133/pp524D.

Barclay, R.S., Johnson, K.R., Betterton, W.J., and Dilcher, D.L., 2003, Stratigraphy and megaflora of a K-T boundary section in the eastern Denver Basin, Colorado: Rocky Mountain Geology, v. 38, p. 45–71, doi:10.2113/gsrocky.38.1.45.

Barnet, J.S.K., Littler, K., Westerhold, T., Kroon, D., Leng, M.J., Bailey, I., Röhl, U., and Zachos, J.C., 2019, A High-Fidelity Benthic Stable Isotope Record of Late Cretaceous–Early Eocene Climate Change and Carbon-Cycling: Paleoceanography and Paleoclimatology, v. 34, p. 672–691, doi:10.1029/2019PA003556.

Barreda, V.D., Cúneo, N.R., Wilf, P., Currano, E.D., Scasso, R.A., and Brinkhuis, H., 2012, Cretaceous/Paleogene Floral Turnover in Patagonia: Drop in Diversity, Low Extinction, and a Classopollis Spike: PLoS ONE, v. 7, doi:10.1371/journal.pone.0052455.

Beane, J.E., Turner, C.A., Hooper, P.R., Subbarao, K.V., and Walsh, J.N., 1986, Stratigraphy, composition and form of the Deccan Basalts, Western Ghats, India: Bulletin of Volcanology, v. 48, p. 61–83, doi:10.1007/BF01073513.

Berger, W.H., and Parker, F.L., 1970, Diversity of Planktonic Foraminifera in Deep-Sea Sediments: Science, v. 168, p. 1345–1347.

Blonder, B., Royer, D.L., Johnson, K.R., Miller, I., and Enquist, B.J., 2014, Plant Ecological Strategies Shift Across the Cretaceous-Paleogene Boundary: PLOS Biology, v. 12, p. 1–9, doi:10.1371/journal.pbio.1001949.

Bray, J.R., and Curtis, J.T., 1957, An Ordination of the Upland Forest Communities of Southern Wisconsin: Ecological Monographs, v. 27, p. 326–349, doi:10.2307/1942268.

Brokaw, N., and Busing, R.T., 2000, Niche versus chance and tree diversity in forest gaps: Trends in Ecology & Evolution, v. 15, p. 183–188, doi:10.1016/S0169-5347(00)01822-X.

Brown, R.W., 1962, Paleocene Flora of the Rock Mountains and Great Plains: United States Geological Survey Professional Paper 375, p. 1–119.

Brown, J.H., 2014, Why are there so many species in the tropics? Journal of biogeography, v. 41, p. 8.

Brusatte, S.L. et al., 2015, The extinction of the dinosaurs: Biological Reviews, v. 90, p. 628–642, doi:10.1111/brv.12128.

Buckley, G.A., 2018, Magnetostratigraphy of Upper Cretaceous (Lancian) to Middle Paleocene (Tiffanian) strata in the northeastern Crazy Mountains Basin, Montana, U.S.A.: Rocky Mountain Geology, v. 53, p. 59–74, doi:10.24872/rmgjournal.53.2.59.

Bullock, S.H., and Solis-Magallanes, J.A., 1990, Phenology of Canopy Trees of a Tropical Deciduous Forest in Mexico: Biotropica, v. 22, p. 22–35, doi:10.2307/2388716.

Burnham, R.J., Wing, S.L., and Parker, G.G., 1992, The Reflection of Deciduous Forest Communities in Leaf Litter: Implications for Autochthonous Litter Assemblages from the Fossil Record: Paleobiology, v. 18, p. 30–49.

Butler, R.F., Krause, D.W., and Gingerich, P.D., 1987, Magnetic Polarity Stratigraphy and Biostratigraphy of Middle-Late Paleocene Continental Deposits of South-Central Montana: The Journal of Geology, v. 95, p. 647–657, doi:10.1086/629161.

Butler, R.F., and Lindsay, E.H., 1985, Mineralogy of Magnetic Minerals and Revised Magnetic Polarity Stratigraphy of Continental Sediments, San Juan Basin, New Mexico: The Journal of Geology, v. 93, p. 535–554, doi:10.1086/628979.

Butler, R.F., Lindsay, E.H., Jacobs, L.L., and Johnson, N.M., 1977, Magnetostratigraphy of the Cretaceous-Tertiary boundary in the San Juan Basin, New Mexico: Nature, v. 267, p. 318–323, doi:10.1038/267318a0.

Butler, R.F., and Taylor, L.H., 1978, A middle Paleocene paleomagnetic pole from the Nacimiento Formation, San Juan Basin, New Mexico: Geology, v. 6, p. 495–498, doi:10.1130/0091-7613(1978)6<495:AMPPPF>2.0.CO;2.

Carmichael, M.J. et al., 2017, Hydrological and associated biogeochemical consequences of rapid global warming during the Paleocene-Eocene Thermal Maximum: Global and Planetary Change, v. 157, p. 114–138, doi:10.1016/j.gloplacha.2017.07.014.

Cather, S.M., 2004, The Laramide orogeny in central and northern New Mexico and southern Colorado, *in* Mack, G.H. and Giles, K.A. eds., The Geology of New Mexico - A Geologic History, New Mexico Geological Society Special Publication, v. 11, p. 203–248.

Cather, S.M., Heizler, M.T., and Williamson, T.E., 2019, Laramide fluvial evolution of the San Juan Basin, New Mexico and Colorado: Paleocurrent and detrital-sanidine age constraints from the Paleocene Nacimiento and Animas formations: Geosphere, v. 15, p. 1–24, doi:10.1130/GES02072.1.

Chapin, C.E., and Cather, S.M., 1983, Eocene tectonics and sedimentation in the Colorado Plateau-Rocky Mountain area: Arizona Geological Society Digest, v. 14, p. 173–198.

Coccioni, R., Frontalini, F., Bancalà, G., Fornaciari, E., Jovane, L., and Sprovieri, M., 2010, The Dan-C2 hyperthermal event at Gubbio (Italy): Global implications, environmental effects, and cause(s): Earth and Planetary Science Letters, v. 297, p. 298–305, doi:10.1016/j.epsl.2010.06.031.

Comer, E.E., Slingerland, R.L., Krause, J.M., Iglesias, A., Clyde, W.C., Raigemborn, M.S., and Wilf, P., 2015, Sedimentary Facies and Depositional Environments of Diverse Early Paleocene Floras, North-Central San Jorge Basin, Patagonia, Argentina: PALAIOS, v. 30, p. 553–573, doi:10.2110/palo.2014.064.

Condit, R., Watts, K., Bohlman, S.A., Pérez, R., Foster, R.B., and Hubbell, S.P., 2000, Quantifying the Deciduousness of Tropical Forest Canopies under Varying Climates: Journal of Vegetation Science, v. 11, p. 649–658, doi:10.2307/3236572.

Connell, J.H., 1978, Diversity in Tropical Rain Forests and Coral Reefs: Science, v. 199, p. 1302–1310, doi:10.1126/science.199.4335.1302.

Connolly, S.R., and Miller, A.I., 2001, Global Ordovician faunal transitions in the marine benthos: proximate causes: Paleobiology, v. 27, p. 779–795, doi:10.1666/0094-8373(2001)027<0779:GOFTIT>2.0.CO;2.

Cope, E.D., 1875, Report on the geology of that part of northwestern New Mexico examined during the field season of 1874, *in* Annual Report to the Chief of Engineering, Washington, D. C., U. S. Army, War Department, p. 981–1017.

Cormack, R.M., 1964, Estimates of Survival from the Sighting of Marked Animals: Biometrika, v. 51, p. 429–438, doi:10.2307/2334149.

Davis, A.J., Peppe, D.J., Atchley, S.C., Williamson, T.E., and Flynn, A.G., 2016, Climate and landscape reconstruction of the Arroyo Chijuillita Member of the Nacimiento Formation, San Juan Basin, New Mexico: Providing environmental context to early Paleocene mammal evolution: Palaeogeography, Palaeoclimatology, Palaeoecology, v. 463, p. 27–44, doi:10.1016/j.palaeo.2016.09.011.

Donovan, M.P., Iglesias, A., Wilf, P., Labandeira, C.C., and Cúneo, N.R., 2016, Rapid recovery of Patagonian plant–insect associations after the end-Cretaceous extinction: Nature Ecology & Evolution, v. 1, p. 5, doi:10.1038/s41559-016-0012.

Dunlop, D.J., and Özdemir, Ö., 1997, Rock Magnetism: Fundamentals and Frontiers: New York, Cambridge University Press, 573 p.

Dunn, R.E., 2003, Correlation of leaf megafossil and palynological data with North American Land Mammal Ages from Paleocene strata of the Ferris and Hanna Formations, Hanna Basin, south-central, Wyoming [M.S. Thesis]: University of Wyoming, 204 p.

Dupuy, B., Maitre, H.F., and Amsallem, I., 1999, Tropical forest management techniques: a review of the sustainability of forest management practices in tropical countries: Rome, FAO Forestry Policy and Planning Division, 50 p.

Edmonds, M., and Wallace, P.J., 2017, Volatiles and Exsolved Vapor in Volcanic Systems: Elements, v. 13, p. 29–34, doi:10.2113/gselements.13.1.29.

Ellis, B., Daly, D.C., Hickey, L.J., Mitchell, J.D., Johnson, K.R., Wilf, P., and Wing, S.L., 2009a, Manual of Leaf Architecture: Ithaca, Comstock Publishing Associates, 190 p.

Ellis, B., Daly, D.C., Hickey, L.J., Mitchell, J.V., Johnson, K.R., Wilf, P., and Wing, S.L., 2009b, Manual of Leaf Architecture: Ithaca, NY, Cornell University Press, 200 p.

Ellis, B., and Johnson, K.R., 2013, Comparison of Leaf Samples from Mapped Tropical and Temperate Forests: Implications for Interpretations of the Diversity of Fossil Assemblages: PALAIOS, v. 28, p. 163–177, doi:10.2110/palo.2012.p12-073r.

Ellis, B., Johnson, K.R., and Dunn, R.E., 2003, Evidence for an in situ early Paleocene rainforest from Castle Rock, Colorado: Rocky Mountain Geology, v. 38, p. 73–100, doi:10.2113/gsrocky.38.1.173.

Fassett, J.E., 1985, Early Tertiary Paleogeography and Paleotectonics of the San Juan Basin, New Mexico and Colorado, *in* Flores, R.M. and Kaplan, S.S. eds., Cenozoic Paleogeography of the West-Central United States, Denver, CO, The Rocky Mountain Section Society of Economic Paleontologists and Mineralogists, p. 317–334.

Fassett, J.E., 2009a, New geochronologic and stratigraphic evidence confirms the Paleocene age of the dinosaur-bearing Ojo Alamo Sandstone and Animas Formation in the San Juan Basin, New Mexico and Colorado: Palaeontologia Electronica, v. 12, p. 146.

Fassett, J.E., 2009b, Revised geochronology and paleomagnetic interpretations of uppermost Cretaceous and lowermost Paleocene rocks in the southern San Juan Basin, New Mexico: Palaeontologia Electronica, v. 12, p. 1–146.

Fassett, J.E., Heaman, L.M., and Simonetti, A., 2011, Direct U-Pb dating of Cretaceous and Paleocene dinosaur bones, San Juan Basin, New Mexico: Geology, v. 39, p. 159–162, doi:10.1130/G31466.1.

Fassett, J.E., Zielinski, R.A., and Budahn, J.R., 2002, Dinosaurs that did not die: Evidence for Paleocene dinosaurs in the Ojo Alamo Sandstone, San Juan Basin, New Mexico: Geological Society of America Special Papers, v. 356, p. 307–336.

Fisher, R.A., 1953, Dispersion of a sphere: Proceedings of the Royal Society A, v. 217, p. 295–305, doi:10.1098/rspa.1953.0064.

Fleck, R.J., Calvert, A.T., Coble, M.A., Wooden, J.L., Hodges, K., Hayden, L.A., van Soest, M.C., du Bray, E.A., and John, D.A., 2019, Characterization of the rhyolite of Bodie Hills and 40Ar/39Ar intercalibration with Ar mineral standards: Chemical Geology, v. 525, p. 282–302, doi:10.1016/j.chemgeo.2019.07.022.

Flynn, A.G., Davis, A.J., Williamson, T.E., Heizler, M., Fenley, C.W.I., Leslie, C.E., Secord, R., Brusatte, S.L., and Peppe, D.J., in press, Early Paleocene Magnetostratigraphy and Revised Biostratigraphy of the Ojo Alamo Sandstone and Lower Nacimiento Formation, San Juan Basin, New Mexico, USA: Geological Society of America Bulletin, doi:https://doi.org/10.1130/B35481.1.

Flynn, A.G., and Peppe, D.J., 2019, Early Paleocene tropical forest from the Ojo Alamo Sandstone, San Juan Basin, New Mexico, USA: Paleobiology, v. 45, p. 612–635, doi:10.1017/pab.2019.24.

Flynn, A.G., Peppe, D.J., and Abbuhl, B., 2018, Rapid floral change in diverse early Paleocene fossil flora from the San Juan Basin, New Mexico, USA, *in* European Palaeobotany and Palynology Conference Program with Abstracts, Dublin, European Palaeobotany and Palynology Congress.

Flynn, A.G., Peppe, D.J., Davis, A.J., Williamson, T.E., Heizler, M.T., Leslie, C.E., Secord, R., Brusatte, S.L., and Fenley, C.W.I., 2019, High-Resolution Latest Cretaceous to Early Paleocene Magnetostratigraphy from the San Juan Basin, New Mexico, USA Constrains the Age of Dinosaur and Mammalian Faunas Across the K/Pg boundary, *in* Geologic Society of America, Abstracts with Programs, 5, v. 51, doi:10.1130/abs/2019AM-340641.

Foote, M., 1992, Rarefaction Analysis of Morphological and Taxonomic Diversity: Paleobiology, v. 18, p. 1–16.

Force, E.R., Butler, R.F., Reynolds, R.L., and Houston, R.S., 2001, Magnetic Ilmenite-Hematite Detritus in Mesozoic-Tertiary Placer and Sandstone-Hosted Uranium Deposits of the Rocky Mountains: Economic Geology, v. 96, p. 1445–1453, doi:10.2113/gsecongeo.96.6.1445.

Frederiksen, N.O., 1987, Tectonic and Paleogeographic Setting of a New Latest Cretaceous Floristic Province in North America: PALAIOS, v. 2, p. 533–542.

Fuentes, A.J., Clyde, W.C., Weissenburger, K., Bercovici, A., Lyson, T.R., Miller, I.M., Ramezani, J., Isakson, V., Schmitz, M.D., and Johnson, K.R., 2019, Constructing a time scale of biotic recovery across the Cretaceous–Paleogene boundary, Corral Bluffs, Denver Basin, Colorado, U.S.A.: Rocky Mountain Geology, v. 54, p. 133–153, doi:10.24872/rmgjournal.54.2.133.

Gilmour, I., Gilmour, M., Jolley, D., Kelley, S., Kemp, D., Daly, R., and Watson, J., 2013, A high-resolution nonmarine record of an early Danian hyperthermal event, Boltysh crater, Ukraine: Geology, v. 41, p. 783–786, doi:10.1130/G34292.1.

Givnish, T.J., 1999, On the causes of gradients in tropical tree diversity: Journal of Ecology, v. 87, p. 193–210, doi:10.1046/j.1365-2745.1999.00333.x.

Granger, W., 1917, Notes on Paleocene and lower Eocene mammal horizons of northern New Mexico and southern Colorado: Bulletin of the American Museum of Natural History, v. 37, p. 821–830.

Grossnickle, D.M., and Newham, E., 2016, Therian mammals experience an ecomorphological radiation during the Late Cretaceous and selective extinction at the K–Pg boundary: Proceedings of the Royal Society B: Biological Sciences, v. 283, p. 20160256, doi:10.1098/rspb.2016.0256.

Hammer, Ø., Harper, D.A.T., and Ryan, P.D., 2001, Past: Paleontological statistics software package for education and data analysis: Palaeontologia Electronica, v. 4, p. 1–9.

Harrington, G.J., and Jaramillo, C.A., 2007, Paratropical floral extinction in the Late Palaeocene–Early Eocene: Journal of the Geological Society, v. 164, p. 323–332, doi:10.1144/0016-76492006-027.

Haufler, C.H., Hooper, E.A., and Therrien, J.P., 2000, Modes and mechanisms of speciation in pteridophytes: Implications of contrasting patterns in ferns representing temperate and tropical habitats: Plant Species Biology, v. 15, p. 223–236, doi:10.1111/j.1442-1984.2000.00042.x.

Hickey, L.J., 1980, Paleocene Stratigraphy and Flora of the Clark's Fork Basin, *in* Gingerich, P.D. ed., Early Cenozoic Paleontology and Stratigraphy of the Bighorn Basin, Wyoming: 1880-1980, University of Michigan Papers on Paleontology, v. 24, p. 33–49.

Hicks, J.F., Johnson, K.R., Obradovich, J.D., Miggins, D.P., and Tauxe, L., 2003, Magnetostratigraphy of Upper Cretaceous (Maastrichtian) to lower Eocene strata of the Denver Basin, Colorado: Rocky Mountain Geology, v. 38, p. 1–27, doi:10.2113/gsrocky.38.1.1.

Hicks, J.F., Johnson, K.R., Obradovich, J.D., Tauxe, L., and Clark, D., 2002, Magnetostratigraphy and Geochronology of the Hell Creek and Basal Fort Union Formations of Southwestern North Dakota and a Recalibration of the Age of the Cretaceous-Tertiary Boundary, *in* Hartman, J.H., Johnson, K.R., and Nichols, D.J. eds., The Hell Creek Formation and the Cretaceous-Tertiary Boundary in the Northern Great Plains: An Integrated Continental Record of the End of the Cretaceous, Geological Society of America Special Paper 361, p. 35–55.

Hobbs, K.M., 2016, Sedimentation, pedogenesis, and paleoclimate conditions in the Paleocene San Juan Basin, New Mexico, USA [Ph.D. Dissertation]: University of New Mexico, 160 p.

Huff, P.M., Wilf, P., and Azumah, E.J., 2003, Digital Future for Paleoclimate Estimation from Fossil Leaves? Preliminary Results: PALAIOS, v. 18, p. 266–274, doi:10.1669/0883-1351(2003)018<0266:DFFPEF>2.0.CO;2.

Hull, P.M. et al., 2020, On impact and volcanism across the Cretaceous-Paleogene boundary: Science, v. 367, p. 266–272, doi:10.1126/science.aay5055.

Hunter, J.P., and Hartman, J.H., 2003, Brown Ranch locality area, "Mid"-Paleocene mammals and the tongues of the Cannonball Formation, Slope County, North Dakota, *in* Hartman, J.H. ed., Vertebrate Paleontology of the High Plains - The Late Mesozoic/Cenozoic Record of North Dakota, St. Paul, Minnesota, Society of Vertebrate Paleontology, p. 1–8.

Iglesias, A., Wilf, P., Johnson, K.R., Zamuner, A.B., Cúneo, N.R., Matheos, S.D., and Singer, B.S., 2007, A Paleocene lowland macroflora from Patagonia reveals significantly greater richness than North American analogs: Geology, v. 35, p. 947–950, doi:10.1130/G23889A.1.

Jaramillo, C. et al., 2010, Effects of Rapid Global Warming at the Paleocene-Eocene Boundary on Neotropical Vegetation: Science, v. 330, p. 957–961, doi:10.1126/science.1193833.

Johnson, K.R., 1989, High-resolution megafloral biostratigraphy spanning the Cretaceous-Tertiary boundary in the northern Great Plains [Ph.D. Dissertation]: Yale University, 556 p.

Johnson, K.R., 2002, Megaflora of the Hell Creek and lower Fort Union Formation in the western Dakotas: Vegetational response to climate change, the Cretaceous-Tertiary boundary event, and rapid marine transgression, *in* Hartman, J.H., Johnson, K.R., and Nichols, D.J. eds., The Hell Creek Formation and the Cretaceous-Tertiary boundary in the northern Great Plains: An integrated continental record of the end of the Cretaceous, Geological Society of America Special Paper, p. 329–391.

Johnson, K.R., and Ellis, B., 2002, A Tropical Rainforest in Colorado 1.4 Million Years after the Cretaceous-Tertiary Boundary: Science, v. 296, p. 2379–2383, doi:10.1126/science.1072102.

Johnson, K.R., and Hickey, L.J., 1990, Megafloral change across the Cretaceous/Tertiary boundary in the northern Great Plains and Rocky Mountains, U.S.A.: Geological Society of America Special Papers, v. 247, p. 433–444, doi:10.1130/SPE247-p433.

Johnson, K.R., Reynolds, M.L., Werth, K.W., and Thomasson, J.R., 2003, Overview of the Late Cretaceous, early Paleocene, and early Eocene megafloras of the Denver Basin, Colorado: Rocky Mountain Geology, v. 38, p. 101–120, doi:10.2113/gsrocky.38.1.101.

Jolly, G.M., 1965, Explicit Estimates from Capture-Recapture Data with Both Death and Immigration-Stochastic Model: Biometrika, v. 52, p. 225–247, doi:10.2307/2333826.

Kirschvink, J.L., 1980, The least-squares line and plane and the analysis of paleomagnetic data: Geophysical Journal International, v. 62, p. 699–718, doi:https://doi.org/10.1111/j.1365-246X.1980.tb02601.x.

Kraft, N.J., Comita, L.S., Chase, J.M., Sanders, N.J., Swenson, N.G., Crist, T.O., Stegen, J.C., Vellend, M., Boyle, B., and Anderson, M.J., 2011, Disentangling the drivers of β diversity along latitudinal and elevational gradients: Science, v. 333, p. 1755–1758.

Kuiper, K.F., Deino, A., Hilgen, F.J., Krijgsman, W., Renne, P.R., and Wijbrans, J.R., 2008, Synchronizing Rock Clocks of Earth History: Science, v. 320, p. 500–504, doi:10.1126/science.1154339.

Labandeira, C.C., Johnson, K.R., and Wilf, P., 2002, Impact of the terminal Cretaceous event on plant–insect associations: Proceedings of the National Academy of Sciences, v. 99, p. 2061–2066, doi:10.1073/pnas.042492999.

Lavorel, S., McIntyre, S., Landsberg, J., and Forbes, T.D.A., 1997, Plant functional classifications: from general groups to specific groups based on response to disturbance: Trends in Ecology & Evolution, v. 12, p. 474–478, doi:10.1016/S0169-5347(97)01219-6.

Lebreton, J.-D., Burnham, K.P., Clobert, J., and Anderson, D.R., 1992, Modeling Survival and Testing Biological Hypotheses Using Marked Animals: A Unified Approach with Case Studies: Ecological Monographs, v. 62, p. 67–118, doi:10.2307/2937171.

LeCain, R., Clyde, W.C., Wilson, G.P., and Riedel, J., 2014, Magnetostratigraphy of the Hell Creek and lower Fort Union Formations in northeastern Montana, *in* Wilson, G.P., Clemens, W.A., Horner, J.R., and Hartman, J.H. eds., Through the End of the Cretaceous in the Type Locality of the Hell Creek Formation in Montana and Adjacent Areas, Geological Society of America Special Paper 503, Geological Society of America Special Paper, v. 503, p. 137–147, doi:10.1130/2014.2503(04).

Lehman, T.M., 1985, Depositional environments of the Naashoibito Member of the Kirtland Shale, Upper Cretaceous, San Juan Basin, New Mexico: New Mexico Bureau of Mines and Mineral Resources Circular, v. 195, p. 55–79.

Lehman, T.M., and Wheeler, E.A., 2009, New Late Cretaceous and Paleocene Dicot Woods of Big Bend National Park, Texas and Review of Cretacous Wood Characteristics: IAWA Journal, v. 30, p. 293–318, doi:10.1163/22941932-90000220.

Leigh, E.G., Davidar, P., Dick, C.W., Puyravaud, J.-P., Terborgh, J., ter Steege, H., and Wright, S.J., 2004, Why Do Some Tropical Forests Have So Many Species of Trees? BIOTROPICA, v. 36, p. 447–473, doi:10.1646/1607.

Leslie, C.E., Peppe, D.J., Williamson, T.E., Heizler, M., Jackson, M., Atchley, S.C., Nordt, L., and Standhardt, B., 2018a, Revised age constraints for Late Cretaceous to early Paleocene terrestrial strata from the Dawson Creek section, Big Bend National Park, west Texas: GSA Bulletin, v. 130, p. 1143–1163, doi:10.1130/B31785.1.

Leslie, C.E., Peppe, D., Williamson, T., Heizler, M., Secord, R., and Leggett, T., 2018b, High-resolution magnetostratigraphy of the upper Nacimiento Formation, San Juan Basin, New Mexico, USA: implications for basin evolution and mammalian turnover: American Journal of Science, v. 318, p. 300–334, doi:10.2475/3.2018.02.

Lesquereux, L., 1878, Contributions to the Fossil Flora of the Western Territories part II, the Tertiary Flora: United States Geological Survey of the Territories, v. 7, 366 p.

Lindsay, E.H., 2003, Chronostratigraphy, biochronology, datum events, land mammal ages, stage of evolution, and appearance event ordination, *in* Flynn, L.J. ed., Vertebrate fossils and their context: contributions in honor of Richard H. Tedford, New York, Bullentin of the American Musuem of NaturalHistory, v. 279, p. 212–230.

Lindsay, E.H., Butler, R.F., and Johnson, N.M., 1981, Magnetic polarity zonation and biostratigraphy of Late Cretaceous and Paleocene continental deposits, San Juan Basin, New Mexico: American Journal of Science, v. 281, p. 390–435, doi:10.2475/ajs.281.4.390.

Lindsay, E.H., Jacobs, L.L., and Butler, R.F., 1978, Biostratigraphy and magnetostratigraphy of Paleocene terrestrial deposits, San Juan Basin, New Mexico: Geology, v. 6, p. 425–429, doi:10.1130/0091-7613(1978)6<425:BAMOPT>2.0.CO;2.

Liow, L.H., and Finarelli, J.A., 2014, A dynamic global equilibrium in carnivoran diversification over 20 million years: Proceedings of the Royal Society B: Biological Sciences, v. 281, p. 20132312, doi:10.1098/rspb.2013.2312.

Liow, L.H., and Nichols, J.D., 2010, Estimating Rates and Probabilities of Origination and Extinction Using Taxonomic Occurrence Data: Capture-Mark-Recapture (CMR) Approaches, *in* Hunt, G. and Alroy, J. eds., Short Courses in Paleontology: Quantitative Paleobiology, New Haven, CT, Yale University Printing and Publishing, p. 81–94.

Liow, L.H., Reitan, T., and Harnik, P.G., 2015, Ecological interactions on macroevolutionary time scales: clams and brachiopods are more than ships that pass in the night: Ecology Letters, v. 18, p. 1030–1039, doi:10.1111/ele.12485.

Liu, Y.-J., Arens, N.C., and Li, C.-S., 2007, Range change in Metasequoia: relationship to palaeoclimate: Botanical Journal of the Linnean Society, v. 154, p. 115–127, doi:10.1111/j.1095-8339.2007.00597.x.

Lofgren, D.L., Lillegraven, J.A., Clemens, W.A., Gingerich, P.D., and Williamson, T.E., 2004, Paleocene Biochronology: The Puercan Through Clarkforkian Land Mammal Ages, *in* Woodburne, M.O. ed., Late Cretaceous and Cenozoic Mammals of North America, New York, Columbia University Press, p. 43–105.

Lowrie, W., 1990, Identification of ferromagnetic minerals in a rock by coercivity and unblocking temperature properties: Geophysical Research Letters, v. 17, p. 159–162, doi:10.1029/GL017i002p00159.

Lucas, S.G., Sullivan, R.M., Cather, S.M., Jasinski, S.E., Fowler, D.W., Heckbert, A.B., Spielmann, J.A., and Hunt, A.P., 2009, No Definitive Evidence of Paleocene Dinosaurs in the San Juan Basin: Palaeontologia Electronica, v. 12, p. 1–10.

Lyson, T.R. et al., 2019, Exceptional continental record of biotic recovery after the Cretaceous–Paleogene mass extinction: Science, doi:10.1126/science.aay2268.

Magurran, A.E., 2004, Measuring Biological Diversity: Maiden, MA, Blackwell Publishing, 264 p.

Marcot, J.D., Fox, D.L., and Niebuhr, S.R., 2016, Late Cenozoic onset of the latitudinal diversity gradient of North American mammals: Proceedings of the National Academy of Sciences, v. 113, p. 7189–7194, doi:10.1073/pnas.1524750113.

Margalef, R., 1958, Information theory in ecology: General Systems, v. 3, p. 36–71.

Mason, I.P., 2013, 40Ar/39Ar Chronostratigraphy of late Cretaceous early Paleocene Rocks of the San Juan Basin, NM [M.S. thesis]: New Mexico Institute of Mining and Technology, 1–25 p.

Matthew, W.D., 1937, Paleocene faunas of the San Juan Basin, New Mexico: Transactions of the American Philosophical Society, v. 30, p. 1–510.

McIver, E.E., 1999, Paleobotanical evidence for ecosystem disruption at the Cretaceous-Tertiary boundary from Wood Mountain, Saskatchewan, Canada: Canadian Journal of Earth Sciences, v. 36, p. 775–789, doi:10.1139/cjes-36-5-775.

McIver, E.E., and Basinger, J.F., 1993, Flora of the Ravenscrag Formation (Paleocene), southwestern Saskatchewan, Canada: Palaeontographica Canadiana, v. 10.

Mehltreter, K., Walker, L.R., and Sharpe, J.M., 2010, Fern Ecology: Cambridge, New York, Cambridge University Press, 474 p.

Miall, A.D., 2010, Alluvial deposits, *in* James, N.P. and Darlrymple, R.W. eds., Facies Models 4, St. John’s, Newfoundland and Labrador, Canada, The Geologic Association of Canada, p. 105–137.

Miller, I.M., Brandon, M.T., and Hickey, L.J., 2006, Using leaf margin analysis to estimate the mid-Cretaceous (Albian) paleolatitude of the Baja BC block: Earth and Planetary Science Letters, v. 245, p. 95–114, doi:10.1016/j.epsl.2006.02.022.

Min, K., Mundil, R., Renne, P.R., and Ludwig, K.R., 2000, A test for systematic errors in 40Ar/39Ar geochronology through comparison with U/Pb analysis of a 1.1-Ga rhyolite: Geochimica et Cosmochimica Acta, v. 64, p. 73–98, doi:10.1016/S0016-7037(99)00204-5.

Mohr, B.A.R., Bernardes-de-Oliveira, M.E.C., Loveridge, R., Pons, D., Sucerquia, P.A., and Castro-Fernandes, M.C., 2015, Ruffordia goeppertii (Schizaeales, Anemiaceae) – A common fern from the Lower Cretaceous Crato Formation of northeast Brazil: Cretaceous Research, v. 54, p. 17–26, doi:10.1016/j.cretres.2014.11.006.

Molino, J.-F., 2001, Tree Diversity in Tropical Rain Forests: A Validation of the Intermediate Disturbance Hypothesis: Science, v. 294, p. 1702–1704, doi:10.1126/science.1060284.

Mooney, H.A., Bullock, S.H., and Medina, E., 1995, Introduction, *in* Bullock, S.H., Mooney, H.A., and Medina, E. eds., Seasonally Dry Tropical Forests, Cambridge, Cambridge University Press, p. 1–9.

Murphy, P.G., and Lugo, A.E., 1986, Ecology of Tropical Dry Forest: Annual Review of Ecology and Systematics, v. 17, p. 67–88, doi:10.1146/annurev.es.17.110186.000435.

Newberry, J.S., 1868, Notes on the later extinct floras of North America, with descriptions of some new species of fossil plants from the Cretaceous and Tertiary strata: Lyceum Natural History New York Annals, v. 9, p. 1–76.

Nichols, D.J., 2003, Palynostratigraphic framework for age determination and correlation of the nonmarine lower Cenozoic of the Rocky Mountains and Great Plains region, *in* Raynolds, R.G. and Flores, R.M. eds., Cenozoic Systems of the Rockey Mountain Region, Denver, CO, Rocky Mountain Section of the Society for Sedimentary Geology (SEPM), p. 107–134.

Nichols, D.J., Fleming, R.F., and Frederiksen, N.O., 1990, Palynological evidence of effects of the terminal Cretaceous event on terrestrial floras in western North America, *in* Kauffman, E.G. and Walliser, O.H. eds., Extinction Events in Earth History, Berlin, Springer-Verlag, Lecture Notes in Earth Sciences, v. 30, p. 351–364, doi:10.1007/BFb0011158.

Nichols, D.J., and Johnson, K.R., 2008, Plants and the K-T Boundary: New York, Cambridge University Press, 292 p.

North, G.R., Cahalan, R.F., and Coakly Jr., J.A., 1981, Energy balance climate models: Reviews of Geophysics, v. 19, p. 91–121.

Ogg, J.G., 2012, Geomagnetic Polarity Timescale, *in* Gradstein, F.M., Ogg, J.G., Schmitz, M., and Ogg, G. eds., The Geologic Timescale, Oxford, United Kingdom, Elsevier Science, p. 85–113.

Osborn, H.F., 1929, The titanotheres of ancient Wyoming, Dakota, and Nebraska: United States Geological Survey Monograph, v. 55, p. 1–701.

O'Sullivan, R.B., Repenning, C.A., Beaumont, E.C., and Page, H.G., 1972, Stratigraphy of the Cretaceous Rocks and the Tertiary Ojo Alamo Sandstone, Navajo and Hopi Indian Reservations, Arizona, New Mexico, and Utah: United States Geological Survey Professional Paper 521-E, p. 1–65.

Peppe, D.J., 2010, Megafloral change in the early and middle Paleocene in the Williston Basin, North Dakota, USA: Palaeogeography, Palaeoclimatology, Palaeoecology, v. 298, p. 224–234, doi:10.1016/j.palaeo.2010.09.027.

Peppe, D.J. et al., 2011a, Sensitivity of leaf size and shape to climate: global patterns and paleoclimatic applications: New Phytologist, v. 190, p. 724–739, doi:10.1111/j.1469-8137.2010.03615.x.

Peppe, D.J. et al., 2011b, Sensitivity of leaf size and shape to climate: global patterns and paleoclimatic applications: New Phytologist, v. 190, p. 724–739, doi:10.1111/j.1469-8137.2010.03615.x.

Peppe, D.J., Baumgartner, A., and Flynn, A.G., in press, Reconstructing paleoclimate and paleoecology using fossil leaves, *in* Croft, D.A., Simpson, S.W., and Su, D.F. eds., Methods in Paleoecology: Reconstructing Cenozoic Terrestrial Environments and Ecological Communities, Dordrect, Springer, Vertebrate Paleobiology and Paleoanthropology.

Peppe, D.J., Evans, D. a. D., and Smirnov, A.V., 2009, Magnetostratigraphy of the Ludlow Member of the Fort Union Formation (Lower Paleocene) in the Williston Basin, North Dakota: Geological Society of America Bulletin, v. 121, p. 65–79, doi:10.1130/B26353.1.

Peppe, D.J., Heizler, M., Williamson, T.E., Mason, I.P., Brusatte, S., Weil, A., and Secord, R., 2013, New Age Constraints on Late Cretaceous through Early Paleocene Age Rocks in the San Juan Basin, New Mexico, *in* Geologic Society of America, Abstracts with Programs, 7, v. 45.

Peppe, D.J., Hickey, L.J., Miller, I.M., and Green, W.A., 2008, A Morphotype Catalogue, Floristic Analysis and Stratigraphic Description of the Aspen Shale Flora (Cretaceous–Albian) of Southwestern Wyoming: Bulletin of the Peabody Museum of Natural History, v. 49, p. 181–208.

Phillips, D., Matchan, E.L., Honda, M., and Kuiper, K.F., 2017, Astronomical calibration of 40Ar/39Ar reference minerals using high-precision, multi-collector (ARGUSVI) mass spectrometry: Geochimica et Cosmochimica Acta, v. 196, p. 351–369, doi:10.1016/j.gca.2016.09.027.

Phillips, O., and Miller, J.S., 2002, Global Patterns of Plant Diversity: Alwyn H. Gentry's Forest Transect Data Set: St. Louis, Mo, Missouri Botanical Garden Press, 319 p.

Pielou, E.C., 1969, An introduction to mathematical ecology: New York, Wiley, 294 p.

Pittermann, J., Stuart, S.A., Dawson, T.E., and Moreau, A., 2012, Cenozoic climate change shaped the evolutionary ecophysiology of the Cupressaceae conifers: Proceedings of the National Academy of Sciences of the United States of America, v. 109, p. 9647–9652, doi:10.1073/pnas.1114378109.

Poorter, H., Niinemets, Ü., Poorter, L., Wright, I.J., and Villar, R., 2009, Causes and consequences of variation in leaf mass per area (LMA): a meta-analysis: New Phytologist, v. 182, p. 565–588, doi:10.1111/j.1469-8137.2009.02830.x.

Powell, J.S., 1973, Paleontology and Sedimentation Models of the Kimbeto Member of the Ojo Alamo Sandstone, *in* Fassett, J.E. ed., Cretaceous and Tertiary Rocks of the Southern Colorado Plateau: a Memoir of the Four Corners Geological Society, Four Corners Geologic Society, p. 111–122.

Pradel, R., 1996, Utilization of Capture-Mark-Recapture for the Study of Recruitment and Population Growth Rate: Biometrics, v. 52, p. 703–709, doi:10.2307/2532908.

Pyke, C.R., Condit, R., Aguilar, S., and Lao, S., 2001, Floristic Composition across a Climatic Gradient in a Neotropical Lowland Forest: Journal of Vegetation Science, v. 12, p. 553–566, doi:10.2307/3237007.

Quillévéré, F., Norris, R.D., Kroon, D., and Wilson, P.A., 2008, Transient ocean warming and shifts in carbon reservoirs during the early Danian: Earth and Planetary Science Letters, v. 265, p. 600–615, doi:10.1016/j.epsl.2007.10.040.

Raup, D.M., and Crick, R.E., 1979, Measurement of faunal similarity in paleontology: Journal of Paleontology, v. 53, p. 1213–1227.

Reich, P.B., Walters, M.B., and Ellsworth, D.S., 1992, Leaf Life-Span in Relation to Leaf, Plant, and Stand Characteristics among Diverse Ecosystems: Ecological Monographs, v. 62, p. 365–392, doi:10.2307/2937116.

Renne, P.R., Sprain, C.J., Richards, M.A., Self, S., Vanderkluysen, L., and Pande, K., 2015, State shift in Deccan volcanism at the Cretaceous-Paleogene boundary, possibly induced by impact: Science, v. 350, p. 76–78, doi:10.1126/science.aac7549.

Riva, E.G. de la, Olmo, M., Poorter, H., Ubera, J.L., and Villar, R., 2016, Leaf Mass per Area (LMA) and Its Relationship with Leaf Structure and Anatomy in 34 Mediterranean Woody Species along a Water Availability Gradient: PLOS One, v. 11, p. 1–18, doi:10.1371/journal.pone.0148788.

Roberts, A.P., 1995, Magnetic properties of sedimentary greigite (Fe3S4): Earth and Planetary Science Letters, v. 134, p. 227–236, doi:10.1016/0012-821X(95)00131-U.

Royer, D.L. et al., 2007, Fossil leaf economics quantified: calibration, Eocene case study, and implications: Paleobiology, v. 33, p. 574–589, doi:10.1666/07001.1.

Royer, D.L., Miller, I.M., Peppe, D.J., and Hickey, L.J., 2010, Leaf economic traits from fossils support a weedy habit for early angiosperms: American Journal of Botany, v. 97, p. 438–445, doi:10.3732/ajb.0900290.

Royer, D.L., Wilf, P., Janesko, D.A., Kowalski, E.A., and Dilcher, D.L., 2005, Correlations of climate and plant ecology to leaf size and shape: potential proxies for the fossil record: American Journal of Botany, v. 92, p. 1141–1151, doi:10.3732/ajb.92.7.1141.

Schmidt, A. et al., 2016, Selective environmental stress from sulphur emitted by continental flood basalt eruptions: Nature Geoscience, v. 9, p. 77–82, doi:10.1038/ngeo2588.

Schoene, B., Eddy, M.P., Samperton, K.M., Keller, C.B., Keller, G., Adatte, T., and Khadri, S.F.R., 2019, U-Pb constraints on pulsed eruption of the Deccan Traps across the end-Cretaceous mass extinction: Science, v. 363, p. 862–866, doi:10.1126/science.aau2422.

Schulte, P. et al., 2010, The Chicxulub Asteroid Impact and Mass Extinction at the Cretaceous-Paleogene Boundary: Science, v. 327, p. 1214–1218, doi:10.1126/science.1177265.

Sibert, E., Friedman, M., Hull, P., Hunt, G., and Norris, R., 2018, Two pulses of morphological diversification in Pacific pelagic fishes following the Cretaceous–Palaeogene mass extinction: Proceedings of the Royal Society B: Biological Sciences, v. 285, p. 20181194, doi:10.1098/rspb.2018.1194.

Sikkink, P.G.L., 1987, Lithofacies relationships and depositional environment of the Tertiary Ojo Alamo Sandstone and related strata, San Juan Basin, New Mexico and Colorado: Special Paper of the Geological Society of America, v. 209, p. 81–104, doi:10.1130/SPE209-p81.

Simpson, G.G., 1959, Fossil Mammals from the Type Area of the Puerco and Nacimiento Strata, Paleocene of New Mexico: American Museum Novitates, v. 1957, p. 1–22.

Sinclair, W.J., and Granger, W., 1914, Paleocene deposits of the San Juan Basin, New Mexico: Bulletin of the American Museum of Natural History, v. 33, p. 297–316.

Smith, S.M., Sprain, C.J., Clemens, W.A., Lofgren, D.L., Renne, P.R., and Wilson, G.P., 2018a, Early mammalian recovery after the end-Cretaceous mass extinction: A high-resolution view from McGuire Creek area, Montana, USA: GSA Bulletin, v. 130, p. 2000–2014, doi:10.1130/B31926.1.

Smith, S.M., Sprain, C.J., Clemens, W.A., Lofgren, D.L., Renne, P.R., and Wilson, G.P., 2018b, Early mammalian recovery after the end-Cretaceous mass extinction: A high-resolution view from McGuire Creek area, Montana, USA: GSA Bulletin, v. 130, p. 2000–2014, doi:10.1130/B31926.1.

Sprain, C.J., Feinberg, J.M., Renne, P.R., and Jackson, M., 2016, Importance of titanohematite in detrital remanent magnetizations of strata spanning the Cretaceous-Paleogene boundary, Hell Creek region, Montana: Geochemistry, Geophysics, Geosystems, v. 17, p. 660–678, doi:10.1002/2015GC006191.

Sprain, C.J., Renne, P.R., Clemens, W.A., and Wilson, G.P., 2018, Calibration of chron C29r: New high-precision geochronologic and paleomagnetic constraints from the Hell Creek region, Montana: GSA Bulletin, v. 130, p. 1615–1644, doi:10.1130/B31890.1.

Sprain, C.J., Renne, P.R., Vanderkluysen, L., Pande, K., Self, S., and Mittal, T., 2019, The eruptive tempo of Deccan volcanism in relation to the Cretaceous-Paleogene boundary: Science, v. 363, p. 866–870, doi:10.1126/science.aav1446.

Sprain, C.J., Renne, P.R., Wilson, G.P., and Clemens, W.A., 2015, High-resolution chronostratigraphy of the terrestrial Cretaceous-Paleogene transition and recovery interval in the Hell Creek region, Montana: GSA Bulletin, v. 127, p. 393–409, doi:10.1130/B31076.1.

Stromberg, J.C., 2001, Biotic integrity of Platanus wrightii riparian forests in Arizona: first approximation: Forest Ecology and Management, v. 142, p. 251–266, doi:10.1016/S0378-1127(00)00355-8.

Subbarao, K.V., and Courtillot, V., 2017, Deccan basalts in and around Koyna — Warna region, Maharashtra: Some reflections: Journal of the Geological Society of India, v. 90, p. 653–662, doi:10.1007/s12594-017-0772-y.

Sullivan, R.M., and Lucas, S.G., 2003, The Kirtlandian, a new land vertebrate “age” for the Late Cretaceous of Western North America: Guidebook of the New Mexico Geological Society, v. 54, p. 369–377.

Sullivan, R.M., Lucas, S.G., and Braman, D.R., 2005, Dinosaurs, pollen, and the Cretaceous-Tertiary boundary in the San Juan Basin: Guidebook of the New Mexico Geological Society, v. 56, p. 395–407.

Taylor, J.R., 1982, An Introduction to Error Analysis: The Study of Uncertainties in Physical Measurements: Mill Valley, CA, University Science Books, 270 p.

Taylor, L.H., and Butler, R.F., 1980, Magnetic-polarity stratigraphy of Torrejonian sediments, Nacimiento Formation, San Juan Basin, New Mexico: American Journal of Science, v. 280, p. 97–115, doi:10.2475/ajs.280.2.97.

Tidwell, W.D., Ash, S.R., and Parker, L.R., 1981, Cretaceous and Tertiary floras of the San Juan Basin, *in* Lucas, S.G., Rigby, J.K., and Kues, B.S. eds., Advances in San Juan Paleontology, Albuquerque, New Mexico, University of New Mexico Press, p. 307–332.

Tomida, Y., 1981, “Dragonian” fossils from the San Juan Basin and the status of “Dragonian” land mammal “age,” *in* Lucas, S.G., Rigby, J.K.Jr., and Kues, B.S. eds., Advances in San Juan Basin Paleontology, Albuquerque, New Mexico, University of New Mexico Press, p. 222–241.

Tomida, Y., and Butler, R.F., 1980, Dragonian mammals and Paleocene magnetic polarity stratigraphy, North Horn Formation, central Utah: American Journal of Science, v. 280, p. 787–811, doi:10.2475/ajs.280.8.787.

Torsvik, T.H., Müller, R.D., Van der Voo, R., Steinberger, B., and Gaina, C., 2008, Global plate motion frames: Toward a unified model: Reviews of Geophysics, v. 46, p. 44, doi:10.1029/2007RG000227.

Trendell, A.M., Atchley, S.C., and Nordt, L.C., 2013, Facies analysis of a probable large fluvial fan depositional system: The Upper Triassic Chinle Formation at Petrified Forest National Park, Arizona, USA: Journal of Sedimentary Research, v. 83, p. 873–895, doi:10.2110/jsr.2013.55.

Tryon, R.M., and Tryon, A.F., 1982, Ferns and Allied Plants: With Special Reference to Tropical America: New York, Springer-Verlag, 858 p.

Vajda, V., and Bercovici, A., 2014, The global vegetation pattern across the Cretaceous–Paleogene mass extinction interval: A template for other extinction events: Global and Planetary Change, v. 122, p. 29–49, doi:10.1016/j.gloplacha.2014.07.014.

Webb, L.J., 1959, A Physiognomic Classification of Australian Rain Forests: Journal of Ecology, v. 47, p. 551–570, doi:10.2307/2257290.

Weissmann, G.S. et al., 2013, Prograding distributive fluvial systems: geomorphic models and ancient examples, *in* Driese, S.G. and Nordt, L.C. eds., New Frontiers in Paleopedology and Terrestrial Paleoclimatology, SEPM Special Publication, v. 104, p. 131–147.

Wheeler, E.A., McClammer, J., and LaPasha, C.A., 1995, Similarities and differences in dicotyledonous woods from the Cretaceous and Paleocene - San Juan Basin, New Mexico, USA: IAWA Journal, v. 16, p. 223–254.

White, G.C., and Burnham, K.P., 1999, Program MARK: survival estimation from populations of marked animals: Bird Study, v. 46, p. S120–S139, doi:10.1080/00063659909477239.

Whittaker, R.H., 1975, Communities and Ecosystems: New York, Macmilan, 1–352 p.

Wilf, P., 1997, When are leaves good thermometers? A new case for Leaf Margin Analysis: Paleobiology, v. 23, p. 373–390, doi:10.1017/S0094837300019746.

Wilf, P., and Johnson, K.R., 2004, Land plant extinction at the end of the Cretaceous: a quantitative analysis of the North Dakota megafloral record: Paleobiology, v. 30, p. 347–368, doi:10.1666/0094-8373(2004)030<0347:LPEATE>2.0.CO;2.

Wilf, P., Johnson, K.R., and Huber, B.T., 2003, Correlated Terrestrial and Marine Evidence for Global Climate Changes before Mass Extinction at the Cretaceous-Paleogene Boundary: Proceedings of the National Academy of Sciences of the United States of America, v. 100, p. 599–604, doi:10.1073/pnas.0234701100.

Wilf, P., Labandeira, C.C., Johnson, K.R., and Ellis, B., 2006, Decoupled plant and insect diversity after the end-Cretaceous extinction: Science, v. 313, p. 1112–1115.

Wilf, P., Wing, S.L., Greenwood, D.R., and Greenwood, C.L., 1998, Using fossil leaves as paleoprecipitation indicators: An Eocene example: Geology, v. 26, p. 203–206, doi:10.1130/0091-7613(1998)026<0203:UFLAPI>2.3.CO;2.

Williamson, T.E., 1996, The beginning of the age of mammals in the San Juan Basin, New Mexico: Biostratigraphy and evolution of Paleocene mammals of the Nacimiento Formation: New Mexico Museum of Natural History and Science Bulletin, v. 8, p. 1–141.

Williamson, T.E., Brusatte, S.L., Secord, R., and Shelley, S., 2016, A new taeniolabidoid multituberculate (Mammalia) from the middle Puercan of the Nacimiento Formation, New Mexico, and a revision of taeniolabidoid systematics and phylogeny: Zoological Journal of the Linnean Society, v. 177, p. 183–208, doi:10.1111/zoj.12336.

Williamson, T.E., and Lucas, S.G., 1992, Stratigraphy and mammalian biostratigraphy of the Paleocene Nacimiento Formation, southern San Juan Basin, New Mexico: New Mexico Geological Society Guidebook, v. 43, p. 265–296.

Williamson, T.E., and Lucas, S.G., 1997, The Chico Springs locality, Nacimiento Formation, San Juan Basin, New Mexico: New Mexico Geological Society Guidebook, v. 48, p. 259–265.

Williamson, T.E., Nichols, D.J., and Weil, A., 2008, Paleocene palynomorph assemblages from the Nacimiento Formation, San Juan Basin, New Mexico, and their biostratigraphic significance: New Mexico Geology, v. 30, p. 3–11.

Williamson, T.E., and Weil, A., 2008a, Metatherian Mammals from the Naashoibito Member, Kirtland Formation, San Juan Basin, New Mexico and Their Biochronologic and Paleobiogeographic Significance: Journal of Vertebrate Paleontology, v. 28, p. 803–815, doi:10.1671/0272-4634(2008)28[803:MMFTNM]2.0.CO;2.

Williamson, T.E., and Weil, A., 2008b, Stratigraphic Distribution of Sauropods in the Upper Cretaceous of the San Juan Basin, New Mexico, with Comments on North America's Cretaceous "Sauropod Hiatus": Journal of Vertebrate Paleontology, v. 28, p. 1218–1223, doi:10.1671/0272-4634-28.4.1218.

Wilson, G.P., 2014, Mammalian extinction, survival, and recovery dynamics across the Cretaceous-Paleogene boundary in northeastern Montana, USA, *in* Wilson, G.P., Clemens, W.A., Horner, J.R., and Hartman, J.H. eds., Through the End of the Cretaceous in the Type Locality of the Hell Creek Formation in Montana and Adjacent Areas, Geological Society of America Special Paper 503, p. 365–392.

Wing, S.L., Alroy, J., and Hickey, L.J., 1995a, Plant and mammal diversity in the Paleocene to early Eocene of the Bighorn Basin: Palaeogeography, Palaeoclimatology, Palaeoecology, v. 115, p. 117–155, doi:10.1016/0031-0182(94)00109-L.

Wing, S.L., Alroy, J., and Hickey, L.J., 1995b, Plant and mammal diversity in the Paleocene to early Eocene of the Bighorn Basin: Palaeogeography, Palaeoclimatology, Palaeoecology, v. 115, p. 117–155, doi:10.1016/0031-0182(94)00109-L.

Wing, S.L., and Currano, E.D., 2013, Plant response to a global greenhouse event 56 million years ago: American Journal of Botany, v. 100, p. 1234–1254, doi:10.3732/ajb.1200554.

Wing, S.L., Harrington, G.J., Smith, F.A., Bloch, J.I., Boyer, D.M., and Freeman, K.H., 2005, Transient Floral Change and Rapid Global Warming at the Paleocene-Eocene Boundary: Science, v. 310, p. 993–996, doi:10.1126/science.1116913.

Wolfe, J.A., and Upchurch, G.R., 1987, Leaf Assemblages across the Cretaceous-Tertiary Boundary in the Raton Basin, New Mexico and Colorado: Proceedings of the National Academy of Sciences of the United States of America, v. 84, p. 5096–5100, doi:10.1073/pnas.84.15.5096.

Wood, H.E., Chaney, R.W., Clark, J., Colbert, E.H., Jepsen, G.L., Reeside, J.B., and Stock, C., 1941, Nomenclature and correlation of the North American Continental Tertiary: Bulletin of the Geological Society of America, v. 52, p. 1–48.

Wright, I.J. et al., 2004, The worldwide leaf economics spectrum: Nature, v. 428, p. 821–827.

Yoshifuji, N., Kumagai, T., Tanaka, K., Tanaka, N., Komatsu, H., Suzuki, M., and Tantasirin, C., 2006, Inter-annual variation in growing season length of a tropical seasonal forest in northern Thailand: Forest Ecology and Management, v. 229, p. 333–339, doi:10.1016/j.foreco.2006.04.013.

Ziegler, A.M., Rees, P.M., Rowley, D.B., Bekker, A., Qing, L., and Hulver, M.L., 1996, Mesozoic assembly of Asia: constraints from fossil floras, tectonics, and paleomagnetism, *in* Yin, A. and Harrison, M. eds., The Tectonic Evolution of Asia, Cambridge University Press, p. 371–400.